Strain Softening and Instability of Sand under Plane-Strain Conditions

Dariusz Wanatowski

SCHOOL OF CIVIL AND ENVIRONMENTAL ENGINEERING

NANYANG TECHNOLOGICAL UNIVERSITY

2005

Strain Softening and Instability of Sand under Plane-Strain Conditions

Dariusz Wanatowski

School of Civil & Environmental Engineering

A thesis submitted to the Nanyang Technological University
in fulfilment of the requirement for the degree of
Doctor of Philosophy

2005

ACKNOWLEDGMENTS

The research work presented in this thesis has been carried out under the supervision of Associate Professor Chu Jian, who has been a constant source of ideas, guidance and support throughout this research. I would like to thank him for his persistence and valuable advices.

Special thanks go to all the technicians from the Geotechnics Laboratory, especially to Mr. Vincent H. K. Heng, Mr. S. L. Tay and Mr. Eugene H. G. Tan for their invaluable assistance in the setting up of the plane-strain apparatus. The experiments would not have been carried out smoothly without your patient guidance and assistance.

I would also like to thank my research colleagues in the School of Civil and Environmental Engineering who have made my stay at NTU so enjoyable and memorable. Special thanks go to Chin Liang, Huili, Meng Hwee, Manish and Claudia for sharing the knowledge of the laboratory work, for being there for a "little chat", and most of all, for being my friends.

My heartfelt thanks and appreciations also go to my Polish friends Piotr and Barbara who have made me feel much closer to Poland, my native county.

I would like to express my gratitude to the Nanyang Technological University in Singapore for granting the scholarship for this Ph.D. programme. I am also extremely grateful to the members of the Institute of Civil Engineering at the Poznań University of Technology in Poland, especially Professor A. Florkiewicz, Head of Division of Geotechnics and Engineering Geology, for allowing me to study in Singapore.

Last but not least, my deepest appreciation goes to my mother Jadwiga, my sister Dorota with her family, and my wife Lina, for their encouragement for my research and for their continued love throughout my life.

TABLE OF CONTENTS

SUMMARY

The majority of experimental studies on strain softening and instability behaviour of sand have been carried out under axisymmetric conditions. However, many geotechnical problems cannot be idealised as axisymmetric conditions, but as plane-strain conditions. Therefore, it is more relevant to study the stress-strain behaviour of soil under plane-strain conditions.

A comprehensive experimental study on the strain softening and instability behaviour of granular soil under plane-strain conditions is presented in this thesis. A new plane-strain apparatus was developed and used in this study. The main features of the new plane-strain apparatus were that free-ends were used and the lateral stress (σ_2) was measured by four submersible load cells. The occurrence of shear bands and non-homogeneous deformations could be detected by comparing the σ_2 versus shear strain curves obtained from the four individual load cells.

A granular fill, the so-called Changi sand, was retrieved from a reclamation site in Singapore and used in the experiments. The study was carried out mainly by conducting specialised plane-strain tests on very loose to medium dense Changi sand using the new plane-strain apparatus. Based on several series of drained and undrained tests conducted on the Changi sand at very loose, medium loose and medium dense states under plane-strain conditions, the drained and undrained characteristics of the sand were studied. The critical state line, the failure lines and the instability lines were established. The tests were conducted under both deformation-controlled and load-controlled loading modes so that the effect of loading mode on the strain softening and instability behaviour could be studied. The test results show that the post-peak behaviour of sand in both drained and undrained tests is affected by the loading mode. Under a deformation-controlled loading mode, strain softening develops, whereas under a load-controlled loading mode, instability occurs. It has also been observed that the critical state line under the plane-strain condition is different from that under the triaxial condition. These

findings have important practical implications and will affect the assumptions that can be made regarding the soil behaviour in mathematical modelling and numerical analysis.

In stress path controlled tests, strain softening in the form of decreasing deviatoric stress may be suppressed. In this study, the strain softening behaviour of sand was investigated by strain path testing, in which $d\varepsilon_v/d\varepsilon_1$ was controlled. Under plane-strain conditions, two types of strain softening, material softening and banding softening were identified. The occurrence of strain softening under plane-strain conditions is affected by the void ratio, the strain increment ratio and the initial effective confining stress. Using strain path tests, the asymptotic behaviour under plane-strain conditions was also established. When medium loose to medium dense sand is sheared along a constant $d\varepsilon_v/d\varepsilon_1$ path, the resulting effective stress path will approach asymptotically a constant stress ratio line (CSRL). The smaller (i.e., more negative) the imposed strain increment ratio, the larger the resultant asymptotic stress ratio, $(q/p')_{asy}$. A relationship between the imposed strain increment ratio and the resultant constant stress ratio has been established experimentally. This relationship is consistent with that established by Chu et al. (1992) under axisymmetric conditions.

Following the previous studies of Leong (2001) and Loke (2004) under axisymmetric conditions, the instability behaviour of both contractive and dilative sand was further studied under various drainage conditions along a constant shear stress path with decreasing mean effective stress. The results have shown that the instability line defined using Lade's method, is the same for both drained and undrained conditions and the instability line defines the lower bound of all the possible unstable conditions regardless of the drainage conditions. Therefore, a zone of instability can be defined as the area bound by the failure line and the instability line. Instability will occur under either undrained or drained condition when the stress state falls into the zone of instability.

A runaway type of instability can occur even for medium dense sand when a constant shear test is conducted under a constant $d\varepsilon_v/d\varepsilon_1$ condition (CSSP test). Similarly to the condition for the occurrence of strain softening, the strain

increment ratio imposed to a specimen has to be adequately low (i.e., negative) to generate pore water pressure. If the $(d\varepsilon_v/d\varepsilon_1)_i$ experienced by the specimen in a strain path test is more negative than the $(d\varepsilon_v/d\varepsilon_1)_{max}$ obtained from a drained test, the specimen will become unstable. The occurrence of this type of instability is associated with the increase in pore water pressure. Therefore, the increase in pore water pressure is the necessary condition for the occurrence of this type of instability. It is also found that the instability line obtained from the CSSP tests coincides with the peak stress line obtained from the strain path tests conducted under deformation-controlled loading mode. This shows that the peak stress line can be used to predict the instability conditions in CSSP tests.

Shear bands always occur during plane-strain tests on medium loose and medium dense sand under drained conditions. However, shear bands do not always occur when very loose sand is tested under drained conditions. Under undrained conditions, shear bands can also develop unless the specimen is looser than the void ratio at the critical state. The measured shear band inclinations for the Changi sand are in the range from 49.6° to 58.6°, giving an average value of 56°. Shear band orientations were best predicted by Roscoe's solution.

LIST OF TABLES

LIST OF FIGURES

LIST OF SYMBOLS

I. NOTATIONS

b	:	magnitude of the intermediate principal stress (*b-value*)
B	:	Skempton's pore water pressure parameter
C_C	:	coefficient of curvature
C_U	:	coefficient of uniformity
C^e_{ijkl}	:	elastic stiffness tensor
$-d\varepsilon_v/d\varepsilon_1$	:	dilatancy ratio
$(-d\varepsilon_v/d\varepsilon_1)_{max}$	:	maximum dilatancy ratio at failure
$d\varepsilon_v/d\varepsilon_1$	:	strain increment ratio
$(d\varepsilon_v/d\varepsilon_1)_f$	:	strain increment ratio at failure
$(d\varepsilon_v/d\varepsilon_1)_i$	:	strain increment ratio imposed
D	:	dilatancy factor $(D = 1 - d\varepsilon_v/d\varepsilon_1)$
D_{50}	:	mean grain size (mm)
Dr_0	:	initial relative density (%)
Dr_c	:	relative density at the end of consolidation (%)
e	:	void ratio
e_0	:	initial void ratio (after saturation)
e_c	:	void ratio after consolidation
e_{cr}	:	void ratio at critical state
e_f	:	void ratio at the end of the experiment
e_{IL}	:	void ratio at the instability point
e_{max}	:	maximum void ratio
e_{min}	:	minimum void ratio
f	:	yield function in stress space
$\hat{f}$	:	yield function in stress space related parameter
g	:	yield function in strain space
$\hat{g}$	:	yield function in strain space related parameter
G	:	plastic potential function
G_s	:	specific gravity of soil

h	:	parameter in Eqn. (2 – 1)
I_1	:	the first principal stress invariant
I_3	:	the third principal stress invariant
K	:	constant in Rowe's stress-dilatancy equation
K_0	:	coefficient of lateral earth pressure at rest
m	:	constant in Lade's failure criterion in Eqn. (5 – 8)
M_{cs}	:	effective stress ratio at critical state
M_d	:	mass of dry sand specimen (g)
M_L	:	gradient of the constant stress ratio line
M_T	:	torque applied in hollow cylinder apparatus (kNm)
M_w	:	mass of pore water in sand specimen (g)
p'	:	mean effective stress (kPa)
p_a	:	atmospheric pressure
p_c'	:	mean effective stress at the end of consolidation (kPa)
p_i	:	inner cell pressure applied in hollow cylinder apparatus (kPa)
p_o	:	outer cell pressure applied in hollow cylinder apparatus (kPa)
q	:	deviatoric stress (kPa)
q_c	:	deviatoric stress at the end of consolidation (kPa)
q/p'	:	effective stress ratio
$(q/p')_{asy}$	:	effective stress ratio at asymptotic state
s	:	maximum shear stress in the plane of shearing
t	:	mean effective stress in the plane of shearing
u	:	pore water pressure
W	:	vertical load applied in hollow cylinder apparatus (kN)
W_p	:	plastic work
α	:	major principal stress direction (°)
β	:	parameter in Eqn. (2 – 7)
δ_{ij}	:	a vector on the hydrostatic axis (Kronecker delta)
Δu	:	excess pore water pressure (kPa)
ε_1	:	axial strain (%)
ε_2	:	lateral strain $\varepsilon_2 = 0$ (%)
ε_3	:	lateral strain (%)
ε_v	:	volumetric strain (%)
ε_s	:	deviatoric strain (%)

$\dot{\varepsilon}_{ij}^{p}$	:	plastic strain increment
$\dot{\varepsilon}_{ij}^{t}$	:	total strain increment
η_1	:	constant in Lade's failure criterion in Eqn. (5 – 8)
η_{IL}	:	effective stress ratio at instability line, $(q/p')_{IL}$
η_f	:	effective stress ratio at failure, $(q/p')_f$
η_p	:	gradient of the peak stress line, $(q/p)_p$
η_{ult}	:	effective stress ratio at ultimate state, $(q/p')_{ult}$
θ	:	angle of the shear band orientation (°)
θ_A	:	Arthur's shear band inclination (°)
θ_C	:	Coulomb's shear band inclination (°)
θ_R	:	Roscoe's shear band inclination (°)
φ'	:	effective friction angle (°)
φ'_{cs}	:	effective friction angle at critical state (°)
φ'_{ps}	:	effective friction angle under plane-strain conditions (°)
φ'_{tri}	:	effective friction angle under triaxial conditions (°)
μ	:	Lode stress parameter in Eqn. (2 – 12)
ν	:	Lode strain parameter in Eqn. (2 – 12)
σ_1	:	total major principal stress (kPa)
σ_2	:	total intermediate principal stress (kPa)
σ_3	:	total minor principal stress (kPa)
σ_1'	:	effective major principal stress (kPa)
σ_2'	:	effective intermediate principal stress (kPa)
σ_3'	:	effective minor principal stress (kPa)
$\dot{\sigma}_{ij}$	:	stress increment
σ_r	:	total radial direct stress in hollow cylindrical sample (kPa)
σ_z	:	total vertical direct stress in hollow cylindrical sample (kPa)
σ_θ	:	total circumferential direct stress in hollow cylindrical sample(kPa)
$\tau_{\theta z}$	:	torsional shear stress in hollow cylindrical sample (kPa)
ψ	:	state parameter
$\bar{\psi}$	:	modified state parameter
ψ_s	:	mobilized dilatancy angle of the soil (°)

II. ABBREVIATIONS

CSD	:	constant-shear drained
CSL	:	critical state line
CSRL	:	constant stress ratio line
CSSP	:	constant shear strain path
DAC	:	data acquisition card
DC	:	deformation-controlled loading mode
DPVC	:	digital pressure/volume controller
FL	:	failure line
HCA	:	hollow cylinder apparatus
ICL	:	isotropic consolidation line
IL	:	instability line
LC	:	load-controlled loading mode
LVDT	:	linear variable differential transformer
MT	:	moist tamping method
NC	:	normally consolidated
OC	:	overconsolidated
PC	:	personal computer
ps	:	plane-strain
PSA	:	plane strain apparatus
PSL	:	peak stress line
SSL	:	steady-state line
tri	:	triaxial
WS	:	water sedimentation method

CHAPTER 1

INTRODUCTION

1.1 Background

Singapore is a country with very limited land resources. Offshore land reclamation has been carried out by using mainly hydraulically deposited granular soils in the past to cater for further economic expansion. At present, more than 15% of the total Singapore area is reclaimed land. Furthermore, the hydraulically deposited sand fill is relatively loose which makes it susceptible to liquefaction or instability. A study on the engineering behaviour of the granular fill, in particular strain softening and instability, is essential.

The fundamental properties and the drained and undrained behaviour of the granular fill were reported by Leong et al. (2000) and Leong (2001). Loke (2004) carried out studies on the effect of various factors such as fines content, strain rate or sample preparation methods on the stress-strain behaviour of the granular fill. Most of the experiments were conducted under axisymmetric conditions except Gan (2002) who studied the effect of principal stress rotation on the liquefaction and the instability behaviour of the granular fill using a hollow cylinder apparatus. However, further studies on strain softening and instability of sand should be carried out under plane-strain or more general stress conditions. This is necessary not only because the stress conditions under plane-strain or three dimensional conditions are more representative of the engineering problems, but also because the effect of shear band formation on the unstable behaviour of sand can be studied.

Although shear band formation has been extensively examined in the past (e.g. Desrues et al., 1985, 1996; Drescher et al., 1990; Han & Drescher, 1993; Chu et al., 1996; Finno et al., 1996, 1997; Alshibli & Sture, 2000; Wang & Lade, 2001; Finno & Rechenmacher, 2003; Alshibli et al., 2003), most of studies have focused on the inclination and patterns of shear bands. Furthermore, few studies on the instability behaviour of sand under plane-strain conditions have been carried out. The interrelation between instability and shear band formation has not been fully studied either.

1.2 Objectives

The objectives of this study are:

a) to study the strength and deformation characteristics of the granular material under plane-strain conditions;
b) to study the mechanisms of strain softening and instability of very loose to medium dense sand under plane-strain conditions and the factors that affect the occurrence of strain softening and instability;
c) to compare the behaviour of sand under axisymmetric conditions with that under plane-strain conditions;
d) to investigate the relationship among strain softening, instability and shear band formation;
e) to discuss the practical implication of the current research.

1.3 Scope of Study

A granular fill material obtained from the Changi reclamation site in Singapore, locally known as Changi sand, was used for this study. A new plane-strain apparatus was used to study experimentally the behaviour of saturated, very loose to medium dense sand under drained, undrained and other drainage conditions. The effects of various factors on the strain softening and instability of granular soils were investigated. In relation to the strain softening behaviour of medium dense sand, the asymptotic behaviour of granular soils was also studied. Based on the experimental data, the conditions under which strain softening and instability can

occur under plane-strain conditions were established. Finally, the influence of the shear band development on the failure mechanisms of granular soils was discussed.

1.4 Outline of Thesis

This thesis consists of 7 chapters. A review of previous theoretical and experimental studies on strain softening and instability behaviour of granular soils is presented in Chapter 2. Chapter 3 presents the testing arrangement and methodology adopted in the study. The stress-strain behaviour of the granular soil under plane-strain conditions is discussed in Chapter 4. The asymptotic behaviour of granular soils under plane-strain conditions is investigated in Chapter 5. The strain softening behaviour under plane-strain conditions is also studied in Chapter 5. The instability of the granular soil under undrained, drained and strain path controlled conditions is studied in Chapter 6. Finally, the conclusions, practical implications and recommendations for future study are made in Chapter 7.

CHAPTER 2

LITERATURE REVIEW

2.1 Introduction

Landslides are commonly classified as falls, topples, slides, spreads and flows based on their ways of movement. This classification, however, does not describe landslide initiation mechanisms which need to be understood in order to propose counter measures to slope failures. A geotechnical classification based on the initiation mechanisms of landslides was proposed by Sassa (1989). He classified slope failures into three groups, slide, liquefaction and creep. It should be pointed out that liquefaction is the most rapid and thus the most dangerous initiation mechanism of landslides. Therefore, it requires the special attention of civil engineers and researchers.

The most common usage of the term static liquefaction includes strain softening phenomenon wherein a mass of soil which is subjected to undrained monotonic loading loses a large percentage of its shear resistance and flows in a liquid manner (Castro, 1969). This definition was adopted in many studies (e.g. Castro & Poulos, 1977; Morris, 1983; Poulos et al., 1985; Kramer & Seed, 1988; Lade, 1992). It is a common understanding that static liquefaction only occurs for loose granular material under undrained conditions. However, this may not be the case in practice. Slope failure in dilating soil has been observed in several cases by Been et al. (1988). The Fort Peck Dam case is one of such failures. Flow failures in Mississippi riverbanks occurring in dense sand was also described by Torrey & Weaver (1984). Furthermore, Been et al. (1987, 1988) argued that a well-documented Nerlerk berm case (Sladen et al., 1985a; Konrad, 1991; Lade, 1993)

might also have occurred for dilating sand. Therefore, liquefaction type of unstable behaviour may occur for sand that is not loose or there are other than liquefaction failure mechanisms of dense granular soil slopes.

Furthermore, numerous failures in granular slopes under other than undrained conditions have been reported in the past (Eckersley, 1985, 1990; Olson et al., 2000; Sassa, 2000; Adalier & Elgamal, 2002). In laboratory model tests, Eckersley (1990) observed that the flow slide in a granular soil slope occurred under a drained conditions. In the analysis of Wachusett Dam case in 1907, Olson et al. (2000) also concluded that the failure was caused by static liquefaction under completely drained conditions. In fact, the possibility of static liquefaction occurring under other than undrained conditions has been recognised for a long time. The failure mechanisms related to the re-distribution of void ratio within a globally undrained sand layer (Fig. 2.1(a)) or spreading of excess pore water pressure with global volume changes along a slope (Fig. 2.1(b)) have been suggested by the National Research Council (NRC, 1985). Adalier & Elgamal (2002) also observed from a series of centrifuge model tests that there is a potential strength loss in the dense sand zone as a result of pore water migration into the dense area from the adjacent loose ground. These observations further indicate that flow slides can also take place under other than undrained or fully drained conditions. Therefore, the failure mechanisms of granular soils under these conditions need to be studied.

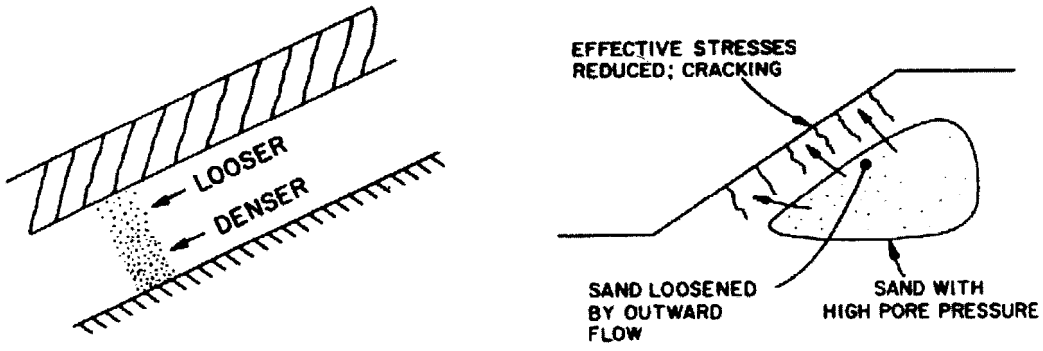

(a) (b)

Fig. 2.1 Failure mechanisms defined by NRC: (a) mechanism B: simulation for void redistribution within a globally sand layer; (b) mechanism C: situation for failure by spreading of excess pore pressure with global volume changes (after NRC, 1985)

The flow slides of granular slopes can also be induced by the instability of soil. Instability is defined as the inability of a material to sustain a given load or stress, and large plastic stains are developed as a result (Chu et al., 1993; Lade et al., 1988; Lade, 1993, 1994). Instability of soils normally occurs when the soil element reaches the failure state. However, instability can also occur at a stress level below the failure and thus it is termed as pre-failure instability. This type of instability behaviour is often characterised by a sudden collapse of a soil specimen accompanied by a rapid increase of pore pressure well within the effective stress failure envelope. Therefore, pre-failure instability is not synonymous to failure. Furthermore, flow slides caused by pre-failure instability usually lead to catastrophic consequences as they occur without any obvious warnings. Although pre-failure instability normally occurs for loose sand, this type of deformation in relatively dense granular materials has also been reported (Torrey & Weaver, 1984; Fleming et al., 1989; Chu et al., 1993; and Sassa, 2000). Little experimental studies have been carried out with relatively dense materials and our understanding of the instability mechanisms of dense soils is still very limited.

Most laboratory studies in the past have been carried out by means of triaxial tests. Therefore majority research findings were established under axisymmetric conditions (Chu et al., 1992, 1993, 2003; Lade & Pradel, 1990; Lade, 1992, 1994, 1999; Sasitharan et al., 1993; Yamamuro & Lade, 1997a). As a large number of geotechnical problems can be idealised into plane-strain conditions, further studies on strain softening and instability behaviour of sand under plane-strain or other general stress conditions should be conducted. Furthermore, it is also important to investigate the effect of shear band formation on the unstable behaviour of dense sand.

This chapter is presented in three parts. Part One focuses on the theoretical background. This includes the basic definitions of strain softening, instability and the critical state concept. A review on the related numerical models is also conducted. Previous experimental studies on the liquefaction and instability of sand are described in Part Two. A review of experimental investigations using various apparatuses on the shear band formation is also presented in Part Two. A summary of the literature is presented in Part Three.

2.2 Strain Softening

2.2.1 Definition of Strain Softening

The phenomenon wherein the shear resistance of a soil element decreases with further shearing after the deviatoric stress reaches its peak value refers to strain softening. A typical strain softening behaviour for dense and loose sand under drained and undrained conditions is given in Fig. 2.2. When the strain softening occurs in loose sand under undrained conditions (Fig. 2.2), the term *static liquefaction* is normally used (Castro, 1969; Morris, 1983).

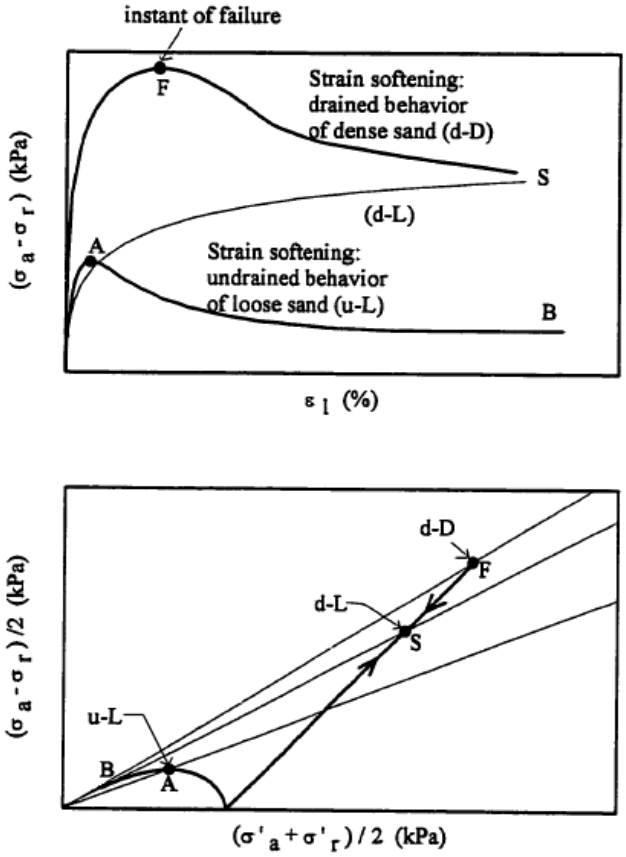

Fig. 2.2 Strain softening response characteristics of dense sand under drained conditions and of loose sand under undrained conditions (after Eliadorani, 2000)

Several definitions of strain softening within the framework of plasticity theory have been proposed in the past. For instance, Prevost & Hoeg (1975) used the stress space formulated plasticity in defining strain softening. They proposed the following mathematical expression:

$h > 0$, strain hardening (2 – 1a)

$h < 0$, strain softening (2 – 1b)

where h is a parameter defined by the following constitutive equation:

$$d\varepsilon_{ij} = C^{e}_{ijkl}\, d\sigma'_{kl} + h\frac{\partial G}{\partial \sigma'_{ij}}\left(\frac{\partial f}{\partial \sigma'_{kl}} d\sigma'_{kl}\right) \qquad (2-1c)$$

where C^{e}_{ijkl} is the elastic stiffness tensor, G is the plastic potential function, and f is the yield function.

Casey & Naghdi (1981) on the other hand defined strain softening based on strain space formulated plasticity. This concept can be expressed mathematically by the following equations:

$$\hat{f} \Big/ \hat{g} > 0 \qquad (2-2a)$$

$$\hat{f} \Big/ \hat{g} < 0 \qquad (2-2b)$$

$$\hat{f} \Big/ \hat{g} = 0 \qquad (2-2c)$$

where f, g are the yield functions defined in stress space and strain space; and $\hat{f}$, $\hat{g}$ are yield functions related parameters, respectively.

It was pointed out by Chu et al. (1992) that the abovementioned definitions of strain softening require the choice of the elasto-plastic yield function and the plastic potential as a prori.

Valanis (1985) proposed a definition of strain softening expressed in terms of total strains instead of plastic strains in elasto-plastic formulations. Assuming that ε_{ij} is a parametric representation of strain path in strain space and σ_{ij}' is the corresponding stress path in stress space, a material exhibits strain softening at a point of the strain path if, at this point:

$$d\sigma'_{ij}\, d\varepsilon_{ij} \le 0 \qquad (2-3)$$

It should be noted that Valanis' definition of strain softening for axisymmetric stress conditions can be rewritten as:

$$d\sigma'_1\, d\varepsilon_1 + 2d\sigma'_3\, d\varepsilon_3 = dp'\, d\varepsilon_v + dq\, d\varepsilon_s < 0 \qquad (2-4)$$

The terms used in Inequality (2 – 4) are defined in Cam-clay theory (Schofield & Wroth, 1968) as:

Deviator stress	$q = \sigma_1 - \sigma_3$
Mean effective stress	$p' = \frac{1}{3}\left(\sigma'_1 + 2\sigma'_3\right)$
Deviator strain	$\varepsilon_s = \frac{2}{3}\left(\varepsilon_1 - \varepsilon_3\right)$
Volumetric strain	$\varepsilon_v = \varepsilon_1 + 2\varepsilon_3$

If $d\varepsilon_1 > 0$, Inequality (2 – 4) implies that $dq < 0$ for drained conditions (i.e. $d\sigma'_3 = 0$ and $dq = d\sigma'_1$). Similarly, using $d\varepsilon_v = 0$ and thus $d\varepsilon_1/d\varepsilon_3 = -2$ in Inequality (2 – 4) will lead to $dq < 0$ for undrained conditions as well. In strain path testing the inequality (2 – 4) becomes:

$$d\varepsilon_1\left(dq + d\sigma'_3 \frac{d\varepsilon_v}{d\varepsilon_1}\right) < 0 \qquad (2-5a)$$

Since $d\varepsilon_1 > 0$ and $d\sigma_3 = 0$ during a strain path test, thus $d\sigma'_3 = -du$. Therefore, Inequality (2 – 5a) can be written as:

$$dq < du \frac{d\varepsilon_v}{d\varepsilon_1} \qquad (2-5b)$$

It can be seen from Inequality (2 – 5b) that the condition of strain softening is related to change in pore water pressure, u, and the strain increment ratio, $d\varepsilon_v/d\varepsilon_1$. For example, if $du > 0$ and $d\varepsilon_v/d\varepsilon_1 < 0$, Inequality (2 – 5b) at least requires $dq < 0$. Under plane-strain conditions, Inequality (2 – 3) becomes:

$$d\sigma'_1\, d\varepsilon_1 + d\sigma'_3\, d\varepsilon_3 = ds'\, d\varepsilon_v + dt\, d\varepsilon_s < 0 \qquad (2-6)$$

The variables in Inequality (2 – 6) are so-called Roscoe planar measures:

Maximum shear stress	$t = (\sigma_1' - \sigma_3')/2$
Mean effective stress	$s' = (\sigma_1' + \sigma_3')/2$
Shear strain	$\varepsilon_s = \varepsilon_1 - \varepsilon_3$
Volumetric strain	$\varepsilon_v = \varepsilon_1 + \varepsilon_3$

Similarly to axisymmetric conditions, Inequality (2 – 6) implies that $dt < 0$ for drained or undrained conditions. However, it should be pointed out that the validity of (2 – 6) is limited to situations in which the principal axes of strain increment and of stress coincide (Wood, 1990). For other stress conditions, taking no account of the directions of the principal stress and strain axes, a generalized form of Valanis' strain softening definition should be used. Using the general stress and strains conditions, Valanis' definition can be expressed as:

$$dp'\,d\varepsilon_v + \beta\, dq\, d\varepsilon_s < 0 \qquad (2-7)$$

where:

$$p' = \left(\sigma_1' + \sigma_2' + \sigma_3'\right)/3 \qquad (2-8)$$

$$q = \frac{1}{\sqrt{2}}\left[\left(\sigma_1 - \sigma_2\right)^2 + \left(\sigma_2 - \sigma_3\right)^2 + \left(\sigma_3 - \sigma_1\right)^2\right]^{\frac{1}{2}} \qquad (2-9)$$

$$\varepsilon_v = \varepsilon_1 + \varepsilon_2 + \varepsilon_3 \qquad (2-10)$$

$$\varepsilon_s = \frac{\sqrt{2}}{3}\left[\left(\varepsilon_1 - \varepsilon_2\right)^2 + \left(\varepsilon_2 - \varepsilon_3\right)^2 + \left(\varepsilon_3 - \varepsilon_1\right)^2\right]^{\frac{1}{2}} \qquad (2-11)$$

$$\beta = \frac{\left(3 + \mu\nu\right)}{\sqrt{\left(3 + \mu^2\right)\left(3 + \nu^2\right)}} \qquad (2-12)$$

$$\mu = \frac{2\sigma_2' - \sigma_3' - \sigma_1'}{\sigma_1' - \sigma_3'} = b + \frac{\sigma_2' - \sigma_1'}{\sigma_1' - \sigma_3'} \qquad (2-13)$$

$$b = \frac{\sigma_2' - \sigma_3'}{\sigma_1' - \sigma_3'} \qquad (2-14)$$

$$\nu = \frac{2d\varepsilon_2 - d\varepsilon_3 - d\varepsilon_1}{d\varepsilon_1 - d\varepsilon_3} \qquad (2-15)$$

in which p', q, ε_v, ε_s are the generalized mean effective stress, deviatoric stress, volumetric stress and deviatoric strain respectively. μ is the Lode stress parameter, ν is the Lode strain parameter and b is a parameter that measures the relative magnitude of the intermediate principal stress.

It was pointed out by Chu et al. (1992) that Valanis' definition has a number of advantages. Firstly, it is stated in terms of total strains instead of plastic strains in elasto-plastic formulation. In this way, the difficulties inherent in decomposing the measured total strains into elastic and plastic components are avoided. Secondly, the definition is expressed in incremental forms and it is not related to stress and strain history. It was also shown by Chu et al. (1996) that strain softening under three dimensional stress conditions occurred in the $dq < 0$ region, as for axisymmetric conditions. These features make Valanis' definition preferable for investigating experimentally, strain softening behaviour along a wide spectrum of paths. It should be pointed out that more precise and satisfactory definition of strain softening may be required under other than axisymmetric stress conditions. However, to the author's knowledge, it has not been given yet. It should also be noted that there is no reference to energy considerations in Valanis' definition. This is because energy considerations are more relevant to instability postulates which are discussed later (see Section 2.3.2). Furthermore, Lade et al. (1987, 1988) have pointed out that energy considerations are not very relevant to strain softening criteria if other factors such drainage conditions or dilatancy are not taken into account.

2.2.2 Modelling of Strain Softening

To model strain softening behaviour of soils successfully is still not an easy task. Although the numerical modelling is beyond the scope of this research, the most important findings are summarized in this section. There are two approaches which have been adopted in modelling of the strain softening behaviour. If strain softening is observed without non-homogeneous deformations, it is considered as a true material behaviour. On the other hand, if strain softening is accompanied by the development of non-homogeneous deformation, it is referred as a bifurcation or strain localization.

2.2.2.1 Modelling of Material Behaviour

Strain softening and strain hardening is often considered to study various geotechnical problems, especially associated with the progressive failure mechanisms. However, one should notice that consideration of strain softening behaviour requires special care when using numerical methods.

One of the first attempts to model strain softening of soils was made by Lo & Lee (1973). They proposed an approximate method of finite element analysis for stresses and displacements in slopes of strain softening material. The simplified stress-strain formulations for brittle material assumed by Lo & Lee (1973) could not incorporate the real behaviour of soil but they showed the capacity of finite element method to study strain softening problems.

Since then, numerous constitutive models for soils have been proposed within the framework of incremental elastoplasticity. The strain softening incremental elastoplastic models are based on the concepts of yield condition, flow rule, and hardening rule. The yield conditions can be expressed in terms of the principal stresses or the stress invariants, and can be represented by a surface in three dimensional space of principal stresses. Inside the yield surface the deformation is purely elastic. A smooth closed yield surface is normally used, for example, Nova & Wood (1979), Lade & Kim (1995), Drescher et al. (1995). Isotropic softening, represented by a shrinkage of the yield surface is generally described by a function of the plastic strains. The volumetric component of the plastic strain was used by Drescher et al. (1995), whereas both volumetric and shear components were incorporated by Nova & Wood (1979), Pestana (1996), and Drescher & Mroz (1997). Lade (1977) and Lade & Kim (1995) on the other hand, have considered the size of the yield surface as a function of plastic work. To define the orientation of the plastic strain increment vector, the non-associated flow rule was used in many models, for example, Nova & Wood (1979), Drescher & Mroz (1997), Pestana (1996), Gajo & Wood (1999b).

In some models, the influence of density has also been analysed by formulating a particular hardening rule. Mroz & Pietruszczak (1983) proposed the concept of

configuration hardening, which assumes that the hardening law is a function of the distance between the yield surface and a surface representing the density state. Pestana (1996) and Drescher & Mroz (1997) used the distance measured along the isotropic stress axis between the yield surface and the reference line. Gajo & Wood (1999b) used the state parameter defined by Been & Jefferies (1985), which measures the vertical distance to the critical state line (CSL) on the *e-p'* plane.

Although elastoplastic models are commonly used to predict the behaviour of granular materials, some fundamental issues are still debatable, e.g. decomposition of strains into elastic and plastic parts or transition between elastic and plastic deformations (Wu & Niemunis, 1996). These difficulties can be overcome within the framework of the hypoplasticity theory. As compared to elastoplasticity, hypoplastic constitutive models are incrementally non-linear. Furthermore, the response of granular material is described without any decomposition of the strain into a reversible and an irreversible part (Wu & Kolymbas, 1990, 2000; Kolymbas, 1991). Wu & Niemunis, (1996, 1997) and Wu et al. (1996) have shown that a hypoplastic model can predict successfully strain softening of granular materials within a wide range of density and stress level.

It has been realized in the past that the simplified models formulated in terms of two stress invariants are adequate for representing the strain softening behaviour only in axisymmetric conditions (Nova & Wood, 1979, Drescher & Mroz, 1997; Boukpeti et al., 2002). However, a realistic description of the strain softening response requires general formulations in terms of three stress invariants (Lade & Duncan, 1975, Lade, 1977, Gajo & Wood, 1999a).

It should also be pointed out that most of the currently existing constitutive soil models are isotropic. Anisotropic models are seldom used mainly because of the lack of experimental data on soil anisotropy, which is a direct result of the inability of conventional laboratory equipment to investigate such behaviour. In reality however, most soils behave in anisotropic manner. This anisotropic behaviour consists of two components, *inherent* and *induced* anisotropy. Inherent anisotropy is controlled by the fabric of the soil before it is loaded. Induced anisotropy arises due to further loading. In most field situations soils possess initial anisotropy which

is a combination of inherent and induced components. Therefore, an anisotropic soil model should be able to simulate both anisotropic components. Anisotropic soil models developed at the Massachusetts Institute of Technology (i.e., MIT–E1 and MIT–E3) are such models (Whittle, 1993; Whittle & Kavvadas, 1994). These models are loosely based on modified Cam clay (Roscoe & Burland, 1968). However, several extensions have been made to enable certain features of soil behaviour not realized by modified Cam clay including anisotropic yield surface, kinematic plasticity, bounding surface plasticity and strain softening behaviour. As a result these models can simulate inherent and induced anisotropic behaviour under various loading paths. This enables more accurate prediction for strain softening behaviour but makes anisotropic models very complex.

Despite the large number of constitutive models proposed in the literature, it is very difficult to judge which model is the most suitable for describing the strain softening of granular materials under various drainage and loading conditions. In most cases the constitutive relations have to be formulated as non-linear differential equations, which cannot be easily solved. Consequently the numerical modelling of strain softening needs to be further developed.

2.2.2.2 Modelling of Strain Localization

Modelling of strain softening by plasticity presumes that strain softening is a material property. It implies that the stress and strain distribution within the soil element is homogeneous in the softening region. However, the occurrence of strain softening is often accompanied by non-homogeneous deformation, such as shear bands. In such case, the soil behaviour cannot be properly modelled by continuum mechanics only. Therefore, the occurrence of non-homogeneous deformations was suggested to be modelled by bifurcation theory (Vardoulakis, 1979, 1980, 1983).

In recent years, the concept of bifurcation in geomechanics has been a subject of extensive research. The classical bifurcation theory assumes that a uniform deformation field is initially induced by the application of uniform stresses on a homogeneous material and at a critical condition it gives way to a strain localization zone in which deformation rates vary with position across the zone but

remain uniform outside the zone. Mathematically, the problem reduces to seeking a non-unique solution to the equations for a given constitutive equation of the material. The basic theoretical principles of bifurcation were developed by Thomas (1961), Hill (1962) and Mandel (1964) for rigid plastic and elasto-plastic solids. Later, the bifurcation theory was applied to soils by Rice (1973), Vardoulakis (1979), Vermeer (1982) and Molenkamp (1985). It has been found that the predictions of shear band initiation are very sensitive to the constitutive models being used. In this section, several numerical approaches of the shear band predictions are reviewed and discussed.

Rudnicki & Rice (1975) applied the bifurcation analysis to predicting the bifurcation conditions in pressure-sensitive dilatant materials. They reported that according to the predictions with constitutive models involving non-associated flow plastic flow, shear bands can occur in the hardening regime. On the other hand, constitutive models assuming normality predict that shear bands are only possible in the softening regime. However, irrespective of the plastic flow rule, shear bands were always predicted to occur in the softening regime for triaxial compression and extension tests.

Vermeer (1982) investigated the condition for shear band initiation and the orientation of shear bands in granular materials by means of a simple compliance analysis with a Mohr-Coulomb type model. A positive hardening model was obtained, showing that shear bands occurred in the hardening regime.

Molenkamp (1985) verified the applicability of some constitutive soil models by comparing experimental results with predicted conditions for shear band initiation. He found that the model with the Lade-Duncan yield surface and plastic potential function (Lade & Duncan, 1975) predicted that shear bands initiated in the plastic hardening regime in plane strain tests and in the softening regime in triaxial tests. The models with Mohr-Coulomb yield surfaces predicted that shear bands always occurred in the plastic hardening regime, which is consistent with Vermeer's analysis.

Peters et al. (1988) evaluated the shear band initiation using a simple constitutive model involving the stress ratio (σ_1/σ_3) as the yield function and Rowe's stress-dilatancy theory. He found that shear bands initiate in the strain softening regime under axisymmetric conditions and in the strain hardening regime under plane-strain conditions, which is consistent with Molenkamp's prediction with the Lade-Duncan yield surface. However, the comparison of modelling predictions and experimental results showed that the constitutive models assuming homogeneous stress-strain behaviour prior to strain localization overestimated the resistance of axisymmetric tests against shear band initiation.

Bardet (1990) found by conducting parametric studies that the critical hardening modulus for the earliest possible occurrence of shear bands is sensitive to Poisson's ratio, the dilatancy angle and the friction angle. However, the critical hardening modulus is also a function of the orientation of potential shear band, which depends largely on the particle size of the granular material. Since the classical bifurcation analysis does not involve the particle size in the constitutive models, it may be inadequate for providing more accurate predictions (Muhlhaus & Vardoulakis, 1987; Fish & Belytschko, 1990).

The classical bifurcation theory, with the concept of continuum mechanics, does not take into account the microstructure of the material. Therefore, many researchers have been extending bifurcation theory on the basis of micromechanics. Bardet (1994) for example, showed that although particle rotation is the dominant microscopic mechanism, especially in the zone of localized deformation, it is largely neglected in bifurcation modelling.

Cosserat continuum mechanics that takes into consideration both particle displacement and particle rotation, has been used for modelling the kinematics of granular soils (Muhlhaus & Vardoulakis, 1987; Bardet & Proubet, 1990; De Borst, 1991; Papanastasiou & Vardoulakis, 1992). In Cosserat continuum mechanics the medium is described by a rigid body $C(x)$ around the point x with a velocity vector v and a particle rotation vector ω^c. The internal length scale is introduced into the modelling through the rotation gradient ω^c which allows analysis of shear band thickness and effects of scale.

Numerous various approaches have further been suggested in the recent years. Among them the most interesting and significant are:

- Hypoplastic models (Wu & Sikora, 1991; Tejchman & Wu, 1993, 1996; Tejchman & Bauer, 1996)
- Gradient dependent models (De Borst & Muhlhaus, 1992; Muhlhaus & Aifantis, 1992; De Borst et al., 1995; Oka et al., 2000)
- Visco-plastic models (Sluys & De Borst, 1992)
- Adaptive mesh models (Ortiz & Quigley, 1991, Larsson et al., 1991; Zienkiewicz et al., 1995)
- Enhanced finite element models (Ortiz et al., 1987; Pietruszczak & Stolle, 1985; Pietruszczak & Niu, 1992; Larsson et al., 1993; Simo et al., 1993)
- Multilaminate elastoplastic models (Pande & Sharma, 1983; Pietruszczak & Pande, 1987; Sadrnejad & Pande, 1989)
- Strong discontinuity models (Borja, 2000; Borja et al., 2000; Borja & Regueiro, 2001; Regueiro & Borja, 2001; Borja & Lai, 2002).

2.3 Instability of Granular Soils

2.3.1 Definition of Instability

Instability in granular materials has been defined (Lade et al., 1987, 1988; Lade & Pradel, 1990; Chu et al., 1993; Yamamuro & Lade, 1997a) as a condition in which large plastic strains are generated rapidly due to the inability of a soil element to carry or sustain a given load. This definition also includes the inability to carry small perturbations in the stress. It should be emphasized that instability is granular materials is not synonymous with failure because it can occur inside the established failure surface.

Instability of granular materials can be either total or temporary. Total instability occurs when the soil loses completely its shear strength. It is often characterized by a sudden collapse accompanied by a rapid increase in pore pressure from the point of unstable behaviour. This phenomenon in soil resembles static liquefaction, in that there is a sudden reduction in soil shear strength under undrained conditions. Temporary instability occurs when the soil reduces some of its shear strength and then recovers to support higher stresses.

2.3.2 Instability Postulates

According to plasticity theory there are two instability postulates for time-independent materials. The first one is Drucker's postulate (Drucker 1951, 1956, 1959), which states that for stability to exist the second increment of plastic work has to be positive or zero:

$$d^2W_P = \dot{\sigma}_{ij}\, d\dot{\varepsilon}_{ij}^{p} \geq 0 \qquad (2-16)$$

where $\dot{\sigma}_{ij}$ is the stress increment and $\dot{\varepsilon}_{ij}^{p}$ is the resulting plastic strain increment (the vector normal to the plastic potential surface). The second is Hill's postulate (Bishop & Hill, 1951; Hill, 1958) developed based on the hypothesis of a rigid plastic material. It states that for stability to exist the second increment of total work must be nonnegative:

$$d^2W_P = \dot{\sigma}_{ij}\, d\dot{\varepsilon}_{ij}^{t} \geq 0 \qquad (2-17)$$

where $\dot{\sigma}_{ij}$ is the stress increment and $\dot{\varepsilon}_{ij}^{t}$ is the resulting total strain increment. The only difference between these two postulates is that Inequality (2 – 16) uses plastic strain increment and Inequality (2 – 17) uses total strain increment.

It can also be noted that Hill's stability postulate expressed by Inequality (2 – 17) can be compared with Valanis' definition of strain softening defined by Inequality (2 – 3). Comparison of (2 – 3) and (2 – 17) would imply that if the measured stress and strain increment response at a given point violates Hill's stability postulate, then strain softening would be equivalent to instability by definition. However, Lade et al. (1987, 1988) have shown that Hill's postulate, although indicating strain softening behaviour, is only sufficient but not necessary condition for instability. The other necessary condition for the occurrence of instability is the generation of pore water pressure. Therefore, the occurrence of strain softening does not imply the occurrence of instability for the same stress or strain conditions and instability is not identical to strain softening by definition. Only if the second work increment together with drainage conditions is considered, a proper comparison of instability and strain softening can be made.

Drucker's and Hill's stability postulates were developed for solid materials. They are adequate to describe the instability behaviour of materials that exhibit the associated plastic flow. However, granular materials behave differently, exhibiting nonassociated flow. Therefore, violation of these postulates cannot be taken as a general instability condition for granular materials, as reported by Lade et al. (1987, 1988).

Lade et al. (1988) modified the instability conditions to be applicable for granular materials. It was found that instability inside the failure surface will occur when the two following conditions are fulfilled:

$$\frac{\partial g}{\partial \sigma_{ij}} \cdot \delta_{ij} > 0 \qquad (2-18)$$

$$\frac{\partial f}{\partial \sigma_{ij}} \cdot \delta_{ij} < 0 \qquad (2-19)$$

where g is a plastic potential function, f is a yield function, and δ_{ij} is a vector on the hydrostatic axis (Kronecker delta). Inequalities (2 – 18) and (2 – 19) dictate instability when (2 – 17) is true. Inequality (2 – 18) requires exhibition of plastic volumetric compression or a tendency for such behaviour when the total volumetric strain is zero. Inequality (2 – 19) specifies that the yield surface must "open up" in the outward direction of the hydrostatic axis (Lade et al., 1988; Lade & Pradel, 1990; Chu et al., 1993). It can be schematically illustrated as a region of potential instability, indicated by the shaded area in Fig. 2.3.

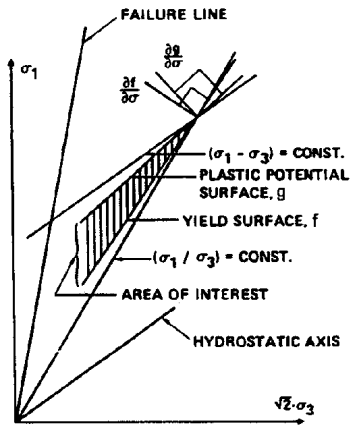

Fig. 2.3 Region of potential instability (after Lade, 1999)

Lo & Chu (1991a) and Chu et al. (1993) argued that above mentioned instability conditions are suitable only for very loose saturated sand under undrained conditions. Therefore, Chu et al. (1993) proposed two instability conditions, which can be considered as an extension of those defined by Lade et al. (1988). These conditions can be expressed as:

$$\frac{\partial f}{\partial p'} < 0 \qquad (2-20)$$

$$\left(\frac{d\varepsilon_v}{d\varepsilon_1}\right)_i \leq \left(\frac{d\varepsilon_v}{d\varepsilon_1}\right)_f \qquad (2-21)$$

where $(d\varepsilon_v/d\varepsilon_1)_i$ is a strain increment ratio imposed on a soil element and $(d\varepsilon_v/d\varepsilon_1)_f$ is the strain increment ratio at failure obtained from a $d\sigma_3' = 0$ test.

Inequality (2 – 20) can be illustrated schematically as an admissible zone for instability, shown in Fig. 2.4. It implies that for a stress state represented by point A in Fig. 2.4, any stress path located within the shaded zone is pointing outward from the yield surface and instability is possible (Chu et al., 1993; Chu, 1998, Chu & Leong, 2001). On the contrary, for a stress state at point B of Fig. 2.4, any stress path will point inward from the current yield surface and instability is not possible. Inequality (2 – 21) should be considered as a condition additional to the former one. Moreover it should be noticed that this inequality is necessary but not sufficient for the occurrence of instability (Chu, 1998; Chu & Leong, 2001).

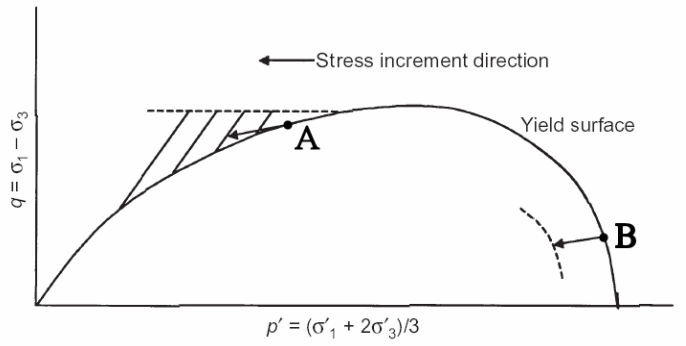

Fig. 2.4 Admissible zone for instability (after Chu & Leong, 2001)

Lade (1994) also expanded his instability definition, presented earlier in Fig. 2.3. He found that the region for potential instability must occur for decreasing stresses where the stress increment vector is inclined in such direction that plastic strains are produced. It means that potential instability does not necessarily occur between the yield and plastic potential surfaces as shown in Fig. 2.3. Fig. 2.3 would have to be modified to extend the shaded region between the $(\sigma_1 - \sigma_3) = constant$ and the yield surface, *f*. This re-evaluation takes into account different possibilities for the plastic potential surfaces, as presented in Fig. 2.5. It can be seen from Fig. 2.5(a) that Inequality (2 – 16) can fail with increasing stresses. Fig. 2.5(b) shows that instability can also occur with a positive work increment.

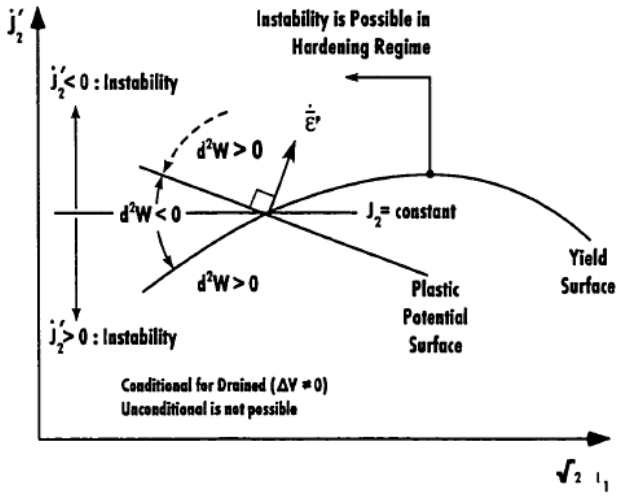

Fig. 2.5(a)

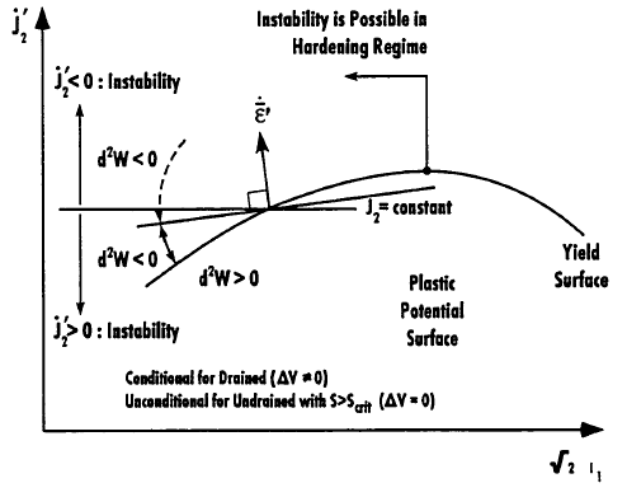

Fig. 2.5(b)

Fig. 2.5 Modified region of potential instability: (a) contractive granular materials; (b) dilative granular materials (after Lade, 1994)

2.3.3 Instability Line and Instability Zone

When the conditions of instability, described above, are reached, soil may not be able to sustain the current stress state. Such stress corresponds to the top of the current yield surfaces (Lade, 1992, 1999). This is schematically shown on the *q-p'* diagram in Fig. 2.6. It can be seen that the top of the undrained effective stress path occurs slightly after, but very close to the top of the yield surface. The difference is due to the stability provided by the elastic strains, as defined by Hill (Lade, 1992, 1993, 1999).

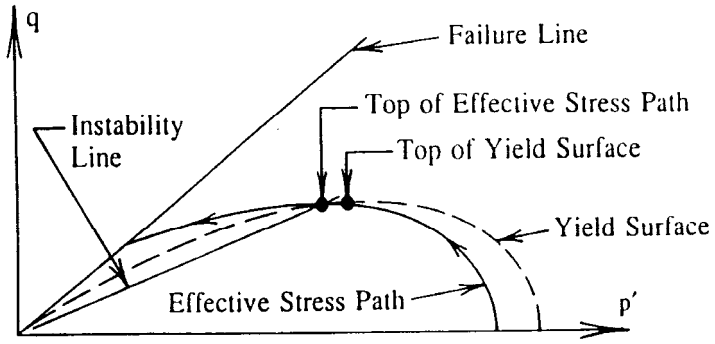

Fig. 2.6 Location of instability line (after Lade, 1999)

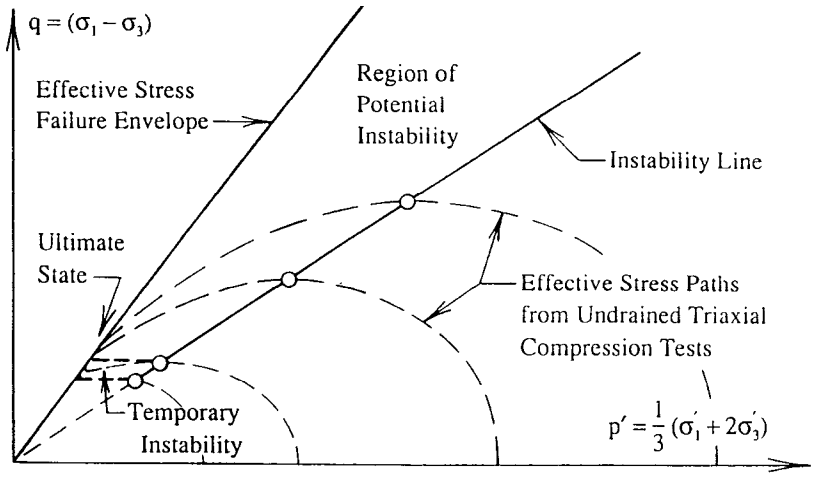

Fig. 2.7 Schematic diagram of instability line and region of potential instability on *q-p'* plane (after Lade, 1994)

Lade (1993) showed that a granular material becomes unstable when the stress state is located on or above a line connecting the peaks of effective stress paths obtained from undrained tests. He defined this line as the instability line and reported that it separates the potentially unstable stress states from the stable stress

states (Fig. 2.7). The line marks the lower limit for the region of potential instability, and defines the condition for the occurrence of pre-failure instability. It can be seen from Fig. 2.7 that the upper limit of potential instability region is defined by the failure line. In this region, loading will take place inside the failure surface and instability may develop in the form of inability to sustain the current deviator stress.

Numerous experiments have shown that the instability line is straight and it passes through the origin of the stress diagram (Lade, 1992, 1994, 1999, Leong et al., 2000; Chu et al., 2003). As the yield surfaces of sand are uniquely located, thus the location of the instability line is also unique for a given sand at a given void ratio (Yamamuro & Lade, 1997a; Chu et al., 2003). Fig. 2.7 also shows the region of temporary instability which is located in the upper part of the dilating zone. Within this area instability may initially occur, but eventually soil will dilate and become stable again.

2.4 Critical State Concept

The concept of a "critical state" of deformation was introduced in the 1930's in an attempt to relate volume change behaviour, specimen density and confining pressure during shearing (Casagrande, 1936). Based on the results of drained direct shear tests, he found there is a critical void ratio for a given sand, dependent only on the confining stress imposed during shearing. Casagrande's concept became a major component of a critical state soil mechanics, developed in the 1960's to characterize soil behaviour in an elasto-plastic framework. According to this theory, the critical state of soil is a state of continued, indefinite plastic shearing without changes in volume and effective stress (Schofield & Wroth, 1968).

At the critical state, there is a unique relationship between the effective stresses and the void ratio of soil. Therefore, critical state conditions can be described by a critical state line (CSL) in the *e-p'-q* space. The projections of the CSL on *q-p'* and *e-p'* planes are schematically presented in Fig. 2.8. Effective stress paths for a CU and a CD triaxial test on normally consolidated (loose) specimens are also shown in this figure. The failure states for both drained and undrained tests are reached on

the CSL. It demonstrates the basic assumption of the critical state concept, that is, the uniqueness of the CSL.

Despite general acceptance of the critical state concept, some researchers have not been satisfied with the critical state definition, as it does not mention of soil structure, particle breakage, and shearing mode or rate. Consequently, the concept of "steady state" was proposed by Poulos (1981). He defined the steady state of deformation as the state at which a mass of soil is continuously deformed at constant volume, constant normal effective stress, constant shear stress, and constant velocity. The steady state is postulated to occur only after all particle reorientation and breakage is complete and the soil has achieved the specific structural flow of particles associated only with the steady state.

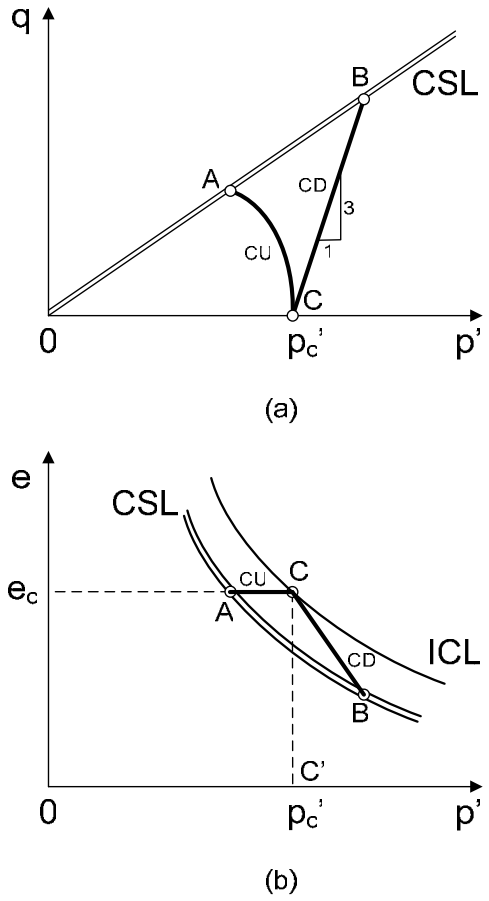

Fig. 2.8 Schematic presentation of CSL: (a) *q-p'* plane; (b) *e-p'* plane

One can notice that the concept of the steady state only differs from the critical state in that steady state requires a constant velocity to be achieved, and specifies that a particular flow structure is associated with its achievement. However, in the

past, the critical state has been typically related to drained behaviour of contractive specimens, while the steady state is normally used in liquefaction analysis of very loose specimens under an undrained condition.

It should also be noted that critical state can be achieved by shearing very loose soil at various confining pressures, but it can also be realized by shearing dense soil at high confining pressures. Several researchers have found that as confining pressure increases the effect of the initial void ratio is diminished (Been at al., 1991; Lade & Yamamuro, 1996; Yamamuro & Lade, 1996, Leroueil, 1997). However, shearing of granular materials at high confining pressures induce grain breakage which has a significant effect on the CSL in the *e-p'* (or *e-log p'*) plot. The CSL, measured for quartz sands on *e-log p'* plane, can only be reasonably approximated by a straight line in the stress range 10–500 kPa (Been et al., 1991; Leroueil, 1997). This is because at low confining pressures there is little particle crushing. However, the amount of particle breakage increases rapidly at higher stresses varying between 500 and 2000 kPa depending on the mineralogy and the grain size distribution of the granular material. As a result, the CSL curves abruptly and becomes bilinear. Furthermore, the CSL and isotropic consolidation line (ICL) on *e-log p'* plane are not necessarily parallel and can be curved. These factors have to be considered when critical state parameters are determined by high pressure tests. More discussion on the critical state and the steady state concepts, based on previous experimental studies, will be presented in the following section.

Been & Jefferies (1985) pointed out that the nature of the steady/critical state implies the limited applicability for characterizing a potentially liquefiable soil. This is because the steady state/critical state line only defines a reference state. However, the behaviour of a granular material should also be related to its initial state. Been & Jefferies (1985) introduced a state parameter, ψ that can express the initial state of soil in terms of its density. The state parameter can be defined as:

$$\psi = e - e_{cr} \qquad (2-22)$$

where e is the void ratio at the initial state and e_{cr} is the void ratio at the critical state at the same mean effective stress, p'. The state parameter definition is

illustrated in Fig. 2.9. It can be seen from Fig. 2.9 that a material with positive ψ is located above the CSL, whereas a material with negative ψ is located below the CSL. In other words positive state parameter defines contractive behaviour and negative state parameter defines dilative behaviour of granular soil.

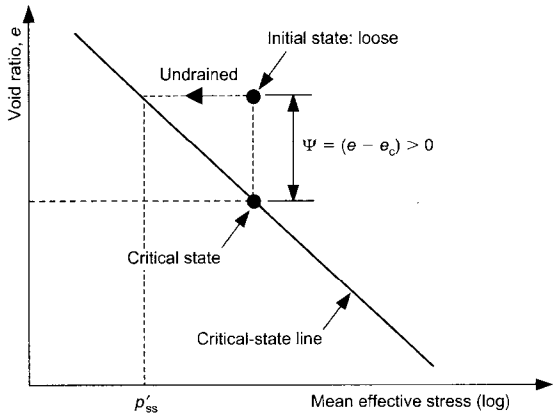

Fig. 2.9 Definition of state parameter (after Yang, 2002)

To facilitate the application of the state parameter concept to slope stability analysis Chu et al. (2003) proposed a modified state parameter, $\bar{\psi}$. The modified state parameter is defined as:

$$\bar{\psi} = e_{IL} - e_{cr} \qquad (2-23)$$

where e_{IL} is the void ratio at the instability point and e_{cr} is the void ratio at the critical state at the same mean effective stress, p'. The difference between ψ and $\bar{\psi}$ is that $\bar{\psi}$ defines the state at instability line rather than the state after consolidation, as initially proposed by Been & Jefferies (1985).

2.5 Review of Previous Experimental Studies

2.5.1 Strain Softening as Material Behaviour

To date, extensive experimental works, mostly under axisymmetric stress conditions, have been carried out to study strain softening behaviour of granular soils. Majority of these investigations have been focused on strain softening of dense sand under drained conditions and the strain softening of loose sand under undrained conditions.

Although, the strain softening of dense granular material has been extensively studied in the past, most of the experiments are limited to conventional triaxial tests without properly lubricated end platens. Therefore, considerable non-homogeneous deformations were often developed in the strain softening region. Experimental studies have shown that this type of behaviour can be related to the friction developed between specimens and platen interfaces (Rowe & Barden, 1964; Bishop & Green, 1965). Drescher & Vardoulakis (1982) also showed that with the improvement in the end restraint, the softening observed in a drained test can be significantly reduced. Therefore, it has been argued by some researchers that the strain softening as a true material property cannot be developed in the specimen under axisymmetric stress conditions (Drescher & Vardoulakis, 1982; Hettler & Vardoulakis, 1984). Moreover, it has been observed that even experiments with "perfect" boundary conditions do not ensure homogeneous deformation. Non-homogenous deformations can still occur in the form of buckling, bulging, and shear banding in triaxial tests conducted on dense sand (Vardoulakis, 1979, Hettler & Vardoulakis, 1984).

Strain softening of loose sand under an undrained condition, commonly referred as a static liquefaction, has been investigated in the past by number of researchers (e.g. Castro, 1969; Castro & Poulos, 1977; Poulos et al., 1985; Sladen et al., 1985b; Alarcon-Guzman et al., 1988; Ishihara, 1993; Yamamuro & Lade, 1997b; Vaid & Eliadorani, 1998; Leong et al., 2000). This phenomenon is characterized by large pore pressure development that can result in zero effective confining pressure and stress difference at low axial strains.

The typical stress-strain behaviour of sand in an undrained triaxial test is presented in Fig. 2.10. It can be seen that dense sand tends to exhibit strain-hardening behaviour (curve 1), in which shear stress increases with increasing shear strain. Curve 1 shows the behaviour of dense sand in the non-flow state. Loose sand, on the other hand, tends to exhibit strain softening behaviour (curve 3), where shear stress decreases with increasing shear strain. Loose sand in such a state is referred to, as the *steady flow state*. For medium loose sand (curve 2), strain softening behaviour is observed at lower strain, followed by strain hardening at larger strain. Such behaviour is referred to, as the *quasi-steady state* (Been et al., 1991; Verdugo

& Ishihara, 1996; Zhang & Garga, 1997) or *limited liquefaction* (Castro, 1969). Fig. 2.10 indicates that the strain softening resistance increases with increasing relative density. In other words, under undrained conditions, the potential for the occurrence of strain softening decreases with increasing relative density (Kramer & Seed, 1988). Sometimes only a slight change in density can convert the soil specimen from a strain hardening state to a strain softening state (Poulos et al., 1985).

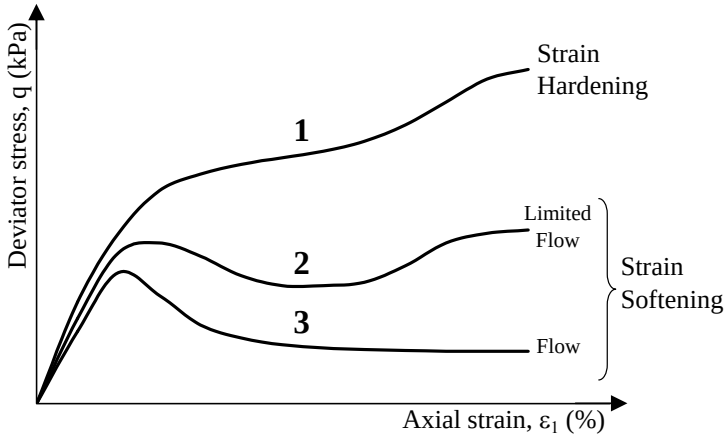

Fig. 2.10 Classification of undrained behaviour of sand

It is well known that behaviour of granular soils is strongly dependent on drainage conditions. However, as mentioned before, majority of experimental studies on strain softening is conducted under either drained or undrained conditions. Limited amount of data is published under other drainage conditions (Chu et al., 1992; Chu & Leong, 2001; Vaid & Eliadorani, 1998; Lancelot et al., 2004).

The study of Chu et al. (1992) shows that strain softening is a behaviour more closely related to strain path control rather than stress path control. The latter approach may force a specimen into an inadmissible state, while the former allows strain softening, if any, to develop freely. It should be noted that an undrained test is a strain path test. An undrained condition is only a special case of the general strain path controlled conditions (Chu, 1991; Chu et al., 1993). Furthermore, strain path tests can better simulate real field situations, where a soil element will normally experience changes in both volume and pore water pressure simultaneously and a fully drained or an undrained condition is exceptional.

2.5.2 Instability

2.5.2.1 Undrained Behaviour

The first experimental study on pre-failure instability of granular soils was conducted by Lade et al. (1988). By performing several triaxial tests on saturated sand, Lade et al. (1988) showed that a compressive specimen was unable to sustain a constant load under an undrained condition when a stress point was below but close to instability line. This is because pore water pressure will increase under creep and the effective stress path will move into the region of potential instability, inducing the pre-failure instability. During instability the pore water pressure and the axial strain rate shoot up and a loose specimen physically collapses. Lade et al. (1988) concluded that for instability to occur, the soil element must exhibit compressive behaviour. Lade et al. (1988) also observed that instability may not occur, if the response of the soil is dilative.

A number of other experimental studies on loose granular soils under undrained conditions have been reported in the literature (Lade & Pradel, 1990; Lade, 1992; Konrad, 1990, 1993; Sasitharan et al., 1993; Leong et al., 2000). It was also reported that for dilative sand, instability will not occur under undrained conditions (Chu et al., 1993, Chu & Leong 2001; Chu et al., 2003).

2.5.2.2 Drained Behaviour

It has been established by several researchers that instability will not occur for loose or dense sand under a drained condition if the stress state imposed into a soil element does not change (Lade et al., 1987; Pradel & Lade, 1990; Chu, 1991; Leong et al., 2000). Therefore, it is believed that the soil behaviour is always stable under a fully drained condition. However, there are practical cases where instability might have occurred in granular soils under a fully drained condition. The flow slide at Wachusett Dam (Olson et al., 2000) is an example of such flow slides. Slope failures can also be caused by a reduction in the mean effective stress, because of water infiltration into slopes. Such conditions can be idealized by stress paths with constant deviator stress, but decreasing mean effective stress. This type of test is referred as a constant shear-drained test (Brand, 1981; Anderson &

Riemer, 1995; Anderson & Sitar, 1995; Chu et al., 2003). The constant shear-drained (CSD) path can be obtained in the laboratory by either decreasing the cell pressure while maintaining constant back pressure, or by increasing back pressure at constant cell pressure. Although both procedures results in the same nearly horizontal stress paths, the latter simulates better the real path generated in the field (Anderson & Sitar, 1995; Farooq et al., 2002).

Leong (2001) and Chu et al. (2003) conducted several CSD tests on loose and dense Changi sand under axisymmetric conditions. They concluded that a reduction in confining stress is a necessary condition for instability to occur in granular soils. Therefore, this type of instability has been termed as *conditional instability*. In addition Chu et al. (2003) proposed a new framework for the interpretation of slope failure mechanisms. They reported that the conditions for the occurrence of instability can be uniquely described by the modified stress parameter and the critical state line. Loke (2004) also found that the conditional instability that occurs under drained conditions can evolve into a runaway instability when the drainage is impeded or when the soil cannot accommodate the large volume change induced by drained instability. In other words, a soil element may become unstable initially under a drained condition, and evolve into a runaway instability if the amount of volume change generated during the drained instability cannot be accommodated.

2.5.2.3 Behaviour in Strain Path Testing

Strain softening or instability of sand has often been investigated experimentally under undrained conditions. However, in most practical problems, a soil element may experience both volume change and pore water pressure change simultaneously (Chu, 1991; Vaid & Eliadorani, 1998). Furthermore, failure mechanisms related to a re-distribution of void ratio within a globally undrained sand layer and the spreading of excess pore pressure with global volume changes has also been defined by National Research Council (see Fig. 2.1). Adalier & Elgamal (2002) also reported a pore water pressure increase and a potential strength loss in the dense granular soil due to the migration of pore water into the dense zone from the adjacent loose zone. These situations can be simulated in the laboratory by controlling the strain increment ratio, $d\varepsilon_v/d\varepsilon_1$, imposed to a specimen

(Chu, 1991). This condition, in which the dilation of the sand is controlled, has been termed as the *non-undrained* condition (Chu, 1991) or the *partially drained* condition (Vaid & Eliadorani, 1998; Eliadorani, 2000). However, to avoid any misconception about drainage conditions, the term *strain path controlled* condition will be used in this thesis.

Experimental studies on the instability of granular soils under strain path controlled conditions (Chu, 1991; Chu et al., 1993; Vaid & Eliadorani, 1998) can been carried out using the strain path testing technique developed by Chu & Lo (1991). In this method an undrained test is only a special case of general drainage conditions with $d\varepsilon_v/d\varepsilon_1 = 0$. All the other drainage conditions can be simulated by $d\varepsilon_v/d\varepsilon_1 \neq 0$. Chu (1991), Chu et al. (1993), Vaid & Eliadorani (1998), and Lancelot et al. (2004) have observed that pre-failure strain softening and pre-failure instability can occur for dense sand when tested along a strain path with $d\varepsilon_v/d\varepsilon_1 < 0$.

Chu et al. (1993) stated that when $d\varepsilon_v/d\varepsilon_1 > 0$, the soil specimen will compress and water will flow out of the sample with axial deformation. On the other hand, when $d\varepsilon_v/d\varepsilon_1 < 0$, the sample will dilate and water will flow into the specimen. Chu et al. (1993) also proposed a comparison of $d\varepsilon_v/d\varepsilon_1$ imposed to the specimen with the maximum dilation rate at failure, measured by $d\sigma_3' = 0$ test, as the criterion for instability to occur (see Inequality 2 – 20 and 2 – 21).

Chu (1991) and Chu & Leong (2001) have conducted a number of tests on loose and dense granular materials under strain path controlled conditions. A large reduction in the shear resistance and runaway flow failure is observed after instability occurred. Chu (1991) stated that although this kind of instability exhibits a flow state similar to that of the liquefaction in undrained tests, these two types of behaviour are still different. The liquefied soil in an ordinary undrained test reaches eventually a steady state, but the unstable soil in a strain path test collapses with a pore water pressure increase to the cell pressure level.

A similar study was carried out by Vaid & Eliadorani (1998). The authors reported that the small expansive volumetric strains resulting from the strain path controlled condition could render an initial state that would have been stable under undrained

deformation into an unstable state. Therefore, an undrained condition, commonly assumed as the most conservative, may not be the most dangerous situation.

Although a number of studies have been carried out on the influence of strain path on the occurrence of instability in granular soils, most of the studies were carried out using triaxial tests. As such, a further research under plane-strain conditions was carried out in this study.

2.5.3 Strain Softening versus Instability

Strain softening is referred to the reduction in the shear resistance of a soil element with further shearing after the deviatoric stress reaches its peak value. Instability, on the other hand, is defined as a condition in which large plastic strains are generated rapidly due to the inability of a soil element to carry or sustain a given load. It needs to be pointed out that liquefaction is instability behaviour not strain softening behaviour. However, in the previous studies, the differentiation was not made. For example, liquefaction is often studied using deformation-controlled tests, where strain softening instead of instability occurs.

Chu & Leong (2001) have observed that strain softening behaviour of sand is different from instability. They reported that upon the onset of instability, a specimen will collapse suddenly, whereas during the strain softening, a specimen will not collapse and the deviator stress will reduce gradually. However, the conditions that lead to strain softening and instability are the same, except that the former occurs under deformation-controlled loading conditions and the latter under load-controlled loading conditions (Chu, 1998; Chu & Leong, 2001).

Based on experimental results, Chu (1998) has shown that the occurrence of pre-failure strain softening is affected not only by the strain increment ratio but also by the density of the soil and the effective confining stress. These effects can be illustrated as:

- the strain increment ratio – the smaller the $d\varepsilon_v/d\varepsilon_1$ ratio, the higher the tendency for strain softening to occur

- the density of the soil – the looser the soil, the higher the tendency for strain softening to occur
- the effective confining stress – the higher the confining stress, the higher the tendency for strain softening to occur
- the effective stress ratio – strain softening only occurs when the initial stress ratio is adequately high.

The above factors also affect the instability.

It should also be pointed out that the occurrence of strain softening is a necessary, but not sufficient condition for instability, and instability is a sufficient, but not necessary condition for strain softening (Chu & Leong, 2001). In other words, pre-failure strain softening is related to pre-failure instability. Therefore, these two types of sand behaviour should be studied together.

2.5.4 The Uniqueness of Critical State

A uniqueness of the critical state (or steady state) is a very important concept in strain softening and instability analysis. Therefore, several researchers have investigated this uniqueness in the past (Kuerbis et al., 1988; Vaid et al., 1990; Been et al., 1991; Castro et al., 1992; Negussey & Islam; 1994; Verdugo & Ishihara, 1996; Yamamuro & Lade, 1998).

Castro et al. (1992), for example, conducted drained and undrained triaxial tests on loose samples and found that the location of steady state line was not affected by initial state and sample preparation method. Negussey & Islam (1994) carried out triaxial compression and extension tests on loose sand and reported that the SSL was unique only for particular mode of loading. Vaid et al. (1990) also found that the location of the SSL derived from extension tests is affected by the void ratio. Based on these findings, the uniqueness of steady state appears to be dependent on shearing mode (Vaid et al., 1990; Riemer & Seed, 1997; Yamamuro & Lade, 1998).

It should be pointed out that the majority of the existing data, which address the uniqueness of critical and steady states, is based on the response of loose sand. It

was because the importance of the critical (steady) state in evaluating liquefaction potential of contractive granular soils. Moreover, technical problems have been associated with defining the critical state line by triaxial tests on dense sands. Particularly, the non-homogeneous deformations were usually observed before the critical state was reached and thus a true material behaviour could not be assured. Therefore, dense specimens were not used in defining the location of the CSL, unless some techniques to avoid shear band occurrence were adopted (Chu & Lo, 1993).

Majority of experimental studies on the uniqueness of the critical state has been conducted under axisymmetric stress conditions. Since shear bands normally occur under plane-strain conditions, the critical state has seldom been investigated by plane-strain tests. Mooney et al. (1998) carried out plane-strain tests on dense sand and found that there was no apparent unique critical state line defined on e-p' plane, but a unique critical state line existed on the q-p' plane regardless of the initial void ratio and stress level, as shown in Fig. 2.11.

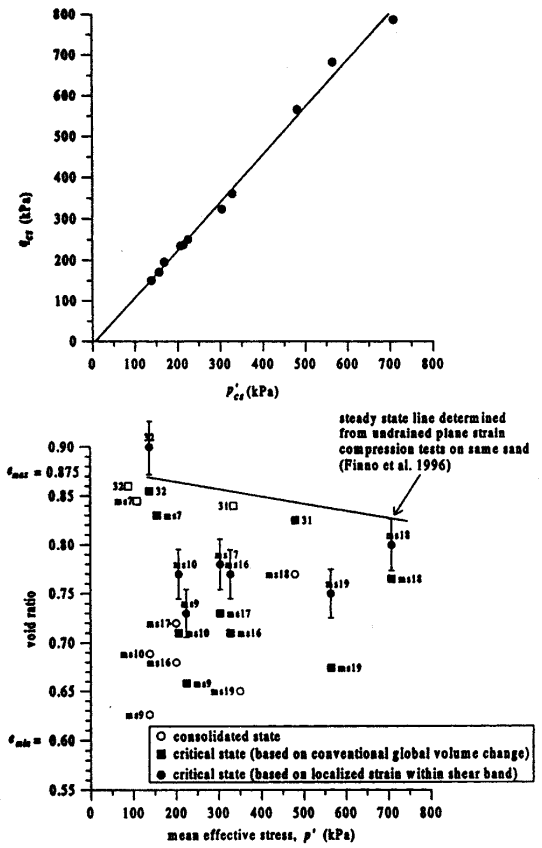

Fig. 2.11 Consolidated and critical states of drained plane-strain compression tests (after Mooney et al., 1998)

Mooney et al. (1998) suggested that previously determined critical state lines might have been found unique because they were derived from the same consolidation state. Mooney et al. (1998) further reported that in order to obtain reliable position of the CSL, void ratios within shear bands have to be determined. More recently, Finno & Rechenmacher (2003) also conducted drained, plane strain compression tests to evaluate the relationship between the void ratio and the effective stress at critical state. They reported that the relationship between void ratio and mean effective stress is indeed not unique but depends on consolidation history and the initial state of sand. Therefore, it may be expected that the CSL established under triaxial conditions would not be in general applicable to the plane-strain conditions. Comparative studies however must be carried out to confirm this observation.

Traditionally, it is thought that shear bands do not occur in the plane-strain tests conducted on loose sand. However, experimental results obtained by Finno et al. (1996, 1997) have shown that shear bands occur in loose sand in both drained and undrained plane-strain compression tests. Nevertheless, Finno et al. (1996) found that the effect of shear bands on the critical state in loose sand was minimal. Desrues et al. (1996) also observed that the density variations between the shear bands and the surrounding material in loose specimens were insignificant. Based on these findings it can be concluded that the critical state can be correctly determined by plane-strain tests conducted on loose sand. However, to accurately measure the critical state of sand using dense specimens, the behaviour inside shear bands needs to be analysed.

2.5.5 Shear Band Formation

2.5.5.1 Introduction

Shear band in soil element is defined as a thin layer that is bounded by the two material discontinuity surfaces of the velocity gradient (Muhlhaus & Vardoulakis, 1987). In other words, it is the localization of deformation in a thin layer of intensively shearing material (Vermeer, 1990), as shown in Fig. 2.12.

Many geotechnical engineering problems such as slopes, embankments, or retaining walls are associated with shear bands. Consequently, shear band

formation has been one of the most active and visible areas of research in soil mechanics over the past 40 years. A large number of experimental studies have been conducted to investigate this phenomenon. In this section, some important findings on shear band formation obtained from different devices such as triaxial, plane-strain, true triaxial and hollow cylinder apparatus are reviewed.

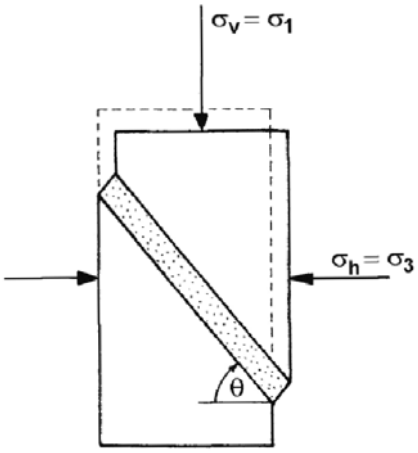

Fig. 2.12 Shear band in soil sample (after Vermeer, 1990)

2.5.5.2 Conventional Triaxial Tests

It has been thought for many years that shear bands can occur during conventional triaxial tests. However, Rowe & Barden (1964) showed that it was the result of non-homogeneous deformations developed in a triaxial test with unlubricated platens. Rowe & Barden (1964) also reported that a proper lubrication of end platens can delay significantly non-homogeneous deformations. Therefore, many researchers have studied effects of various boundary conditions on the behaviour of granular soils.

Bishop & Green (1965) investigated the effect of end restraint and specimen size on the strength and deformation characteristics of granular soils. They carried out several triaxial compression tests on specimens with different degrees of end restraint and different H/D ratios. Bishop & Green (1965) found that non-homogeneous deformations induced by end restraint promoted shear band development and resulted in strength decrease. They also concluded that taller specimens will always fail earlier than shorter specimens, if the same free-end system is used.

Kirkpatrick & Belshaw (1968) studied triaxial specimens using *X*-ray technique. They showed that specimens with conventional rigid platens barrelled and developed significant non-homogeneous deformations. However, the specimens with lubricated end platens remained uniform and in cylindrical shape throughout shearing.

It was also reported by Drescher & Vardoulakis (1982) that strain softening observed in triaxial tests conducted on dense granular soils is related to the friction presented on the specimen and platen interfaces. Drescher & Vardoulakis (1982) showed that with the improvement in the free-end techniques, the strain softening observed in a drained test can be considerably reduced. They also pointed out that if the H/D ratio of the specimen is relatively small the bulging effect can also be suppressed. Hettler & Vardoulakis (1984) on the other hand reported that even with "perfect" boundary conditions strain softening caused by non-homogeneous deformation could still occurred at larger strains. Therefore, it would be difficult to conclude if strain softening is purely a result of non-homogeneous deformations. Their experimental results also indicated that in triaxial compression tests the homogeneous deformation mode can change spontaneously to the non-homogeneous mode during shearing.

Peters et al. (1988) studied the effect of shear band formation on the behaviour of granular materials in triaxial and plane-strain tests. The triaxial compression tests showed that shear band developed in the strain softening region after the peak had occurred. Therefore, it was indicated that the stress-strain behaviour prior to failure in triaxial tests should not be affected by shear banding. However, if a proper lubrication of the end platens is not used, the non-homogenous deformations can developed too early causing premature failure. Peters et al. (1988) also pointed out that if the specimen deforms uniformly without the formation of shear band the stress-strain response is smooth. On the other hand, if the shear band occurs, the failure will be reached rapidly.

Chu & Lo (1993) also reported that the technique used to prepare the free-ends may have a significant effect on the occurrence of non-homogeneous deformations. Fig. 2.13 compares the results of four drained tests conducted on dense specimens

with similar void ratios, but with different end platen conditions. From the comparison of tests # 2, 3, and 4, it is evident that the occurrence of non-homogeneous deformation is sensitive to details of free ends. Furthermore, Chu & Lo (1993) observed that non-homogeneous deformations are not always associated with the formation of a distinct shear band. This suggests that the occurrence of shear bands may be dependent on to the apparatus type and may not be directly comparable. It can also be seen from Fig. 2.13 that with the use of very good quality free-ends, non-homogeneous deformation will be significantly delayed until a large deformation is reached.

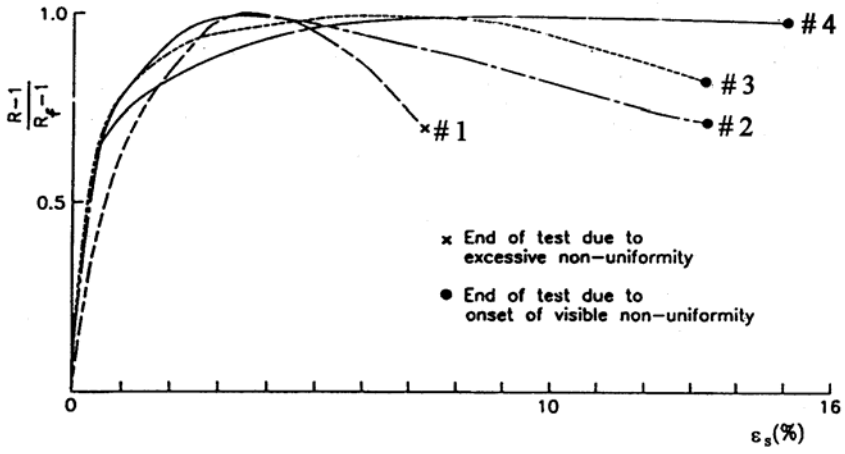

Test	H/D	Free-end	Grease	t/d_{50}	D_p/D	Platen condition
1	2	No	----	----	1	NS
2	1	Yes	ordinary	0.85	1.10	NS
3	1	Yes	HVS	0.85	1.15	NS
4	1	Yes	HVS	2	1.15	PM

H = height of specimen
D = diameter of specimen
t = thickness of latex disc
d_{50} = grain size
D_p = diameter of enlarged platen
NS = no specification
PM = polished to mirror finish
HVS = high vacuum silicone grease

Fig. 2.13 Drained triaxial test results with different end conditions (after Chu & Lo, 1993)

Desrues et al. (1996) pointed out that in the axisymmetric triaxial test localization patterns are most difficult to detect and describe. The results of triaxial tests conducted on dense and loose specimens with and without lubrication showed that more or less complex localization patterns can be developed depending on test conditions. The complexity of shear bands development in triaxial compression experiments was also emphasized by Alshibli et al. (2003) who studied the

localization phenomena in sands under very low confining pressures. Desrues et al. (1996) suggested that symmetry of the specimen state is a factor that influences shear band formation under axisymmetric stress conditions. Therefore, unique and severe localization modes can be produced if the symmetry of the specimen is disturbed by various factors such as incorrect centring of the specimen, tilted platens or local weakness of specimens. Desrues et al. (1996) also indicated that despite different localization patterns, both loose and dense specimens tested at the same confining pressure achieved the same critical state void ratio within localization zones. Frost & Jang (2000) supported these findings using the image analysis-based measurements during drained triaxial tests conducted on dense specimens.

Although many triaxial compression experiments have been performed in the past, triaxial extension tests received less attention. The main reason is that the extension test has substantially more problems associated with strain localization than the compression test (Yamamuro & Lade, 1995). As necking is a dominant deformation mode in the triaxial extension test, it leads to underestimation of the deviatoric stress at the neck area (Roscoe et al., 1963). Therefore, it appears that the extension test does not provide a reliable method to determine the strength of granular soils. The unstable nature of the extension test is explained in Figs. 2.14 and 2.15, in which triaxial compression and extension tests are schematically compared (Yamamuro & Lade, 1995).

Lade et al. (1996) also reported that conventional extension tests are always subject to non-homogeneous deformations in the hardening regime, in the form of either necking or shear banding. They concluded that the conventional extension test is unsuitable for determination of soil parameters. Therefore, the strength characteristics of soils should be determined based on the results from the tests with more uniform stress-strain behaviour than that obtained from conventional extension tests. Lade et al. (1996) have suggested that the uniformity of a specimen in the extension test can be improved by enforcing a rubber membrane with thin steel plates.

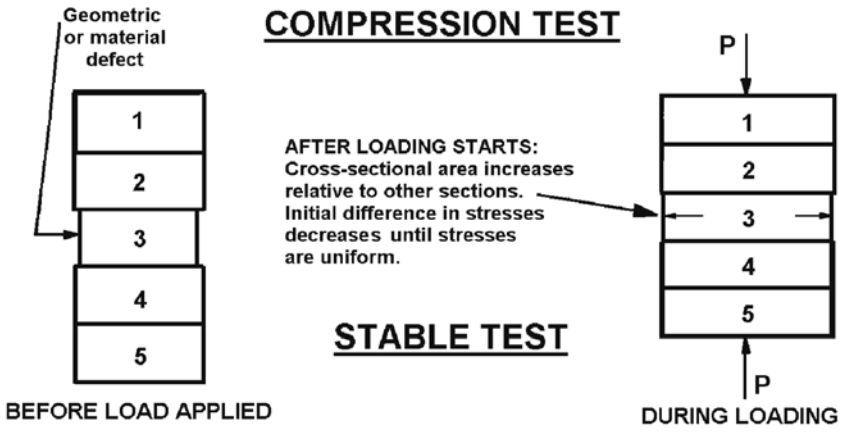

Fig. 2.14 Diagram showing stable nature of compression test during loading indicated by redistribution of initial stress concentrations formed from initial imperfections (after Yamamuro & Lade, 1995)

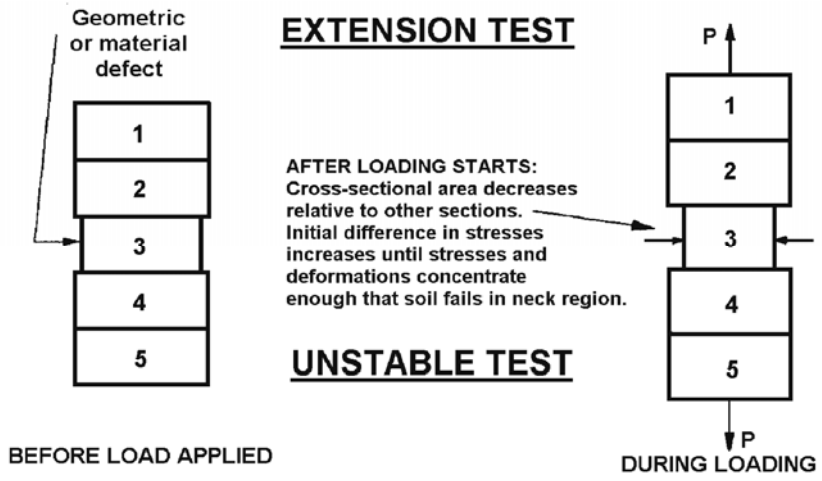

Fig. 2.15 Diagram showing unstable nature of extension test indicated by accumulation of initial stress concentrations formed from initial imperfections (after Yamamuro & Lade, 1995)

2.5.5.3 Plane-Strain Tests

The importance of studying the stress-strain behaviour of sand under plane-strain conditions has been highlighted by a number of researchers (e.g. Bishop, 1966; Lee, 1970; Green, 1971; Marachi et al., 1981). Many common field problems, e.g. slopes, embankments, and retaining walls, approximate closely to plane-strain conditions. Furthermore, strain localization problems observed in the field can be better understood using a plane-strain apparatus. Several plane-strain or biaxial

devices have been developed in the past to study the strength and deformation characteristics of soils under plane-strain conditions (e.g. Cornforth, 1964; Duncan & Seed, 1966; Drescher et al., 1990; Tatsuoka et al., 1986, 1994; Finno et al., 1996, 1997; Yasin et al. 1999, Alshibli et al., 2003, 2004). Many valuable comparisons between triaxial and plane-strain test results have also been reported (Cornforth, 1964; Lee & Shubeck, 1971; Marachi et al., 1981; Alshibli et al., 2003). Table 2-1 presents a summary of most of the plane-strain devices that have been developed in the past by various research groups.

In the early stage of experimental investigations under plane-strain conditions, several researchers focused on the strength and deformation characteristics of granular materials. It was showed that the shear strength of granular soils under plane-strain conditions is higher than that under axisymmetric stress conditions. Furthermore, the difference between plane-strain test results and triaxial test results becomes higher with increasing soil density (Cornforth, 1964; Rowe, 1969; Lee, 1970; Green, 1971; Green & Reades, 1975; Oda et al., 1978). It was also observed that specimens in plane-strain tests are stiffer and experience smaller volume changes than those in triaxial tests (Cornforth, 1964; Bishop, 1966; Barden et al., 1969; Lee, 1970, Green & Reades, 1975; Marachi et al., 1981). Typical stress-strain curves for plane-strain and triaxial tests are shown in Fig. 2.16.

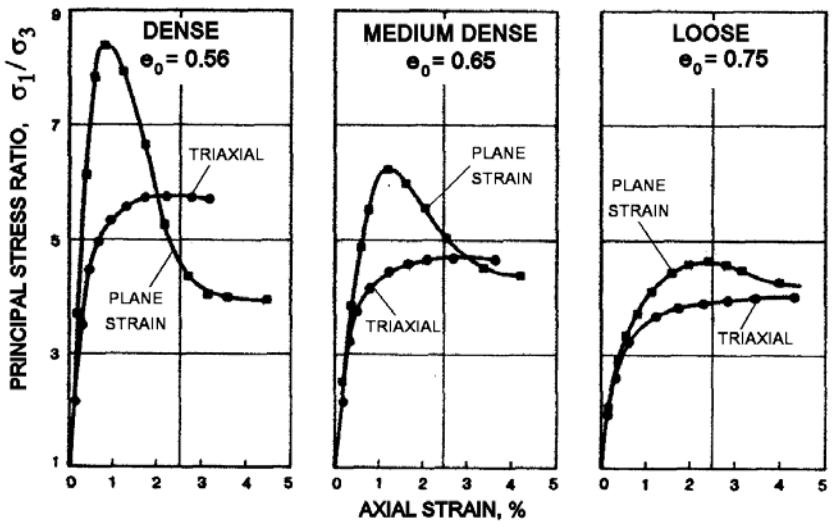

Fig. 2.16 Stress-strain relationship for plane-strain and triaxial specimens (after Marachi et al., 1981)

Table 2-1 Summary of plane-strain devices used by different researchers.

Location	Specimen size (W × L × H) (mm)	Specimen – boundary interface	Type of lubrication	Measurement of "out-of-plane" stress	Remarks	Reference
Imperial College, London, UK	51 × 406 × 102	σ_1, σ_2 – rigid	silicone grease	Yes	Null technique used to measure σ_2	Bishop (1958), Cornforth (1961, 1964)
Technical University of Karlsruhe, Germany	200× 1000 × 600	σ_1, σ_2 – rigid	soft soap	Yes	Suitable for large scale model testing	Leussink & Wittke (1964)
University of California, Berkeley, USA	28 × 71 × 61 28 × 71 × 71	σ_1, σ_2 – rigid σ_3 – can be flexible	silicone grease	No	Both side plates – stainless steel	Duncan & Seed (1966) Lee (1970)
University of Cambridge, UK	70-130 × 70-130 × 50	σ_1, σ_2, σ_3– rigid	silicone grease	Yes	σ_1, σ_3 – aluminium plates σ_2 – glass plate	Hambly & Roscoe (1969) Hambly (1969, 1972)
University of British Columbia, Canada	25 × 100 × 57	σ_1, σ_2 – rigid σ_3 – flexible	silicone grease	Yes	Both side plates – stainless steel	Campanella & Vaid (1973)
University College, London, UK	100 × 100 × 100	σ_1, σ_3 – flexible σ_2 – rigid	latex sheet + silicone grease	Yes	One side plate – steel; the other – Acryle	Arthur et al. (1985) Yasin et al. (1999)
University of Karlsruhe, Germany	45-133 × 45-133 × 50	σ_1, σ_2, σ_3– rigid	silicone grease	Yes	Modification of Hambly (1969) apparatus	Topolnicki et al. (1990)
University of Minnesota, USA	40 × 80 × 140	σ_1, σ_2 – rigid	glass lined plates + grease	No	Unrestrained bottom end platen	Drescher et al. (1990)
Northwestern University, USA	40 × 80 × 140	σ_1, σ_2 – rigid	glass lined plates + grease	Yes	Modification of Drescher et al. (1990) apparatus	Finno et al. (1996, 1997)
Laboratoire 3S-IMG, Grenoble, France	35 × 90-135 × 75-350	σ_1, σ_2 – rigid	glass plates + silicone grease	No	Unrestrained top end platen	Desrues et al. (1985, 1996), Desrues & Viggiani (2004)
University of Tokyo, Japan	40 × 80 × 105 80 × 160 × 140	σ_1, σ_2 – rigid	latex sheet + silicone grease	Yes	ε_1 measured by proximity transducers	Tatsuoka et al. (1986, 1994), Yasin et al. (1999)
Louisiana State University, USA	60 × 120 × 180	σ_1, σ_2 – rigid	glass lined plates	No	Unrestrained bottom end platen	Alshibli et al. (2004)

Comparison of the stress-strain behaviour in plane-strain and triaxial tests indicates that the stress conditions have large influence not only on the strength of soils but also on the shear band formation. In early 1960s, Cornforth (1961, 1964) did not observed apparent shear bands in any of the triaxial and plane-strain tests stopped at the maximum deviatoric stresses. However, if a plane-strain test was continued to the ultimate state, a visible shear bands developed. With the progress in experimental techniques and equipment used in soil mechanics laboratories, more researchers have realized that stress-strain behaviour in plane-strain tests is significantly influenced by shear band formation. It was observed that the peak failure in plane-strain tests is associated with the shear band development. Therefore, many studies have been conducted in order to determine whether the failure under plane-strain conditions is the cause or the result of shear band formation. Peters et al. (1988) found that shear bands occur in the hardening regime and cause the peak deviatoric stress behaviour. It was concluded that once the shear band occurs, the constitutive relationship is no longer valid. These finding were further confirmed by Peric et al. (1993) who also observed that under plane-strain conditions shear bands occur in the hardening regime before significant plastic deformations take place. Therefore, in the post-bifurcation regime, the stress-strain characteristics do not follow the constitutive behaviour under plane-strain conditions.

Drescher et al. (1990) developed a new biaxial apparatus for testing growth of shear bands. The apparatus is schematically shown in Fig. 2.17.

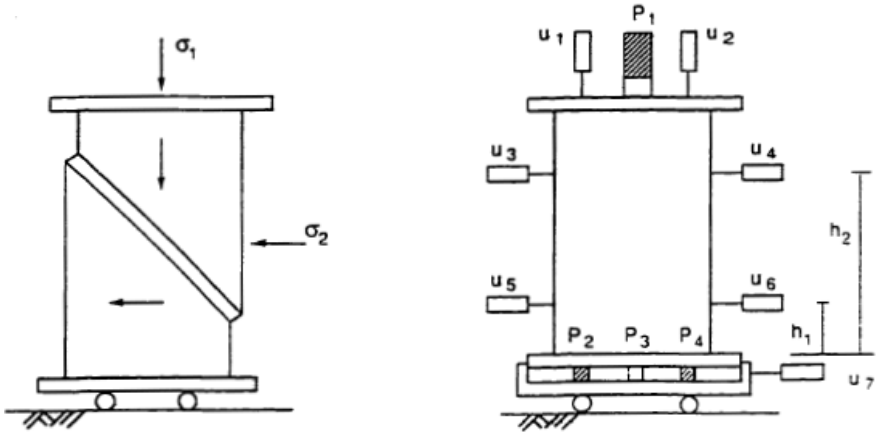

(a) (b)

Fig. 2.17 Biaxial apparatus: (a) schematic; (b) arrangement of load cells and LVDTs (after Drescher et al., 1990)

It can be seen from Fig. 2.17 that the biaxial apparatus has a unique feature that is a linear bearing platform which allows free lateral displacement of the lower part of the specimen once a shear band develops. Thus, the shear band formation will not be affected by the end friction or boundary effects. Another way of achieving this is to use properly lubricated free-ends. It should be pointed out that the lateral out-of-plane stress (σ_3) was not measured in the biaxial apparatus.

Based on the experiments conducted on dry dense sand, Drescher et al. (1990) concluded that shear bands developed before the peak is reached. However, they pointed out that shear banding can be affected by confining pressure or sand gradation and γ–ray or *X*-ray techniques should be employed to confirm these observations. Using the same biaxial apparatus, Han & Vardoulakis (1991) conducted plane-strain tests on loose and dense sand under both drained and undrained conditions. The shear bands were observed using *X*-ray radiographs. Han & Vardoulakis (1991) reported that shear bands occurred in dense specimens. However they did not find any shear bands in loose specimens. Furthermore, they observed that shear bands in undrained tests occurred in strain softening regime, whereas in drained tests shear bands developed in the hardening regime.

The biaxial apparatus developed by Drescher et al. (1990) was further modified by Harris et al. (1995) to allow the measurement of the load-displacement characteristics within the failure zone. The modified biaxial apparatus is presented in Fig. 2.18.

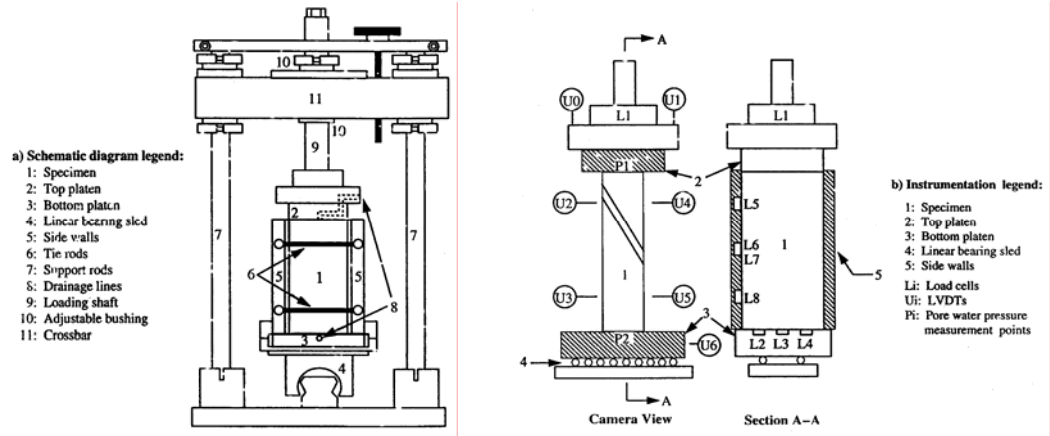

(a) (b)

Fig. 2.18 Modified biaxial apparatus: (a) schematic diagram; (b) instrumentation (after Finno et al., 1997)

A total of 19 sensors are used in the system. Four internally located load cells (L1, L2, L3, L4) allow accurate measurement of axial force. Another four load cells (L5, L6, L7, L8) are embedded in an aluminium side plate to measure out-of-plane forces. The displacements of the specimen and the horizontal movement of the base plate are measured by seven displacement transducers. One of the side plates is a Plexiglas window that permits a view of the specimen side during the test.

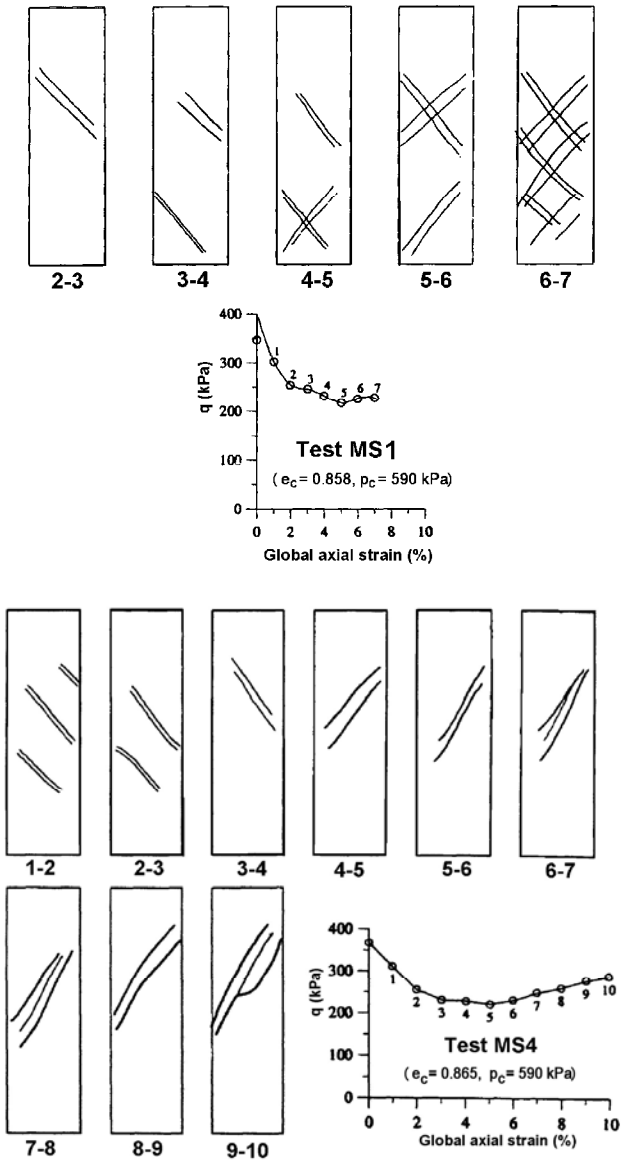

Fig. 2.19 Comparison of shear band evolutions observed in two undrained tests MS1 and MS4 carried our by Harris et al. (1995)

Harris et al. (1995) and Finno et al. (1996, 1997) have conducted several tests on loose granular soils using this biaxial apparatus. They have shown that the strain localizations can develop in loose specimens. The two examples of shear band

development as observed by Harris et al. (1995) are presented in Fig. 2.19. Both tests were on loose sand under the same test conditions. However, the patterns of non-homogeneous deformations in the two tests are different. It was reported by Finno et al. (1996, 1997) that the first appearance of the persistent shear band consistently occurred before the maximum effective stress ratio.

It should be pointed out that there are discrepancies among different studies on the occurrence of shear bands in loose specimens. The results obtained by Finno et al. (1996, 1997) agree with that by Mokni & Desrues (1998), but not with Han & Vardoulakis (1991) who did not observe any distinct shear bands in contractive specimens. Han & Vardoulakis (1991) have only reported diffuse modes of localization and concluded that specimens with these so-called “wrinkling” modes of deformation could still be considered as fairly homogeneous. Typical loose specimen observed at the end of a plane-strain test by Han & Vardoulakis (1991) is shown in Fig. 2.20.

Fig. 2.20 Typical deformation mode of a loose specimen at the end of plane-strain test (after Han & Vardoulakis, 1991)

In fact, Finno et al. (1997) also reported few plane-strain tests conducted on loose sand in which the overall deformation was uniform. In those tests, neither a distinct shear band nor barrelling of the specimens was observed. It has been observed that mobilized friction in those tests has increased monotonically and has asymptotically approached a peak value at the end of shearing. This is in agreement with the study by Cornforth (1964) who reported that it might be possible to shear a

very loose specimen under plane-strain conditions directly to an ultimate state without a peak in the stress-strain curve and without dilating.

It has been reported that the global measurement of displacements and volume changes of specimens do not capture the behaviour in thin shear bands (Desrues et al., 1985, 1996; Harris et al., 1995, Finno et al., 1997; Mooney et al., 1997, 1998). The significant progress made in shear band monitoring techniques during the last decade, provided the opportunity for precise measurement of shear band inclination and thickness. Following techniques are normally used:

- *X*-ray radiography (Vardoulakis & Graf, 1982; Michalowski, 1990; Han & Vardoulakis, 1991)
- γ-ray absorption (Desrues et al., 1985)
- Laser speckle method (Tatsuoka et al., 1990)
- Stereophotogrammetry (Mokni & Desrues, 1998; Desrues & Viggiani, 2004; Yoshida et al., 1994; Harris et al., 1995; Finno et al., 1996, 1997; Mooney et al., 1997, 1998)
- *X*-ray Computed Tomography (Desrues et al., 1996; Alshibli et al., 2000; Batiste et al., 2004; Sun et al., 2004)
- Digital image analysis (Liang et al., 1997; Alshibli & Sture, 2000)
- Digital Image Correlation (Finno & Rechenmacher, 2003; Rechenmacher & Finno, 2004)

In classical soil mechanics the orientation of a shear band is determined by (Coulomb, 1776)

$$\theta_C = 45° + \varphi/2 \qquad (2-24)$$

where φ is the angle of internal friction. Such a direction coincides with a plane of maximum stress obliquity.

Another solution for the shear band orientation was proposed by Roscoe (1970). He described the angle θ, using a plastic flow rule, as:

$$\theta_R = 45° + \psi_s/2 \qquad (2-25)$$

where ψ_s is the angle of dilatancy.

It can be seen that the difference between the Coulomb orientation and the Roscoe orientation is significant because the dilatancy angle is usually much smaller than the friction angle (Vermeer, 1990; Tatsuoka et al., 1990). Therefore, Arthur et al. (1977) proposed that the average of these two angles should be used to define the direction of shear bands

$$\theta_A = 45° + (\varphi + \psi_s)/4 \qquad (2-26)$$

All of the Coulomb, Roscoe and Arthur inclinations are defined with respect to the direction of minor principal stress.

One of the first attempts to measure shear band orientation was made by Cornforth (1964). He reported that shear bands directions were in agreement with Coulomb's solution. Similar observations were also made by Desrues et al. (1985) and Finno et al. (1996). Drescher et al. (1990) on the other hand suggested that shear band inclinations in poorly graded dry Ottawa sand were in agreement with Roscoe's theory. Several experimental results have also shown that the orientation of shear bands varies between the limits of Roscoe's and Coulomb's solutions (Tatsuoka et al., 1990; Vermeer, 1990; Han & Drescher, 1993; Peric et al., 1993; Finno et al., 1997; Finno & Rechenmacher, 2003). These experimental findings have supported Arthur's inclination.

Vermeer (1990) also observed that shear band inclination is related to particle size distribution. He reported that coarse sands tend to give Roscoe's orientation, whereas fine sands tend to give Coulomb's orientation. Mokni & Desrues (1998) and Alshibli & Sture (2000) also observed that lower shear band inclination is associated with larger grain sizes.

It has also been observed that shear band inclination varies with confining pressure and specimen density. Several researchers (Han & Drescher, 1993; Yoshida et al., 1994, Alshibli & Sture, 2000) have reported that shear band inclination decreases with increasing confining pressure. Furthermore, Alshibli & Sture (2000) reported that larger shear band inclination is obtained for dense specimens compared to that for loose specimens. The same observation was reported by Mokni & Desrues (1998).

Based on the experimental data published in the literature, it can be concluded that all shear band inclination solutions proposed by Coulomb, Roscoe and Arthur are favoured by some researchers. This suggests that shear band inclination is sensitive to the apparatus type and may not be directly comparable, as pointed out by Finno et al. (1997).

Another aspect of shear band formation which has been investigated in the past is its thickness. Although there is ample experimental evidence that shear bands in granular materials involve a significant number of grains, the thickness of shear bands does not seem to be unique (Muhlhaus & Vardoulakis, 1987; Finno et al., 1997). Shear band thickness is commonly associated by researchers with mean grain size, D_{50}. For example, Roscoe (1970) indicated that the width of shear band is 10 times D_{50}. On the other hand, Muhlhaus & Vardoulakis (1987) showed that it is 16 times D_{50}. Yoshida et al. (1994) reported that the thickness of shear bands varied from 10 to 30 times D_{50}. Finally recent data presented by Finno et al. (1997) and Finno & Rechenmacher (2003) have indicated that the width of the shear bands vary from 10 to 25 times the mean grain size. In addition, Finno et al. (1997) suggested that thicknesses of shear bands can vary along their length and can change during shearing process.

2.5.5.4 True Triaxial Tests

A number of various true triaxial apparatuses have been developed in the past. Three different types of true triaxial devices are described in the literature. The difference among them lies in the applied boundary conditions and loading procedures.

1) Flexible Boundary

In this category all six surfaces of the cubical specimens are loaded by flexible rubber bags. Examples of such designs are described by Ko & Scott (1967, 1968), Arthur & Menzies (1972), Arthur et al. (1977), Yamada & Ishihara (1979), Sture & Desai (1979), Haruyama (1985) and Prashant & Penumadu (2004). The main advantage of flexible boundaries is uniformity of stresses applied to the specimen surfaces. However, due to the flexibility of rubber bags, serious errors can be induced in the measurement of displacements.

2) Rigid Boundary

In this category all the six surfaces of the specimen are loaded by rigid platens in three orthogonal directions. The basic design was proposed by Hambly (1969). Roscoe (1970), Pearce (1971) and Goldscheider (1982) also used rigid boundaries. However, because of complexity of loading systems and large stress concentrations only limited data has been published.

3) Mixed Boundaries

True triaxial cells in this category consist of both flexible and rigid boundaries to apply principal stresses. Two modes of loading for intermediate stresses application are commonly used. Shibata & Karube (1965), Sutherland & Mesdary (1969) used designs in which the major principal stress was applied through the rigid platens and the intermediate stress was applied by two rubber bags filled with water or oil. On the other hand, Green (1971), Lade & Duncan (1973), Reades & Green (1976), Wang & Lade (2001), Shapiro & Yamamuro (2003) used rigid platens instead of rubber bags to apply the intermediate stresses. Chu et al. (1996) also applied so called “composite boundary” loading system which consists of a piece of undersized metal platen bounded on the loading surface of a flexible bag. Such a design combines the advantages of both rigid and flexible loading boundaries.

Most of the abovementioned true triaxial apparatuses were used to investigate the strength and deformation characteristics of soils under generalized stress conditions. The influence of the intermediate principal stress on the behaviour of soils has also been studied. However, only few experimental studies on the shear band formation have been reported. It might be because of difficulties in detecting shear bands under three dimensional stress conditions. Therefore, the process of shear band formation under three dimensional stress conditions is still not clarified.

Arthur et al. (1977) carried out series of drained tests conducted on dense sand under generalized stress conditions using flexible boundary cell. They recorded shear bands radiographically and observed that shear bands were initiated before peak stress ratio was attained. Based on their experimental results, Arthur et al. (1977) proposed the solution for shear band inclination, known as Arthur’s

orientation (see Eqn. 2 – 26). Arthur & Dunstan (1982) further reported that shear band orientation is independent of the intermediate principal stress value.

Chu et al. (1996) studied strain softening behaviour and shear band formation using the multi-axial cell. They conducted several constant b-value tests and detected shear bands using a photographic technique. Chu et al. (1996) found that shear bands under generalized stress conditions became visible only in the post-failure region. Therefore, they suggested that the necessary conditions for the initiation of the shear bands are shearing beyond failure state and $\sigma_2' \neq \sigma_3'$. Chu e al. (1996) also indicated that the final shear band can follow one of the two modes, as presented in Fig. 2.21.

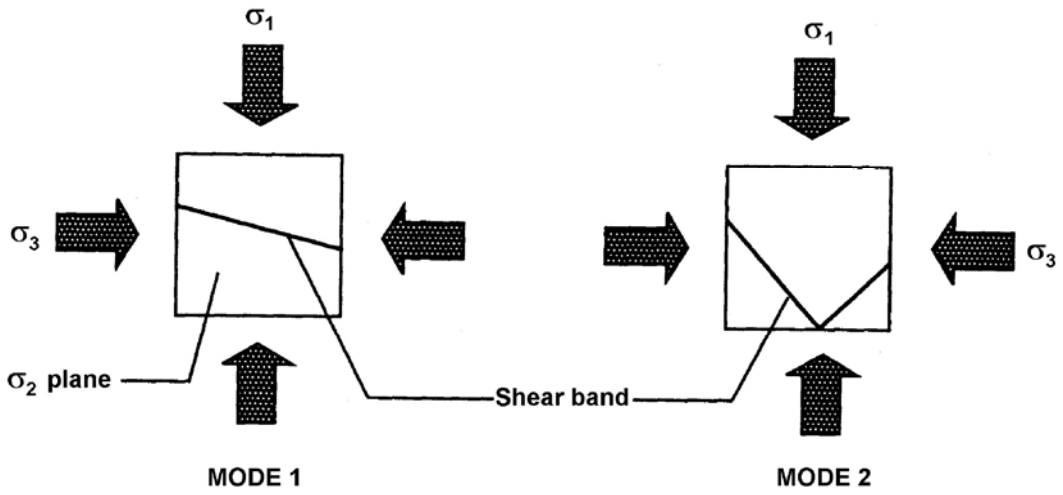

Fig. 2.21 Two modes of shear bands observed in multi-axial cell (after Chu et al., 1996)

Lade & Wang (2001) conducted series of tests on tall (H/D = 2.47) prismatic sand specimens under generalized stress conditions. They observed the same mode of shear bands in all the tests (Fig. 2.22(a)) with exception of tests with $b = 1$ (Fig. 2.22(b)). Lade & Wang (2001) also measured the orientation of shear bands and compared them with the theoretical predictions, as shown in Fig. 2.23. They observed that the measured shear band inclinations are located between Arthur's and Coulomb's values. However, when the sand becomes denser the shear band inclinations are essentially equal to the Coulomb's solution (Fig. 2.23(a)).

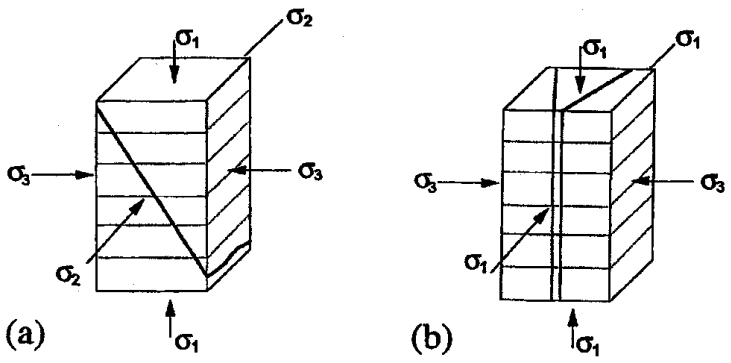

Fig. 2.22 Modes of shear banding observed in prismatic specimens of Santa Monica Beach sand: (a) failure in vertical direction for tests with $0 \leq b < 1$; (b) failure in horizontal direction for tests with $b = 1$ (after Lade & Wang, 2001)

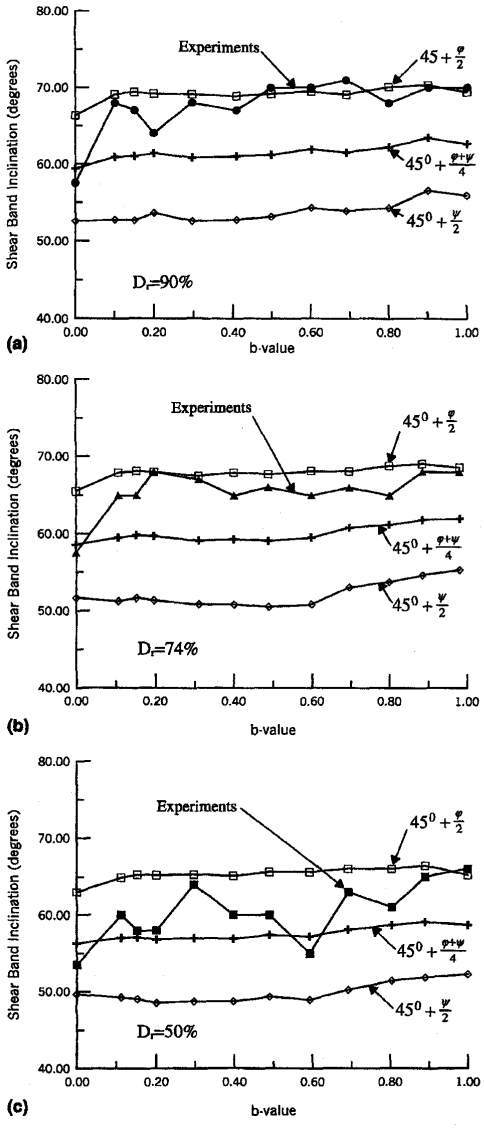

Fig. 2.23 Experimental shear band directions compared with three theoretical values for Santa Monica Beach Sand: (a) dense; (b) medium; (c) loose (after Lade & Wang, 2001)

Wang & Lade (2001) also observed that the peak failure in true triaxial tests appears to be the result of the instability rather than a continuum response of granular material. They demonstrated that shear bands were initiated before peak failure was reached. Therefore, the failure seems to be a consequence of the shear band development. Similar conclusions were made by Desrues et al. (1985), Yoshida et al. (1994), Finno et al. (1996, 1997), Finno & Rechenmacher (2003) and Alshibli et al. (2004) under plane-strain conditions. Furthermore, Wang & Lade (2001) suggested that the breaks in the stress-strain curve and ε_1-ε_2 curve are good indicators of the onset of shear banding.

Shapiro & Yamamuro (2003) employed the true triaxial apparatus similar to that described by Lade (1978) to study the effect of silt on three-dimensional stress-strain behaviour of loose sand. They observed that shear bands have caused failure during all true triaxial tests when *b-value* was greater than zero. However, no shear bands occurred when specimens were undergoing volumetric contraction. The shear bands observed by Shapiro & Yamamuro (2003) were generally paired and symmetrical to the centre axis of the specimen perpendicular to the σ_2 face, as shown in Fig. 2.24. Shapiro & Yamamuro (2003) also pointed out that the exact point at which the shear bands develop under generalized stress conditions is difficult to determine because most of true triaxial devices do not allow the observation of the shear bands until the specimen is removed at the end of the test.

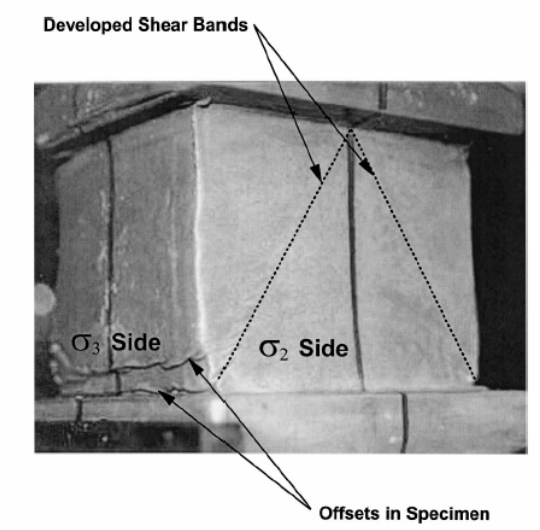

Fig. 2.24 Photograph of true triaxial specimen at conclusion of test (after Shapiro & Yamamuro, 2003)

2.5.5.5 Hollow Cylinder Tests

Unconfined hollow cylinder soil specimens subjected to torque were used as early as 1936 when Cooling & Smith (1936) studied the resistance of soils in pure shearing. Later on Broms & Casbarian (1965) introduced the idea of combining axial and torsional stresses in thin long hollow cylinder specimens to study the effect of the principal stress rotation on the strength parameters of soils.

Hight et al.(1983) reported that the effect of principal stress rotation in soil can be studied by controlling both the direction of the major principal stress (σ_1), which is defined in terms of its angle to the vertical (α), and the magnitude of the intermediate principal stress (σ_2), which is defined in terms of b-value. The influence of such stress rotation on the behaviour of sands cannot be derived from conventional triaxial tests in which triaxial compression ($\alpha = 0°$ and $b = 0$) or triaxial extension ($\alpha = 90°$ and $b = 1$) tests can only be conducted. Moreover, the hollow cylinder apparatus (HCA) is the only equipment in which α and b can be independently controlled. (Hight et al., 1983; Symes et al., 1984; Zdravkovic, 1996; Zdravkovic & Jardine, 2000, 2001; Sivathayalan & Vaid, 2002).

In HCA, an axial load (W), a torque (M_T), internal (p_i) and external (p_o) pressures are applied. The stress conditions are represented by stresses σ_z, $\tau_{\theta z}$, σ_r and σ_θ in the wall of the specimen (Fig. 2.25). By controlling these stresses the magnitude of the principal stresses σ_1, σ_2, and σ_3 can be independently determined, together wit the orientation of the major principal stress, α (Hight et al., 1983; Symes et al., 1984). As the HCA is computer controlled, a wide range of effective stress paths, as well as strain paths can be applied under both drained and undrained conditions (Zdravkovic, 1996).

Although the HCA provides a valuable tool for soil testing, it has one major disadvantage that is, the existence of non-uniformities in stress and strain distribution due to end restraints arising from the top and bottom platens (Saada & Townsend, 1981; Zdravkovic, 1996; Gan, 2002, Sivathayalan & Vaid, 2002). However, Hight et al. (1983) and Symes et al., (1984) have demonstrated that the

non-uniformities can be minimized by careful selection of sample geometry. As a result the HCA is still the most suitable equipment for advanced soil testing. In addition, some experimental works have shown that the HCA can also be used to conduct experiments under plane-strain conditions (Yoshimine et al., 1999), as well as under simple shear modes (Shibuya & Hight, 1987).

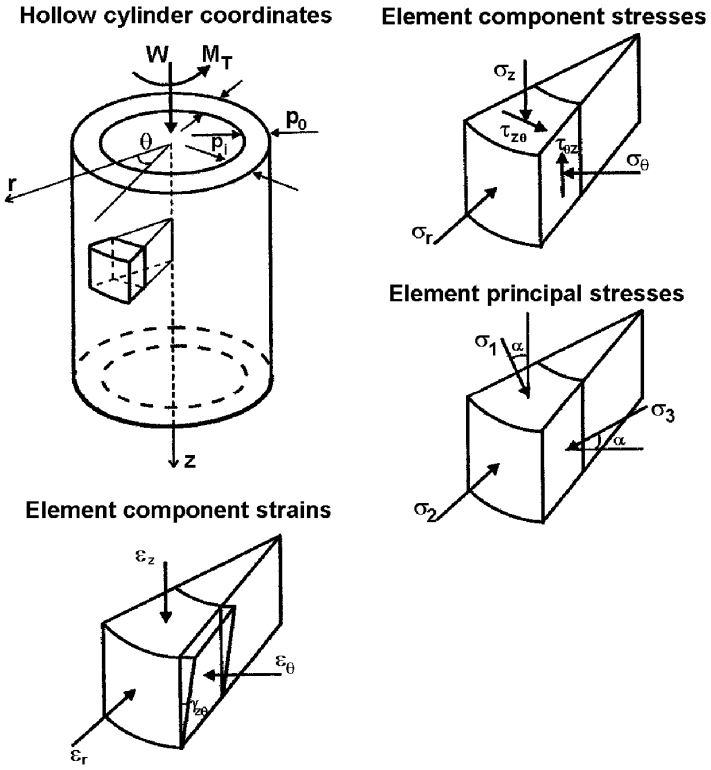

Fig. 2.25 Stress and strain components within the HCA (after Zdravkovic & Jardine, 1997)

Rotation of principal stress directions and changes in the relative magnitude of the intermediate principal stress are strongly associated with most field loading and unloading problems (Hight et al., 1983). The ability of HCA to vary α continuously between 0° and 90°, and b between 0 and 1, allowed a wide range of engineering problems to be considered that could not be simulated in triaxial or plane strain apparatus. Therefore, the HCA has widely been used for studying of the soil anisotropy (Hight et al., 1983; Zdravkovic, 1996; Zdravkovic & Jardine, 2000, 2001). However, only few experimental studies in HCA have been focused on the shear band formation.

Hight et al. (1983) described a new HCA and conducted a series of tests on dense Ham River sand to demonstrate the capabilities of the apparatus. To obtained reliable information on overall uniformity of the specimens, photogrammetric measurements of a grid inscribed on the outer membrane were adopted. Hight et al. (1983) reported that non-uniform deformations obtained during the tests in pre-failure region were insignificant. The shear zones were only observed in post-failure regime and there was no tendency for them to initiate at any preferred location.

Saada et al. (1994) studied the influence of the cracks and shear bands on the kinematics and strength of over consolidated and normally consolidated clay specimens. To study the non-uniform deformation patterns at the end of tests, the specimens were rotated in a front of a camera and photographs were taken for small rotation increments. Those photographs were then overlapped with matching grids and deformation patterns were examined. Saada et al. (1994) observed that bifurcations in the form of shear bands appeared near the peak stress in hollow cylinder experiments. Initially, they were well distributed along the length of the specimens, but eventually they progressed to persistent bands along which the material failed in a catastrophic way. Most of the shear bands were nearly horizontal with only a few inclined. Saada et al. (1994) also observed that the shear bands that developed in the OC clays were thinner and more pronounced than those that developed in the NC clays.

Saada et al. (1999) studied effects of principal stress rotation, the relative density, the confining pressure and grain size distribution on the shear band formation. They examined shear bands by analyzing digital images taken by four cameras located around the hollow cylinder apparatus, as described by Liang et al. (1997). It was observed that a dominant shear band is always initiated in the vicinity of the peak deviatoric stress. Saada et al. (1999) reported that shear band inclination agrees with Arthur's solution and does not seem to be influenced by density and changes in confining pressure. They also indicated that thickness of the persistent shear band is not constant while it is developing. Furthermore, the thickness can vary with b-value, the confining pressure and the density of granular materials.

Most recently, the results of some novel experiments using *X*-ray radiography and microstructural observations of shear band formation in granular materials under drained and undrained conditions were reported by Nemat-Nasser & Okada (2001). Columns of lead silicate granules of distinct colour were embedded within the thin wall of a large hollow cylinder specimen. The deformation of these columns was then radiographically recorded during the shearing. In addition, upon the completion of a shearing, the specimens were frozen and the shear bands were studied by optical microscopy. Nemat-Nasser & Okada (2001) observed extensive dilative deformations along shear bands, accompanied by contractive deformations in planes normal to the centreline of the shear bands. They also pointed out that the shear strains measured inside of a fully developed shear band can exceed 500% for overall nominal specimen strains of about 10%. Finally, they indicated that the shear band thickness is affected by the mean grain size and is approximately 10 – 15 times larger than D_{50}.

2.6 Summary

The literature review presented in Chapter 2 shows that strain softening and instability behaviour of soil have been one of the most active areas of research in geotechnical engineering over the past 30 years. Although significant progress in experimental and analytical research has been made, most of the studies have been performed under axisymmetric stress conditions. Therefore, more experiments should be conducted under plane-strain or more generalized stress conditions.

Instability of loose granular soils under undrained conditions has been well understood and established (Lade, 1992, 1993, 1994; Leong, 2001, Chu et al., 2003). It has also been demonstrated by Chu (1991), Chu et al. (1993, 2003) Chu & Leong (2001), Loke (2004) and Vaid & Eliadorani (1998) that granular soils can become unstable under drained or strain path controlled conditions. The instability behaviour of granular soils under other than drained or undrained conditions and generalised stress states need to be further studied.

There are experimental data (Peters et al., 1988; Han & Vardoulakis, 1991, Finno & Rechenmacher, 2003) and theoretical studies (Vardoulakis, 1978, 1980, 1983;

Peric et al., 1993) that suggest the occurrence of shear bands in the hardening regime under plane-strain conditions. However, all the studies presented in the literature were conducted under conventional drained or undrained conditions and the specimens were sheared under a deformation-controlled loading mode. The shear band formation in constant load testing under both drained and strain path controlled conditions has not been studied yet.

Although the formation of shear bands under plane-strain conditions have been studied in the past by number of researchers, most experimental studies have been focused on the inclination of shear bands. The effect of shear bands on the strain softening and instability of granular soils under plane-strain conditions has seldom been investigated. Therefore, more studies under plane-strain conditions are required to investigate relationship between strain softening or instability and the shear band formation.

CHAPTER 3

MATERIALS & METHODOLOGY

3.1 Introduction

A new plane-strain apparatus together with the computer control system is described in this chapter. The specimen preparation methods and testing procedures are also elaborated. Test errors and error minimization techniques are also discussed. Some experimental results are presented to demonstrate the performance and reliability of the plane-strain testing system. Finally the experimental programme is presented.

3.2 Plane-Strain Apparatus

The design of the plane-strain apparatus is schematically shown in Fig. 3.1 and a picture of the apparatus is shown in Fig. 3.2. It accommodated a 120 mm in height and 60 x 60 mm in cross-section prismatic soil specimen (Fig. 3.1). The lateral loading platens were fixed in position by two pairs of horizontal tie rods. The rods were located two on each side of specimen, one above and one below, as shown in Fig. 3.1(a). Therefore no lateral movement in the horizontal direction along the rods was allowed during a test and thus the plane-strain condition was imposed. Drainage was provided by two 38 mm in diameter porous discs installed in the top cap and the base pedestal. All rigid platens were properly enlarged and lubricated using the free-end technique (Rowe & Barden, 1964) to reduce the boundary restraints and to delay the occurrence of non-homogeneous deformations. Two types of free-end were used. One, consisted of a layer of high vacuum silicone grease and a latex rubber, was used for the top and bottom loading platens. Another

free-end with a layer of high vacuum silicone grease and a Teflon sheet was used for the lateral loading platens.

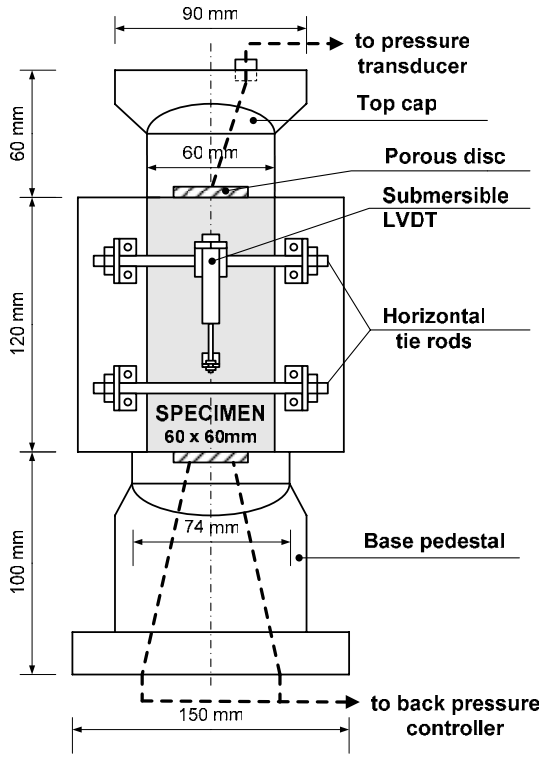

(a)

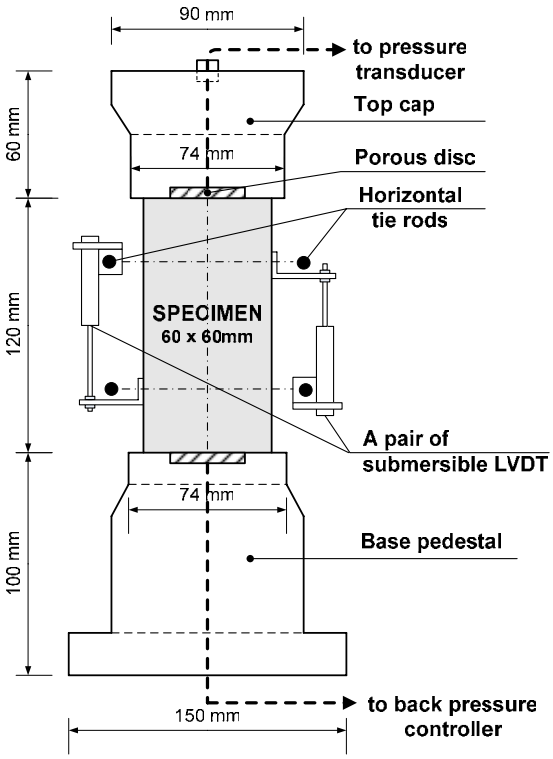

(b)

Fig. 3.1 Plane-strain apparatus: (a) the elevation view; (b) the cross section view

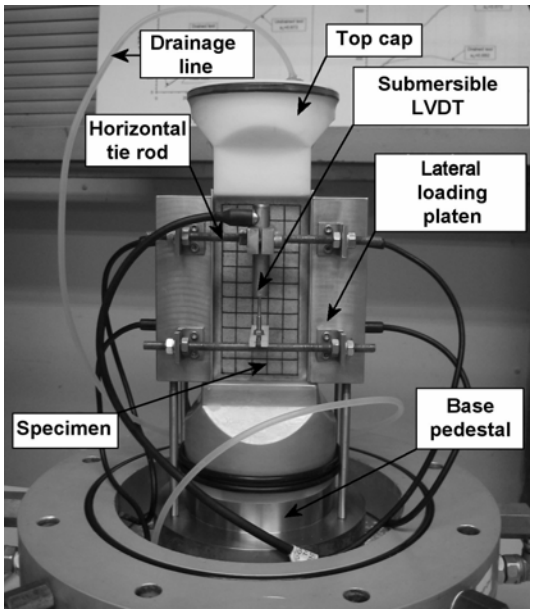

Fig. 3.2 Photograph of the plane-strain apparatus

The plane-strain apparatus shown in Fig. 3.2 was hosted inside a large triaxial cell of 460 mm in height and 220 mm in inner diameter. The cell had a capacity of 1700 kPa.

The computer control system for the plane-strain testing is shown in Fig. 3.3. A hydraulic force actuator mounted at the bottom of a loading frame was used to apply the axial load. The actuator was controlled by a computer via a digital load/displacement control box. The control box adjusted the movement of the base pedestal to achieve desired rate of load or rate of displacement. The cell pressure was applied through a digital pressure/volume controller (DPVC). Another DPVC was used to control the back pressure from the bottom of the specimen and measure the volumetric change in a drained test, or the pore water pressure change in an undrained test. A pore pressure transducer was also used to record the pore water pressure at the top of the specimen.

The lateral stress (σ_2) was measured by four submersible total pressure transducers. The pressure transducers were embedded in the two vertical platens. As shown in Fig. 3.4, two transducers were used for each platen, so that the lateral pressures at both the top and the bottom positions of the specimen could be measured and any non-uniform stress distribution could be detected. The total lateral pressure was

evaluated as an average value obtained from the four individual transducers. The maximum deviation of the σ_2 recorded in the homogeneous regime (i.e., before the occurrence of shear band) was 13 kPa (1.3% of the maximum capacity). An elevated-diaphragm type of soil pressure cell manufactured by Kyowa Electronic Instrument Co. Ltd. was used (Fig. 3.4). The transducer had a capacity of 1000 kPa and a resolution of 0.01 kPa. The diameter of the transducer and the elevated sensing diaphragm was 30 and 23 mm, respectively. Calibrations of the pressure transducers were made by placing the loading platen shown in Fig. 3.4 in a triaxial cell and loading it with water pressure. The maximum error determined from the linear regression of the output recorded during the calibration was 0.1 kPa (i.e., 0.01% of the maximum capacity).

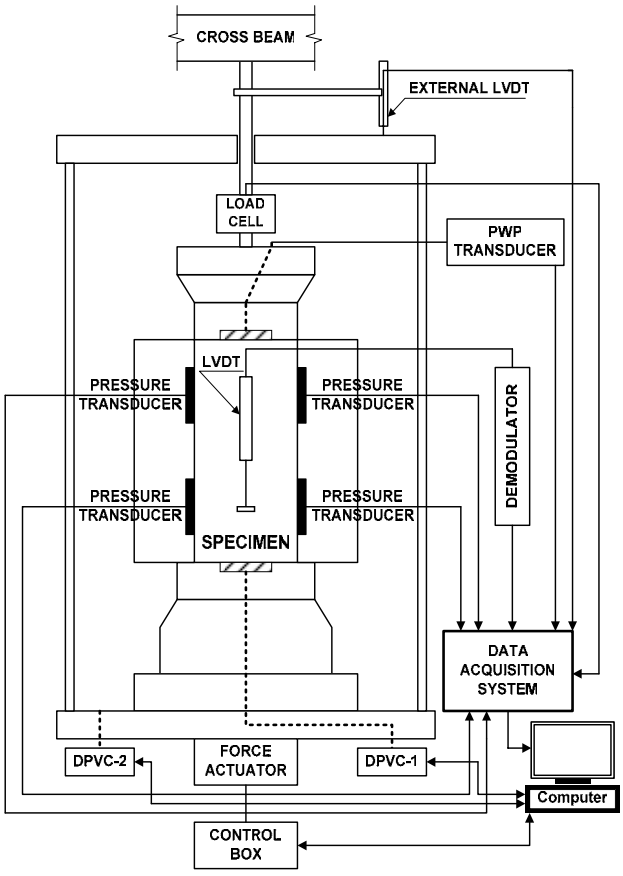

Fig. 3.3 Plane-strain testing system

A pair of miniature submersible linear variable differential transformers (LVDT) was used to measure the vertical displacement, as shown in Figs. 3.1 and 3.2. The internal LVDT had a maximum range of ±5 mm. An external LVDT was also used (Fig. 3.3) to measure the axial strain when the internal LVDTs run out of travel.

Data acquisition was performed by IEEE–PC488 card and Data Acquisition Card (DAC). The former card was used to control the DPVCs and the digital load/displacement control box via personal computer (PC). The latter was used to convert the analogue data from all the transducers to digital format. The data was scanned continuously during the test and stored in the PC.

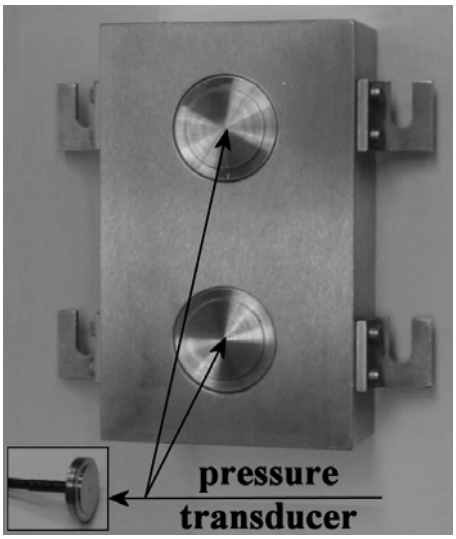

Fig. 3.4 The lateral loading platen

All the measuring devices were calibrated before each series of tests. An input voltage of 5–10V was used on all bridges, both during calibrations and during tests. The corresponding values of load, pressure or deformation and measured output (in mV) showed a little scatter during the calibrations. All established calibration relationships were linear with R-squared values between 0.992–1.000. Therefore, any inaccuracies in the measurement were assumed to be negligible. A summary of errors involved in all the measurements is presented in Table 3-1.

Table 3-1 Summary of accuracy and stability of all the transducers.

Transducer type	Capacity (range)	Accuracy*	Stability#
Vertical load cell	10 kN	0.001 kN	±0.005 kN
Lateral pressure transducer	1000 kPa	0.1 kPa	±0.5 kPa
Pore water pressure transducer	1000 kPa	0.1 kPa	±1.0 kPa
External LVDT	50 mm	0.05 mm	±0.06 mm
Internal LVDT	10 mm	0.001 mm	±0.002 mm

* Maximum error determined from a linear regression during calibration
# Based on the scatter observed for a period of 24 hours prior to calibration

A computer control programme, originally written to conduct general stress and strain path tests (Chu & Lo, 1994), was further modified to conduct various sophisticated stress/strain tests under plane strain condition, including stress paths such as drained $(d\sigma_3' = 0)$, $\sigma_1' = const$, $\sigma_1'/\sigma_3' = const$, $d\sigma_1'/d\sigma_3' = const$, strain paths such as undrained $(d\varepsilon_v/d\varepsilon_1 = 0)$, $d\varepsilon_v/d\varepsilon_1 = const$ and instability (constant shear stress) tests. The structural layout of the main control programme is presented in Fig. 3.5.

During the strain path control, the strain increment ratio $d\varepsilon_v/d\varepsilon_1$ was controlled to a specified value. Such a path could be imposed on a specimen by controlling the volume change of the sample through the DPVC, in accordance with the measured change in axial strain. The cell pressure is kept constant. As a result, the control of volume change of the specimen caused a change in pore water pressure leading to a change in effective confining stress. The control loop for strain path tests was as follows:

a) read LVDT and compute ε_1
b) compute ε_v and volumetric change to be targeted by DPVC
c) send signal to DPVC to target volume change
d) read all transducers, plot the effective stress path and strain path, record stress-strain parameters and return to step (a).

Stress path control during a plane-strain test could be achieved by continuous regulation of the cell pressure targeted by the DPVC in accordance with σ_1' measurement. Consequently the control procedure for a stress path test was as follows:

a) read signal from load cell and calculate σ_1'
b) calculate σ_3' based on the value of σ_1' measured in (a) and the mathematical specification of the stress path
c) calculate the pressure(s) to be targeted by the DPVC(s) and send digital signal(s) to DPVC(s) to target the respective pressure
d) read the LVDTs and volume change of the sample (through the DPVC) for updating the area correction to convert load to stress
e) read all transducers, plot the effective stress path and strain path, record the stress-strain data and return to step (a).

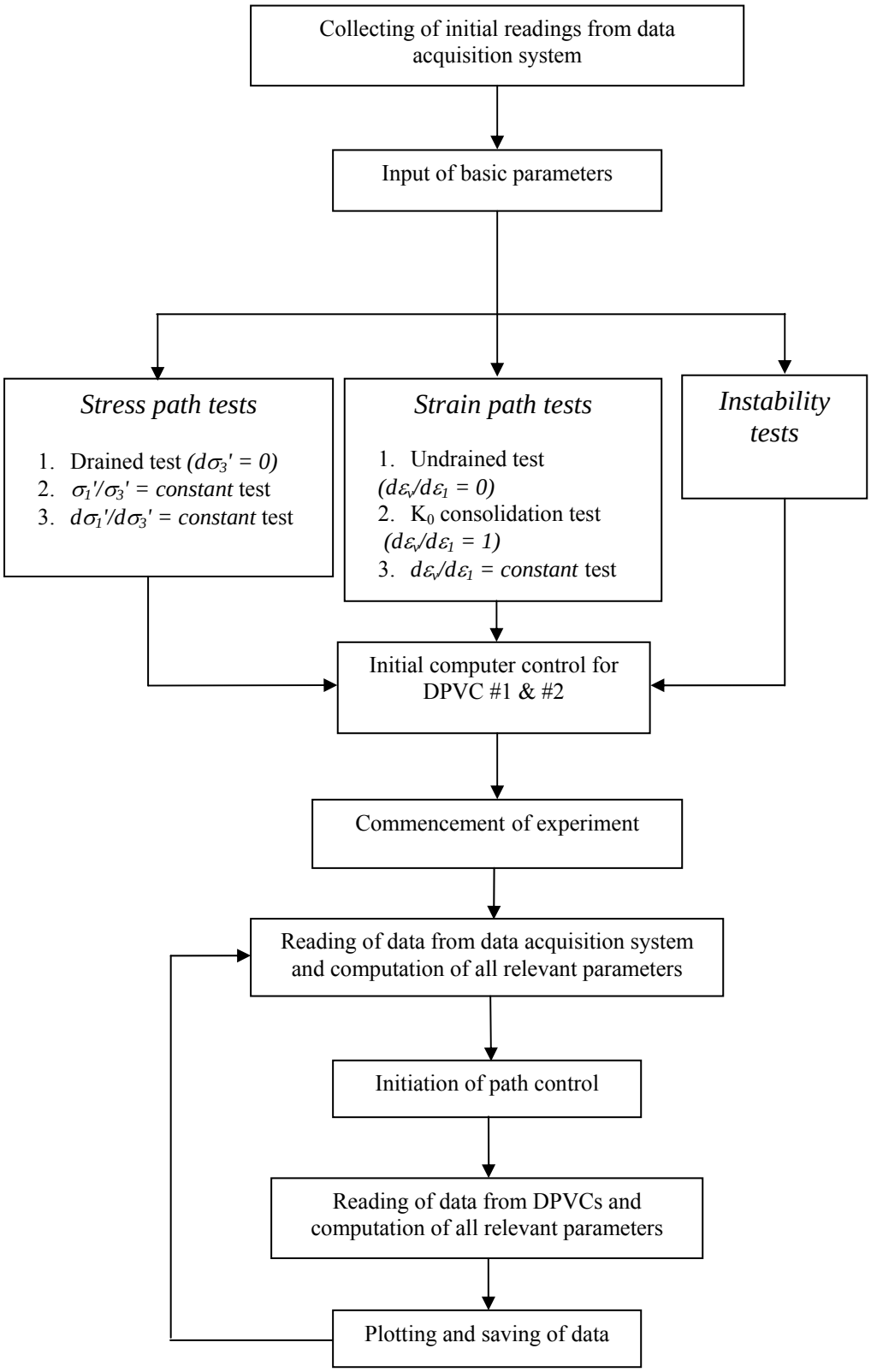

Fig. 3.5 Structural layout of the control programme

3.3 Material Tested

The plane-strain tests were conducted on the marine dredged silica sand, so-called Changi sand, used for the Changi land reclamation project in Singapore. The same sand was also used in previous studies on liquefaction and instability behaviour of granular fill (Leong, 2001; Gan, 2002; Loke, 2004). The average grain size distribution of the sand is shown in Fig. 3.6 and the basic properties of the sand are given in Table 3-2.

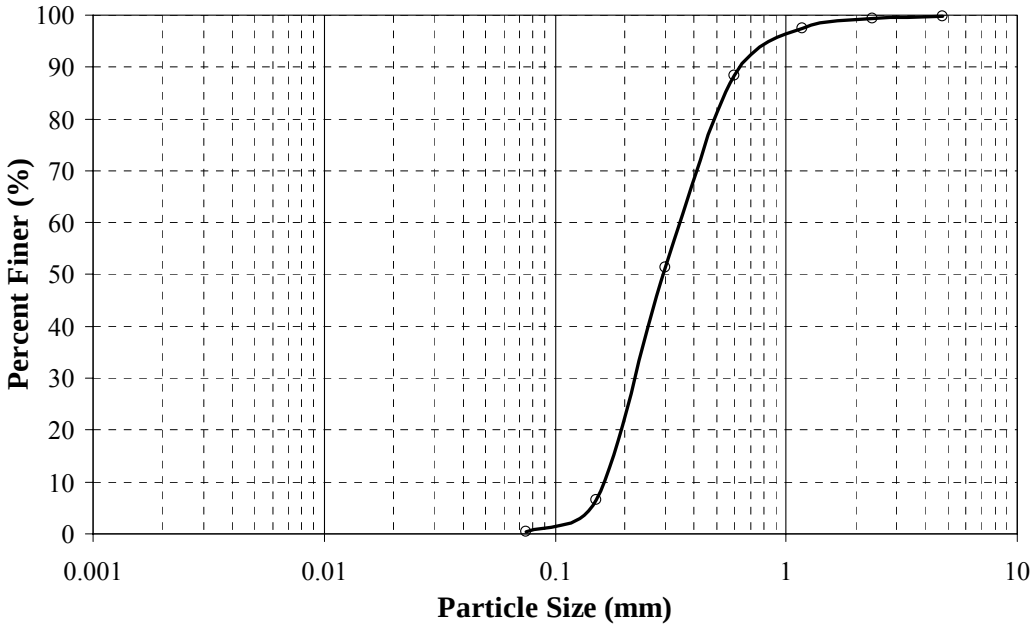

Fig. 3.6 Grain size distribution curve of Changi sand

The Changi sand has the mean grain size *(D_{50})* of approximately 0.30–0.35 mm, the coefficient of uniformity *(C_U)* of 2.0, and coefficient of curvature *(C_C)* of 0.8. The fines content is approximately 0.4%. Therefore, according to Unified Soil Classification System (ASTM: D 2487) it is medium grained, poorly graded, clean sand. The individual particles of the sand are mainly sub-angular in shape. Since the Changi sand was dredged from the seabed, it contained shells of various sizes ranging from 0.2 to 10 mm. The shell content of the granular material varied from 12% to 14%. It was defined by the standard procedure for the determination of the organic content of soils given in BS 1377-3: 1990. The method, which uses dichromate oxidation, is known as Walkley & Black's method.

Table 3-2 Basic properties of the Changi sand.

Specific gravity	Mean size (mm)	Coefficient of uniformity	Coefficient of curvature	Max. void ratio	Min. void ratio	Fines content (%)	Shell content (%)
2.60	0.30–0.35	2.0	0.8	0.916	0.533	0.4	12–14

The specific gravity of the Changi sand is 2.60 as determined by standard water pycnometer test (ASTM: D 854). The minimum and maximum void ratios were found to be 0.533 and 0.916 respectively. The minimum void ratio (e_{min}) was determined according to ASTM: D 4253 using a vibratory table. The maximum void ratio (e_{max}) was measured according to the method developed by Kolbuszewski (1948). In this method the loosest state is obtained by tilting a cylinder (2000 cm^3) containing 1000g of sand through 180 degrees from one vertical position to the other.

3.4 Specimen Preparation Method

Laboratory reconstituted specimens were used in this study. Two specimen preparation methods were used, namely the water sedimentation (WS) and the moist tamping (MT). The WS method was used for medium loose and medium dense samples, while the MT method was used to prepare very loose specimens.

3.4.1 Water Sedimentation Method

A four-part split mould, shown in Fig. 3.7 was used for the preparation of plane-strain specimens. Before placing the mould on the base pedestal, high vacuum silicone grease was applied on all sides of the base and the top cap. Two porous stones, 38 mm in diameter each, were placed on the base and top cap respectively. All drainage lines were saturated with de-aired water. A fixed mass of oven-dried sand was prepared and cooled to room temperature just before the sample preparation.

A 0.4 mm latex membrane was then sealed to the base pedestal by O-rings and stretched against the wall of the mould. A small vacuum suction of 5–10 kPa was used to achieve a tight fit between the mould and the membrane. The mould was

half-filled with de-aired water. Deposition of sand was done by moving the tip of the funnel in a circular motion 1–5 mm above the water surface. During this stage great care was taken to ensure that sand was pluviated continuously without causing any significant segregation of the material particles. For the preparation of denser specimens compaction was applied by knocking the side of the mould. The number of knocks on each side of the mould was controlled to achieve a high degree of sample homogeneity as well as test reproduction.

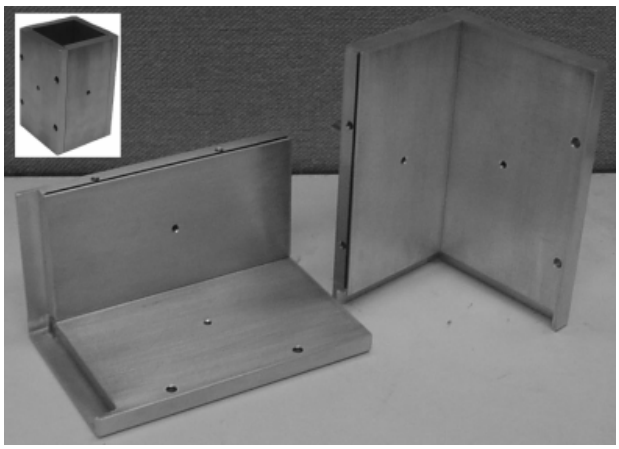

Fig. 3.7 Four-part split mould used for specimen preparation

After completion of the sand placement, the top cap was placed on the specimen surface. The membrane was then carefully pulled over the top cap and secured to it with two O-rings, as shown in Fig. 3.8.

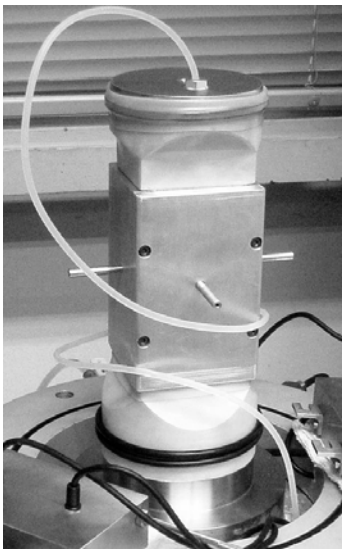

Fig. 3.8 A typical specimen with the top cap installed

A vacuum of approximately 20 kPa was applied to the sample using a burette before the mould was removed. Fig. 3.9 presents a sand specimen after the mould was dismantled. Next, the bottom drainage line was closed. The confinement of 20 kPa was therefore maintained. Moreover, no volume change was taken place at this stage. Direct measurement of the specimen dimensions was then made and the initial void ratio (e_0) was calculated. The two lateral loading platens together with the internal LVDTs were installed. Finally, the cell was assembled and filled with distilled water.

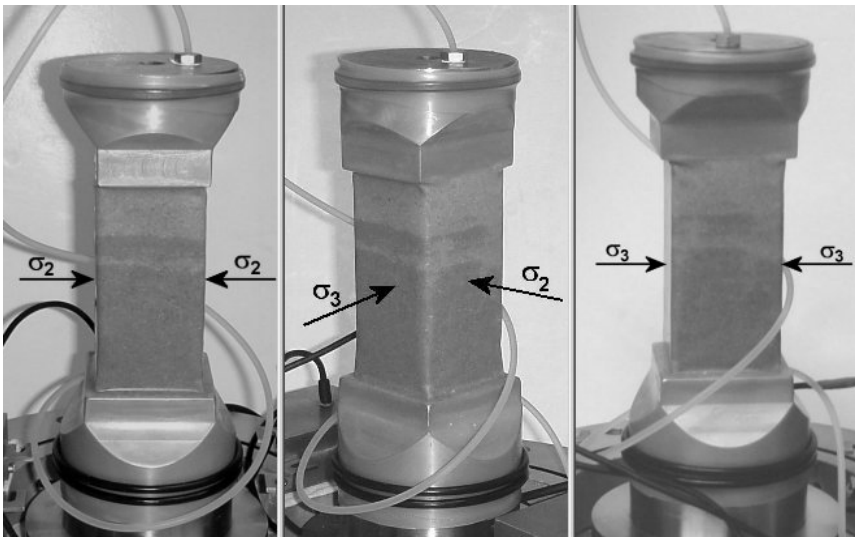

Fig. 3.9 A typical specimen after the mould was dismantled

3.4.2 Moist Tamping Method

The specimen preparation by the MT method was almost identical to that by the WS method. However, in the MT method, the oven-dried sand was mixed with 5% of de-aired water prior to the placement to the mould. After mixing, the moist sand was deposited into the mould and compacted in five layers. For each layer, slight tamping was applied with a small tamper. The amount of energy used in the tamping process was carefully controlled. The compactive effort was increased towards the top of the specimen to achieve greater uniformity, as suggested by Ladd (1974), Mulilis et al. (1977), and Hird & Hassona (1990). Although the capillary suction between the sand particles was able to stabilize the specimen after the top cap was installed, a vacuum of about 20 kPa was still applied to the sample through the bottom drainage line. After the mould was dismantled, the dimensions

of the specimen were taken and the initial void ratio, e_0, was calculated. Similarly to the WS method, the sample preparation phase was finished after filling the cell with distilled water.

3.5 Testing Procedures

3.5.1 Saturation

After filling the cell with distilled water a cell pressure of 20 kPa was applied. The specimen was then flushed with de-aired water from the bottom for a period of 60 minutes under a small water head of about 0.5 m. The bottom drainage line was then connected to a DPVC and the cell pressure and back pressure were increased simultaneously with an effective stress of 10 kPa under undrained conditions. A back pressure of 400 to 600 kPa was used. The particular back pressure values were chosen based on the previous experiments on Changi sand by Leong (2001), Gan (2002), and Loke (2004). For all the specimens *B* values of approximately 0.96-0.97 were achieved when the back pressure reached 400 kPa. However, back pressure values higher than 400 kPa had to be used to K_0 consolidate some specimens to $p_c' > 400$ kPa.

3.5.2 Consolidation & Aging

All the specimens tested were consolidated from an isotropic stress state of 20 kPa to the required anisotropic stress state along the K_0 path. The K_0 condition was imposed by regulating the volume change of the specimen in accordance with the axial strain to maintain $d\varepsilon_V/d\varepsilon_1 = 1$, a method described by Lo & Chu (1991b). The consolidation was carried out under a deformation-controlled loading mode at a constant rate of 0.05 mm/min. The K_0 consolidation of sand under plane-strain conditions is described in more details in Appendix A. At the end of consolidation, an aging period of 30 minutes was imposed to each specimen with the stresses maintained constant. Therefore, the effect of aging time on the stress-strain behaviour of sand, if any, was consistent in all plane-strain tests.

3.5.3 Shearing

Shearing was carried out using either stress path or strain path control. A drained test was conducted using stress path control with $d\sigma_3' = 0$. An undrained test was a special case of strain path test with $d\varepsilon_v/d\varepsilon_1 = 0$. All tests were carried out using either deformation-controlled (DC) or load-controlled (LC) loading mode. The DC mode allowed strain softening behaviour to be observed. The LC mode was used to investigate instability behaviour of sand. All the deformation-controlled tests were conducted at a constant rate of 0.05 mm/min (drained) or 0.10 mm/min (undrained and strain paths). The particular shearing rates were chosen in accordance with previous experiments on Changi sand in triaxial cells by Leong (2001), Gan (2002), and Loke (2004). Therefore, plane-strain tests and triaxial tests could be easily compared. The loading rate for load-controlled tests varied between 0.010 kN/min and 0.015 kN/min. These rates were selected in such way that the expected maximum deviatoric stress obtained from load-controlled test would be reached in the same time as that in deformation-controlled test on an identical specimen. This was done to ensure that the average loading rates in both deformation-controlled and load-controlled tests would be the same.

3.5.4 Void Ratio Calculation

The accurate determination of the void ratio of specimen plays an important role in the analysis of the behaviour of sand. Therefore, it is necessary to adopt a reliable method for void ratio calculation (Sladen & Handford, 1987; Vaid & Sivathayalan, 1996). The most common procedure to determine the void ratio of granular soil specimen is based on a direct measurement of the specimen dimensions. However, serious errors can occur in the computed void ratio of the sand specimen due to the low resolution of instruments used in the evaluation of its physical dimensions. Several other techniques have also been proposed. Sladen & Handford (1987) for example, froze the sample after testing and determined its bulk density. Konrad (1990) used a method in which the diameter of the sample remained constant during saturation and the axial deformation was recorded. The change in void ratio was then computed.

In the present study, a procedure proposed by Verdugo & Ishihara (1996) was adopted. This method was developed using the water content of the specimen at the end of test. It involves the following steps:

1) At the end of test, the drainage valve was closed, so that no further volume change was permitted. The cell pressure was also increased to 1000 kPa.
2) The burette was connected to the bottom drainage line and the valve was opened. The level of water in the burette was measured.
3) The cell pressure was increases once again to the maximum capacity in order to remove as much water as possible from the specimen.
4) The cell pressure was released and the triaxial cell was dismantled. A small suction applied via burette allowed the sample to remain stable.
5) The top cap and the membrane were removed. All the soil with remaining water was carefully collected.
6) The void ratio at the end of test, e_f, was calculated from the following equation:

$$e_f = \frac{M_w}{M_d} G_s \qquad (3-1)$$

where, M_w is the mass of pore water in the tested specimen (the sum of the water remained within the specimen and the water collected via burette at the end of test), M_d is the dry weight of the specimen and G_s is the specific gravity of the soil.

7) The void ratio after consolidation, e_c, and the and the initial void ratio after saturation, e_0, were back calculated using the volumetric change of the specimen recorded from back pressure DPVC.

3.6 Error Minimization Techniques

Two major errors are involved in the experimental investigations of granular soils. These are membrane penetration and bedding errors. To maintain the accuracy of the measurement, it is essential to minimize or correct these errors. In this study, experimental techniques were adopted to reduce both membrane penetration and bedding errors. These methods have been confirmed to be effective by Lo et al. (1989), Chu (1991) and Loke (2004).

3.6.1 Membrane Penetration

The importance of the membrane penetration effect has been recognized by a number of previous researchers (Roscoe et al., 1963; Molenkamp & Luger, 1981; Baldi & Nova, 1984; Vaid & Negussey, 1984). The membrane penetration can affect both the pore water pressure in an undrained and the volume change in a drained test. Furthermore, the control of a strain path test will also be affected if the volume change cannot be measured correctly.

A liquid rubber technique was adopted in this research to reduce the effect of membrane penetration. The method involved the use of a silicon rubber for treating the membrane. It was firstly proposed by Kiekbusch & Schuppener (1977) and further modified by Lo et al. (1989). In this method a thin layer of the liquid rubber was coated onto the inner sides of the membrane before the placement of sand. The liquid rubber was prepared as a mixture of the silicon rubber and the catalyst. The proportion of the silicon rubber to catalyst of 4:6 was used. The thickness of the coating was about 0.4 mm. Plane-strain tests were only commenced after the liquid rubber had hardened.

3.6.2 Bedding Errors

Although the free-end system minimizes significantly the development of non-homogeneous deformation, it also causes bedding errors in the measurement of axial and volumetric strains. In this research, internal LVDTs were used. However, as the LVDT was not mounted fully to the specimen, the readings were still affected by the bedding errors at the base. To reduce the bedding errors at the base, top and bottom rigid platens with free-ends installed were preloaded against flat surfaces to the maximum vertical pressure to be applied in tests (i.e. about 600–800 kPa for very loose, 800–1000 kPa for medium dense and 1000–1500 kPa for dense sand). Furthermore, bedding errors were also reduced by using the liquid rubber to treat the free-ends used for the top and bottom platens. Preloading of free-ends and liquid rubber technique have been proven to be effective in reducing bedding errors, in both stress and strain path tests (Lo et al. 1989; Chu and Lo 1993; Chu et al. 1996).

3.7 Repeatability in Test Results

Confidence in any experimental investigation is highly dependent on the consistency and repeatability of test results. The duplication of the methodology described previously, ensured that reproduction of specimens was achieved in all the tests.

Fig. 3.10 presents the results obtained from two tests CK_0D13 and CK_0D15 conducted in the same way on specimens with similar void ratios. The specimens were K_0 consolidated to a mean effective stress p_c' = 200 kPa and void ratios at the end of consolidation were e_c = 0.686 and e_c = 0.681 respectively. Both specimens were sheared to failure along a drained path. Good consistency in stress-strain behaviour, volume change, pore water pressure and lateral stress responses were observed, as shown in Fig. 3.10.

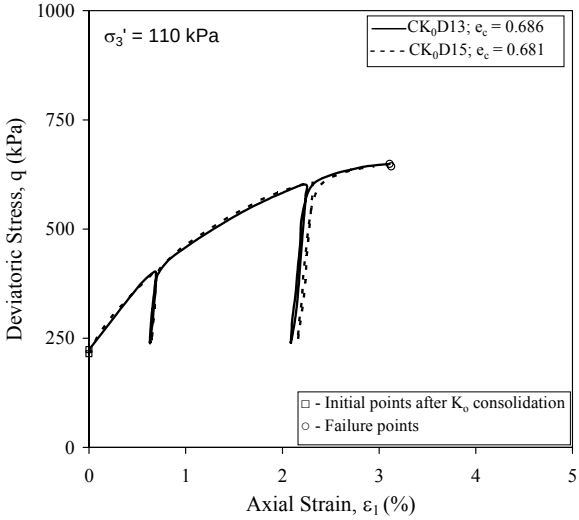

Fig. 3.10(a)

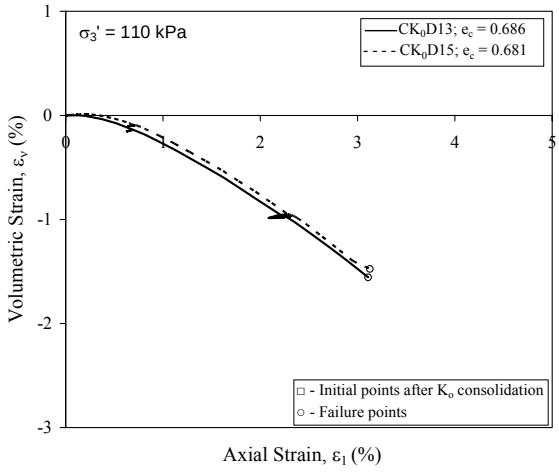

Fig. 3.10(b)

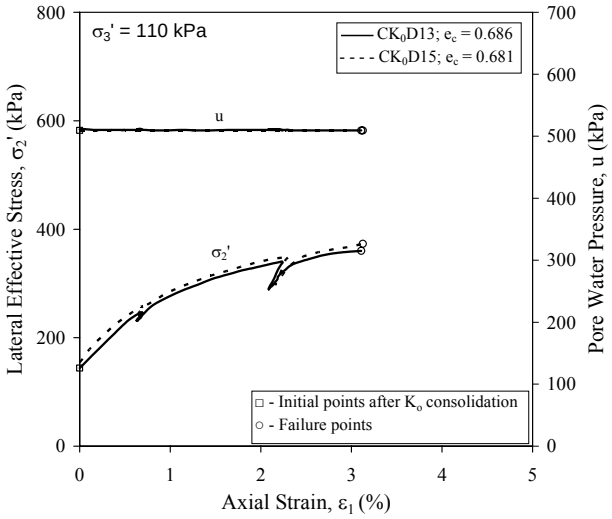

Fig. 3.10(c)

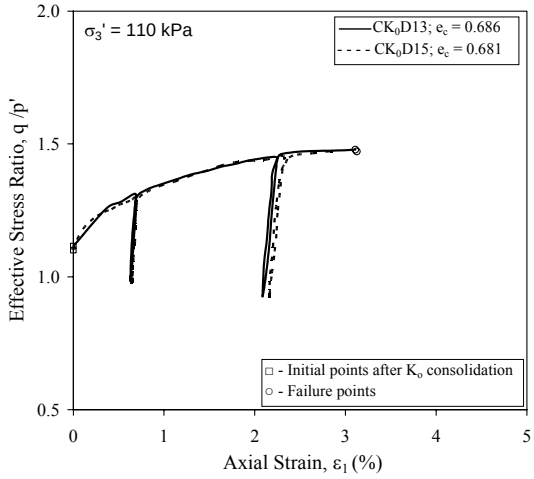

Fig. 3.10(d)

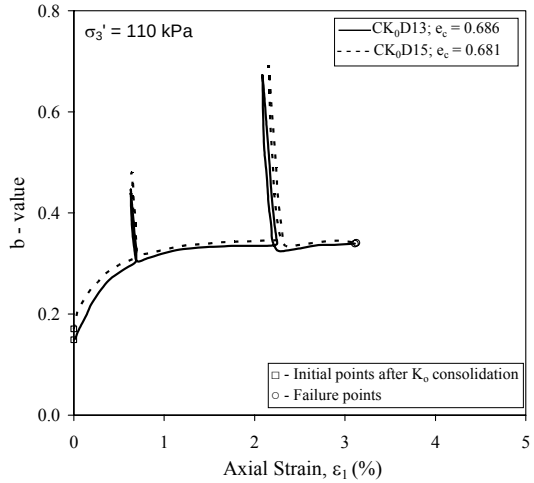

Fig. 3.10(e)

Fig. 3.10 Repeatability of drained tests under plane-strain condition: (a) stress-strain curves; (b) volumetric strain curves; (c) lateral stress and pore water pressure response; (d) *q/p' – ε_1* curves; (e) *b-value – ε_1* curves

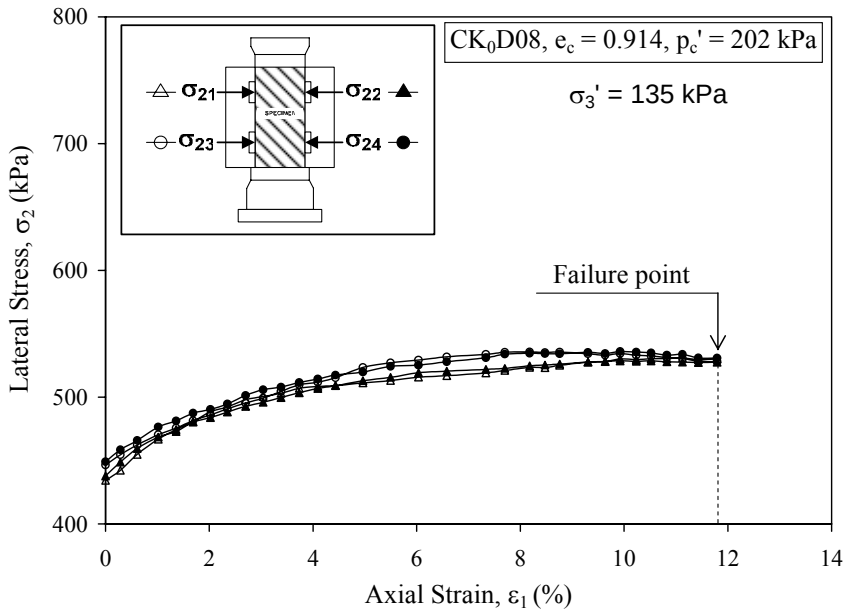

(a)

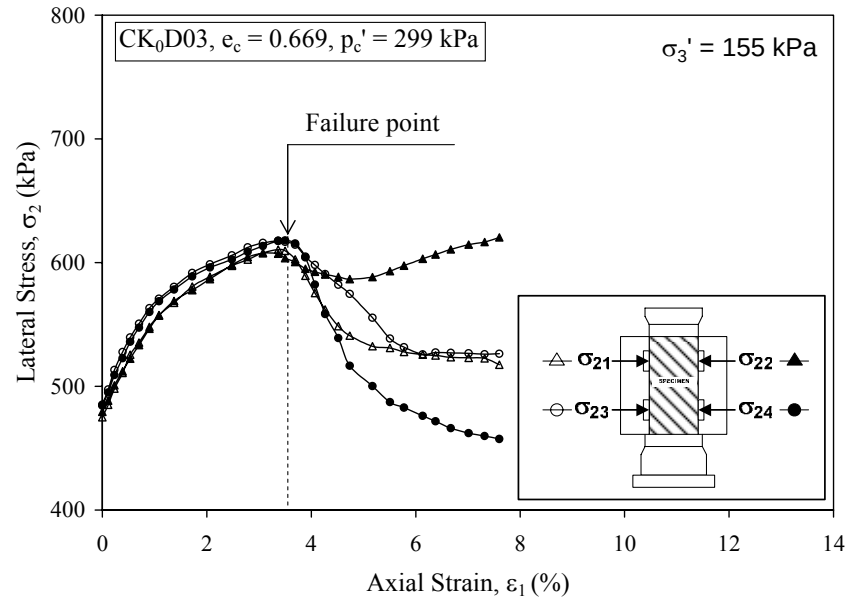

(b)

Fig. 3.11 The σ_2 versus ε_1 curves: (a) very loose specimen; (b) medium dense specimen

As mentioned earlier, the total lateral stress (σ_2) was calculated as an average value obtained from four individual pressure transducers installed in the two lateral loading platens. Therefore, it was essential to ensure that σ_2 values measured by the four individual transducers were consistent and reliable. Typical σ_2 versus ε_1 curves obtained from drained tests on very loose (CK_0D08) and medium dense (CK_0D03) specimens are shown in Fig. 3.11. It can be seen that all the four σ_2

values measured in the two tests were quite consistent until failure was reached. For the medium dense specimen, the lateral stress distributions became highly non-uniform after shear band occurred in the post-failure region and four local values of σ_2 started to diverge (Fig. 3.11(b)). The point where the σ_2–ε_1 curves started to diverge coincided with the point where shear band has occurred, as will be shown in Chapter 4. Therefore, the occurrence of the shear bands could be detected by comparing the σ_2 versus ε_1 curves obtained from the four individual pressure transducers.

3.8 Experimental Programme

The experimental programme undertaken in this research involved mainly plane-strain compression tests. The experiments included drained and strain path *($d\varepsilon_v/d\varepsilon_1$ = const)* tests under both deformation-controlled and load-controlled loading modes. Most of the tests were conducted on medium loose to medium dense sand. Some tests on very loose sand were also carried out. The mean effective stress ranged from 100 to 400 kPa after K_0 consolidation. The tests were categorized into six series, as follows:

1) Series A were drained and undrained tests conducted to determine basic engineering properties of Changi sand, such as failure line (FL), critical state line (CSL), constant stress ratio line (CSRL), and instability line (IL) under plane-strain conditions. The deformation-controlled loading mode was used.

2) Series B was carried out to investigate general behaviour of sand under load-controlled loading mode. The results were compared with those obtained from Series A. The relationship between strain softening and instability was studied.

3) Series C involved the strain path tests with various strain increment ratios. The effect of dilation, drainage conditions, strain rate, and void ratio on the behaviour of sand under strain path controlled conditions was studied in this series.

4) Series D consisted of constant stress tests conducted under both drained and undrained conditions. The results obtained from this series of tests were used to establish factors that affect the occurrence of instability under plane-strain conditions.

5) Series E was performed to investigate the instability behaviour of sand under strain path controlled conditions. The effect of void ratio and the strain increment ratio imposed during a constant load test on the instability behaviour of granular soil was discussed.

During all the experiments, the shear band formation process was monitored by taking photos at a close time interval using a high resolution digital camera.

3.9 Summary

A new plane-strain apparatus together with a computer-controlled system have been described in this chapter. The developed automated plane-strain testing system enables both stress and strain paths to be controlled accurately. The system also enables deformation-controlled and load-controlled loading modes to be used. The main feature of the new plane-strain apparatus (PSA) is that the lateral stress (σ_2) can be measured by four submersible load cells. In some existing plane-strain devices (Drescher et al., 1990; Finno et al., 1996, 1997; Alshibli et al., 2004) a linear bearing platform is used to allow lateral displacement of the specimen to develop freely once a shear band develops. In this new PSA, properly lubricated free-ends are used instead. This will not only reduce the boundary effect on the stress-strain behaviour, but also allow shear bands to develop freely. Furthermore, by measuring the σ_2 in four different locations, the onset of non-homogeneous stress and deformation can be identified. It has been shown in this chapter that good repeatability of the test data was obtained. Therefore, the PSA was proved to be reliable equipment for granular soil testing and a suitable device to fulfil the research objectives in this study.

CHAPTER 4

GENERAL STRESS-STRAIN BEHAVIOUR OF SAND UNDER PLANE-STRAIN CONDITIONS

4.1 Introduction

The fundamental characteristics and the strain softening and instability behaviour of the granular material used in this study, i.e., the Changi sand, have been investigated under axisymmetric conditions by Leong (2001), Gan (2002) and Loke (2004) through triaxial compression tests. However, the general stress-strain behaviour of Changi sand under plane-strain conditions has not been studied before. In this study, several series of drained and undrained $(d\varepsilon_v/d\varepsilon_1 = 0)$ tests were conducted on Changi sand using the plane-strain apparatus described in Chapter 3. To study the effect of loading modes, plane-strain tests under both deformation-controlled and load-controlled loading modes were conducted. Based on these results, the drained, undrained and static liquefaction behaviour of sand was described. The critical state line (CSL), failure lines (FL), instability lines (IL), and constant stress ratio lines (CSRL) under plane-strain conditions were also established. The results obtained from plane-strain tests were compared with those obtained from triaxial tests conducted by Leong (2001) and Loke (2004).

4.2 Testing Programme

The drained and undrained plane-strain tests were conducted on samples with various densities, ranging from very loose to medium dense states. To study influence of the initial confining pressure, samples with the same void ratios but different confining stresses were tested. A summary of the tests conducted under drained conditions is given in Table 4-1. A summary of the tests carried out under undrained conditions is presented in Table 4-2.

Table 4-1 Summary of the plane-strain tests conducted under drained conditions.

Test No	Preparation method	e_c	Density state*	Stress state after consolidation		Mode of shearing	Rate of shearing
				p_c' (kPa)	q_c (kPa)		
CK_0D01	WS	0.678	Medium dense	100	100	Deformation controlled (mm/min)	0.05
CK_0D02		0.665		201	230		0.05
CK_0D03		0.669		299	351		0.05
CK_0D04	WS	0.784	Medium loose	102	88		0.05
CK_0D05		0.771		201	188		0.05
CK_0D06		0.760		300	293		0.05
CK_0D07	MT	0.932	Very loose	99	71		0.06
CK_0D08		0.914		202	166		0.06
CK_0D09		0.900		298	275		0.06
CK_0D01L	WS	0.687	Medium dense	100	81	Load controlled (kN/min)	0.012
CK_0D02L		0.681		200	210		0.015
CK_0D03L		0.674		297	328		0.015
CK_0D04L	WS	0.773	Medium loose	102	82		0.010
CK_0D05L		0.768		201	186		0.012
CK_0D06L		0.758		299	268		0.015
CK_0D07L	MT	0.922	Very loose	97	76		0.010
CK_0D08L		0.905		200	160		0.010
CK_0D09L		0.908		302	261		0.010

*The classification of relative density is given in Appendix B

Table 4-2 Summary of the plane-strain tests conducted under undrained conditions.

Test No	Preparation method	e_c	Density state	Stress state after consolidation		Mode of shearing	Rate of shearing
				p_c' (kPa)	q_c (kPa)		
CK_0U01	WS	0.696	Medium dense	98	93	Deformation controlled (mm/min)	0.1
CK_0U02		0.695		202	219		0.1
CK_0U03		0.694		299	329		0.1
CK_0U13		0.692		406	436		0.1
CK_0U04	MT	0.935	Very loose	97	70		0.1
CK_0U05		0.915		198	157		0.1
CK_0U06		0.899		298	245		0.1
CK_0U07		0.911		199	154		0.1
CK_0U08		0.902		198	168		0.1
CK_0U09		0.893		198	174		0.1
CK_0U10		0.888		199	186		0.1
CK_0U11		0.884		199	191		0.1
CK_0U12		0.868		198	205		0.1
CK_0U01L	WS	0.714	Medium dense	102	90	Load controlled (kN/min)	0.02
CK_0U02L		0.712		202	185		0.02
CK_0U03L		0.707		301	280		0.02
CK_0U04L	MT	0.946	Very loose	96	73		0.01
CK_0U05L		0.911		199	150		0.01
CK_0U06L		0.900		299	276		0.01

* The classification of relative density is given in Appendix B

The stress parameters used in the data analysis throughout this and next chapters are defined as follows:

$$p' = \frac{1}{3}\left(\sigma_1' + \sigma_2' + \sigma_3'\right) \qquad (4-1)$$

$$q = \frac{1}{\sqrt{2}}\left[(\sigma_1 - \sigma_2)^2 + (\sigma_2 - \sigma_3)^2 + (\sigma_3 - \sigma_1)^2\right]^{1/2} \qquad (4-2)$$

$$b = \frac{(\sigma_2 - \sigma_3)}{(\sigma_1 - \sigma_3)} \qquad (4-3)$$

where *p'*, *q* and *b* are mean effective stress, deviatoric stress and so-called *b-value*, respectively.

4.3 Drained Behaviour

4.3.1 Deformation-Controlled Loading Mode

4.3.1.1 Medium Dense Sand

The results of three K_0 consolidated drained (CK_0D) tests conducted on medium dense specimens, CK_0D01, CK_0D02, and CK_0D03, are shown in Fig. 4.1. All specimens were K_0 consolidated to a mean effective stress, p_c' = 100, 201, and 299 kPa respectively. The specimens were then sheared under drained conditions with σ_3' maintained constant. During shearing, the deviatoric stress firstly reached a peak and then reduced gradually to a constant ultimate value, as shown in Fig. 4.1(b). The peak point was taken as the failure point. It should be pointed out that shear bands were detected in all the tests before the peak points. The gradient of the failure line obtained from the three peak points is η_f = 1.53 (Fig. 4.1(a)). The gradient of the ultimate state line obtained from the three ultimate state points is η_{ult} = 1.43. It can be seen from Fig. 4.1(b) that the peak (i.e. the failure) deviatoric stress occurred at an axial strain ε_1 ranging from 3% to 4%. The higher the p_c', the higher the failure deviatoric stress and the higher the ε_1. The volumetric strain behaviour of the three tests is presented in Fig. 4.1(c). The curves show an initial volumetric contraction and a subsequent volumetric dilation in all specimens. It can be observed from Fig. 4.1(c) that the higher the p_c', the smaller the amount of

dilation. The effective stress ratio, *q/p'* versus ε_1 curves and the *b-value* versus ε_1 curves are presented in Fig. 4.1(d). It can be seen that all the specimens failed at the maximum effective stress ratio *q/p'* = 1.53 and reached the same effective stress ratio *q/p'* = 1.43 at the ultimate state. The *b-value* varied from 0.18 to 0.34 during shearing.

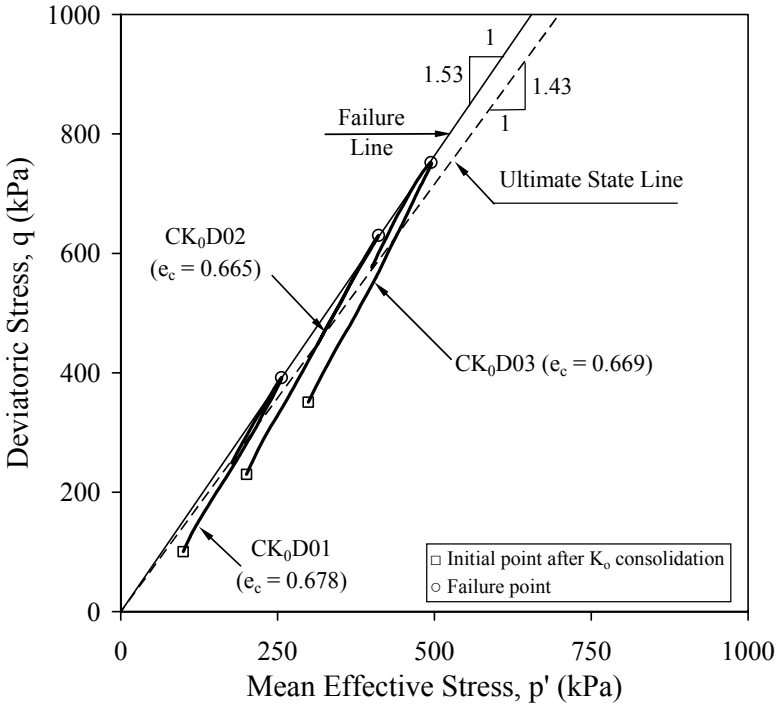

Fig. 4.1(a)

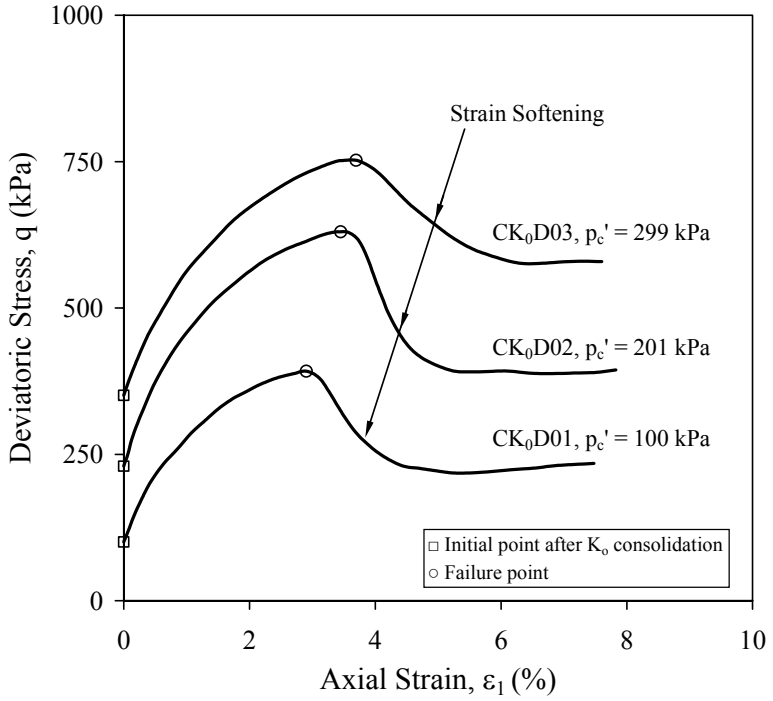

Fig. 4.1(b)

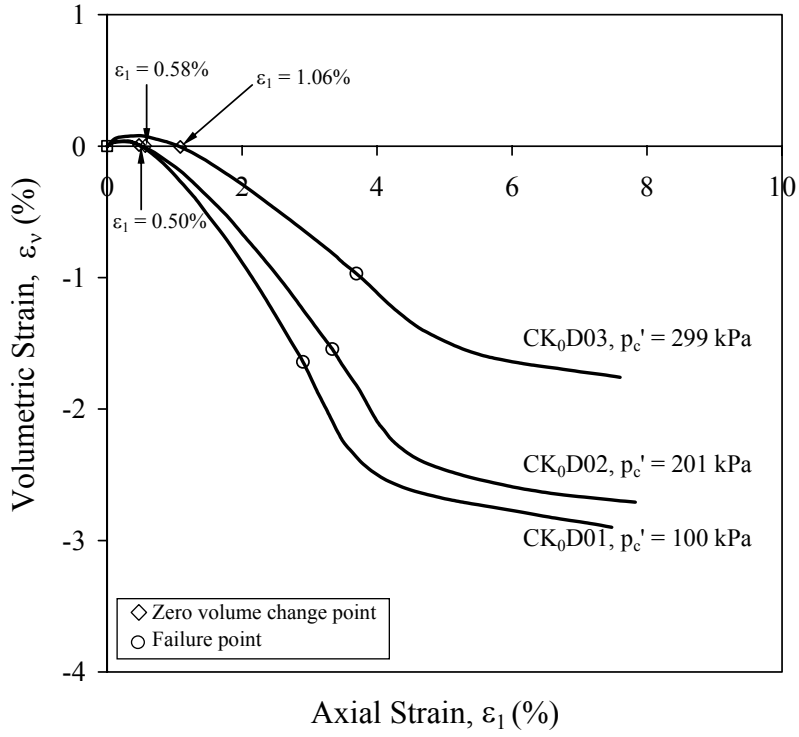

Fig. 4.1(c)

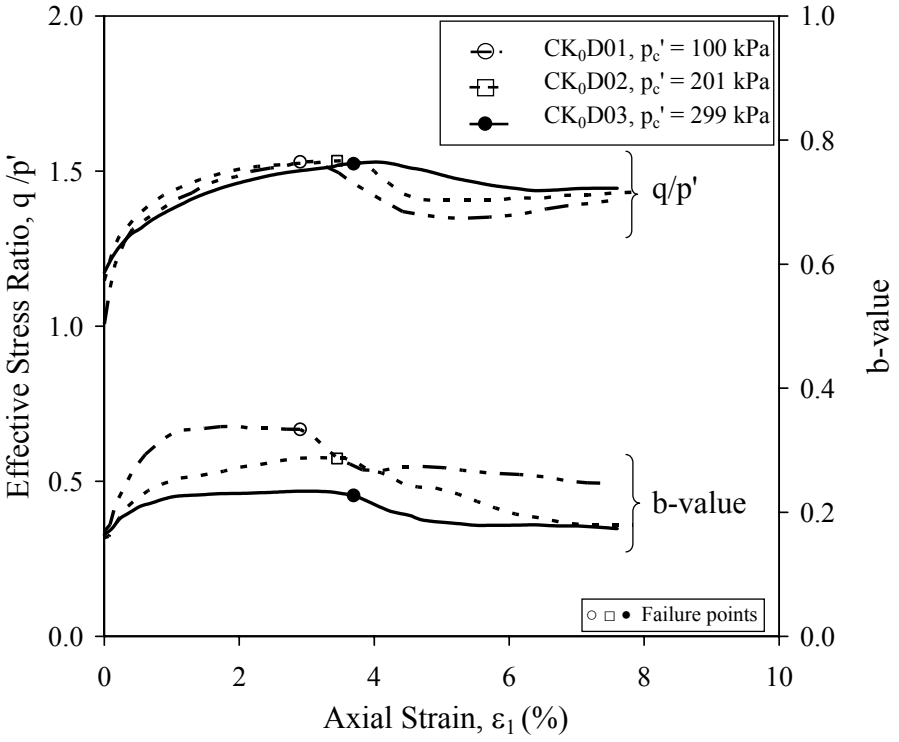

Fig. 4.1(d)

Fig. 4.1 Drained behaviour of medium dense sand under deformation-controlled loading mode: (a) effective stress paths; (b) stress-strain curves; (c) volumetric strain versus axial strain curves; (d) *q/p'* and *b-value* versus axial strain curves

4.3.1.2 Medium Loose Sand

The results of CK_0D tests on medium loose specimens CK_0D04, CK_0D05, and CK_0D06, are presented in Fig. 4.2. The effective stress paths are shown in Fig. 4.2(a). The gradient of the failure line obtained is $\eta_f = 1.35$, which is smaller than that obtained for medium dense specimens (Fig. 4.1(a)). The gradient of the ultimate state line obtained is $\eta_{ult} = 1.32$, which is different from that obtained for medium dense specimens. As shown in Fig. 4.2(b), the stress-strain behaviour for medium loose sand is similar to that observed for medium dense sand. The deviatoric stress firstly reached a peak, which was accompanied by shear band formation, and then reduced gradually to a constant ultimate value. However, there is less strain softening for medium loose specimens compared with that for medium dense specimens. The failure axial strain obtained was in the range from 3% to 6%, which is larger than that obtained for medium dense specimens. Fig. 4.2(c) presents the volumetric strain versus axial strain curves, which are similar to those for medium dense specimens, but the amount of dilation was smaller. The effective stress ratio, *q/p'* versus ε_1 and *b-value* versus ε_1 curves are shown in Fig. 4.2(d). It is again seen that failure occurred at the maximum point and *b-values* varied from 0.23 to 0.32 during shearing.

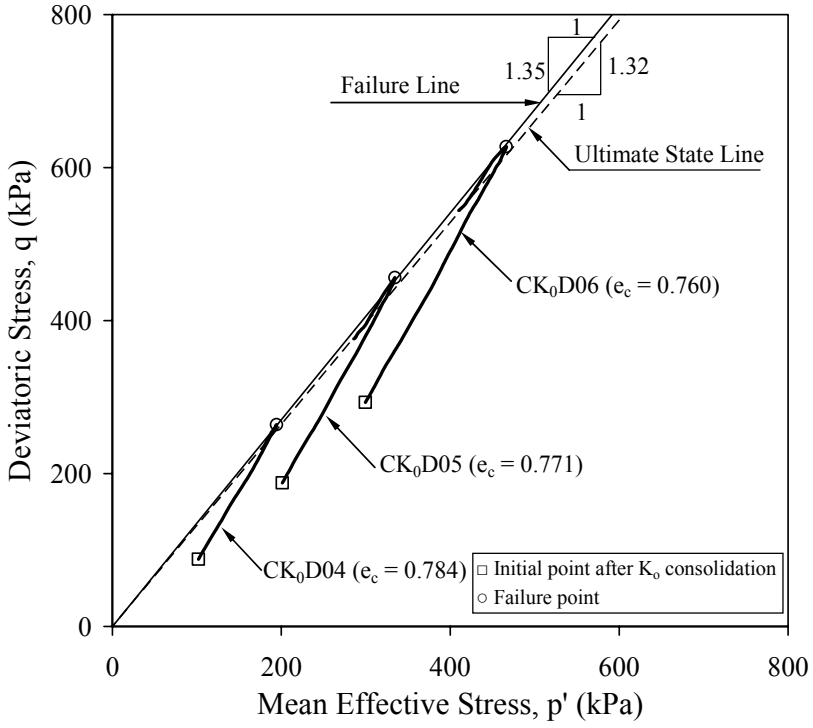

Fig. 4.2(a)

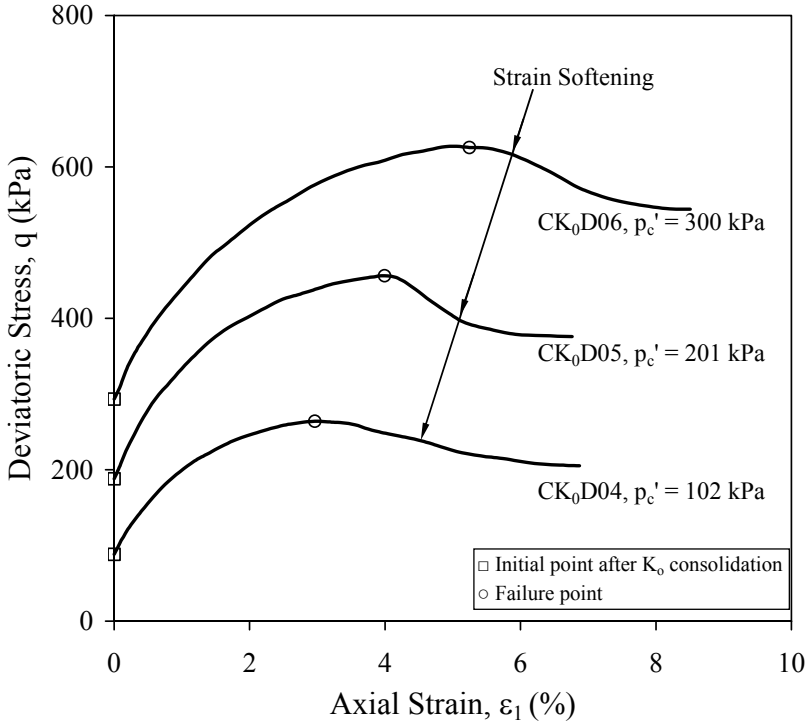

Fig. 4.2(b)

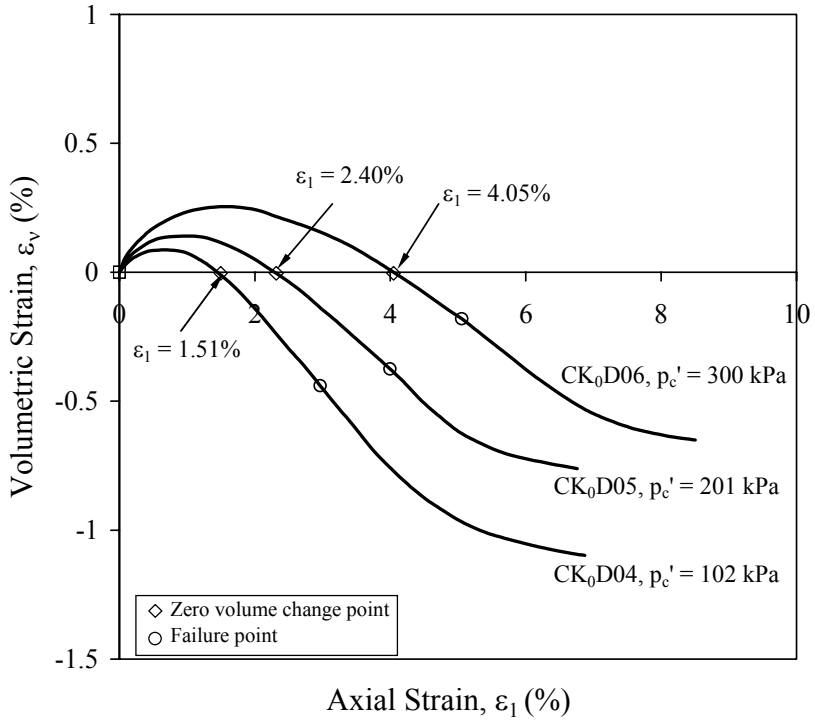

Fig. 4.2(c)

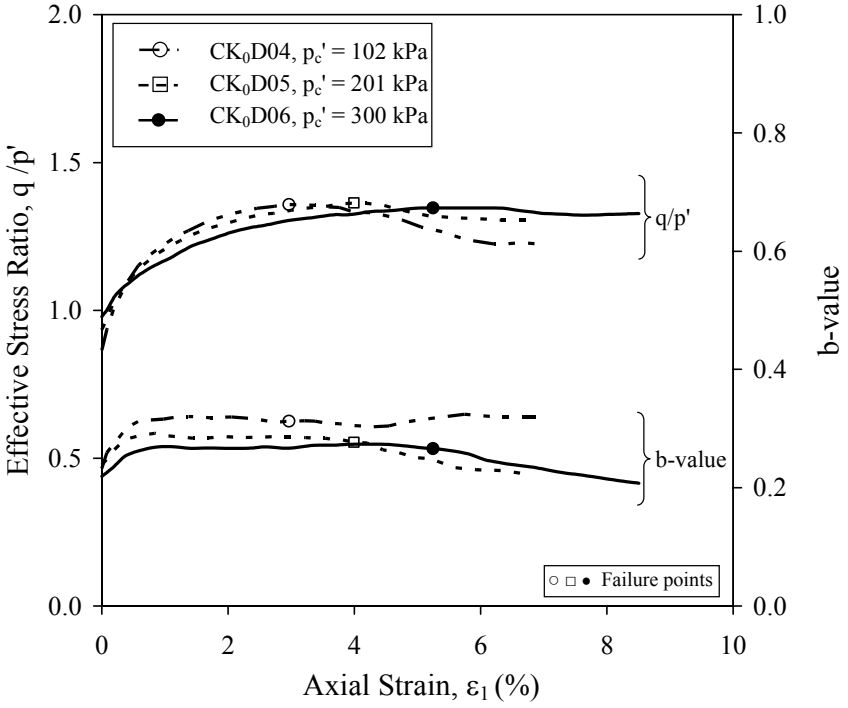

Fig. 4.2(d)

Fig. 4.2 Drained behaviour of medium loose sand under deformation-controlled loading mode: (a) effective stress paths; (b) stress-strain curves; (c) volumetric strain versus axial strain curves; (d) *q/p'* and *b-value* versus axial strain curves

4.3.1.3 Very Loose Sand

The results of CK_0D tests on very loose sand are presented in Fig. 4.3. The gradient of the failure line obtained is 1.16, as shown in Fig. 4.3(a). This value is smaller than the gradients obtained for medium dense sand (η_f = 1.53) and medium loose sand (η_f = 1.35), reflecting the dependence of failure on the void ratio of sand. The stress-strain curves are shown in Fig. 4.3(b). The deviatoric stress approached a constant value at the end of each test. There was no indication of shear band occurrence in the three tests. The volumetric strain also approached a constant value at the end of each test, as shown in Fig. 4.3(c). Therefore, the failure line in Fig. 4.3(a) is also the critical state line (CSL). The effective stress ratio and the *b-value* versus axial strain curves are presented in Fig. 4.3(d). It can be observed that each specimen failed at approximately the same effective stress ratio *q/p'* = 1.16 and the *b-value* at failure was 0.28.

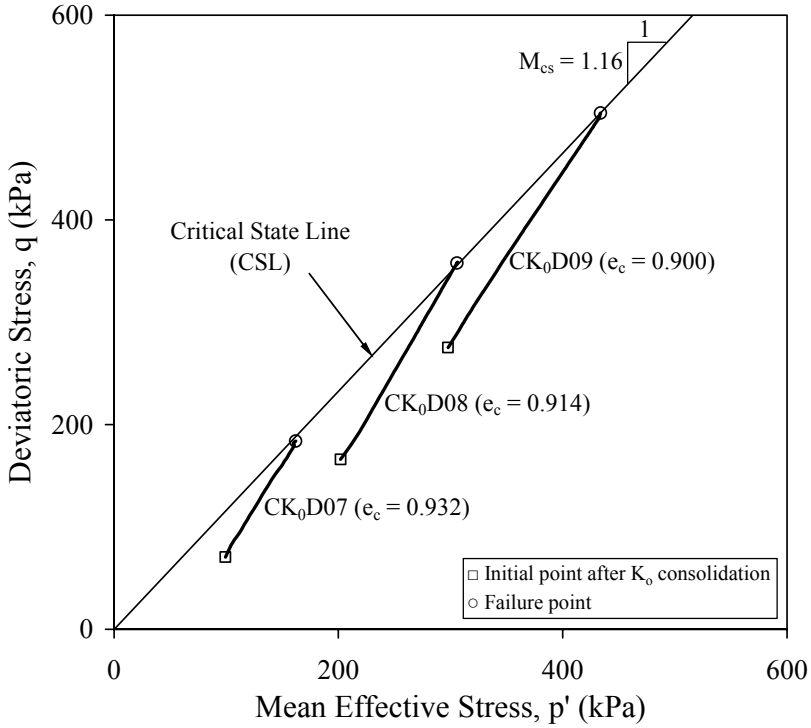

Fig. 4.3(a)

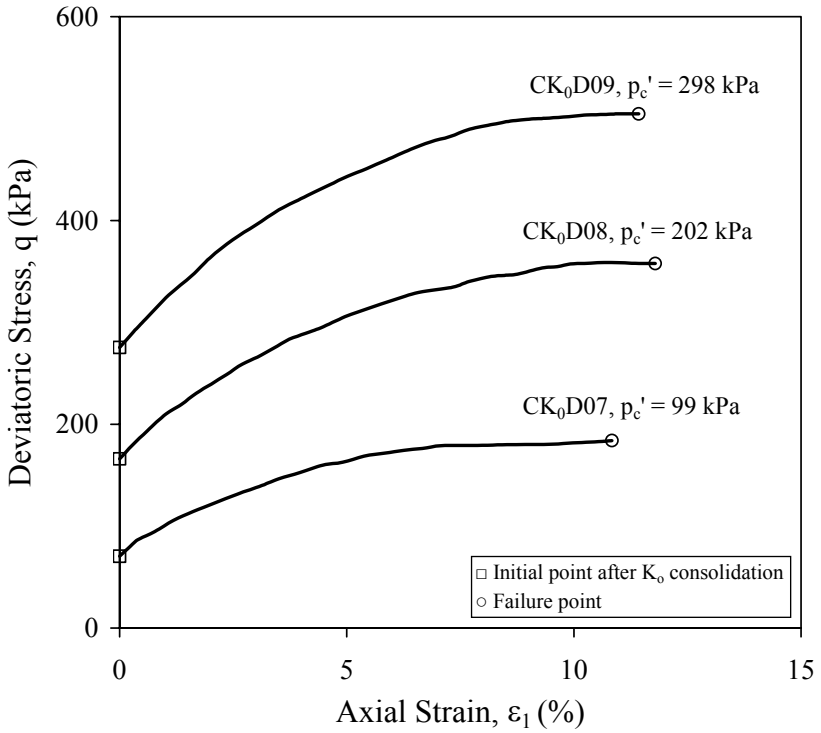

Fig. 4.3(b)

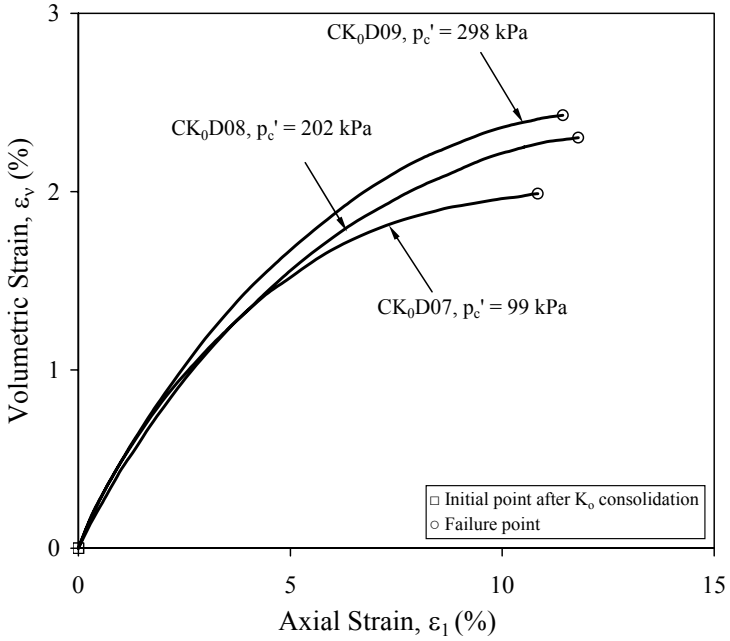

Fig. 4.3(c)

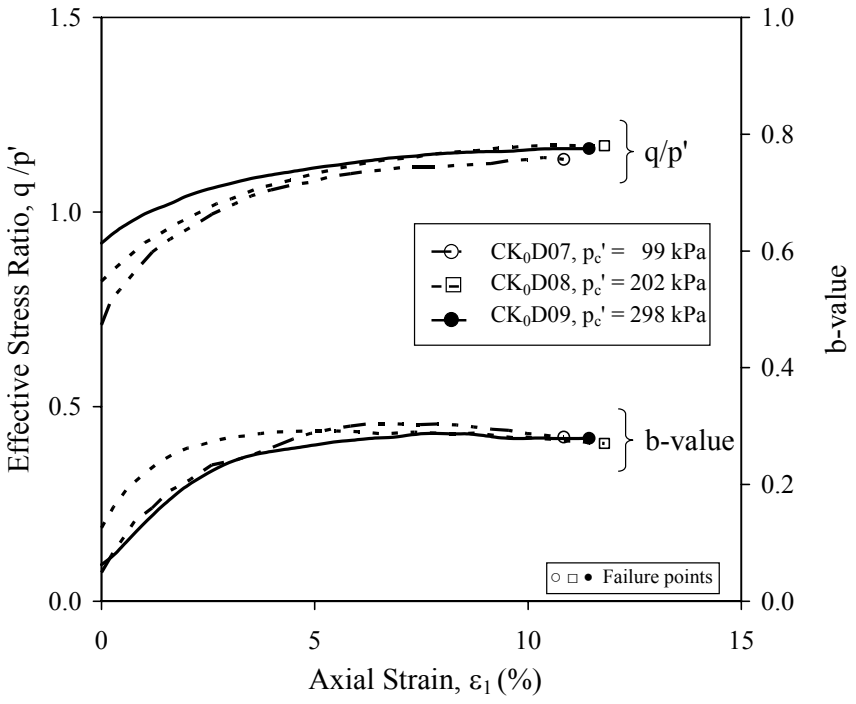

Fig. 4.3(d)

Fig. 4.3 Drained behaviour of very loose sand under deformation-controlled loading mode: (a) effective stress paths; (b) stress-strain curves; (c) volumetric strain versus axial strain curves; (d) *q/p'* and *b-value* versus axial strain curves

4.3.2 Load-Controlled Loading Mode

4.3.2.1 Medium Dense Sand

The results of three CK_0D tests on medium dense specimens, CK_0D01L, CK_0D02L, and CK_0D03L, conducted under load-controlled loading mode are shown in Fig. 4.4. All specimens were K_0 consolidated to a mean effective stress, p_c' = 100, 200, and 297 kPa respectively. The void ratios of the specimens after consolidation were e_c = 0.687, 0.681 and 0.674. The shearing rate used was 0.012 kN/min for CK_0D01L and 0.015 kN/min for CK_0D02L and CK_0D03L.

The effective stress paths obtained from these tests are shown in Fig. 4.4(a). It can be seen that all the specimens failed along the same failure line. The gradient of the failure line obtained from the three stress paths was η_f = 1.53. The stress-strain curves obtained from the tests are presented in Fig. 4.4(b). In all the tests the deviatoric stress dropped suddenly, immediately after the peak, as shown in Fig. 4.4(a). Shear bands were detected in pre-peak region in all the tests. The axial strain versus time curves are plotted in Fig. 4.4(c). It can be seen that the sudden drop in the deviatoric stress was accompanied by a sudden increase in axial strain, that is, the collapse of the specimen. Therefore, the specimen became unstable when the peak stress was reached. Shear bands had further developed in the post-peak region. Therefore, the stress-strain curves measured after the peak under load-controlled loading mode do not represent an element behaviour anymore, as pointed out by Chu (1999) and Chu & Leong (2001). Thus, an ultimate state is not determined in load-controlled tests.

The volumetric strain versus axial strain curves obtained from the three load-controlled tests on medium dense sand are plotted in Fig. 4.4(d). The volumetric strain behaviour shown in Fig. 4.4(d) is similar to that shown in Fig. 4.1(c) for tests under deformation-controlled mode except in the post-peak region. As shear bands occurred just before the peak, the volumetric strain measured in the post-peak region is no longer representative of element behaviour. The *q/p'* and the *b-value* versus ε_1 curves are presented in Fig. 4.4(e). It can be seen that the *q/p'* at failure is the same for the three tests. The failure *b-values* obtained in the three tests are in the range between 0.28 and 0.35.

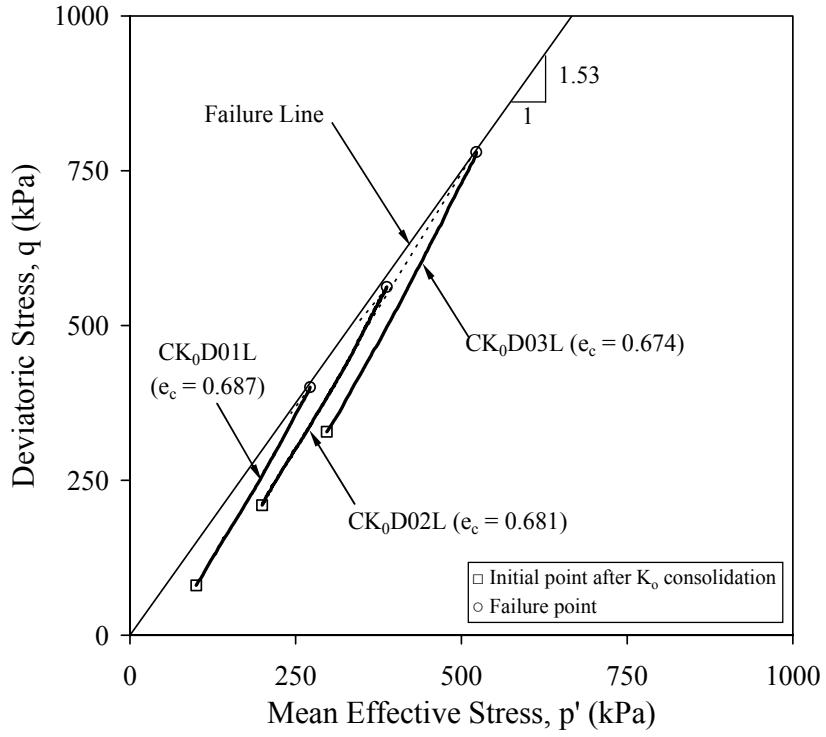

Fig. 4.4(a)

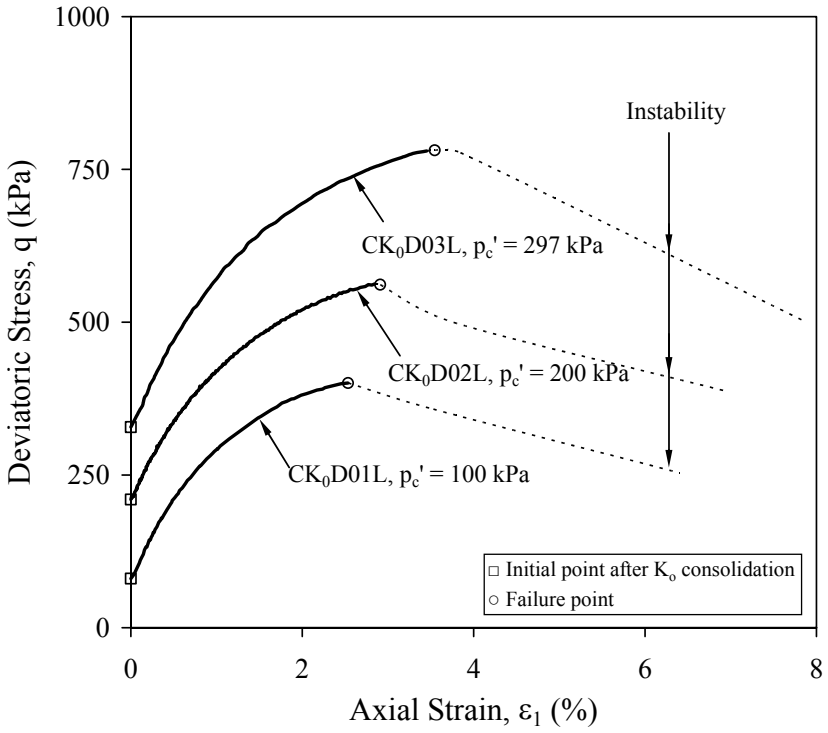

Fig. 4.4(b)

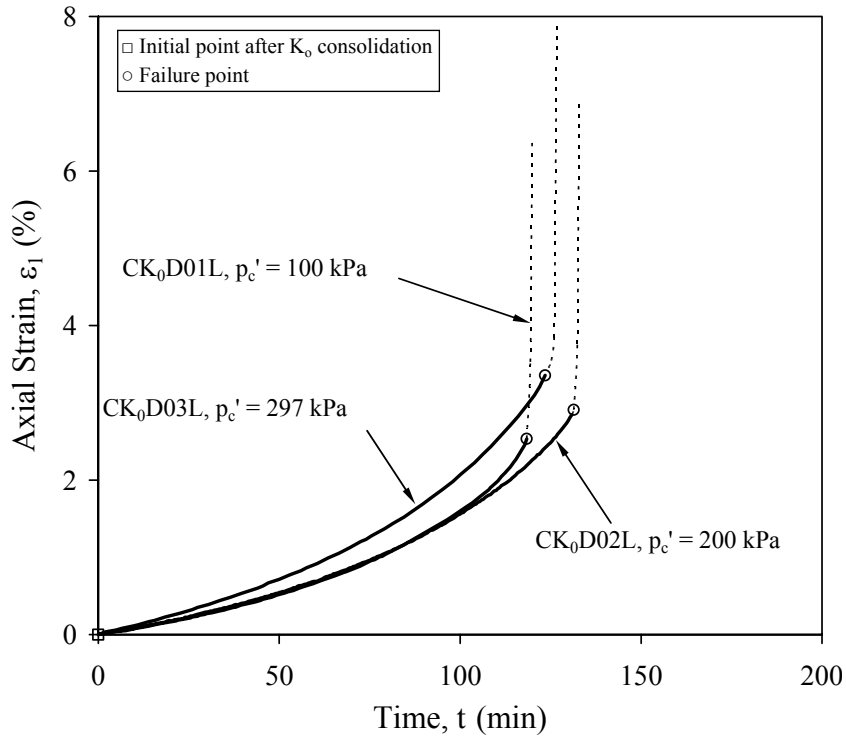

Fig. 4.4(c)

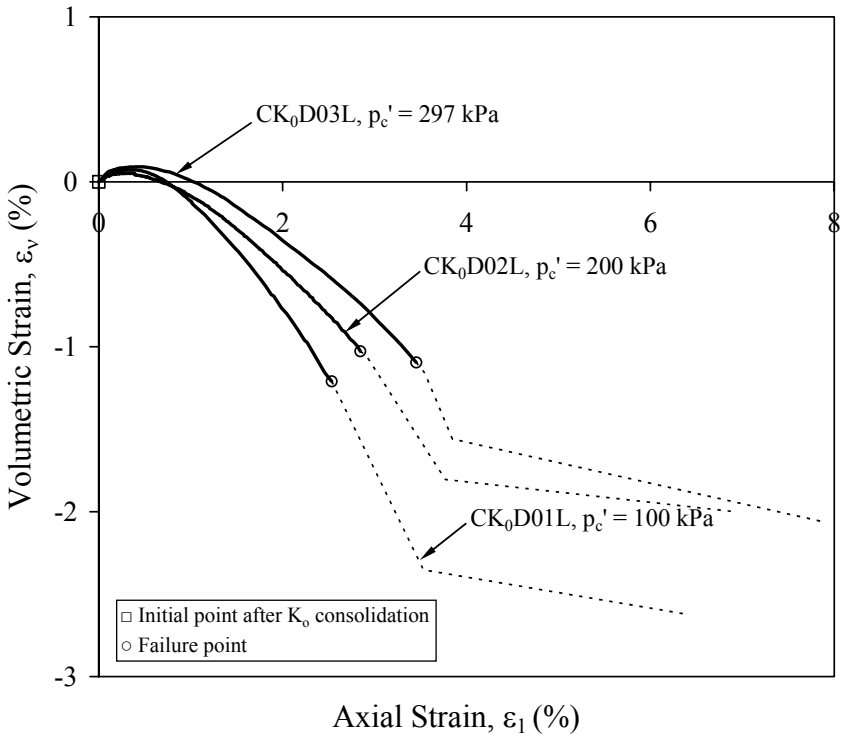

Fig. 4.4(d)

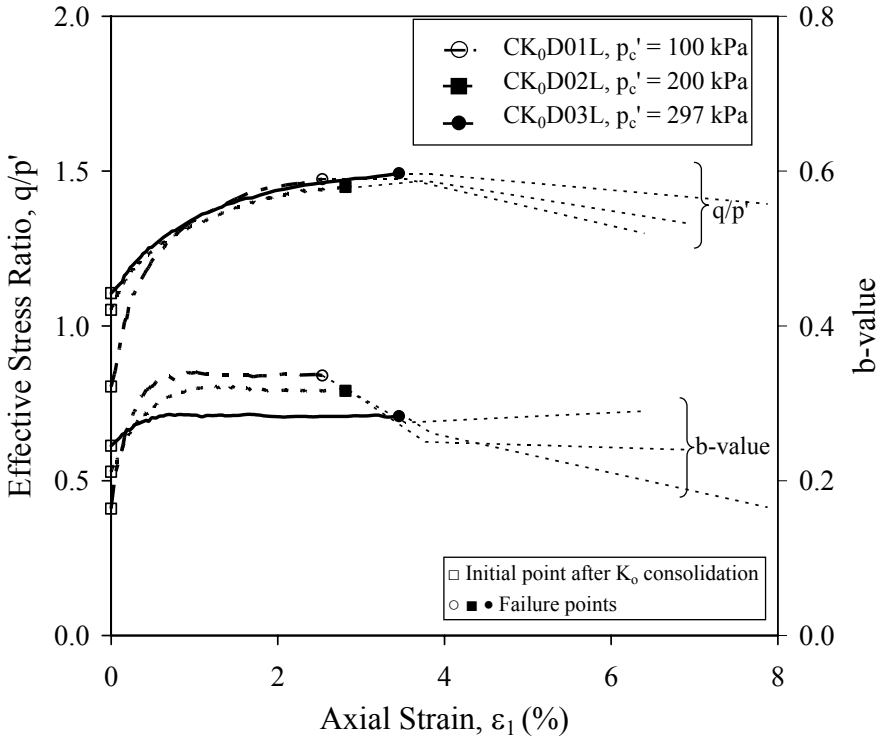

Fig. 4.4(e)

Fig. 4.4 Drained behaviour of medium dense sand under load-controlled loading mode: (a) effective stress paths; (b) stress-strain curves; (c) ε_1 versus *time* curves; (d) volumetric strain versus axial strain curves; (e) *q/p'* and *b-value* versus axial strain curves

4.3.2.2 Medium Loose Sand

The results of three tests on medium loose specimens CK_0D04L, CK_0D05L, and CK_0D06L, are presented in Fig. 4.5. The effective stress paths are shown in Fig. 4.5(a). The gradient of the failure line obtained is $\eta_f = 1.35$. As can be observed from Fig. 4.5(b), the stress-strain behaviour for medium loose sand is very similar to that observed for medium dense sand. The deviatoric stress firstly reached a peak, and then dropped suddenly. The sudden drop in the deviatoric stress was accompanied by a sudden increase in axial strain, as shown in Fig. 4.5(c). The samples therefore, collapsed at the peak. The ε_v versus ε_1 curves are shown in Fig. 4.5(d). Similarly to the medium dense specimens, shear bands have been detected just before the peak points were reached. Therefore, the volumetric strain measured in the post-peak region no longer represents an element behaviour. The amount of dilation obtained in those tests was smaller than that for medium dense specimens

(see Fig. 4.4(d)). The effective stress ratio, *q/p'* versus ε_1 and the *b-value* versus ε_1 curves are shown in Fig. 4.5(e). It is again seen that the *q/p'* at peak is about the same for all the three tests. The *b-values* varied from 0.30 to 0.33 at the peak.

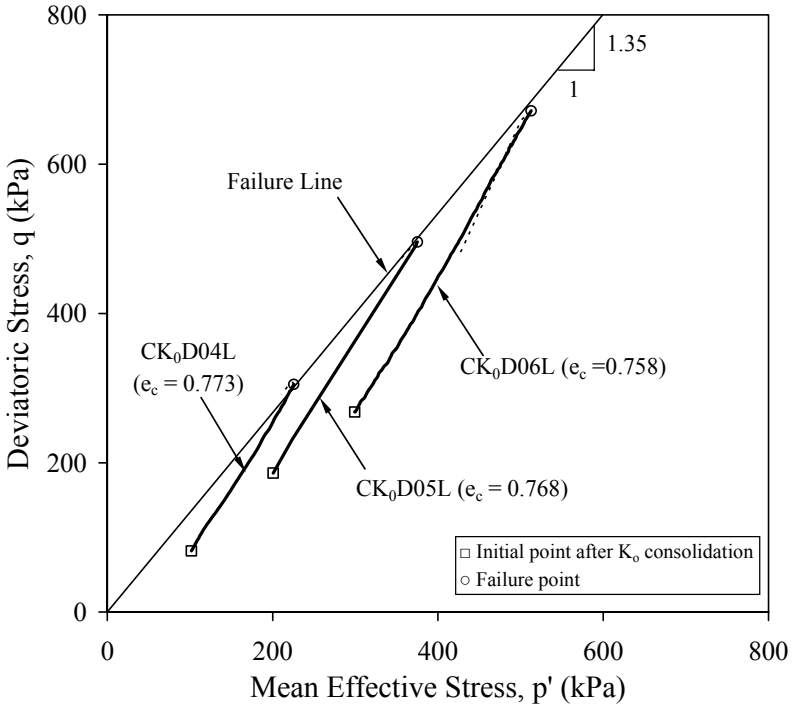

Fig. 4.5(a)

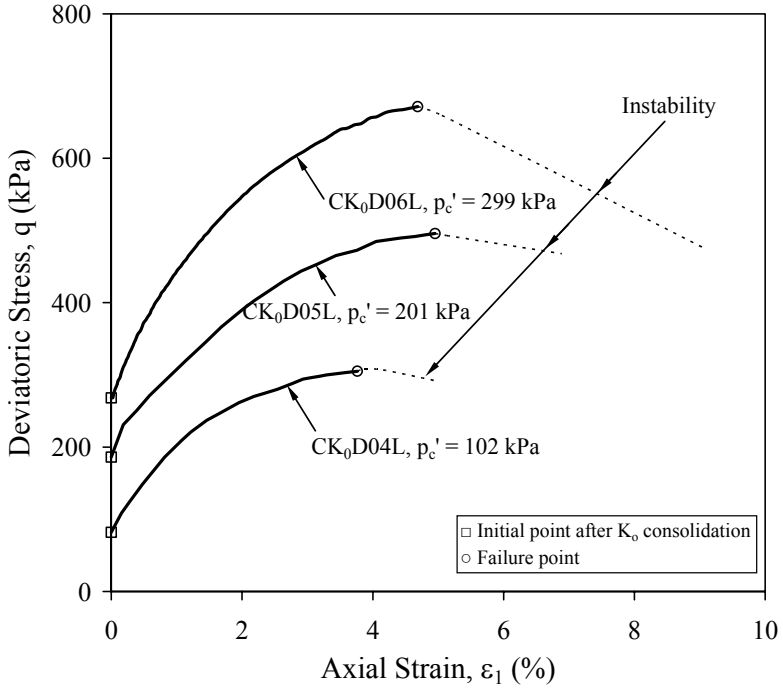

Fig. 4.5(b)

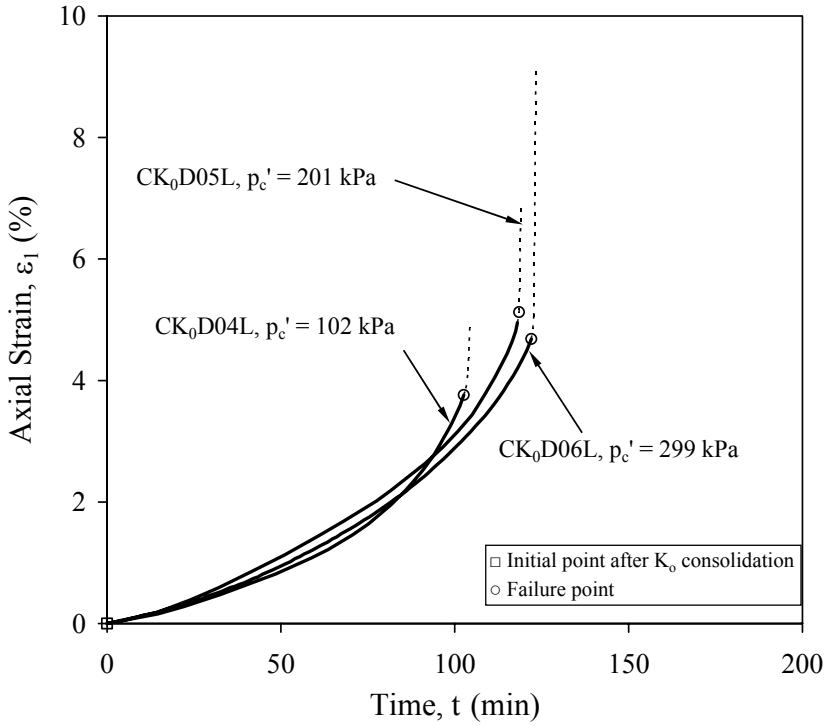

Fig. 4.5(c)

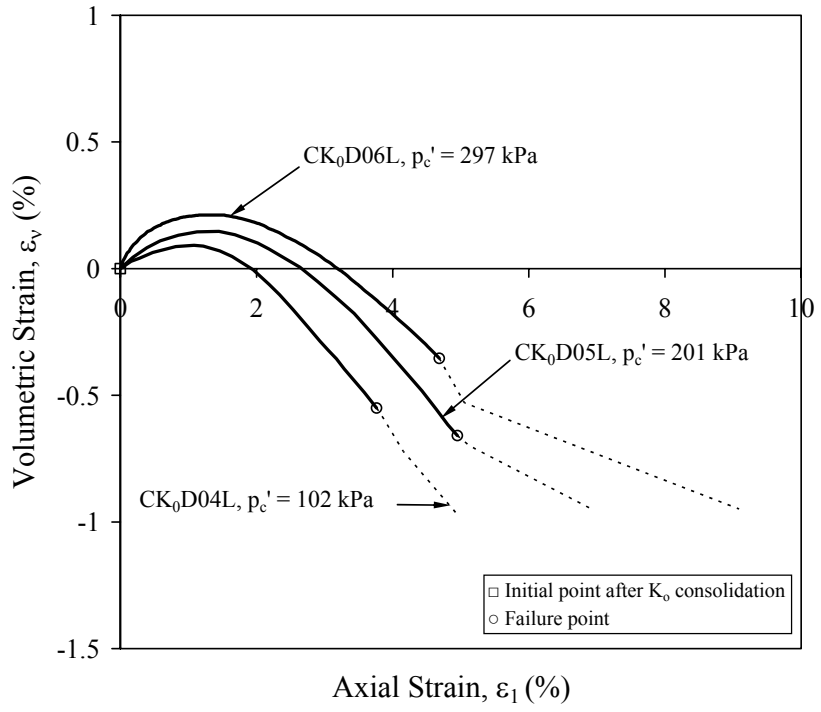

Fig. 4.5(d)

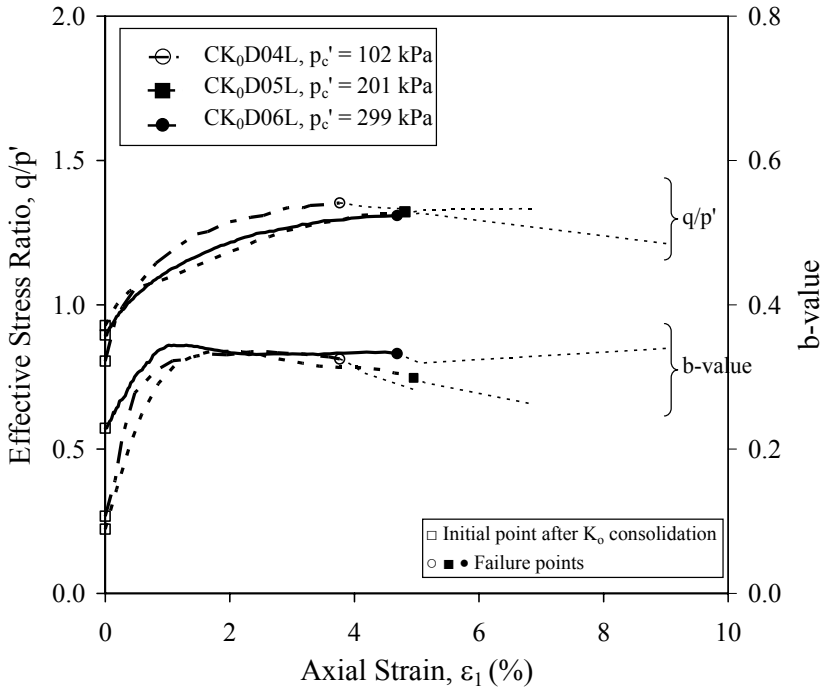

Fig. 4.5(e)

Fig. 4.5 Drained behaviour of medium loose sand under load-controlled loading mode: (a) effective stress paths; (b) stress-strain curves; (c) ε_1 versus *time* curves; (d) volumetric strain versus axial strain curves; (e) *q/p'* and *b-value* versus axial strain curves

4.3.2.3 Very Loose Sand

The results of CK_0D tests on very loose sand under load-controlled mode are given in Fig. 4.6. The gradient of the failure line obtained is 1.16, as shown in Fig. 4.6(a). The stress-strain curves are shown in Fig. 4.6(b) and the axial strain versus time curves are presented in Fig. 4.6(c). Similarly to medium dense and medium loose specimens, the axial strain for very loose samples increased rapidly at the failure point, as shown in Fig. 4.6(c). However, the deviatoric stress remained almost constant, as shown in Fig. 4.6(b) and there was no shear band detected during shearing. The volumetric strain also approached a constant value at the end of each test, as shown in Fig. 4.6(d). As both the stresses and volumetric strains maintained constant in the post-peak region, the failure line in Fig. 4.6(a) also defines the critical state line (CSL). The effective stress ratio and the *b-value* versus axial strain curves are presented in Fig. 4.6(e). It can be observed that all specimens

failed at approximately the same effective stress ratio *q/p'* = 1.16. The *b-value* at the failure varied from 0.24 to 0.29.

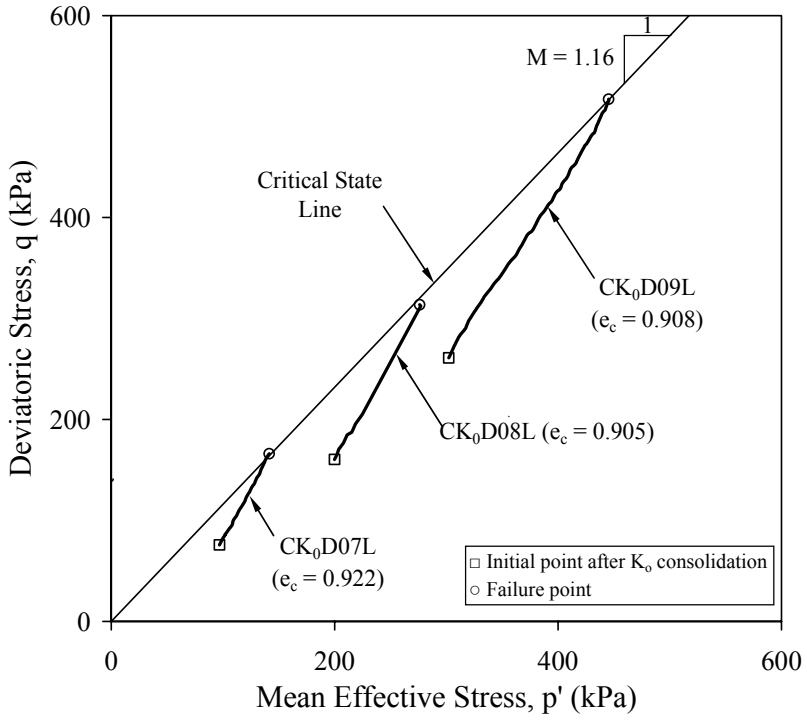

Fig. 4.6(a)

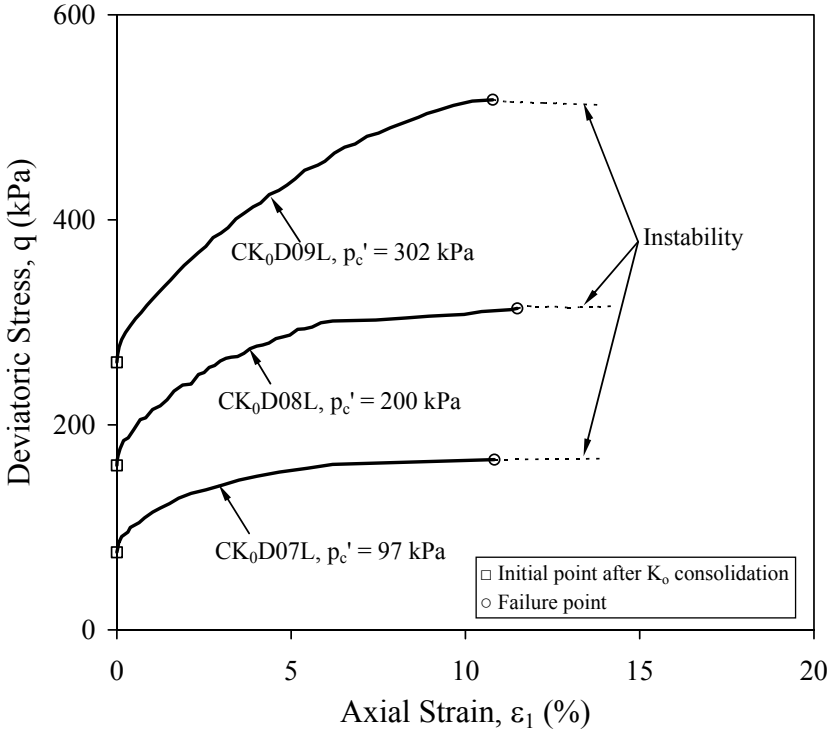

Fig. 4.6(b)

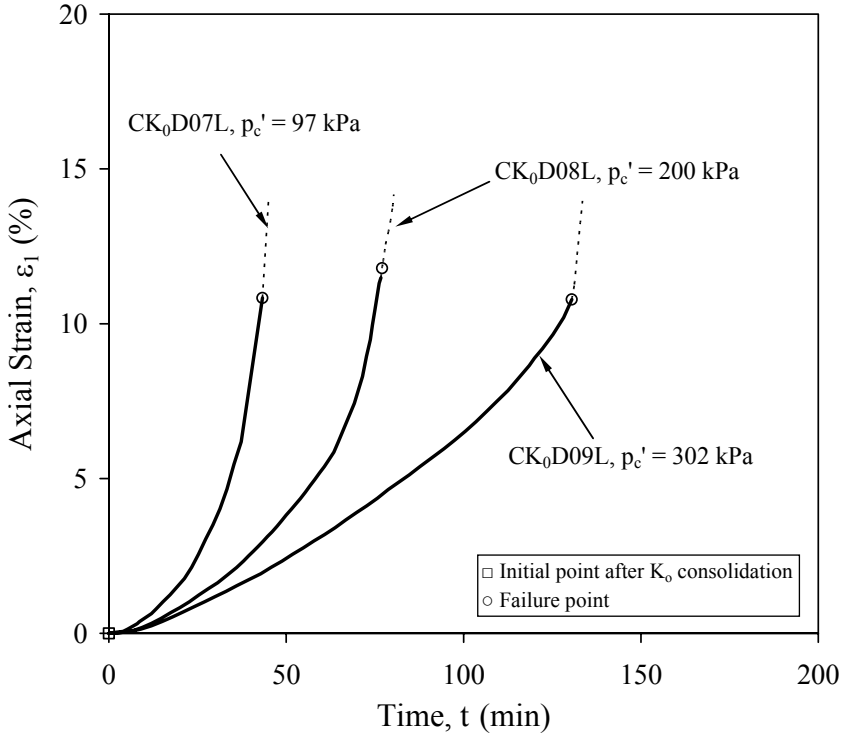

Fig. 4.6(c)

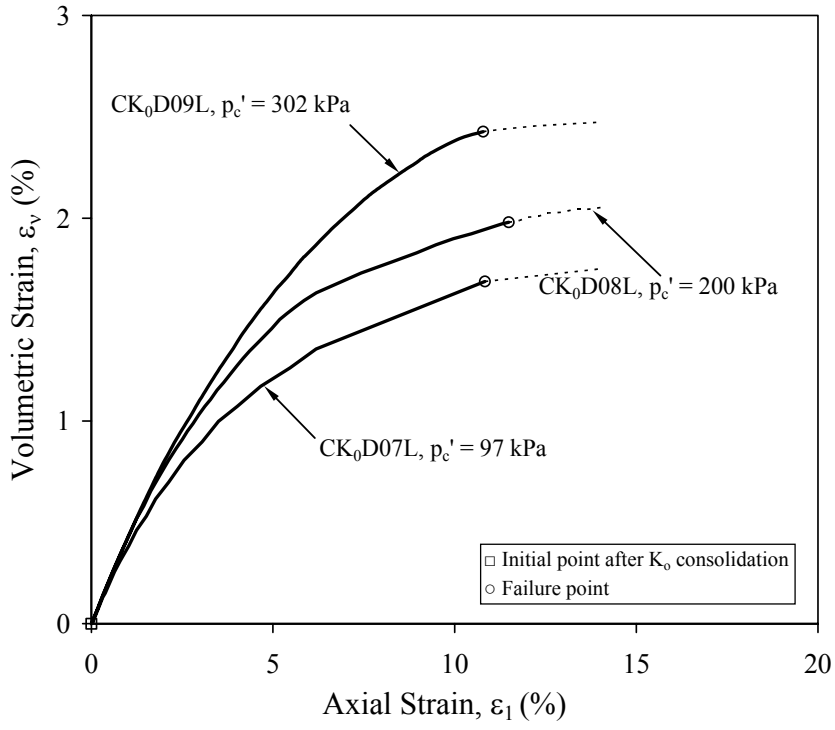

Fig. 4.6(d)

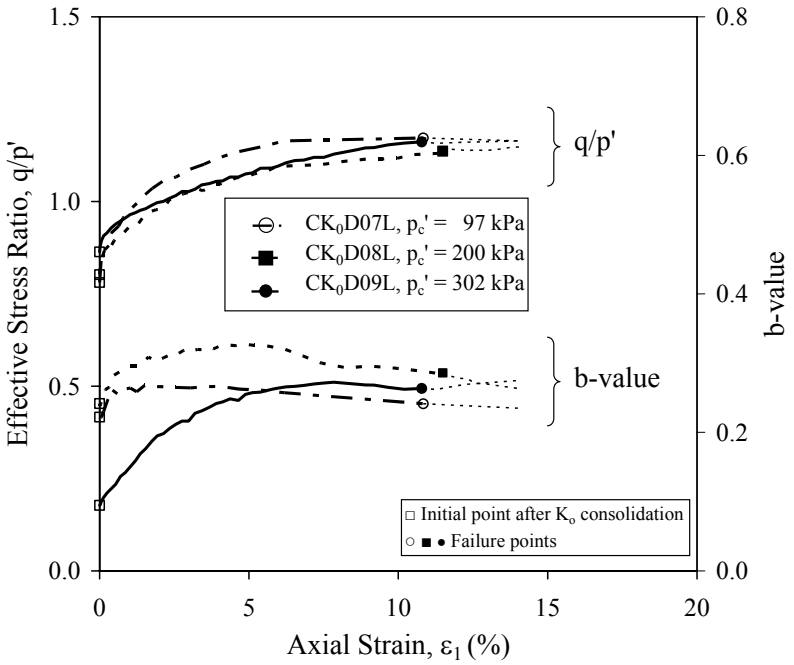

Fig. 4.6(e)

Fig. 4.6 Drained behaviour of very loose sand under load-controlled loading mode: (a) effective stress paths; (b) stress-strain behaviour; (c) ε_1 versus *time* curves; (d) volumetric strain versus axial strain curves; (e) *q/p'* and *b-value* versus axial strain curves

4.3.3 Comparison of Drained Behaviour under Deformation-Controlled and Load-Controlled Loading Modes

4.3.3.1 Medium Dense Sand

The results of two CK_0D tests conducted on medium dense specimens with comparable void ratios, CK_0D03 and CK_0D03L, are presented in Fig. 4.7. Test CK_0D03 was conducted under deformation-controlled (DC) loading mode, and test CK_0D03L under load-controlled (LC) loading mode.

The effective stress paths obtained from the two tests are compared in Fig. 4.7(a). Although the two paths are slightly different due to the different initial stress states, they eventually reached the same failure line with a gradient η_f = 1.53. The deviatoric stress versus axial strain curves for the two tests are plotted in Fig. 4.7(b). The stress-strain curves in the pre-peak region are quite similar. Both peaks

occurred at around the same axial strain of 3.5%. However, the post-peak behaviours are different. In the DC test (CK_0D03), strain softening occurred, whereas in the LC test (CK_0D03L), instability occurred. The difference in the two tests may be better illustrated in Fig. 4.7(c) where the deviatoric stresses versus time curves for both tests are plotted. The deviatoric stress in the LC test (CK_0D03L) increased linearly until reaching the peak and then dropped suddenly in post-peak region. On the other hand, the deviatoric stress in the DC test (CK_0D03) increased non-linearly with time, then reduced gradually and reached an ultimate state at the end of the test. The volumetric strain behaviour of the two tests is compared in Fig. 4.7(d). The ε_v versus ε_1 curves of the two tests are similar in the pre-peak region, but different in the post-peak region.

The axial strain versus time and volumetric strain versus time curves are presented in Figs. 4.7(e) and 4.7(f) respectively. In the DC test, ε_1 increased almost linearly with time. However, in the LC test, the $d\varepsilon_1/dt$ rate was increasing continuously and the specimen became unstable at the peak point. Instability behaviour could not be observed in a DC test because the specimen was forced to deform at a constant rate even after reaching its peak deviatoric stress. In this case, the specimen would undergo strain softening, that is, the deviatoric stress is reducing gradually. Therefore, strain-softening behaviour is manifested in deformation-controlled tests and instability behaviour in load-controlled tests. Similar behaviour was also observed from the tests on medium loose specimens.

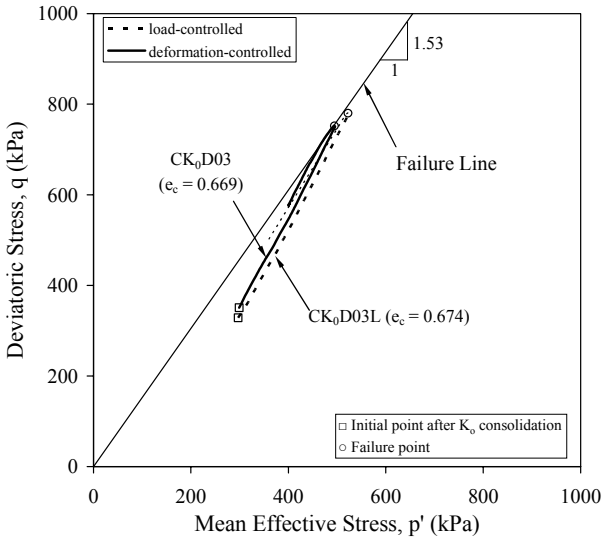

Fig. 4.7(a)

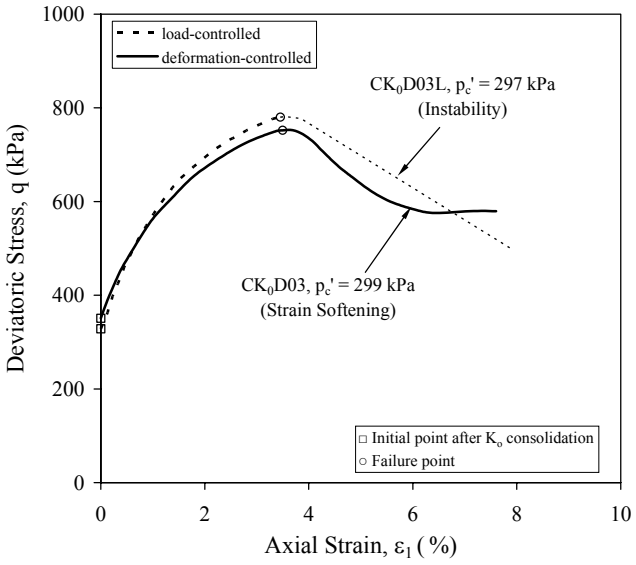

Fig. 4.7(b)

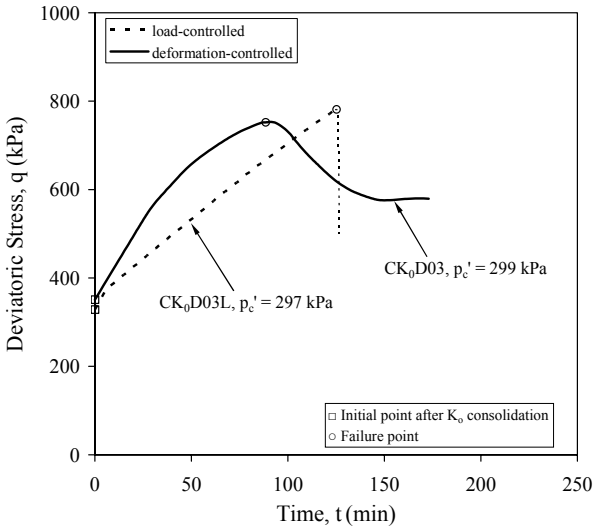

Fig. 4.7(c)

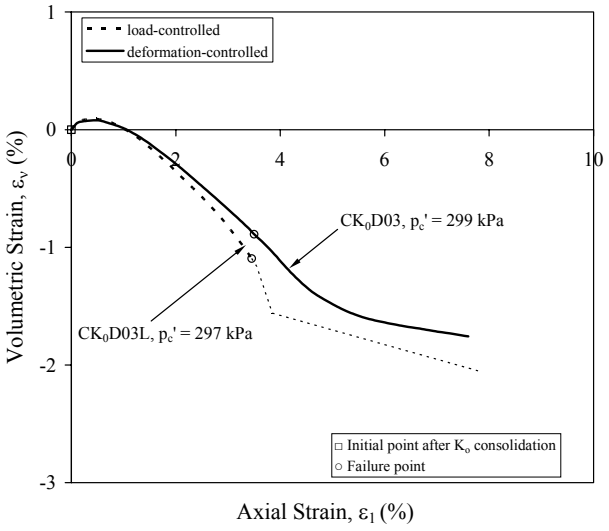

Fig. 4.7(d)

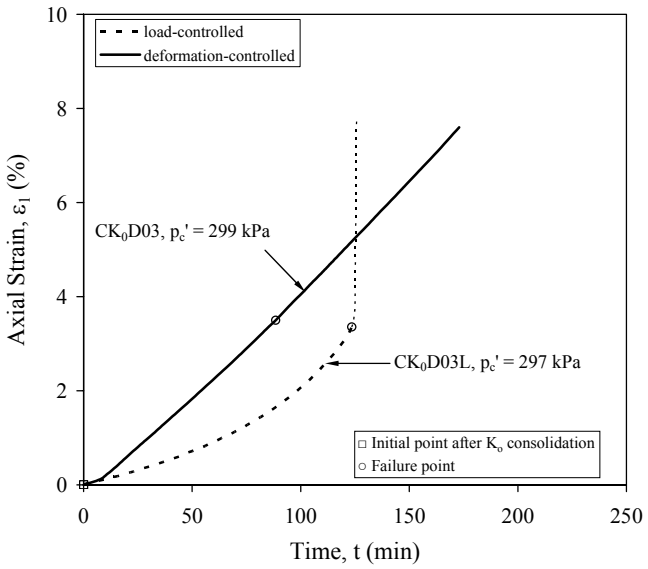

Fig. 4.7(e)

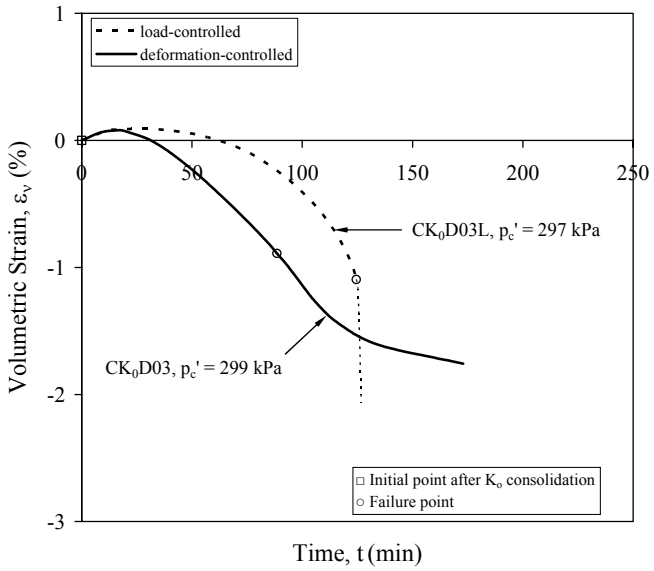

Fig. 4.7(f)

Fig. 4.7 Comparison of drained tests conducted on medium dense sand under deformation-controlled and load-controlled loading modes: (a) effective stress paths; (b) stress-strain curves; (c) deviatoric stress versus time curves; (d) ε_v versus ε_1 curves; (e) ε_1 versus *time* curves; (f) ε_v versus *time* curves

4.3.3.2 Very Loose Sand

The results of two tests, CK_0D09 and CK_0D09L, conducted on very loose sand are compared in Fig. 4.8. The specimens were K_0 consolidated to mean effective stresses, p_c' of 298 and 302 kPa respectively. Test CK_0D09 was conducted under

deformation-controlled mode with a rate of 0.06 mm/min, while Test CK_0D09L was carried out under load-controlled mode with a rate of 0.01 kN/min.

The effective stress paths obtained from the two tests are compared in Fig. 4.8(a). It can be seen that both tests ended at the same failure line which has a gradient *q/p'* = 1.16. The stress-strain behaviours are compared in Fig. 4.8(b). The deviatoric stress versus axial strain curves in the pre-peak region were similar. The deviatoric stress approached a constant value at the end of the DC test (CK_0D09), whereas a slight reduction in the deviatoric stress was observed in the LC test after the specimen became unstable.

The variation of the deviatoric stress with time in both types of tests is shown in Fig. 4.8(c). The deviatoric stress in the LC test (CK_0D09L) increased linearly until reaching the maximum value and then dropped. The deviatoric stress in the DC test (CK_0D09) increased with decreasing rate and reached a constant value at the end of the test.

The volumetric strain versus axial strain curves of the two tests are shown in Fig. 4.8(d). The two curves were almost identical except a sudden increase in ε_1 in the LC test after the peak. Both curves showed volumetric contraction throughout the tests. The volumetric strain also approached a constant value at the end of each test. Therefore, a critical state was attained at the end of the DC test.

The axial strain versus time and the volumetric strain versus time curves are shown in Figs. 4.8(e) and 4.8(f). The axial strain rate increased continuously in the LC test while the axial strain rate was kept constant throughout the DC test. At the failure point in the LC test, the specimen became unstable and the axial strain increased very rapidly as shown in Fig. 4.8(e). In the LC test the volumetric strain increased almost linearly with time before the failure point. On the other hand, in the DC test, the rate of volumetric strain decreased gradually and reached almost constant value at failure (Fig. 4.8(f)).

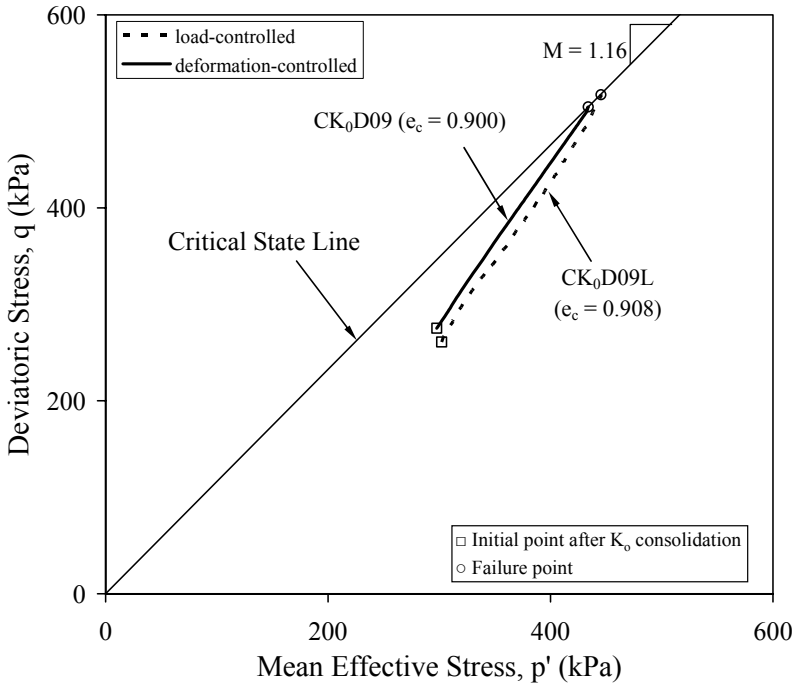

Fig. 4.8(a)

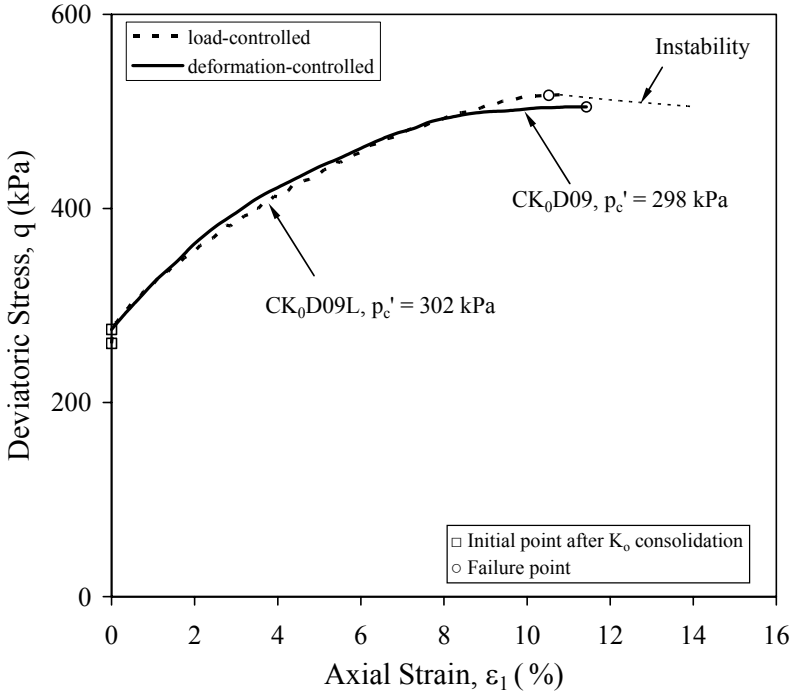

Fig. 4.8(b)

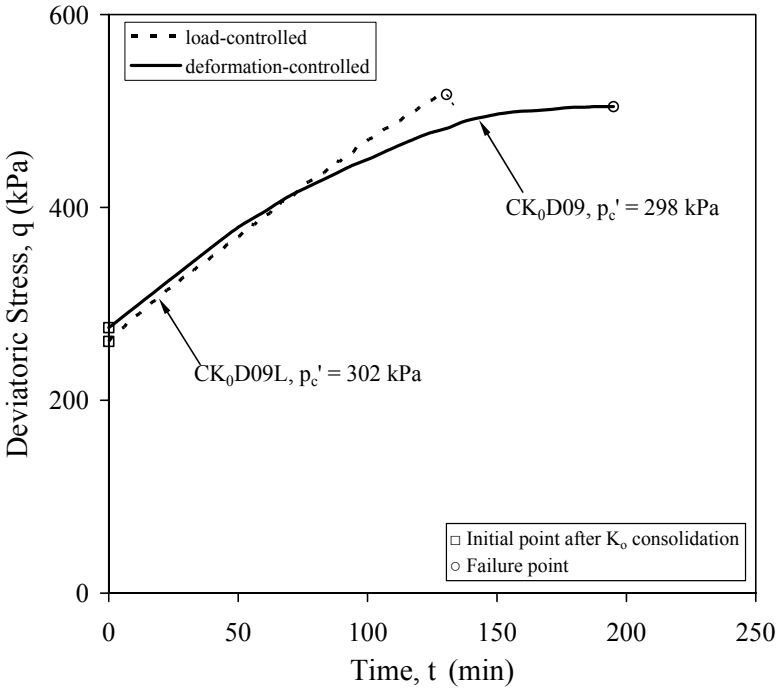

Fig. 4.8(c)

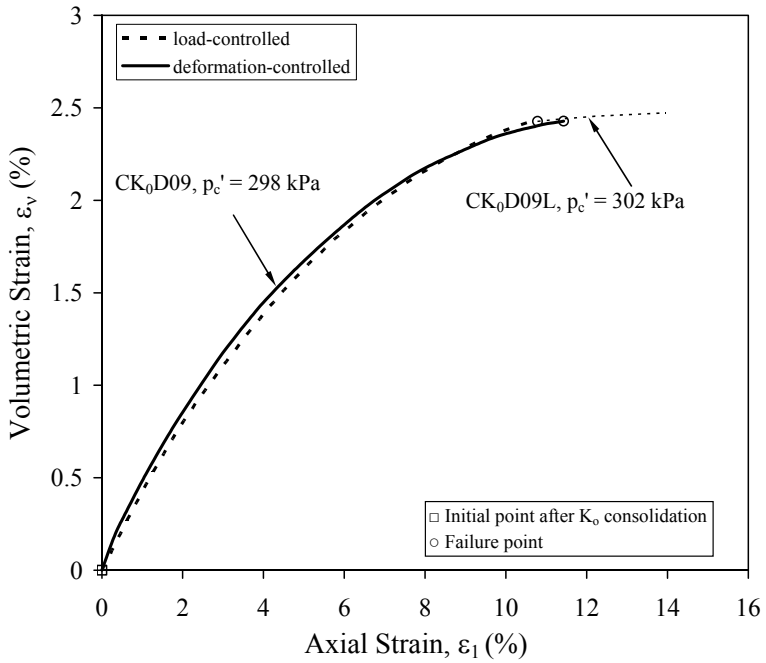

Fig. 4.8(d)

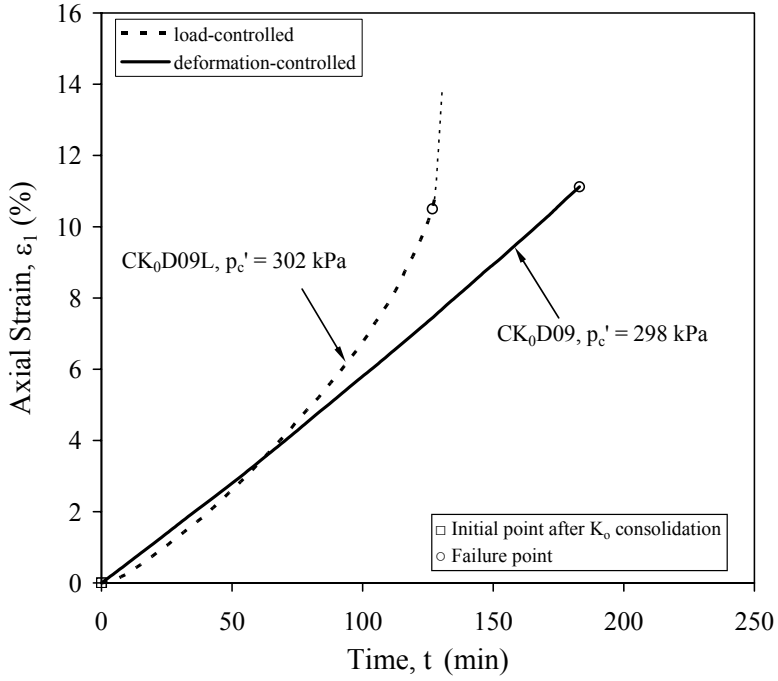

Fig. 4.8(e)

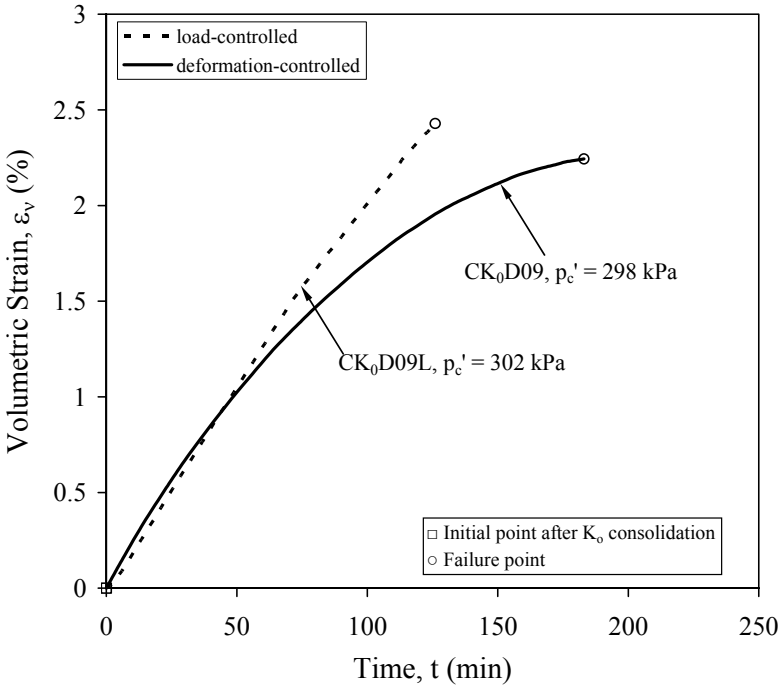

Fig. 4.8(f)

Fig. 4.8 Comparison of drained tests conducted on very loose sand under deformation-controlled and load-controlled loading modes: (a) effective stress paths; (b) stress-strain curves; (c) deviatoric stress versus time curves; (d) ε_v versus ε_1 curves; (e) ε_1 versus *time* curves; (f) ε_v versus *time* curves

4.3.4 Summary of Drained Tests

The failure lines obtained from the drained tests conducted under both deformation-controlled and load-controlled loading modes are plotted in Fig. 4.9 on both the *q-p'* and the *e-p'* planes. The data indicate that the failure lines on both the *q-p'* and the *e-p'* planes are not affected by the loading mode. As the failure line obtained for very loose sand is also the CSL, the CSL is not affected by the loading mode either. These findings are consistent with the observations made by other researchers based on triaxial test results (Poulos et al., 1988; De Gregorio, 1990; Been et al., 1991; Chu & Leong, 2001). They reported that the failure line, the SSL or the CSL is not affected by the loading modes. However, it should be pointed out that the post-peak behaviour is significantly affected by the loading mode.

The dependence of shear strength on the density of sand is shown in Fig. 4.9(a). The gradients of failure lines, η_f, on the *q-p'* plane for very loose, medium loose and medium dense sand are 1.16, 1.35, and 1.53 respectively. The corresponding friction angles are 36.0°, 43.4°, and 49.7°. These values are unique for both modes of loading. The ultimate state lines obtained from drained tests conducted on medium loose and medium dense specimens under the DC lading mode are also plotted in Fig. 4.9. It can be observed that the ultimate states of medium loose and medium dense specimens in plane-strain tests do not form a single line, neither on the *q-p'* (Fig. 4.9(a)) nor on the *e-p'* (Fig. 4.9(b)) plane. However, the ultimate state lines, the failure lines, and the CSL are approximately parallel on the *e-p'* plane, as shown in Fig. 4.9(b). These findings are consistent with the observations made by Finno & Rechenmacher (2003). They reported that the relationship between void ratio and mean effective stress is not unique but depends on consolidation history and the initial state of sand.

A further comparison of all the failure states is given in Fig. 4.10. By plotting the values of η_f together with void ratio, e_c, an exponential relationship between the two parameters can be established, as shown in Fig. 4.10(a). It can be noticed that the gradient of failure line, η_f decreases with increasing void ratio, e_c. There is also an exponential relationship between maximum dilatancy ratio $(-d\varepsilon_v/d\varepsilon_1)_{max}$ and

void ratio, e_c, as presented in Fig. 4.10(b). It should be noted that this relationship is affected by p_c'. For a given e_c, the higher the p_c', the smaller the $(-d\varepsilon_v/d\varepsilon_1)_{max}$.

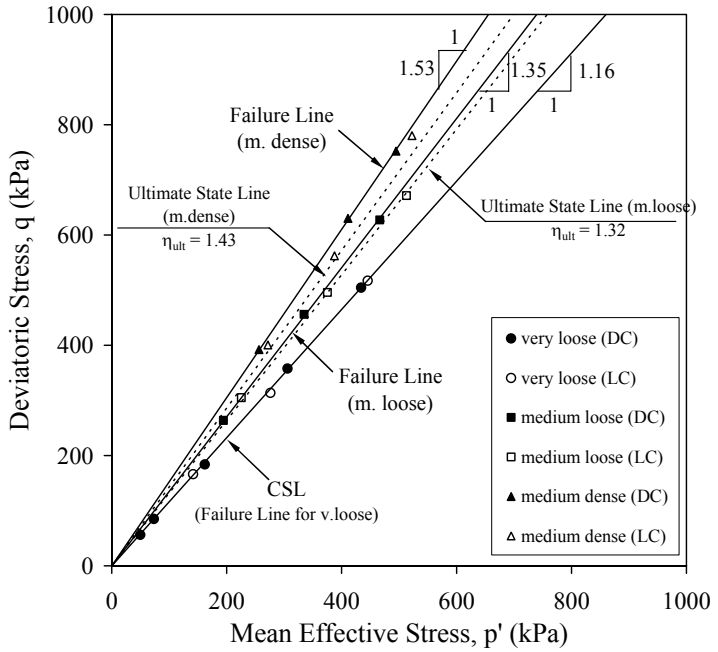

Fig. 4.9(a)

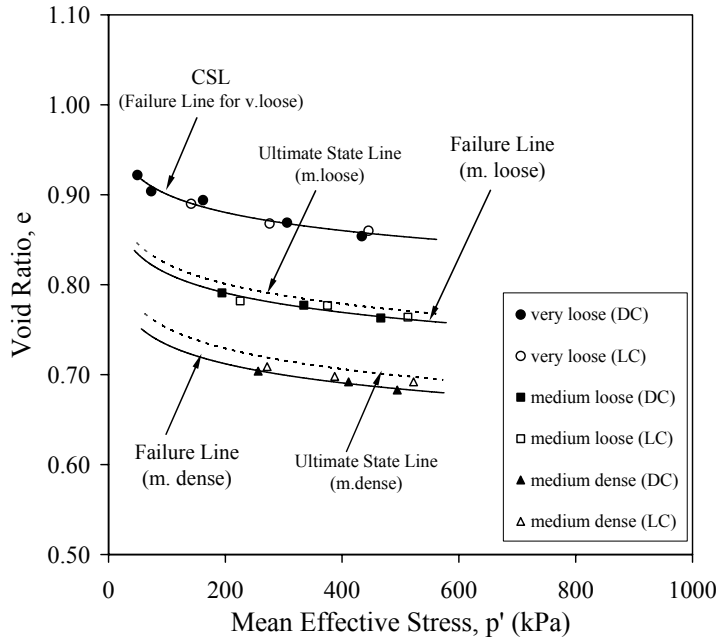

Fig. 4.9(b)

Fig. 4.9 Summary of drained tests conducted under deformation-controlled and load-controlled loading modes: (a) *q-p'* plane; (b) *e-p'* plane

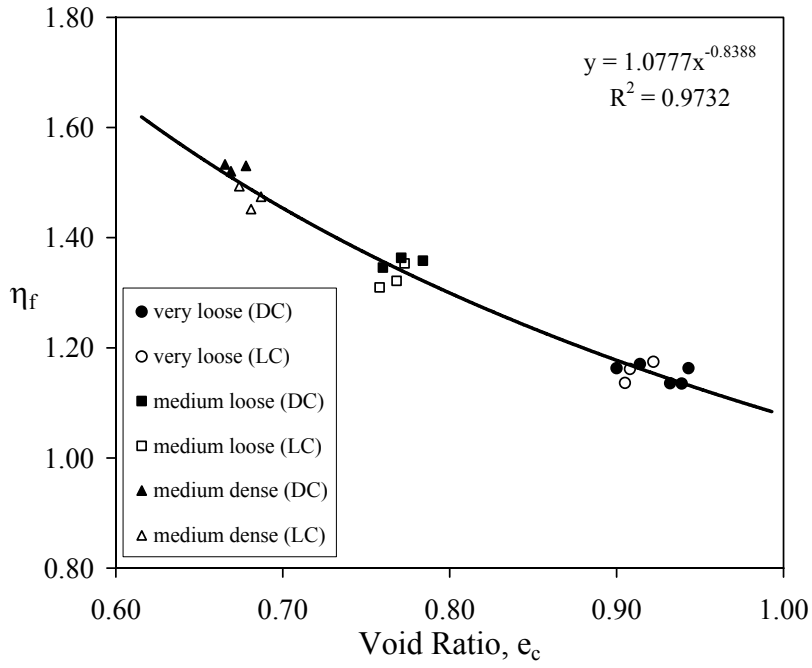

Fig. 4.10(a)

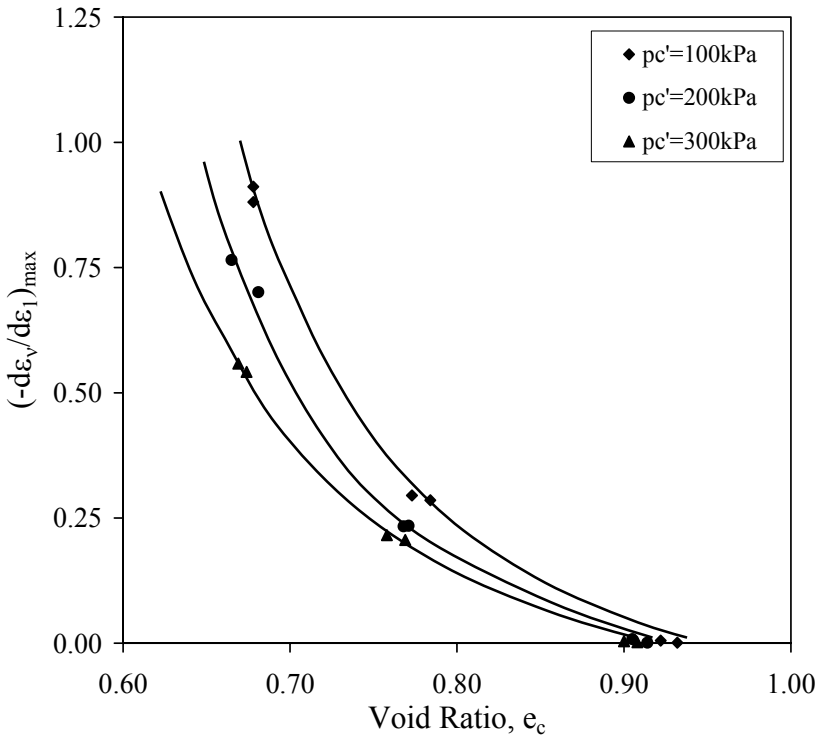

Fig. 4.10(b)

Fig. 4.10 Summary of failure states obtained from drained tests: (a) relationship between η_f and e_c; (b) relationship between $(-d\varepsilon_v/d\varepsilon_1)_{max}$ and e_c

4.4 Undrained Behaviour

4.4.1 Deformation-Controlled Loading Mode

4.4.1.1 Very Loose Sand

The results of five K_0 consolidated undrained tests, CK_0U04, CK_0U05, CK_0U06, CK_0U11 and CK_0U12 are presented in Fig. 4.11. These tests were conducted on very loose sand under a DC loading mode. The void ratios, e_c, of the five specimens after K_0 consolidation were 0.935, 0.915, 0.899, 0.884 and 0.868 respectively. The specimen CK_0U04 was K_0 consolidated to p_c' = 97 kPa and CK_0U06 to p_c' = 298 kPa. All the other specimens were consolidated to p_c' = 198 – 199 kPa.

The effective stress paths obtained from the above five tests are presented in Fig. 4.11(a). The critical state line (CSL) as determined by drained tests on very loose sand is also shown in Fig. 4.11(a). It can be seen that the effective stress paths resulting from the tests with strain softening behaviour approached the CSL. Therefore, the CSL is unique for both undrained and drained tests. The stress-strain curves of the five tests are presented in Fig. 4.11(b). The deviatoric stress in Test CK_0U11 became constant after reaching the peak value. The excess pore water pressure generated during this test also became constant after reaching the peak value, as shown in Fig. 4.11(c). Therefore, a critical state behaviour was obtained in Test CK_0U11 and the critical void ratio was e_{cr} = 0.884.

Tests CK_0U04, CK_0U05 and CK_0U06 with $e_c > e_{cr}$ exhibited strain softening behaviour. Test CK_0U12 with $e_c < e_{cr}$ experienced strain hardening behaviour before the peak was reached. For specimens looser than e_{cr} (Tests CK_0U04, CK_0U05 and CK_0U06), the excess pore water pressures increased continuously throughout shearing, as shown in Fig. 4.11(c). For the same p_c', the larger the e_c, the greater the excess pore water pressure. On the other hand, for specimen denser than e_{cr} (Test CK_0U12), the excess pore water pressure increased initially and then decreased, and reached a constant value at the end of the test.

The *q/p'* versus ε_1 and the *b-value* versus ε_1 curves are shown in Fig. 4.11(d). The *b-values* varied from test to test within the 0.29 to 0.40 range. It appears that the looser the sand, the higher the *b-value*.

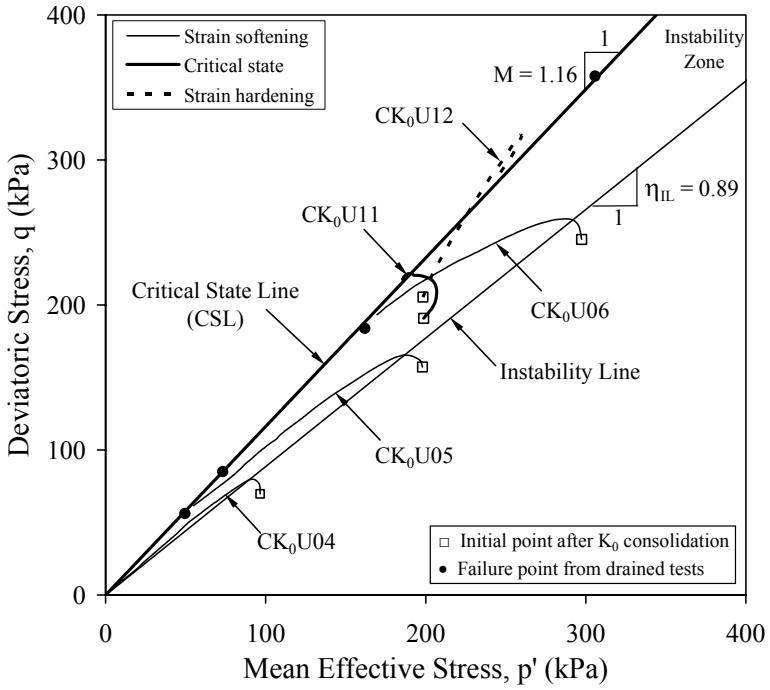

Fig. 4.11(a)

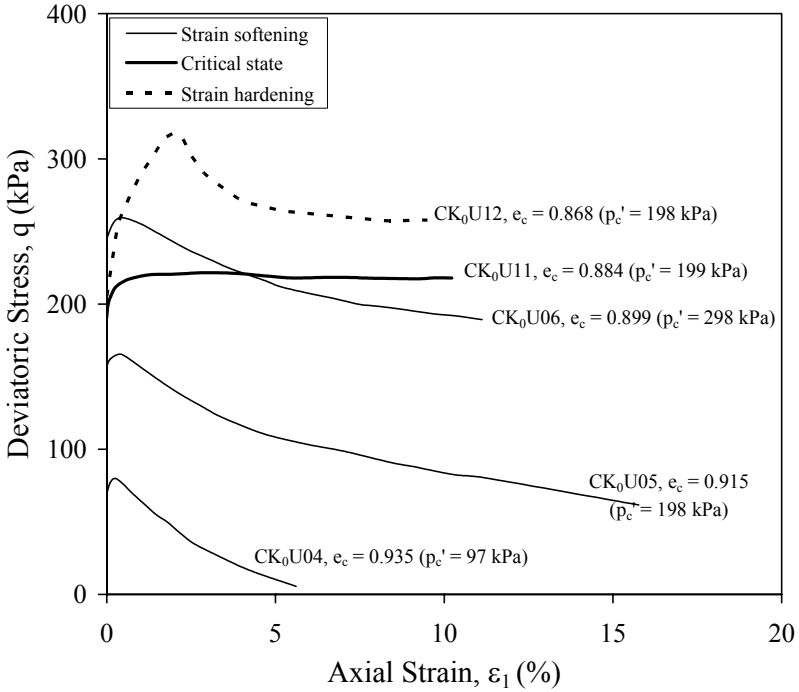

Fig. 4.11(b)

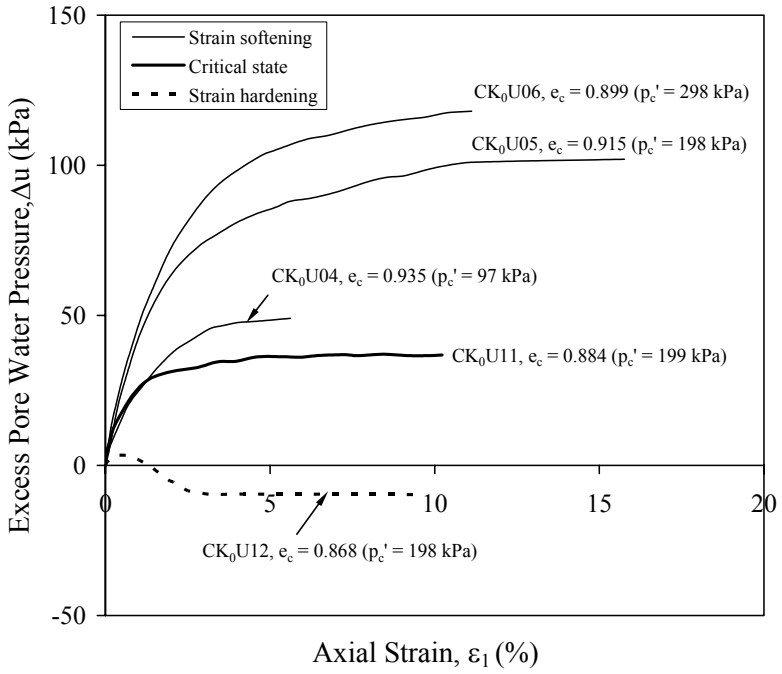

Fig. 4.11(c)

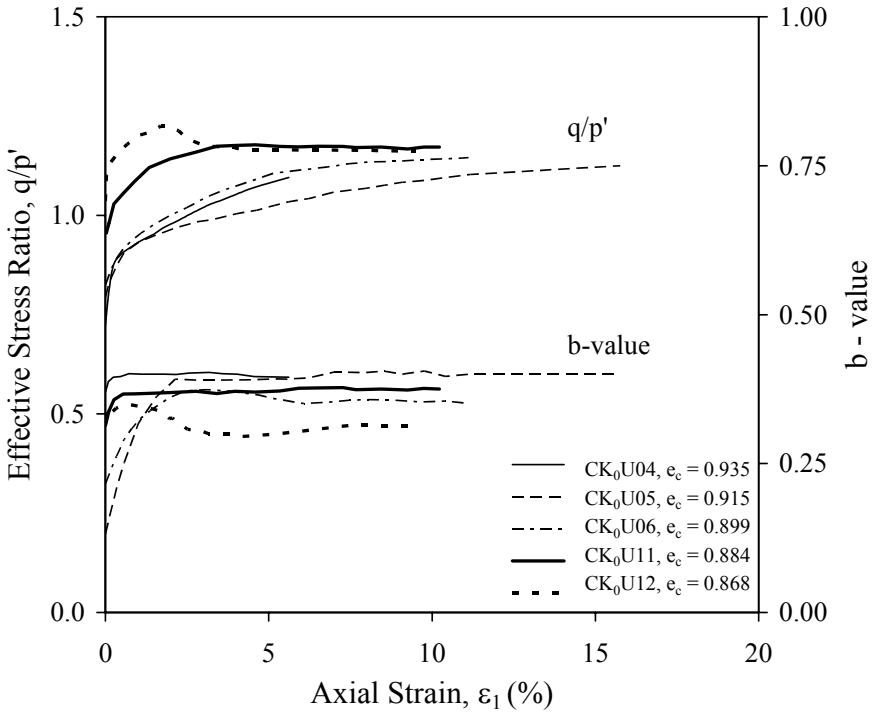

Fig. 4.11(d)

Fig. 4.11 Undrained behaviour of very loose sand under deformation-controlled loading mode: (a) effective stress paths; (b) stress-strain curves; (c) excess pore water pressure versus axial strain curves; (d) *q/p'* and *b-value* versus ε_1 curves

Although Test CK_0U12 exhibited a strain hardening behaviour, strain softening also occurred after the deviatoric stress reached the peak, as shown in Figs. 4.11(a) and 4.11(b). It should be pointed out that the strain softening observed in Test CK_0U12 is different from that in Tests CK_0U04, CK_0U05 and CK_0U06. First, the peak in Test CK_0U12 was reached at $\varepsilon_1 \approx 2\%$, whereas the peak points in the other tests were reached at ε_1 within 0.2 to 0.4%. Second, in Test CK_0U12, the peak occurred together with shear band formation. However, in the other tests, shear bands did not occur. Therefore, the strain softening observed in Test CK_0U12 is due to the development of shear band rather than an element behaviour.

A line can be drawn through the peak points of the undrained effective stress paths as shown in Fig. 4.11(a). This line has been called the instability line by Lade (1993). The zone bounded by the instability line and the CSL is called the zone of instability, in which loose sand can become unstable under undrained conditions (Lade & Pradel, 1990; Leong et al., 2000). As shown by Imam et al. (2002) and Chu et al. (2003) under triaxial conditions, the instability line is not unique, but varies with the void ratio and stress level. Fig. 4.12 shows the effective stress paths obtained from a series of CK_0U tests conducted on specimens with different e_c, but under the same mean effective stress, p_c'. It can be seen that the smaller the e_c, the higher the slope of the instability line. Based on Fig. 4.12, relationship between the slope of instability line η_{IL} and e_c can be established, as shown in Fig. 4.13.

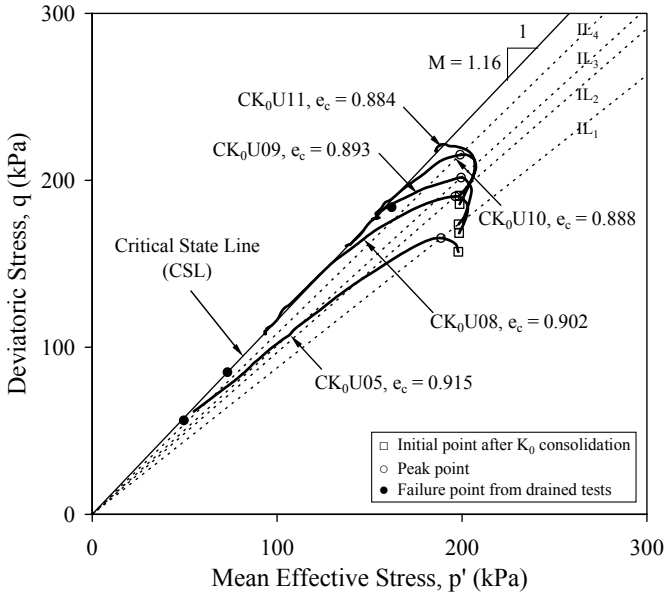

Fig. 4.12 Undrained tests on very loose sand showing the variation of the instability line with the void ratio

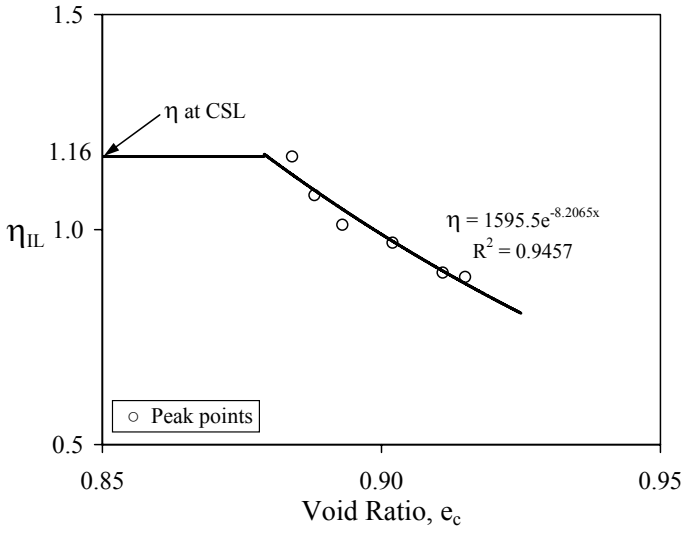

Fig. 4.13 Relationship between η_{IL} and e_c for plane-strain conditions

4.4.1.2 Medium Dense Sand

The results of four undrained tests CK_0U01, CK_0U02, CK_0U03 and CK_0U13 conducted on medium dense sand are presented in Fig. 4.14. The four specimens were firstly K_0 consolidated to a mean effective stress p_c' = 98, 202, 299 and 406 kPa respectively, and then sheared under undrained conditions.

Fig. 4.14(a) shows the effective stress paths obtained from the four tests. The failure line obtained from drained tests on medium dense sand and the CSL are also plotted in Fig. 4.14(a). Strain hardening behaviour was observed in all the tests. All the effective stress paths approach asymptotically a straight line as shown in Fig. 4.14(a). This line has been called the constant stress ratio line (CSRL) by Chu et al. (2003). The gradient of this line is M_L = 1.39. Similar behaviour has also been observed for other soils under axisymmetric conditions (Zhang & Garga, 1997; Chu et al., 2003), plane-strain conditions (Topolnicki et al., 1990) and three-dimensional conditions (Chu & Lo, 1994). This type of behaviour has been termed as the asymptotic behaviour by Gudehus et al. (1977).

The stress-strain curves of the four undrained tests are plotted in Fig. 4.14(b). It can be seen that after the stress-strain reached a peak, strain softening occurred in every test at an axial strain ranging from 4.7% to 5.7%. The higher the p_c', the smaller the

strain value at peak. The strain softening behaviour was accompanied by non-homogeneous deformations and the formation of shear band. Therefore, the strain softening behaviour in the post-peak region may not be a material behaviour. This argument is also supported by the pore water pressure curves shown in Fig. 4.14(c). When the shear bands occurred the changes in pore water pressures ceased.

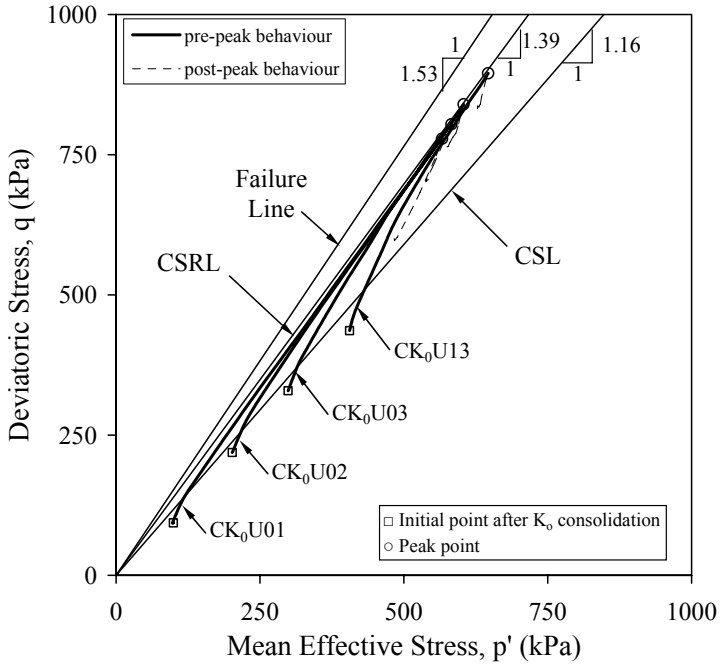

Fig. 4.14(a)

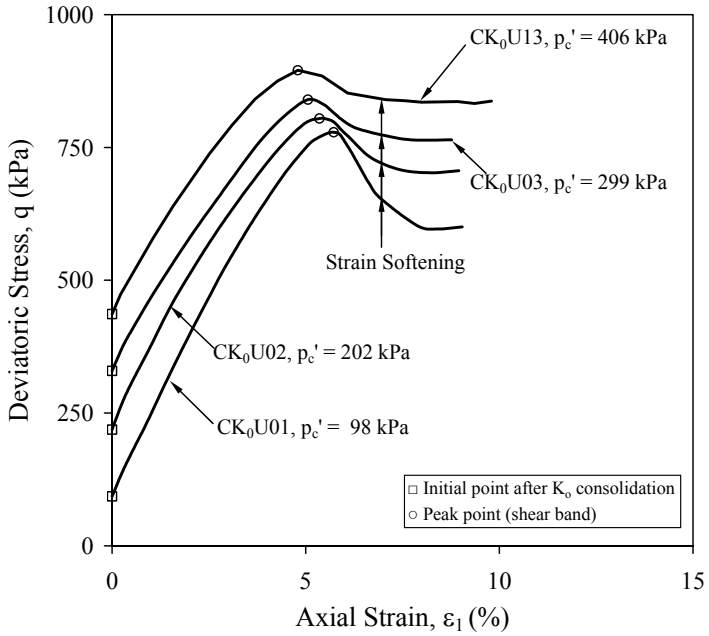

Fig. 4.14(b)

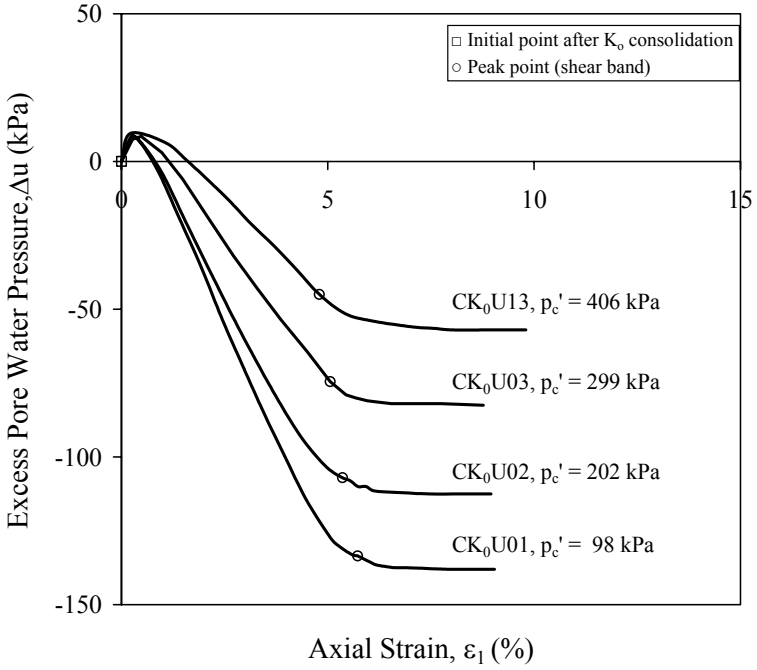

Fig. 4.14(c)

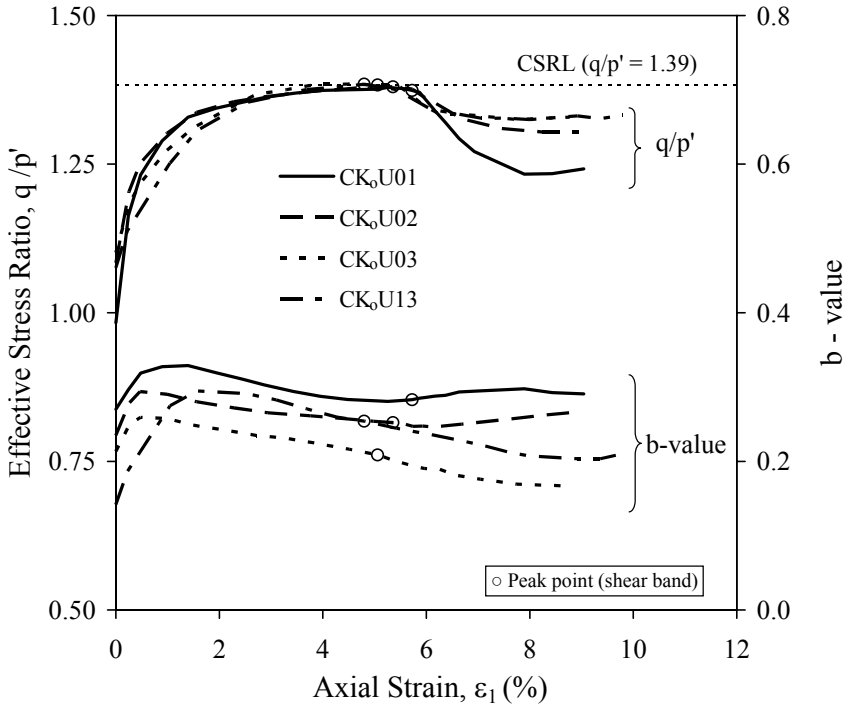

Fig. 4.14(d)

Fig. 4.14 Undrained behaviour of medium dense sand under deformation-controlled loading mode: (a) effective stress paths; (b) stress-strain curves; (c) excess pore water pressure versus axial strain curves; (d) *q/p'* and *b-value* versus ε_1 curves

The *q/p'* versus ε_1 and the *b-value* versus ε_1 curves are presented in Fig. 4.14(d). It is again seen that the *q/p'* curves reach asymptotically the same ratio 1.39 irrespective of p_c'. The *q/p'* reduces when shear bands occurred. The *b-values* during shearing varied in the range between 0.18 and 0.31.

4.4.2 Load-Controlled Loading Mode

4.4.2.1 Very Loose Sand

The results of three CK_0U tests, CK_0U04L, CK_0U05L, and CK_0U06L, conducted on very loose specimens under a LC loading mode are shown in Fig. 4.15. The specimens were K_0 consolidated to mean effective stresses, p_c' = 96, 199, and 299 kPa respectively. The void ratios of the specimens after consolidation were e_c = 0.946, 0.911 and 0.900. All the specimens were sheared with a rate of 0.01 kN/min.

The effective stress paths obtained from the three tests are shown in Fig. 4.15(a). Behaviour similar to the undrained tests conducted under a DC loading mode (Fig. 4.14(a)) was observed. Using the peak points the instability line can be determined as shown in Fig. 4.15(a). The gradient of the instability line obtained is η_{IL} = 0.89.

The stress-strain curves obtained from the tests are presented in Fig. 4.15(b). The peaks occurred around an axial strain of 0.3 – 0.4%. The axial strain versus time curves are plotted in Fig. 4.15(c). It can be seen that once the peak deviatoric stress was reached, the axial strain would increase suddenly and the specimen would collapse. In other words, the specimen became unstable when the peak stress was reached. It should be pointed out however, that shear bands were not detected in all the three tests.

The excess pore water pressure versus axial strain curves obtained from the three load-controlled tests on very loose sand are presented in Fig. 4.15(d). It can be seen that all the pore water pressures reached constant values at the end of tests. The higher the p_c', the greater the Δu generated during shearing. The pore water pressure at the point where the peak deviatoric stress was attained was much smaller than the maximum pore water pressure value. Therefore, the majority of

the pore water pressure was generated after the specimen became unstable. The *q/p'* versus ε_1 and the *b-value* versus ε_1 curves are shown in Fig. 4.15(e). The three curves are quite similar. The *b-values* varied mainly in the range of 0.37 to 0.40.

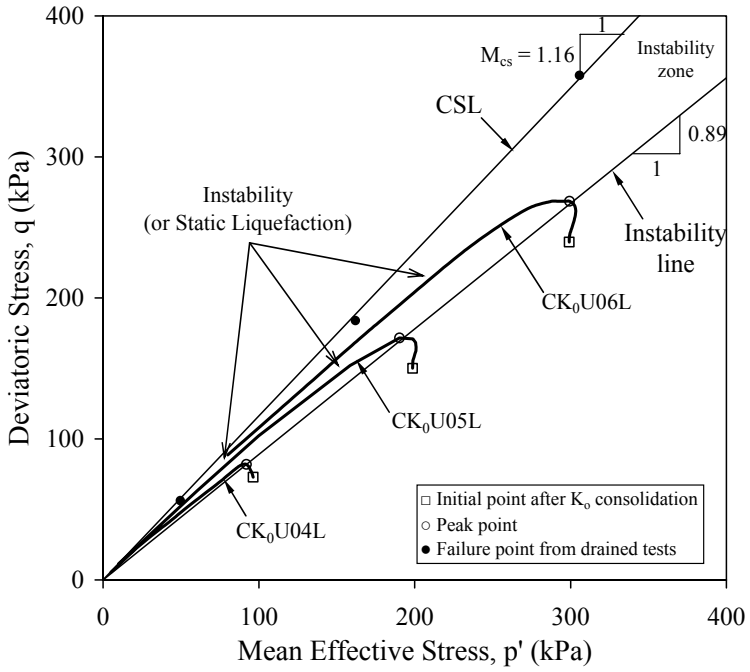

Fig. 4.15(a)

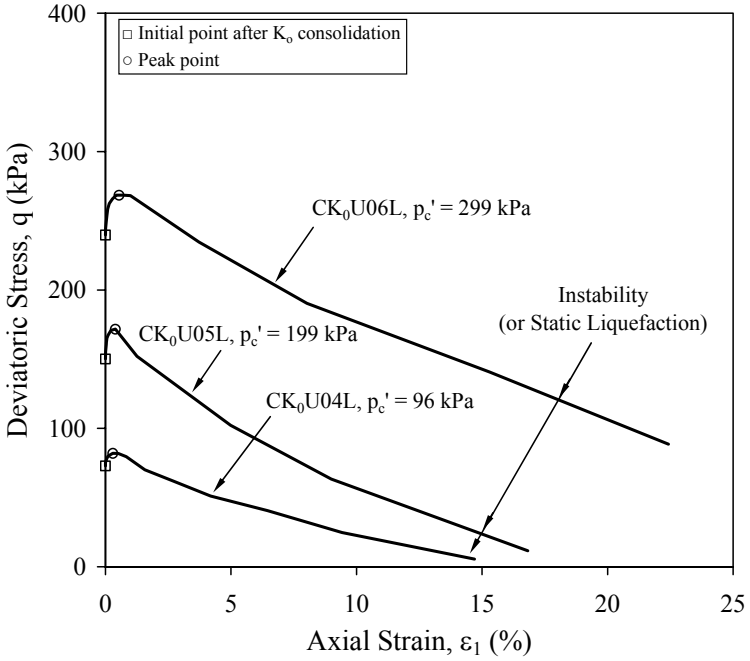

Fig. 4.15(b)

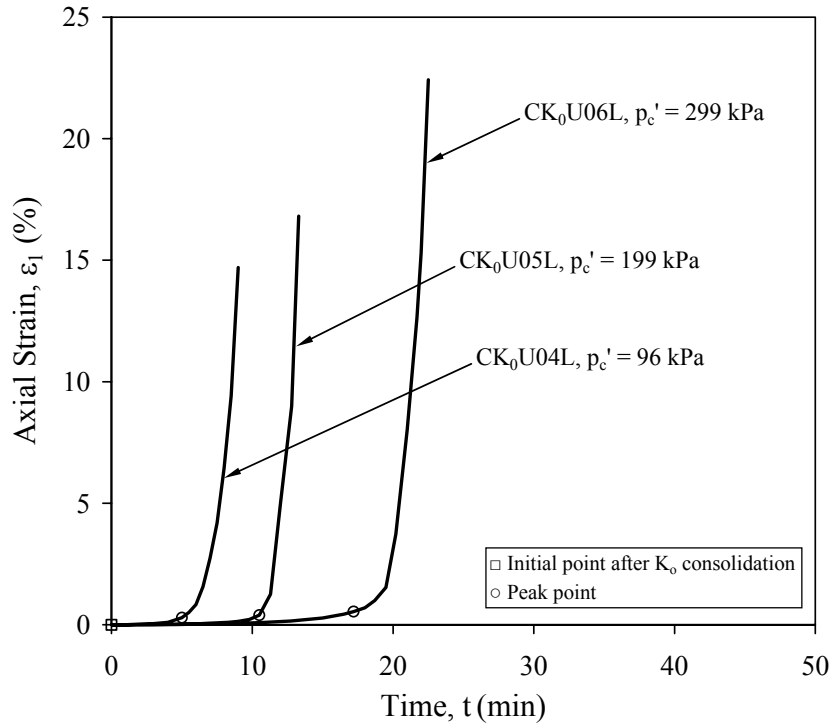

Fig. 4.15(c)

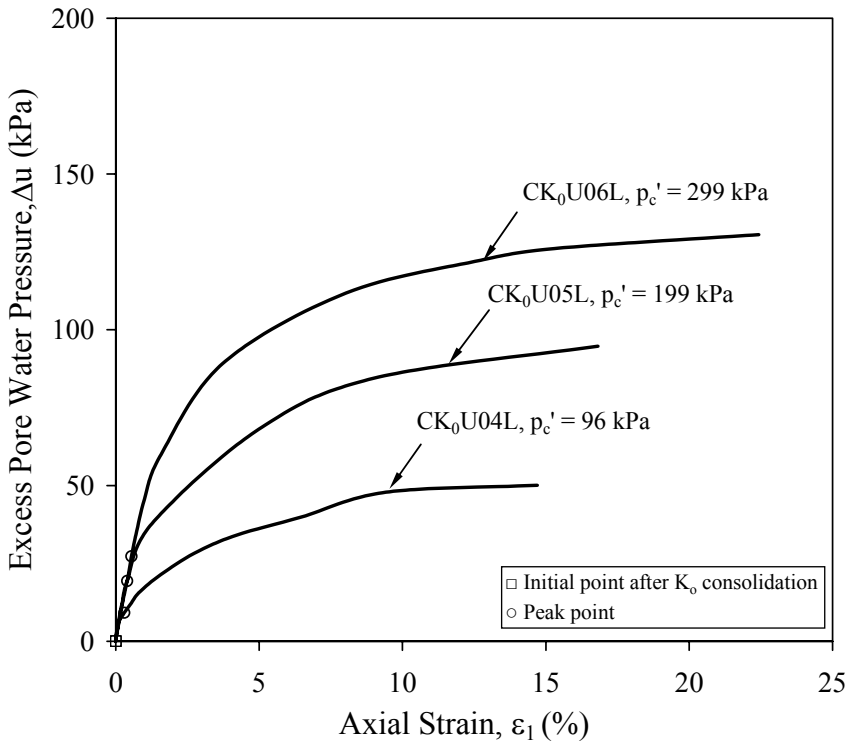

Fig. 4.15(d)

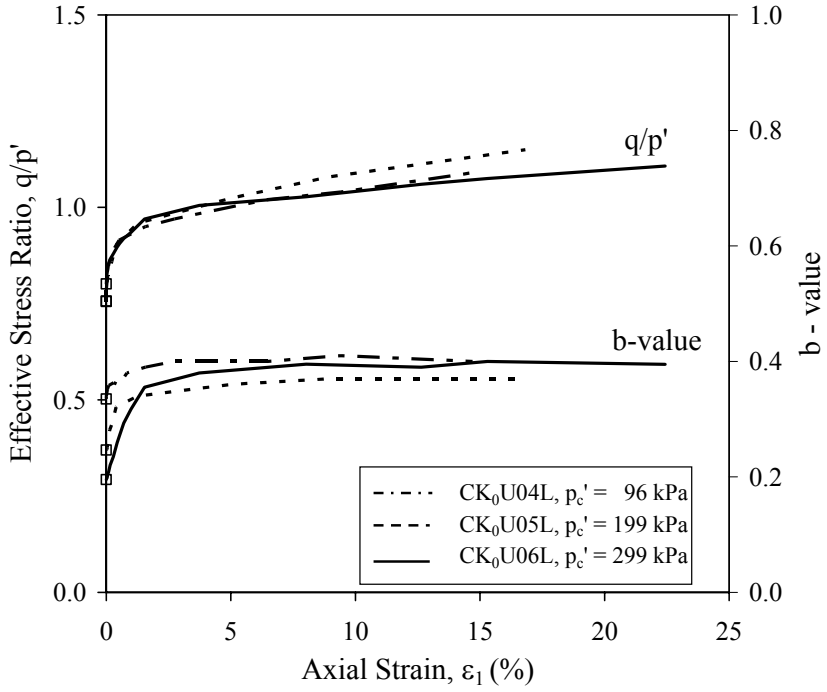

Fig. 4.15(e)

Fig. 4.15 Undrained behaviour of very loose sand under load-controlled loading mode: (a) effective stress paths; (b) stress-strain curves; (c) ε_1 versus *time* curves; (d) excess pore water pressure versus axial strain curves; (e) *q/p'* and *b-value* versus axial strain curves

4.4.2.2 Medium Dense Sand

The results of three CK_0U tests on medium dense specimens CK_0U01L, CK_0U02L, and CK_0U03L, are presented in Fig. 4.16. The specimens were K_0 consolidated to mean effective stresses, p_c' = 102, 202, and 301 kPa. The void ratios after consolidation were e_c = 0.714, 0.712 and 0.707 respectively. All the specimens were sheared with a rate of 0.02 kN/min.

The effective stress paths obtained from the three tests are shown in Fig. 4.16(a). The CSL and the failure line determined in drained tests on the specimens with comparable void ratios are also presented in Fig. 4.16(a). All the effective stress paths approached asymptotically a CSRL. The gradient of the CSRL is M_L = 1.35. However, shear bands eventually occurred before the peak in all the specimens and deviatoric stresses started to decrease, as shown in Fig. 4.16(b). The curves in the

region where shear bands had occurred are plotted in dashed lines. It can be seen from Fig. 4.16(b) that the peak deviatoric stress increases with the mean effective consolidation stress, p_c'. The peaks occurred at an axial strain ranging from 6.6 to 7.1%.

The axial strain versus time curves are given in Fig. 4.16(c). Before the peak was reached, the axial strain increased almost linearly with time in all the three tests. After shear bands had developed, the axial strain increased suddenly, as shown in Fig. 4.16(c). The specimens became unstable. The excess pore water pressure versus axial strain curves are presented in Fig. 4.16(d). All the curves show that the pore water pressure ceded to change in the post-peak region.

The *q/p'* versus ε_1 and the *b-value* versus ε_1 curves are presented in Fig. 4.16(e). It is seen that the *q/p'* in the pre-peak region was the same, reflecting the fact that all the curves approached asymptotically the CSRL. The *b-values* at peak measured in the three tests are in the range between 0.17 and 0.41. The looser the specimen, the higher the *b-value* observed.

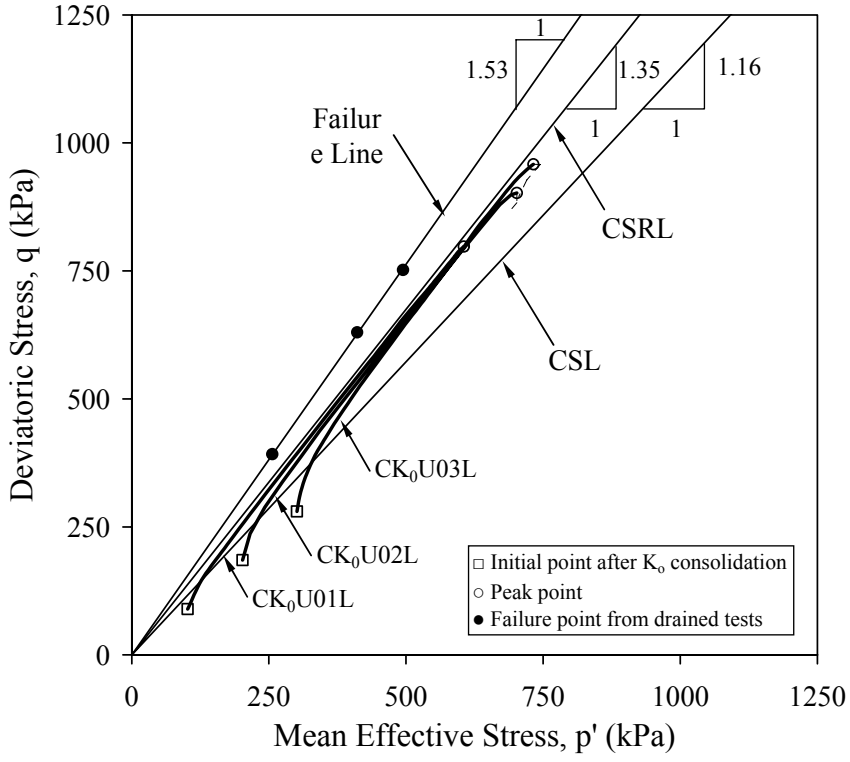

Fig. 4.16(a)

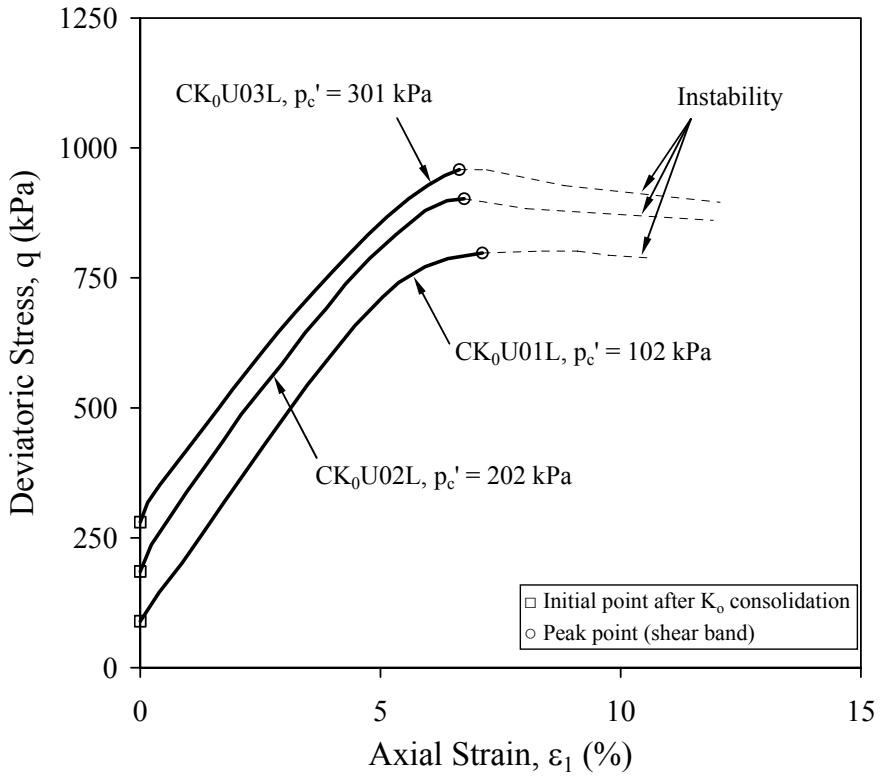

Fig. 4.16(b)

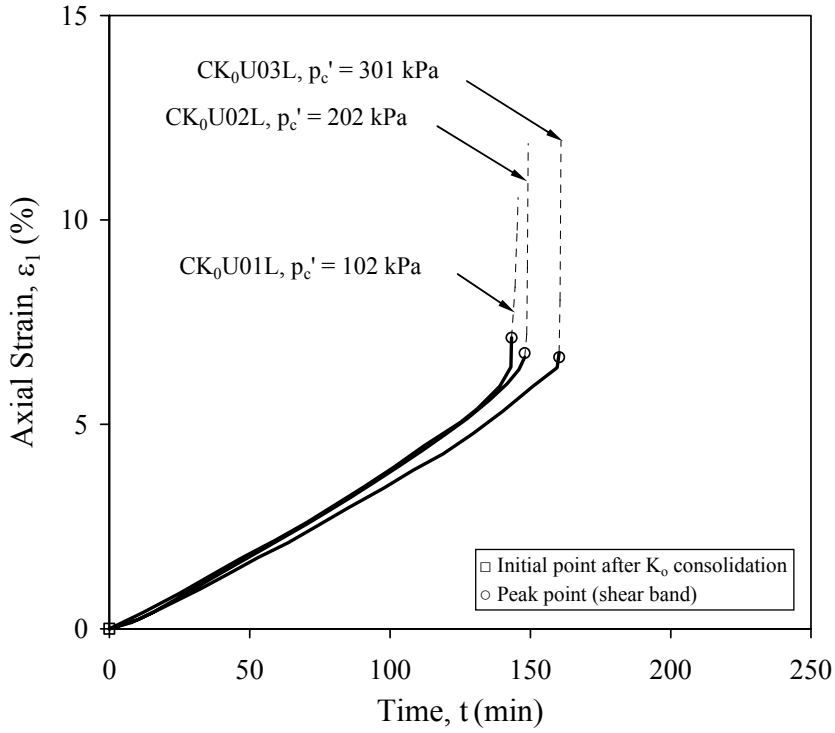

Fig. 4.16(c)

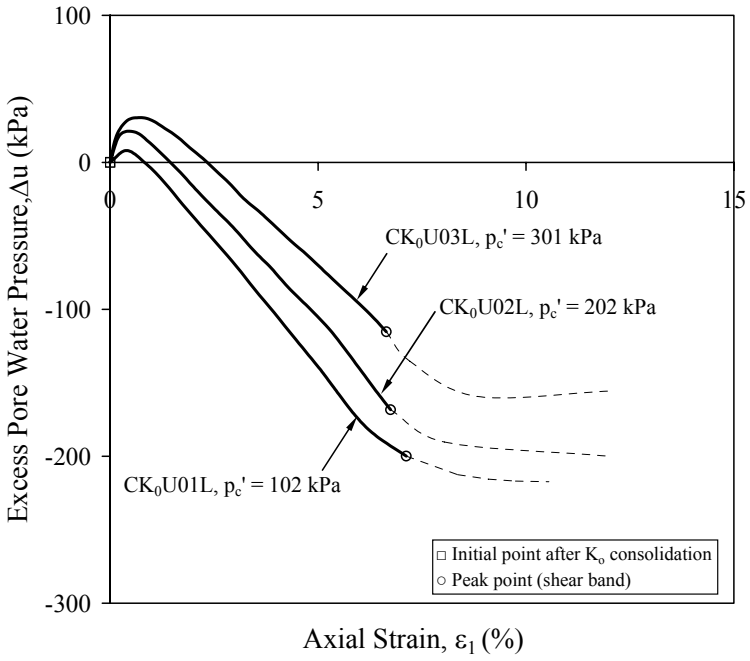

Fig. 4.16(d)

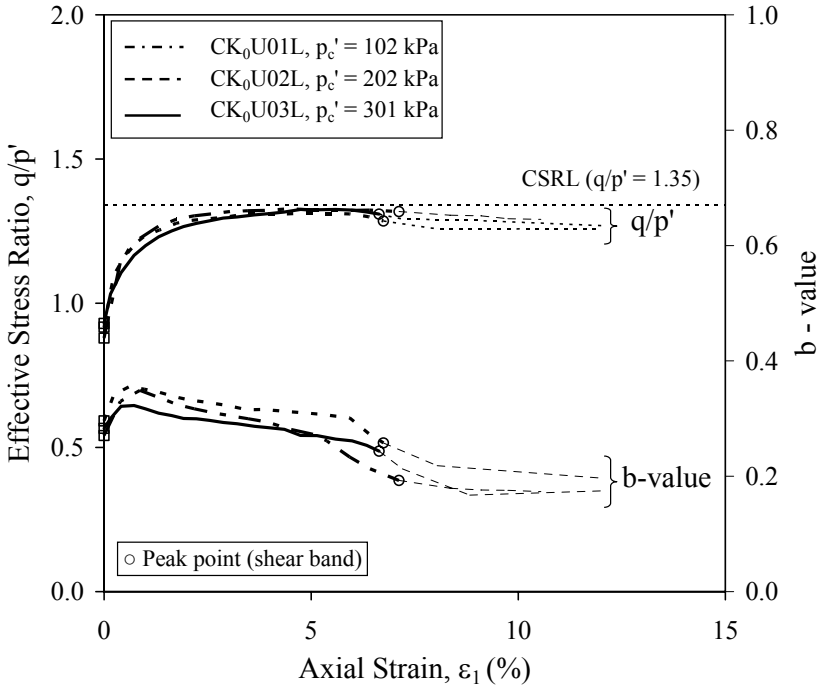

Fig. 4.16(e)

Fig. 4.16 Undrained behaviour of medium dense sand under load-controlled loading mode: (a) effective stress paths; (b) stress-strain curves; (c) ε_1 versus *time* curves; (d) excess pore water pressure versus axial strain curves; (e) *q/p'* and *b-value* versus axial strain curves

4.4.3 Comparison of Undrained Behaviour under Deformation-Controlled and Load-Controlled Loading Modes

4.4.3.1 Very Loose Sand

The results of two CK_0U tests conducted on very loose specimens with comparable void ratios are presented in Fig. 4.17. Test CK_0U05 was conducted under a DC loading mode and Test CK_0U05L under a LC loading mode. The effective stress paths of the two tests are compared in Fig. 4.17(a). The two paths in the pre-peak range are different. This could be due to the difference in the shearing rates used in the two tests. Nevertheless, the peak points occurred along the same instability line with a gradient η_{IL} = 0.89. After the peak both stress paths plunged towards the CSL.

The deviatoric stress versus axial strain curves for the two tests are plotted in Fig. 4.17(b). The trends of two curves are similar. The peak occurred at around an axial strain of 0.4% and followed by a drastic reduction in the deviatoric stress for both tests. The deviatoric stress versus time curves and the axial strain versus time curves are plotted in Figs. 4.17(c) and 4.17(d) respectively. In Test CK_0U05L the deviatoric stress dropped suddenly at the peak (Fig. 4.17(c)) and the axial strain also increased suddenly at the peak (Fig. 4.17(d)). Thus, the specimen became unstable at the peak and instability occurred in Test CK_0U05L. On the other hand, in Test CK_0U05, the deviatoric stress reduced gradually (Fig. 4.17(c)) and the axial strain increased almost linearly with time (Fig. 4.17(d)) in the post-peak region. Therefore, strain softening occurred in Test CK_0U05.

The excess pore water pressure versus axial strain and versus time curves are also shown in Figs. 4.17(e) and 4.17(f) respectively. The amount of pore water pressure generated in the two tests is different. In Test CK_0U05, the pore water pressure increased gradually and reached a constant value at the end of shearing, whereas in Test CK_0U05L, the pore water pressure shot up after the specimen became unstable at the peak (Fig. 4.17(f)).

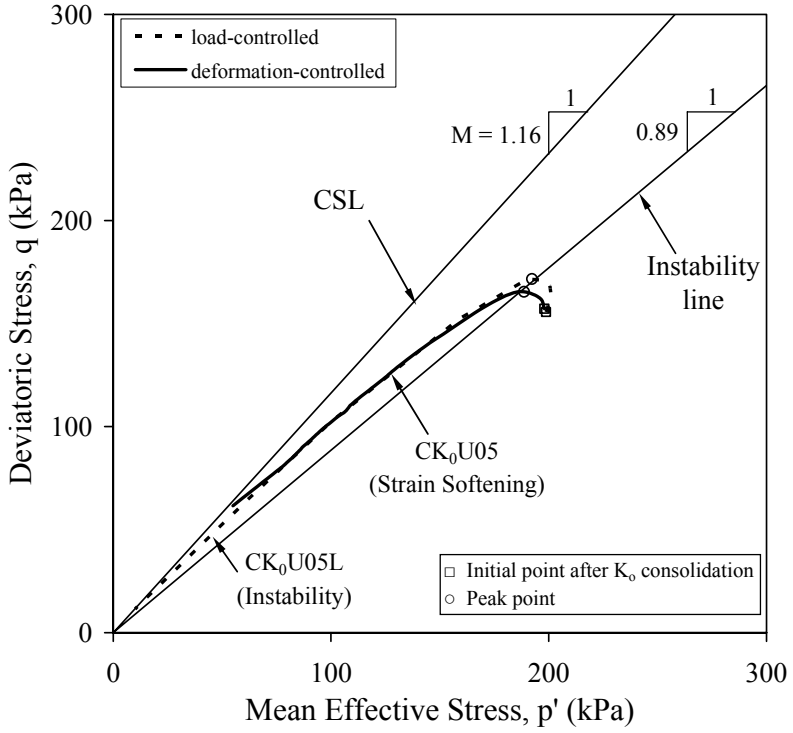

Fig. 4.17(a)

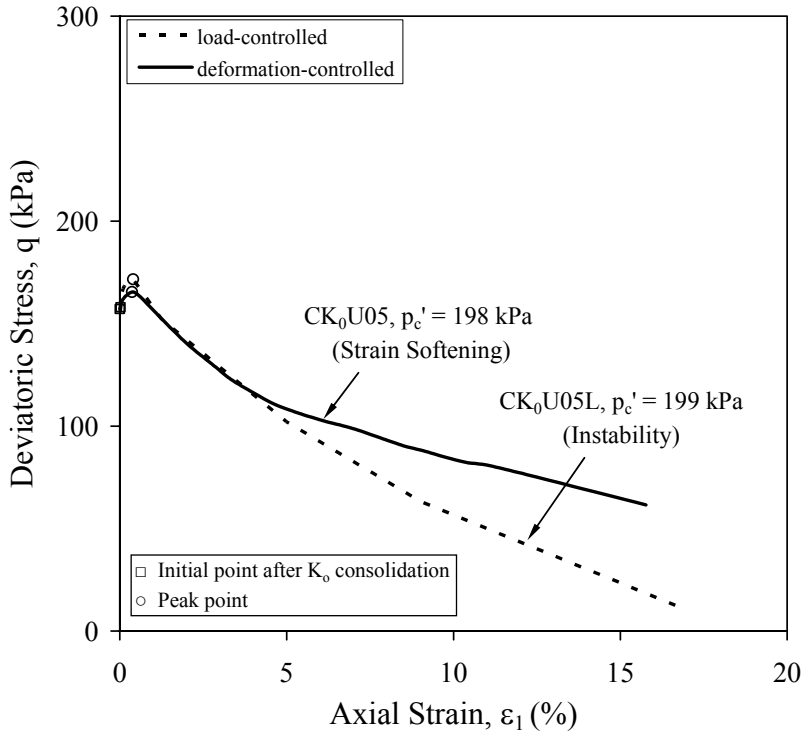

Fig. 4.17(b)

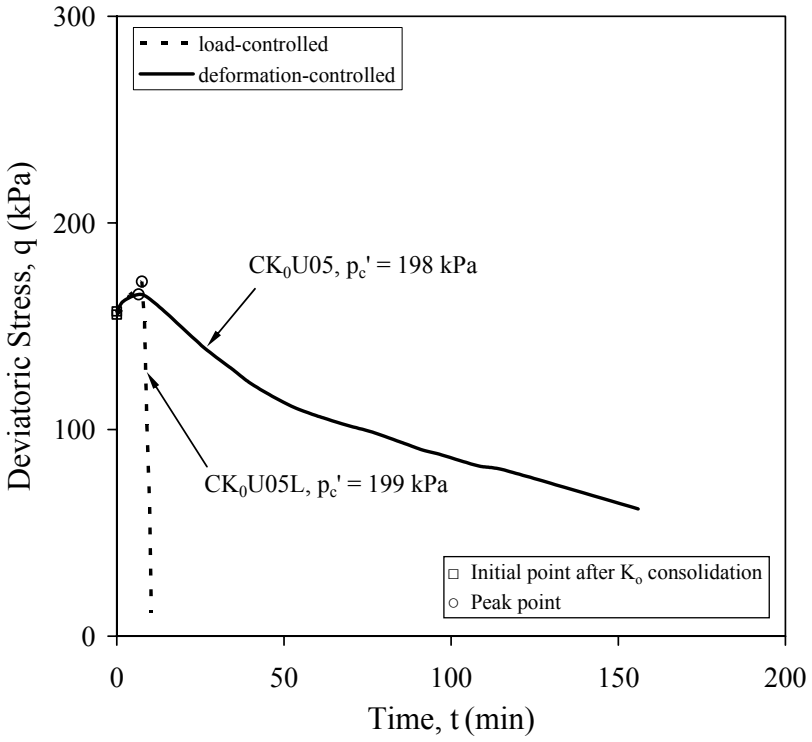

Fig. 4.17(c)

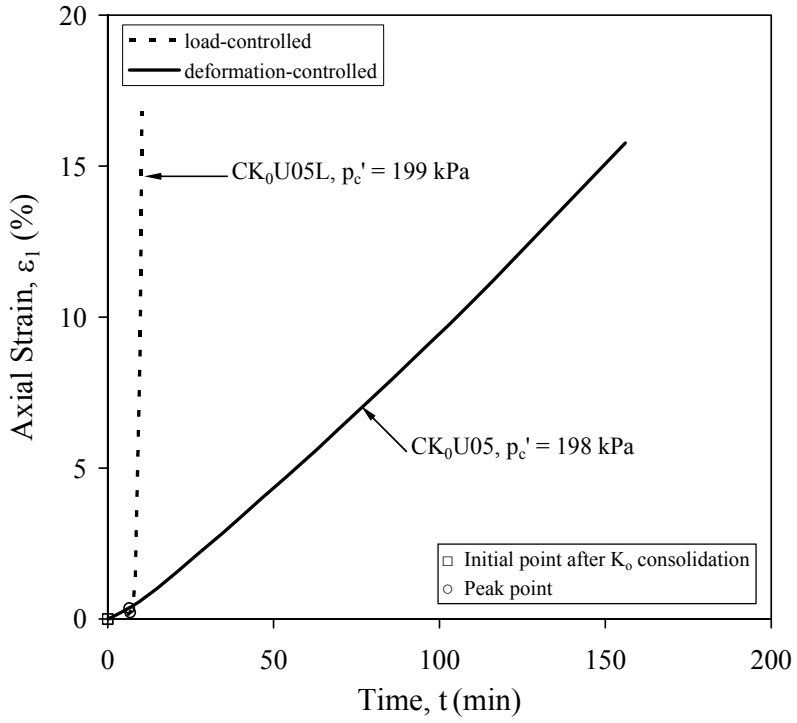

Fig. 4.17(d)

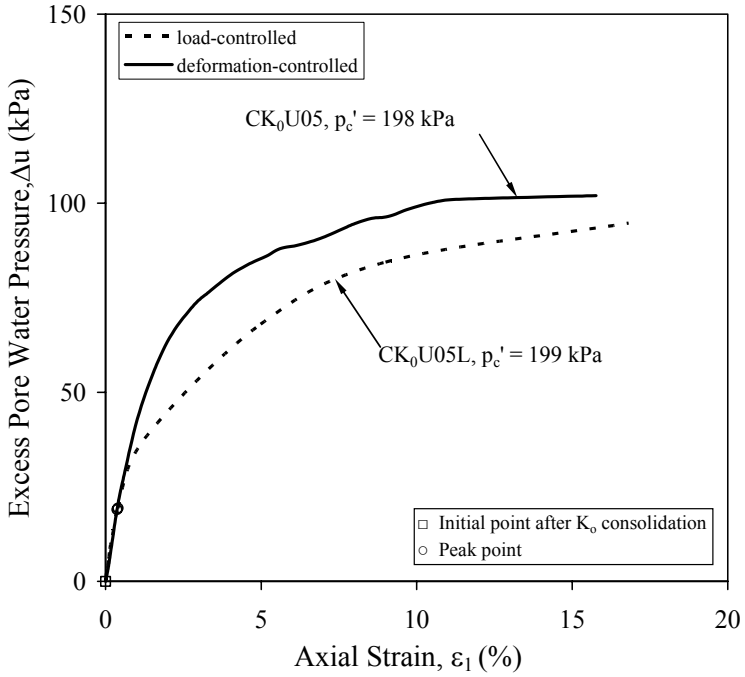

Fig. 4.17(e)

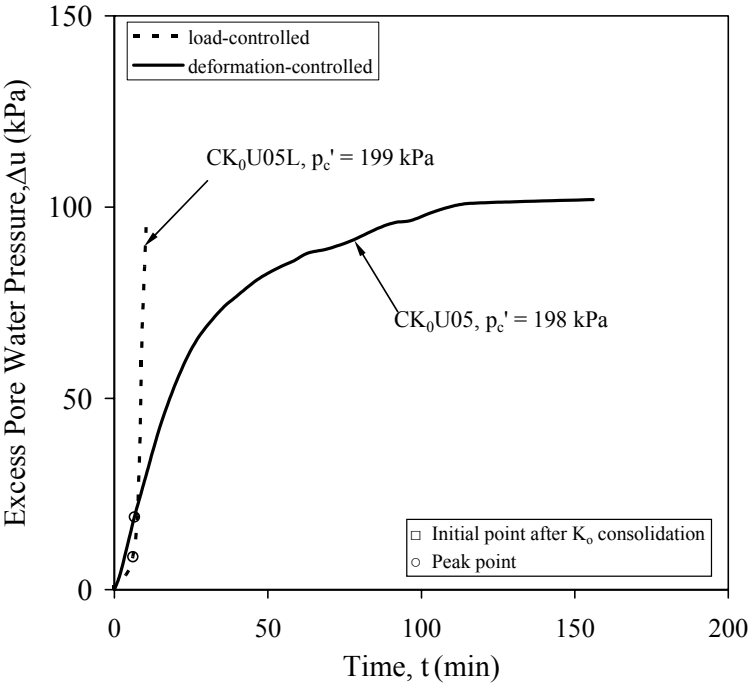

Fig. 4.17(f)

Fig. 4.17 Comparison of undrained tests conducted on very loose sand under deformation-controlled and load-controlled loading modes: (a) effective stress paths; (b) stress-strain curves; (c) deviatoric stress versus time curves; (d) ε_1 versus *time* curves; (e) Δu versus ε_1 curves; (f) Δu versus *time* curves

4.4.3.2 Medium Dense Sand

The results of Tests CK_0U03 and CK_0U03L conducted on medium dense sand are compared in Fig. 4.18. The specimens were K_0 consolidated to mean effective stresses, p_c' of 299 and 301 kPa respectively. Test CK_0U03 was conducted under a DC loading mode and Test CK_0U03L under a LC loading mode. The effective stress paths obtained from the two tests are compared in Fig. 4.18(a). Although the stress paths in the two tests are quite similar, they end up at slightly different CSRLs. The gradient of the CSRL obtained from Test CK_0U03 is $(q/p')_{DC}$ = 1.39, and from Test CK_0U05L is $(q/p')_{LC}$ = 1.35. Whether the differences are due to the difference in loading mode or the difference in strain rate or void ratio needs to be investigated further.

The deviatoric stress versus axial strain curves for the two tests are plotted in Fig. 4.18(b). The stress-strain curves in the pre-peak region are quite similar. However the peak values are different and the axial strains at the peak are also different. It can be seen from Figs. 4.18(a) & 4.18(b) that the higher peak deviatoric stress was obtained from Test CK_0U03L. This effect may be attributed to the different strain rates used in the two tests. As shown in Fig. 4.18(d), in Test CK_0U03L, a much lower axial strain rate was used. Therefore, a negative strain rate effect on the peak deviatoric stress was observed from the two tests. The negative strain rate effect observed herein has also been reported in the past by other researchers (Seed & Lundgren, 1954, Nash & Dixon, 1961, Whitman & Healy, 1962).

The deviatoric stress versus time and axial strain versus time curves are presented in Fig. 4.18(c) and Fig. 4.18(d). It can be seen from Fig. 4.18(c) that in Test CK_0U03L the deviatoric stress increased linearly with time until the peak and then dropped suddenly at the peak point, whereas in Test CK_0U03, the deviatoric stress reduced gradually with time in the post-peak region. In Test CK_0U03, the deformation rate was controlled constant, so $d\varepsilon_1/dt$ maintains at more or less the same rate in both the pre-peak and post-peak regions, as shown in Fig. 4.18(d). In Test CK_0U03L, load was controlled to increase at a given rate. When the deviatoric stress reached the peak, the specimen could not take up any extra load and became unstable. As a result, ε_1 shot up almost instantly at the peak, as shown in Fig.

4.18(d). Therefore, in post-peak region, instability occurred in Test CK_0U03L and strain softening occurred in Test CK_0U03.

The excess pore water pressure versus axial strain curves in the two tests are compared in Fig. 4.18(e). In Test CK_0U03L, a greater excess pore water pressure was generated at the peak point. In Test CK_0U03, the pore water pressure stopped changing soon after the peak where the shear band occurred.

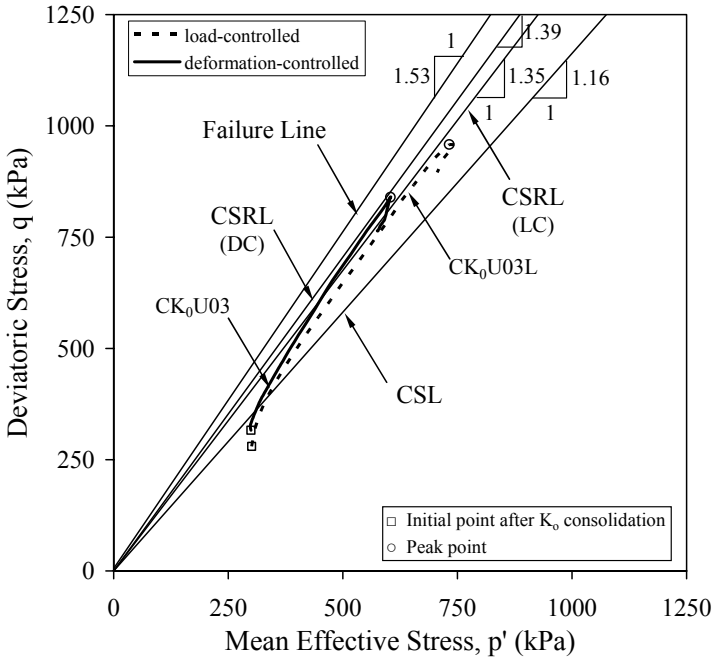

Fig. 4.18(a)

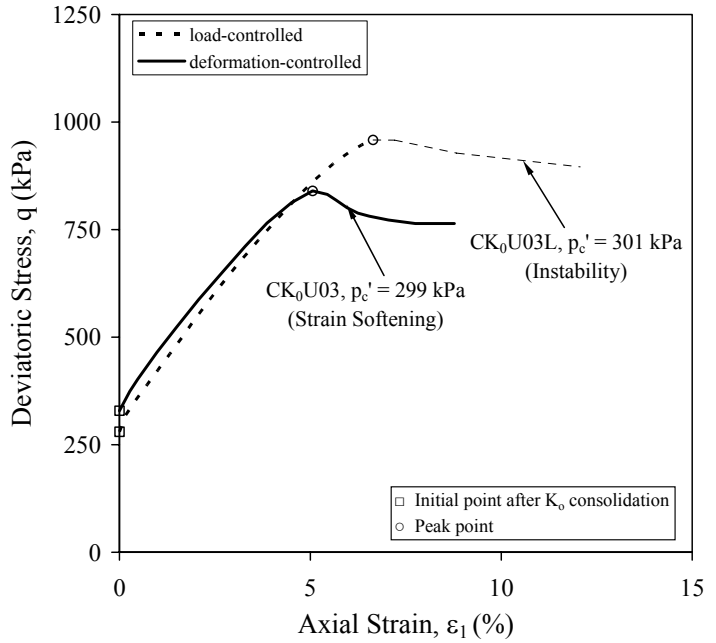

Fig. 4.18(b)

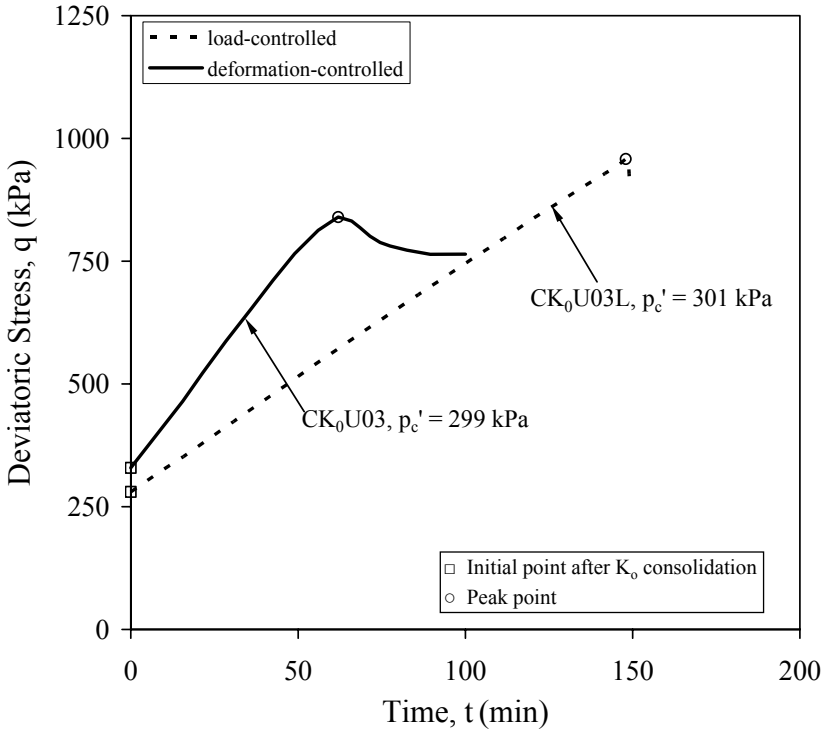

Fig. 4.18(c)

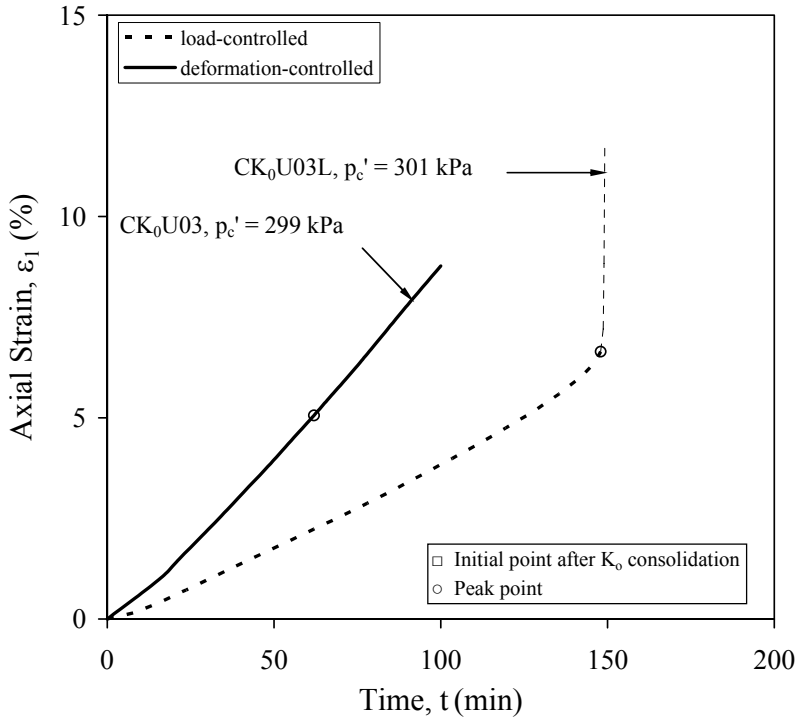

Fig. 4.18(d)

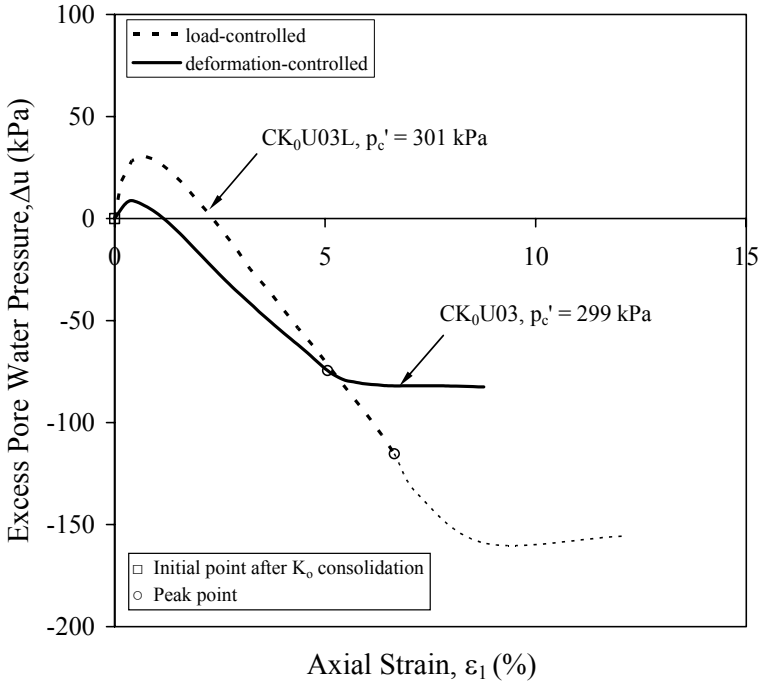

Fig. 4.18(e)

Fig. 4.18 Comparison of undrained tests conducted on medium dense sand under deformation-controlled and load-controlled loading modes: (a) effective stress paths; (b) stress-strain curves; (c) deviatoric stress versus time curves; (d) ε_1 versus *time* curves; (e) Δu versus ε_1 curves

4.4.4 Summary of Undrained Tests

The results obtained from all the undrained tests conducted under both DC and LC loading modes are presented in Fig. 4.19 on both the *q-p'* and the *e-p'* planes. The failure line for medium dense sand as determined by drained tests is also shown in Fig. 4.19. As the instability line is not unique (see Fig. 4.12), only the lower bound of instability line is presented. The data indicate that the CSL on both the *q-p'* and the *e-p'* planes is unique and is not affected by the loading mode. For a given void ratio, the instability line is also independent of the loading mode. The CSRLs obtained from undrained tests conducted on medium dense specimens are also shown in Fig. 4.19. It can be seen that the CSRL is in between the failure line and the CSL. The CSRL appears to be affected by the loading mode, as shown in Fig. 4.19, although the difference is small.

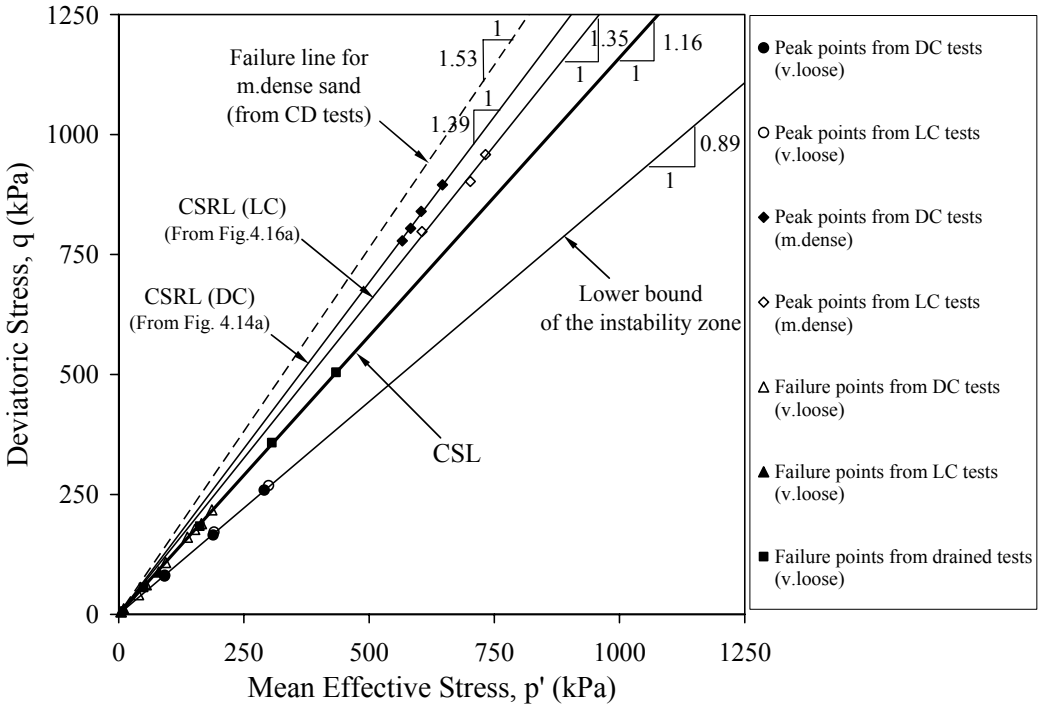

Fig. 4.19(a)

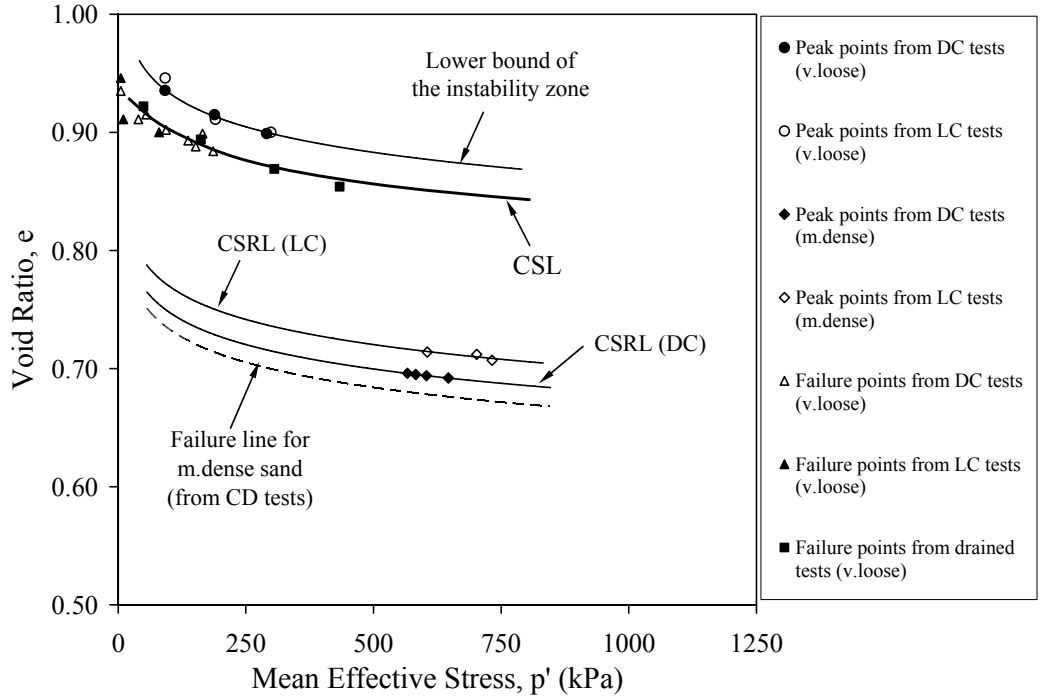

Fig. 4.19(b)

Fig. 4.19 Summary of undrained tests conducted under deformation-controlled and load-controlled loading modes: (a) *q-p'* plane; (b) *e-p'* plane

4.5 Comparison of Plane-Strain and Triaxial Tests

Many valuable comparisons between triaxial and plane-strain test results have been reported in the past (Cornforth, 1964; Lee & Shubeck, 1971; Marachi et al., 1981; Alshibli et al., 2003). It has been shown that the shear strength of granular soils under plane-strain conditions is higher than that under axisymmetric stress conditions. It has also been established that the difference between plane-strain test results and triaxial test results becomes higher with increasing soil density (Cornforth, 1964; Rowe, 1969; Lee, 1970; Green, 1971; Green & Reades, 1975; Oda et al., 1978). However, whether a unique critical state can be obtained under plane-strain and axisymmetric stress conditions should also be verified.

A comparison of the test results obtained under plane-strain conditions with those obtained under axisymmetric conditions by Chu et al. (2003) are presented in Table 4-3. It can be seen that the gradient of the CSL, CSRL, instability line and failure line obtained from plane-strain tests are lower than those obtained from triaxial tests within comparable range of void ratios.

Table 4-3 Comparison between plane-strain and triaxial test results

Line	Plane-strain			Triaxial		
	Void ratio	q/p'	φ'	Void ratio	q/p'	φ'
CSL	0.884 – 0.946	1.16	36.0°	0.864 – 0.972	1.35	33.4°
Instability Line	0.884 – 0.946	0.89 – 1.16	–	0.864 – 0.916	0.94 – 1.35	–
CSRL	0.696 – 0.692	1.39	–	0.643 – 0.695	1.50	–
Failure Line	0.665 – 0.678	1.53	49.7°	0.654 – 0.663	1.63	40.1°
Failure Line	0.760 – 0.784	1.35	43.4°	0.724 – 0.767	1.53	38.1°

The CSLs and the FLs for medium dense sand determined under plane-strain and axisymmetric conditions are also compared in Fig. 4.20. The ILs are also plotted in Fig. 4.20. It can be seen that the FL, CSL and IL obtained from plane-strain tests are different from that obtained from triaxial tests on both *q-p'* and *e-log p'* planes. It should be particularly noted that the gradient of the CSL under plane-strain and triaxial conditions is different. The gradient of the CSL on the *q-p'* plane for plane-strain conditions is 1.16 whereas the gradient of the CSL for axisymmetric conditions is 1.35. In terms of friction angle, φ'_{cs} is 36.0° under the plane-strain

condition and 33.4° under the triaxial condition. It should also be noted that the failure line determined under triaxial conditions is above the failure line under plane-strain conditions, as shown in Fig. 4.20(a). However, in terms of friction angle, φ'_{tri}' is 40.1° and φ'_{ps} is 49.7°. Therefore, under plane-strain or three dimensional conditions, φ' may not be a good failure parameter.

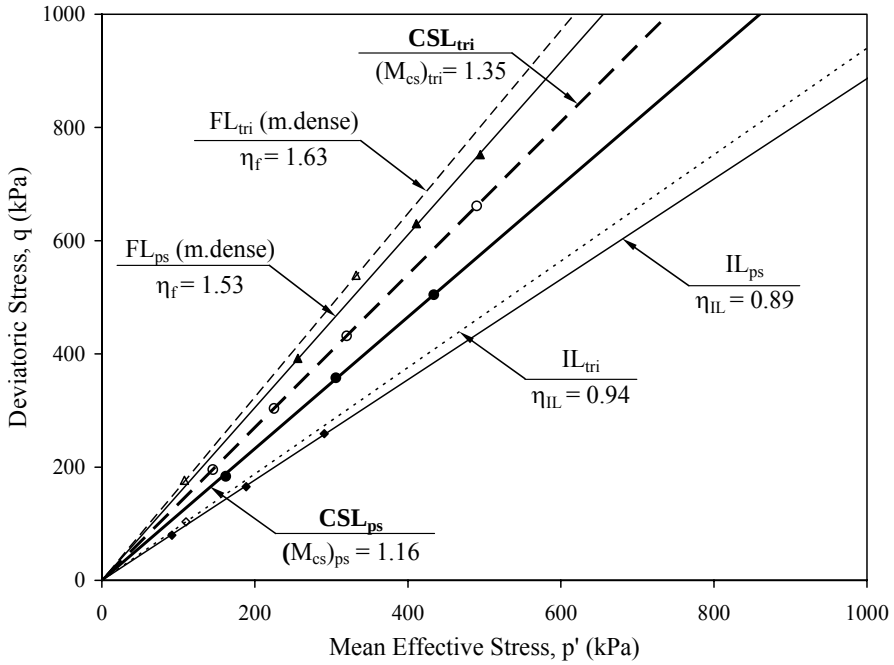

Fig. 4.20(a)

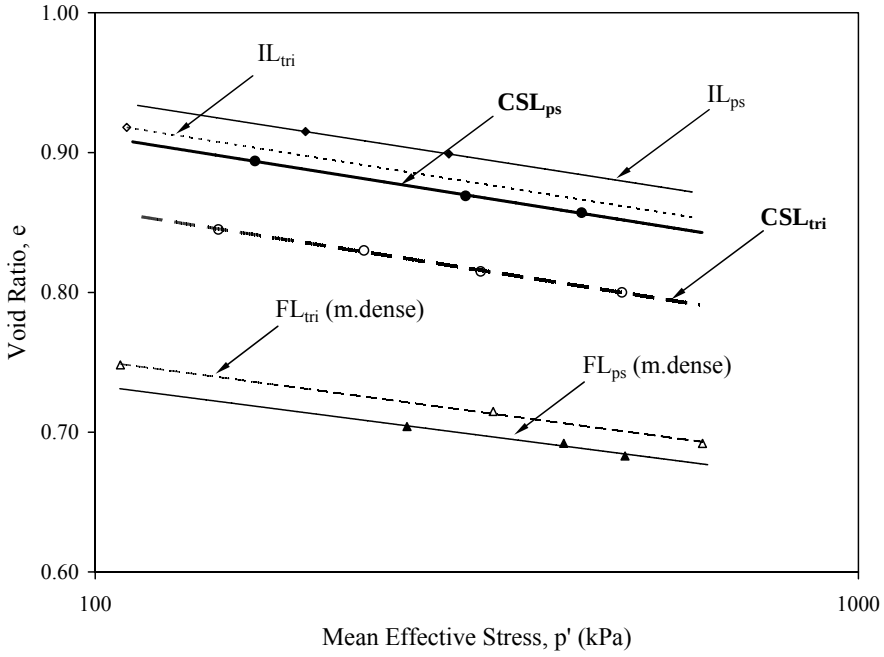

Fig. 4.20(b)

Fig. 4.20 Comparison of plane-strain and triaxial tests: (a) *q-p'* plane; (b) *e-log p'* plane

The failure states obtained from plane-strain tests and triaxial tests under drained conditions are further compared in Fig. 4.21. It can be observed from Fig. 4.21(a) that the relationships between effective stress ratio at failure, η_f, and void ratio, e_c, determined by plane-strain and triaxial tests are different. The friction angles obtained from plane-strain and triaxial tests are also different, as shown in Fig. 4.21(b). The higher the void ratio, the smaller the difference between the friction angles.

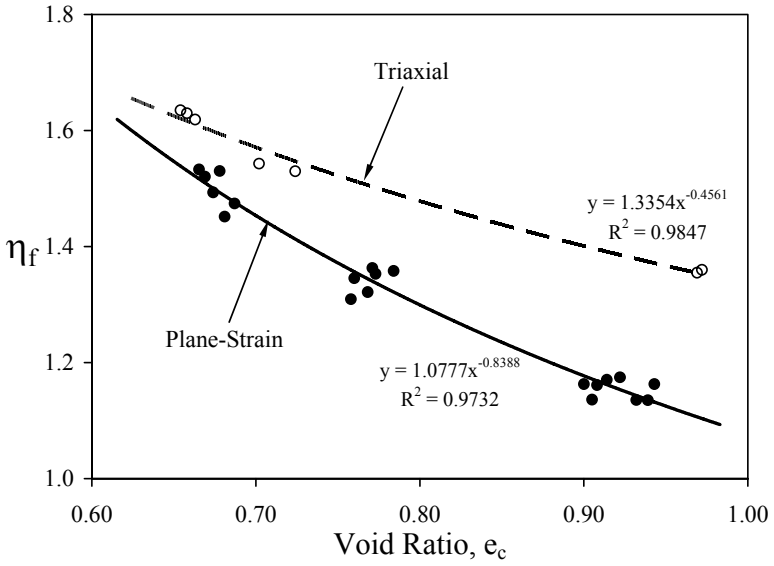

Fig. 4.21(a)

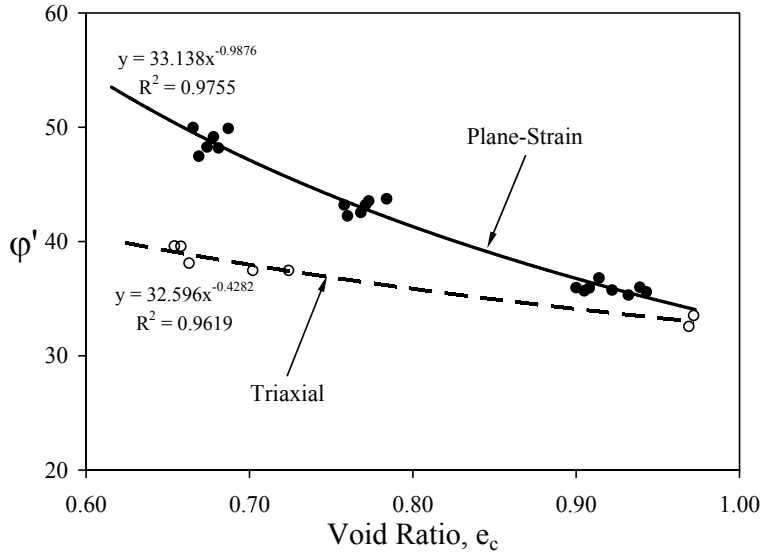

Fig. 4.21(b)

Fig. 4.21 Comparison of failure states under plane-strain and axisymmetric conditions: (a) relationship between η_f and e_c; (b) relationship between φ' and e_c

4.6 Shear Band Formation

4.6.1 Introduction

The objective of this research was not to investigate the evolution or to measure the thickness of shear bands. Therefore, sophisticated techniques such as stereophotogrammetry, *X*-ray Computed Tomography and Digital Image Correlation were not used in this study. Nevertheless, during a plane-strain test, the shear band formation process was monitored by taking photos at a close time interval using a high resolution digital camera. Grid lines were marked on the surface of the specimen facing the camera to facilitate the observation of the shear band. The occurrence of the shear bands was also detected by comparing the σ_2 versus ε_1 curves obtained from the four individual pressure transducers used to measure σ_2.

It was shown in sections 4.3 and 4.4 that shear bands affect the stress-strain behaviour of medium loose to medium dense specimens under plane-strain conditions. Moreover, the failure mechanism of medium dense specimens is closely related to the shear band formation. In this section typical stress-strain curves obtained from drained and undrained plane-strain tests are presented and the methods used to detect shear bands are described. Typical modes of shear bands obtained from plane-strain tests are also presented.

4.6.2 Drained Tests

4.6.2.1 Medium Dense Sand

The results of Test CK_0D03 conducted on medium dense specimen (e_c = 0.699) under a drained condition have been presented in Fig. 4.1. During the test, photos were taken continuously at a time interval of 2 minutes. The photographs taken during the test (points 0 – 10) are given in Appendix C (Fig. C.1). Selected photos around the formation of shear band are also shown in Fig. 4.22(a). The points 0 to 10 refer to the points marked on the stress-strain curves shown in Fig. 4.22.

The σ_2 versus ε_1 curves obtained from the four load cells are presented in Fig. 4.22(b). It can be seen that at point 4(O), the σ_2 values measured by each load cell start to diverge. Compared with the photos shown in Fig. 4.22(a), the shear band became visible at point 5(B), which was one point after point 4(O). Therefore, point 4(O), where σ_2 starts to diverge can be used as an indicator for the onset of the shear band. As shown in Fig. 4.22(c), point 5(B) is at the peak of the q-ε_1 curve. After point 6(F), strain softening occurred (Fig. 4.22(c)). The ε_v versus ε_1 curve is shown in Fig. 4.22(d). No obvious indication of the shear band occurrence can be seen from Fig. 4.22(d). Similar observations were made for all other drained tests conducted on medium dense and medium loose specimens. Based on the results, it may be concluded that shear bands occur at the point where the peak deviatoric stress is about to be reached. Strain softening occurs after shear bands have developed. Although by observation, strain softening occurs after the development of shear band, in terms of mechanisms it is still difficult to conclude whether strain softening is a result of shear band.

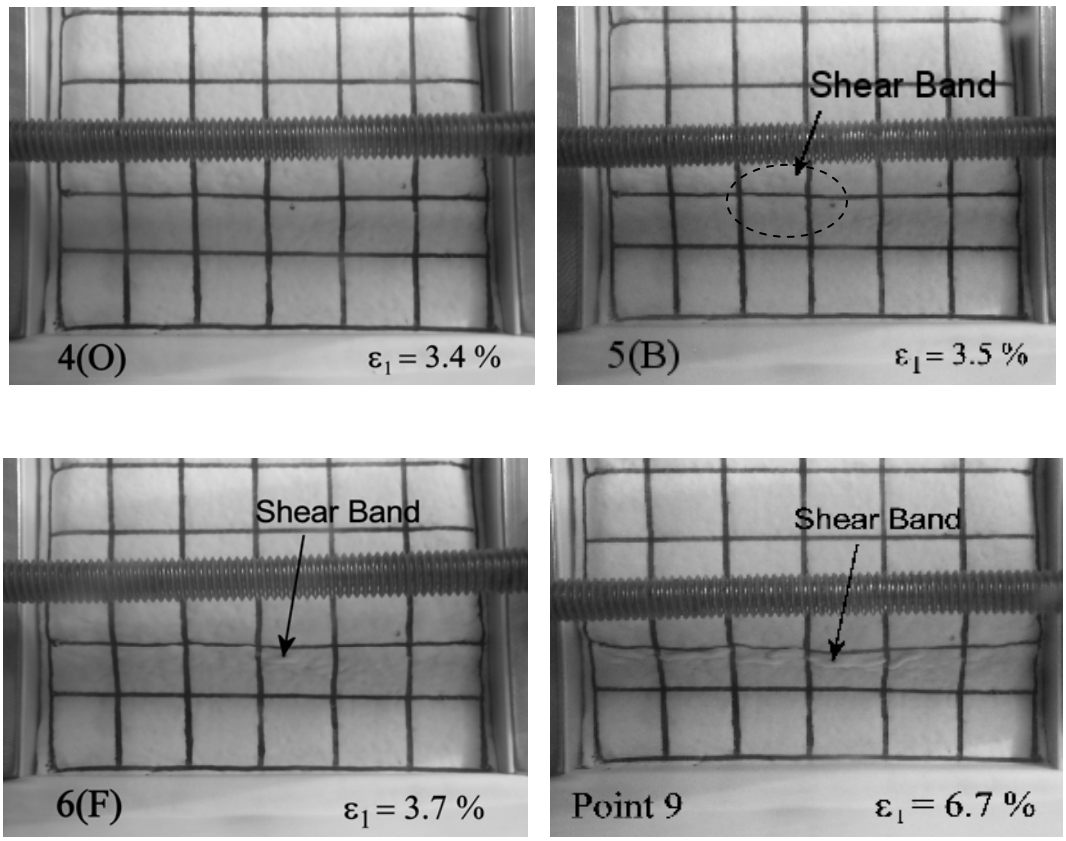

Fig. 4.22(a)

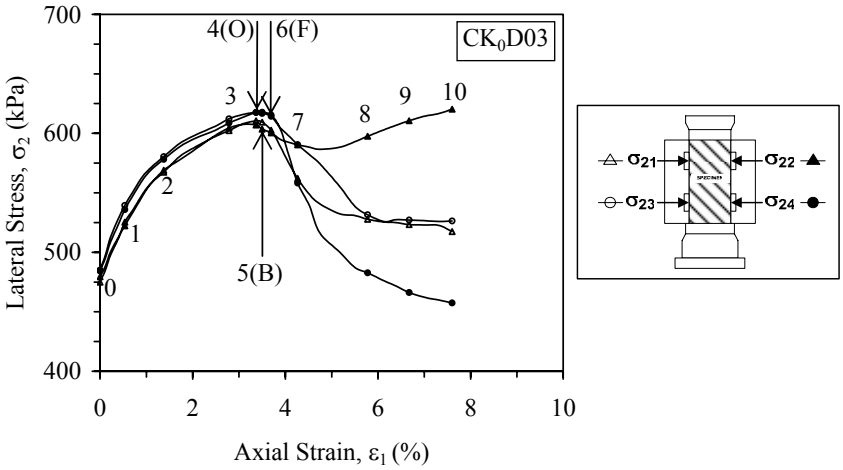

Fig. 4.22(b)

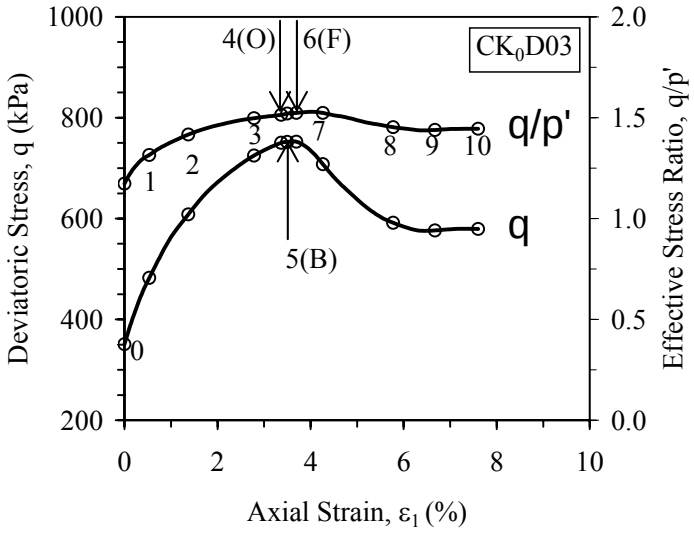

Fig. 4.22(c)

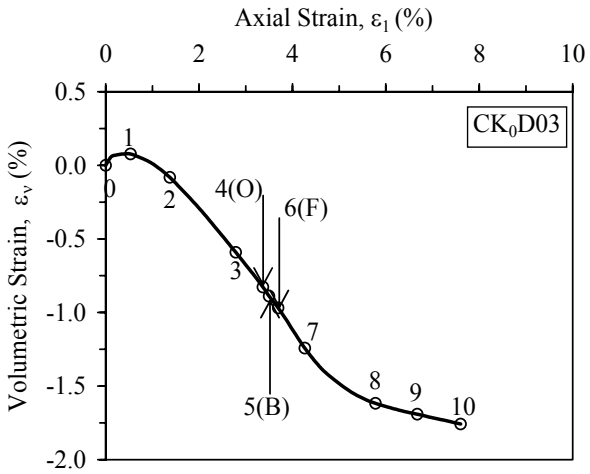

Fig. 4.22(d)

Fig. 4.22 Shear band development in Test CK_0D03: (a) selected photos; (b) σ_2 versus ε_1 curves; (c) q versus ε_1 and q/p' versus ε_1 curves; (d) ε_v versus ε_1 curves

The photos of the shear band developed in Test CK_0D03 are shown in Fig. 4.23. The photos were taken after the cell was dismounted and a suction was applied to hold the specimen. It can be seen from Fig. 4.23 that the specimen slides towards the σ_3 direction. Therefore, the shear band on the σ_3 plane is essentially horizontal and the shear band on the σ_2 plane is inclined (Fig. 4.23).

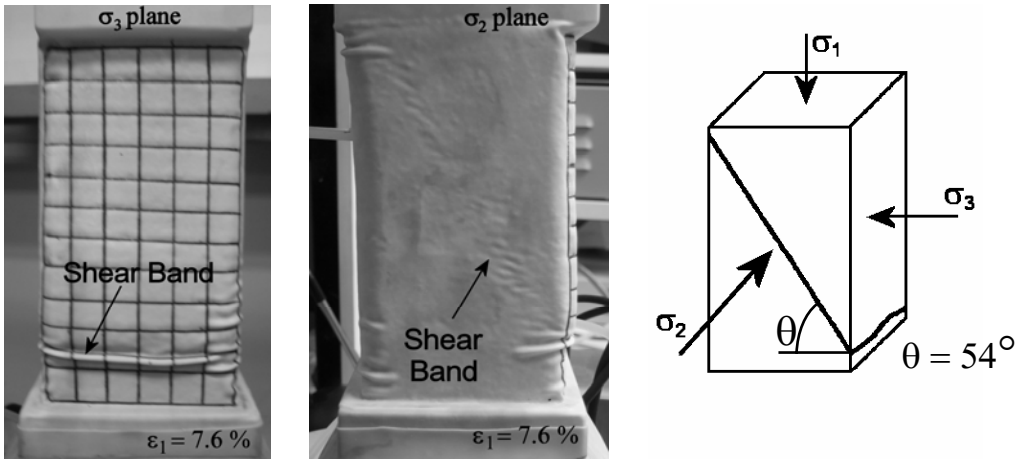

Fig. 4.23 The shear band observed at the end of Test CK_0D03

4.6.2.2 Very Loose Sand

The results of drained test CK_0D08, conducted on very loose specimen (e_c = 0.914) have been presented in Fig. 4.3. The photographs taken during the test are presented in Appendix C (Fig. C.2). Two selected photos are also shown in Fig. 4.24(a).

The σ_2 versus ε_1 curves obtained from four individual load cells are shown in Fig. 4.24(b). It can be seen that all the four curves are close to each other until the end of the test. There was no visible shear band observed during the entire duration of the test (see Fig. 4.24(a) or Fig. C.2 in Appendix C). The q-ε_1 and q/p'-ε_1 curves are shown in Fig. 4.24(c). No strain softening has occurred either. The ε_v versus ε_1 curve is given in Fig. 4.24(d). The volumetric strain approached a constant value at the end of shearing, thus indicating that the critical state was achieved in Test CK_0D08. Similar observations were made from other drained tests conducted on very loose sand. Based on the evidences stated above, it may be concluded that the development of shear band does not dominate the drained behaviour of very loose

sand, even though there might be some possibility for shear band to develop. This is consistent with the observations made in triaxial tests.

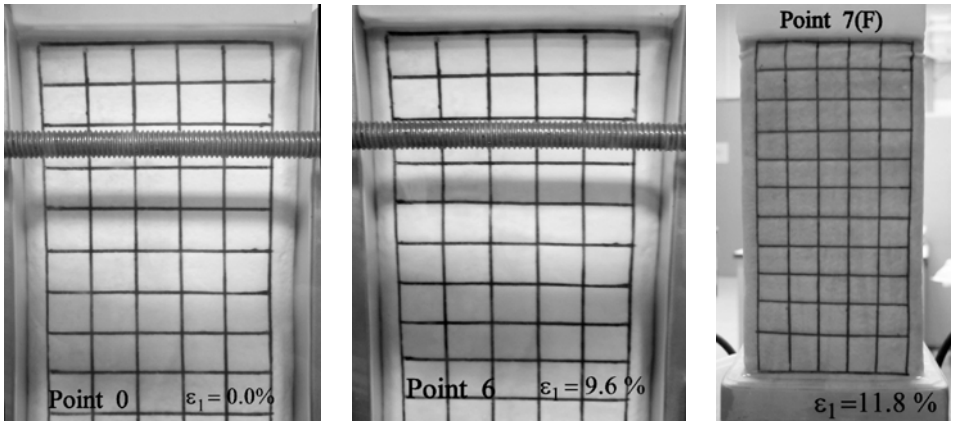

Fig. 4.24(a)

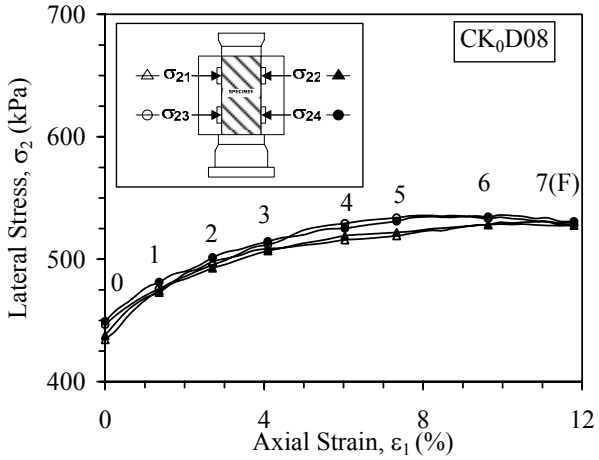

Fig. 4.24(b)

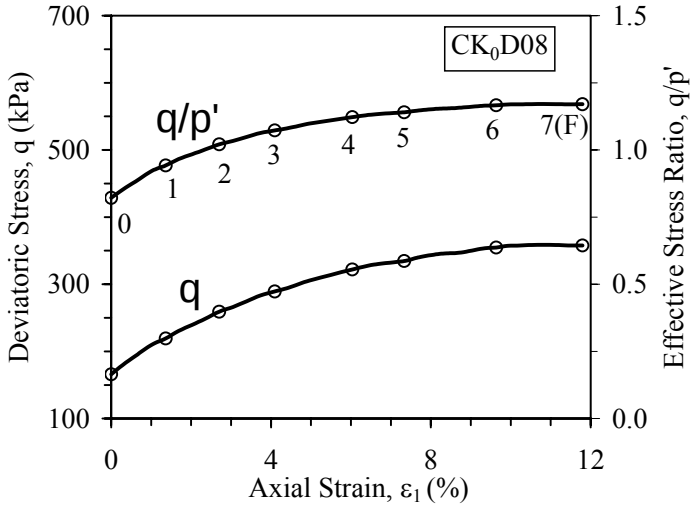

Fig. 4.24(c)

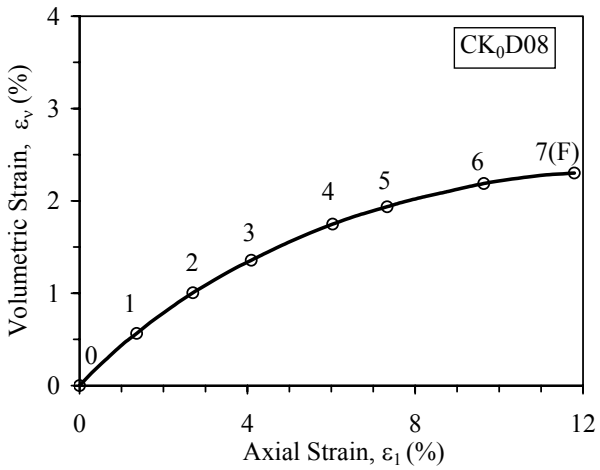

Fig. 4.24(d)

Fig. 4.24 Test CK_0D08: (a) selected photos; (b) σ_2 versus ε_1 curves; (c) q versus ε_1 and q/p' versus ε_1 curves; (d) ε_v versus ε_1 curves

4.6.3 Undrained Tests

4.6.3.1 Medium Dense Sand

The results of Test CK_0U02 conducted on medium dense specimen (e_c = 0.695) under an undrained condition have been presented in Fig. 4.14. The photographs taken during the test are given in Appendix C (Fig. C.3). Selected photos around the formation of shear band are also shown in Fig. 4.25(a).

It can be seen from the σ_2 versus ε_1 curves shown in Fig. 4.25(b) that σ_2 starts to diverge at point 3(O). The onset of shear band formation, as shown in Fig. 4.25(a), is point 5(B,P). This point coincides with the peak deviatoric stress, as shown in Fig. 4.25(c). On the pore water pressure curve, shown in Fig. 4.25(d), the pore water pressure change seems to become gentle at the point of shear band formation and eventually approaches a constant value (Fig. 4.25(d)).

The shear band observed at the end of Test CK_0U02 is shown in Fig. 4.26. Similar to the specimen in Test CK_0D03 (see Fig. 4.23), the specimen in Test CK_0U02 slides towards the σ_3 direction, as shown in Fig 4.26.

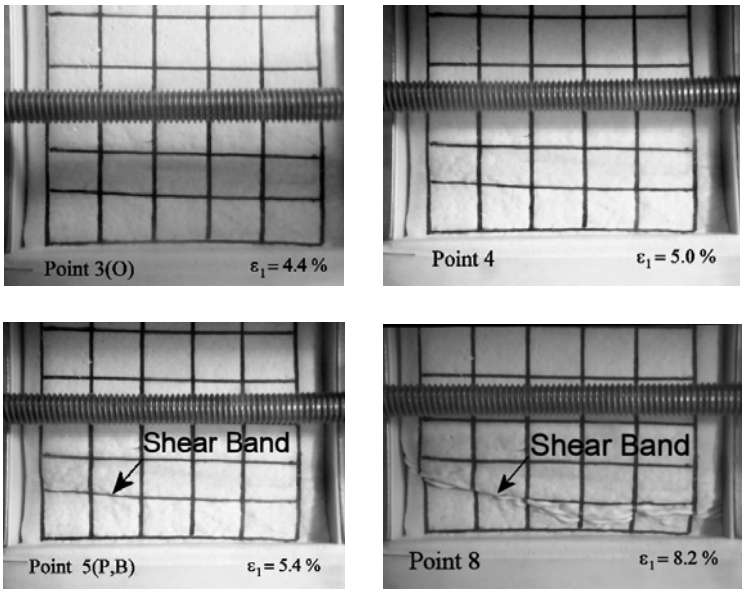

Fig. 4.25(a)

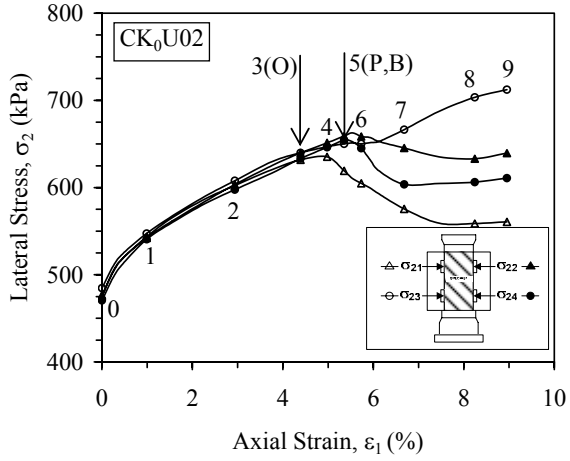

Fig. 4.25(b)

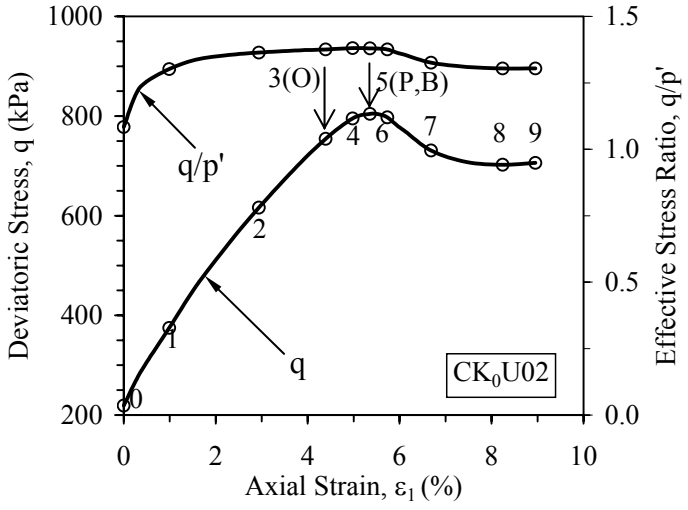

Fig. 4.25(c)

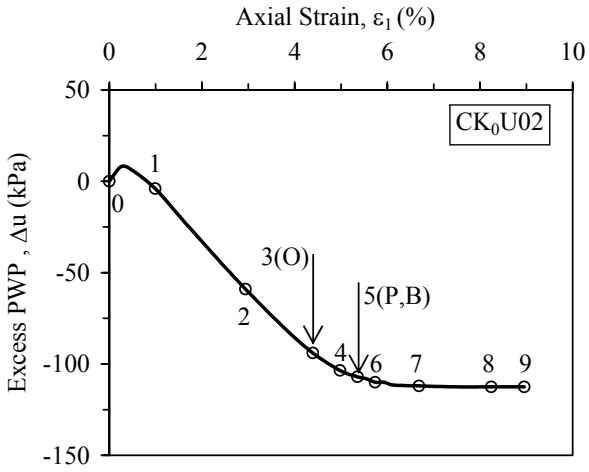

Fig. 4.25(d)

Fig. 4.25 Shear band development in Test CK_0U02: (a) selected photos; (b) σ_2 versus ε_1 curves; (c) q versus ε_1 and q/p' versus ε_1 curves; (d) Δu versus ε_1 curve

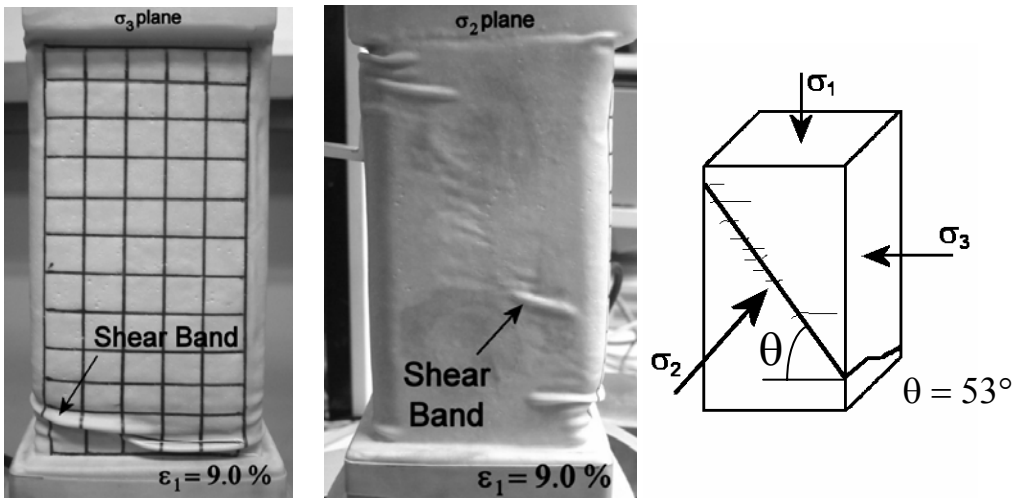

Fig. 4.26 The shear band observed at the end of Test CK_0U02

4.6.3.2 Very Loose Sand

The results of Test CK_0U05, conducted on very loose specimen have been presented in Fig. 4.11. The void ratio of the specimen after K_0 consolidation was e_c = 0.915. Please note that e_c = 0.915 is higher than the critical void ratio e_{cr} = 0.884 determined in Test CK_0U11 (see Fig. 4.11). Therefore, strain softening behaviour was observed in Test CK_0U05. The photographs taken during the test are given in Appendix C (Fig. C.4). Two photographs of the specimen taken at the end of the test are also shown in Fig. 4.27(a). It can bee seen from Fig. 4.27(a) that there was

no distinct shear band observed in Test CK_0U05. Only a few diffuse deformations were detected at the end of the test on the specimen surface. Similar *'wrinkling'* modes of localization have also been observed in loose specimens by Han & Vardoulakis (1991). They have reported however, that the specimens with this type of deformations can still be considered as homogeneous.

The σ_2 versus ε_1 curves obtained from Test CK_0U05 are shown in Fig. 4.27(b). It can be seen that there is little variation in σ_2 values obtained from the four different load cells. The q-ε_1 and q/p'-ε_1 curves of Test CK_0U05 are also shown in Fig. 4.27(c). It can be observed from the q-ε_1 curve that strain softening occurred at small axial strain (Fig. 4.27(b)). Based on all the evidences stated above, it may be concluded that shear band did not occur in Test CK_0U05. Therefore, strain softening observed in Test CK_0U05 is an element behaviour. Similar observations were made in all the undrained tests conducted on very loose specimens with $e_c > e_{cr}$.

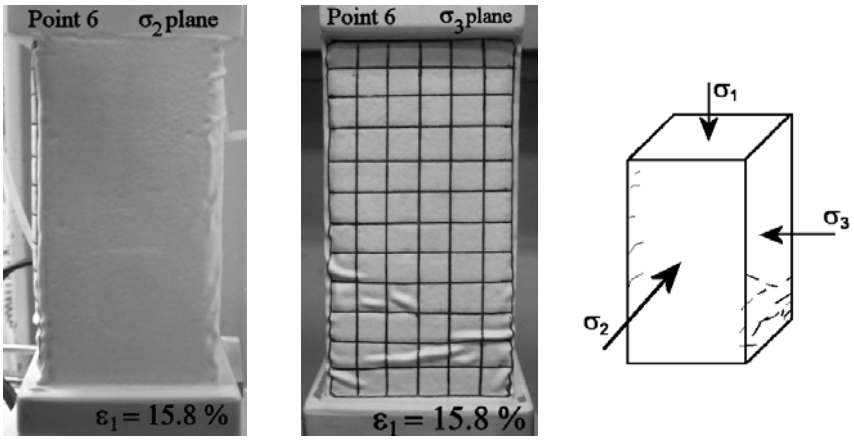

Fig. 4.27(a)

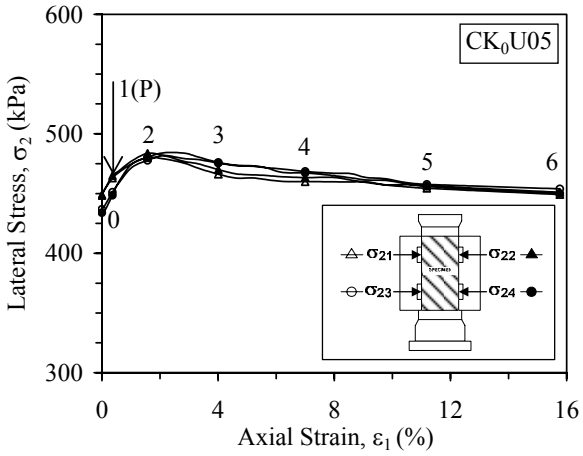

Fig. 4.27(b)

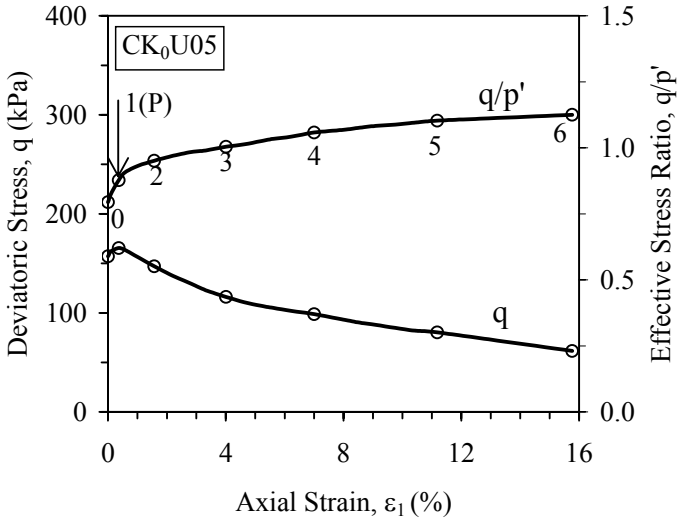

Fig. 4.27(c)

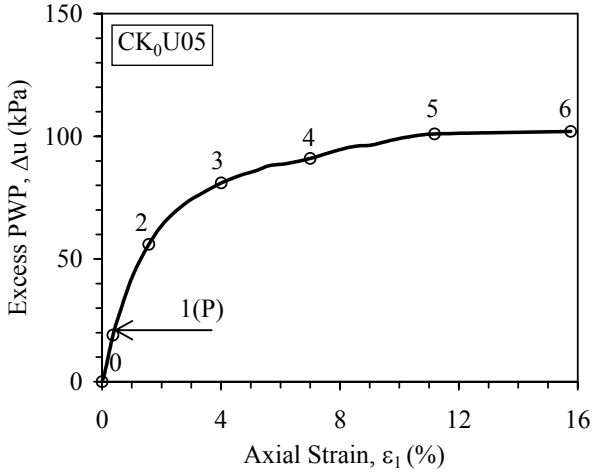

Fig. 4.27(d)

Fig. 4.27 Test CK_0U05: (a) selected photos; (b) σ_2 versus ε_1 curves; (b) q versus ε_1 and q/p' versus ε_1 curves; (c) Δu versus ε_1 curve

The results of Test CK_0U12, conducted on very loose specimen have been presented in Fig. 4.11 and discussed in Section 4.4.1.1. The void ratio of the specimen after K_0 consolidation was $e_c = 0.868$ ($Dr_c = 12.5\%$), which is lower than $e_{cr} = 0.884$. Therefore, strain hardening behaviour was initially observed in Test CK_0U12. The photographs taken during the test are given in Appendix C (Fig. C.5). Selected photographs of the specimen in Test CK_0U12 are also shown in Fig. 4.28(a). It can be seen that the shear band became visible on the specimen surface at point 3(B), which is just before the peak of the q-ε_1 curve (point 4(P)), as shown in Fig. 4.28(c). After point 4(P), the banding softening has occurred.

The σ_2 versus ε_1 curves obtained from the four load cells are presented in Fig. 4.28(b). It can be seen that at point 2(O), the σ_2 value measured by each load cell starts to diverge. Compared with the photos shown in Fig. 4.28(a), the shear band became visible at point 3(B), which was one point after point 2(O). Therefore, point 2(O), where σ_2 starts to diverge indicates the onset of the shear band. The Δu-ε_1 curve of Test CK_0U12 is shown in Fig. 4.28(d). It is observed that the change in pore water pressure ceased after the shear band was fully developed.

The photograps of the shear band observed at the end of Test CK_0U12 are shown in Fig. 4.29. Similarly to the other tests in which shear bands occurred, the specimen in Test CK_0U12 slides towards the σ_3 direction.

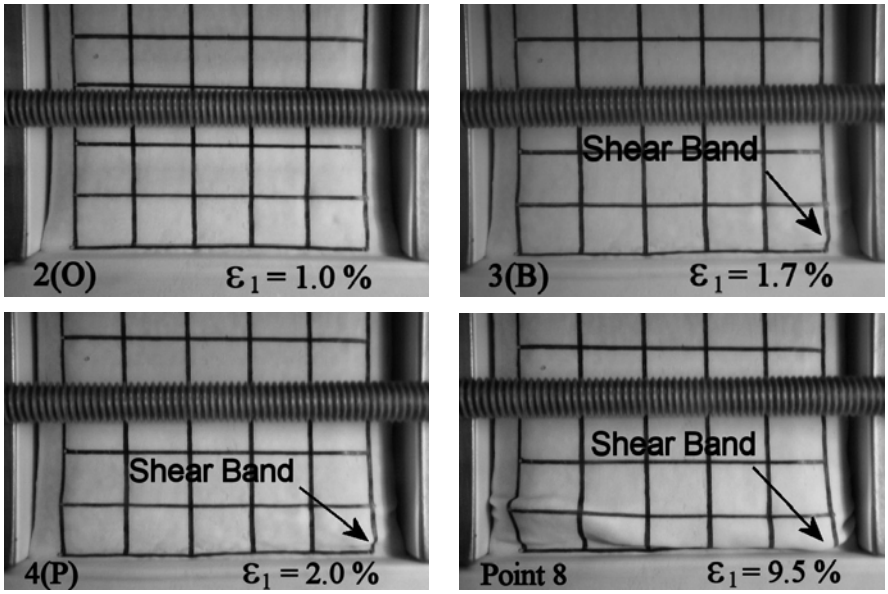

Fig. 4.28(a)

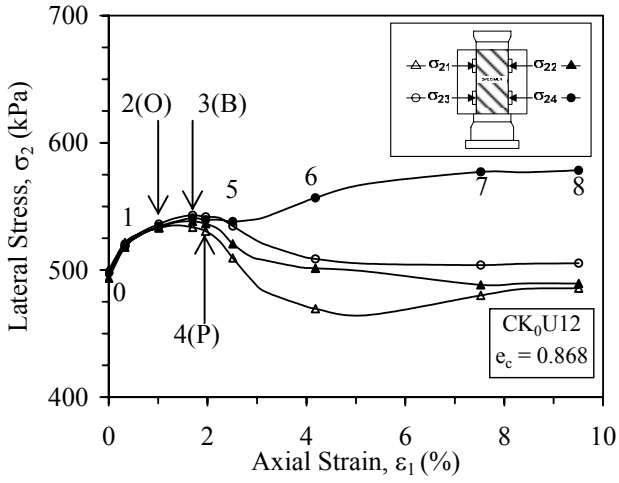

Fig. 4.28(b)

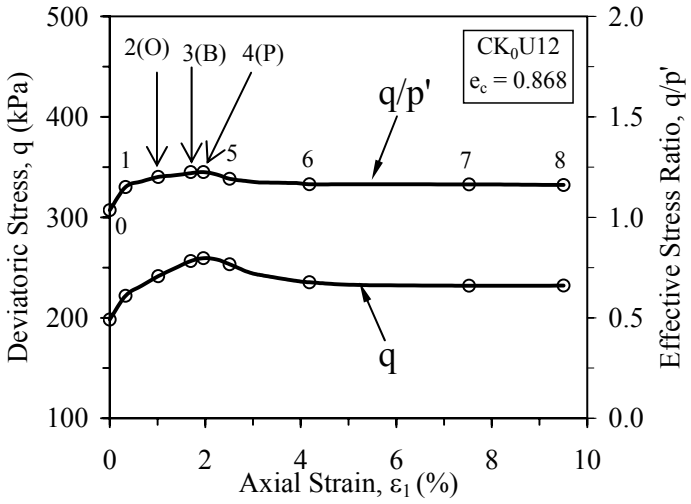

Fig. 4.28(c)

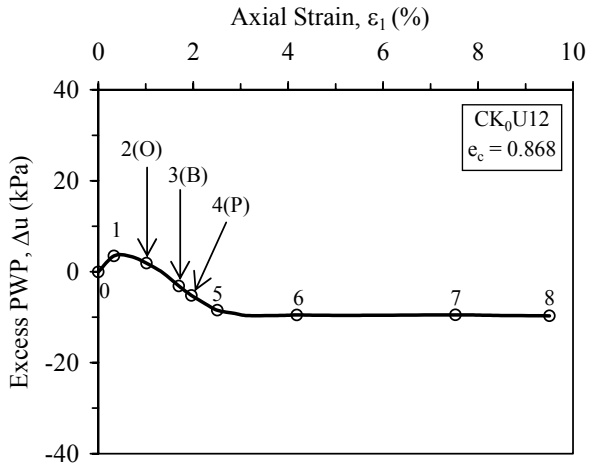

Fig. 4.28(d)

Fig. 4.28 Shear band development in Test CK_0U12: (a) selected photos; (b) σ_2 versus ε_1 curves; (b) q versus ε_1 and q/p' versus ε_1 curves; (c) Δu versus ε_1 curve

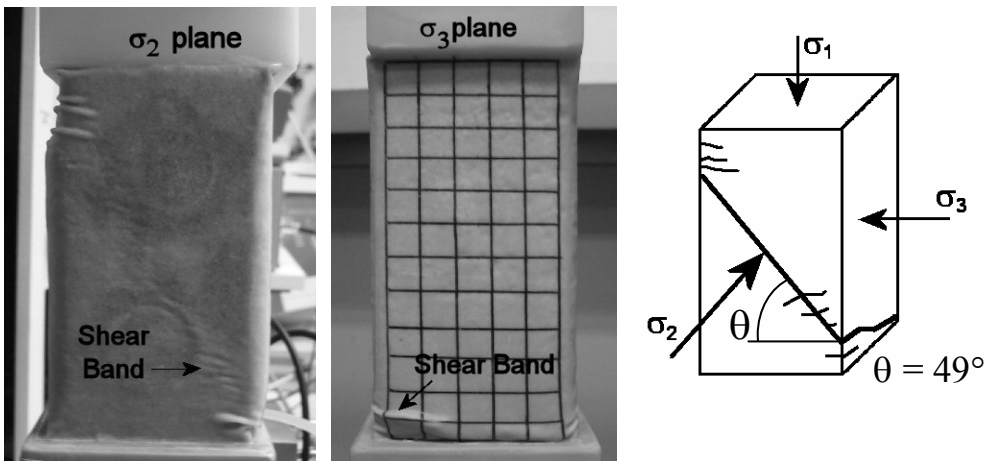

Fig. 4.29 The shear band observed at the end of Test CK_0U12

4.6.4 Shear Band Description

The shear band developments in Test CK_0D03 conduceted under drained conditions and in Tests CK_0U02 & CK_0U12 conducted under undrained conditions have been described in the preceding section. The photographs of shear bands observed in two more tests, Test CK_0D05L and Test CK_0U03L are also presented in Fig. 4.30. Tthe photos shown in Fig. 4.30 were taken at the end of each test when the cell was dismounted and a suction was applied to hold the specimen. As described earlier, the shear bands on the σ_3 plane are nearly horizontal bands and the shear bands on the σ_2 plane are inclined shear bands with an angle θ (Fig. 4.30).

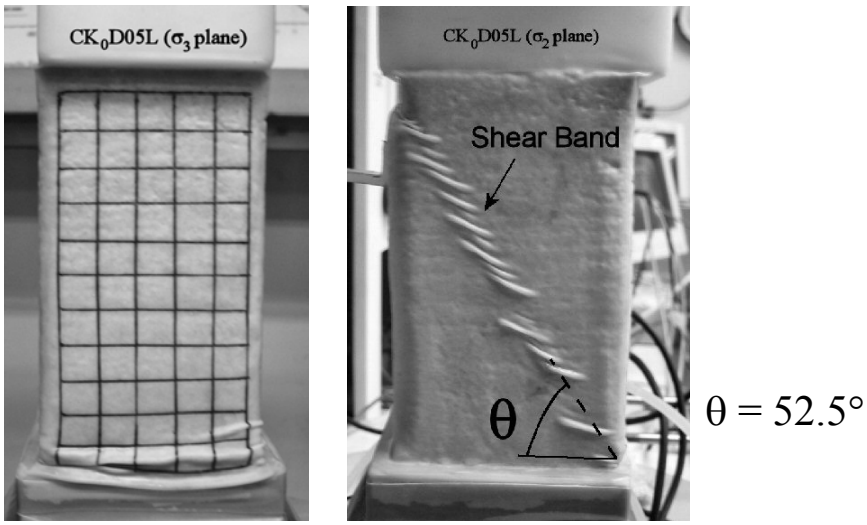

Fig. 4.30(a)

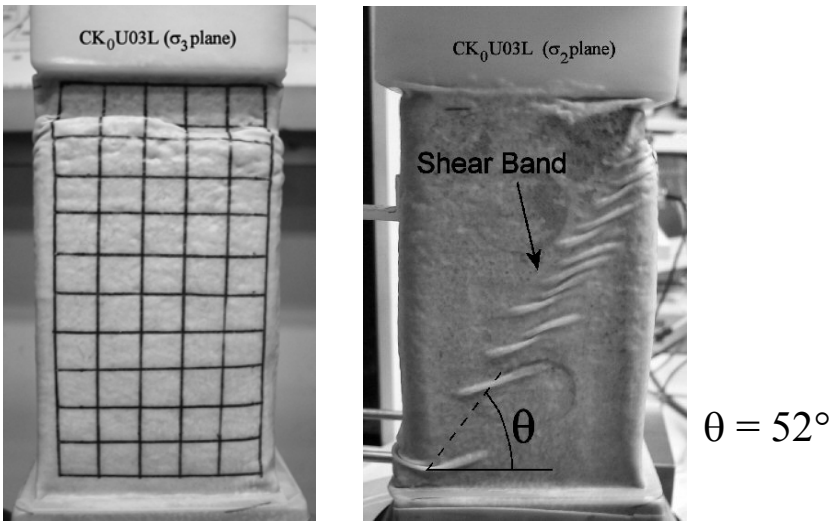

Fig. 4.30(b)

Fig. 4.30 Examples of shear bands observed at the end of plane-strain tests: (a) Test CK_0D05L; (b) Test CK_0U03L

After each test, the surfaces where σ_2 was acting were examined. The liquid rubber technique used in this research to minimize bedding and membrane penetration errors (described in Chapter 3) helped to analyze the shear bands because shear bands created fracture lines in the liquid rubber layer, as shown in Fig. 4.31. Therefore, the inclination of the shear bands along the σ_2 surface at the end of test could be measured.

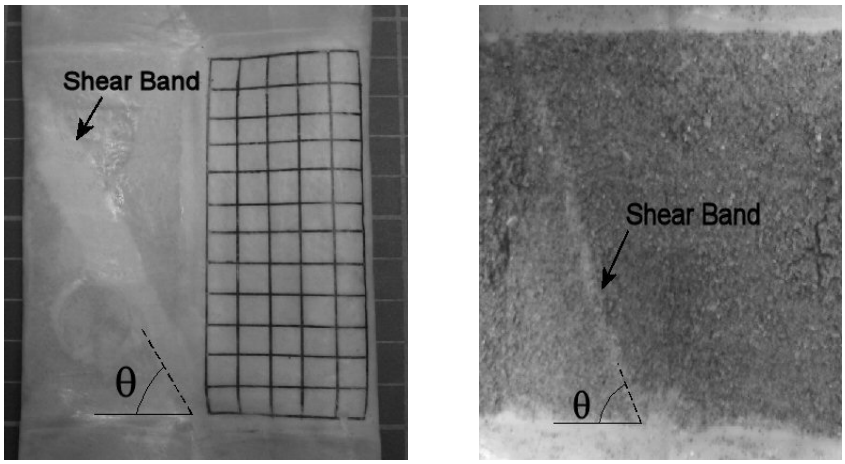

(a) (b)

Fig. 4.31 Photographs of the membrane at the end of Test CK_0D02: (a) the outer surface; (b) the inner surface

For plane-strain tests conducted on medium loose to dense sand the angles θ are between 49.6° and 58.6°, giving an average value of 56°. The typical mode of shear band obtained in this study is illustrated in Fig. 4.32. It has been observed that the shear band inclination is not significantly affected by confining pressure or relative density.

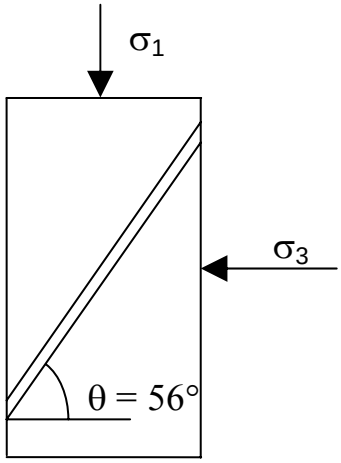

Fig. 4.32 Typical mode of the shear band observed in plane-strain tests

For comparison, the Coulomb, Roscoe and Arthur inclination solutions for Changi sand were computed. The average shear band inclinations predicted by these solutions are presented in Table 4-4. The φ' and ψ_s values were taken at peak deviatoric stress so that the comparison among the predictions and measured values would be consistent. For Changi sand, shear band inclinations were best predicted by the Roscoe solution.

Table 4-4 Comparison among the Coulomb, Roscoe and Arthur solutions for Changi sand

Density state*	φ'	ψ_s	Coulomb $45° + \varphi'/2$	Roscoe $45° + \psi_s/2$	Arthur $45° + (\varphi' + \psi_s)/4$
Medium Loose	43.4	14.0	66.7	52.0	59.4
Medium dense	49.7	37.2	69.9	63.6	66.7

* The classification of relative density is given in Appendix B

4.6.5 Discussion

The above results indicate that when a shear band occurs, the lateral stress distributions become highly non-uniform. Therefore, the point where the σ_2 curves start to diverge indicates the point where shear band has occurred. The results obtained from drained and undrained plane-strain tests also show that the shear band develops in the specimen earlier than its physical appearance on the membrane surface. It is also observed that shear bands in plane-strain tests are initiated before the peak deviatoric stress. Furthermore, strain softening always occurs after the development of shear bands. However, in terms of mechanism, it is difficult to conclude whether strain softening is a result of the shear band.

The results obtained from plane-strain tests have shown that shear bands do not occur in very loose specimens under drained conditions. Under undrained conditions, shear bands can also develop unless the specimen is looser than the void ratio at the critical state (e_{cr}).

4.7 Summary

The drained and undrained stress-strain and strength characteristics of Changi sand under plane-strain conditions have been studied. The effect of loading mode, i.e., whether the test is conducted under deformation-controlled or load-controlled loading mode has also been investigated. Based on the experimental results, the critical state line (CSL), failure lines (FL), instability lines (IL), and constant stress ratio lines (CSRL) under plane-strain conditions have been established. The results presented in Chapter 4 can be summarized as follows:

- A relationship between the gradient of the failure line, η_f, and the consolidated void ratio, e_c, is established. The value of η_f ranges from 1.53 for medium dense sand to 1.16 for very loose sand. The slope of the critical state line is M_{cs} = 1.16. The corresponding friction angle, φ', is in the range from 36.0° to 49.7°. The φ' value is 7% to 19% higher than that obtained from triaxial tests for the soil at the same void ratio. It is particularly noted that critical state line on both *q-p'* and *e-p'* planes obtained under the plane-strain conditions is different from that obtained under the triaxial conditions. In terms of friction angle, the friction angle at the critical state measured under plane-strain conditions ($(\varphi_{cs}')_{ps}$ = 36.0°) is also different from that obtained under axisymmetric conditions ($(\varphi_{cs}')_{tri}$ = 33.4°).

- Plane-strain tests under both deformation-controlled and load-controlled conditions were conducted. A comparison of the two tests indicate that the failure line and the critical state line on both the *q-p'* and the *e-p'* planes are not affected by the loading mode. However, the post-peak behaviour of sand in both drained and undrained tests is affected by the loading mode. Under a deformation-controlled loading mode, strain softening develops, whereas under a load-controlled loading mode, instability occurs.

- When very loose sand is tested under undrained conditions, strain softening, strain hardening or critical state behaviour can be obtained. Specimens with $e_c > e_{cr}$ exhibit strain softening behaviour, whereas specimen with $e_c < e_{cr}$ experience strain hardening behaviour. A critical state behaviour is observed when $e_c = e_{cr}$. The critical void ratio determined under plane-

strain conditions for p_c' = 200 kPa is e_{cr} = 0.884. When medium dense sand is sheared under an undrained condition the effective stress path approaches a constant stress ratio line (CSRL). The gradient of the CSRL determined under plane-strain conditions is M_L = 1.39. However, as a result of shear band formation, a peak state followed by an ultimate state is eventually obtained from each test conducted on medium dense sand.

- A series of plane-strain tests conducted on very loose sand under undrained conditions indicate that the instability line under plane-strain conditions can be defined using the method suggested by Lade (1993) for axisymmetric conditions. Similar to the observations made under axisymmetric conditions, the instability line is not unique, but varies with the void ratio of the sand. The smaller the e_c, the higher the gradient of the instability line. However, the position of the instability line does not seem to be affected by the loading mode, that is, whether the tests are conducted under a deformation-controlled mode or a load-controlled mode.

- Shear bands will eventually occur during plane-strain tests on medium loose and medium dense sand under drained conditions. However, shear bands do not always occur when very loose sand is tested under drained plane-strain conditions. Under undrained conditions, shear bands can also develop unless the specimen is looser than the void ratio at the critical state under a given mean effective stress. The measured shear band inclination for the Changi sand is in the range from 49.6° to 58.6°, giving an average value of 56°. Shear band inclinations were best predicted by Roscoe's solution.

CHAPTER 5

ASYMPTOTIC & STRAIN SOFTENING BEHAVIOUR OF SAND

5.1 Introduction

The stress-strain behaviour of soils is path dependent. The stress-strain response of soil can be entirely different when a specimen is sheared under different paths. The influence of paths on the stress-strain behaviour of soils has been studied by conducting stress path tests (Lade & Duncan, 1976; Lo & Lee, 1990) and strain path tests (Chu, 1991; Eliadorani, 2000; Leong, 2001; Loke, 2004; Lancelot et al., 2004). However, most of the studies were carried out under axisymmetric conditions. No study on the stress-strain behaviour of sand along strain path testing has been conducted under plane-strain conditions.

Another important characteristic of sand is strain softening. Strain softening is a phenomenon when the shear resistance decreases with the development of axial strain after the deviatoric stress reaches its peak value. Previous studies on strain softening behaviour have been reviewed in Chapter 2. As discussed by Chu et al. (1992), under three dimensional loading conditions, a decrease in shear resistance cannot be judged simply from the stress-strain curve. Therefore, Valanis' strain softening definition needs to be used to define the occurrence of strain softening (Valanis, 1985).

The objective of this chapter is to study the strain softening of sand in strain path testing under plane-strain conditions. The results of the strain path ($d\varepsilon_v/d\varepsilon_1$ =

constant) tests conducted on very loose to medium dense sand are presented. The asymptotic behaviour of granular soil under plane-strain conditions is investigated. The Lade's criterion that was used to define failure is discussed. Finally, various factors affecting the occurrence of strain softening under plane-strain conditions are described.

5.2 Testing Programme

The behaviour of sand under plane-strain condition in the present study was investigated under a wide range of linear strain paths. The strain paths used in the experiments, in the form of strain increment ratios $(d\varepsilon_v/d\varepsilon_1)$ are schematically presented in Fig. 5.1.

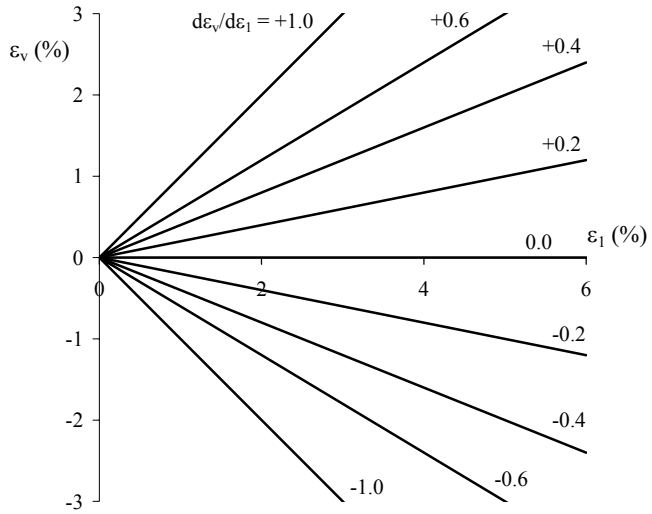

Fig. 5.1 Typical range of imposed strain paths under plane-strain conditions

All the specimens were K_0 consolidated under the designed initial effective confining pressures and sheared along either a dilative $(d\varepsilon_v/d\varepsilon_1 < 0)$ or compressive $(d\varepsilon_v/d\varepsilon_1 > 0)$ strain increment path. To study the effect of the initial effective confining stress, tests with different initial confining stresses were conducted. The tests were carried out under both deformation-controlled and load-controlled modes with different strain rates. It should be pointed out that the back pressure level at the end of K_0 consolidation was taken as the datum and the decrease in pore water pressure was noted as negative. All the strain path tests conducted under plane-strain conditions are summarized in Table 5-1.

Table 5-1 Summary of strain path tests conducted under plane-strain conditions.

Test No	Preparation method	e_c	Dr_c (%)	Density state*	p_c' (kPa)	q_c (kPa)	$d\varepsilon_v/d\varepsilon_1$
SP01	WS	0.660	67	dense	202.1	226.4	
SP02	WS	0.684	61	m. dense	201.0	211.1	
SP03	WS	0.753	43	m. loose	200.2	196.0	-0.2
SP04	MT	0.897	5	v. loose	195.9	169.8	
SP25	WS	0.691	59	m. dense	402.6	433.2	
SP05	WS	0.677	62	m. dense	198.2	220.3	
SP06	WS	0.728	49	m. loose	199.2	200.7	
SP07	WS	0.781	35	m. loose	201.3	198.7	-0.4
SP08	MT	0.890	7	v. loose	200.6	172.4	
SP26	WS	0.731	48	m. loose	404.5	421.7	
SP09	WS	0.679	62	m. dense	200.0	222.4	
SP10	WS	0.754	42	m. loose	202.0	203.5	
SP11	WS	0.784	34	loose	200.4	190.1	
SP12	MT	0.887	8	v. loose	199.8	169.0	
SP27	WS	0.748	44	m. loose	451.0	476.2	
SP28	WS	0.750	43	m. loose	880.4	918.6	-0.6
SP29	WS	0.671	64	m. dense	703.3	777.3	
SP33L	WS	0.672	64	m. dense	201.7	227.0	
SP34L	WS	0.751	43	m. loose	202.0	203.8	
SP35L	WS	0.776	37	m. loose	199.6	194.0	
SP36L	MT	0.883	9	v. loose	199.4	170.0	
SP13	WS	0.682	61	m. dense	201.5	210.7	-1.0
SP14	WS	0.694	58	m. dense	202.9	218.1	
SP15	WS	0.759	41	m. loose	199.5	201.4	+0.2
SP16	MT	0.888	7	v. loose	197.8	174.3	
SP17	WS	0.682	61	m. dense	200.5	227.3	
SP18	WS	0.756	42	m. loose	202.9	203.5	+0.4
SP19	MT	0.878	10	v. loose	199.6	174.3	
SP20	WS	0.681	61	m. dense	206.2	226.4	
SP21	WS	0.754	42	m. loose	201.7	206.3	+0.6
SP22	MT	0.903	3	v. loose	197.5	171.9	
SP23	WS	0.686	60	m. dense	202.8	226.6	+1.0
SP24	WS	0.762	40	m. loose	196.2	196.7	
CK_0U01	WS	0.696	57	m. dense	97.7	93.1	
CK_0U02	WS	0.695	58	m. dense	201.9	218.8	
CK_0U03	WS	0.694	58	m. dense	298.8	329.1	0.0
CK_0U08	MT	0.902	4	v. loose	198.4	168.4	
CK_0U13	WS	0.692	58	m .dense	405.7	436.3	
SP42	WS	0.678	62	m. dense	200.8	223.3	changed
SP43	WS	0.771	38	m. loose	199.6	200.1	in steps

*The classification of relative density is given in Appendix B

5.3 Asymptotic Behaviour of Sand

It has been shown by Chu (1991) and Chu et al. (1992) that for medium dense specimens tested under strain path with $d\varepsilon_v/d\varepsilon_1 \geq 0$, strain hardening behaviour is observed. The effective stress paths in these tests approach asymptotically a straight line, called the constant stress ratio line (CSRL) by Chu et al. (2003). This type of behaviour had been termed as the asymptotic behaviour by Gudehus et al. (1977) to describe a response of soil along proportional stress/strain paths. The results presented by Gudehus et al. (1977) show that when a soil is sheared along some $\sigma_1'/\sigma_3' = const$ paths, the strain approach a $d\varepsilon_v/d\varepsilon_1 = const$ state, instead of a critical state. Experimental data presented by Topolnicki et al. (1990) on clay using a biaxial cell and Chu & Lo (1994) on sand using triaxial and multi-axial cells indicated further that when a soil is sheared along some $d\varepsilon_v/d\varepsilon_1 = const$ paths, the stress ratio will approach constant. Therefore, the asymptotic state may be defined as the state where a soil element deforms under a constant stress mobilized level and a constant dilatancy ratio state, that is when $q/p' = const$ and $d\varepsilon_v/d\varepsilon_1 = const$.

5.3.1 Medium Dense Sand

The influence of a strain path on the stress-strain behaviour of sand is clearly demonstrated in Fig. 5.2, where the results of a series of strain path tests conducted on medium dense sand with different strain increment ratios, $d\varepsilon_v/d\varepsilon_1$, are presented. The void ratios of specimens after K_0 consolidation, e_c, ranged from 0.677 to 0.695, corresponding to relative densities Dr_c = 58–62%. All the specimens were prepared by the WS method. It can be seen from Fig. 5.2(a) that for a given axial strain, the larger the strain increment ratio, the stiffer the stress-strain curve. Within the range of $d\varepsilon_v/d\varepsilon_1$ used, both strain hardening and strain softening was observed.

The excess pore water pressures developed in the tests are shown in Fig. 5.2(b). It can be seen that the larger the strain increment ratio imposed, the more negative the pore water pressure change. It is noted that the pore water pressure developed in an undrained test is not the largest, as often assumed. The pore water generation for the undrained path is in between that for a negative (dilative) strain increment ratio path and a positive (compressive) strain increment ratio path.

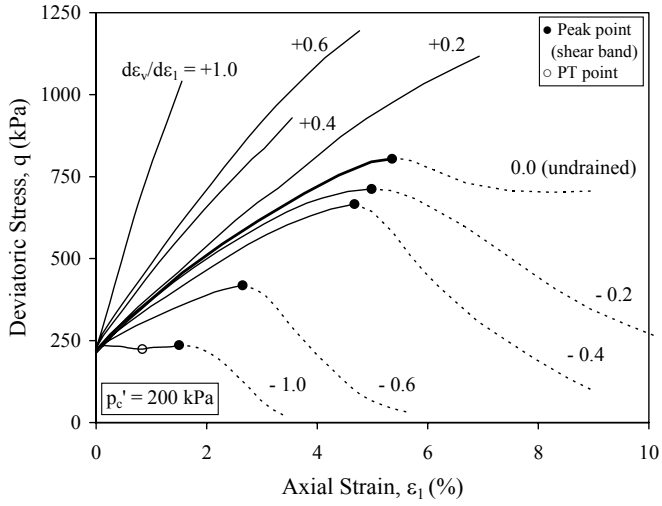

Fig. 5.2(a)

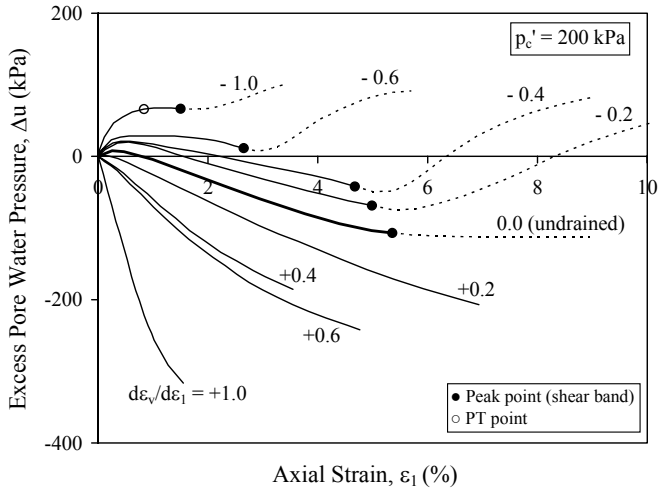

Fig. 5.2(b)

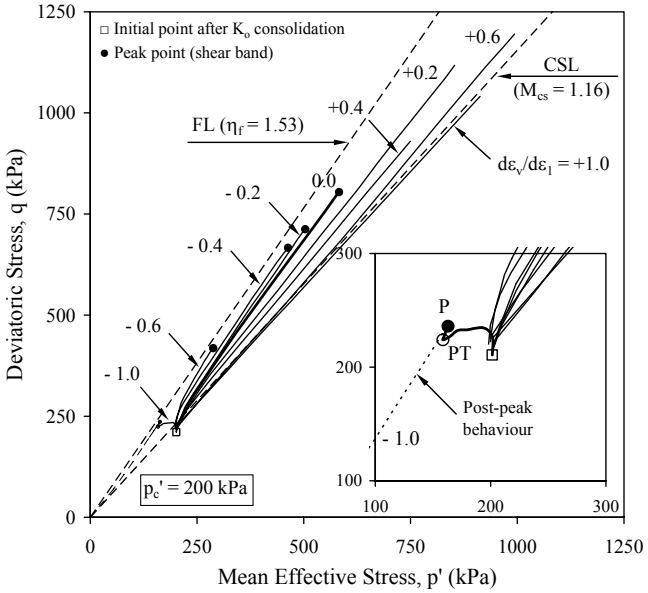

Fig. 5.2(c)

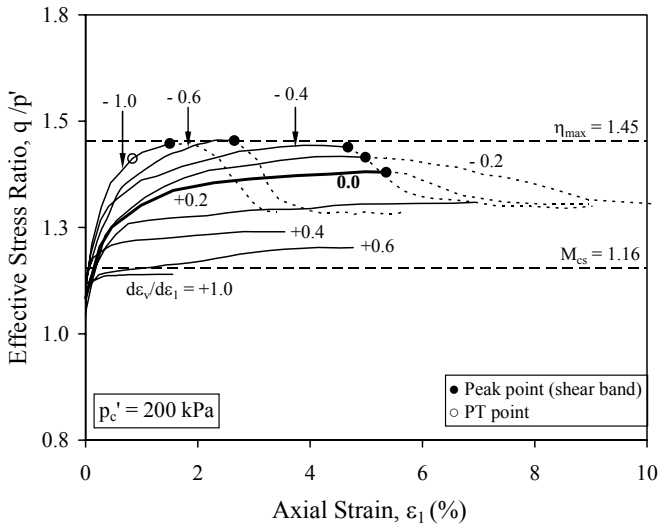

Fig. 5.2(d)

Fig. 5.2 Strain path dependent behaviour of medium dense sand: (a) stress-strain curves; (b) excess pore water pressure versus axial strain curves; (c) effective stress paths; (d) effective stress ratio versus axial strain curves

The effective stress paths obtained from the strain paths tests are plotted in Fig. 5.2(c). Except the test with $d\varepsilon_v/d\varepsilon_1$ = -1.0, all the other paths show a tendency to approach the asymptotic line. It can be observed that the larger (i.e., the more positive) the strain increment ratio, the lower the asymptotic stress ratio η_{asy}. This can also be seen from the *q/p'* versus ε_1 curves are shown in Fig. 5.2(d). However due to shear band formation, strain softening and thus a reduction in *q/p'* occurred in some tests (Figs. 5.2(a) and 5.2(d)). It is also observed that although η_{asy} increases with increasing dilation $(-d\varepsilon_v/d\varepsilon_1)$, the η_{asy} approached by the tests with $d\varepsilon_v/d\varepsilon_1$ = -0.4, -0.6, and -1.0 is about the same value of η_{max} = 1.45. Therefore, there appears to be a limiting value, η_{max}. When $(-d\varepsilon_v/d\varepsilon_1)$ exceeds a certain value, η_{asy} will reach the limiting value.

5.3.2 Very Loose Sand

The results of a series of strain path tests conducted on very loose sand with strain increment ratios, $d\varepsilon_v/d\varepsilon_1$, ranging from +0.6 to -0.6 are presented in Fig. 5.3. The void ratios of specimens after consolidation, e_c, ranged between 0.887 and 0.903, corresponding to relative densities Dr_c = 3–10%. All the specimens were prepared by the MT method. The effect of strain paths on the stress-strain behaviour of very

loose sand can be seen in Fig. 5.3(a) where stress-strain curves are plotted. By imposing a more compressive (positive) strain increment ratio, a sand specimen shows a stiffer behaviour. Similarly, when the strain increment ratio becomes more negative (dilative) a specimen exhibits more pronounced strain softening. It is also observed that under an undrained condition $(d\varepsilon_v/d\varepsilon_1 = 0)$ strain softening occurs for very loose sand.

The excess pore water pressure versus axial strain curves obtained for very loose sand are presented in Fig. 5.3(b). The positive pore water pressure development was observed when $d\varepsilon_v/d\varepsilon_1 < 0$. Negative pore water pressure response was obtained when $d\varepsilon_v/d\varepsilon_1 > 0$. The more negative the $d\varepsilon_v/d\varepsilon_1$ imposed, the more positive the excess pore water pressure change.

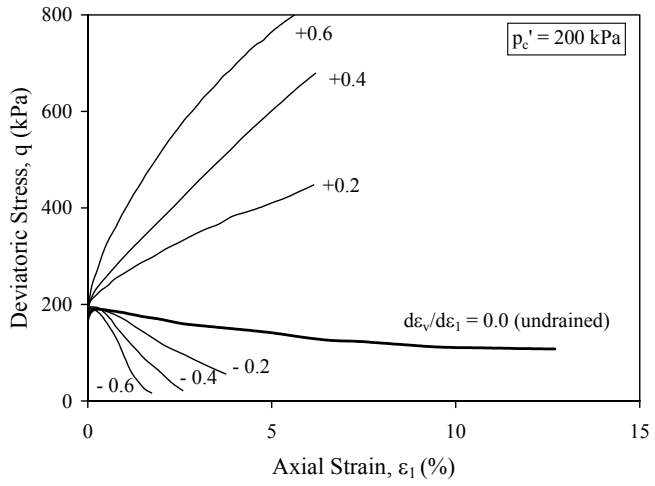

Fig. 5.3(a)

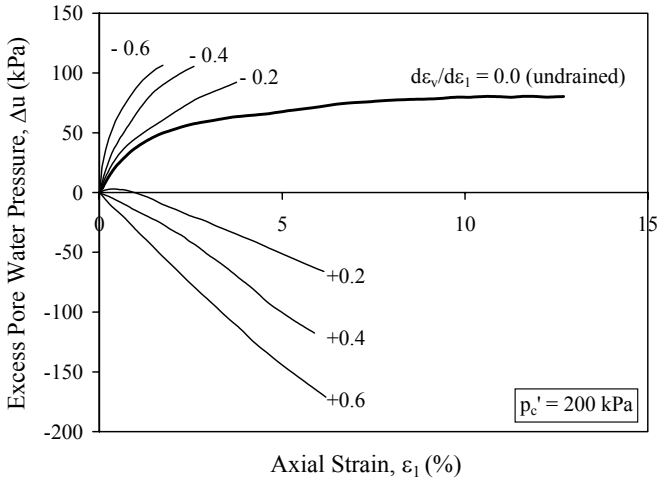

Fig. 5.3(b)

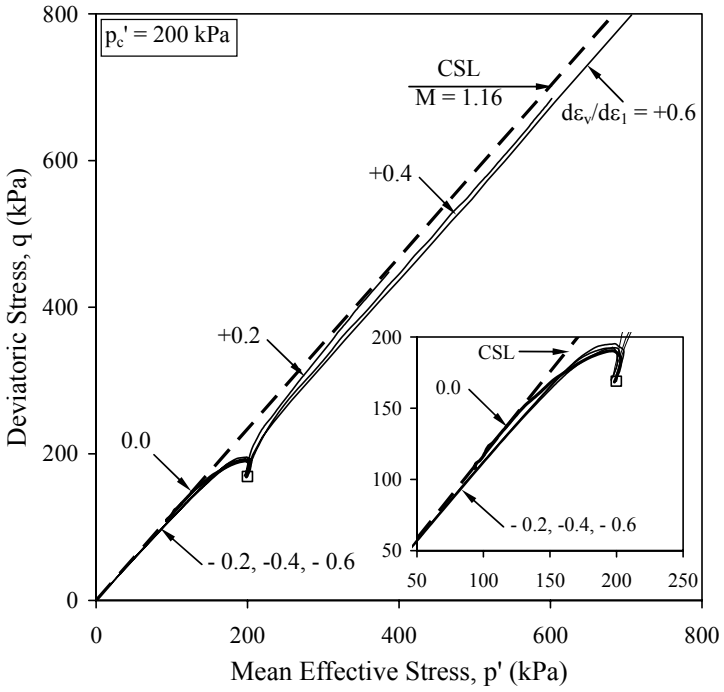

Fig. 5.3(c)

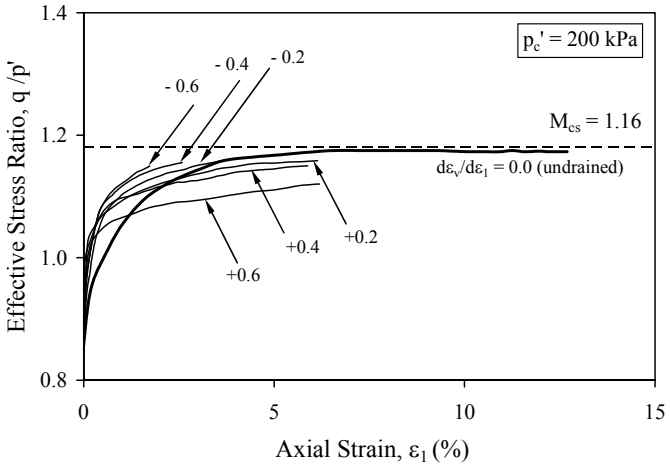

Fig. 5.3(d)

Fig. 5.3 Strain path dependent behaviour of very loose sand: (a) stress-strain curves; (b) excess pore water pressure versus axial strain curves; (c) effective stress paths; (d) effective stress ratio versus axial strain curves

The excess pore water pressure versus axial strain curves obtained for very loose sand are presented in Fig. 5.3(b). The positive pore water pressure development was observed when $d\varepsilon_v/d\varepsilon_1 < 0$. Negative pore water pressure response was obtained when $d\varepsilon_v/d\varepsilon_1 > 0$. The more negative the $d\varepsilon_v/d\varepsilon_1$ imposed, the more positive the excess pore water pressure change.

The effective stress paths obtained from the tests on very loose sand are presented in Fig. 5.3(c). The CSL line obtained from drained plane-strain tests on very loose sand (see Chapter 4) is also plotted in Fig. 5.3(c). The stress paths obtained from compressive strain paths exhibit strain hardening behaviour while the stress paths obtained from dilative strain paths exhibit strain softening behaviour. Nevertheless, it can be seen from Fig. 5.3(c) that the stress paths resulting from tests with $d\varepsilon_v/d\varepsilon_1$ < 0.2 approached the CSL. The stress paths obtained from tests with $d\varepsilon_v/d\varepsilon_1$ = 0.4 and 0.6 approached the asymptotic lines. The *q/p'* versus ε_1 curves are presented in Fig. 5.3(d). It is seen that all the curves tend to approach asymptotically a constant *q/p'* value. The limiting stress ratio, η_{max}, for loose sand appears to be M_{cs} = 1.16. This is consistent with previous studies using undrained tests.

5.3.3 Discussion

The experimental results presented above clearly demonstrated that stress-strain behaviour of sand under plane-strain condition is strain path dependent. The result show that a more positive strain increment ratio leads to a stiffer response. Depending on the density, when a $d\varepsilon_v/d\varepsilon_1$ more negative than a certain value is imposed, strain softening will occur. It is consistent with the observations made for axisymmetric conditions based on triaxial test results (Chu, 1991; Eliadorani, 2000; Leong, 2001; Loke, 2004). However, under plane-strain conditions shear bands would occur in medium loose and medium dense specimens. The occurrence of shear bands can lead to strain softening behaviour in post-peak region. Under axisymmetric conditions, shear bands would not occur, if free-ends were used to reduce end frictions. Therefore, the strain softening behaviour under plane-strain conditions as presented above, are classifieds into two types. The first type is the pre-failure strain softening occurring for very loose sand as shown in Fig. 5.3(a) for tests with $d\varepsilon_v/d\varepsilon_1$ of 0.0 (undrained), -0.2, -0.4, and -0.6. This type of softening is a true material behaviour and it reflects the response of loose granular soils to the imposed strain path. The second type is the strain softening observed in hardening regime for medium loose and dense sand after the occurrence of shear band, for example, test $d\varepsilon_v/d\varepsilon_1$ = 0.0 (undrained), -0.2, -0.4, or -0.6 for medium dense sand in Fig. 5.2. This type of strain softening is caused by the formation of shear band in

the hardening regime. This type of strain softening has been called the *banding softening* by Chu et al. (1996).

The asymptotic state of sand has been investigated by Chu (1991) and Chu & Lo (1994) under axisymmetric and three-dimensional stress conditions. It was found that the $(q/p')_{asy}$ is independent of the soil stress history and the initial effective confining stress. Chu (1991) and Chu & Lo (1994) also concluded that there is a relationship between the controlled strain increment ratio $d\varepsilon_v/d\varepsilon_1$ and the asymptotic stress ratio $(q/p')_{asy}$. This relationship is independent of the initial effective confining stress, the loading mode and shearing rate and is not significantly affected by the void ratio.

The experimental data obtained from the strain path tests conducted on medium dense sand (e_c = 0.67–0.71) and commenced from p_c' = 200 kPa is presented in Fig. 5.4. It can be see from Fig. 5.4 that there is a relationship between $(q/p')_{asy}$ and $d\varepsilon_v/d\varepsilon_1$ at the asymptotic state. By fitting the line through all the data points, the empirical equation between the asymptotic stress ratio and strain increment ratio in a strain path test for $-0.6 \le d\varepsilon_v/d\varepsilon_1 \le 1$, can be established:

$$\left(\frac{q}{p'}\right)_{asy} = M_0 - \mu\left(\frac{d\varepsilon_v}{d\varepsilon_1}\right) \qquad (5-1)$$

where M_0 =1.37 and μ = 0.23 are the experimental constants.

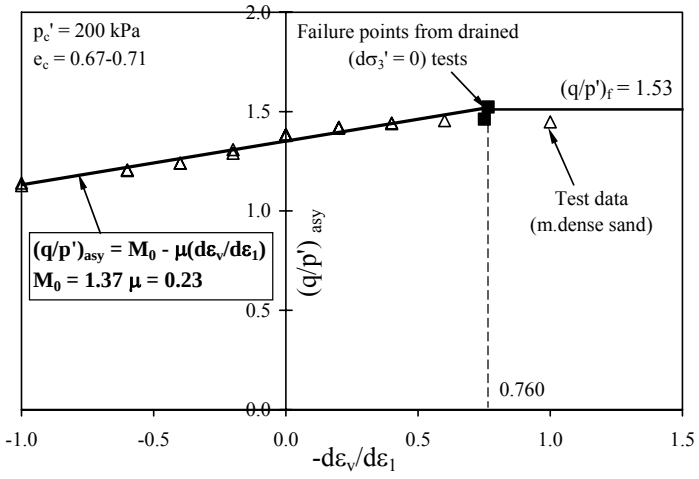

Fig. 5.4 Relationship between $(q/p')_{asy}$ and $(-d\varepsilon_v/d\varepsilon_1)$

The presented relationship shows that the asymptotic stress ratio increases with the decrease in the controlled strain increment ratio. However, as discussed earlier, the achievable stress ratio is bounded by a limiting value of $(q/p')_{asy}$. Furthermore, it has been established by Chu & Lo (1994) under axisymmetric conditions that the maximum achievable asymptotic stress ratio, η_{max}, is bounded by the failure line determined by drained tests. In other words, when the controlled strain increment ratio, $(d\varepsilon_v/d\varepsilon_1)_i$, is more negative than the strain increment ratio at failure, $(d\varepsilon_v/d\varepsilon_1)_f$, the asymptotic stress ratio can only reach its limit value, the failure stress ratio $(q/p')_f$.

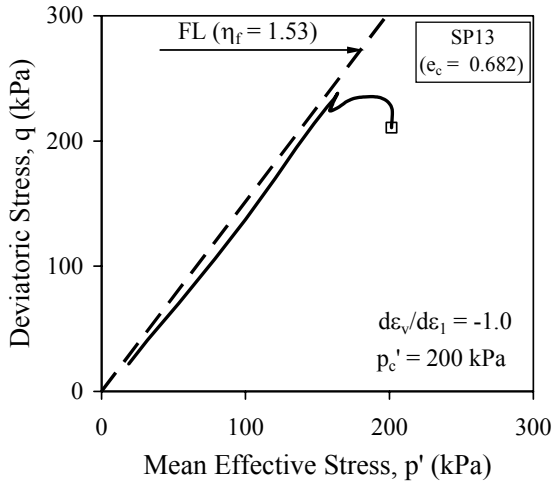

Fig. 5.5 Effective stress path of a $d\varepsilon_v/d\varepsilon_1$ = -1.0 test

The effective stress path resulted from a $d\varepsilon_v/d\varepsilon_1$ = -1.0 test is presented in Fig. 5.5. More detailed results of this test have been given earlier in Fig. 5.2. Although the strain increment ratio imposed in the test is more negative than $(d\varepsilon_v/d\varepsilon_1)_f$, = *-0.76* determined for the same p_c' = 200 kPa (see Fig. 4.10(b)), the effective stress path approaches the failure line. Therefore, similarly to the axisymmetric conditions, $(d\varepsilon_v/d\varepsilon_1)_f$ seems to be a threshold strain increment ratio under plane-strain conditions. When the controlled strain increment ratio is more negative than the strain increment ratio at failure, which in this case is -0.760, the asymptotic stress ratio can only reach its limit value, the failure stress ratio $(q/p')_f$. Thus, for the strain path tests with $d\varepsilon_v/d\varepsilon_1 < (d\varepsilon_v/d\varepsilon_1)_f$:

$$\left(\frac{q}{p'}\right)_{asy} = \left(\frac{q}{p'}\right)_f \qquad (5-2)$$

where $(q/p')_f$ is the failure stress ratio.

Combining Eqns. (5 – 1) and (5 – 2), the empirical relationship between the asymptotic stress ratio in a constant strain increment ratio path test can be established:

$$\left(\frac{q}{p'}\right)_{asy} = \begin{cases} M_0 - \mu\left(d\varepsilon_v / d\varepsilon_1\right), & for \quad d\varepsilon_v / d\varepsilon_1 \geq \left(d\varepsilon_v / d\varepsilon_1\right)_f \\ \left(\frac{q}{p'}\right)_f & for \quad d\varepsilon_v / d\varepsilon_1 < \left(d\varepsilon_v / d\varepsilon_1\right)_f \end{cases} \qquad (5-3)$$

For the data shown in Fig. 5.4, M_0 = 1.37, μ = 0.23, and $(q/p')_f$ = 1.53. This relationship is consistent with that obtained under axisymmetric conditions by Chu & Lo (1994).

In Fig. 5.6, the data obtained from the strain path tests is compared with the Rowe's stress-dilatancy equation (Rowe, 1962, 1971) for drained tests, expressed as:

$$\frac{\sigma_1'}{\sigma_3'} = K\left(1 - \frac{d\varepsilon_v}{d\varepsilon_1}\right) \qquad (5-4)$$

where K is an experimental constant related to the friction angle at the critical state. For the Changi sand tested under plane-strain conditions, K = 3.85. The failure points obtained from drained tests are also plotted in Fig. 5.6. It should be mentioned that in Rowe's stress-dilatancy theory it is assumed that the stress-dilatancy behaviour is independent of the initial effective confining stress. However, it has been shown in Chapter 4 that this assumption is not valid for Changi sand tested under plane-strain conditions. Since all the strain path tests presented in Fig. 5.6 were commenced from the initial effective confining stress of 200 kPa, only the failure points obtained for the same p_c' were presented in this figure. By comparing the curve obtained from the experiments with that obtained from the modified Rowe's stress-dilatancy theory, it can be seen that the stress ratio mobilized in a constant strain increment ratio path test is higher than that in a drained test for the same amount of dilatancy. Thus, it is clear that Eqn. (5 – 4) cannot predict the asymptotic response in a strain path test. The two curves only merge at the failure state, indicating that stress ratio at failure is independent of the

stress/strain path leading to the failure. A horizontal line drawn to the right-hand side of the failure points in Fig. 5.6 represents the limit surface expressed by Eqn. (5 – 2).

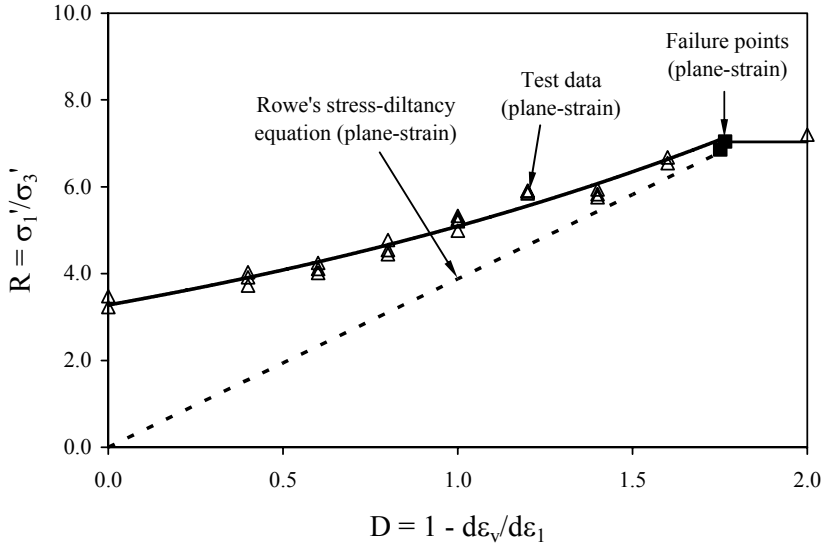

Fig. 5.6 Stress ratio versus dilatancy plot

The data obtained from the strain path tests under plane-strain conditions is also compared with the *original* Cam clay model (Roscoe & Schofield, 1963; Schofield & Wroth, 1968) and the *modified* Cam clay model (Roscoe & Burland, 1968), as shown in Fig. 5.7. In the *original* Cam clay model the stress-dilatancy relation is defined by

$$\frac{q}{p'} = M - \frac{d\varepsilon_v}{d\varepsilon_s} \qquad (5-5)$$

where M = 1.16 is the stress ratio at the critical state, as determined by drained tests. The *modified* Cam clay equation is expressed as:

$$\frac{d\varepsilon_v}{d\varepsilon_s} = \frac{M^2 - \eta^2}{2\eta} \qquad (5-6)$$

where $\eta = q/p'$.

It can be seen from Fig. 5.7 that Eqns. (5 – 5) and (5 – 6) cannot predict the asymptotic behaviour of sand in a strain path test under plane-strain conditions.

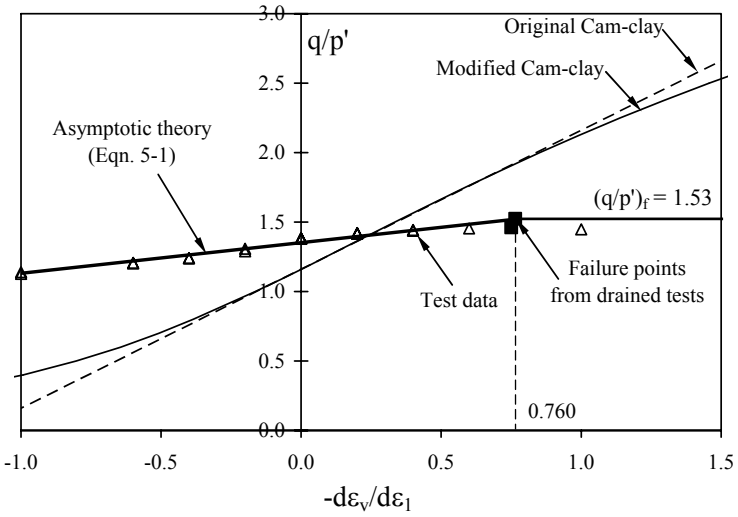

Fig. 5.7 Comparison of stress-dilatancy plots obtained from asymptotic theory and Cam clay models

5.4 Strain Softening Behaviour of Sand

5.4.1 Introduction

It has been shown by Chu et al. (1992) that strain softening as material behaviour can occur in sand and the strain increment ratio influences the occurrence of strain softening under axisymmetric and three-dimensional loading conditions. As established by Chu et al. (1992) for axisymmetric conditions, whether a soil element will undergo strain hardening or softening depends on the relative magnitude of the strain increment ratio of the soil obtained from conventional drained test, $(d\varepsilon_v/d\varepsilon_1)_{max}$ and the strain increment ratio, $(d\varepsilon_v/d\varepsilon_1)_i$ imposed during the test. It means that a soil specimen undergoing contractive volumetric change can experience strain softening behaviour if the strain increment ratio imposed during the strain path test, $(d\varepsilon_v/d\varepsilon_1)_i$ is smaller (i.e. less compressive) than the maximum dilation rate of the soil obtained from a drained test, $(d\varepsilon_v/d\varepsilon_1)_{max}$. The conditions for the occurrence of strain softening and strain hardening established by Chu et al. (1992) are presented below:

$$(d\varepsilon_v/d\varepsilon_1)_i - (d\varepsilon_v/d\varepsilon_1)_{max} > 0 \quad \rightarrow \quad \text{hardening} \qquad (5-7a)$$

$$(d\varepsilon_v/d\varepsilon_1)_i - (d\varepsilon_v/d\varepsilon_1)_{max} = 0 \quad \rightarrow \quad \text{perfectly plastic} \qquad (5-7b)$$

$$(d\varepsilon_v/d\varepsilon_1)_i - (d\varepsilon_v/d\varepsilon_1)_{max} < 0 \quad \rightarrow \quad \text{softening} \qquad (5-7c)$$

where $(d\varepsilon_v/d\varepsilon_1)_{max}$ – the maximum dilation rate of the soil obtained from drained test and $(d\varepsilon_v/d\varepsilon_1)_i$ – the strain increment ratio imposed during the strain path test. In this section, the findings established by Chu et al. (1992) are verified under plane-strain conditions.

5.4.2 Definition of Failure

Failure is one of the most important characteristics of soil that needs to be discussed. Under axisymmetric conditions, failure can be defined as the state where q_{max} or $(q/p')_{max}$ is reached. However, under more generalized loading conditions, failure needs to be defined by a failure criterion.

In this study, the failure criterion proposed by Lade (1977) was adopted. Lade's failure criterion is expressed as:

$$\left(\frac{I_1^3}{I_3} - 27\right)\left(\frac{I_1}{p_a}\right)^m = \eta_1 \qquad (5-8)$$

where $I_1 = \sigma_1 + \sigma_2 + \sigma_3$ and $I_3 = \sigma_1 \sigma_2 \sigma_3$ are the first and third principal stress invariants respectively. The p_a is the value of atmospheric pressure in consistent units. m and η_1 are dimensionless parameters to be determined by experimental data.

Fig. 5.8 presents the data for the failure stresses obtained from three sets of drained plane-strain tests conducted for very loose, medium loose and medium dense sand. Three values of η_1 were calculated from the three sets of data: η_1 = 51.8 for medium dense sand, η_1 = 32.7 for medium loose sand, and η_1 = 18.8 for very loose sand respectively. m = 0.1024 was calculated as the slope of the lines, which is about the same for all the densities. Parameters η_1 and m determined under plane-strain conditions are summarized in Table 5-2. The failure η_1 values obtained from the drained tests will be used to define failure for the strain path tests used in studying the strain softening behaviour. Nevertheless, it can be proved mathematically that η_1 is related to q/p' (Chu, 1991). Furthermore, if generalized

forms of q and p' are used (see Eqns. 4 – 1 and 4 – 2 in Chapter 4), both η_1 and q/p' reach the maximum values simultaneously.

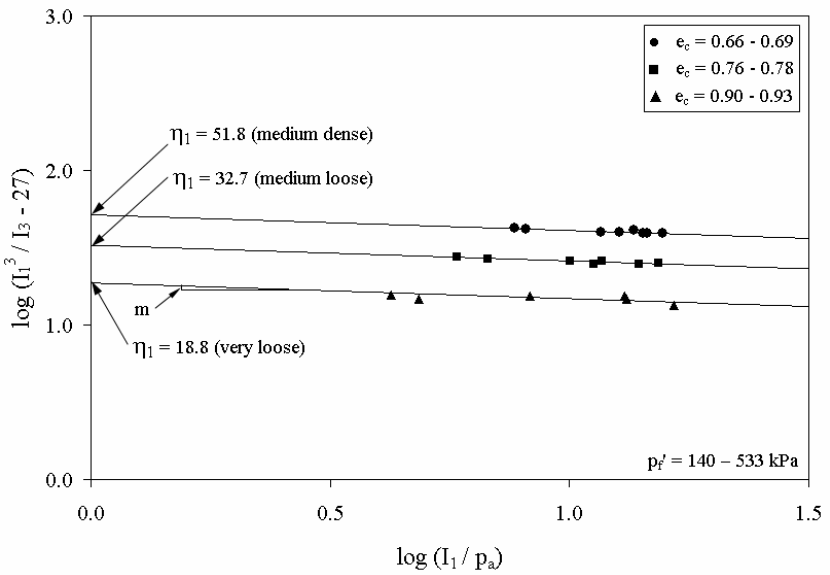

Fig. 5.8 Determination of parameters η_1 and m in Lade's failure criterion under plane-strain conditions

Table 5-2 Parameters η_1 and m determined under plane-strain conditions

	Very loose	Medium loose	Medium dense
D_r (%)	≤ 15	35 – 50	50 – 65
η_1	18.8	32.7	51.8
m	0.1024	0.1024	0.1024

5.4.3 Pre-Failure Strain Softening

5.4.3.1 Effect of Strain Increment Ratio

The stress-strain curve of strain path test SP42 is presented in Fig. 5.9(a). The test was commenced from an initial effective confining stress of p_c' = 201 kPa. The value of the imposed $d\varepsilon_v/d\varepsilon_1$ decreased in steps from +1.0 to -2.5. It can be seen from Fig. 5.9(a) that strain softening occurred in Test SP42 when $d\varepsilon_v/d\varepsilon_1$ = -0.8 (point A). The variation of $d\sigma'_{ij}d\varepsilon_{ij}$ with the axial strain is plotted in Fig. 5.9(b). It can be seen by comparing Fig. 5.9(a) with Fig. 5.9(b) that the sign of $d\sigma'_{ij}d\varepsilon_{ij}$ became negative in the $dq < 0$ region. It means that strain softening occurred in the

$dq < 0$ region. When strain softening occurred there was not any shear band formation within the specimen.

The influence of strain increment ratio on the occurrence of strain softening can also be observed in Fig. 5.9(c) where the effective stress path obtained from Test SP42 is presented. With every decrease in the strain increment ratio, the effective stress path turned more towards the failure line. Eventually, strain softening occurred when $d\varepsilon_v/d\varepsilon_1$ = -0.8. It can be seen from Figs. 5.9(c) and 5.9(d) that the strain softening occurred before the failure state was reached. Therefore, the strain softening obtained in Test SP42 was a pre-failure strain softening. It should be pointed out that a shear band only occurred when failure was reached. Thus, the pre-failure strain softening in Test SP42 is a material behaviour.

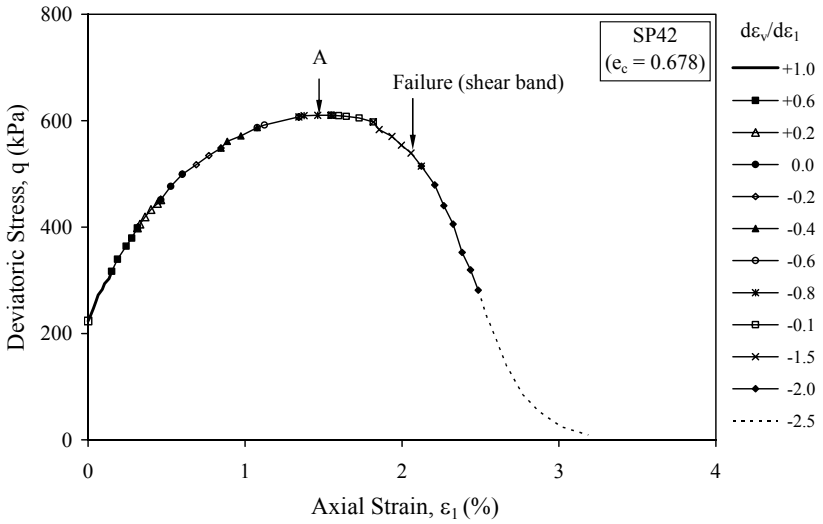

Fig. 5.9(a)

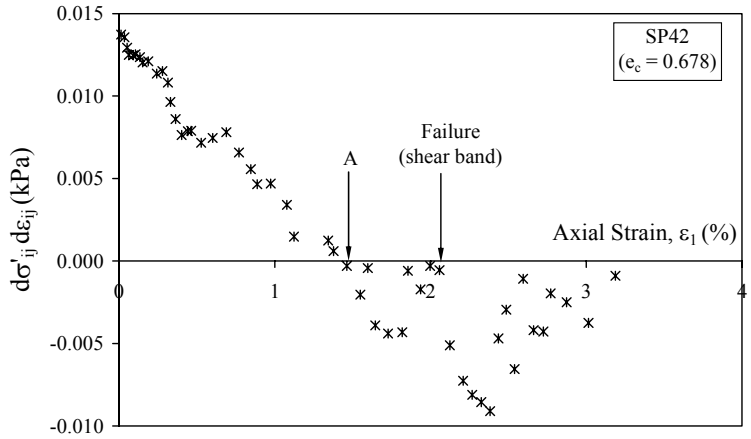

Fig. 5.9(b)

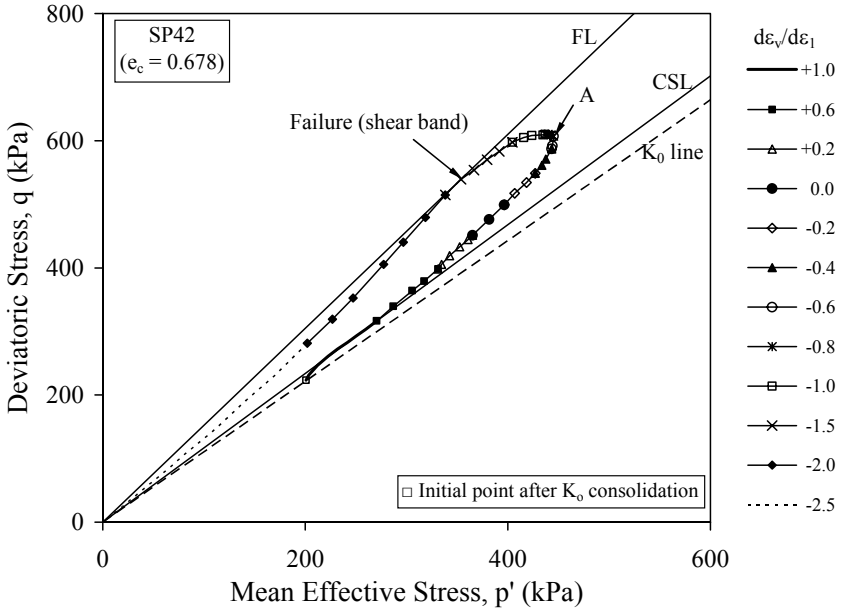

Fig. 5.9(c)

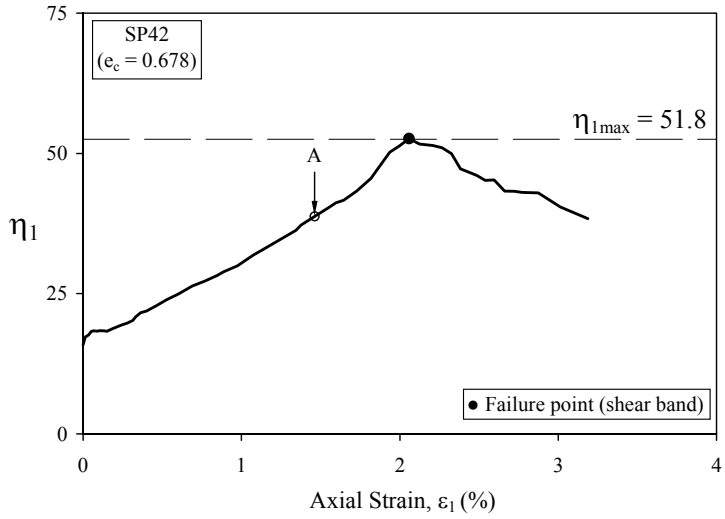

Fig. 5.9(d)

Fig. 5.9 Results of Test SP42 conducted on medium dense sand: (a) stress-strain curve; (b) $d\sigma'_{ij}d\varepsilon_{ij}$ versus ε_1 curve; (c) effective stress path; (d) η_1 versus ε_1 curve

To further discuss the pre-failure softening behaviour of sand under plane-strain conditions, the results of two constant $d\varepsilon_v/d\varepsilon_1$ path tests, SP09 and SP13, are presented in Fig. 5.10. The two tests were conducted with the same initial effective confining stress of p_c' = 200 kPa, but different stress increment ratios. The $d\varepsilon_v/d\varepsilon_1$ = -0.6 was used for Test SP09 and $d\varepsilon_v/d\varepsilon_1$ = -1.0 for Test SP13. It should be noted that in Fig. 5.10, the dashed line represents the region where shear bands became visible. The stress-strain curves of the two tests are compared in Fig. 5.10(a). In

Test SP09, strain softening was associated with shear band formation at point D. In Test SP13, however, two types of strain softening are identified. Firstly, strain softening as a material behaviour occurred at point A. It was followed by a local strain hardening behaviour in the region BC. Finally, banding softening occurred at point C, which was accompanied by a shear band. Since a true material strain softening occurred for Test SP13 but not for Test SP09, it can be concluded that $d\varepsilon_v/d\varepsilon_1$ affected the occurrence of strain softening. The smaller the strain increment ratio, the greater the tendency for strain softening to occur.

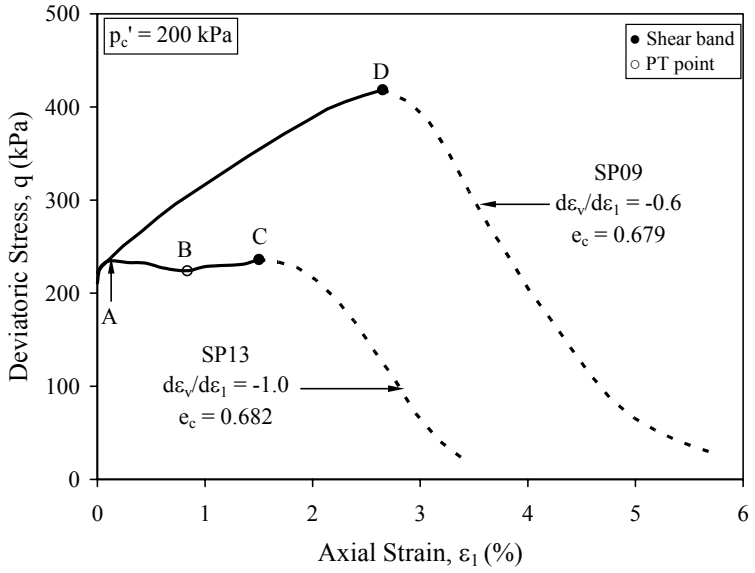

Fig. 5.10(a)

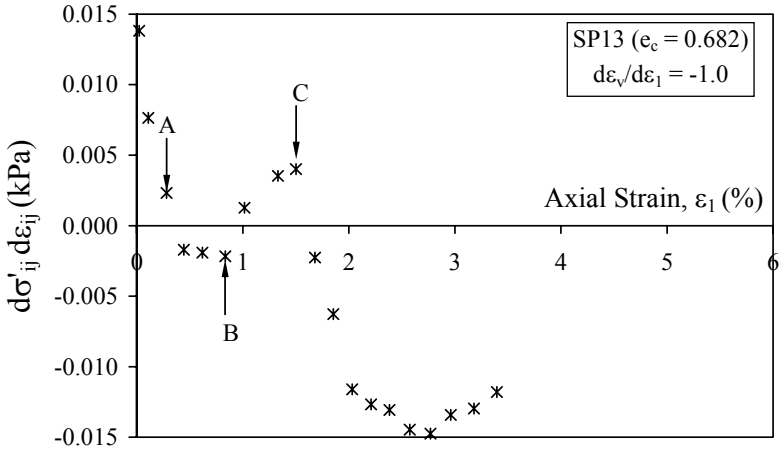

Fig. 5.10(b)

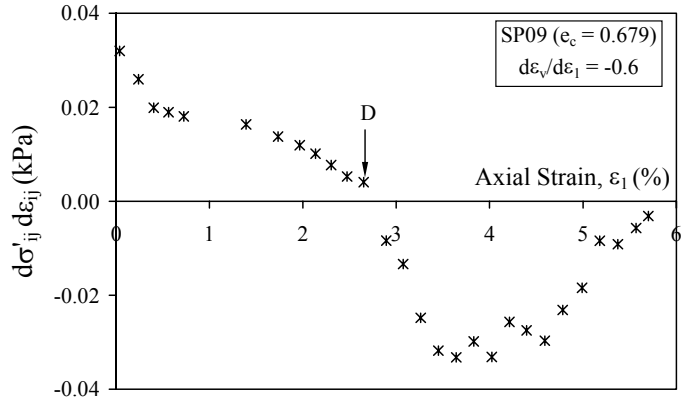

Fig. 5.10(c)

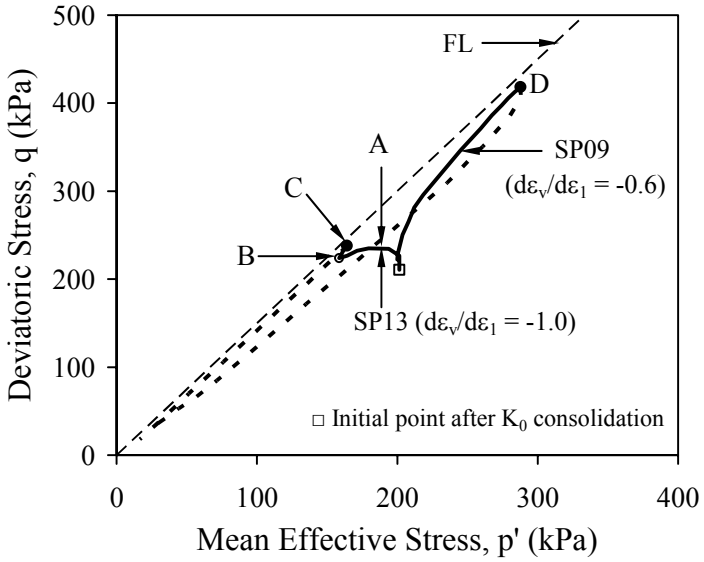

Fig. 5.10(d)

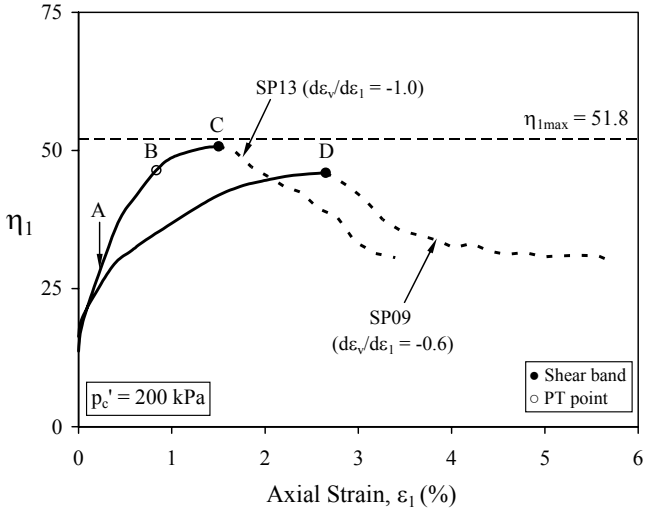

Fig. 5.10(e)

Fig. 5.10 Comparison of Tests SP09 and SP13: (a) stress-strain curves; (b) $d\sigma'_{ij}d\varepsilon_{ij} - \varepsilon_1$ curve for Test SP13; (c) $d\sigma'_{ij}d\varepsilon_{ij} - \varepsilon_1$ curve for Test SP09; (d) effective stress paths; (e) η_1 versus ε_1 curves

The variation of $d\sigma'_{ij}d\varepsilon_{ij}$ with the axial strain for Test SP13 and Test SP09 is plotted in Figs. 5.10(b) and 5.10(c) respectively. This data again shows that $d\sigma'_{ij}d\varepsilon_{ij} < 0$ was associated with $dq < 0$, that is, strain softening occurred in the $dq < 0$ region. The resulting effective stress paths for the two tests are plotted in Fig. 5.10(d). It is seen that a slight increase in q, observed in Test SP13 (point B), led to a transition to the failure point (point C). Such a local hardening behaviour in an overall softening region has also been observed for some undrained triaxial tests on loose sand when studying the liquefaction behaviour. This phenomenon has been termed as *limited flow* behaviour (Castro, 1969).

The η_1 versus ε_1 curves for the two tests are plotted in Fig. 5.10(e). By comparing the η_1 value with η_{1max} value, it can be seen that Test SP13 has reached a failure state at point C. Therefore, the strain softening occurred at point A is a pre-failure strain softening and the strain softening occurred at point C is a post-failure strain softening. In Test SP09, a failure state has not been reached. This is because the effective stress path reaches the asymptotic line which is slightly below the failure line. The strain softening occurred after point D was associated with the onset of the shear band. Therefore, it was banding softening.

5.4.3.2 Effect of Void Ratio

To discuss the effect of void ratio on the strain softening behaviour of sand in strain path testing, the four strain path tests with $d\varepsilon_v/d\varepsilon_1 = -0.4$ imposed are compared. All the specimens were K_0 consolidated to a mean effective stress, $p_c' = 200$ kPa. A summary of testing conditions is given in Table 5-3.

Table 5-3 Summary of testing conditions for $d\varepsilon_v/d\varepsilon_1 = -0.4$ path tests.

Test No	$d\varepsilon_v/d\varepsilon_1$	e_c	Dr_c (%)	Density state	$(q/p')_{asy}$	Softening/ Hardening	Shear band
SP05	-0.4	0.677	62	m. dense	1.45	hardening	Yes
SP06		0.728	49	m. loose	1.43	hardening	Yes
SP07		0.781	35	loose	1.34	limited soft.	Yes
SP08		0.890	7	v. loose	1.16	Softening	No

The results of the four strain path tests conducted on very loose to medium dense sand are presented in Fig. 5.11. The effect of void ratio on the stress-strain behaviour of sand is demonstrated in Fig. 5.11(a), where stress-strain curves obtained from all the four tests are plotted. Although the same negative strain increment ratio was imposed to all the specimens, different types of behaviour, mainly strain hardening, limited strain softening and strain softening was observed. The response at denser states was strongly strain hardening compared to that at loose states. For example, the medium dense specimen SP05 (e_c = 0.677) exhibited strain hardening, the medium loose specimen SP07 (e_c = 0.781) limited strain softening, and the very loose specimen SP08 (e_c = 0.890) full strain softening. It can be seen from Fig. 5.11(a) that the higher the void ratio, the higher the peak deviatoric stress. It should be pointed out that the peak deviatoric stress in Tests SP05 and SP06 coincides with shear band formation, whereas a shear band does not occur in Test SP08 and the peak is a material behaviour. Consequently, banding softening behaviour is observed in Tests SP05 and SP06, whereas material strain softening is observed in Test SP08. As shown in Fig. 5.11(a), the limited strain softening was observed in Test SP07. In this test, the material strain softening first occurred and the minimum value of deviatoric stress was reached. After that a strain hardening behaviour was observed and eventually banding strain softening occurred. The excess pore water pressure curves obtained from the four tests are presented in Fig. 5.11(b). The looser the specimen, the larger the excess pore water pressure was developed.

The effective stress paths obtained from the four tests are plotted in Fig. 5.11(c). It can be seen that all the effective stress paths approach asymptotically the constant stress ratio line (CSRL). It can also be observed that the CSRL is not unique. The higher the void ratio the lower the asymptotic stress ratio, $(q/p')_{asy}$. The same can be seen in Fig. 5.11(d) where q/p' versus ε_1 curves are presented. Please note that the failure stress ratios change with void ratio. The relationship between the asymptotic stress ratio, $(q/p')_{asy}$, and void ratio, e_c, is plotted in Fig. 5.12. As shown in Fig. 5.12, the $(q/p')_{asy}$ decreases with increasing void ratio. For very loose sand, $(q/p')_{asy}$ is the same as the stress ratio at critical state M_{cs}. Therefore, the critical state seems to be the lower bound of the asymptotic state for very loose sand.

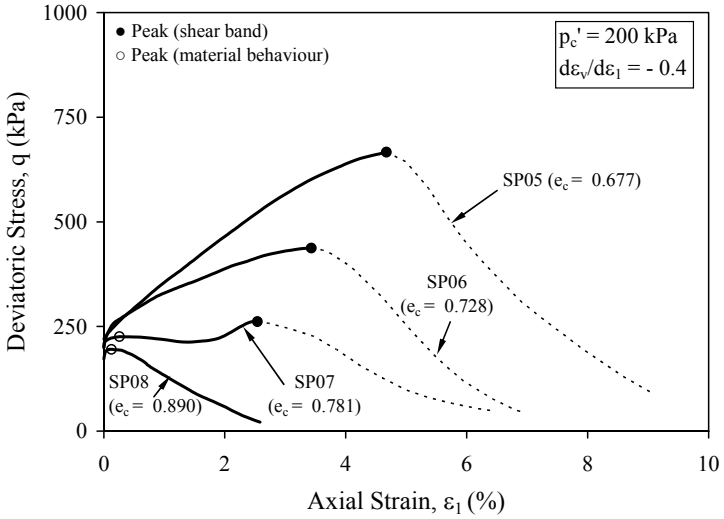

Fig. 5.11(a)

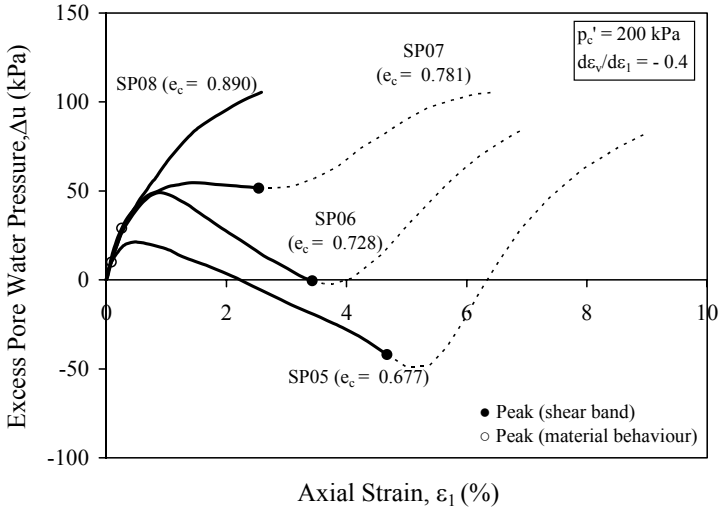

Fig. 5.11(b)

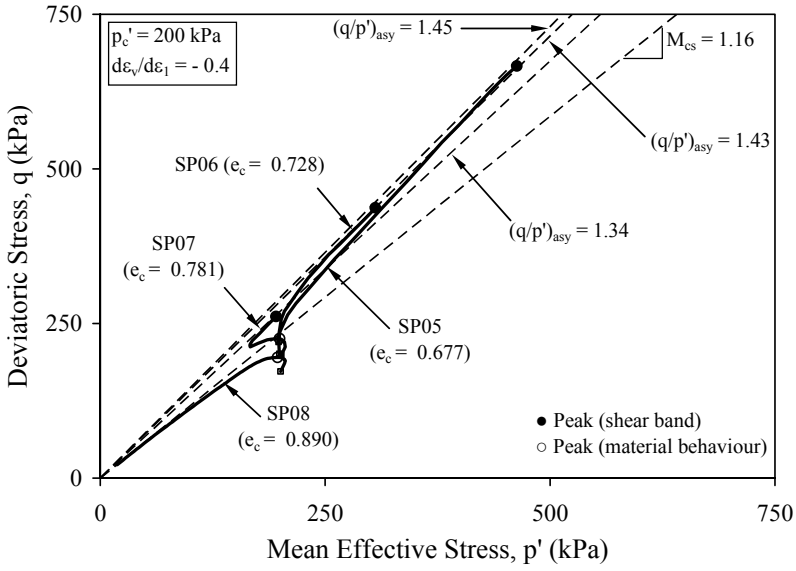

Fig. 5.11(c)

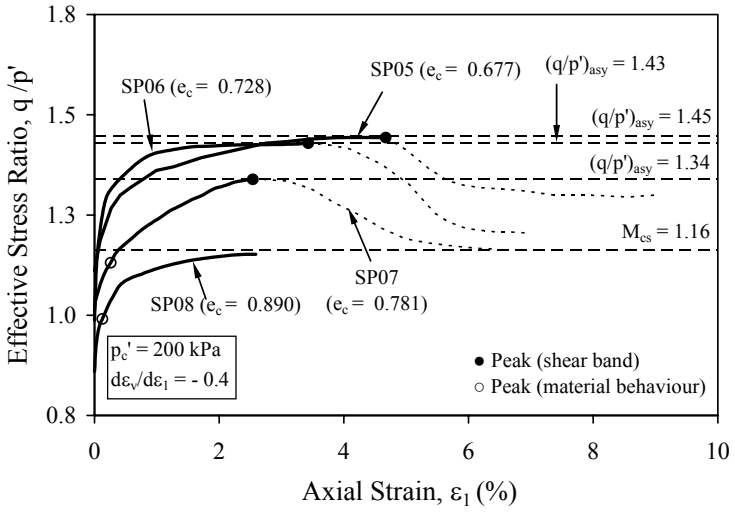

Fig. 5.11(d)

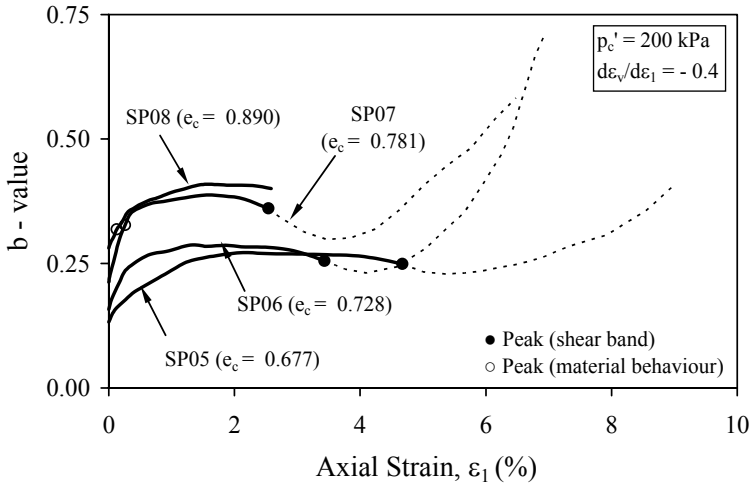

Fig. 5.11(e)

Fig. 5.11 Results of $d\varepsilon_v/d\varepsilon_1$ = -0.4 path tests: (a) stress-strain curves; (b) excess pore water pressure curves; (c) effective stress paths; (d) *q/p'* versus ε_1 curves; (e) *b-value* versus ε_1 curves.

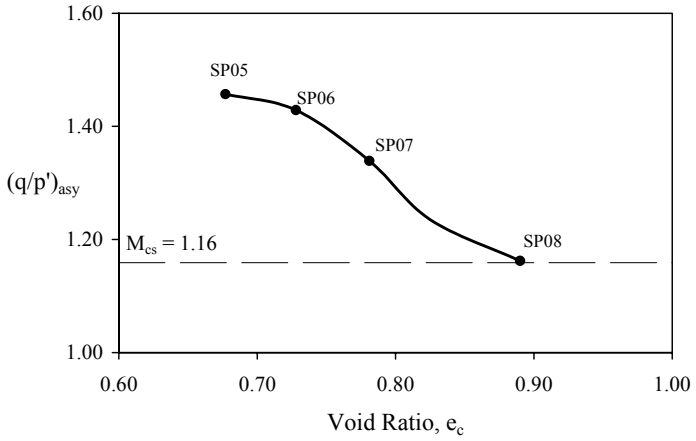

Fig. 5.12 Relationship between $(q/p')_{asy}$ and e_c obtained from $d\varepsilon_v/d\varepsilon_1$ = -0.4 path tests

The *b-value* versus axial strain curves obtained from the $d\varepsilon_v/d\varepsilon_1$ = -0.4 path tests are shown in Fig. 5.11(e). The *b-values* measured in the four tests are in the range between 0.17 and 0.40. The relationship between *b-value* at the asymptotic state and void ratio, e_c, is presented in Fig. 5.13. It is observed that the looser the specimen, the higher the *b-value*.

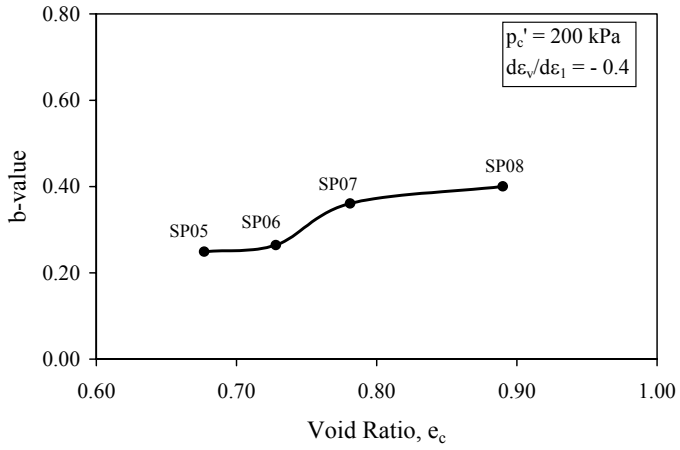

Fig. 5.13 Relationship between *b-value* and e_c obtained from $d\varepsilon_v/d\varepsilon_1$ = -0.4 path tests

The experimental data presented in this section shows that the behaviour of sand in strain path testing is influenced by void ratio. By imposing the same constant strain increment ratio to specimens with different densities, both strain hardening and strain softening can be obtained. The looser the soil, the easier for strain softening to occur.

The initial testing conditions of all the strain path tests conducted under plane-strain conditions are plotted on $d\varepsilon_v/d\varepsilon_1$ versus e_c plane in Fig. 5.14. Based on the data points, a response boundary can be obtained, as shown in Fig. 5.14. The boundary divides the plane into a hardening region and a softening region. It reflects the influence of both $d\varepsilon_v/d\varepsilon_1$ and e_c. The higher the e_c and the lower the $d\varepsilon_v/d\varepsilon_1$, the greater the tendency for strain softening to occur. Therefore, for a given $d\varepsilon_v/d\varepsilon_1$ there is a critical void ratio, at which the strain softening can be initiated. For example, for $d\varepsilon_v/d\varepsilon_1$ = -0.4 the critical point is C_1, as shown in Fig. 5.14, and for $d\varepsilon_v/d\varepsilon_1$ = 0 there is a critical point is C_0, at which e_{cr} = 0.884 (see Fig. 5.14). This e_{cr} has been discussed in Chapter 4. Similarly, for a given void ratio, there is a

critical value of $d\varepsilon_v/d\varepsilon_1$, at which strain softening can be initiated. For instance, corresponding to e_c = 0.68, point C_2 represents the lowest strain increment ratio required to cause strain softening. The data presented in Fig. 5.14 verifies that the response boundary of strain softening under plane-strain conditions can be determined in the same way to that established under axisymmetric conditions by Chu (1991).

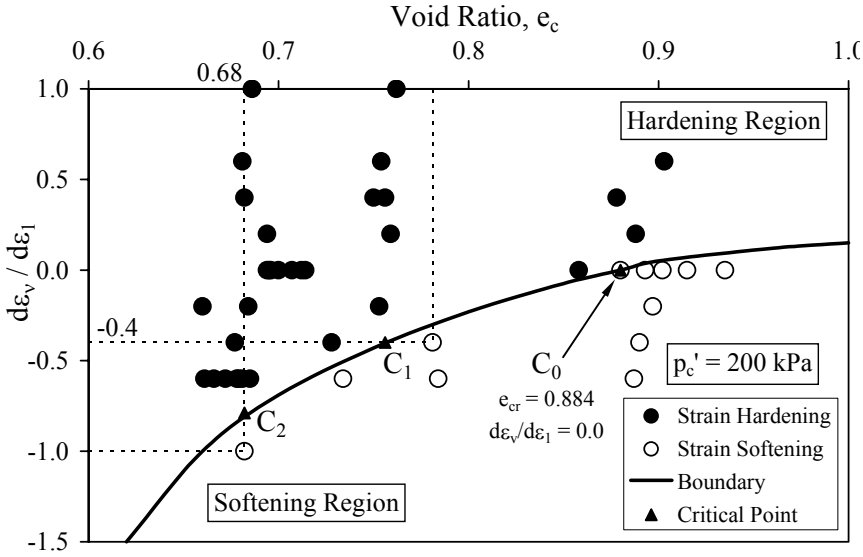

Fig. 5.14 Response boundary on $d\varepsilon_v/d\varepsilon_1$ versus e_c plane determined under plane-strain conditions

5.4.3.3 Effect of Initial Effective Confining Stress

The effect of the initial effective confining stress, p_c', on the occurrence of strain softening is demonstrated in Fig. 5.15, where the results of Tests SP09 and SP29 are compared. The two tests were conducted by following the same strain path of $d\varepsilon_v/d\varepsilon_1$ = -0.6 but commenced from different initial effective confining stresses of 200 kPa and 703 kPa respectively. As shown in Fig. 5.15(a) the effective stress paths traced by these two tests are different. Strain softening is observed in Test SP29 but not in Test SP09. Shear bands occurred in both tests. In Test SP29, the shear band is observed in the post-peak region (point B), whereas in Test SP09, the shear band coincided with the peak (point C). Therefore, strain softening as a material behaviour was observed in Test SP29 and banding softening was observed in Test SP09.

The η_1 versus ε_1 curve obtained from the two tests are plotted in Fig. 5.15(c). It can be seen that in both tests shear bands occurred at points where η_1 reached its peak value. However, η_{1max} has not been reached yet. This shows that under strain path controlled conditions, failure state determined by drained tests, may not be reached due to shear band formation. Therefore, it appears that the failure state under plane-strain conditions is closely related to the shear band formation. This is consistent with conclusions made by Wang & Lade (2001) based on true triaxial tests. Wang & Lade (2001) have observed that the failure state for dense sand is a consequence of the shear band development. Based on the results presented above it can be further concluded that the failure criterion determined under drained conditions may not be applicable for all the strain path tests conducted under plane-strain conditions.

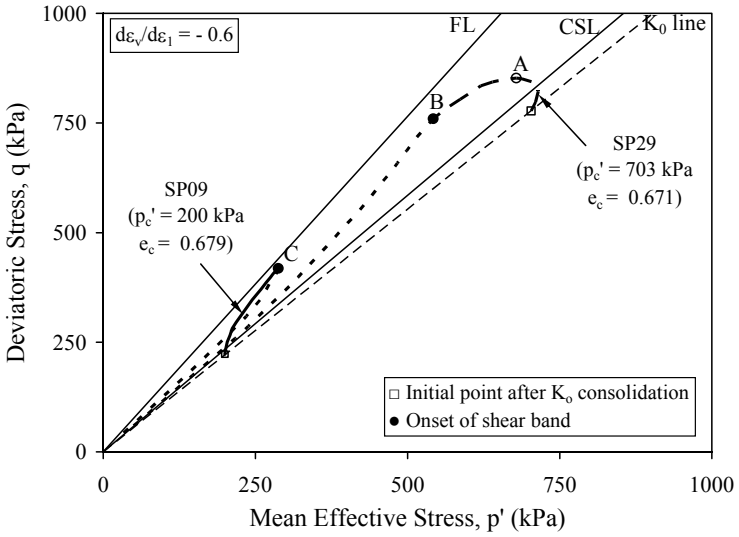

Fig. 5.15(a)

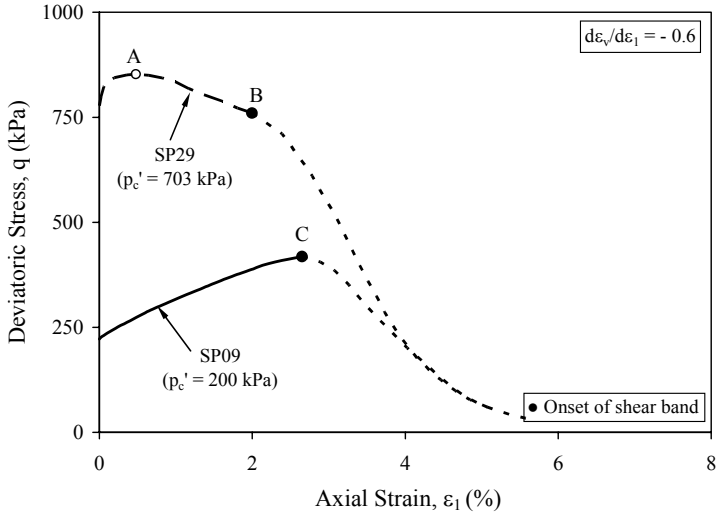

Fig. 5.15(b)

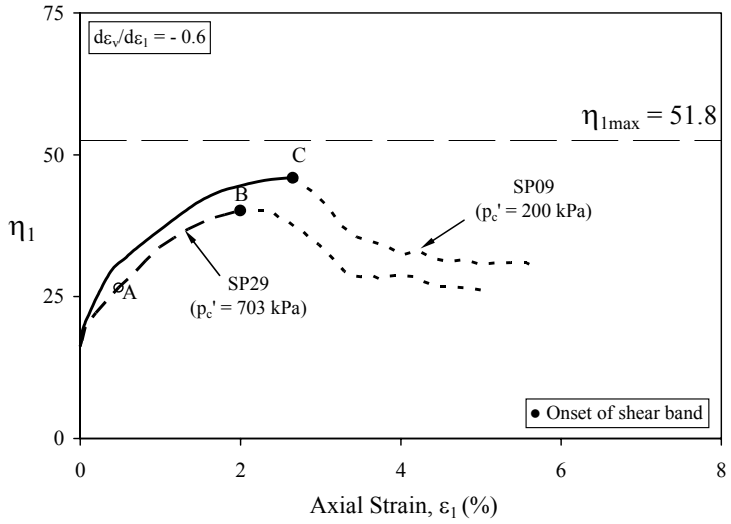

Fig. 5.15(c)

Fig. 5.15 Effect of p_c' on the strain softening behaviour of medium dense sand: (a) effective stress paths; (b) stress-strain curves; (c) η_1 versus ε_1 curves

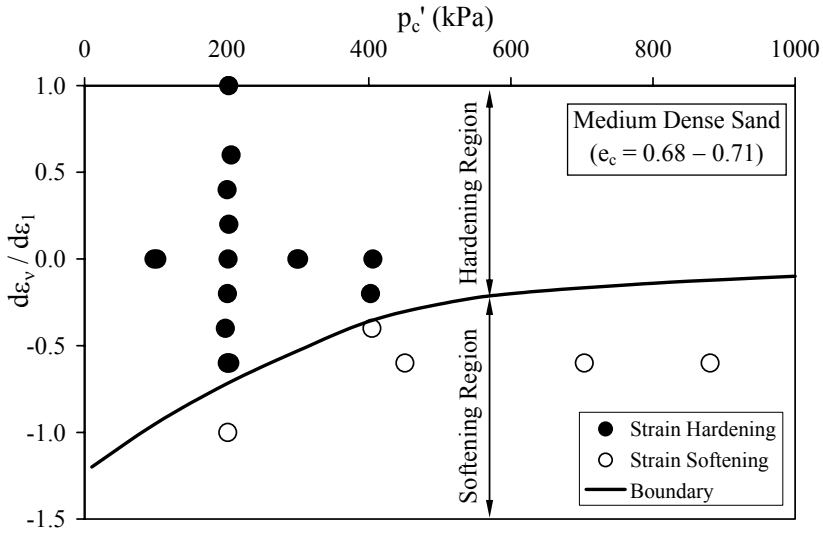

Fig. 5.16 Response boundary on $d\varepsilon_v/d\varepsilon_1$ versus p_c' plane determined for medium dense sand under plane-strain conditions

Fig. 5.16 presents all the strain path tests conducted on medium dense specimens as points on the $d\varepsilon_v/d\varepsilon_1$ versus p_c' plane. It can be observed from Fig. 5.16 that there is a response boundary, which divides the plane into a softening region and a hardening region. Points located exactly on the response boundary represent critical test conditions when pre-failure strain softening can be initiated. As established by Chu et al. (1992) under axisymmetric conditions, this boundary can be used to estimate whether strain softening or strain hardening occur under a given initial

effective confining stress and a constant strain increment ratio condition. The data presented in this section verifies that the response boundary of pre-failure strain softening is also applicable under plane-strain conditions. If the influence of void ratio, e_c, is taken into consideration (see Fig. 5.14), a critical surface can be formed in three dimensional $p_c' - e_c - (-d\varepsilon_v/d\varepsilon_1)$ space, as schematically shown in Fig. 5.17. The critical surface illustrates the mutual influence of p_c', e_c, and $d\varepsilon_v/d\varepsilon_1$ on the occurrence of strain softening under plane-strain conditions. However, more tests with various initial conditions are needed to determine the critical surface for strain softening precisely.

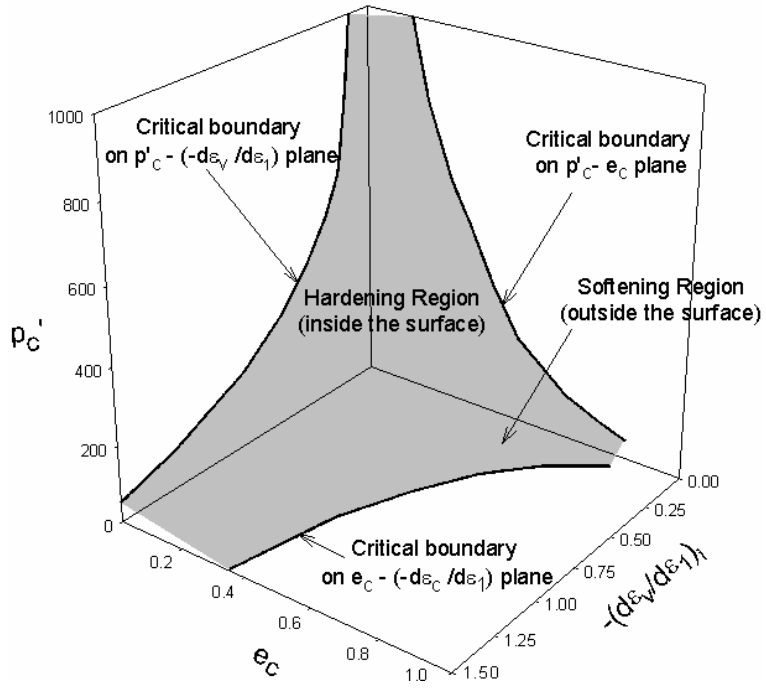

Fig. 5.17 Critical surface for the occurrence of strain softening

5.4.4 Post-Failure Strain Softening

The data presented in the preceding section shows that pre-failure strain softening can occur as a material property in some plane-strain tests. On the other hand, it was demonstrated that the shear band development was closely related to the failure under plane-strain conditions. Therefore, the post-failure strain softening behaviour observed in these tests is always a strain localization type. To study the post-failure behaviour of sand under plane-strain conditions, another series of strain

path tests was conducted. The testing conditions of all the tests are summarised in Table 5-4. All the specimens were prepared using the WS method and K_0 consolidated to p_c' = 200 kPa before shearing. In conducting the test, all the specimens were brought to the failure state by drained stress paths. Then, a $d\varepsilon_v/d\varepsilon_1$ = *constant* path was imposed. The imposed strain increment ratio ranged from +0.6 to -1.0. The $d\varepsilon_v/d\varepsilon_1$ path was imposed when q/p' just reached $(q/p')_f$ = 1.53.

Table 5-4 Summary of testing conditions in post-failure strain path testing.

Test No	e_c	Dr_c (%)	Density state	p_c' (kPa)	q_c (kPa)	$(d\varepsilon_v/d\varepsilon_1)_i$	$(d\varepsilon_v/d\varepsilon_1)_f$
SP01F	0.688	59	medium dense	199.5	221.0	+0.60	-0.80
SP02F	0.681	61		201.1	221.6	0.00	-0.81
SP03F	0.675	63		199.8	221.2	-0.20	-0.81
SP04F	0.682	61		198.1	222.4	-0.60	-0.82
SP05F	0.685	60		200.4	222.7	-1.00	-0.81

The stress-strain curves of these tests are presented in Fig. 5.18(a). It can be seen from Fig. 5.18(a) that prior to reaching the failure state the stress-strain curves are almost identical, indicating a good repeatability of test results. After $d\varepsilon_v/d\varepsilon_1$ was imposed, the post-failure behaviour of the four tests became different. The imposed strain increment ratio affects the post-failure behaviour. The specimens tested with $(d\varepsilon_v/d\varepsilon_1)_i$ = 0.0, -0.2, and -0.6 manifested post-failure strain hardening behaviour whereas the specimen tested with $(d\varepsilon_v/d\varepsilon_1)_i$ = -1.0 exhibited post-failure strain softening behaviour. However, shear bands soon became visible in the two tests with $(d\varepsilon_v/d\varepsilon_1)_i$ = -0.2 and -0.6, and strain softening occurred at points B_2 and B_3. The test with $(d\varepsilon_v/d\varepsilon_1)_i$ = 0.0 was terminated before strain softening was observed. However, it would occur with further shearing, as shear band was also developed in this test. For the test with $(d\varepsilon_v/d\varepsilon_1)_i$ = -1.0, it can also be observed from Fig. 5.18(a) that after the shear band was fully developed at point B_1 the post-failure strain softening became more significant. The effective stress ratio, q/p', against axial strain, ε_1, curves for the four tests are plotted in Fig. 5.18(b). The q/p' decreases gradually for all the tests and approached an ultimate state after the shear bands are fully developed. However, no unique ultimate state was observed.

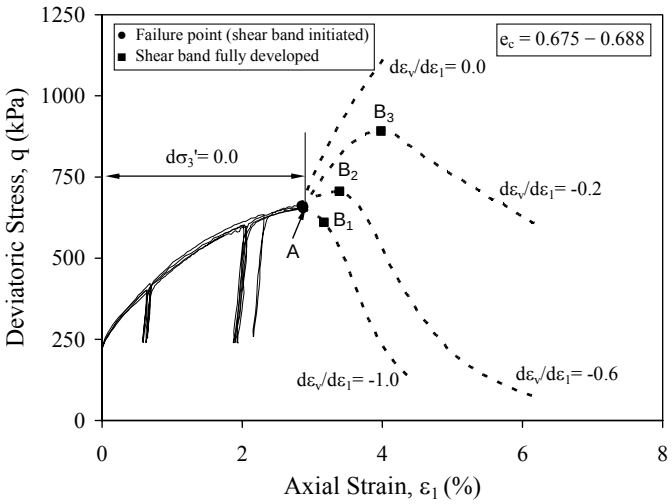

Fig. 5.18(a)

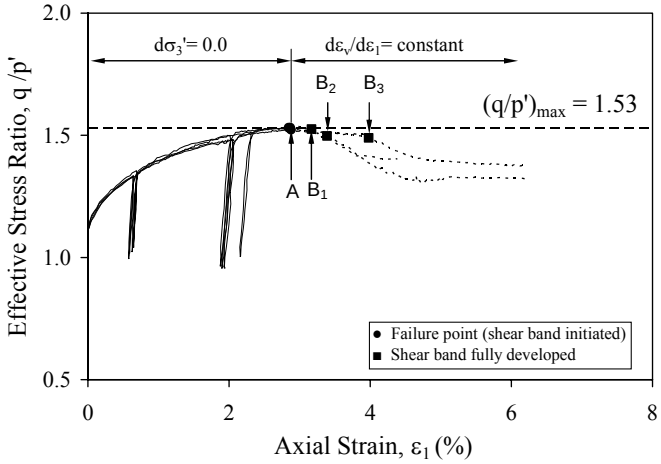

Fig. 5.18(b)

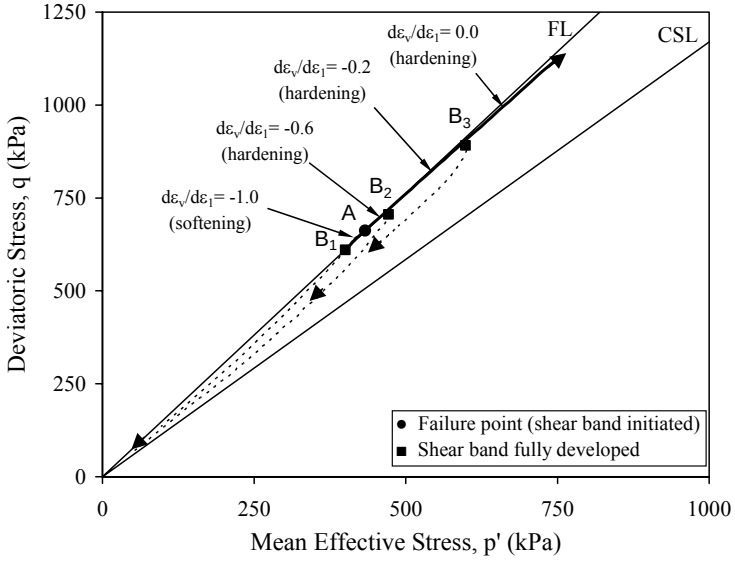

Fig. 5.18(c)

Fig. 5.18 Post-failure response of sand under plane-strain conditions: (a) stress-strain curves; (b) *q/p'* versus ε_1 curves; (c) effective stress paths

The effective stress paths resulted from the above tests are shown in Fig. 5.18(c). It can be seen from Fig. 5.18(c) that the post-failure strain hardening path was obtained from $d\varepsilon_v/d\varepsilon_1$ = 0.0 (undrained) test. The effective stress path obtained from test $d\varepsilon_v/d\varepsilon_1$ = -0.2 was also a strain hardening type, as shown by line A – B_3. However at point B_3, shear bands occurred and both q and p' began to decrease towards the origin. Similar post-failure stress path was obtained from test with $d\varepsilon_v/d\varepsilon_1$ = -0.6. The strain hardening response was observed between point A and B_2, followed by strain softening after shear band formation at point B_2. However, the strain hardening path in test $d\varepsilon_v/d\varepsilon_1$ = -0.6 was shorter than that in test $d\varepsilon_v/d\varepsilon_1$ = -0.2. The effective stress path resulted from test $d\varepsilon_v/d\varepsilon_1$ = -1.0 is also plotted in Fig. 5.18(c). It can be seen that the effective stress path traces down along the failure line immediately after point A. At point B_1, when the shear band is fully developed, the path begins to trace down towards the origin.

It has been illustrated in Fig. 5.18 that the strain increment ratio affects the post-failure behaviour of sand under plane-strain conditions. It was consistently observed that strain softening occurred when the differences between the imposed strain increment ratios and the strain increment ratios at failure were negative. On the other hand, strain hardening occurred when the differences were positive. For example, in Test SP04F $(d\varepsilon_v/d\varepsilon_1)_i$ = -0.60 and $(d\varepsilon_v/d\varepsilon_1)_f$ = -0.82. Consequently, $[(d\varepsilon_v/d\varepsilon_1)_i - (d\varepsilon_v/d\varepsilon_1)_f]$ = 0.22 and strain hardening behaviour prevails in the post-failure region. In Test SP05F however, $[(d\varepsilon_v/d\varepsilon_1)_i - (d\varepsilon_v/d\varepsilon_1)_f]$ = -0.19. Therefore, post-failure strain softening is observed in Test SP05F. The results presented above shows that the post-failure response under plane-strain conditions depends on the relative change in the strain increment ratio. Therefore, the conditions for the occurrence of strain softening (Inequality 5 – 7) established under axisymmetric conditions by Chu et al. (1992) are also applicable under plane-strain conditions. However, the post-failure behaviour under plane-strain conditions is dominated by shear band formation and banding softening eventually occurs.

5.4.5 Discussion

The pre-failure and post-failure strain path tests conducted on medium loose and medium dense sand have shown that under plane-strain conditions strain softening

is associated with the development of shear bands. Furthermore, the failure state under plane-strain conditions is related to the development of shear bands and the peak strength may be largely dependent on the conditions at which shear banding occurs.

It has been observed from the experimental data that even if material softening occurs in the pre-failure region, shear bands will also occur in the post-failure region and banding softening will occur subsequently. During the material softening stage, the deviatoric stress decreases slowly and the effective stress path approaches the failure line. When the specimen reaches the banding softening stage, the deviatoric stress decreases abruptly and the shear band fully develops. The strain softening behaviour observed for very loose sand is an exception because shear band formation does not occur and the critical state is eventually reached. For a test in which a shear band is initiated in the hardening region, only banding softening will occur. A material softening will not take place and failure is likely caused by shear band development.

The post-failure strain path test results presented in the preceding section show that the formation of shear bands in plane-strain tests is not instantaneous but progressive. Therefore, a temporary strain hardening can be observed in post-failure region even though strain hardening criterion is met. After shear bands are fully developed in specimens, post-failure strain softening occurred. The experimental results show that under plane-strain conditions, the behaviour in the post-failure region is dominated by banding softening irrespective of what kind of strain path is used.

5.5 Effect of Loading Mode on Stress-Strain Behaviour of Sand in Strain Path Testing

The effect of loading mode on the drained and undrained behaviour of sand was discussed in Chapter 4. It has been shown that the failure line, the CSL and instability lines were not affected by the loading mode. However, the CSRL obtained from undrained test conducted on medium dense sand might be influenced by the loading mode. To study whether the loading mode has any effect on the

behaviour of sand in strain path testing, two sets of tests conducted on medium dense and very loose specimens under both the deformation-controlled (DC) and the load-controlled (LC) loading modes are compared. The strain increment ratio $d\varepsilon_v/d\varepsilon_1$ = -0.6 was imposed in all the tests. The DC tests were conducted at a rate of 0.05 mm/min and the LC tests at a rate of 0.01 kN/min. A summary of the testing conditions is given in Table 5-5.

Table 5-5 Summary of the plane-strain tests conducted under different loading modes.

Test No	Preparation method	e_c	Dr_c (%)	Density state	$d\varepsilon_v/d\varepsilon_1$	p_c' (kPa)	q_c (kPa)	Loading mode
SP09	WS	0.679	62	medium	-0.6	200.0	222.4	DC
SP33L		0.672	64	dense		201.7	227.0	LC
SP12	MT	0.887	8	very	-0.6	199.8	169.0	DC
SP36L		0.883	9	loose		199.4	170.0	LC

5.5.1 Medium Dense Sand

The results of the two tests SP09 and SP33L conducted on medium dense sand are compared in Fig. 5.19. The specimens were K_0 consolidated to mean effective stresses, p_c' of 200 kPa and 202 kPa respectively. Test SP09 was conducted under a DC loading mode and Test SP33L under a LC loading mode. The effective stress paths obtained from the two tests are compared in Fig. 5.19(a). The stress paths in the two tests are similar and end up at the same CSRL.

The stress-strain curves for the two tests are plotted in Fig. 5.19(b). The stress-strain curves in the pre-peak region are very similar. Both specimens exhibited strain hardening behaviour and reached peak deviatoric stress values due to shear band formation. However, the peak values and the axial strains at the peak are different. It can be seen from Fig. 5.19(b) that the higher peak deviatoric stress was obtained from Test SP33L. This effect may be attributed to the different strain rates used in the two tests. As shown in Fig. 5.19(c), in Test SP33L, a lower $d\varepsilon_1/dt$ was used. Therefore, a negative strain rate effect on the peak deviatoric stress was observed from the two tests. The negative strain rate effect observed here has been

reported by a few other researchers in the past as well (Seed & Lundgren, 1954, Nash & Dixon, 1961, Whitman & Healy, 1962). It should be noted from Figs. 5.19(b) and 5.19(c) that the post-peak behaviour observed in the two tests is also different. In Test SP33L the deviatoric stress dropped suddenly at the peak point, whereas in Test SP09 the deviatoric stress reduced gradually with axial strain in the post-peak region. In Test SP09, the deformation rate was controlled constant, so $d\varepsilon_1/dt$ maintained at the same rate in both the pre-peak and post-peak regions (Fig. 5.19(c)). In Test SP33L, the load was controlled to increase at a given rate. When the deviatoric stress reached the peak, the specimen could not sustain any extra load and became unstable. As a result, ε_1 shot up almost instantly at the peak, as shown in Fig. 5.19(c). Therefore, instability occurred in Test SP33L and strain softening occurred in Test SP09. It should be pointed out that shear bands occurred at the peaks in both tests. However, the specimen in the LC test collapsed after the shear band occurred whereas the specimen in the DC test remained stable.

The excess pore water pressure versus axial strain curves obtained from the two tests are compared in Fig. 5.19(d). Similar behaviour is observed in the two tests. However, in the LC test, a more negative excess pore water pressure is generated at the peak point. The *q/p'* versus ε_1 curves and *b-value* versus ε_1 plots are presented in Fig. 5.19(e). It can be seen that the two specimens reached the same asymptotic stress ratio, $(q/p')_{asy}$ = 1.45. The *b-values* obtained from the two tests before the peaks were also similar and varied between 0.23 and 0.40.

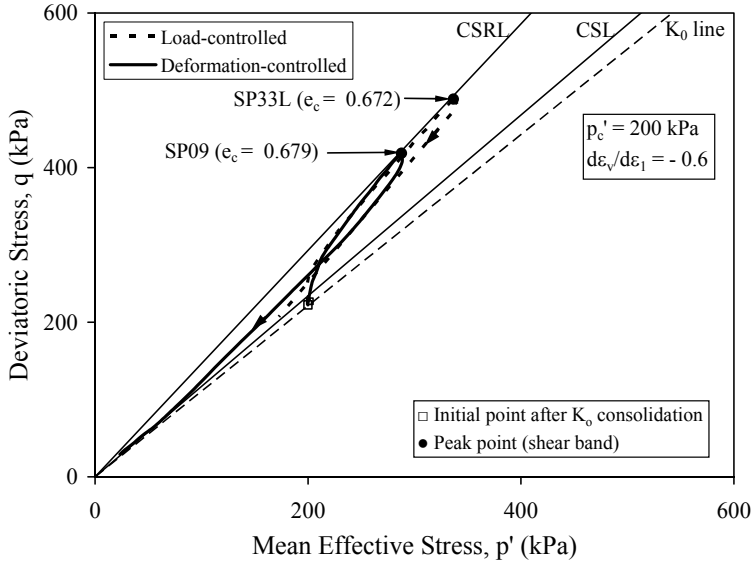

Fig. 5.19(a)

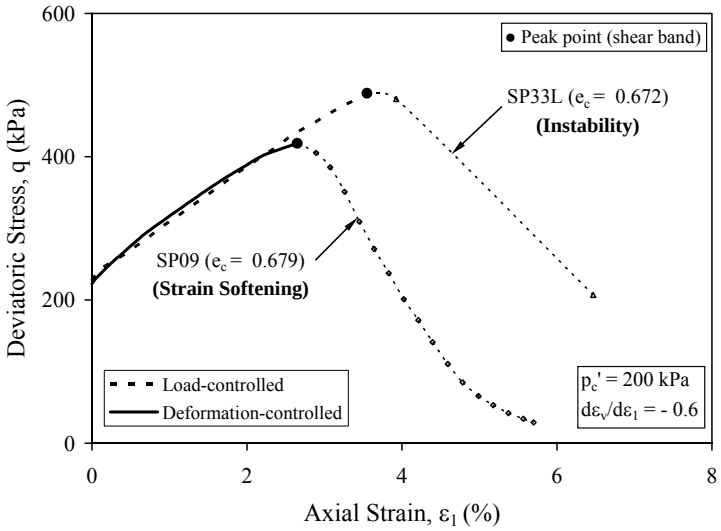

Fig. 5.19(b)

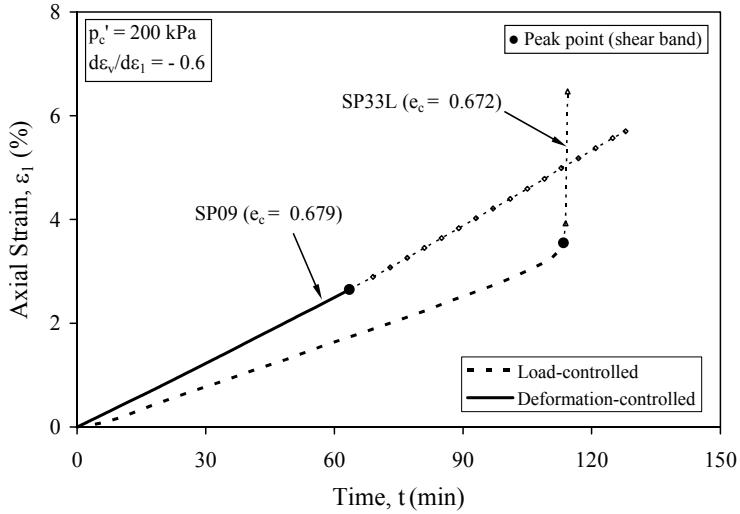

Fig. 5.19(c)

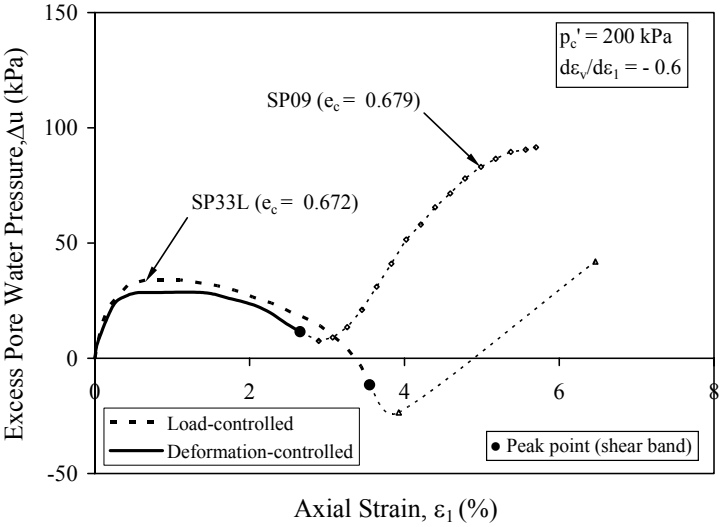

Fig. 5.19(d)

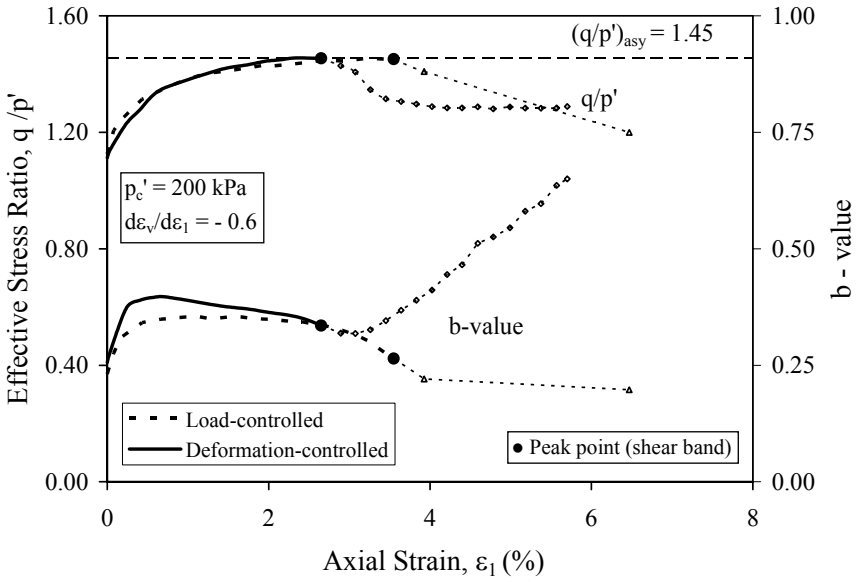

Fig. 5.19(e)

Fig. 5.19 Comparison of strain path tests conducted on medium dense sand under deformation-controlled and load-controlled loading modes: (a) effective stress paths; (b) stress-strain curves; (c) ε_1 versus *time* curves; (d) Δu versus ε_1 curves; (e) *q/p'* and *b-value* versus ε_1 curves

5.5.2 Very Loose Sand

The results of two tests conducted on very loose specimens with comparable void ratios are presented in Fig. 5.20. Test SP12 was conducted under a DC loading mode and Test SP36L under a LC loading mode. The specimens were K_0 consolidated to initial effective confining stresses of 200 kPa and 199 kPa respectively. The effective stress paths of the two tests are compared in Fig. 5.20(a). It can be seen that the two paths are very similar. The peak points occurred along the same peak stress line. After the peak both stress paths traced towards the CSL.

The deviatoric stress versus axial strain curves for the two tests are plotted in Fig. 5.20(b). The two curves are similar only in the pre-peak region. The peak occurred at around an axial strain of 0.1% in both tests. However, the post-peak behaviour observed in the two tests is different. In Test SP36L the deviatoric stress dropped suddenly and the axial strain increased suddenly, as shown in Fig. 5.20(c). Thus, the specimen became unstable at the peak and instability occurred in the LC test.

The specimen physically collapsed. On the other hand, in Test SP12, the deviatoric stress reduced gradually (Fig. 5.20(b)) and the axial strain increased linearly with time (Fig. 5.20(c)). Therefore, strain softening occurred in the DC test.

The excess pore water pressure versus axial strain curves are shown in Fig. 5.20(d). The two curves are almost the same. However, in Test CK_0U05L, the pore water pressure increased more significantly after the specimen became unstable at the peak.

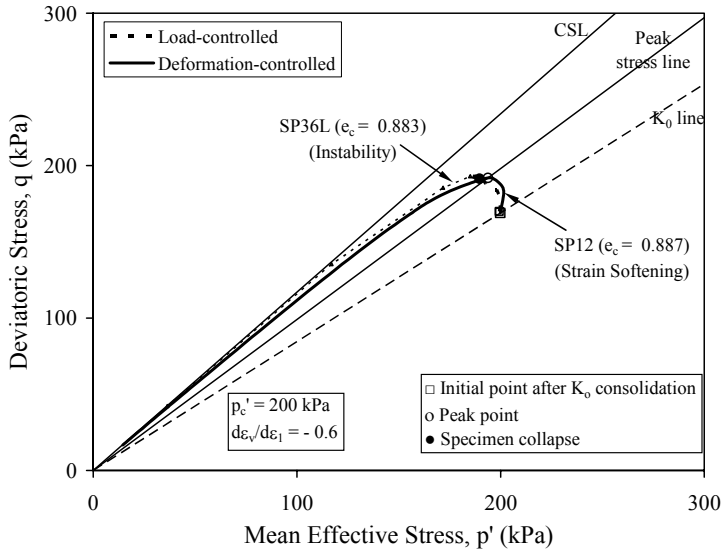

Fig. 5.20(a)

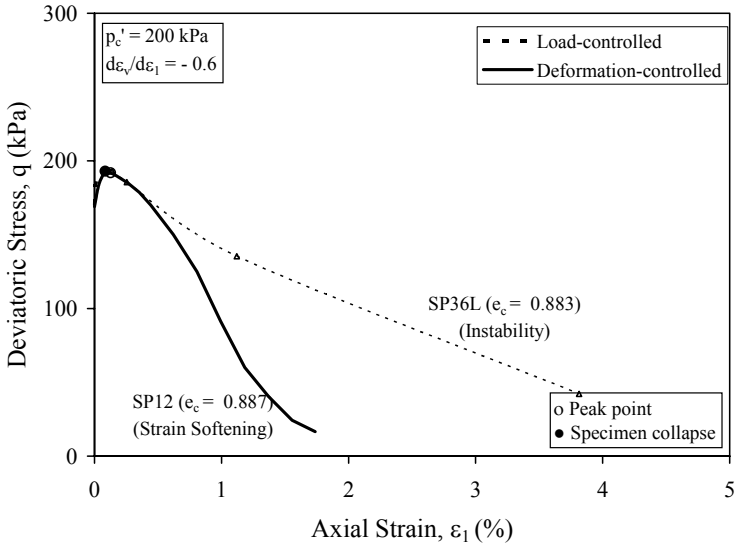

Fig. 5.20(b)

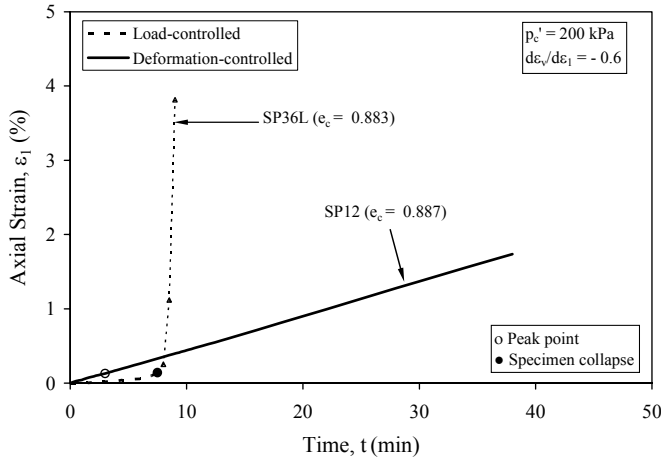

Fig. 5.20(c)

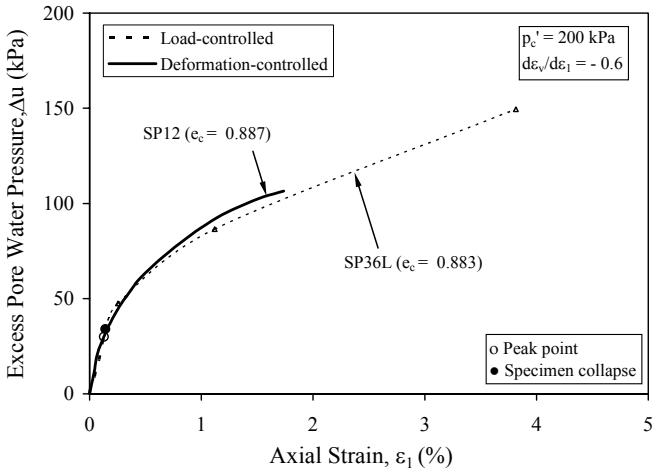

Fig. 5.20(d)

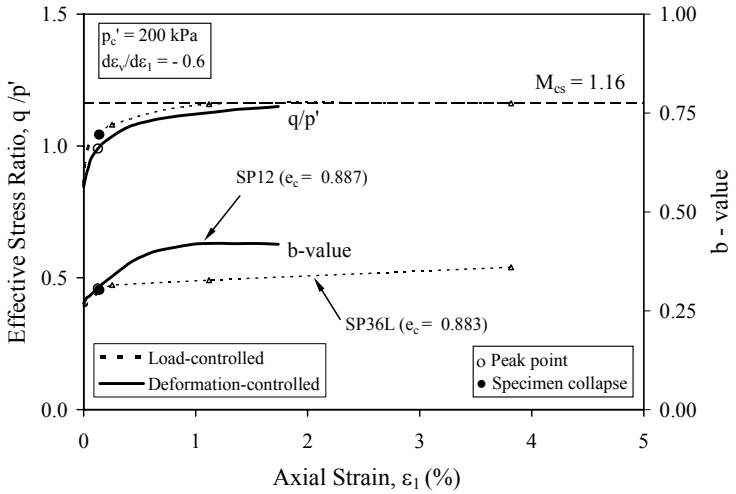

Fig. 5.20(e)

Fig. 5.20 Comparison of strain path tests conducted on very loose sand under deformation-controlled and load-controlled loading modes: (a) effective stress paths; (b) stress-strain curves; (c) ε_1 versus *time* curves; (d) Δu versus ε_1 curves; (e) *q/p'* and *b-value* versus ε_1 curves

The *q/p'* versus ε_1 curves and the *b-value* versus ε_1 curves are shown in Fig. 5.20(e). It can be seen that the specimens in the two tests approached asymptotically the same *q/p'* ratio, that is, M_{cs} = 1.16. The *b-values* observed in the pre-peak region were quite similar for both tests but diverged after the peak. The *b-value* was in the range between 0.26 and 0.42.

5.5.3 Discussion

The results obtained from the $d\varepsilon_v/d\varepsilon_1$ = -0.6 path tests conducted under both DC and LC loading modes showed that the CSRL for medium dense sand and the peak stress line for very loose sand are independent of the loading mode. Stress-strain behaviour observed in load-controlled and deformation-controlled tests is similar in the pre-peak region. However, the behaviour in the post-peak region is different. In the post-peak region, instability occurs in load-controlled tests, whereas strain softening develops in deformation-controlled tests. Similar conclusions were made for drained and undrained conditions, as presented in Chapter 4.

5.6 Shear Band Formation

The results of a strain path test SP05 conducted on a medium dense specimen (e_c = 0.677) using $d\varepsilon_v/d\varepsilon_1$ = -0.4 have been presented in Fig. 5.11 (see Section 5.4.3.2). The photographs taken during the test are given in Fig. C.6 in Appendix C. Selected photos taken around the shear band formation are shown in Fig. 5.21(a). It can be seen that shear band occurred at point 5. The σ_2 versus ε_1 curves as measured by four different load cells are shown in Fig. 5.21(b). It can be seen that σ_2 versus ε_1 curves start to diverge at point 4(O). As discussed in Chapter 4, the divergence in the $\sigma_2 - \varepsilon_1$ curves is an indication that shear bands might have occurred at point 4(O). As shown in Fig. 5.21(c), point 5(P,B) where the shear band became visible is the peak point on the $q - \varepsilon_1$ curve. It can also be seen from Fig. 5.21(d) that the pore water pressure started to increase soon after point 5(P,B) which is another indication that shear band had occurred. As discussed in Chapter 4, shear band only becomes visible when it is fully developed. Therefore, the shear band is likely to have started at point 4(O). Similar behaviour of medium loose sand can also be observed in Fig. 5.22, where results of Test SP26 are presented.

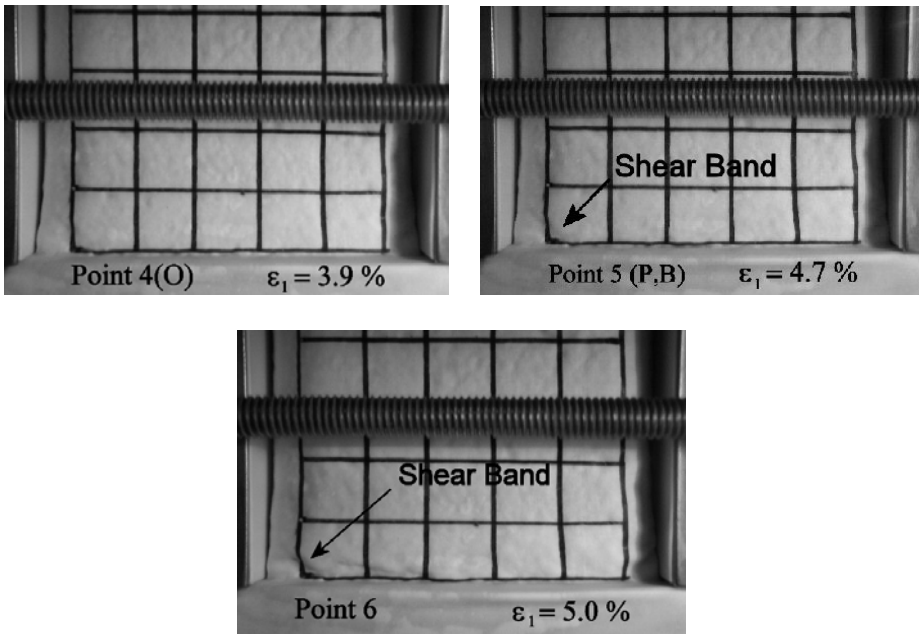

Fig. 5.21(a)

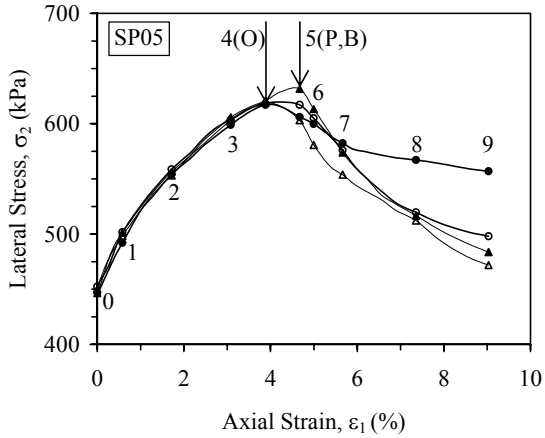

Fig. 5.21(b)

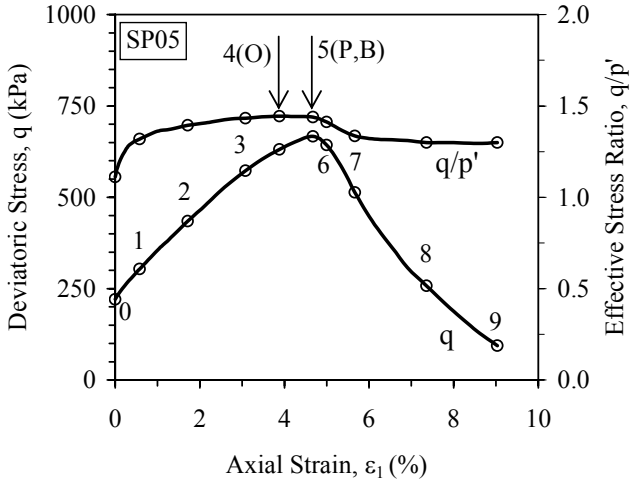

Fig. 5.21(c)

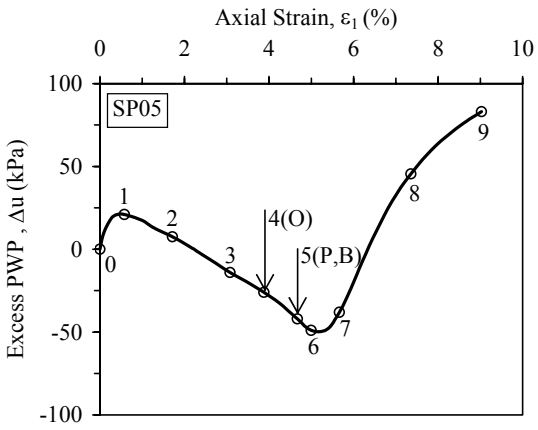

Fig. 5.21(d)

Fig. 5.21 Shear band development in Test SP05: (a) selected photos; (b) σ_2 versus ε_1 curves; (c) q versus ε_1 and q/p' versus ε_1 curves; (d) Δu versus ε_1 curves

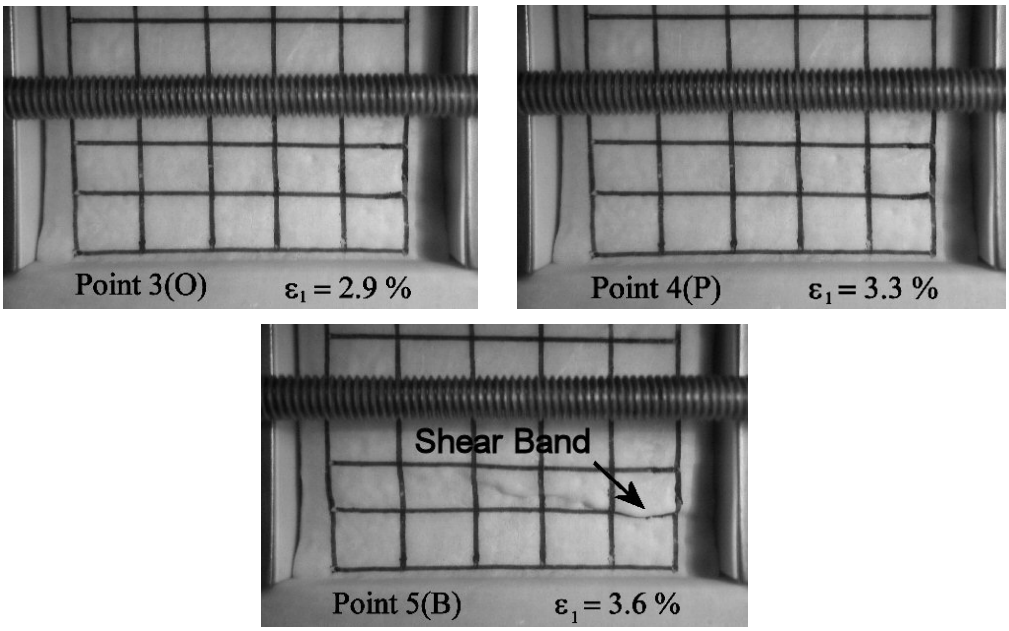

Fig. 5.22(a)

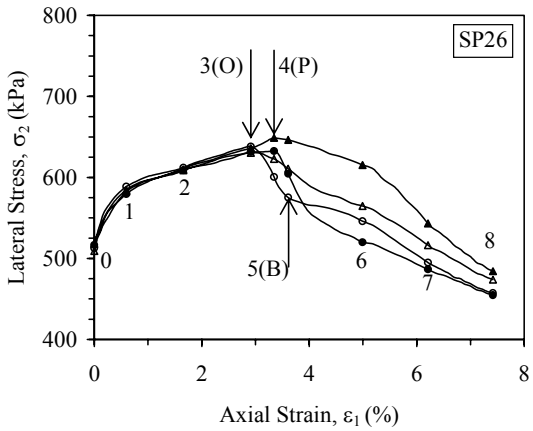

Fig. 5.22(b)

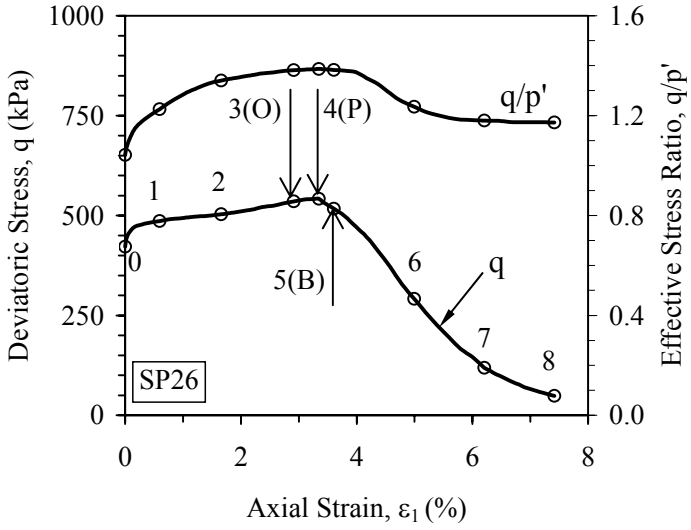

Fig. 5.22(c)

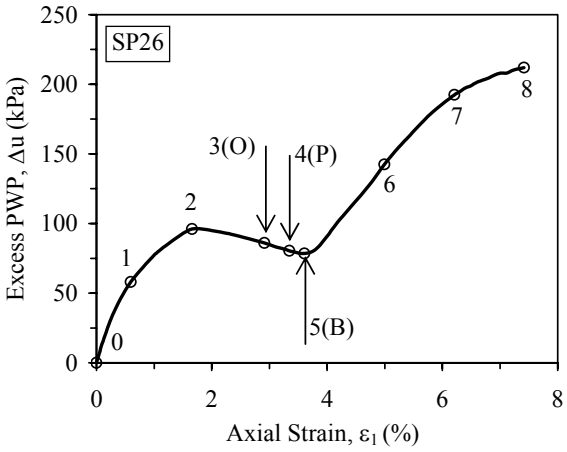

Fig. 5.22(d)

Fig. 5.22 Shear band development in Test SP26: (a) selected photos; (b) σ_2 versus ε_1 curves; (c) q versus ε_1 and q/p' versus ε_1 curves; (d) Δu versus ε_1 curve

The results of Test SP28 conducted on medium loose specimen (e_c = 0.750) are presented in Fig. 5.23. In Test SP28 the specimen was K_0 consolidated to p_c' = 880 kPa. After that the strain increment ratio of -0.6 was imposed. The photographs taken during the test are presented in Fig. C.8 (Appendix C). Selected photos taken around the shear band are also shown in Fig. 5.23(a). From the σ_2–ε_1 curves shown in Fig. 5.23(b), there is little variation in σ_2 values obtained from the four different load cells before point 3(O) is reached. It is indicative that the shear band has occurred at point 3(O). It can be seen from the q–ε_1 curve shown in Fig. 5.23(c) that strain softening occurred at point 1(P). As the axial strain at point 1(P) is only

less than 1% where shear band would not occur, the strain softening occurred at point 1(P) was element behaviour. The excess pore water pressure versus axial strain curve obtained from Test SP28 is presented in Fig. 5.23(d). It can be seen that pore water pressure started to increase at higher rate at point 4(B) where the shear band became visible.

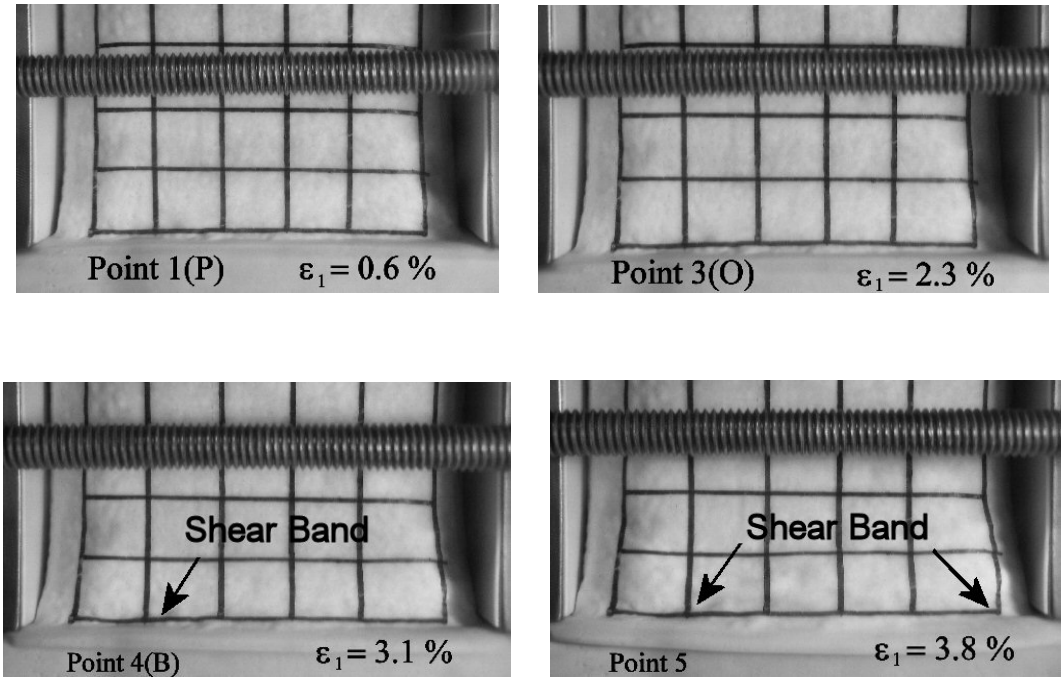

Fig. 5.23(a)

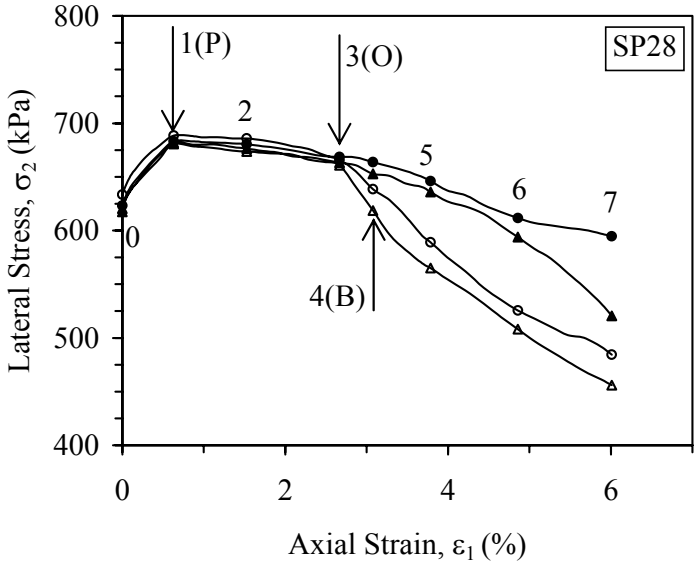

Fig. 5.23(b)

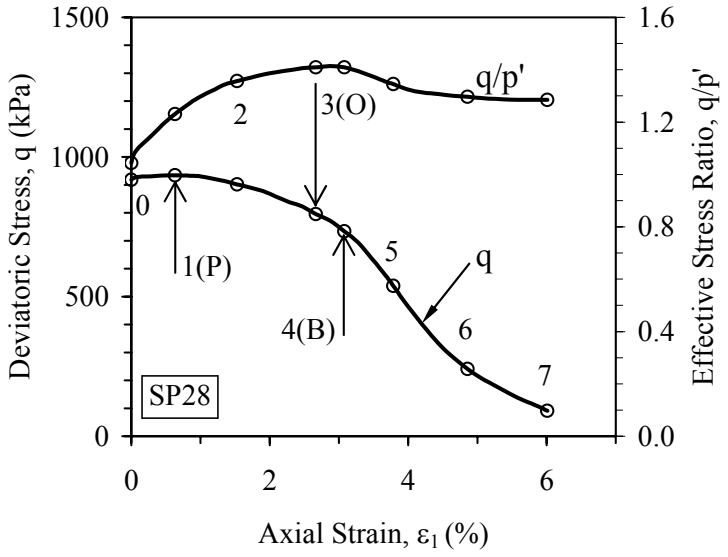

Fig. 5.23(c)

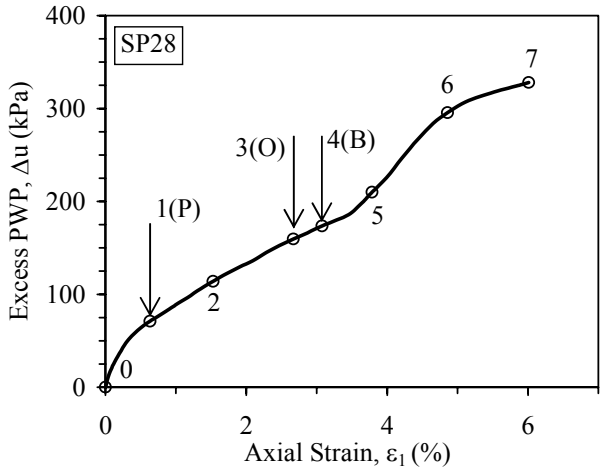

Fig. 5.23(d)

Fig. 5.23 Shear band development in Test SP28: (a) selected photos; (b) σ_2 versus ε_1 curves; (c) q versus ε_1 and q/p' versus ε_1 curves; (d) Δu versus ε_1 curve

The typical mode of the shear bands developed during strain path tests is identical with that observed under drained and undrained conditions (see Fig. 4.32 in Chapter 4). The shear band on the σ_3 plane is indicated by a nearly horizontal band and the shear band on the σ_2 plane is inclined with an angle θ. The average value of the angle θ is 56°. An example of shear band observed in Test SP26 is presented in Fig. 5.24.

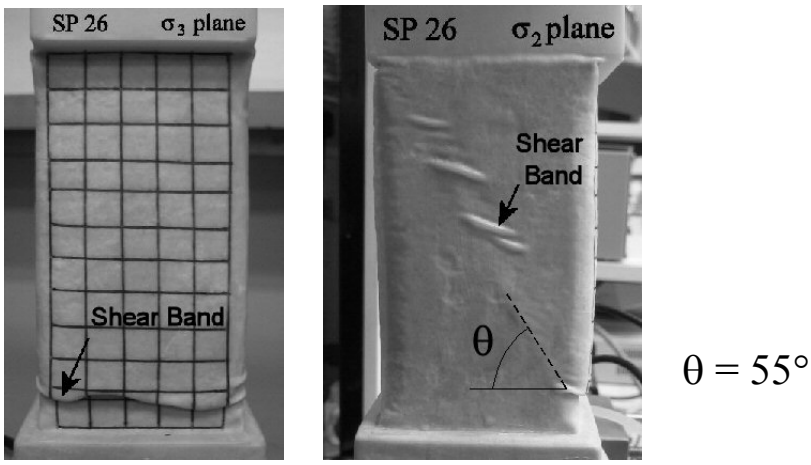

Fig.5.24 A shear band observed at the end of Test SP26

5.7 Summary

The asymptotic state and strain softening response of a granular soil under plane-strain conditions was studied. The results presented in Chapter 5 can be summarized as follows:

- In a strain path test, both pore water pressure and volume are changed. Therefore, it can be used to simulate various drainage conditions. The stress-strain behaviour of soil under strain path controlled conditions is not bound by undrained $(d\varepsilon_v/d\varepsilon_1 = 0)$ and drained behaviour.

- The stress-strain behaviour of sand under plane-strain conditions is strain path dependent. When the strain increment ratio imposed, $(d\varepsilon_v/d\varepsilon_1)_i$, is larger (i.e., more positive) than a threshold value, strain hardening behaviour will prevail. On the other hand, when the $(d\varepsilon_v/d\varepsilon_1)_i$ is smaller (i.e., more negative) than a threshold value, strain softening will occurs. The threshold strain increment ratio is defined as $(d\varepsilon_v/d\varepsilon_1)_f$, that is the strain increment ratio at failure as measured in a drained test.

- When medium dense sand is sheared under $d\varepsilon_v/d\varepsilon_1 = const$ path, the resulting effective stress path will approach asymptotically a constant stress ratio line (CSRL). The smaller (i.e., more negative) the imposed strain increment ratio, the larger the resultant asymptotic stress ratio, $(q/p')_{asy}$. The relationship between the imposed strain increment ratio and the resultant

constant stress ratio can be experimentally determined. For plane-strain conditions, the relationship can be expressed as:

$$\left(\frac{q}{p'}\right)_{asy} = \begin{cases} M_0 - \mu\left(d\varepsilon_v / d\varepsilon_1\right), & for \quad d\varepsilon_v / d\varepsilon_1 \geq \left(d\varepsilon_v / d\varepsilon_1\right)_f \\ \left(\frac{q}{p'}\right)_f & for \quad d\varepsilon_v / d\varepsilon_1 < \left(d\varepsilon_v / d\varepsilon_1\right)_f \end{cases}$$

where M_0 = 1.37 and μ = 0.23 are the experimental constants. This relationship is consistent with that obtained under axisymmetric conditions by Chu & Lo (1994).

- Under plane-strain conditions, two types of strain softening behaviour, the pre-failure softening and the post-failure softening are identified. A pre-failure strain softening behaviour may consist of three stages, namely, material softening, banding softening, and ultimate state. During the first stage, the deviatoric stress decreases slowly and the effective stress path plunges towards the failure line. As the specimen reaches the banding softening stage the deviatoric stress will decrease abruptly at an accelerated rate and shear bans are developed. At the final stage, shear bands are fully developed and an ultimate state is approached. However, the strain softening behaviour observed for very loose sand is an exception because shear band may not occur even when the critical state is reached. For a test in which material softening does not occur, strain softening will occur only in two stages, i.e., banding softening and ultimate state.

- The occurrence of pre-failure strain softening under plane-strain conditions is affected by the void ratio, the strain increment ratio and the initial effective confining stress. The higher the void ratio, the smaller the strain increment ratio and the larger the initial effective confining stress, the greater tendency for strain softening to occur. Therefore, a response surface can be determined in three dimensional p_c'–e_c–$(-d\varepsilon_v/d\varepsilon_1)$ space. This surface represents the critical conditions for strain softening to occur. This is consistent with findings established by Chu et al. (1992) under axisymmetric conditions.

- The post-failure strain softening under plane-strain conditions is also studied. Although the strain hardening can be observed under some strain paths, it is only temporary, as shear band will occur and lead to strain softening. Before a shear band is fully developed in a specimen, the effective stress path can trace upwards along the failure line determined by drained tests. However, after the shear band is fully formed, the effective stress path will go downwards and approach an ultimate state.

- The results obtained from strain path tests conducted under both DC and LC loading modes show that the constant stress ratio line for medium dense sand and the peak stress line for very loose sand are independent of the loading mode. Furthermore, the stress-strain behaviour observed in load-controlled and deformation-controlled tests is similar in the pre-peak region. However, the behaviour in the post-peak region is different. In the post-peak region, instability occurs in load-controlled tests, whereas strain softening develops in deformation-controlled tests. This is consistent with the observations made in Chapter 4 under drained and undrained conditions.

CHAPTER 6

INSTABILITY BEHAVIOUR OF SAND

6.1 Introduction

Catastrophic failures in geotechnical structures can be initiated by the instability of soil. Instability refers to a phenomenon in which large plastic strains are generated rapidly due to the inability of the soil element to sustain a given load or stress, including small perturbations. Liquefaction and pre-failure instability under undrained condition has often been considered as the triggering factors for the failure of loose granular slopes (Castro, 1969; Ishihara, 1993; Lade, 1993). Furthermore, there are cases where instability occurred under essentially drained or other drainage conditions (Been et al., 1988; Eckersley, 1990; Olson et al., 2000). Although several studies on instability of sand have been reported in the literature (e.g. Lade & Pradel, 1990; Lade 1992, 1993; Chu et al., 1993, 2003; Vaid & Eliadorani, 1998; Leong et al., 2000), most of them were conducted under axisymmetric stress conditions.

The objective of this chapter is to investigate the instability behaviour of sand under plane-strain conditions and to verify whether the studies conducted under axisymmetric conditions are still applicable to plane-strain conditions. Instability tests on very loose to medium dense specimens under various drainage conditions were conducted. The factors affecting the instability behaviour of sand under plane-strain conditions are studied. Finally, the effect of shear band formation on the instability of sand is discussed.

6.2 Testing Programme

Three series of instability tests were conducted to study the pre-failure instability behaviour and to investigate the factors that influence the instability of Changi sand under undrained, drained and strain path controlled conditions. Two specimen preparation methods, the moist tamping (MT) and the water sedimentation (WS) were used. The MT method was used for the preparation of very loose specimens and the WS method for medium loose or medium dense specimens. All the specimens were K_0 consolidated to the designed initial mean effective stress.

6.3 Instability Behaviour of Sand under Undrained Conditions

6.3.1 Introduction

The unstable behaviour of Changi sand under undrained conditions in triaxial compression and extension tests was studied by Leong (2001), Gan (2002) and Loke (2004). It has been established that only loose granular soil becomes unstable under undrained conditions. The instability will not occur for dense sand under undrained conditions (Chu et al., 1993; Chu & Leong, 2001). Furthermore, stress level has a dominant effect on the pre-failure instability as discussed by Leong et al. (2000). Whether these findings are still applicable to plane-strain conditions needs to be verified. For this purpose, a series of five undrained instability tests was conducted. A summary of the testing conditions is presented in Table 6-1.

Table 6-1 Summary of instability tests conducted under undrained conditions.

Test No	Preparation method	Density state	e_c	p_c' (kPa)	q_c (kPa)	Remarks
INU01	MT	very loose	0.907	150.2	126.1	Unstable
INU02			0.910	120.1	101.3	Unstable
INU03			0.894	180.0	151.6	Stable
INU04			0.893	190.8	181.8	Unstable
INU05	WS	medium dense	0.653	200.3	221.2	Stable

6.3.2 Very Loose Sand

The results of three instability tests INU01, INU02, and INU03 are presented in Fig. 6.1. Test INU01 was performed by shearing the specimen from the K_0 condition (point A_1) to an effective stress ratio of $q/p' = 1.04$ (point B_1) along a drained path, as shown in Fig. 6.1(a). Upon reaching point B_1, an undrained condition was imposed while the deviatoric stress was maintained constant. The void ratio at point B_1 was $e = 0.889$. The instability line (IL) corresponding to $e = 0.888$ as determined by the undrained test conducted on very loose sand (see Figs. 4.12 and 4.13 in Chapter 4) is also plotted in Fig. 6.1(a).

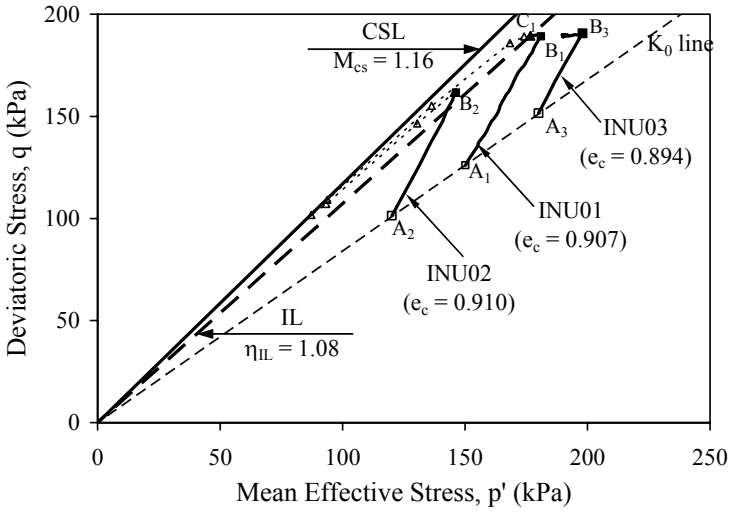

Fig. 6.1(a)

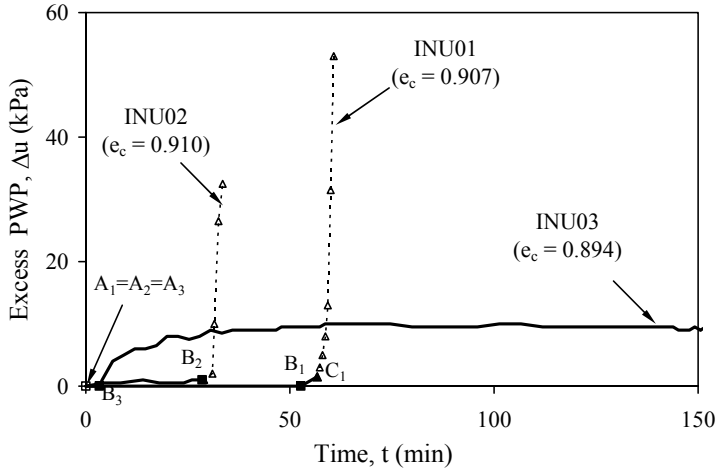

Fig. 6.1(b)

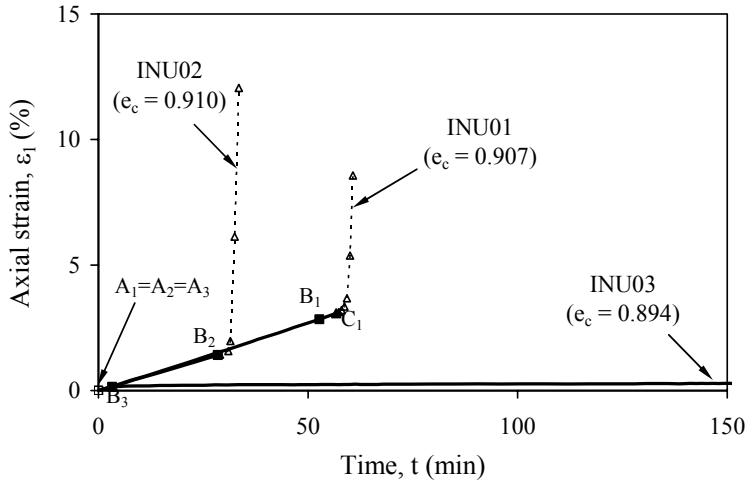

Fig. 6.1(c)

Fig. 6.1 Results of undrained instability tests conducted on very loose specimens: (a) effective stress paths; (b) excess pore water pressure against time curves; (c) axial strain against time curves

The excess pore water pressure and the axial strain development during the instability test are shown in Figs. 6.1(b) and 6.1(c) respectively. It can be seen from Fig. 6.1(b) that in Test INU01, the pore water pressure started to increase immediately after drainage conditions were changed from drained to undrained at point B_1. Within next few minutes the pore water pressure shot up and instability occurred at point C_1. This was accompanied by a sudden increase in axial strain rate, as shown in Fig. 6.1(c). The effective stress at point C_1 is shown in Fig. 6.1(a). It can be seen that C_1 is close to the IL. When instability occurred, the specimen physically collapsed.

Test INU02 was conducted in a way similar to Test INU01. After K_0 consolidation the stress state was brought to point B_2 (q/p' = 1.11). The void ratio at point B_2 was e = 0.888. It can be seen from Fig. 6.1(a) that point B_2 is slightly above the IL, corresponding to e = 0.888. Upon reaching point B_2, the deviatoric stress was maintained constant and an undrained condition was imposed. Under such conditions, the pore water pressure and axial strain increased rapidly at point B_2, as shown in Figs. 6.1(b) and 6.1(c). The instability occurred and the specimen physically collapsed.

Test INU03 was carried out in a way similar to Test IND02, except that the consolidation stresses are higher. As shown in Fig. 6.1(a), the specimen was brought from point A_3 to point B_3 along a drained path. The deviatoric stress at point B_3 is the same as that in Test INU01 (q = 190 kPa). However, in terms of effective stress ratio, the q/p' at point B_3 is 0.96, which is lower than that at point B_1 (for Test INU01). The void ratio at B_3 is 0.886. Upon reaching point B_3, the deviatoric stress was kept constant and an undrained condition was imposed. During a period of 150 min, the pore water pressure and the axial strain did not change much (Figs. 6.1(b) and 6.1(c)). The specimen was at a stable state.

The results of the above three tests indicate that the undrained instability can occur for very loose sand under plane-strain conditions. The occurrence of undrained instability appears to be controlled by the stress ratio q/p'. When q/p' reaches the q/p' of the instability line, instability occurs, as in Tests INU01 and INU02. However, if q/p' is much smaller than q/p' of the IL, instability will not occur even if the same q is used. The above observation is consistent with that made in triaxial tests (Leong, 2001).

6.3.3 Medium Dense Sand

To investigate whether the dense specimen will become unstable under plane-strain conditions, Test INU05 was conducted on dense sand in a way similar to Test INU01. The results obtained from Test INU05 are presented in Fig. 6.2. The CSL and the FL obtained from CK_0D tests conducted on specimens with comparable void ratios are also shown in Fig. 6.2(a). The specimen was K_0 consolidated to an effective confining stress p_c' = 200 kPa (point A in Fig. 6.2(a)). The void ratio at point A was e_c = 0.653. At point A, an undrained condition was imposed and the load was maintained constant for a period of 30 minutes (A – A'). As shown in Fig. 6.2(b), during this period there was only small increase in the pore water pressure at the beginning. There was very little increase in the axial strain too (Fig. 6.2(c)). The specimen was in a stable state. The specimen was further sheared from point A' to point B to an effective stress ratio q/p' = 1.34 along a drained path. Upon reaching point B (Fig. 6.2(a)), an undrained condition was again imposed and the load was maintained constant for a period of 30 minutes. As shown in Fig.

6.2(b), during this period the pore water pressure decreased. The axial strain increased only a little (Fig. 6.2(c)). Therefore, the specimen was perfectly stable (point B'). The same specimen was subsequently sheared to higher stress ratios of *q/p'* = 1.42 (point C) and *q/p'* = 1.49 (point D) along the drained path. Undrained conditions and constant deviatoric stresses were imposed at points C and D for 30 minutes. As shown in Fig. 6.2(b), during these periods the pore water pressures decreased (C – C' and D – D'). Therefore, the effective stress paths moved away from the FL to the right (Fig. 6.2(a)). Along this stress path the deformation behaviour of the soil is essentially elastic. The axial strains observed in the periods C – C' and D – D' were also very small, as shown in Fig. 6.2(c). Therefore, the specimen was stable and pre-failure instability did not occur. After point D' the specimen was sheared further to failure at point F (Fig. 6.2(a)). As the test was conducted under load-controlled loading mode, the failure was manifested in the form of instability. The axial strain increased rapidly at point F (Fig. 6.2(c)) and shear band also occurred. The effective stress path eventually dropped towards the CSL, as shown in Fig. 6.2(a). It may be concluded from this test that pre-failure instability will not occur for dense sand under undrained conditions. This is consistent with the observations made under axisymmetric conditions (Chu & Leong, 2001; Chu et al., 2003).

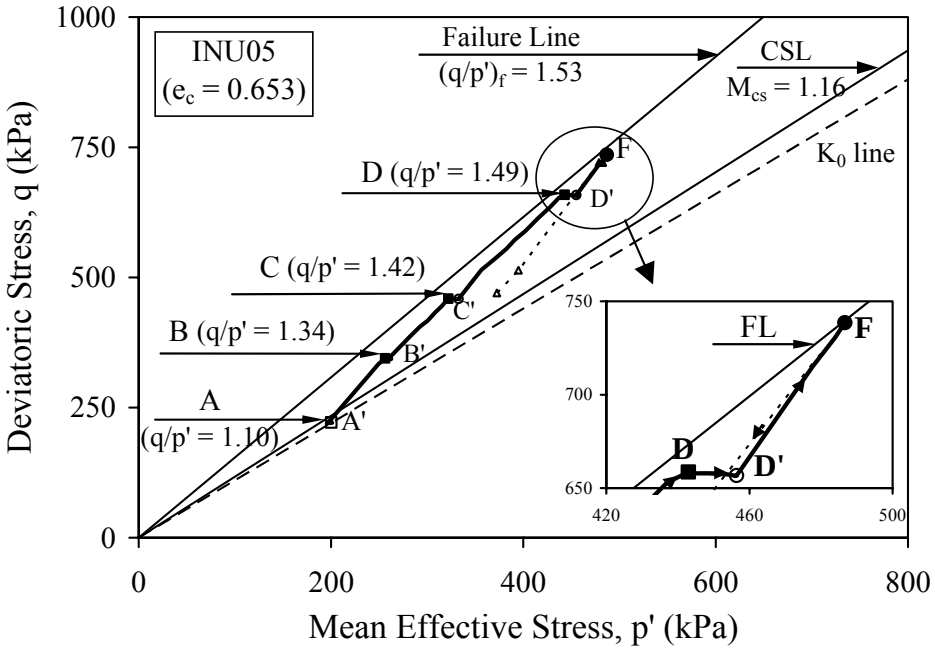

Fig. 6.2(a)

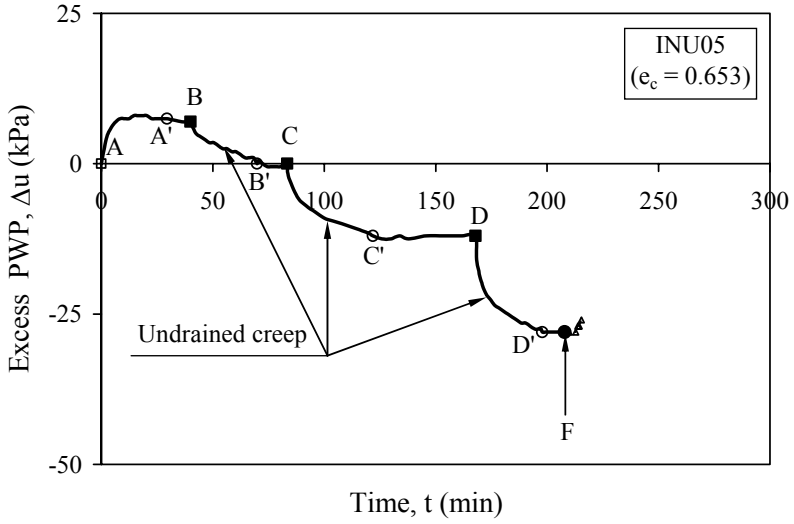

Fig. 6.2(b)

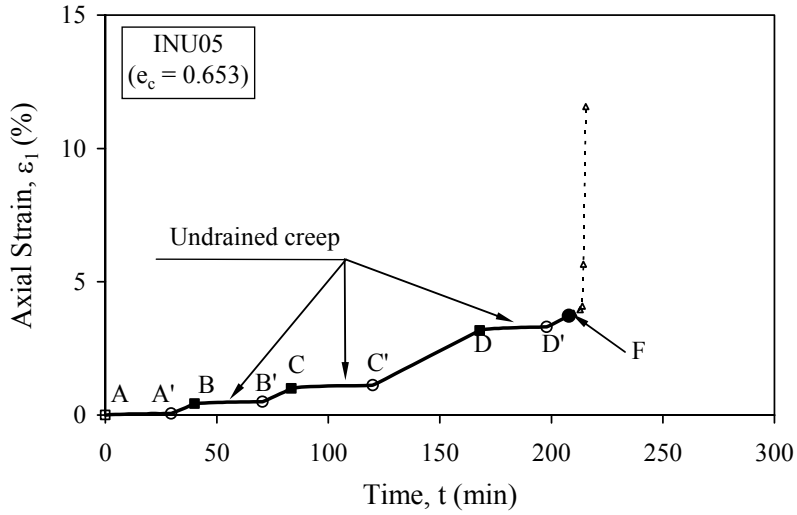

Fig. 6.2(c)

Fig. 6.2 Results of Test INU05 conducted on medium dense sand:
(a) effective stress path; (b) excess pore water pressure versus time curve;
(c) axial strain versus time curve

6.3.4 Discussion

The results of the above four tests indicate that the undrained instability in a form of run-away deformation occurs for very loose sand under plane-strain conditions in the same way as that under axisymmetric conditions. The condition for instability to occur is also the same, that is, the stress state needs to be above the IL. The test results also show that the IL as defined by Lade (1993) is still applicable to the plane-strain conditions. The IL can be obtained by connecting the

peak points of the effective stress paths resulting from undrained tests (see Fig. 4.12 in Chapter 4). Therefore, the IL determined in this way can be used to predict the instability conditions. Instability may also possibly occur even when the initial stress state is slightly below the IL as shown by Leong & Chu (2002) under axisymmetric conditions and Test INU01 under plane-strain conditions. This is because under undrained creep the stress state moves to the left into the instability zone, as shown in Fig. 6.1(a) for Test INU01. When instability occurs, the specimen physically collapses.

The results of Test INU05 indicate that for dilative sand, instability will not occur under undrained conditions. This is in agreement with the results obtained under axisymmetric conditions (Lade & Pradel, 1990; Lade, 1992, 1993; Sasitharan et al., 1993; Leong et al., 2000; Chu & Leong, 2001; Leong & Chu, 2002; Chu et al., 2003). Therefore, it can be concluded that the conditions for the occurrence of instability under undrained conditions are the same for both plane-strain and axisymmetric conditions.

6.4 Instability Behaviour of Sand under Drained Conditions

6.4.1 Introduction

It has been reported by Leong et al. (2000), Chu et al. (2003), and Loke (2004) that instability will not occur under drained conditions if the effective stress state is maintained constant,. However, granular soil can become unstable at a stress state below the failure line under a fully drained condition when the effective stress path is controlled to move into the zone of potential instability. Such conditions can be obtained in the laboratory by a test with constant deviatoric stress, but decreasing mean effective stress. This type of test is referred as a constant shear-drained (CSD) test by Anderson & Riemer (1995) and Anderson & Sitar (1995).

A study on the instability behaviour of loose and dense sand in CSD tests under axisymmetric conditions has been carried out by Leong (2001) and Chu et al. (2003). They have concluded that along a CSD path instability can occur for both loose and dense granular soils. However, this type of drained instability is not the

same as the runaway instability occurring for loose sand under undrained conditions. Therefore, the drained instability has been termed as *conditional* instability by Chu et al. (2003). Loke (2004) has further shown that a conditional instability can evolve into a runaway instability if the amount of volume change generated during the drained instability cannot be accommodated. All the above observations were made under axisymmetric stress conditions. Whether these results can be generalized into plane-strain conditions needs to be studied. Furthermore, shear bands may develop under plane-strain conditions. Whether instability is coupled with the shear band formation needs to be also investigated.

Table 6-2 Summary of instability tests conducted under drained conditions.

Test No	e_c	Density state	p_c' (kPa)	q_c (kPa)	ψ	$\bar{\psi}$	η_{IL}	Shear band
IND01	0.902	v. loose	199.7	173.5	0.022	0.019	1.05	No
IND02	0.903	v. loose	203.5	177.6	0.023	0.018	1.06	No
IND03	0.679	m. dense	206.1	185.2	-0.200	-0.208	1.44	Yes
IND04	0.682	m. dense	206.2	183.1	-0.198	-0.207	1.43	Yes
IND05	0.878	v. loose	299.5	259.6	0.011	0.008	1.10	No
IND06	0.891	v. loose	200.5	177.9	0.011	0.009	1.10	No
IND07	0.870	v. loose	250.1	177.3	-0.004	-0.002	1.14	No
IND08	0.741	m. loose	303.3	295.1	-0.127	-0.125	1.33	Yes
IND09	0.709	m. dense	207.0	201.3	-0.170	-0.172	1.40	Yes
IND10	0.678	m. dense	313.0	276.8	-0.194	-0.192	1.40	Yes
IND11	0.699	m. dense	158.3	138.7	-0.194	-0.192	1.42	Yes
IND12	0.654	m. dense	282.1	265.5	-0.210	-0.208	1.42	Yes
IND13	0.675	m. dense	281.6	184.9	-0.199	-0.208	1.43	Yes

Several drained instability tests were conducted under plane-strain conditions to study the pre-failure instability behaviour and to investigate the factors that influence the instability behaviour of sand. In terms of testing methods, a CSD test can be conducted in two ways. The first is to shear a specimen along a constant shear path by increasing the back pressure while maintaining the confining pressure constant. The second is to decrease the confining pressure while maintaining the pore water pressure constant. It should be noted that even when there is change in back pressure or pore water pressure, it is still considered as a "drained" test, because the volume of the specimen is changing. The study of Leong (2001)

indicates that there is no difference between the two types of testing methods. A comparison of the two testing methods was also made in this study under plane-strain conditions. A summary of all the instability tests conducted under drained conditions is presented in Table 6-2 (see the previous page).

6.4.2 Results

6.4.2.1 Very Loose Sand

The results of two instability tests IND01 and IND02 conducted on very loose specimens are presented in Fig. 6.3. The specimens were anisotropically consolidated to the mean effective stresses of 200 kPa and 204 kPa (Fig. 6.3(a)). The void ratios of the specimens after consolidation were e_c = 0.902 and 0.903, respectively. After consolidation the specimens were sheared along constant shear drained paths. As shown in Fig. 6.3(c) two different procedures were used to impose a constant shear path. In Test IND01, the back pressure was increased with the confining pressure kept constant, whereas in Test IND02, the back pressure was maintained constant while the confining pressure was reduced. A constant decrease/increase rate of 0.5 kPa/min was used in both tests.

The effective stress paths obtained from the two tests are plotted in Fig. 6.3(a). It can be seen that due to the reduction of the effective confining stress, the effective stress paths moved from points A_1, A_2 to points I_1, I_2. There were little axial strain developments until points I_1 and I_2, where the axial strains in both tests started to develop at faster rates, as shown in Fig. 6.3(b). According to the definition given by Chu et al. (2003), instability occurred at points I_1 and I_2. Using points I_1 and I_2, the IL can be determined, as shown in Fig. 6.3(a). The gradient of the IL, η_{IL}, is 1.06. This is smaller than the gradient of the CSL, M_{cs} = 1.16. Thus, instability observed in Tests IND01 and IND02 is a pre-failure instability.

The effective stresses obtained from the two tests are plotted against time in Fig. 6.3(d). It can be seen that before the onset of instability the resulting effective stresses for the two tests are almost the same, despite the difference in testing procedures. It can also be observed from Figs. 6.3(b) to 6.3(d) that the instability in Test IND01 (point I_1) occurred earlier than that in Test IND02 (point I_2). This is

because the distance between the initial state and the onset of instability in Test IND01 ($A_1 - I_1$) is larger than that in Test IND02 ($A_2 - I_2$). Therefore, more time was needed in Test IND01 for instability to occur.

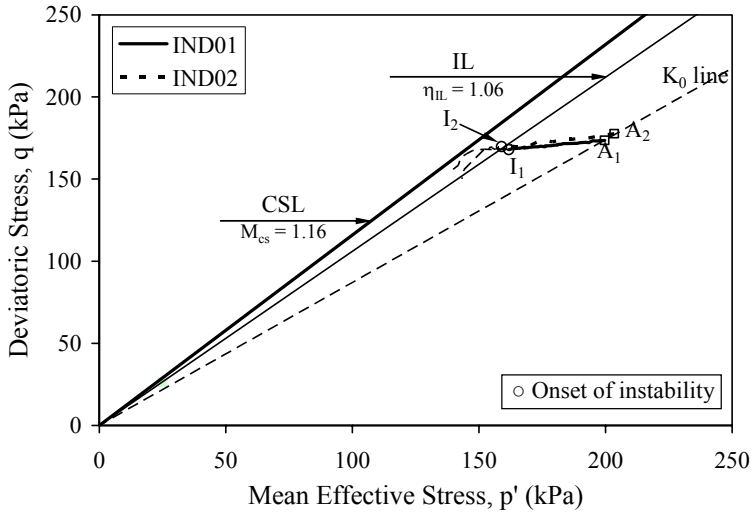

Fig. 6.3(a)

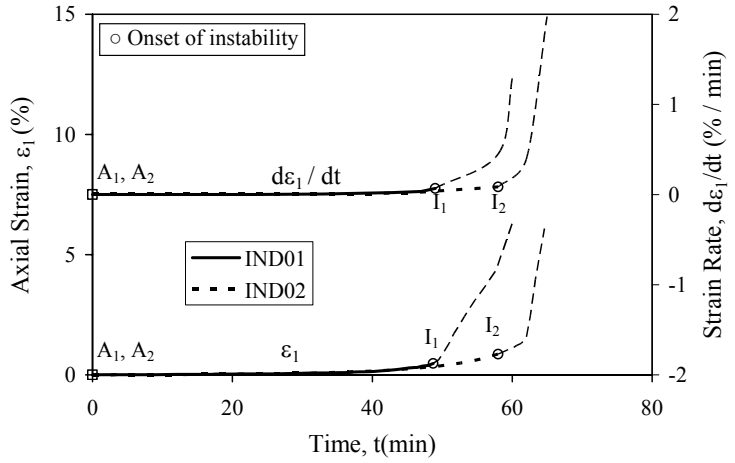

Fig. 6.3(b)

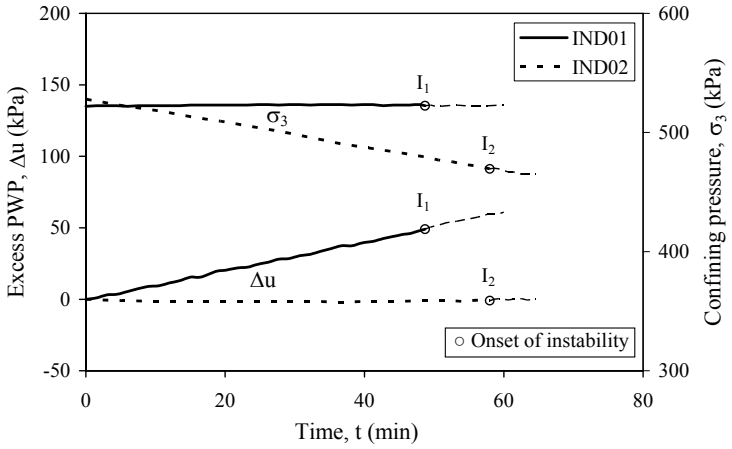

Fig. 6.3(c)

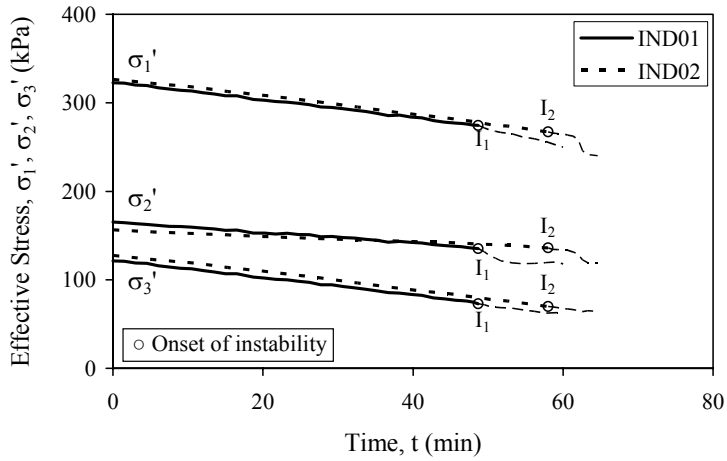

Fig. 6.3(d)

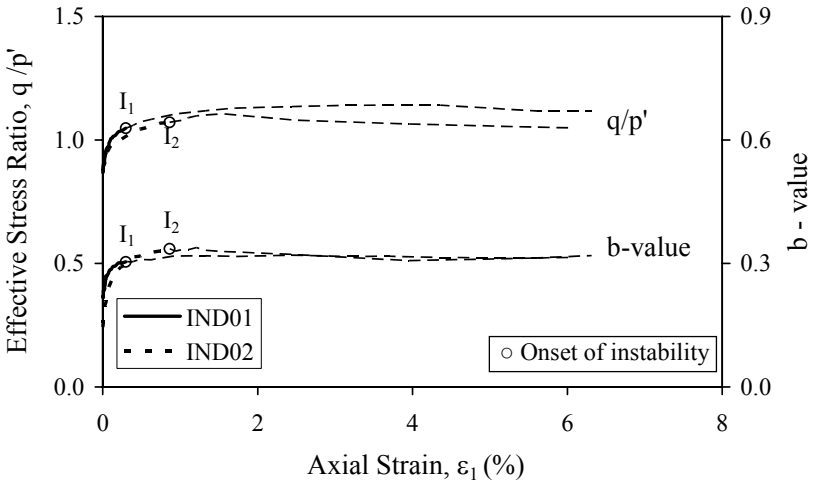

Fig. 6.3(e)

Fig. 6.3 Results of drained instability tests conducted on very loose sand: (a) effective stress paths; (b) ε_1 and $d\varepsilon_1/dt$ versus time curves; (c) Δu and σ_3 versus *time* curves; (d) effective stress versus time curves; (e) *q/p'* and *b-value* versus ε_1 curves

The *q/p'* versus ε_1 and *b-value* versus ε_1 curves are presented in Fig. 6.3(e). It is seen that the testing procedure has little effect on the *q/p'* and *b-value*. The axial strain at the onset of instability is larger in Test IND02, in which the confining pressure was reduced. The b-value obtained from the two tests is in the range between 0.15 and 0.32.

It should be pointed out that there was no visible shear band observed in the two tests. The σ_2 versus ε_1 curves did not diverge either, as shown in Fig. 6.4 for Test IND01. It can be seen that all the four σ_2 values were very similar until the end of

the test. The same observations were made from other instability tests conducted on very loose sand under drained conditions. This implies that shear bands did not occur in very loose specimens. Therefore, it can be concluded that instability behaviour of very loose sand observed under plane-strain conditions is not due to shear band formation.

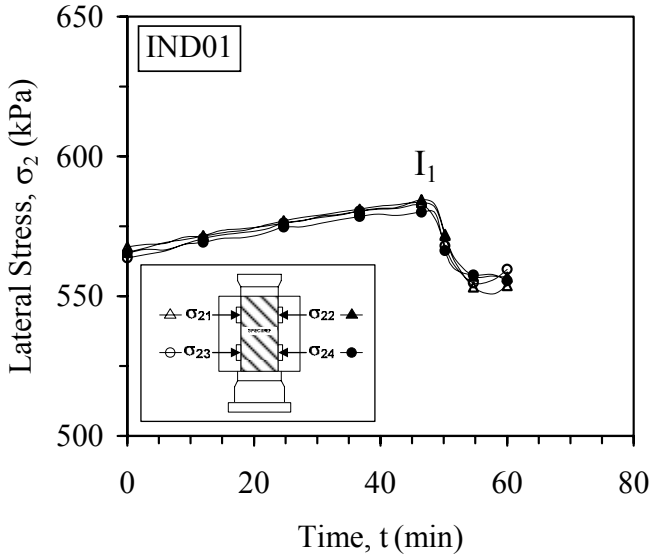

Fig. 6.4 Lateral stress versus time curves obtained from Test IND01

6.4.2.2 Medium Dense Sand

A comparison of two instability tests IND03 and IND04 conducted on medium dense specimens using two different procedures is given in Fig. 6.5. The specimens were anisotropically consolidated to the mean effective stresses of 206 kPa and 205 kPa. The void ratios of the specimens after K_0 consolidation were e_c = 0.679 and 0.682, respectively. During instability tests, the back pressure was increased in Test IND03, whereas the confining pressure was reduced in Test IND04, as presented in Fig. 6.5(c). A constant decrease/increase rate of 0.5 kPa/min was used in both tests.

The effective stress paths of the two tests are presented in Fig. 6.5(a). The CSL and the FL as defined by drained tests are also plotted in Fig. 6.5(a). The ε_1 versus time and $d\varepsilon_1/dt$ versus time curves are shown in Fig. 6.5(b). It can be seen that the axial strain started to increase abruptly at points I_3 and I_4, indicating the onset of instability. As shown in Fig. 6.5(a), the instability points in both tests occurred at around the same stress state. Therefore, the line passing through points I_3 and I_4

defines the IL, with the gradient η_{IL} = 1.45. It can also be seen from Figs. 6.5(a) and 6.5(b) that shear band initiation points were detected in the two tests before the instability have occurred.

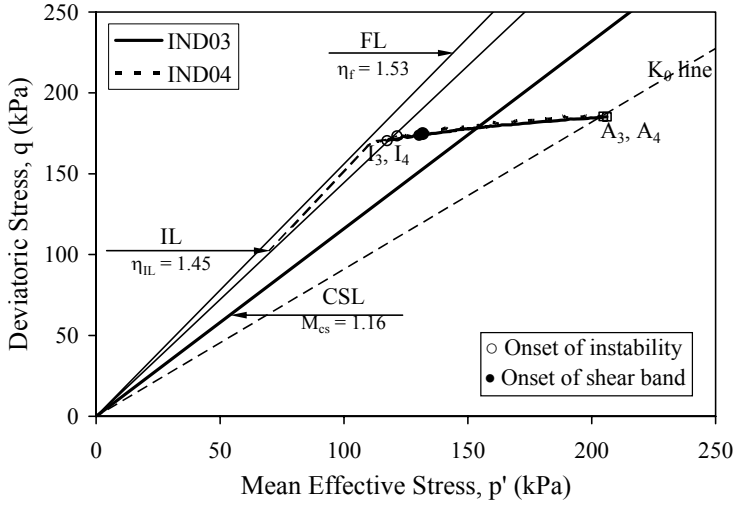

Fig. 6.5(a)

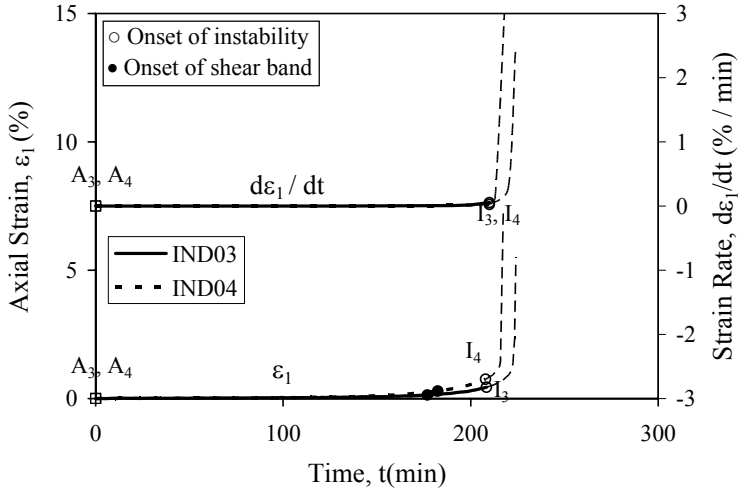

Fig. 6.5(b)

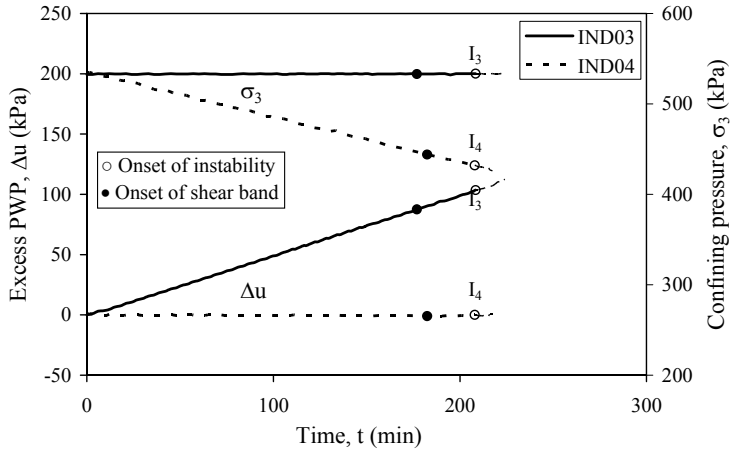

Fig. 6.5(c)

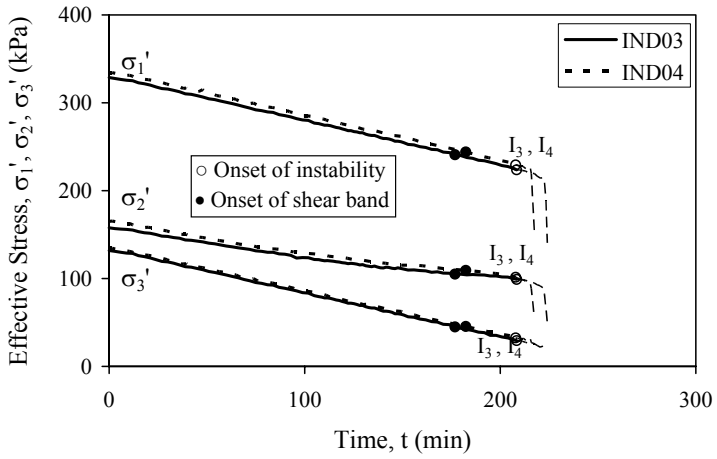

Fig. 6.5(d)

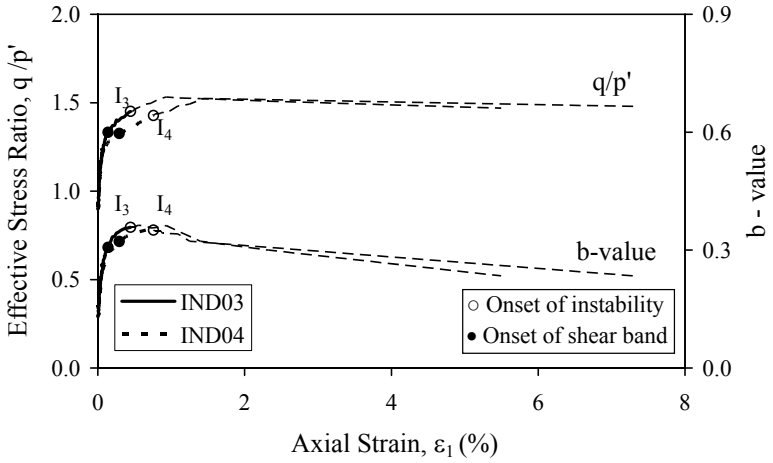

Fig. 6.5(e)

Fig. 6.5 Results of drained instability tests conducted on medium dense sand: (a) effective stress paths; (b) ε_1 and $d\varepsilon_1/dt$ versus time curves; (c) Δu and σ_3 versus time curves; (d) effective stress versus time curves; (e) *q/p'* and *b-value* versus ε_1 curves

The effective stress changes measured in the two tests are presented in Fig. 6.5(d). It is observed from Fig. 6.5(d) that the instability testing procedure does not affect the effective stresses obtained from tests (Fig. 6.5(a)), nor the resulting effective stress paths, as shown in Fig. 6.5(d). The effective stress ratio versus axial strain curves and *b-value* versus axial strain curves are plotted in Fig. 6.5(e). It can be seen that instability point in Test IND04, conducted by decreasing the confining pressure, occurred at larger axial strain than that in Test IND03, conducted by increasing the back pressure. Nevertheless, the difference is small. This is consistent with the results obtained for very loose specimens shown in Fig. 6.3(e). The *b-value* measured in the two tests is in the range of 0.14 – 0.36.

The results presented above for tests conducted on both very loose and medium dense specimens show that CSD tests can be carried out using either one of the following two testing procedures: by increasing the back pressure, or by decreasing the confining pressure. It is observed that both procedures yield the same stress paths and the same instability conditions. In the following plane-strain tests presented in this study, the method of increasing pore water pressure while maintaining σ_3 constant was used.

The shear band development in Test IND03 is shown in Fig. 6.6 and the photographs taken during the test are given in Appendix C (Fig. C.9). Selected photographs from Test IND03 are also shown in Fig. 6.6(a).

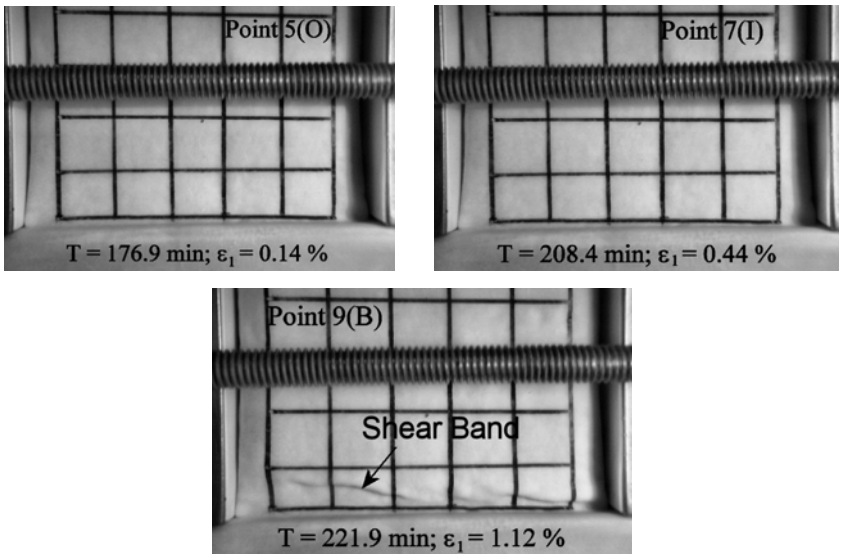

Fig. 6.6(a)

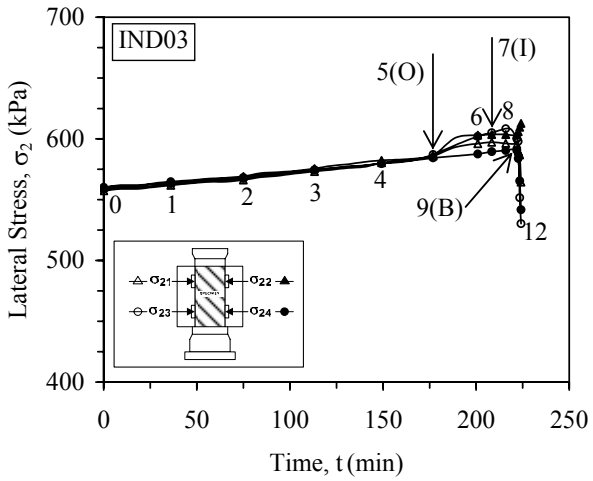

Fig. 6.6(b)

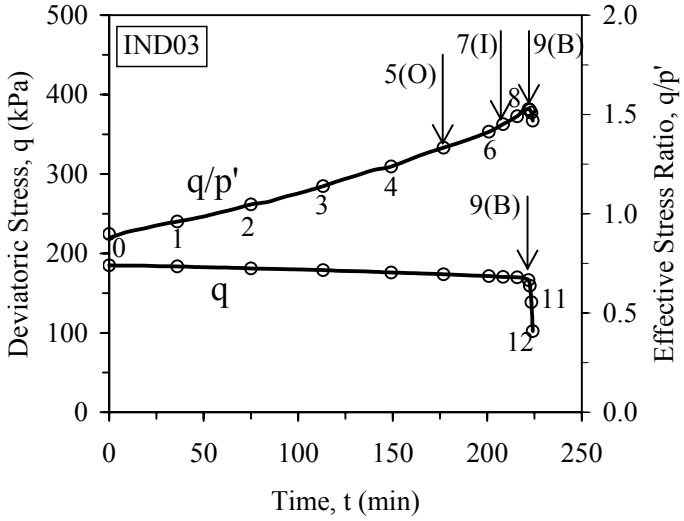

Fig. 6.6(c)

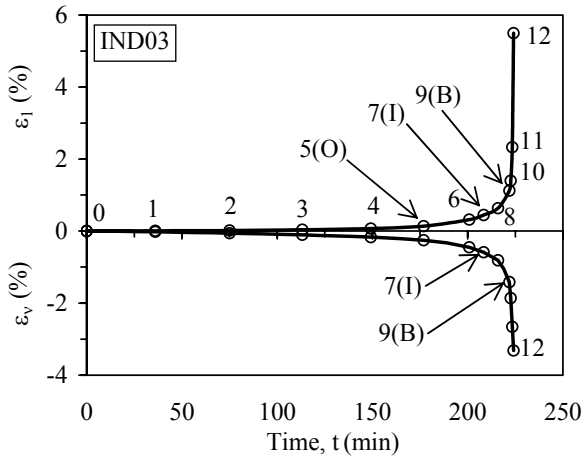

Fig. 6.6(d)

Fig. 6.6 Shear band development in Test IND03: (a) selected photos; (b) σ_2 versus time curves; (c) q versus time and q/p' versus time curves; (d) ε_1 and ε_v versus time curves

The σ_2 against time curves obtained from the test are plotted in Fig. 6.6(b). It is seen that the σ_2 values measured by the four individual load cells were almost identical until point 5(O). It is indicative that the shear band might have occurred at point 5(O). Similarly to the other types of plane-strain tests conducted on medium dense specimens, there was no indication of shear band occurrence on the deviatoric stress or effective stress ratio curves, as shown in Fig. 6.6(c). However, once the shear band was fully developed (point 9(B)), the deviatoric stress and q/p' ratio decreased significantly, as shown in Fig. 6.6(c). The axial strain versus time and volumetric strain versus time curves obtained from Test IND03 are shown in

Fig. 6.6(d). It is seen that instability starts at point 7(I), which is characterised by the shooting up of both ε_1 and ε_v. The point where the shear band was captured by the camera (point 9(B)) is after point 7(I). The same behaviour was observed for all the other instability tests conducted on medium dense specimens under drained conditions.

6.4.2.3 Comparison

The data presented in the preceding section showed that conditional instability under drained conditions could occur for both very loose and medium dense specimens. In this section, the differences and similarities between instability behaviours of loose and dense sand are analyzed further. The results obtained from Tests IND01 and IND03 are compared in Fig. 6.7. Test IND01 was conducted on very loose specimen, whereas Test IND03 on medium dense specimen.

The effective stress paths resulting from the two tests together with the instability lines, the failure line and the CSL are plotted in Fig. 6.7(a). The failure line (FL) for medium dense sand and the CSL determined by drained tests (see Fig. 4.9) are also shown in Fig. 6.7(a). Both specimens were first anisotropically consolidated to points A_1 and A_3 respectively. After that the vertical load was maintained at a constant level and the back pressure was increased at a constant rate. Consequently, the mean effective stresses reduced and the effective stress paths moved towards the FL (Fig. 6.7(a)). Upon reaching points I_1 and I_3, instability occurred in both tests.

It can be seen from Fig. 6.7(a) that instability occurred much earlier in the very loose specimen than in the medium dense specimen. The very loose specimen became unstable before reaching the CSL. On the other hand, the medium dense specimen became unstable after the CSL, but before reaching the FL. Therefore, pre-failure instability occurred in both tests. As can be observed from Fig. 6.7(a), the mean effective stress in Test IND01 reduced about 40 kPa from the initial state to the unstable state. In Test IND03, the mean effective stress had to be reduced about 90 kPa. This corresponds to an increase in pore water pressure equivalent to a rise water head in the field of 4 m and 9 m, respectively. It shows that the loose

granular slopes are more susceptible for the occurrence of pre-failure instability. It should be noticed that in Test IND03 (which was conducted on medium dense specimen), the shear band was detected at point 5(O) which was before the instability point (Fig. 6.7(a)). On the other hand, in Test IND01 conducted on very loose sand, no shear band was observed throughout the test.

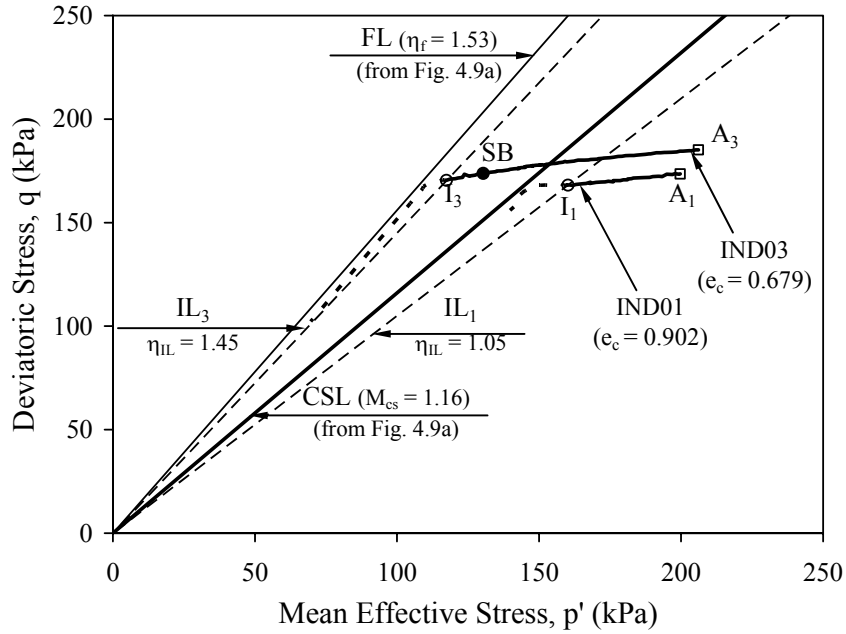

Fig. 6.7(a)

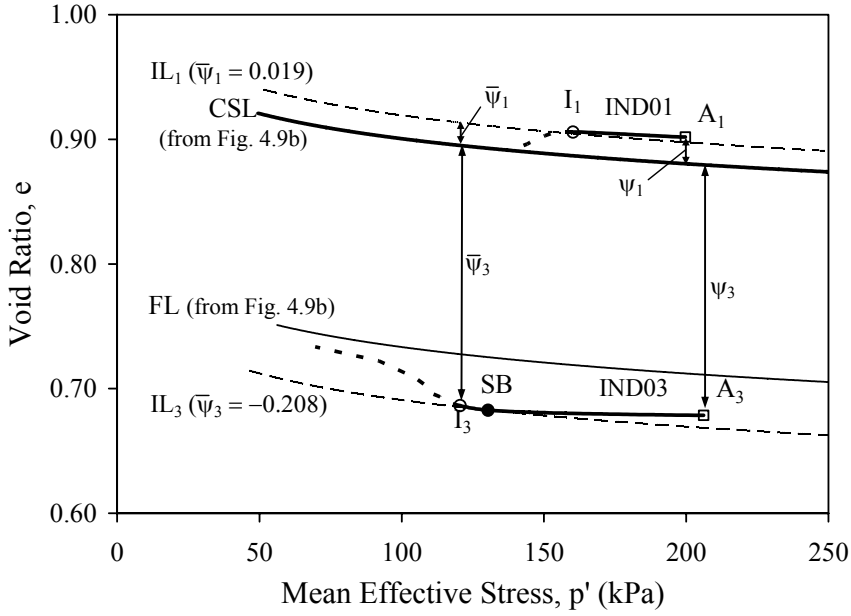

Fig. 6.7(b)

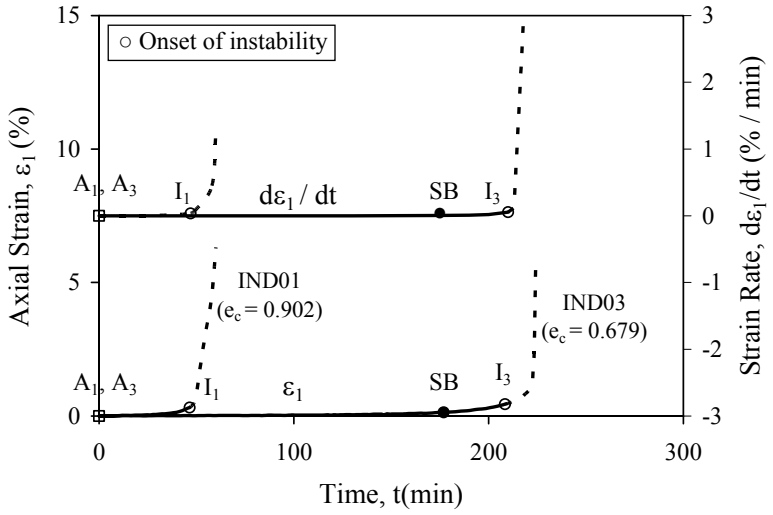

Fig. 6.7(c)

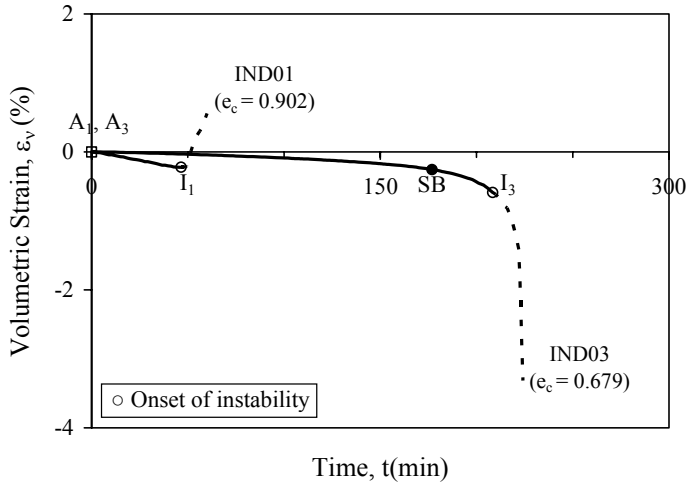

Fig. 6.7(d)

Fig. 6.7 Instability behaviour of very loose and medium dense sand under drained conditions: (a) effective stress paths; (b) *e-p'* plot; (c) axial strain versus time curves; (d) volumetric strain versus time curves

The results of the two tests are also plotted on the *e-p'* plane in Fig. 6.7(b). For each test, the initial state is represented by point A_1 or A_3 and the point at which instability occurred is represented by point I_1 or I_3. The state parameter, ψ, as defined by Been & Jefferies (1985), and the modified state parameter, $\overline{\psi}$ as described by Chu et al. (2003), are also shown schematically in Fig. 6.7(b). The definitions of parameters ψ and $\overline{\psi}$ were given in Chapter 2. These two parameters will be used in the following discussion. It can be seen that for states looser than the critical state, the two state parameters are positive, whereas for states denser than the critical state, the two state parameters are negative.

The changes in axial strain and volumetric strain with time are presented in Figs. 6.7(c) and 6.7(d) respectively. It can be observed from Fig. 6.7(c) that in the stable regions (between points A_1, A_3 and I_1, I_3) the change in axial strains was very small. The two specimens in Tests IND01 and IND03 underwent an axial deformation of approximately 0.32% and 0.44% respectively, which were increased at a constant rate. When the stress states reached points I_1 and I_3, acceleration in the axial strain could be seen evidently (Fig. 6.7(c)). Therefore instability is considered to have occurred at points I_1 and I_3. Fig. 6.7(d) shows that there was very small change in the volumetric strain before instability had occurred in the two tests. Upon reaching the instability points the volumetric strains started to increase rapidly. The medium dense specimen in Test IND03 was in dilation whereas the very loose specimen in Test IND01 was in compression after the occurrence of the instability.

6.4.2.4 Discussion

The results presented in the preceding section showed that instability can take place in both loose and dense sand in plane-strain tests under drained conditions. This is consistent with previous experimental studies conducted under axisymmetric conditions (Chu & Leong, 2001; Chu et al., 2003; Loke, 2004). The studies of Chu & Leong (2001), Chu et al. (2003) and Loke (2004) also show that the IL under axisymmetric conditions is defined based on yielding conditions. Therefore, the IL that control the occurrence of instability is the same for both drained and undrained conditions and the zone of instability is defined regardless of the drainage conditions.

It has been shown earlier (see Figs. 4.12 and 4.13 in Chapter 4) that by connecting the peak points of the undrained stress paths, the η_{IL} for contractive sand can be determined. The IL defined in this way specifies a yielding point where large plastic strain can develop. It has been shown under axisymmetric conditions that for dilative sand, a peak is no longer obtainable to define the IL (Leong et al., 2000; Chu et al., 2003; Loke, 2004). In this case, the effective stress path of an undrained test will increase monotonically and approach the CSRL (defined in Chapter 4).

Chu et al. (2003) has also found that the CSRL coincides with the yielding surface. Therefore, the CSRL can be used to determine the IL for dense sand.

The results of three drained and one undrained tests conducted on medium dense specimens under plane-strain conditions are presented in Fig. 6.8.

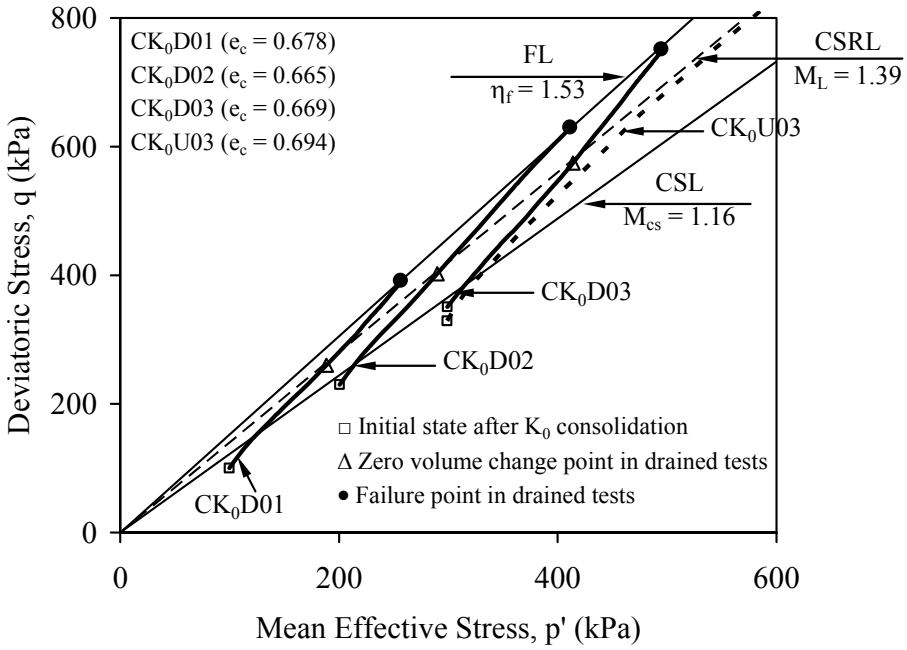

Fig. 6.8(a)

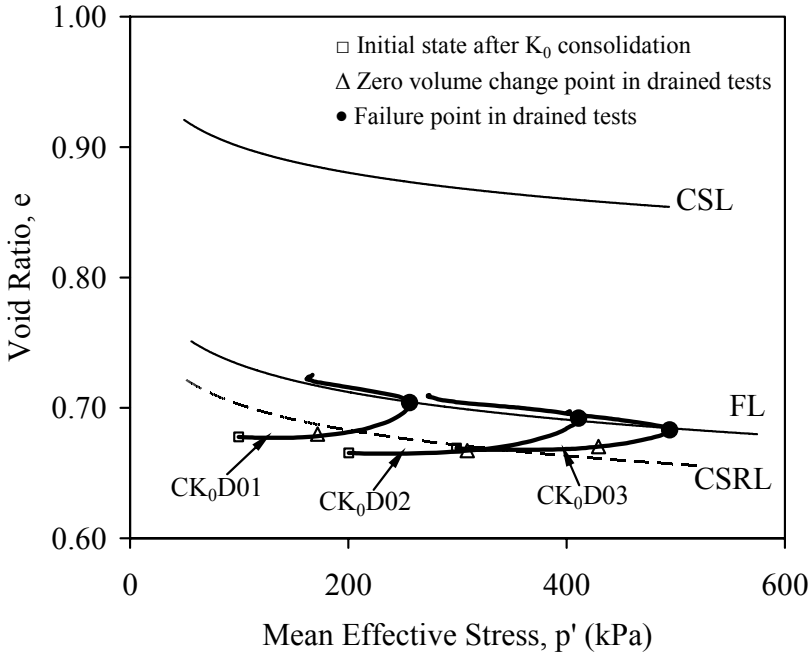

Fig. 6.8(b)

Fig. 6.8 Typical drained and undrained behaviour of medium dense sand under plane-strain conditions: (a) *q-p'* plane; (b) *e-p'* plane

The *e-p'* plot of the three drained tests in Fig. 6.8(b) shows that a large void ratio change started to develop only at the zero volume change points, when dilation begins. Therefore, these points are the yielding points, where large plastic strains can develop. The line connecting those points on the *q-p'* plane defines a yielding surface, as shown in Fig. 6.8(a). It can be seen from Fig. 6.8(a) that the yielding surface coincides with the CSRL obtained from the undrained test conducted on medium dense sand. Therefore, the CSRL obtained from plane-strain tests can be used to determine the yield surface for dense sand. This is consistent with findings reported by Chu et al. (2003). It can be seen from Fig. 6.8(a) that the CSRL lies between the FL and the CSL. The gradients of the FL and the CSRL obtained from Fig. 6.8(a) are $\eta_f = 1.53$ and $M_L = 1.39$, respectively.

Based on the results obtained from medium dense specimens (Fig. 6.8) and the results obtained from very loose specimens (see Chapter 4), the slope of the IL, η_{IL}, is plotted against modified state parameter, $\bar{\psi}$, in Fig. 6.9. It can be seen that the η_{IL} levels off when the soil becomes very dense or very loose. Furthermore, Fig. 6.9 shows that the instability behaviour of sand with the void ratio smaller than the void ratio at critical state coincides with shear band formation. On the other hand, when the void ratio of sand is larger than the void ratio at critical state, a shear band will not occur.

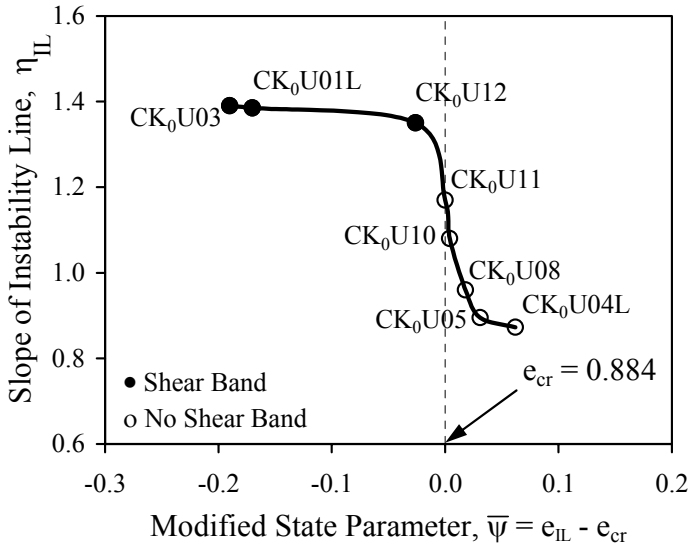

Fig. 6.9 Relationship between the slope on the instability line η_{IL} and modified state parameter $\bar{\psi}$

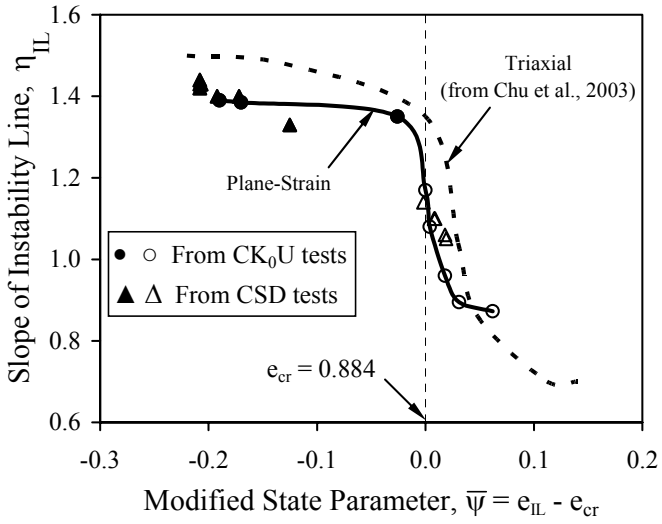

Fig. 6.10 Comparison of slopes of the instability line obtained from undrained and drained instability tests

The η_{IL} versus $\bar{\psi}$ curve obtained in Fig. 6.9, is replotted in Fig. 6.10 together with the instability points obtained from instability tests conducted under drained conditions. The relationship between η_{IL} and $\bar{\psi}$ determined under axisymmetric conditions by Chu et al. (2003), is also plotted in Fig. 6.10. It can be seen from Fig. 6.10 that the η_{IL} obtained from instability tests agrees well with that determined from undrained tests as explained previously. Therefore, the η_{IL} obtained from undrained tests can be used to predict the instability conditions. As shown in Fig. 6.10 the η_{IL} in the contractive side changes more drastically than η_{IL} in the dilative side. This is consistent with the observation made under axisymmetric conditions that the influence of void ratio on the unstable behaviour of loose sand is much greater than that on the behaviour of dense sand. The η_{IL} versus $\bar{\psi}$ curves obtained from triaxial and plane-strain are different. However, both curves are similar and show the same trend, as shown in Fig. 6.10.

In conclusion, the results of CSD tests conducted under plane-strain conditions have shown that instability can take place in both loose and dense sand under drained conditions. The IL defined based on yielding conditions is the same for both drained and undrained conditions and defines the lower bound of all the possible unstable conditions regardless of the drainage conditions. Therefore, instability can occur under both undrained and drained conditions as long as the

stress state falls into the zone of instability. This is consistent with previous experimental studies conducted under axisymmetric conditions (Chu & Leong, 2001; Chu & Leong, 2002; Chu et al., 2003; Loke, 2004).

6.4.3 Comparison of Drained and Undrained Instability

The results presented in the preceding sections have demonstrated that instability can occur in loose sand under both drained and undrained conditions. It was also shown that the IL that controls the occurrence of instability appears to be the same for both types of instability. To verify the above findings, two instability tests, INU04 and IND23, conducted under a drained and an undrained condition are compared. A summary of the two tests are given in Table 6-3.

Table 6-3 Comparison of undrained and drained instability of very loose sand.

Test No	Drainage conditions	e_c	Density state	p_c' (kPa)	q_c (kPa)	η_{IL}	Shear band
INU04	Undrained	0.893	v. loose	190.8	181.8	1.15	No
IND23	Drained	0.893	v. loose	190.7	182.4	1.15	No

The effective stress paths of the two tests are plotted in Fig. 6.11(a). Both specimens were K_0 consolidated to the same stress state with the q/p' = 0.95 (points A, A') and then sheared along a drained path to points B and B' (q/p' = 1.11). Upon reaching points B or B', the load was maintained constant in both tests. For Test INU04, an undrained condition was imposed. For Test IND23, a CSD path was imposed by increasing the back pressure at a rate of 0.5 kPa/min. The two specimens became unstable at points I and I' respectively, as shown in Fig. 6.11(a). Points I and I' are almost identical indicating that the instability line for both types of instability is the same. The slope of the instability line, η_{IL} = 1.15, which is close to the CSL (M_{cs} = 1.16).

The variation of axial strain with time measured in the two tests is presented in Fig. 6.11(b). Although two different drainage conditions were imposed in the two tests, the effective stress paths followed are similar (Fig. 6.11(a)). The axial strain versus time curves are also similar (Fig. 6.11(b)). It is observed from Fig. 6.11(b) that instability under a drained condition occurred earlier than that under an undrained

condition. Once instability started (points I, I'), the axial strain increased rapidly at nearly the same rate in both tests.

The volumetric strain versus time curves of the two tests are plotted in Fig. 6.11(c). For the undrained test, the volumetric strain did not change after an undrained condition was imposed. For the drained test, the specimen started to dilate after the constant load was applied. Upon reaching the instability point, the specimen in Test IND23 started to undergo volumetric contraction (point I').

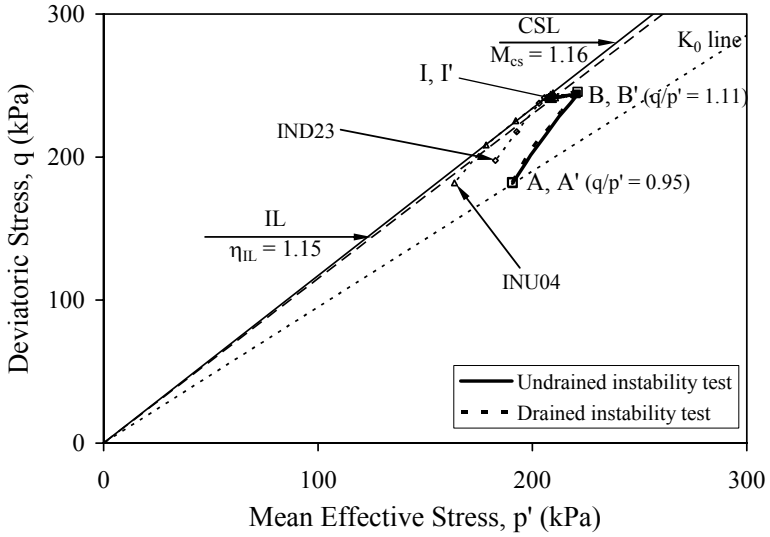

Fig. 6.11(a)

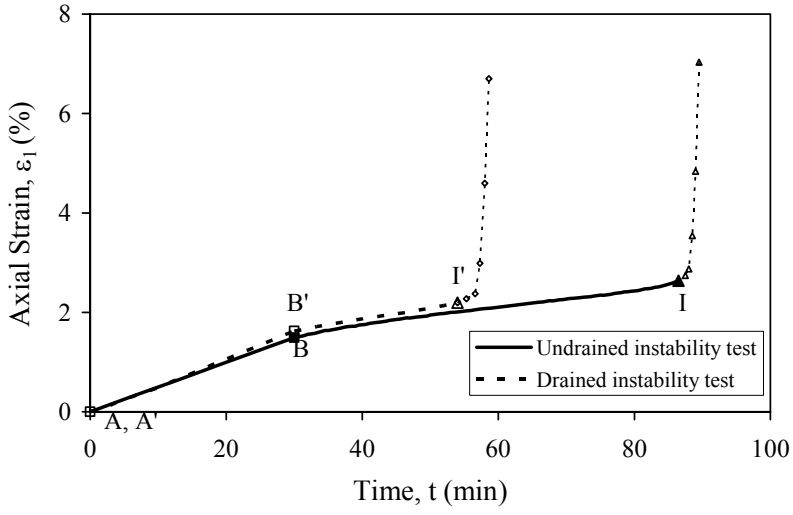

Fig. 6.11(b)

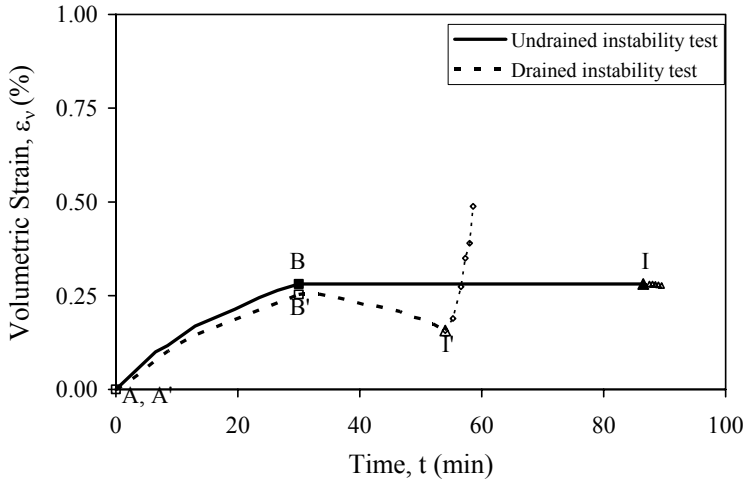

Fig. 6.11(c)

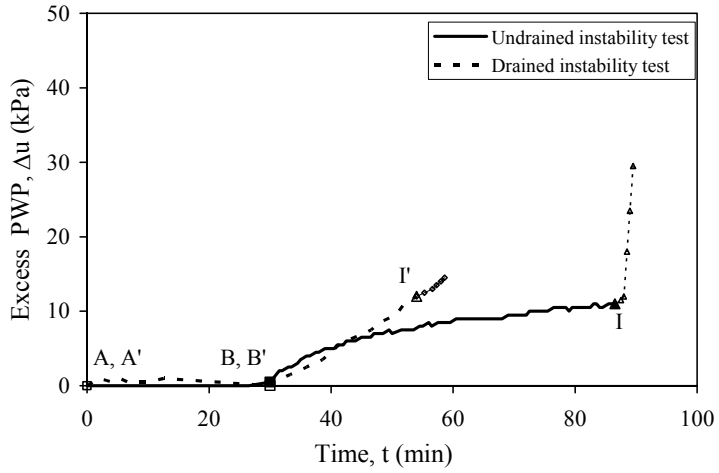

Fig. 6.11(d)

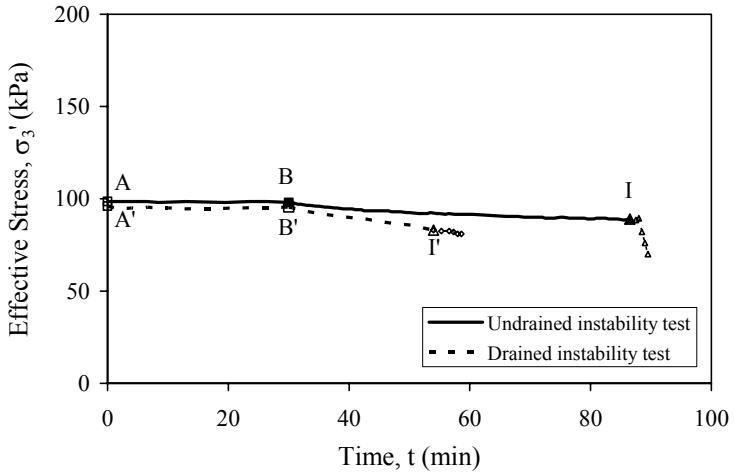

Fig. 6.11(e)

Fig. 6.11 Comparison of drained and undrained instability tests conducted on very loose sand: (a) effective stress paths; (b) axial strain versus time curves; (c) volumetric strain versus time curves; (d) excess pore water pressure versus time curves; (e) σ_3' versus time curves

The excess pore water pressure versus time curves resulting from the two tests are plotted in Fig. 6.11(d). In the drained test, the back pressure was controlled to increase at a given rate (Fig. 6.11(d)). In the undrained test, the pore water pressure increases as a response to undrained loading. At the onset of instability the pore water pressure shot up in Test INU04 (point I), whereas in Test IND23 the pore water pressure was still increasing at the constant rate. Consequently, after instability occurred, the specimen in Test INU04 physically collapsed as in quick sand. However, the specimen in Test IND23 did not "boil" although large deformation was generated suddenly at almost the same rate as in Test INU04 (Fig. 6.11(b)).

The test results presented above support further the conclusion that the conditions under which drained and undrained instability occur for very loose sand are the same. For contractive sand, both drained and undrained instability tests produce stress paths that cross the IL. However, the instability that occurs under an undrained condition is a runaway type, whereas the instability under a drained condition is not, as the pore water pressure does not shoot up, although large deformation occurs. Furthermore, instability under drained conditions can only take place along a stress path with a reduction in mean effective stress. Therefore, instability under drained conditions is a conditional type. This is consistent with previous experiments conducted under axisymmetric stress conditions (Leong, 2001; Chu & Leong, 2001; Chu et al., 2003).

It can be seen from Fig. 6.11(a) that for instability to occur in Tests INU04 and IND23, the stress state moved from point B (B') to point I (I') with a reduction of approximately 12 kPa in the mean effective stress, p'. Practically, it corresponds to an increase in pore water pressure equivalent to a rise of 1.2 m in water head in a granular soil slope. This can be easily achieved during a heavy rainfall. As a result, either drained or undrained instability will occur. Whether it is a drained or an undrained condition will depend on whether the soil undergoes any volume change. If it is an undrained condition, a large increase in pore water pressure can be generated during instability. This large pore water pressure may cause other areas to liquefy and eventually leads to a large scale runaway flow slide.

6.4.4 Effect of Initial State on the Instability Behaviour of Sand

6.4.4.1 Introduction

The instability behaviour of both loose and dense sand in plane-strain tests under fully drained conditions has been presented in the preceding section. The experimental studies under axisymmetric conditions (Leong et al., 2000, Chu & Leong, 2001, Chu et al., 2003) have shown that the occurrence of drained instability is affected by the stress conditions at which instability test is initiated. The effect of initial state, that is, the stress and void ratio state on the instability behaviour of granular soils has been studied by Loke (2004). As described in Chapter 2, the state parameter, ψ, can be used to describe the initial state of soil in terms of the difference between the initial state after consolidation and the critical state in the *e-p'* plane. A positive state parameter defines contractive behaviour and a negative state parameter defines dilative behaviour of granular soil.

Typical results of two drained instability tests, ISTD03 and ISTD06, obtained by Loke (2004) under axisymmetric conditions, are shown in Fig. 6.12. The effective stress paths obtained from the two tests are plotted in Fig. 6.12(a). It can be seen that although the constant load in both tests were applied from two different stress states (points A and A'), both specimens became unstable when their stress states reached the instability line at the same point (points B and B').

The *e-p'* plot of the two tests is presented in Fig. 6.12(b). As can be observed from Fig. 6.12(b), although the state parameters, ψ, for the two tests are different, instability occurred at the same point in both tests. Therefore, the state parameter concept (Been & Jefferies, 1985) does not seem to be suitable for the interpretation of instability behaviour of granular soils. However, these findings have been established under axisymmetric conditions. Whether similar observations can be made under plane-strain conditions needs to be investigated. For this purpose, some instability tests on very loose to medium dense sand were conducted. The results are presented as follows.

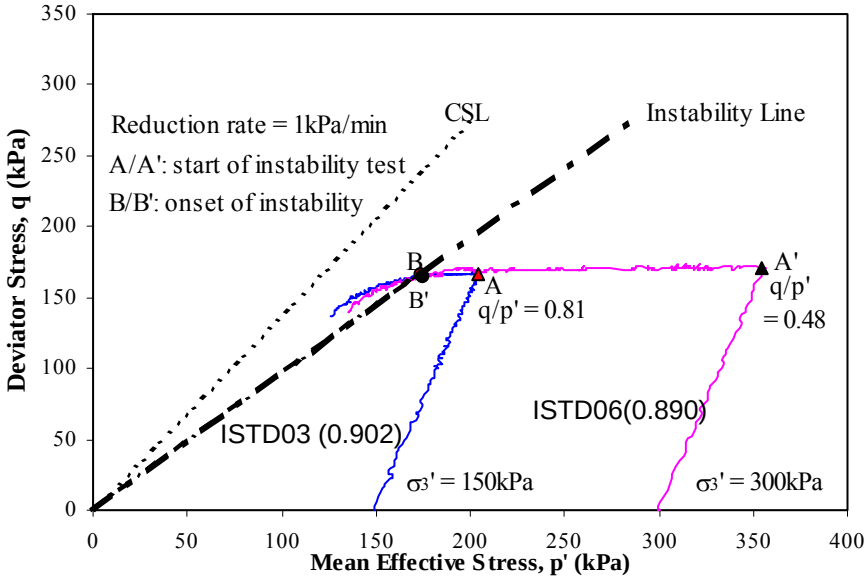

Fig. 6.12(a)

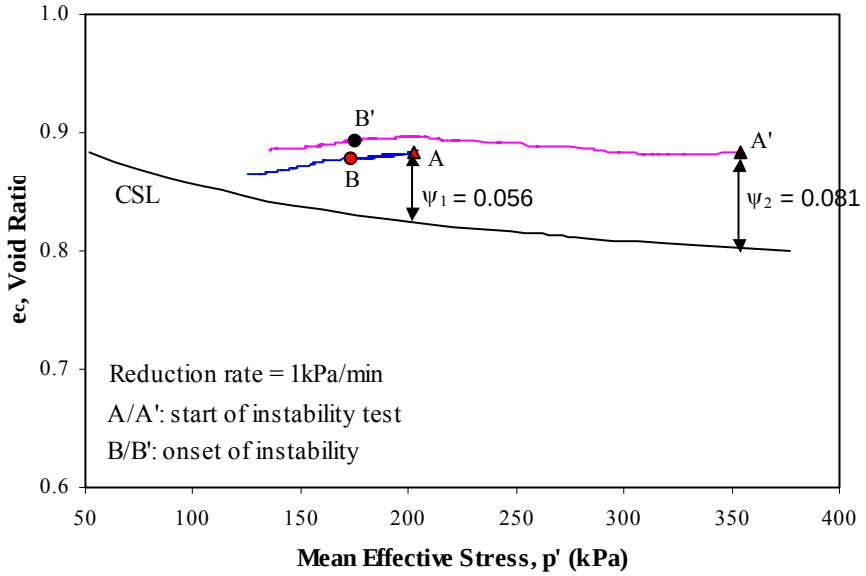

Fig. 6.12(b)

Fig. 6.12 Effect of initial state on the instability behaviour of sand under axisymmetric conditions: (a) *q-p'* plane; (b) *e-p'* plane (after Loke, 2004)

6.4.4.2 Results

To investigate the effect of initial stress state on the instability behaviour of medium dense sand under plane-strain conditions, two instability tests, IND12 and IND13, were conducted by following the same testing procedure. The results of the two tests are presented in Fig. 6.13.

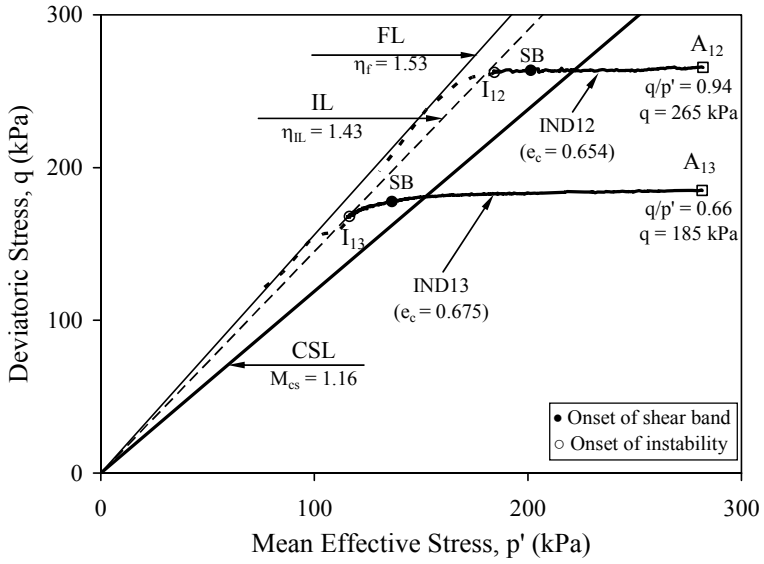

Fig. 6.13(a)

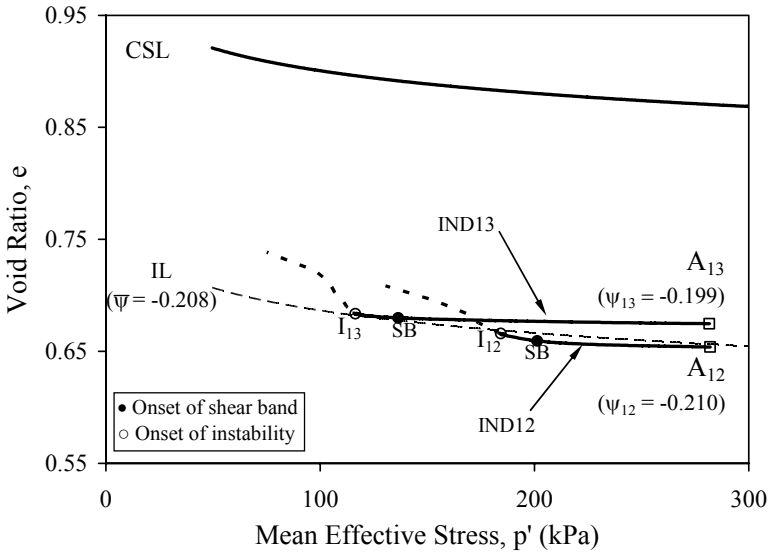

Fig. 6.13(b)

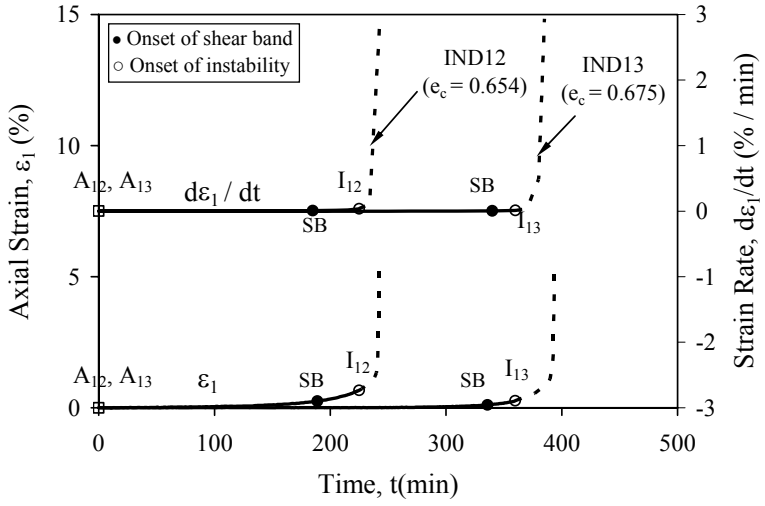

Fig. 6.13(c)

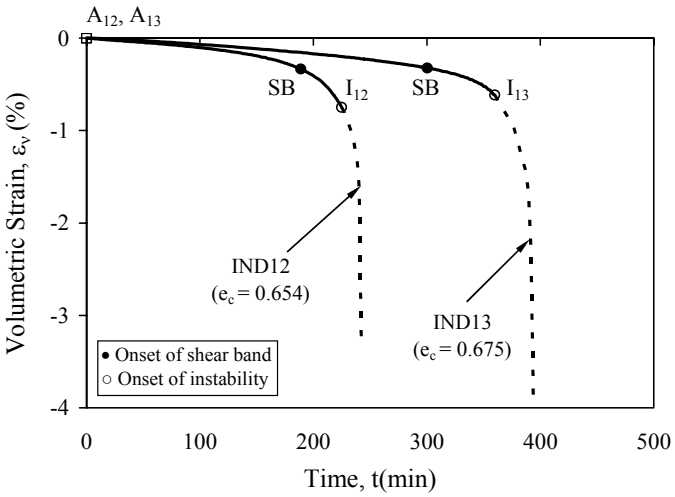

Fig. 6.13(d)

Fig. 6.13 Effect of initial state on the instability of sand under plane-strain conditions: (a) effective stress paths; (b) *e-p'* plot; (c) axial strain versus time curves; (d) volumetric strain versus axial strain curves

As shown in Fig. 6.13(a), the two specimens were anisotropically consolidated to the same mean effective stress of 282 kPa but to different stress levels. The specimen in Test IND12 was consolidated to the q_c = 265 kPa (point A_{12}) whereas the specimen in Test IND13 was consolidated to q_c = 185 kPa (point A_{13}). As a result, the constant load tests were commenced from different effective stress ratios. Test IND12 started from q/p' = 0.94 and Test IND13 from q/p' = 0.66, as shown in Fig. 6.13(a). Although the initial stress states in the two tests were different, both specimens became unstable when their stress states reached the same instability line with a slope, η_{IL} = 1.43 (points I_{12} and I_{13}). The *e-p'* plot of Tests IND12 and IND13 is given in Fig. 6.13(b). Despite different state parameters in the two tests, the same instability line with $\bar{\psi}$ = -0.208 was obtained. Thus, the state parameter is not suitable for the interpretation of instability behaviour of granular soils under plane-strain conditions. It can also be seen from Fig. 6.13(b) that the void ratios increased rapidly at the onset of instability, indicating large yielding. After the onset of instability, the two curves moved towards the CSL.

The axial strain versus time curves are shown in Fig. 6.13(c). It can be again seen from Fig. 6.13(c) that the axial strain in both tests started to increase rapidly at points I_{12} and I_{13}. Thus, instability has occurred at points I_{12} and I_{13} in Tests IND12 and IND13 respectively. It can also be observed from Fig. 6.13(c) that Test IND13,

which started at q/p' = 0.66 (point A_{13}), took a longer time than Test IND12, which started at q/p' = 0.94 (point A_{12}) to initiate instability. This is because Test IND13 started at a lower q/p' ratio than Test IND12. Thus, it requires a larger amount of reduction in p' to reach the instability line.

The volumetric strain versus time curves of the two tests are presented in Fig. 6.13(d). Despite different time taken for instability to occur (225 min. in Test IND12 and 360 min. in Test IND13), similar behaviour was obtained in the two tests. The specimens in the two tests experienced gradual dilation before the instability occurred. Upon the onset of instability at points I_{12} and I_{13}, the dilation in both specimens started to accelerate at similar rate as shown in Fig. 6.13(d).

6.4.4.3 Discussion

The experimental data presented above shows that the occurrence of instability under plane-strain conditions does not depend entirely on the initial state of soil. The initial state affects the time taken for instability to occur and the rate of axial deformation prior to instability. The lower the initial effective stress ratio, q/p', the more time needed for instability to occur and the slower the rate of axial deformation is developed prior to instability. As can be seen from Fig. 6.13(b), although the state parameters, ψ, of the two tests are different, instability occurred along the same instability line in both tests. Therefore, it can be concluded that the occurrence of instability is not controlled solely by the initial state and the state parameter (Been & Jefferies, 1985) is not suitable for the interpretation of slope stability in granular soils. Similar behaviour has also been observed by Loke (2004) under axisymmetric conditions. In this case, the modified state parameter, $\bar{\psi}$, (Chu et al., 2003) may be used.

6.4.5 Effect of Reduction Rate on the Instability Behaviour of Sand

6.4.5.1 Introduction

As discussed earlier, the major difference between an undrained and a drained instability test is that in an undrained test, the pore water pressure generates as a response to an undrained condition, whereas in a drained test the change in p' is

controlled artificially. It needs to be studied whether the rate used to reduce *p'* affects the instability behaviour. On the other hand, it can be conceived that when the *p'* reduction rate becomes equivalent to or higher than the rate at which the excess pore pressure is generated in an undrained condition, a runaway type instead of a conditional type of instability might possibly occur even under a drained condition. It is also possible that when drained instability occurs, the amount of volumetric strain becomes so large that there is no sufficient time for the excess pore water pressure to be dissipated efficiently. As such, the instability that has occurred initially under a drained condition may evolve into a runaway instability, as has been observed by Chu et al. (2003) and Loke (2004) under triaxial testing conditions. To verify the above conjecture under plane-strain conditions, several tests with different σ_3' reduction rates were conducted. A summary of testing conditions is given in Table 6-4.

Table 6-4 Summary of drained instability tests conducted with different σ_3' reduction rates.

Test No	e_c	Density state	p_c' (kPa)	q_c (kPa)	Reduction rate (kPa/min)	$(q/p')_{IL}$	Shear band
IND14	0.900	v. loose	202.0	177.0	0.25	1.05	No
IND15	0.899	v. loose	202.4	178.0	0.50	1.06	No
IND01	0.902	v. loose	199.7	173.5	1.00	1.05	No
IND16	0.898	v. loose	206.2	182.3	3.00	1.05	No
IND17	0.899	v. loose	209.2	185.5	5.00	1.05	No
IND18	0.658	m. dense	197.0	211.3	0.25	1.44	Yes
IND19	0.662	m. dense	195.9	209.1	0.50	1.43	Yes
IND20	0.663	m. dense	194.2	203.6	1.00	1.44	Yes
IND21	0.660	m. dense	196.6	208.2	3.00	1.43	Yes
IND22	0.659	m. dense	191.2	204.5	5.00	1.44	Yes

6.4.5.2 Very Loose Sand

The effect of *p'* reduction rate on the instability behaviour of very loose sand was investigated by conducting five instability tests under drained conditions, with different reduction rates. The experimental results obtained from all the tests are presented in Fig. 6.14. The reduction rates used for the five tests were 0.25, 0.50, 1.00; 3.00, and 5.00 kPa/min (Fig. 6.14(a)).

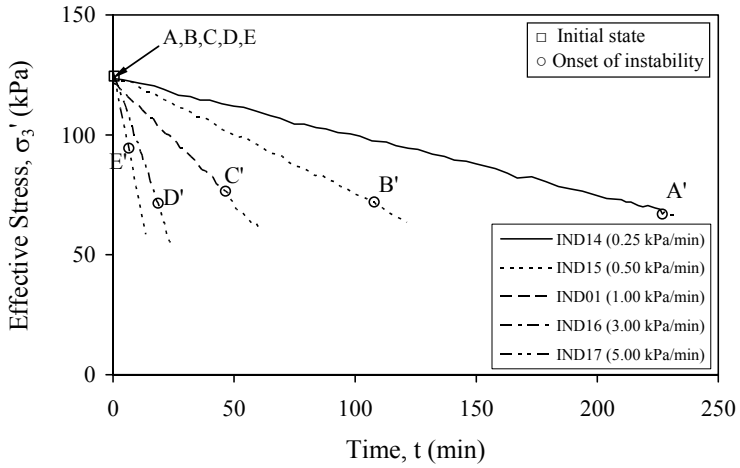

Fig. 6.14(a)

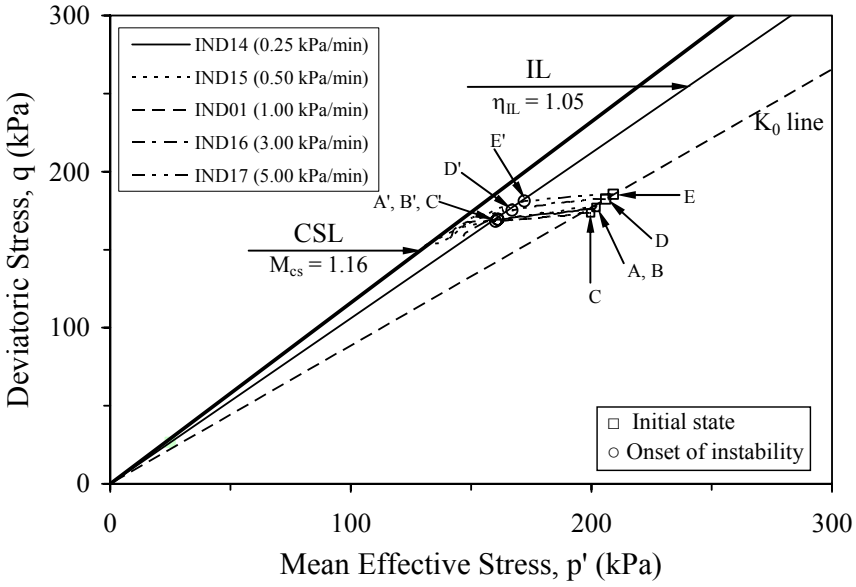

Fig. 6.14(b)

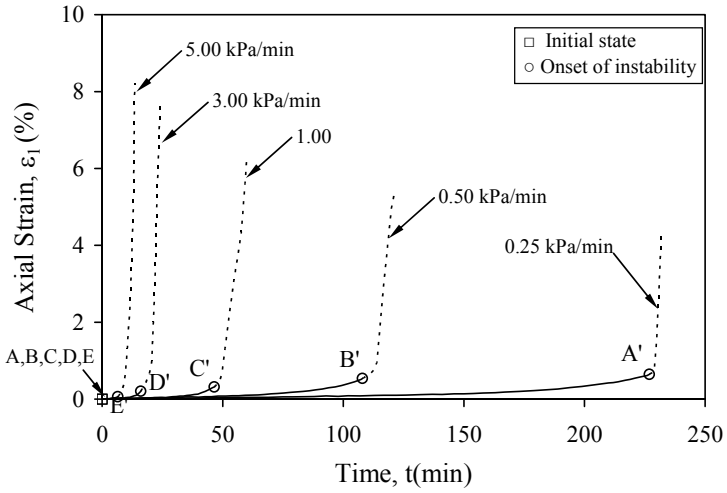

Fig. 6.14(c)

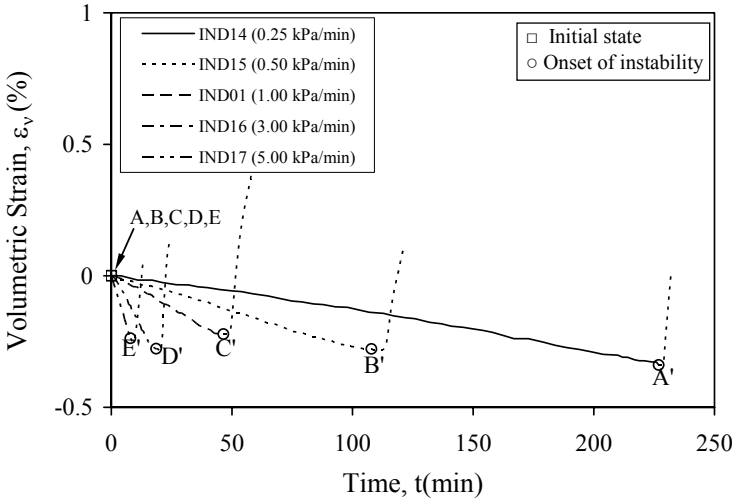

Fig. 6.14(d)

Fig. 6.14 Effect of σ_3' reduction rate on the instability of very loose sand: (a) σ_3' versus time curves; (b) effective stress paths; (c) axial strain versus time curves; (d) volumetric strain versus time curves

The effective stress paths resulted from the five tests are plotted in Fig. 6.14(b). All the tests were K_0 consolidated to the effective stress ratio q/p' = 0.88 (points A, B, C, D, E). After that, a load was maintained constant and a back pressure was increased with a constant rate. As a result, the effective confining stress, σ_3', was reduced at a constant rate (Fig. 6.14(a)). From the effective stress paths in Fig. 6.14(b), it can be seen that although the effective confining pressure of the five tests were reduced at different rates during the instability tests, all the specimens became unstable at the stress states located on the same instability line (point A', B', C', D', and E'). The gradient of the IL is η_{IL} = 1.05. This observation clearly demonstrates that the effective stress path is independent of the reduction rate, or in other words, that the reduction rate does not affect the occurrence of instability. However, the time taken by the five specimens to reach the IL was different. From the axial strain versus time curves presented in Fig. 6.14(c), it can be seen that the amount of time taken for instability to occur becomes shorter as the reduction rate increases. The relationship between the time taken to instability and the reduction rate is presented later in Fig. 6.16. Despite the differences in the time taken for instability to occur upon the onset of instability at point A' (or B', C', D', E'), the axial strain and volumetric strain started to increase rapidly almost at the same rate, as shown in Figs. 6.14(c) and 6.14(d). It can also be observed from Fig. 6.14(c) that less axial deformation is developed in a constant load test when higher p' reduction

rate is used. The relationship between the axial strain at the onset of instability and reduction rate is plotted in Fig. 6.17 (see page 238).

6.4.5.3 Medium Dense Sand

A similar study was also carried out on medium dense sand using five tests conducted at different *p'* reduction rates. The reduction rates used for the five tests were 0.25, 0.50, 1.00, 3.00, and 5.00 kPa/min respectively, as shown in Fig. 6.15(a). It can be seen from the effective stress paths shown in Fig. 6.15(b) that all the specimens were K_0 consolidated to the same effective stress ratio, q/p' = 1.08 (points A, B, C, D, E). After that, a load was maintained constant and a back pressure was increased with a constant rate. As a result the effective confining stress, σ_3', reduced at a constant rate too (Fig. 6.15(a)). From the stress paths in Fig. 6.15(b), it can be seen that although the effective confining pressures of the five tests were reduced at different rates, all the specimens became unstable at the stress states located on the same instability line (point A', B', C', D', and E'). The gradient of the IL is η_{IL} = 1.44. On the other hand, the time taken by the five specimens for the instability to occur was different. Similarly to very loose specimens, the amount of time taken for instability to occur becomes shorter as the reduction rate increases, as shown in Figs. 6.15(c) and 6.15(d).

The relationship between the time taken to instability and the reduction rate used is plotted in Fig. 6.16, for both very loose and medium dense sand. It can be seen that there is a significant reduction in the time taken for instability to occur when the *p'* reduction rate was increased from 0.25 kPa/min to 1.0 kPa/min. However, subsequent increase in the reduction rate does not influence the time taken significantly. Despite the differences in the *p'* reduction rate, upon the onset of instability (points A', B', C', D', E'), the axial strain and volumetric strain started to increase rapidly at the same rate, as shown in Figs. 6.15(c) and 6.15(d). This behaviour is consistent with that observed for very loose specimens. It can also be seen from Fig. 6.15(c) that less axial deformation is developed during the constant load test with increasing reduction rate. The relationship between the axial strain at the onset of instability and reduction rate is plotted in Fig. 6.17.

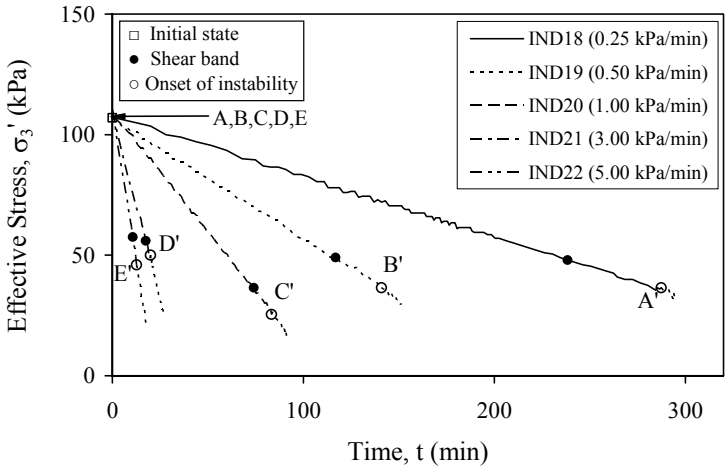

Fig. 6.15(a)

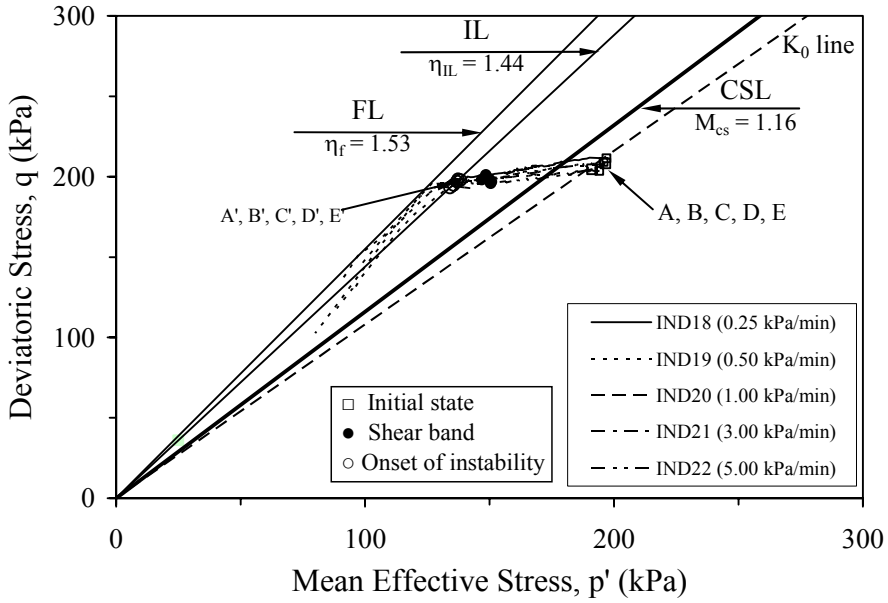

Fig. 6.15(b)

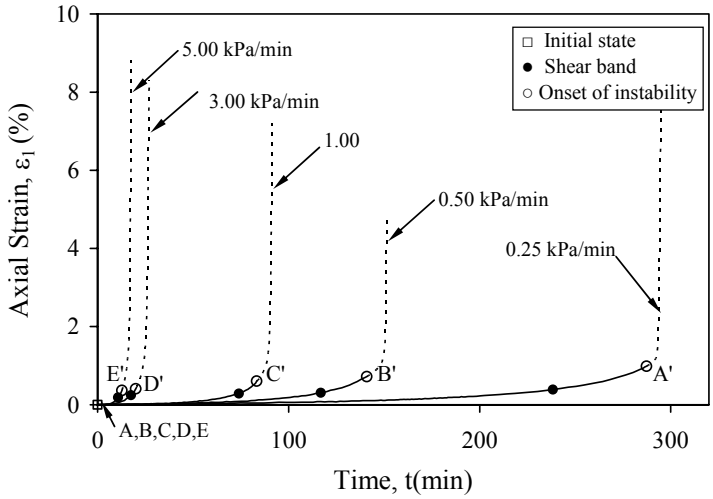

Fig. 6.15(c)

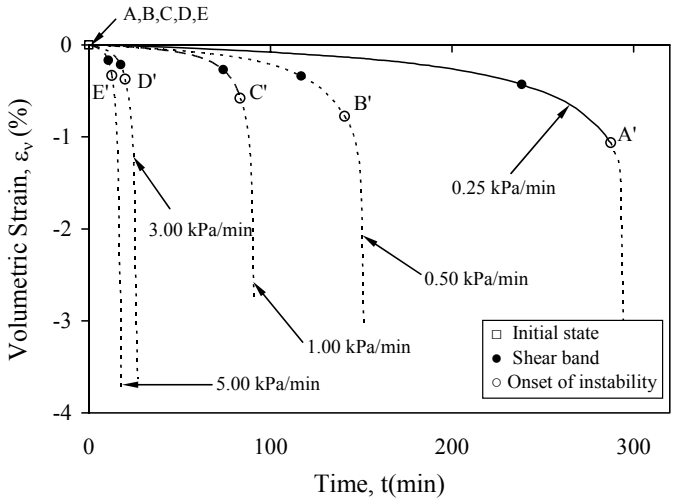

Fig. 6.15(d)

Fig. 6.15 Effect of σ_3' reduction rate on the instability of medium dense sand: (a) σ_3' versus time curves; (b) effective stress paths; (c) axial strain versus time curves; (d) volumetric strain versus time curves

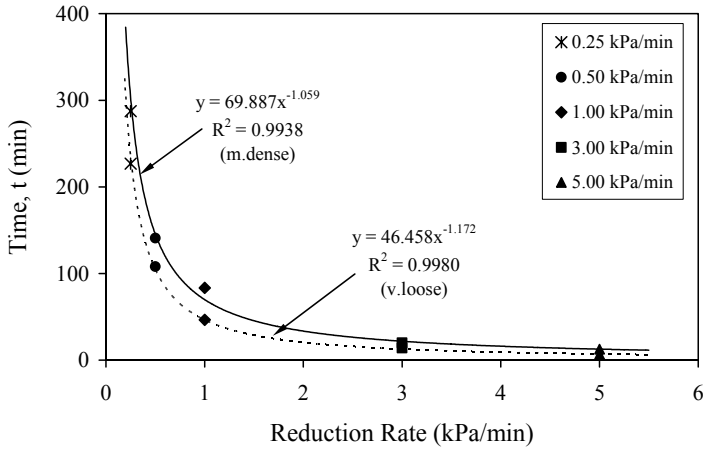

Fig. 6.16 Relationship between time taken to instability and σ_3' reduction rate for very loose and medium dense sand

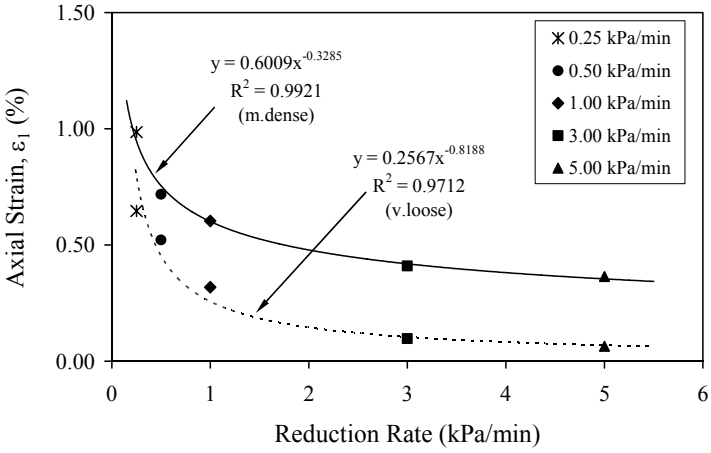

Fig. 6.17 Relationship between axial strain developed in the CSD test and σ_3' reduction rate for very loose and medium dense sand

6.4.5.4 *Special Instability Test*

A special instability test IND24 was conducted on loose sand to study the response of granular soil when an undrained condition is imposed after instability is developing under a drained condition. This is to simulate the condition where the amount of excess pore water pressure generated during instability under a drained loading condition becomes too large for the soil mass to dissipate efficiently.

The effective stress path obtained from Test IND24 is presented in Fig. 6.18(a). The specimen was K_0 consolidated to a mean effective stress of 200 kPa (point A in Fig. 6.18(a)). The void ratio of the specimen after K_0 consolidation was e_c = 0.903. From point A, the deviator load was controlled to be constant. At the same time, the back pressure was increased at a constant rate of 0.5 kPa/min. The drainage valves were closed when point C was reached. The drained instability began to evolve at point B (Fig. 6.18(c)). As shown in Fig. 6.18(a), the deviatoric stress reduced suddenly upon the closure of the drainage valves. This was because the specimen had collapsed, as indicated by the sudden increase in the excess pore water pressure and axial strain (Figs. 6.18(b) and 6.18(c)). A photograph of the specimen at the end of Test IND24 is shown in Fig. 6.18(f). After an undrained condition was imposed, both axial strain rate and pore water pressure increased suddenly and the specimen collapsed instantly.

It should be pointed out that the specimen would not collapse so fast, if the drainage valves were kept open at point C. This is because at the onset of undrained instability the pore water pressure shoots up without any control, whereas the pore water pressure only increases at a constant rate during drained instability, as discussed earlier (see Fig. 6.11(d) in section 6.4.3). Fig. 6.18(e) shows the volumetric strain versus time curve of Test IND24. The specimen underwent volumetric dilation during the constant load test (from point A to B). At the onset of drained instability (point B), the specimen started to contract with high rate. This is consistent with all the drained instability tests conducted on very loose sand.

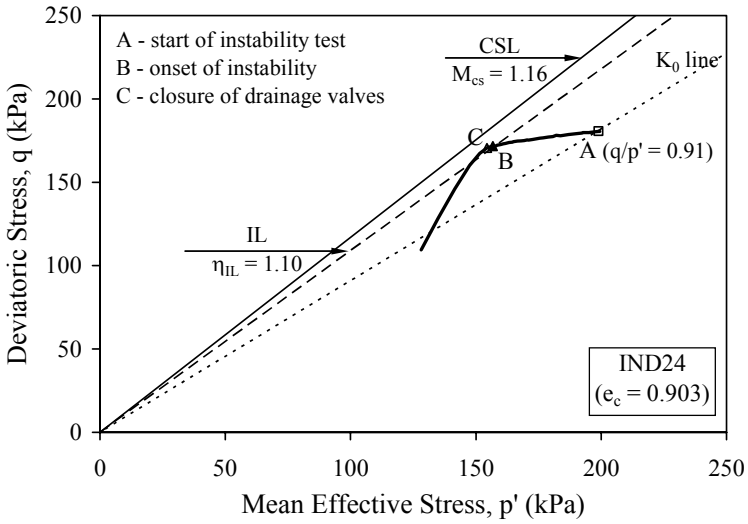

Fig. 6.18(a)

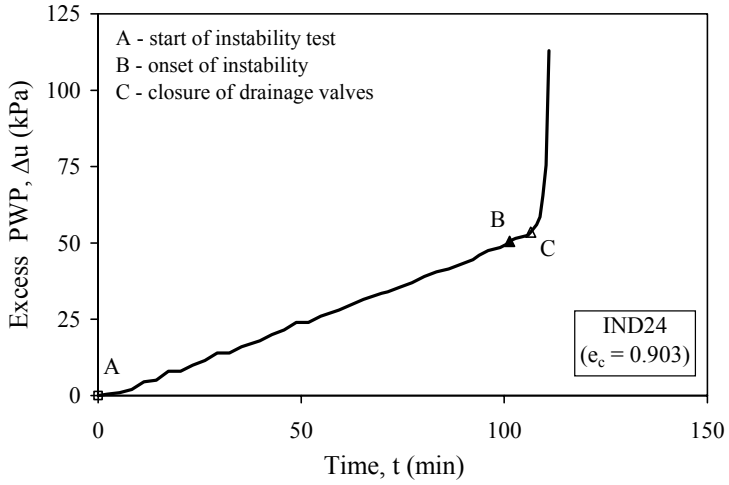

Fig. 6.18(b)

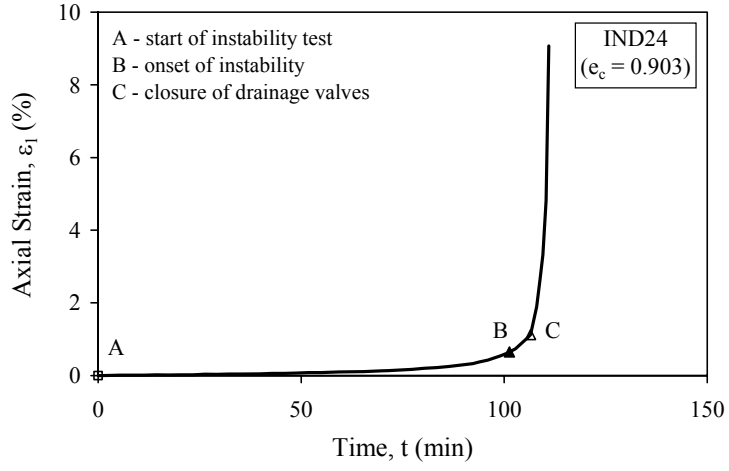

Fig. 6.18(c)

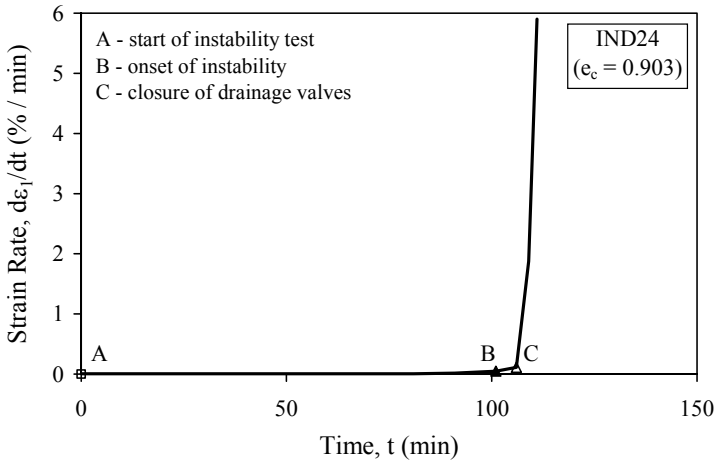

Fig. 6.18(d)

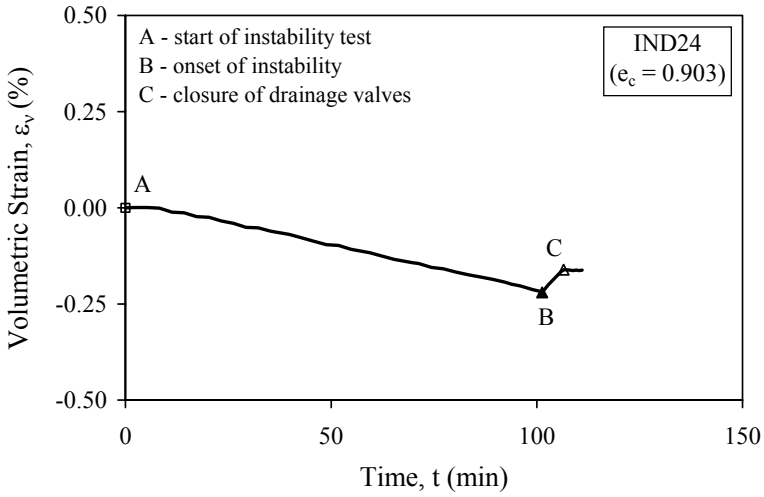

Fig. 6.18(e)

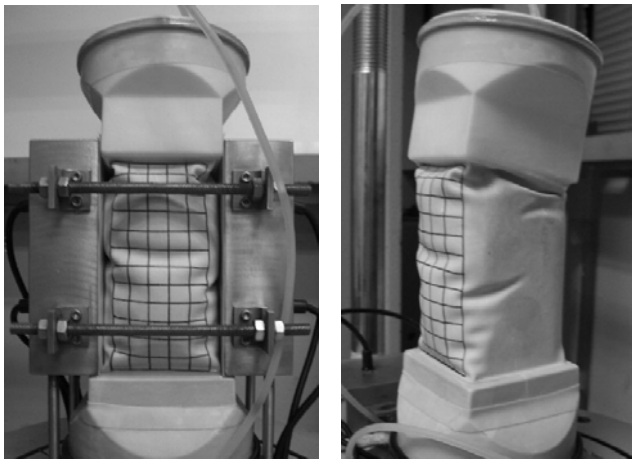

Fig. 6.18(f)

Fig. 6.18 Instability behaviour of very loose sand under drained/undrained conditions: (a) effective stress path; (b) Δu versus time curve; (c) ε_1 versus time curve; (d) $d\varepsilon_1/dt$ versus time curve; (e) ε_v versus time curve; (f) specimen at the end of Test IND24

6.4.5.5 Summary

From the results of drained instability tests conducted with different reduction rates, it can be seen that for both very loose and medium dense sand, instability occurred at the same point on the instability line even though the σ_3' reduction rate was different. The reduction rate however, affects the duration of a constant load test under a drained condition and the amount of axial strain developed upon the instability point (Figs. 6.16 and 6.17). It was observed that the higher the reduction rate, the less time and the less axial deformation is needed for instability to occur. The data obtained from the special instability test conducted under plane-strain conditions also imply that a conditional instability occurring under a drained condition can evolve into a runaway instability when the drainage is stopped. This is consistent with observation made by Chu et al. (2003) and Loke (2004) under axisymmetric conditions.

6.5 Instability Behaviour of Sand in Strain Path Testing

6.5.1 Introduction

Granular soil slope failures have often been attributed to the instability of loose saturated granular soils under undrained conditions. However, the undrained condition may not be necessary. There are failure cases that occurred under drained or other than undrained conditions (Torrey & Weaver, 1984; Eckersley, 1985; Gu et al, 1993; Olson et al., 2000; Adalier & Elgamal, 2002; Sento et al., 2004). Failure mechanisms related to the redistribution of void ratio within a globally undrained sand layer and the spreading of excess pore pressure with global volume changes have been identified by the American National Research Council (1985), as reviewed in Chapter 2. Although many studies have been conducted to understand the behaviour of dilating sand (Chu, 1991; Chu & Leong, 2001; Vaid & Eliadorani, 1998; Eliadorani, 2000; Chu et al., 2003; Loke, 2004), the mechanisms of instability in strain path testing under plane-strain conditions have not been studied yet.

This section presents the results of the constant load tests conducted on both very loose and medium dense sand under plane-strain conditions. The instability

mechanisms of very loose to medium dense sand in strain path testing are studied. Factors that can affect the instability of the granular soil under strain path-controlled conditions are discussed.

6.5.2 Testing Programme

A series of instability tests under strain-path controlled loading conditions was conducted to study the instability behaviour of granular soils in strain path testing. All the instability tests were conducted by imposing negative strain increment ratio to the specimens, while the load was maintained constant. A summary of the tests conducted under strain path controlled conditions is presented in Table 6-5.

Table 6-5 A summary of strain path instability tests.

Test No	Preparation Method	$d\varepsilon_v/d\varepsilon_1$	e_c	p_c' (kPa)	q_c (kPa)	η_{IL}	Stable / Unstable
INSP01	MT	-0.60	0.898	198.8	175.1	1.06	Unstable
INSP02	WS	-0.60	0.754	199.2	191.9	1.27	Unstable
INSP03	WS	-0.40	0.797	210.0	200.3	1.25	Unstable
INSP04	WS	-0.20	0.760	190.4	180.7	1.33	Unstable
INSP06	WS	-0.60	0.685	200.7	211.8	1.53	Unstable
INSP07	WS	-0.60	0.692	200.6	213.9	1.53	Unstable
INSP09	WS	-0.40	0.651	198.2	211.5	-----	Stable
INSP10	WS	-0.20	0.681	200.0	213.1	-----	Stable
INSP11	WS	-0.60	0.798	200.9	198.0	1.19	Unstable

6.5.3 Results

6.5.3.1 Very Loose Sand

The results of the instability test, INSP01, conducted on very loose sand under a strain path controlled condition are presented in Fig. 6.19. The specimen was K_0 consolidated to a mean effective stress of 199 kPa. The void ratio after K_0 consolidation was e_c = 0.898. Upon reaching point A (q/p' = 0.88), the K_0 condition was changed to a strain path control of $d\varepsilon_v/d\varepsilon_1$ = -0.60 with the deviator load maintained constant. During the strain path control, the pore water pressure

increased gradually (Fig. 6.19(c)) and the effective stress path moved towards the CSL, as shown in Fig. 6.19(a). The specimen became unstable when the stress state reached point I. At point I, the axial strain and volumetric strain started to accelerate, as shown in Figs. 6.19(d) and 6.19(e). At the same time, the excess pore water pressure also began to increase rapidly. Therefore, it is evident that instability has occurred at point I. Using point I, the instability line can be determined, as shown in Fig. 6.19(a). The gradient of the instability line, η_{IL} = 1.06. Since the instability was initiated before the CSL, which is also the FL for very loose sand, this is a pre-failure instability. The specimen physically collapsed after instability has occurred, as in undrained instability tests. Therefore, the instability in Test INSP01 is the runaway type. It should also be mentioned that there was no visible shear band detected in Test INSP01.

The undrained stress path obtained from Test INU03 in Fig. 6.1(a), conducted on very loose sand (e_c = 0.894) under an undrained condition, is also replotted in Fig. 6.19(a) for comparison. Although point B is represented by q/p' = 0.96 which is higher than that at point A (q/p' = 0.88), undrained instability did not occur in Test INU03. Therefore, the specimen in Test INSP01 would also be stable at point A if an undrained condition was imposed. However, under a strain path control of $d\varepsilon_v/d\varepsilon_1$ = -0.60, the runaway instability has occurred in Test INSP01.

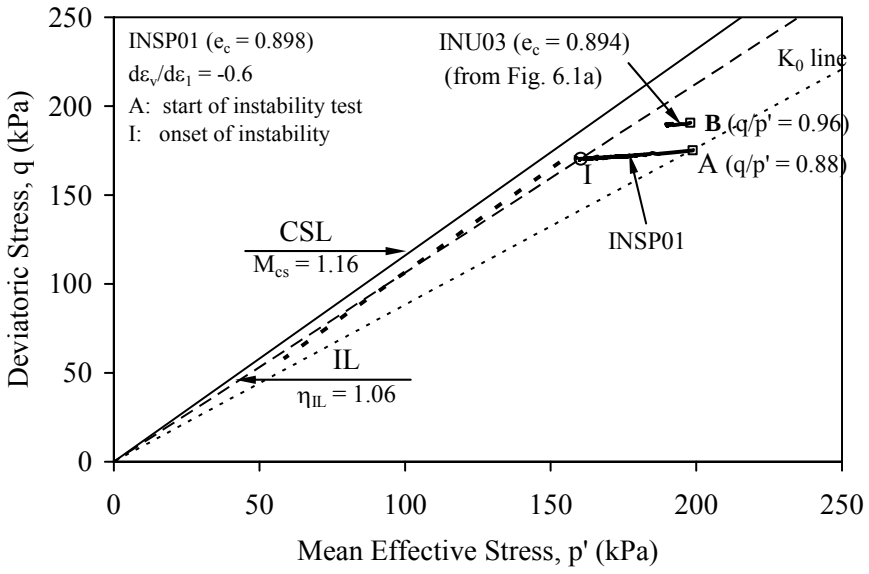

Fig. 6.19(a)

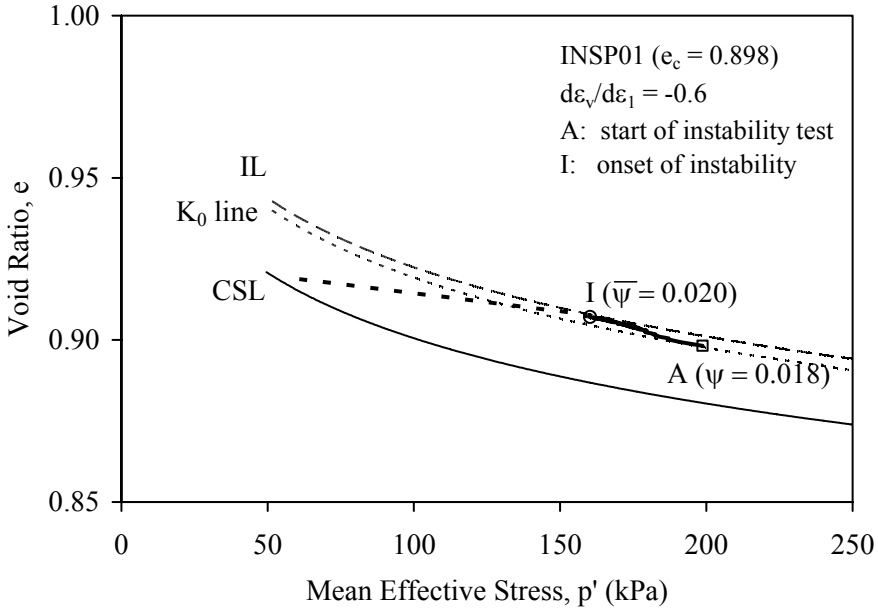

Fig. 6.19(b)

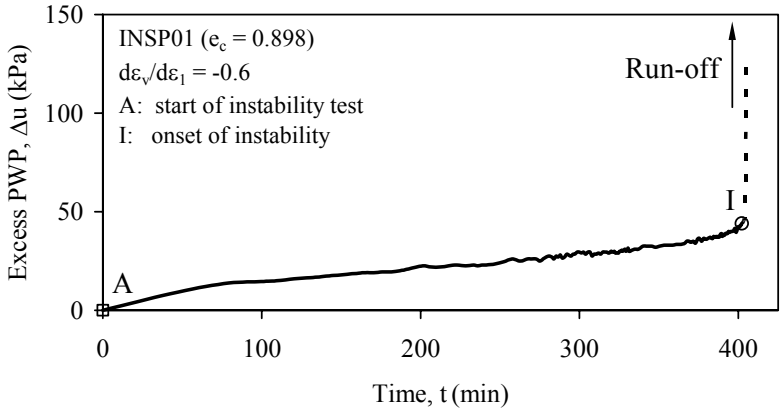

Fig. 6.19(c)

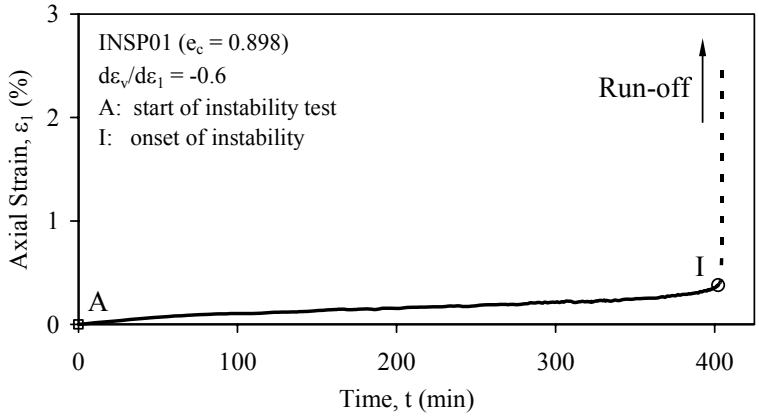

Fig. 6.19(d)

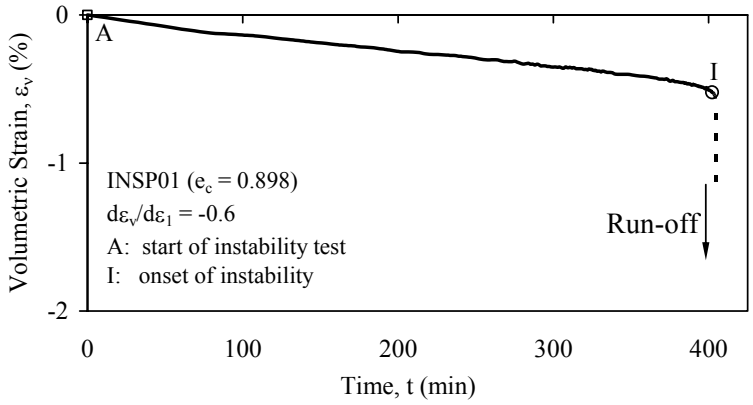

Fig .6.19(e)

Fig. 6.19 Instability behaviour of very loose sand in strain path testing: (a) effective stress path; (b) *e-p'* plot; (c) excess pore water pressure versus time curve; (d) axial strain versus time curve; (e) volumetric strain versus time curve

6.5.3.2 Medium Loose Sand

It was shown above that an otherwise stable specimen can exhibit a runaway instability when a dilative strain increment ratio is imposed to it. Another test, INSP02, was carried on medium loose sand under a strain path controlled condition. The results of Test INSP02 are presented in Fig. 6.20. As shown in Fig. 6.20(a), the specimen was first K_0 consolidated to point A (q/p' = 0.96) and then sheared along a drained path until point B (q/p' = 1.23). Upon reaching point B, a strain path of $d\varepsilon_v/d\varepsilon_1$ = -0.60 was imposed with the deviator load kept constant.

It can be seen from Figs. 6.20(c) and 6.20(d) that the axial strain and pore water pressure started to accelerate when the stress state reached point I. Thus, instability occurred at point I. As can be seen from the stress paths plotted in Fig. 6.20(a), the deviatoric stress started to reduce rapidly at point I, where instability occurred. This reduction in q was caused by a large axial strain and a rapid volumetric dilation, as shown in Figs. 6.20(d) and 6.20(e). Using point I, where large plastic strains are developed, the instability line can be determined. As shown in Fig. 6.20(a), the instability occurred at the stress point with η_{IL} = 1.27, that is, before the failure state (η_f = 1.35), as determined by drained tests conducted on specimens with the same void ratio (see Chapter 4). Thus, the instability in Test INSP02 is a pre-failure instability.

After instability took place in Test INSP02, the specimen physically collapsed, as shown in Fig. 6.21. Therefore, the instability observed in Test ISP02 is a runaway type. This behaviour is similar to the runaway instability observed by Leong (2001) in loose sand under an undrained condition. This shows that a medium loose specimen that exhibits strain hardening behaviour under an undrained condition can liquefy like a loose specimen when subjected to a dilative strain path. Similarly to the very loose specimen in Test INSP01, there was no visible shear band in Test INSP02.

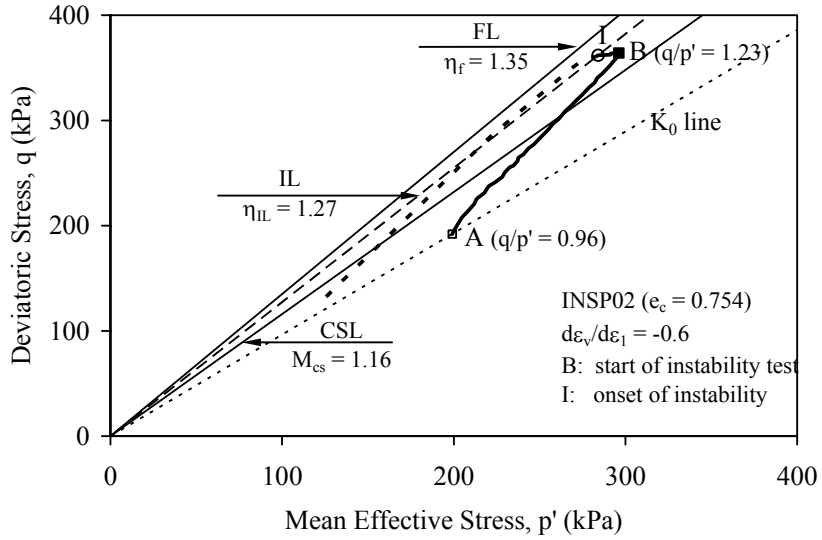

Fig. 6.20(a)

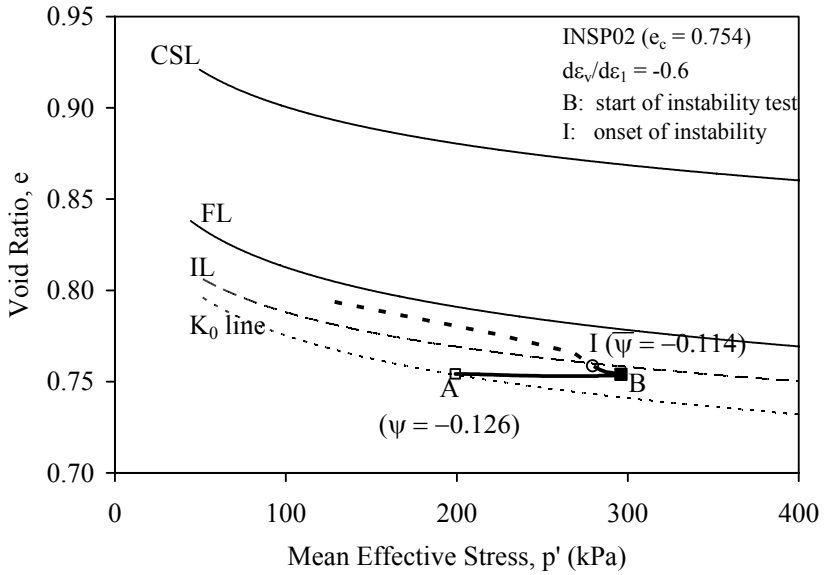

Fig. 6.20(b)

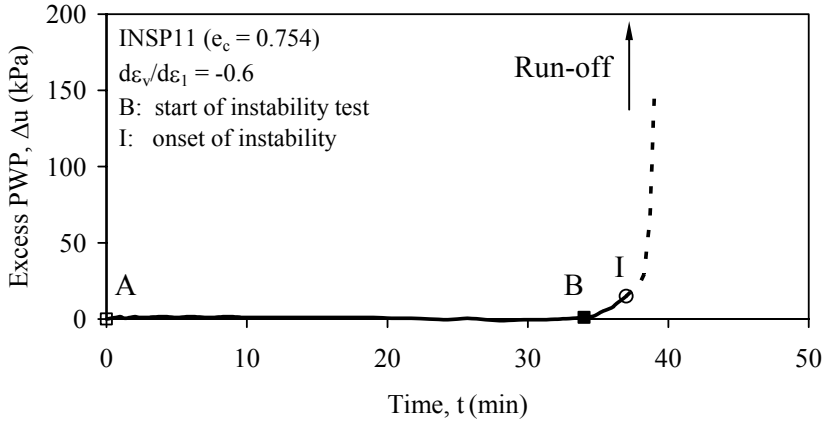

Fig. 6.20(c)

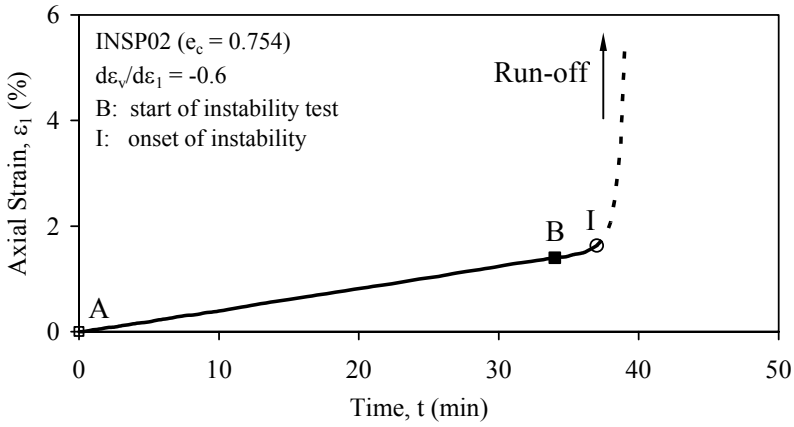

Fig. 6.20(d)

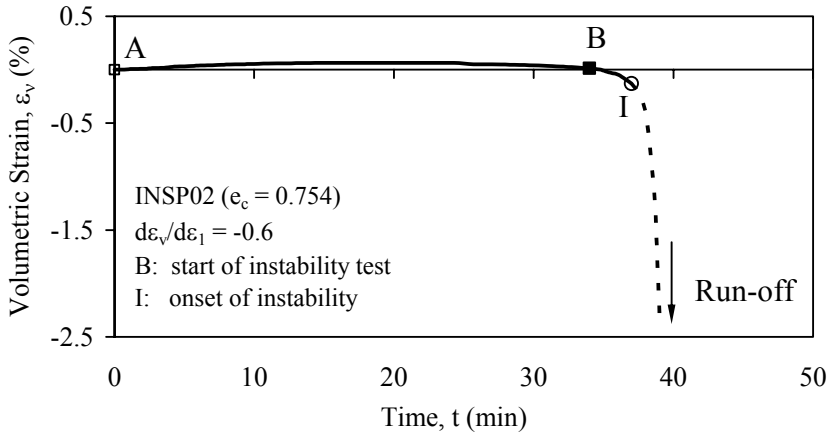

Fig. 6.20(e)

Fig. 6.20 Instability behaviour of medium loose sand in strain path testing: (a) effective stress path; (b) *e-p'* plot; (c) excess pore water pressure versus time curve; (d) axial strain versus time curve; (e) volumetric strain versus time curve

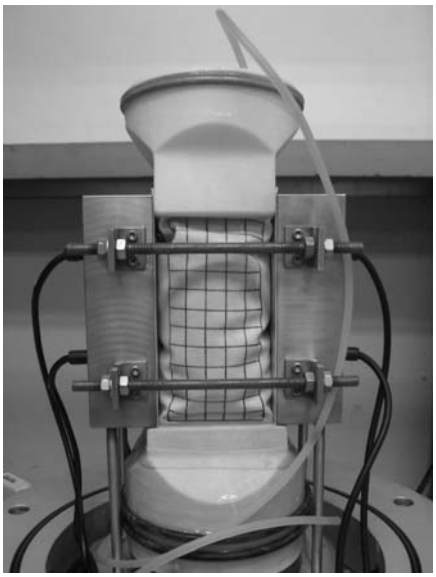

Fig. 6.21 The specimen in Test INSP02 after the occurrence of runaway instability

6.5.3.3 *Medium Dense Sand*

To verify whether runaway type of instability can be observed for medium dense sand, Test INSP06 was carried out. The effective stress path of Test INSP06 is plotted in Fig. 6.22(a). The *e-p'* plot obtained from Test INSP06 is given in Fig. 6.22(b). The CSL and the FL obtained from CK_0D tests on comparable void ratios are also shown in Fig. 6.22(a). The slope of the CSL and the FL is M_{cs} = 1.16 and η_f = 1.53, respectively. After the specimen was K_0 consolidated to point A (q/p' = 1.06, e_c = 0.685), a strain increment ratio of $d\varepsilon_v/d\varepsilon_1$ = -0.60 was imposed while keeping the deviator load constant. Under this strain path, the pore water pressure increased gradually (Fig. 6.22(c)). It can be seen from Figs. 6.22(d) and 6.22(e) that the axial and volumetric strains developed slowly until a shear band occurred at point SB. The pore water pressure was almost constant before the shear band had occurred (Fig. 6.22(c)). During this period, the axial strain and the volumetric strain rate increased steadily at a very slow rate of 0.002 %/min for ε_1 and 0.0015 %/min for ε_v (Figs. 6.22(d) and 6.22(e)). However, soon after the shear band formation (point SB), the excess pore water pressure shot up (Fig. 6.22(c)). The axial and volumetric strains increased suddenly (Fig. 6.22(d) and 6.22(e)). The specimen physically collapsed and the runaway instability had occurred at point F. As shown in Fig. 6.22(a), point F coincides with the failure line determined by drained tests.

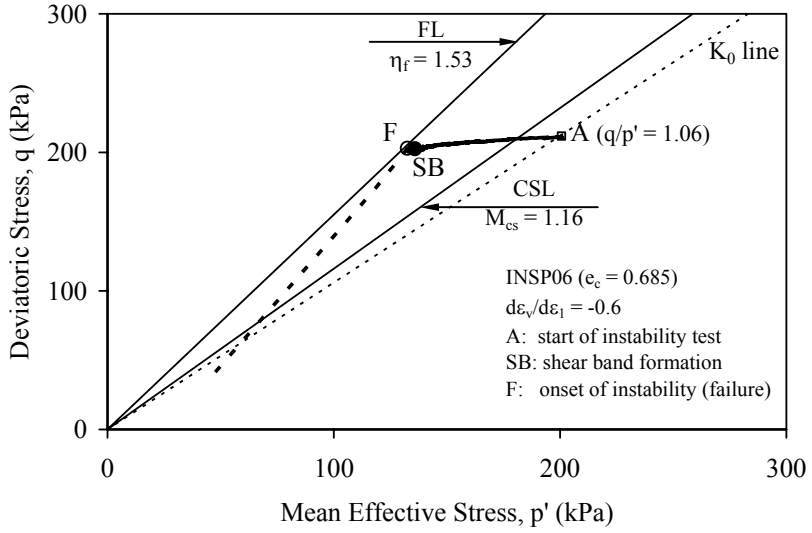

Fig. 6.22(a)

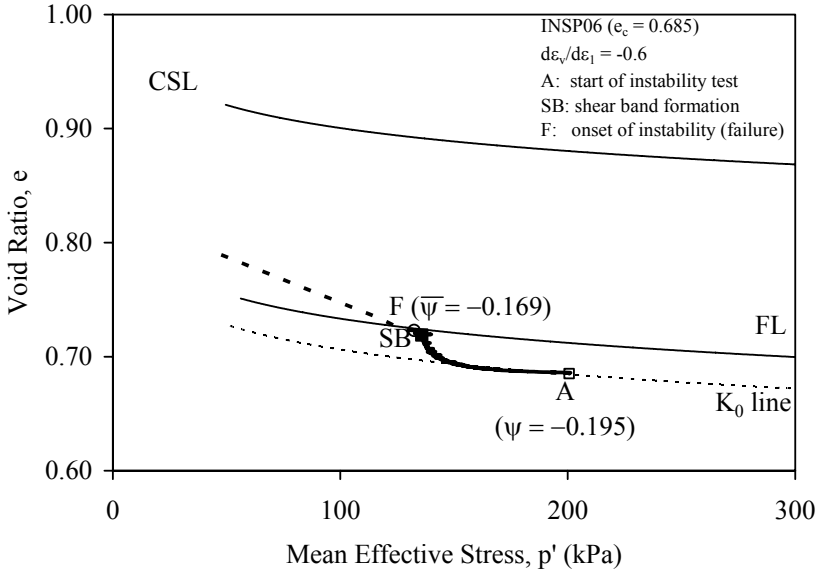

Fig. 6.22(b)

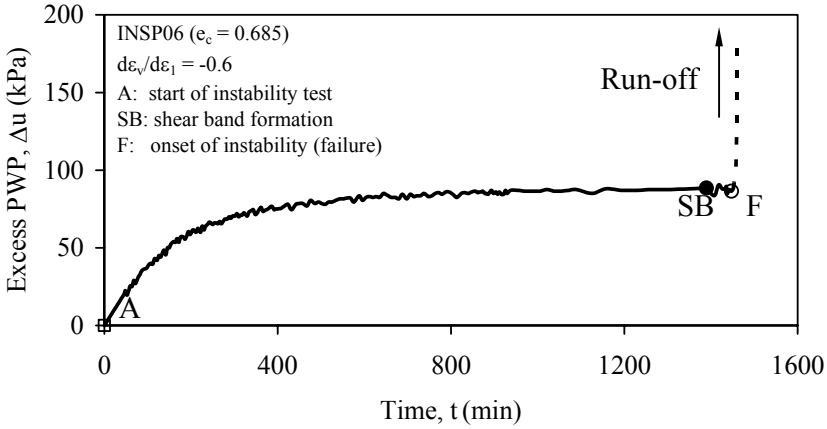

Fig. 6.22(c)

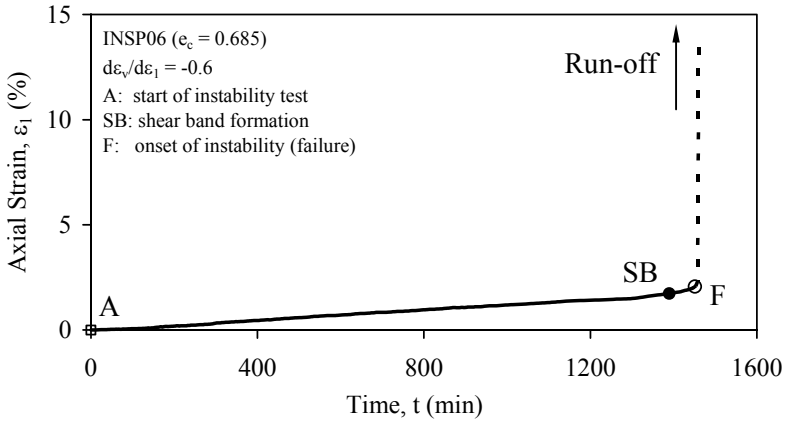

Fig. 6.22(d)

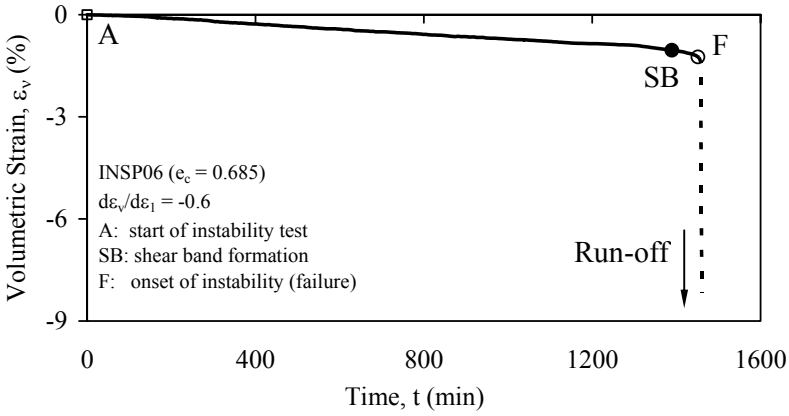

Fig. 6.22(e)

Fig. 6.22 Instability behaviour of medium dense sand in strain path testing: (a) effective stress path; (b) *e-p'* plot; (c) excess pore water pressure versus time curve; (d) axial strain versus time curve; (e) volumetric strain versus time curve

The shear band development in Test INSP06 is shown in Fig. 6.23 and the photos taken during the test are given in Appendix C (Fig. C.10). Selected photos around shear band are also shown in Fig. 6.23(a). The behaviour similar to that in Test IND03, described earlier (see Fig. 6.6), was observed.

The σ_2 against time curves obtained from Test INSP06 are plotted in Fig. 6.23(b). It is seen that the σ_2 values measured by the four individual load cells were almost identical until point 7(O). It is indicative that the shear band might have occurred at point 7(O). Similarly to the other types of plane-strain tests conducted on medium dense specimens there was no indication of shear band occurrence on the deviatoric stress or effective stress ratio curves, as shown in Fig. 6.23(c). Furthermore, there was no visible shear band at point 7(O) either (Fig. 6.23(a)). However, once the

shear band was captured by a camera (point 9(B)), the deviatoric stress and *q/p'* ratio decreased significantly, as shown in Fig. 6.23(b). The excess pore water pressure versus time and axial strain versus time curves obtained from Test INSP06 are shown in Fig. 6.23(d) and Fig. 6.23(e) respectively. It is seen that soon after the shear band was fully developed (point 9(B)), both Δu and ε_1 shot up and the specimen collapsed within a minute. This behaviour is typical for all the other instability tests conducted on medium dense sand with dilative strain increment ratio imposed. It can be concluded that the instability in this test is likely caused by the shear band, which occurred in the vicinity of failure. Therefore, the instability in Test INSP06 is a type of on-failure instability.

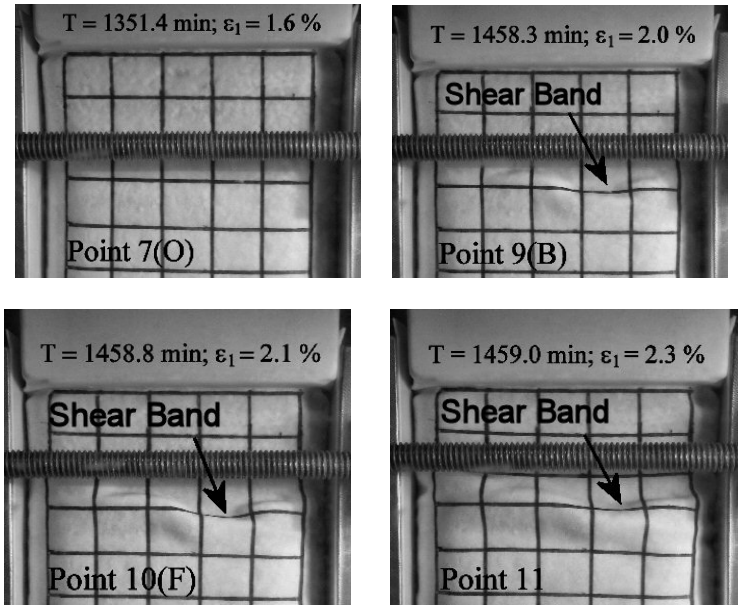

Fig. 6.23(a)

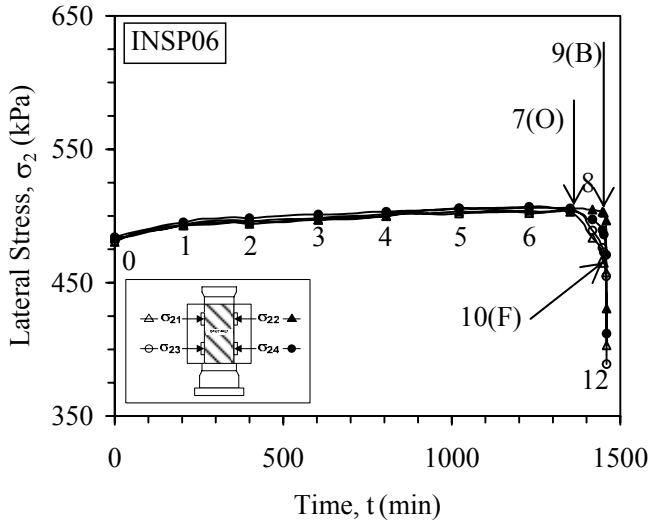

Fig. 6.23(b)

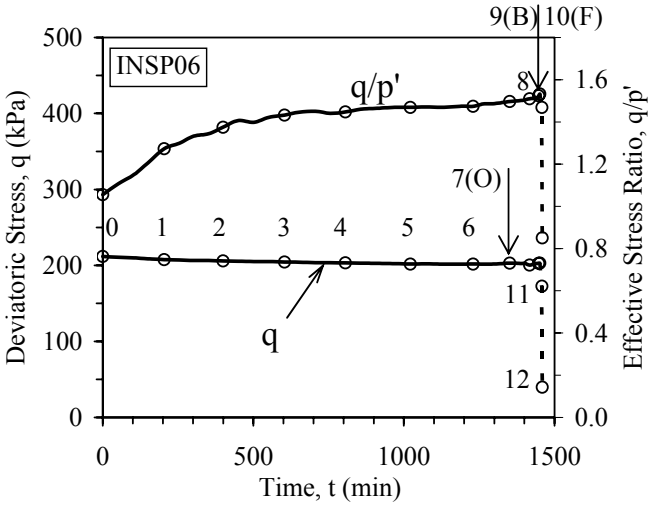

Fig. 6.23(c)

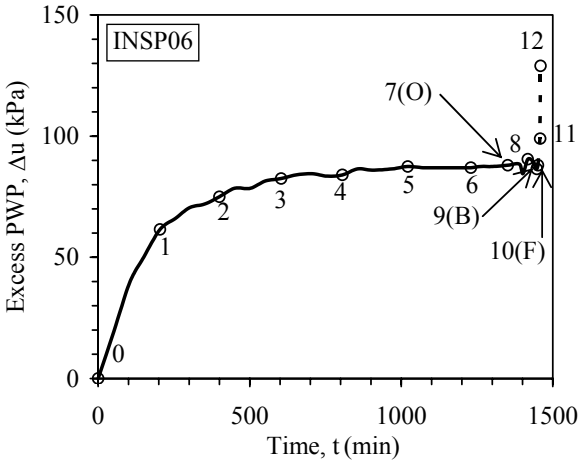

Fig. 6.23(d)

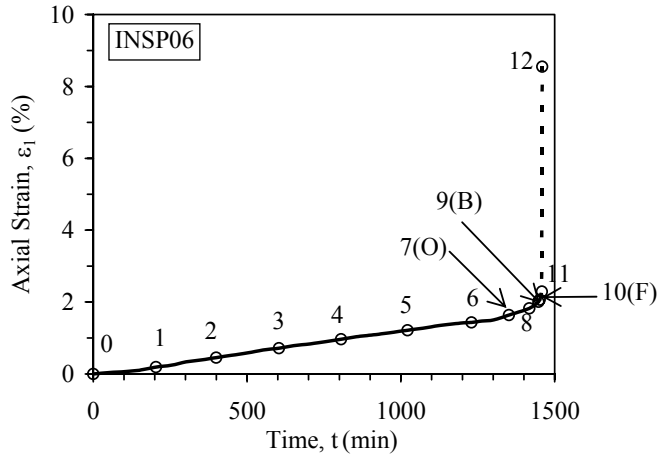

Fig. 6.23(e)

Fig. 6.23 Shear band development in Test INSP06: (a) selected photos; (b) σ_2 versus time curves; (c) q versus time and q/p' versus time curves; (d) Δu versus time curve; (e) ε_v versus time curve

6.5.4 Discussion

The experimental data presented above show that runaway instability can occur for very loose to medium dense sand in a constant load test under strain path controlled conditions. Similarly to the instability behaviour of granular soils under drained condition, the instability behaviour of granular soils in strain path testing is also affected by void ratio. It was observed that the higher the void ratio the lower the gradient of the instability line. On the other hand, once instability occurs, the specimen collapses irrespective of the void ratio.

It has been shown earlier (see section 4.4.1 in Chapter 4) that the instability line for very loose sand can be determined by joining the peak points of the effective stress paths obtained under undrained conditions. Furthermore, the constant stress ratio line obtained from undrained tests can be used to predict the occurrence of instability for medium dense sand. Loke (2004) also reported that similar method can be used to determine the instability line under strain path controlled conditions. By conducting $d\varepsilon_v/d\varepsilon_1 = const$ path tests at different effective confining pressure, using a deformation-controlled loading mode, a peak stress line (PSL) can be determined. Loke (2004) further suggested that the PSL can be used to predict the occurrence of instability under a load-controlled loading mode.

Fig. 6.24 shows the results of three strain path tests SP10, SP27 and SP28 with $d\varepsilon_v/d\varepsilon_1$ = -0.60 imposed. The void ratios of the specimens SP10, SP27 and SP28 after K_0 consolidation were 0.734, 0.728 and 0.730 respectively. Strain-softening behaviour was observed for all the three specimens, as shown in Fig. 6.24(a). From the *e-p'* plot presented in Fig. 6.24(b), it can be seen that plastic yielding occurred at points Y_A, Y_B and Y_C for all the three tests. As shown in Fig. 6.24(a), these points correspond to the peak of the effective stress paths. By joining these three points with the origin, a peak stress line (PSL) can be established. The PSL has a gradient of η_p = 1.25, as shown in Fig. 6.24(a). By joining the three yielding points Y_A, Y_B, and Y_C together on the *e-p'* plane, the PSL on the *e-p'* plane can also be obtained, as shown in Fig. 6.24(b).

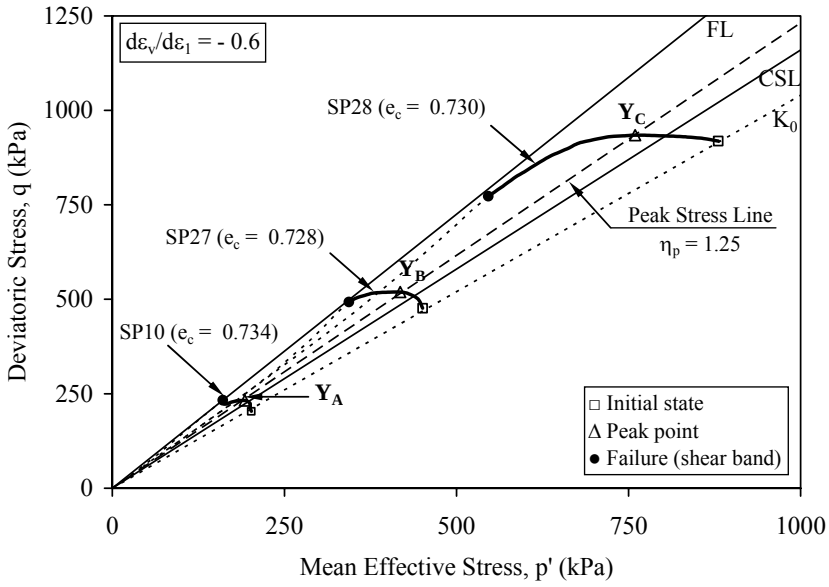

Fig. 6.24(a)

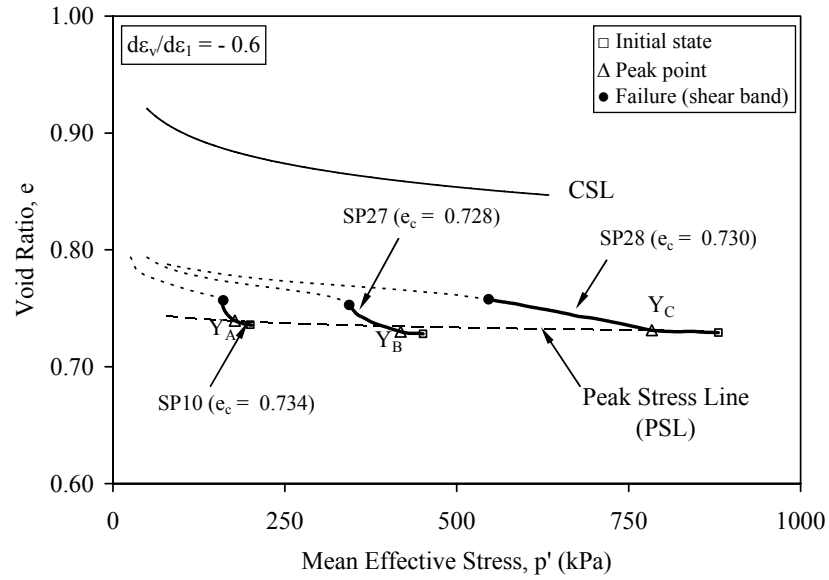

Fig. 6.24(b)

Fig. 6.24 The peak stress line determined by $d\varepsilon_v/d\varepsilon_1 = -0.6$ path tests: (a) *q-p'* plane; (b) *e-p'* plane

From the study of instability behaviour of sand under undrained conditions, it is known that the IL is determined by joining the peak points of the undrained stress paths. Therefore, the PSL obtained in Fig. 6.24(a) for strain path tests conducted under a deformation-controlled loading mode could also be the IL for strain path tests conducted under a load-controlled loading mode. A comparison of the PSL obtained for medium loose sand (Fig. 6.24(a)) and the IL determined for medium

loose specimen with comparable void ratio in Test INSP02 is presented in Fig. 6.25. As can be seen from Fig. 6.25, the two lines are very close to each other. Therefore, the PSL obtained from the strain path tests conducted under a deformation-controlled loading mode and the IL line obtained from constant load tests can be considered as equivalent lines defined under different loading modes.

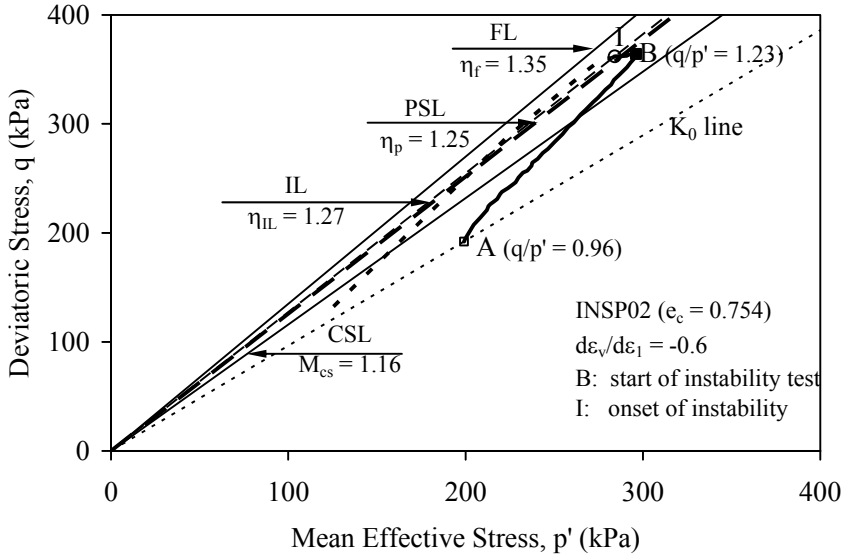

Fig. 6.25 Comparison between the IL and the PSL for Test INSP02

The slope of the PSL, η_p, obtained from $d\varepsilon_v/d\varepsilon_1$ = -0.6 tests conducted under a deformation-controlled loading mode is plotted versus the void ratio, e_c, in Fig. 6.26. The data obtained from the instability tests conducted with $d\varepsilon_v/d\varepsilon_1$ = -0.6 controlled are also plotted in Fig. 6.26. For each test, a solid symbol indicates the instability behaviour coupled with the shear band formation and an open symbol indicates the instability behaviour not related to the shear band formation. It can bee seen that the slope obtained from the instability tests agrees reasonably well with that determined from strain path tests conducted with the same $d\varepsilon_v/d\varepsilon_1$. Therefore, the occurrence of instability in the constant load tests can be predicted by the PSL obtained from the strain path tests, conducted with the same $d\varepsilon_v/d\varepsilon_1$. The relationship between the slope of the IL, η_{IL}, and the void ratio, e_c, obtained from undrained $(d\varepsilon_v/d\varepsilon_1 = 0)$ tests is also shown in Fig. 6.26. It can be observed that the curve obtained from $d\varepsilon_v/d\varepsilon_1$ = 0 tests is different from that obtained from $d\varepsilon_v/d\varepsilon_1$ = -0.6 tests. For a given η_p (or η_{IL}), the soil needs to be much looser to manifest instability under an undrained condition ($d\varepsilon_v/d\varepsilon_1 = 0$) than that under a $d\varepsilon_v/d\varepsilon_1$ = -0.6 condition. This again suggests that the occurrence of instability is

affected not only by the void ratio but also by the strain increment ratio or the drainage conditions imposed.

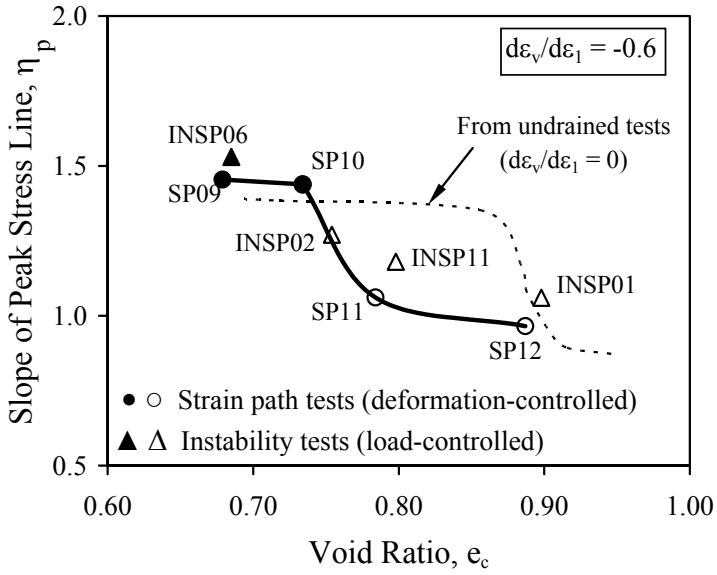

Fig. 6.26 Relationship between the slope on the peak stress line, η_p, and void ratio, e_c, for $d\varepsilon_v/d\varepsilon_1$ = *-0.6* path tests

The influence of strain increment ratio, $d\varepsilon_v/d\varepsilon_1$, on the instability behaviour of medium loose sand was investigated by conducting two tests, INSP03 (e_c = 0.797) and INSP11 (e_c = 0.798) under the same testing conditions but with a different $(d\varepsilon_v/d\varepsilon_1)_i$ ratio. The strain increment ratio of -0.40 was imposed in Test INSP03, whereas the strain increment ratio of -0.60 was imposed in Test INSP11. The results of the two tests are compared in Fig. 6.27.

From the axial strain versus time curves of the two tests, presented in Fig. 6.27(d), it can be seen that the axial strains in both tests started to accelerate at points I and I'. Therefore, instability occurred at points I and I'. Using points I and I', the instability line for each of the test can be determined on the *q-p'* plane, as shown in Fig. 6.27(a). It can be seen from Fig. 6.27(a) that although the constant load tests were started from the same K_0 consolidation state (point A or A'), the two different instability lines were obtained. In test INSP03, the specimen became unstable when the stress path reached the stress state at η_{IL} = 1.25 (point I'). In test INSP11, the specimen became unstable at η_{IL} = 1.19 (point I). Two separate instability lines were thus obtained on the *e-p'* plot, as shown in Fig. 6.27(b). It can also be observed that the specimen in Test INSP11 $(d\varepsilon_v/d\varepsilon_1$ = *-0.6)* exhibits larger

volumetric dilation than the specimen in Test INSP03 *($d\varepsilon_v/d\varepsilon_1$ = -0.4)*. This is also seen in Fig. 6.23(e) where the volumetric strain against time curves of the two tests are plotted. During the constant load test, the specimen with imposed $d\varepsilon_v/d\varepsilon_1$ = -0.6 experienced a volumetric dilation of 0.27%, whereas the specimen with $d\varepsilon_v/d\varepsilon_1$ = -0.4 exhibited a much smaller volumetric dilation of 0.17%. It shows that the plastic yielding in a specimen will occur earlier when more negative $d\varepsilon_v/d\varepsilon_1$ is imposed. Therefore, the specimen in Test INSP11 became unstable faster than the specimen in Test INSP03 (Fig. 6.27(d)). The specimen in Test INSP11 *($d\varepsilon_v/d\varepsilon_1$ = -0.6)* took a much shorter time (≈ 392 minutes) than the specimen in test INSP03 ($d\varepsilon_v/d\varepsilon_1$ = -0.4; ≈ 660 minutes) to reach the stress state at point I or I' where instability occurred. At the same time, it can be seen that both specimens experienced similar axial strains during the constant load tests. The specimen with imposed $d\varepsilon_v/d\varepsilon_1$ = -0.6 experienced an axial strain of 0.45%. For the specimen with imposed $d\varepsilon_v/d\varepsilon_1$ = -0.4, an axial strain of 0.42% was observed. The excess pore water pressures developed in the two tests were also similar (Δu = 60–66 kPa) before the occurrence of instability. After the onset of instability, the axial deformation and pore water pressures in both tests shot up and the specimens physically collapsed.

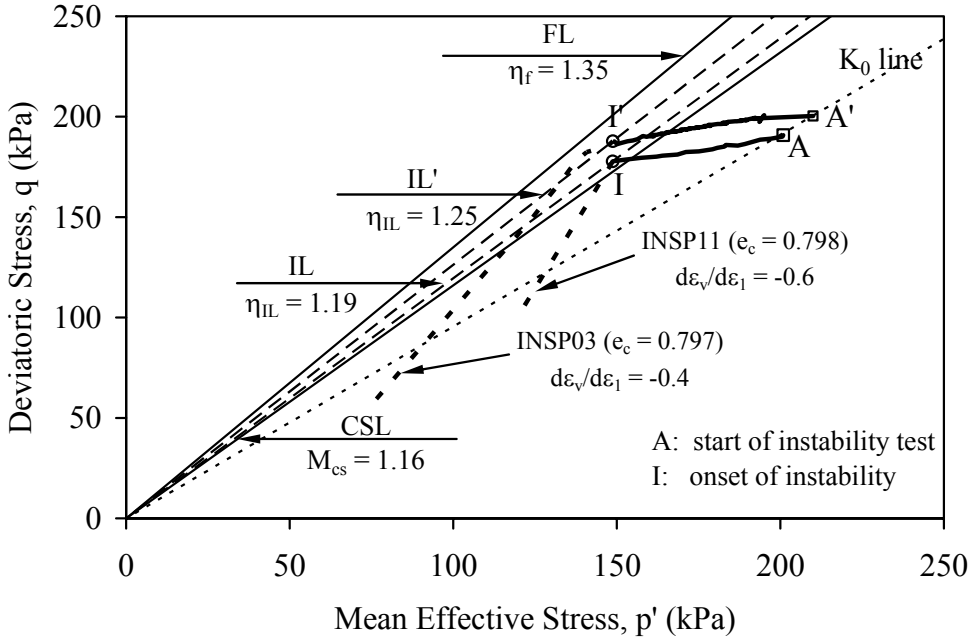

Fig. 6.27(a)

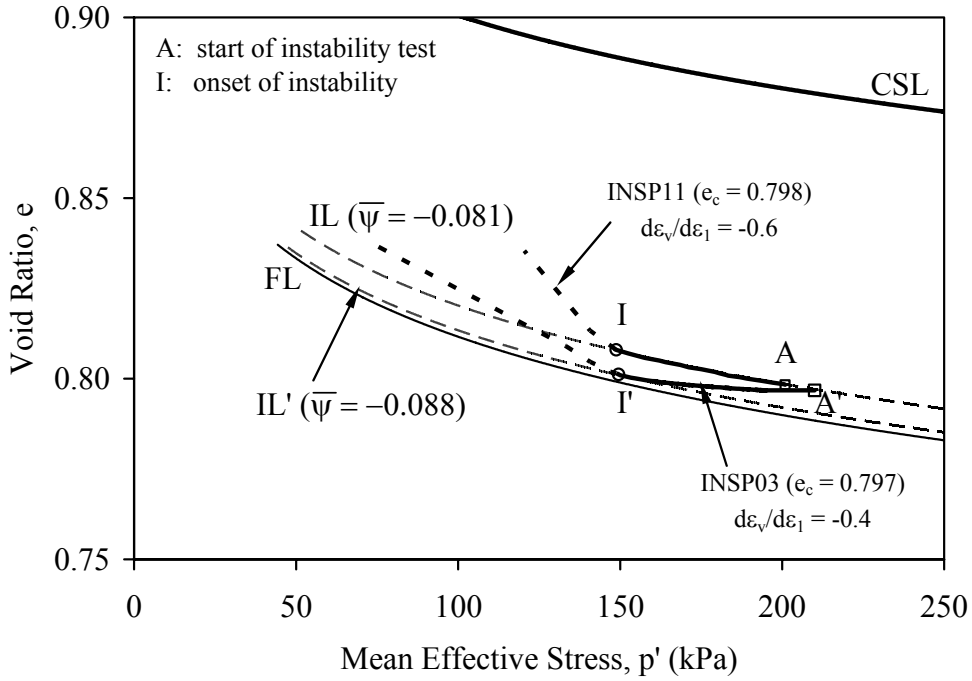

Fig. 6.27(b)

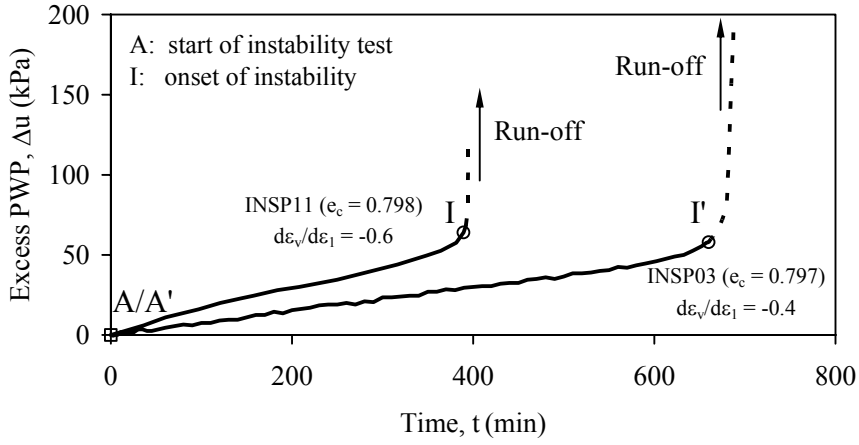

Fig. 6.27(c)

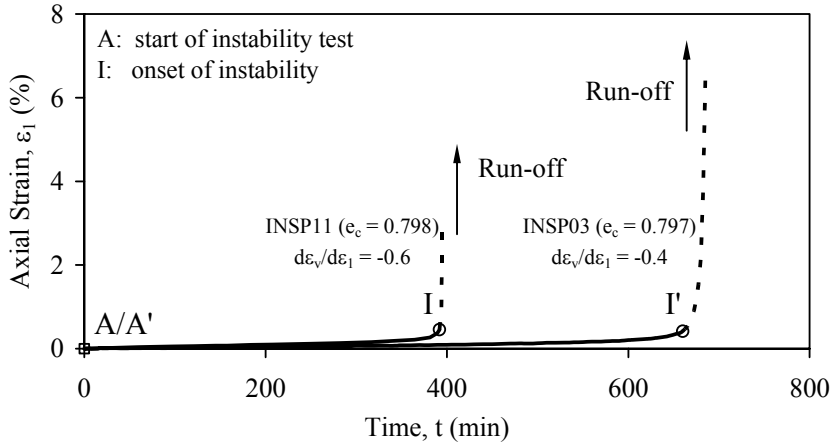

Fig. 6.27(d)

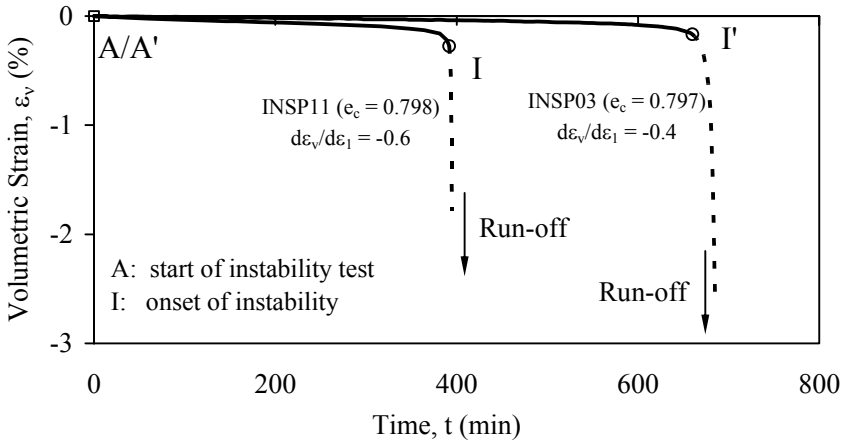

Fig. 6.27(e)

Fig. 6.27 Effect of strain increment ratio on the instability of medium loose sand in strain path testing: (a) effective stress paths; (b) *e-p'* plot; (c) excess pore water pressure versus time curve; (d) axial strain versus time curves; (e) volumetric strain versus time curves

From the experimental results presented above, it can be seen that the strain increment ratio affects the instability behaviour of sand in strain path testing. It was shown that the more dilative the $d\varepsilon_v/d\varepsilon_1$ imposed to the specimen, the higher the tendency for instability to occur. This is because when a $d\varepsilon_v/d\varepsilon_1$ larger than the dilatancy ratio of the soil is imposed, the pore water pressure will increase. This in turn leads to a decrease in effective confining stress and causes instability when the instability line is crossed. It was discussed in Chapters 4 & 5 that generation of pore water pressure can be investigated by reference to drained tests. Therefore, similarly to the condition for the occurrence of strain softening, a strain increment ratio imposed to a specimen has to be adequately low (or more negative) to ensure the generation of pore water pressure. If the $(d\varepsilon_v/d\varepsilon_1)_i$ is more negative than the dilatancy ratio of the soil, $(d\varepsilon_v/d\varepsilon_1)_{max}$, which is obtained from drained (or zero pore water pressure) tests, the pore water pressure will increase and the specimen will become unstable. For example, in Test INSP11 $(d\varepsilon_v/d\varepsilon_1)_i$ = -0.60 and $(d\varepsilon_v/d\varepsilon_1)_{max}$ = -0.19. (see Fig. 4.10(b) in Chapter 4). Consequently, $[(d\varepsilon_v/d\varepsilon_1)_i - (d\varepsilon_v/d\varepsilon_1)_{max}]$ = -0.41 and pre-failure instability occurs in Test INSP11. Similarly, in Test INSP03, $(d\varepsilon_v/d\varepsilon_1)_i$ = -0.40 and $(d\varepsilon_v/d\varepsilon_1)_{max}$ = -0.19. Thus, $[(d\varepsilon_v/d\varepsilon_1)_i - (d\varepsilon_v/d\varepsilon_1)_{max}]$ = -0.21 and pre-failure instability also occurs. In Test INSP06 however, $(d\varepsilon_v/d\varepsilon_1)_i$ = -0.60 but $(d\varepsilon_v/d\varepsilon_1)_{max}$ = -0.79. (see Fig. 4.10(b) in Chapter 4). Therefore, $[(d\varepsilon_v/d\varepsilon_1)_i$ –

$(d\varepsilon_v/d\varepsilon_1)_{max}]$ = 0.19 and pre-failure instability does not occur in Test INSP06 (see Fig. 6.22).

Since the occurrence of instability in strain path testing is influenced by both, the void ratio and the strain increment ratio, there is an instability boundary on the e_c versus $(d\varepsilon_v/d\varepsilon_1)_i$ plane, which represents the critical conditions for instability to occur (Chu, 1991). The initial states of the instability tests conducted under strain path controlled conditions are plotted in Fig. 6.28. It can be seen that the two stable points are on the left top corner, that is, where $(d\varepsilon_v/d\varepsilon_1)_i$ is larger (less negative) or where the void ratio is smaller. There appears to be a boundary that separates the e_c versus $(d\varepsilon_v/d\varepsilon_1)_i$ plane into a stable and an unstable zone, as shown in Fig. 6.28. This is similar to the boundary plotted in Fig. 5.14 for strain softening, which is also replotted in Fig. 6.28. The similarity indicates that the condition for the occurrence of instability is analogous to that for the occurrence of strain softening. Similar observations were also made by Chu (1991) and Chu & Leong (2001) under axisymmetric conditions. They have concluded that if strain softening occurs for a soil specimen under a deformation-controlled loading mode, instability will occur for the same specimen under a load-controlled loading mode and vice-versa.

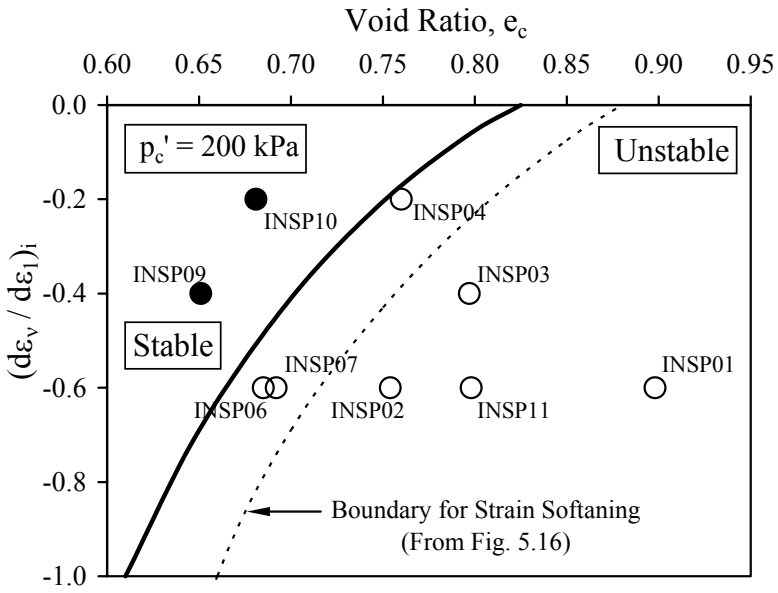

Fig. 6.28 Instability boundary for plane-strain conditions

It should be pointed out that the instability boundary in Fig. 6.28 is determined only for p_c' = 200 kPa. If the influence of p_c' is taken into consideration, a critical surface for the occurrence of instability can be formed in the $p_c' - e_c - (-d\varepsilon_v/d\varepsilon_1)_i$ space. This surface would be similar to the critical surface plotted in Fig. 5.17 for strain softening.

6.6 Summary

Several series of constant load tests were conducted under undrained, drained and strain path controlled conditions using the plane-strain apparatus. The results presented in this chapter can be summarized as follows:

- When very loose sand is tested under an undrained condition using the plane-strain apparatus, a runaway instability, the so-called "undrained instability" can occur. However, undrained instability does not occur for sand at other than very loose states. This is consistent with the experimental results obtained under axisymmetric stress conditions using the triaxial cell.

- Both contractive and dilative sand can become unstable at a stress state below the failure line under a drained condition. The specimen does not collapse instantly during drained instability; however the axial strain is increasing at accelerating rate. As a reduction in the mean effective stress is the necessary condition for the occurrence of drained instability, this type of pre-failure instability has been called the conditional instability. This is consistent with previous studies conducted under axisymmetric conditions (Leong, 2001; Chu & Leong, 2001; Chu et al., 2003; Loke, 2004).

- The results obtained from plane-strain tests have shown that the occurrence of instability under drained conditions is not controlled by the initial state or the state parameter, ψ, but by the modified state parameter, $\bar{\psi}$, which is defined by Chu et al. (2003) as $e_{IL} - e_{cr}$, where e_{IL} is the void ratio at the instability point, and e_{cr} is the void ratio at the critical state at the same mean effective stress. This is consistent with the observations made by Chu et al. (2003) and Loke (2004) under axisymmetric conditions.

- The results of constant load tests conducted under plane-strain conditions have shown that the instability line defined using Lade's method (Lade, 1992) is the same for both drained and undrained conditions and the instability line defines the lower bound of all the possible unstable conditions regardless of the drainage conditions. Therefore, instability will occur under either undrained or drained condition when the stress state falls into the zone of instability. Because the conditions for both types of instability are the same, a conditional instability that occurs under drained conditions can evolve into a runaway instability if the amount of pore water is too large to be dissipated fully from the soil

- The position of instability line determined based on the instability observed in the CSD test is not affected by the rate of reduction in the effective confining stress. The reduction rate, however, affects the time taken for instability to occur and the amount of axial strain developed upon the instability point. It was observed that the higher the reduction rate, the less time and the less axial deformation is needed for instability to occur.

- A runaway type of instability can occur even for medium dense sand when a constant load test is conducted under a strain path controlled condition. Similarly to the condition for the occurrence of strain softening, a strain increment ratio imposed to a specimen has to be adequately low (i.e., negative) to generate the pore water pressure. If the $(d\varepsilon_v/d\varepsilon_1)_i$ experienced by the specimen in a strain path test is more negative than the $(d\varepsilon_v/d\varepsilon_1)_{max}$ obtained from a drained test, the specimen will become unstable. The occurrence of this type of instability is associated with the increase in pore water pressure. Therefore, the increase in pore water pressure is the necessary condition for the occurrence of this type of instability.

- The instability line obtained from strain path tests under constant load conditions coincides with the peak stress line obtained from strain path tests conducted with the same $d\varepsilon_v/d\varepsilon_1$ under a deformation-controlled loading mode. This suggests that the peak stress line can be used to predict the occurrence of instability under strain path controlled conditions.

CHAPTER 7

CONCLUSIONS & RECOMMENDATIONS

7.1 Conclusions

An experimental study on the strain softening and instability behaviour of Changi sand under plane-strain conditions has been carried out. A new plane-strain apparatus has been developed and used in this study. Several series of drained, undrained, strain path controlled and other special tests have been conducted. The measurements of σ_2 at different locations have helped in the detection of the shear band formation. A number of important observations have been made from the study. The main conclusions and contributions of this thesis are summarized below.

- The developed plane-strain apparatus and the testing system are suitable for the study of strain softening and instability behaviour of sand. The computer controlled plane-strain testing system enables various stress and strain path tests to be conducted accurately under both deformation-controlled and load-controlled loading modes. Lubricated loading platens are used, so that the effect of boundary conditions on the stress and strain measurements can be significantly reduced. The obtained data can thus be interpreted as element tests.

- The drained and undrained stress-strain and strength characteristics of Changi sand under plane-strain conditions were studied. The failure lines of the soil at different void ratios were determined. A relationship between the gradient of the failure line, η_f, and the consolidated void ratio, e_c, is established. The value of η_f ranges from 1.53 for medium dense sand to

1.16 for very loose sand. The slope of the critical state line is M_{cs} = 1.16. The corresponding friction angle, φ', is in the range from 36.0° to 49.7°. This φ' value is 7% to 19% higher than that obtained from triaxial tests for the soil at the same void ratio. It is particularly noted that the friction angle at the critical state measured under plane-strain conditions ($(\varphi_{cs}')_{ps} = 36.0^{o}$) is different from that obtained under axisymmetric conditions ($(\varphi_{cs}')_{tri}$ = 33.4°).

- Plane-strain tests under both deformation-controlled and load-controlled conditions were conducted. A comparison of the two tests indicate that the failure line and the CSL on both the *q-p'* and the *e-p'* planes are not affected by the loading mode. However, the post-peak behaviour of sand in both drained and undrained tests is affected by the loading mode. Under a deformation-controlled loading mode strain softening develops, whereas under a load-controlled loading mode instability occurs.

- A series of plane-strain tests conducted on very loose sand under undrained conditions indicate that the instability line under plane-strain conditions can be defined using the method suggested by Lade (1993) for axisymmetric conditions. Similar to the observations made under axisymmetric conditions, the instability line is not unique, but varies with the void ratio of the sand. The smaller the e_c, the higher the gradient of the instability line. However, the position of the instability line does not seem to be affected by the loading mode, that is, whether the tests are conducted under a deformation-controlled mode or a load-controlled mode.

- A number of strain path tests were conducted to investigate strain path dependent behaviour of sand under plane-strain conditions. It is established experimentally that when the strain increment ratio imposed, $(d\varepsilon_v/d\varepsilon_1)_i$ is larger (i.e., more positive) than a threshold value, a strain hardening behaviour will prevail. On the other hand, when the $(d\varepsilon_v/d\varepsilon_1)_i$ is smaller (i.e., more negative) than a threshold value, strain softening will occur. Here, the threshold value refers to the strain increment ratio at failure $(d\varepsilon_v/d\varepsilon_1)_f$, as measured in a drained test. The occurrence of strain softening

under plane-strain conditions is affected by the void ratio, the strain increment ratio and the initial effective confining stress. A response boundary can be identified on the $d\varepsilon_v/d\varepsilon_1 - e$ and $d\varepsilon_v/d\varepsilon_1 - p'$ planes or in the $d\varepsilon_v/d\varepsilon_1 - e - p'$ space. This boundary represents the critical condition for strain softening to occur. This is consistent with the findings established by Chu et al. (1992) under axisymmetric conditions.

- Under plane-strain conditions, two types of strain softening behaviour, the pre-failure softening and the post-failure softening are identified. A pre-failure strain softening behaviour may consist of three stages, namely, material softening, banding softening, and ultimate state. During the first stage, the deviatoric stress decreases slowly and the effective stress path plunges towards the failure line. As the specimen reaches the banding softening stage the deviatoric stress will decrease abruptly at an accelerated rate and shear bands are developed. At the final stage, shear bands are fully developed and an ultimate state is approached. However, the strain softening behaviour observed for very loose sand is an exception because shear band may not occur even if the critical state is reached. For a test in which material softening does not occur, strain softening will occur only in two stages, i.e., banding softening and ultimate state.

- When medium dense sand is sheared under $d\varepsilon_v/d\varepsilon_1 = const$ path, the resulting effective stress path will approach asymptotically a constant stress ratio line (CSRL). The smaller (i.e., more negative) the imposed strain increment ratio, the larger the resultant asymptotic stress ratio, $(q/p')_{asy}$. The relationship between the imposed strain increment ratio and the resultant constant stress ratio can be experimentally determined. For plane-strain conditions, the relationship can be expressed as:

$$\left(\frac{q}{p'}\right)_{asy} = \begin{cases} M_0 - \mu\left(d\varepsilon_v / d\varepsilon_1\right), & for \quad d\varepsilon_v / d\varepsilon_1 \geq \left(d\varepsilon_v / d\varepsilon_1\right)_f \\ \left(\dfrac{q}{p'}\right)_f & for \quad d\varepsilon_v / d\varepsilon_1 < \left(d\varepsilon_v / d\varepsilon_1\right)_f \end{cases}$$

where M_0 and μ are experimental constants.

For medium dense sand tested under plane-strain conditions M_0 = 1.37 and μ = 0.23. This relationship is consistent with that obtained under axisymmetric conditions by Chu & Lo (1994).

- When very loose sand is tested under an undrained condition using the plane-strain apparatus, a runaway instability can occur. When the runaway instability occurs, the specimen collapses almost instantly. However, undrained instability does not occur for sand at other than very loose state. This is consistent with the experimental results obtained under axisymmetric stress conditions using the triaxial cell.

- Both contractive and dilative sand can become unstable at a stress state below the failure line under a drained condition. The specimen does not collapse instantly during drained instability; however, the axial strain is increasing at accelerating rate. As a reduction in the mean effective stress is the necessary condition for the occurrence of drained instability, this type of pre-failure instability has been called the conditional instability. This is consistent with previous studies conducted under axisymmetric conditions (Leong, 2001; Chu & Leong, 2001; Chu et al., 2003; Loke, 2004).

- Despite the differences in the two types of instability, the conditions for the occurrence of both types of instability are the same. The results of constant load tests conducted under plane-strain conditions have shown that the instability line defined using Lade's method, is the same for both drained and undrained conditions and the instability line defines the lower bound of all the possible unstable conditions regardless of the drainage conditions. Therefore, instability can occur under both undrained and drained conditions as long as the stress state falls into the zone of instability. Because the conditions for both types of instability are the same, a conditional instability that occurs under drained conditions can evolve into a runaway instability if the amount of pore water pressure is too large to be dissipated fully from the soil.

- The position of instability line determined based on the instability observed in the CSD test is not affected by the rate of reduction in the effective

confining stress. The reduction rate, however, affects the time taken for instability to occur and the amount of axial strain developed upon the instability point. It was observed that the higher the reduction rate, the less time and the less axial deformation is needed for instability to occur.

- The results obtained from plane-strain tests have shown that the occurrence of instability under drained conditions is not controlled by the initial state or the state parameter, ψ, but by the modified state parameter, $\bar{\psi}$, which is defined by Chu et al. (2003) as $e_{IL} - e_{cr}$, where e_{IL} is the void ratio at the instability point, and e_{cr} is the void ratio at the critical state at the same mean effective stress. This is consistent with the observations made by Chu et al. (2003) and Loke (2004) under axisymmetric conditions

- A runaway type of instability can occur even for medium dense sand when a constant load test is conducted under a strain path $(d\varepsilon_v/d\varepsilon_1)$ controlled condition. Similarly to the condition for the occurrence of strain softening, a strain increment ratio imposed to a specimen has to be adequately low (i.e. negative) to generate the pore water pressure. If the $(d\varepsilon_v/d\varepsilon_1)_i$ experienced by the specimen in a strain path test is more negative than the $(d\varepsilon_v/d\varepsilon_1)_{max}$ obtained from a drained test, the specimen will become unstable. The occurrence of this type of instability is associated with the increase in pore water pressure. Therefore, the increase in pore water pressure is the necessary condition for the occurrence of this type of instability.

- The instability line obtained from strain path tests under constant load conditions coincides with the peak stress line obtained from the strain path tests conducted with the same $d\varepsilon_v/d\varepsilon_1$ under a deformation-controlled loading mode. This suggests that the peak stress line can be used to predict the occurrence of instability under strain path controlled conditions.

- Shear bands always occur during plane-strain tests on medium loose and medium dense sand under drained conditions. However, shear bands do not occur in plane-strain tests conducted on very loose specimens under drained conditions. Under undrained conditions, shear bands can also develop unless the specimen is looser than the void ratio at the critical state. The

measured shear band inclination for the Changi sand is in the range from 49.6° to 58.6°, giving an average value of 56°. Shear band orientations were best predicted by Roscoe's solution.

7.2 Practical Implications

The following practical implications can be drawn from the study:

- The test data confirms that most of the fundamental findings established on strain softening and instability in triaxial tests can be extended to the plane-strain conditions. Therefore, in general, triaxial test can be used to study the strain softening and instability behaviour of sand. However, the comparison of plane-strain and triaxial tests has shown that for a given modified state parameter, $\bar{\psi}$, the slope of instability line (η_{IL}), is lower under plane-strain conditions than that under axisymmetric conditions (see Fig. 6.10). In other words, for a given η_{IL}, the soil needs to be looser to manifest instability in triaxial tests than that in plane-strain tests. This suggests that the occurrence of instability is affected by stress conditions and that granular soil is more vulnerable for instability to occur under plane-strain conditions. Furthermore, there is a fundamental difference between triaxial and plane-strain tests. In triaxial tests, shear bands will not occur for dense sand if the friction between the specimen and loading platens can be eliminated (Chu, 1991). In plane-strain tests, shear band will always occur for dense sand as a response to the plane-strain conditions even if the boundary conditions are 'perfect'. Therefore, it is suggested that a plane-strain test instead of a triaxial test should be used in slope stability analysis.

- Many geotechnical problems such as slopes, embankments, and retaining walls cannot be approximated as axisymmetric conditions. However, the stress-strain behaviour of soil is often studied using triaxial tests. The soil parameters are also usually determined using triaxial tests. One argument for such a practice is that the friction angle obtained from triaxial tests is smaller than that from plane-strain conditions. However, in terms of the failure line defined on the q-p' plane, the failure line for triaxial tests is

actually above the failure line obtained from the plane-strain tests. Therefore, for a soil element sheared along a drained path, failure will occur at a lower deviatoric stress in a plane-strain test (Fig. 7.1). This is the fact that has often been neglected by geotechnical engineers. It also highlights the deficiency of using φ' for plane-strain conditions as φ' does not show the influence of σ_2.

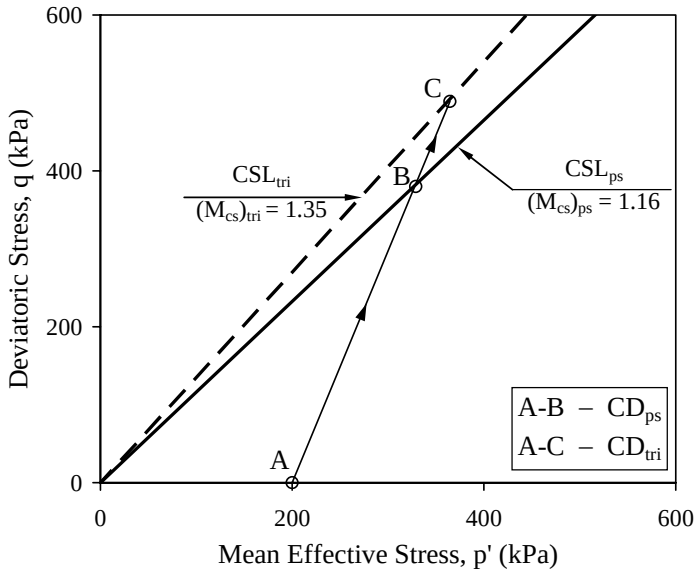

(a)

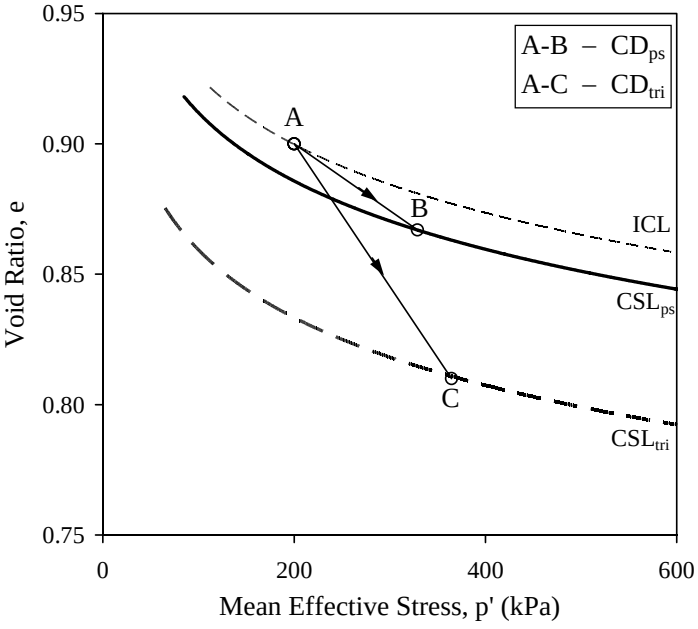

(b)

Fig. 7.1 Critical States Lines for plane-strain and triaxial test results

- The existence of a unique critical state wherein indefinite shearing occurs is a major assumption of the family of elasto-plastic models known as critical state soils mechanics (Schofield & Wroth, 1968). According to the critical state theory, there is a unique void ratio for each state of effective stress at critical state. Therefore, critical state conditions can be described by a critical state line (CSL) in the $e-p'-q$ space. The determination and overall validity of a critical state in sand is essential, because it provides the basis for many constitutive models. Despite the general acceptance of the critical state concept, a question arises on whether the CSL line is unique for axisymmetric, plane-strain and three dimensional stress conditions. The triaxial and plane-strain data obtained from this study show that the CSL obtained under plane-strain conditions is different from that under axisymmetric conditions. For Changi sand, the slope of the CSL under plane-strain conditions is $(M_{cs})_{ps}$ = 1.16 and under axisymmetric conditions is $(M_{cs})_{tri}$ = 1.35, as show in Fig. 7.1(a). The position of the CSL on the *e-p'* plane is also different (Fig. 7.1(b)). Thus, it is not appropriate to assume that the critical state is unique for all stress conditions and the critical state parameters can be measured using triaxial tests. This point is particular important for the use of elasto-plastic models for plane-strain conditions.

- Another important practical implication is related to the loading mode. It is shown that pre-peak behaviour of soil is not significantly affected by the loading mode. However, the post-peak behaviour of sand in both drained and undrained tests is affected by the loading mode. Under a deformation-controlled loading mode, strain softening develops, whereas under a load-controlled loading mode, instability occurs. The effect of the loading mode is also reflected in geotechnical practice, e.g., static pile load tests. The load-settlement curves obtained from a pile load test conducted under a load-controlled loading mode are different from that under deformation-controlled loading mode. A constitutive model of soils describes a unique stress-strain behaviour for a given stress path irrespective of the loading mode adopted. Therefore, a constitutive model may be able to predict when instability or strain-softening occurs, but may not be able to distinguish whether instability or strain softening will occur.

- Since load-controlled tests are characterised by a sudden collapse of a specimen, it may be difficult to define failure unambiguously, especially in loose sand. Fig. 7.2 presents schematically the effective stress paths obtained from two undrained tests conducted on loose sand, one under a DC loading mode (Fig. 7.2(a)) and another under a LC loading mode (Fig. 7.2(b)). The failure line defined by drained tests is also shown in Fig. 7.2. For the deformation-controlled test, failure can be defined either as q_{max} (point B) or $(q/p')_{max}$ (point C). The $(q/p')_{max}$ should be used, so the failure line defined by drained tests will be the same as that by undrained tests. However, for the load-controlled test, instability occurs at point B. The stress-strain behaviour after instability cannot be defined properly. As the sample has collapsed at point B or soon after point B, this point should be defined as the failure point.

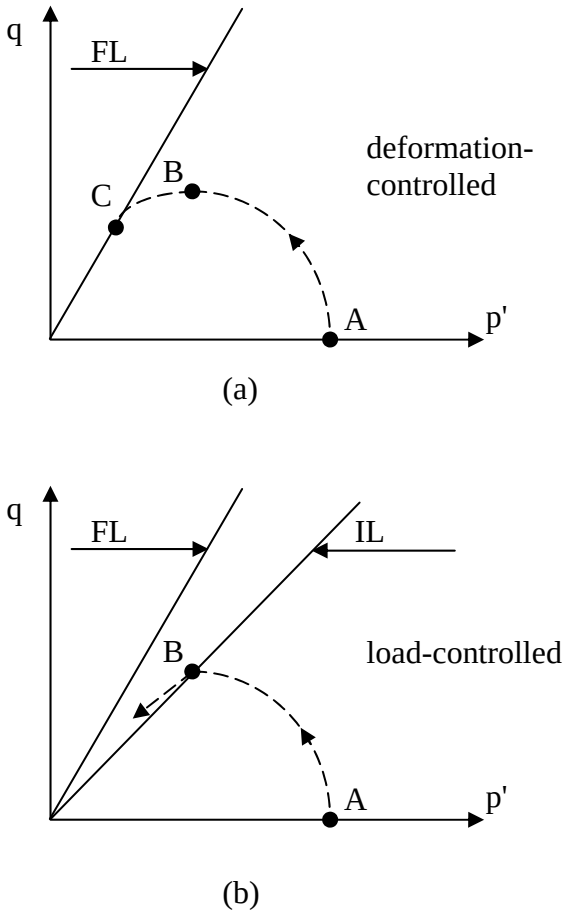

Fig. 7.2 Effective stress paths obtained from undrained tests conducted on loose sand: (a) deformation-controlled loading mode; (b) load-controlled loading mode

7.3 Recommendations

Several interesting findings have been presented in this thesis. However, due to time constraint, several important factors have not been studied. The following recommendations can me made for future research.

- The developed plane-strain testing system can be modified to conduct extension tests. It would be useful to study the strain softening and instability behaviour of sand under extension paths.

- The study presented in this thesis was conducted within a limited range of void ratio, strain increment ratio and initial effective confining stress. To determine the response and instability boundaries in the three dimensional p'–$d\varepsilon_v/d\varepsilon_1$–$e$ space, the wider range of those factors should be used.

- Further study on the shear band formation under a constant shear condition is required to fully understand interrelation between the shear band formation and the occurrence of instability. For this purpose, the plane-strain apparatus used in this study should be modified to accommodate at least one transparent sidewall. This will make possible to detect shear band formation on the σ_2 plane. More sophisticated techniques (e.g. stereophotogrammetry or digital image correlation) should also be used to analyze shear band development in specimens. This may enable studying of the effect of shear band propagation and growth on the instability behaviour of sand.

- A constitutive model should be developed or used to model the experimental data obtained in this study.

REFERENCES

ASTM: D 854-02 (2002). Standard Test Methods for Specific Gravity of Soil Solids by Water Pycnometer.

ASTM: D 2487-00 (2002). Standard Practice for Classification of Soils for Engineering Purposes (Unified Soil Classification System).

ASTM: D 4253-00 (2000). Standard Test Methods for Maximum Index Density and Unit Weight of Soils Using a Vibratory Table.

BS 1377: Part 3: (1990). British Standard Methods of Tests for Soils for Civil Engineering Purposes, Part 3: Chemical and electro-chemical tests.

Adalier, K. & Elgamal, A.-W. (2002). Seismic response of adjacent dense and loose saturated sand columns. *Soil Dynamics and Earthquake Engng*, **22**, 115-127.

Alarcon-Guzman, A., Leonards, G. A. & Chameau, J. L. (1988). Undrained monotonic and cyclic strength of sand. *J. Geotech. Engng, ASCE* **114**, No.10, 1089-1109.

Alshibli, A. K. & Sture, S. (2000). Shear band formation in plane strain experiments of sand. *J. Geotech. Geoenviron. Engng, ASCE* **126**, No.6, 495-503.

Alshibli, K. A., Sture, S., Costes, N. C., Frank, M. L., Lankton, M. R., Batiste, S. N. & Swanson, R. A. (2000). Assessment of localized deformations in sand using X-Ray computed tomography. *Geotech. Testing J.* **23**, No. 3, 274–299.

Alshibli, A. K., Batiste, S. N. & Sture, S. (2003). Strain localization in sand: plane strain versus triaxial compression. *J. Geotech. Geoenviron. Engng, ASCE* **129**, No.6, 483-494.

Alshibli, A. K., Godbold, D. L. & Hoffman, K. (2004). The Louisiana plane strain apparatus for soil testing. *Geotech. Testing J., ASTM* **27**, No.4, 1-10.

Anderson, S. A. & Riemer, M. F. (1995). Collapse of saturated soil due to reduction in confinement. *J. Geotech. Engng, ASCE* **121**, No.2, 216-219.

Anderson, S. A. & Sitar, N. (1995). Analysis of rainfall-induced debris flows. *J. Geotech. Engng, ASCE* **121**, No.7, 544-552.

Arthur, J. R. F. & Menzies, B. K. (1972). Inherent anisotropy in sand. *Géotechnique* 22, No.1, 115-128.

Arthur, J. R. F., Dunstan, T., Al-Ani, Q. A. J. L. & Assadi, A. (1977). Plastic deformation and failure in granular media. *Géotechnique* **27**, No.1, 53-74.

Arthur, J. R. F. & Dunstan, T. (1982). Rapture layers in granular media. *Proc. IUTAM Conf. on Deformation and Failure of Granular Materials*, (*eds. Vermeer & Luger)*, Delft, 453-459.

Arthur, J. R. F., Dunstan, T. & Enstad, G. G. (1985). Determination of the flow function by means of a cubic plane strain tester. *Int. J. Bulk Storage Silos* **1**, No.2, 7-10.

Baldi, G. & Nova, R. (1984). Membrane penetration effects in triaxial testing. *J. Geotech. Engng, ASCE* **110**, No.3, 403-419.

Barden, L., Ismail, H. & Tong, P. (1969). Plane strain deformation of granular material at low and high pressures. *Géotechnique* **19**, No.4, 441-452.

Bardet, J. P. (1990). Hypoplastic model for sands. *J. Engng. Mech., ASCE* **116**, No.9, 1973-1994.

Bardet, J. P. & Proubet, J. (1990). Shear band analysis in idealized granular material. *J. Engng Mech.* **118**, No.2, 387-415.

Bardet, J. P. (1994). Observations on the effects of particle rotations on the failure of idealized granular materials. *Mech. Materials* **18**, 159-182.

Batiste, S. N., Alshibli, K. A., Sture, S. & Lankton, M. (2004). Shear band characterization of triaxial sand specimen using computed tomography. *Geotech. Testing J., ASTM* **27**, No.6, 1-12.

Been, K. & Jefferies, M. G. (1985). A state parameter for sand. *Géotechnique* **35**, No.2, 99-112.

Been, K., Crooks, J. H. A., Colin, B. H. & Horsfield, D. (1988). Liquefaction of hydraulically placed sand fills. *Conference on Hydraulic Fill Structures, ASCE Geotechnical Special Publication **21***, 330-345.

Been, K., Jefferies, M. G. & Hachey, J. E. (1991). The critical state of sands. *Géotechnique* **35**, No.2, 99-112.

Bishop, J. F. W. & Hill, R. (1951). A theory of the plastic distortion of a polycrystalline aggregate under combined stresses. *Philosophical Magazine* **42**, No.327, 414-427.

Bishop, A. W. (1958). The requirements for measuring the coefficient of earth pressure at rest. *Proc. European Conf. Earth Pressures, Brussels*, **1**, 1-7.

Bishop, A. W. & Green, G. E. (1965). The influence of end restraint on the compression strength of a cohesionless soil. *Géotechnique* **15**, No.3, 243-266.

Bishop, A. W. (1966). Strength of soil as engineering materials (6^{th} Rankine Lecture). *Géotechnique* **16**, No.2, 89-130.

Borja, R. I. (2000). A finite element model for strain localization analysis of strongly discontinuous fields based on standard Galerkin approximation. *Comp. Meth. Appl. Mech. Engng* **190**, No.11–12, 1529–1549.

Borja, R. I., Regueiro, R. A. & Lai, T. Y. (2000). FE modelling of strain localization in soft rocks. *J. Geotech. Geoenviron. Engng, ASCE* **126**, No.4, 335–343.

Borja, R. I. & Regueiro, R. A. (2001). Strain localization in frictional materials exhibiting displacement jumps. *Comp. Meth. Appl. Mech. Engng* **190**, No.20–21, 2555–2580.

Borja, R. & Lai, T. Y. (2002). Propagation of localization instability under active and passive loading. *J. Geotech. Geoenviron. Engng, ASCE* **128**, No.1, 64-75.

Boukpeti, N., Mroz, Z. & Drescher, A. (2002). A model for static liquefaction in triaxial compression and extension. *Can. Geotech. J.* **39**, 1243-1253.

Brand, E. W. (1981).Some thoughts on rain-induced slope failures. *Proc. 10^{th} Int. Conf. Soil Mech. Found. Engng, Stockholm,* **3**, 373-376.

Broms, B. B. & Casbarian, A. O. (1965). Effects of rotation of the principal stress axes and of the intermediate stress on shear strength. *Proc. 6th Int. Conf. Soil Mech. Found. Engng, Montreal,* **1**, 179-183.

Campanella, R. G. & Vaid, Y. P. (1973). Influence of stress path on the plane-strain behaviour of a sensitive clay. *Proc. 8^{th} Int. Conf. Soil Mech. Found. Engng, Moscow,* **1**, 85-92.

Casagrande, A. (1936). Characteristics of cohesionless soils affecting the stability of earth fills. *Contributions to Soil Mechanics: 1925-1940*. Boston Society of Civil Engineers, 257-276.

Casey, J. & Naghdi, P. M. (1981). On the characterization of strain-hardening in plasticity. *J. Appl. Mech., ASME* **48**, 285-296.

Castro, G. (1969). Liquefaction of sands. *Harvard Soil Mech. Series*, No.81, 1-112.

Castro, G. & Poulos, S. J. (1977). Factors affecting liquefaction and cyclic mobility. *J. Geotech. Engng Div., ASCE* **102**, No.6, 501-516.

Castro, G., Seed, R. B., Keller, O. T. & Seed, H. B. (1992). Steady-state strength analysis of Lower San Fernando Dam slide. *J. Geotech. Engng, ASCE* **118**, No.3, 406-427.

Chu, J. (1991). *Strain softening behaviour of granular soils under strain path testing.* PhD thesis, The University of New South Wales, Australia.

Chu, J. & Lo, S.-C. R. (1991). On the implementation of strain path testing. *Proc. 10th Eur. Conf. Soil Mech., Florence*, 53-56.

Chu, J., Lo, S.-C. R. & Lee, I. K. (1992). Strain-softening behaviour of a granular soil in strain-path testing. *J. Geotech. Engng, ASCE* **118**, No.2, 191-208.

Chu, J., Lo, S.-C. R. & Lee, I. K. (1993). Instability of granular soils under strain path testing. *J. Geotech. Engng, ASCE* **119**, No.5, 874-892.

Chu, J. & Lo, S.-C. R. (1993). On the measurement of critical state parameters of dense granular soils. *Geotech. Testing J., ASTM* **16**, No.1, 27-35.

Chu, J. & Lo, S.-C. R. (1994). Asymptotic behaviour of a granular soil in strain path testing. *Géotechnique* **44**, No.1, 65-82.

Chu, J., Lo, S.-C. R. & Lee, I. K. (1996). Strain softening and shear band formation of sand in multi-axial testing. *Géotechnique* **46**, No.1, 63-82.

Chu, J. (1998). Pre-failure strain softening and pre-failure instability of a granular soil. *Pre-failure deformation behaviour of geomaterials,* Thomas Telford, London, 337-344

Chu, J. (1999). Discussion on 'Quasi-steady state: a real behaviour?'. *Can. Geotech. J.* **36**, 190-191.

Chu, J. & Leong, W. K. (2001). Pre-failure strain softening and pre-failure instability of sand: a comparative study. *Géotechnique* **51**, No.4, 311-321.

Chu, J. & Leong, W. K. (2002). Effect of fines on instability behaviour of loose sand. *Géotechnique* **52**, No.10, 751-755.

Chu, J., Leroueil, S. & Leong, W. K. (2003). Unstable behaviour of sand and its implication for slope stability. *Can. Geotech. J.* **40**, 873-885.

Chu, J. & Gan, C. L. (2004). Effect of void ratio on K_0 of loose sand. *Géotechnique* **54**, No.4, 285-288.

Cooling, L. F. & Smith, D. B. (1936). The shearing resistance of soils. *Proc. Ins. Civ. Engrs*, London **3**, 333-343.

Cornforth, D. H. (1961). *Plane strain failure characteristics of a saturated sand.* PhD thesis, University of London.

Cornforth, D. H. (1964). Some experiments on the influence of strain conditions on the strength of sand. *Géotechnique* **14**, No. 2, 143-167.

Coulomb, C. A. (1776). Essai sur une application des règles de Maximus et Minimis à quelques Problèmes de Statique, relatifs á l'Archtecture. *Mémoires de Mathématique et de Physique* **7**, 343-382.

De Borst, R. (1991). Simulation of strain localization: A reappraisal of the Cosserat continuum. *Engng Comp.* **8**, 317-332.

De Borst, R. & Muhlhaus, H.-B. (1992). Gradient-dependent plasticity: Formulation and algorithmic aspects. *Int. J. Num. Meth. Engng.* **35**, 521-539.

De Borst, R., Pamin, J. & Sluys, L. J. (1995). Computational issues in gradient plasticity. *Continuum models for materials with microstructures (ed. Muhlhaus)*, Wiley, New York, 159-200.

De Greorgio, V. B. (1990). Loading systems, sample preparation, and liquefaction. *J. Geotech. Engng, ASCE* **116**, No.5, 805-821.

Desrues, J., Lanier, J. & Stutz, P. (1985). Localization of the deformation in tests on sand sample. *Engng Fracture Mech.* **21**, No.4, 909-921.

Desrues, J., Chambon, R., Mokni, M., & Mazerolle, F. (1996). Void ratio evolution inside shear bands in triaxial sand specimens studied by computed tomography. *Géotechnique* **46**, No.3, 529-546.

Desrues, J. & Viggiani, G. (2004). Strain localization in sand: an overview of the experimental results obtained in Grenoble using stereophotogrammetry. *Int. J. Numer. Anal. Meth. Geomech.* **28**, 279-321.

Drescher, A. & Vardoulakis, I. (1982). Geometric softening in triaxial tests on granular material. *Géotechnique* **32**, No.4, 291-303.

Drescher, A., Vardoulakis, I. G. & Han, C. (1990). A biaxial apparatus for testing soils. *Geotech. Testing J., ASTM* **13**, No.3, 226-234.

Drescher, A., Birgisson, B. & Shah, K. (1995). A model for water saturated loose sand. *Numerical Models in Geomechanics, (eds. Pande & Pietruszczak)*, 109-112.

Drescher, A. & Mroz, Z. (1997). A refined superior sand model. *Numerical Models in Geomechanics, (eds. Pande & Pietruszczak)*, 21-26.

Drucker, D. C. (1951). A more fundamental approach to stress-strain relations. *Proc. 1st U.S. National Congress of Appl. Mech.*, 487-491.

Drucker, D. C. (1956). On uniqueness in the theory of plasticity. *Quarterly Appl. Math.* **14**, 35-42.

Drucker, D. C. (1959). A definition of stable inelastic material. *J. Appl. Mech., ASME* **26**, 101-106.

Duncan, J. M. & Seed, H. B. (1966). Strength variation along failure surfaces in clay. *J. Soil Mech. Found. Div., ASCE* **92**, No.6, 81-104.

Eckersley, J. D. (1985). Flowslides in stockpiled coal. *Engng Geol.*, **22**, 13-22.

Eckersley, J. D. (1990). Instrumented laboratory flowslides. *Géotechnique* **40**, No.3, 489-502.

Eliadorani, A. A. (2000). *The response of sands under partially drained states with emphasis on liquefaction.* PhD thesis, The University of British Columbia, Canada.

Farooq, K., Orense, R. P. & Towhata, I. (2002). Mechanism of rain-induced failure in sandy slopes based on field stress path. *Proc. 3rd Int. Conf. on Landslides, Slope Stability and the Safety of Infra-Structures, Singapore*, 159-166.

Finno, R. J., Harris, W. W. & Viggiani, G. (1996). Strain localization and undrained steady state of sand. *J. Geotech. Engng, ASCE* **122**, No.6, 462-473.

Finno, R. J., Harris, W. W., Mooney, M. A. & Viggiani, G. (1997). Shear bands in plane strain compression of loose sand. *Géotechnique* **47**, No.1, 149-165.

Finno, R. J., & Rechenmacher, A. L. (2003). Effects of consolidation history on critical state of sand. *J. Geotech. Geoenviron. Engng, ASCE* **129**, No.4, 350-360.

Fish, J. & Belytschko, T. (1990). A finite element with undirectionally enriched strain field for localization analysis. *Comp. Meth. Appl. Mech. Engng* **78**, No.2, 181-200.

Fleming, R. W., Ellen, S. D. & Algus, M. A. (1989). Transformation of dilative and contractive landslide debris into debris flows – an example from Marin County, California. *Engng Geol.*, **27**, 201-223.

Frost, J. D. & Jang, D.-J. (2000). Evolution of sand microstructure during shear. *J. Geotech. Geoenviron. Engng, ASCE* **126**, No.2, 116-130.

Gajo, A. & Wood, D. M. (1999a). A kinematic-hardening constitutive model for sands: the multiaxial formulation. *Int. J. Num. Anal. Meth. Geomech.* **23**, 925-965.

Gajo, A. & Wood, D. M. (1999b). Severn-Trent sand: a kinematic-hardening constitutive model: q-p formulation. *Géotechnique* **49**, No.5, 595-614.

Gan, C. L. (2002). *Instability of granular soil under general stress conditions.* MEng thesis, Nanyang Technological University, Singapore.

Goldscheider, M. (1982). True triaxial tests on dense sand. *Results Int. Workshop on constitutive Relations for Soils (eds. Gudehus, Darve & Vardoulakis)*, Balkema, Rotterdam, 11-54.

Green, G. E. (1971). Strength and deformation of sand measured in an independent stress control cell. *Proc. Roscoe Memorial Symposium: "Stress-strain behaviour of soils"*, Cambridge University, 285-323.

Green, G. E. & Reades, A. W. (1975). Boundary conditions, anisotropy and sample shape effects on the stress-strain behaviour of sand in triaxial compression and plane strain. *Géotechnique* **25**, No.2, 333-356.

Gu, W. H., Morgenstern, N. R. & Robertson, P. K. (1993). Progressive failure of lower San Fernando dam. *J. Geotech. Engng, ASCE* **119**, No.2, 333-349.

Gudehus, G., Goldscheider, M. & Winter, H. (1977). Mechanical properties of sand and clay and numerical integration methods: some sources of errors and bounds of accuracy. *Finite Elements in Geomechanics, (ed. Gudehus)*, 121-150.

Hambly, E. C. (1969). A new true triaxial apparatus. *Géotechnique* **19**, No.2, 307-309.

Hambly, E. C. & Roscoe, K. H. (1969). Observations and predictions of stresses and strains during plane-strain of "wet" clays. *Proc. 7th Int. Conf. Soil Mech. Found. Engng, Mexico,* **1**, 173-181.

Hambly, E. C. (1972). Plane strain behaviour of remoulded normally consolidated kaolin. *Géotechnique* **22**, No.2, 301-317.

Han, C. & Vardoulakis, I. G. (1991). Plane-strain compression experiments on water-saturated fine-grained sand. *Géotechnique* **41**, No.1, 49-78.

Han, C. & Drescher, A. (1993). Shear bands in biaxial tests on dry coarse sand. *Soils Found.* **33**, No.1, 118-132.

Harris, W. W., Viggiani, G., Mooney, M. A. & Finno, R. J. (1995). Use of stereophotogrammetry to analyze the development of shear bands in sand. *Geotech. Testing J., ASTM* **18**, No.4, 405-420.

Haruyama, M. (1985). Drained deformation-strength characteristics of loose Shirasu (volcanic sandy soil) under three dimensional stresses. *Soils Found.* **25**, No.1, 65-76.

Hettler, A. & Vardoulakis, I. (1984). Behaviour of dry sand tested in a large triaxial apparatus. *Géotechnique* **34**, No.2, 183-197.

Hight, D. W., Gens, A. & Symes, M. J. (1983). The development of a new hollow cylinder apparatus for investigating the effect of principal stress rotation in soils. *Géotechnique* **33**, No.4, 355-383.

Hight, D. W., Georgiannou, V. N., Martin, P. L. & Mundegar, A. K. (1999). Flow slides in micaceous sands., *Problematic Soils, (eds. Moroto & Mitachi*), Balkema, Rotterdam, 945-958.

Hill, R. (1958). A general theory of uniqueness and stability in elastic-plastic solids. *J. Mech. Phys. Solids* **6**, No.3, 236-249.

Hill, R. (1962). Acceleration waves in solids, *J. Mech. Phys. Solids* **10**, No.1, 1-16.

Hird, C. C. & Hassona, F. A. K. (1990). Some factors affecting the liquefaction and flow of saturated sands in laboratory tests. *Engng Geol.,* **28**, 149-170.

Imam, S. M. R., Morgenstern, N. R., Robertson, P. K. & Chan, D. H. (2002). Yielding and flow liquefaction of loose sand. *Soils Found.* **42**, No.3, 19-31.

Ishihara, K. (1993), Liquefaction and flow failure during earthquakes. *Géotechnique* **43**, No.3, 351-415.

Jaky, J. (1944). The coefficient of earth pressure at rest. *J. Soc. Hungarian Arch. Engrs*, **78**, No.22, 355-358.

Kiekbusch, M. & Schuppener, B. (1977). Membrane penetration and its effect on pore water pressures. *J. Geotech. Engng Div., ASCE* **103**, No.11, 1267-1279.

Kirkpatrick, W. M. & Belshaw, D. J. (1968). On the interpretation of the triaxial test. *Géotechnique* **18**, No.3, 336-350.

Ko, H. Y. & Scott, R. F. (1967). A new soil testing apparatus. *Géotechnique* **17**, 40-57.

Ko, H. Y. & Scott, R. F. (1968). Deformation of sand at failure. *J. Soil Mech. Found. Div., ASCE* **94**, No.4, 883-898.

Kolbuszewski, J. J. (1948). An experimental study of the maximum and minimum porosities of sand. *Proc. 2nd Int. Conf. Soil Mech. Found. Engng, Rotterdam,* **1**, 158-165.

Kolymbas, D. (1991). An outline of hypoplasticity. *Arch. Appl. Mech.* **61**, 143-151.

Konrad, J.-M. (1990). Minimum undrained strength of two sands. *J. Geotech. Engng, ASCE* **116**, No.6, 932-947.

Konrad, J. -M. (1991). The Nerlerk berm case history: some considerations for the design of hydraulic sand fills. *Can. Geotech. J.* **28**, 601-612.

Konrad, J.-M. (1993). Undrained response of loosely compacted sands during monotonic and cyclic compression tests. *Géotechnique* **43**, No.1, 69-89.

Kramer, S. L. & Seed, H. B. (1988). Initiation of soil liquefaction under static loading conditions. *J. Geotech. Engng, ASCE* **114**, No.4, 412-430.

Kuerbis, R., Negussey, D. & Vaid, Y. P. (1988). Effect of gradation and fines content on the undrained response of sand. *Proc. Conf. on Hydraulic Fill Structures, Fort Collins, Colorado,* ASCE, 330-345.

Ladd, R. S. (1974). Specimen preparation and liquefaction of sand. *J. Soil Mech. Found. Div., ASCE* **100**, No.10, 1180-1184.

Lade, P. V. & Duncan, J. M. (1973). Cubical triaxial tests on sand. *J. Soil Mech. Found. Div., ASCE* **99**, No.10, 793-812.

Lade, P. V. & Duncan, J. M. (1975). Elasto-plastic stress-strain theory for cohesionless soil. *J. Geotech. Engng Div., ASCE* **101**, No.10, 1037-1053.

Lade, P. V. & Duncan, J. M. (1976). Stress path dependent behaviour of cohesionless soil. *J. Geotech. Engng Div., ASCE* **102**, No.1, 51-56.

Lade, P. V. (1977). Elasto-plastic stress-strain theory for cohesionless soil with curved yield surfaces. *Int. J. Solids Struct.* **13**, 1019-1035.

Lade, P. V. (1978). Cubical triaxial apparatus for soil testing. *Geotech. Testing J., ASTM* **1**, No.2, 93-101.

Lade, P. V., Nelson, R. B. & Ito, Y. M. (1987). Nonassociated flow and stability of granular materials. *J. Engng. Mech., ASCE* **113**, No.9, 1302-1318.

Lade, P. V., Nelson, R. B. & Ito, Y. M. (1988). Instability of granular materials with nonassociated flow. *J. Engng Mech., ASCE* **114**, No.12, 2173-2191.

Lade, P. V. & Pradel, D. (1990). Instability and flow of granular materials. I: Experimental observations. *J. Engng Mech., ASCE* **116**, No.11, 2532-2550.

Lade, P. V. (1992). Static instability and liquefaction of loose fine sandy slopes. *J. Geotech. Engng,* ASCE **118**, No.1, 51-71.

Lade, P. V. (1993). Initiation of static instability in the submarine Nerlerk Berm. *Can. Geotech. J.* **30**, 895-904.

Lade, P. V. (1994). Instability and liquefaction of granular materials. *Comp. Geotech.*, **16**, No.2, 123-151.

Lade, P. V. & Kim, M. (1995). Single hardening constitutive model for soil, rock and concrete. *Int. J. Solids Struct.* **32**, No.14, 1963-1978.

Lade, P. V. & Yamamuro, J. A. (1996). Undrained sand behavior in axisymmetric tests at high pressures. *J. Geotech. Engng, ASCE* **122**, No.2, 120-129.

Lade, P. V, Yamamuro, J. A. & Skyers, B. D. (1996). Effects of shear band formation in triaxial extension tests. *Geotech. Testing J., ASTM* **19**, No.4, 398-410.

Lade, P. V. (1999). Instability of granular materials. *Physics & Mech. of Soil Liquefaction, (eds. Lade & Yamamuro),* Balkema, Rotterdam, 3-16.

Lade, P. V. & Wang, Q. (2001). Analysis of shear banding in true triaxial tests on sand. *J. Engng Mech., ACSE* **127**, No.8, 762-768.

Lancelot, L., Shahrour, I. & Al Mahmoud, M. (2004). Instability and static liquefaction on proportional strain paths for sand at low stresses. *J. Engng Mech., ASCE* **130**, No.11, 1365-1372.

Larsson, R., Runesson, K. & Sture, S. (1991). Finite element simulation of localized plastic deformation. *Arch. Appl. Mech.* **61**, 305-317.

Larsson, R., Runesson, K. & Ottosen, N. S. (1993). Discontinuous displacement approximation for capturing plastic localization. *Int. J. Num. Meth. Engng* **36**, 2087–2105.

Lee, K. L. (1970). Comparison of plane strain and triaxial tests on sand. *J. Soil Mech. Found. Div., ASCE* **96**, No.3, 901-923.

Lee, K. L. & Shubeck, R. J. (1971). Plane-strain undrained strength of compacted clay. *J. Soil Mech. Found. Div., ASCE* **97**, No.1, 219-234.

Leong, W. K., Chu, J. & Teh, C. I. (2000). Liquefaction and instability of a granular fill material. *Geotech. Testing J., ASTM* **23**, No. 2, 178-192.

Leong, W. K. (2001). *Instability behaviour of granular fill material*. PhD thesis, Nanyang Technological University, Singapore.

Leong, W. K. & Chu, J. (2002). Effect of undrained creep on instability behaviour of loose sand. *Can. Geotech. J.* **39**, 1399-1405.

Leroueil, S. (1997). Critical state soil mechanics and the behaviour of real soils. *Recent Developments in Soil and Pavement Mechanics, (ed. Almeida),* Balkema, Rotterdam, 41-80.

Leussink, H. & Wittke, W. (1964). Difference in triaxial and plane strain shear strength. *Laboratory shear testing of soils, ASTM STP **361***, 77-89.

Liang, L., Saada, A. S., Figueroa, J. L. & Cope, C. T. (1997). The use of digital image processing in monitoring shear band development. *Geotech. Testing J., ASTM* **20**, No. 3, 324-339.

Lo, K. Y. & Lee, C. F. (1973). Stress analysis and slope stability in strain softening materials. *Géotechnique* **23**, No.1, 1-11.

Lo, S.-C. R., Chu, J. & Lee, I. K. (1989). A technique for reducing membrane penetration and bedding errors. *Geotech. Testing J., ASTM* **12**, No.4, 311-316.

Lo, S.-C. R. & Lee, I. K. (1990). Response of a granular soil along constant stress increment ratio path. *J. Geotech. Engng, ASCE* **116**, No.3, 355-376.

Lo, S.-C. R. & Chu, J. (1991a). Discussion on instability of granular materials with nonassociated flow. *J. Engng Mech., ASME* **117**, No.4, 930.

Lo, S.-C. R. & Chu, J. (1991b) The measurement of K_0 by triaxial strain path testing. *Soils Found.* **31**, No.2, 181-187.

Loke, W. L. (2004). *Failure mechanisms of gentle granular slopes.* MEng thesis, Nanyang Technological University, Singapore.

Mandel, J. (1964). Conditions de stabilite et postulat de Drucker. *Proc. IUTAM Symposium on Theology and Soil Mechanics*, Grenoble, 58-68.

Marachi, N. D., Duncan, J. M, Chan, C. K. & Seed, H. B. (1981). Plane-strain testing of sand. *Laboratory shear strength of soil, ASTM STP **740***, 294-302.

Michalowski, R. L. (1990). Strain localization and periodic fluctuations in granular flow processes from hoppers. *Géotechnique* **40**, No.3, 389-403.

Mokni, M. & Desrues, J. (1998). Strain localisation measurements in undrained plane-strain biaxial tests on Hostun RF sand. *Mech. Cohesive-Frictional Mater.* **4**, No.4, 419-441.

Molenkamp, F. & Luger, H. J. (1981). Modelling and minimization of membrane penetration effects in tests on granular soils. *Géotechnique* **31**, No.4, 471-486.

Molenkamp, F. (1985). Comparison of frictional material models with respect to shear band initiation. *Géotechnique* **35**, No.2, 127-143.

Mooney, M. A., Viggiani, G. & Finno, R. J. (1997). Undrained shear band deformation in granular media. *J. Engng Mech., ASCE* **123**, No.6, 577-585.

Mooney, M. A., Finno, R. J. & Viggiani, M. G. (1998). A unique critical state for sand. *J. Geotech. Geoenviron. Engng, ASCE* **124**, No.11, 1100-1108.

Morris, D. V. (1983). A note on earthquake-induced liquefaction. *Géotechnique* **33**, No.4, 541-454.

Mroz, Z. & Pietruszczak, S. (1983). A constitutive model for sand with anisotropic hardening rule. *Int. J. Num. Anal. Meth. Geomech.* **7**, 305-320.

Muhlhaus, H.-B. & Vardoulakis, I. (1987). The thickness of shear bands in granular materials. *Géotechnique* **37**, No.3, 271-283.

Muhlhaus, H.-B. & Aifantis, E. C. (1992). A variational principle for gradient plasticity. *Int. J. Solids Struct.* **28**, No.7, 845-857.

Mulilis, J. P., Seed, H. B., Chan, C. K., Mitchell, J. K. & Arulanandan, K. (1977). Effect of sample preparation on sand liquefaction. *J. Soil Mech. Found. Div., ASCE* **103**, No.2, 91-108.

Nash, K. L. & Dixon, R. K. (1961). The measurement of pore pressure in sand under rapid triaxial tests. *Proc. Int. Conf. on the Pore Pressure and Suction in Soils, London*, 21-25.

Negussey, D. & Islam, M. S. (1994). Uniqueness of steady state and liquefaction potential. *Can. Geotech. J.* **31**, 132-139.

Nemat-Nasser, S. & Okada, N. (2001). Radiographic and microscopic observation of shear bands in granular materials. *Géotechnique* **51**, No.9, 753-765.

Nova, R. & Wood, D. M. (1979). A constitutive model for sand in triaxial compression. *Int. J. Num. Anal. Meth. Geomech.* **3**, 255-278.

National Research Council (1985). *Liquefaction of soils during earthquakes.* National Academies Press, Washington, D.C.

Oda, M., Koshikawa, I. & Higuchi, T. (1978). Experimental study of anisotropic shear strength of sand by plane strain test. *Soils Found.* **18**, No.1, 25-38.

Oka, F., Yashima, A., Sawada, K. & Aifantis, E. C. (2000). Instability of gradient-dependent elastoviscoplastic model for clay and strain localization analysis. *Comp. Meth. Appl. Mech. Engng* **183**, 67–86.

Olson, S. M., Stark, T. D., Walton, W. H., & Castro, G. (2000). Static Liquefaction Flow Failure of the North Dike of Wachusett Dam. *J. Geotech. Geoenviron. Engng, ASCE* **126**, No.12, 1184-1193.

Ortiz, M., Leroy, Y. & Needleman, A. (1987). A finite element method for localized failure analysis. *Comp. Meth. Appl. Mech. Engng* **61**, 189–214.

Ortiz, M. & Quigley, J. J. (1991). Properties of discontinuous bifurcation solutions in elasto-plasticity. *Comp. Meth. Appl. Mech. Engng* **90**, 781-804.

Pande, G. N. & Sharma, K. G. (1983). Multi-laminate model of clays – a numerical evaluation of the influence of rotation of the principal stress axes. *Int. J. Num. Anal. Meth. Geomech.* **7**, 397-418.

Papanastasiou, P. C. & Vardoulakis, I. G. (1992). Numerical treatment of progressive localization in relation to borehole stability. *Int. J. Num. Anal. Meth. Geomech.* **16**, 389-424.

Pearce, J. A (1971). A new true triaxial apparatus. *Proc. Roscoe Memorial Symposium: "Stress-strain behaviour of soils"*, Cambridge University, 330-339.

Peric, D., Runesson, K. & Sture, S. (1993). Prediction of plastic localization using MRS-Lade model. *J. Geotech. Engng, ASCE* **119**, No.4, 639-661.

Pestana, J. (1996). A unified description of soil behaviour. *Proc. 11th Conf. Eng. Mech., (eds. Lin & Su),* **2**, 281-284.

Peters, J. F., Lade, P. V. & Bro, A. (1988), Shear band formation in triaxial and plane strain tests. *Advanced Triaxial Testing of Soil and Rock, ASTM STP **977***, 604-627.

Pietruszczak, S. & Stolle, D. F. E. (1985). Deformation of strain softening materials. Part I: Objectivity of finite element solutions based on conventional strain softening formulations. *Comp. Geotech*. **1**, 99-115.

Pietruszczak, S. & Pande, G. N. (1987). Multilaminate framework of soil models – Plasticity formulation. *Int. J. Num. Anal. Meth. Geomech*. **11**, 651-658.

Pietruszczak, S. & Niu, X. (1992). Numerical evaluation of bearing capacity of a foundation in strain softening soil. *Comp. Geotech.* **13**, 187-198.

Poulos, S. J. (1981). The Steady State of Deformation. *J. Geotech. Engng Div., ASCE* **107**, No.5, 553-562.

Poulos, S. J., Castro, G. & France, J. W. (1985). Liquefaction evaluation procedure. *J. Geotech. Engng, ASCE* **111**, No.6, 772-791.

Poulos, S. J., Castro, G. & France, J. W. (1988). Liquefaction evaluation procedure: closure to discussion. *J. Geotech. Engng, ASCE* **114**, No.2, 251-259.

Pradel, D. & Lade, P. V. (1990). Instability and plastic flow of soils II: Analytical Investigation. *J. Engng Mech., ASCE* **116**, No.11, 2551-2566.

Prashant, A. & Penamadu, D. (2004). Effect of intermediate principal stress on overconsolidated Kaolin clay. *J. Geotech. Geoenviron. Engng, ASCE* **130**, No.3, 284-292.

Prevost, J.-H. & Hoeg, K. (1975). Soil mechanics and plasticity analysis of strain softening. *Géotechnique* **25**, No.2, 279-297.

Reades, D. W. & Green, G. E. (1976). Independent stress control and triaxial extension tests on sand. *Géotechnique* **26**, No.4, 551-576.

Rechenmacher, A. L. & Finno, R. J. (2004). Digital image correlation to evaluate shear banding in dilative sands. *Geotech. Testing J., ASTM* **27**, No.1, 1-10.

Regueiro, R. A. & Borja, R. I. (2001). Plane strain finite element analysis of pressure-sensitive plasticity with strong discontinuity. *Int. J. Solids Struct.* **38**, 3647–3672.

Rice, J. R. (1973). Plasticity and soil mechanics. *Proc. Symposium on the Role of Plasticity in Soil Mechanics,* Cambridge. England. pp. 263.

Riemer, M. F. & Seed, R. B. (1997). Factors affecting apparent position of steady-state line. *J. Geotech. Geoenviron. Engng, ASCE* **123**, No.3, 281-288.

Roscoe, K. H. & Schofield, A. N. (1963). Mechanical behaviour of an idealised 'wet' clay. *Proc. European Conf. Soil Mech. Found. Engng,* Wiesbaden, Germany, **1**, 47-54.

Roscoe, K. H., Schofield, A. N., & Thurairajah, A. (1963). An evaluation of test data for selecting a yield criterion for soils. *Laboratory Shear Testing of Soils, ASTM STP* ***301***, 111-128.

Roscoe, K. H. & Burland, J. B. (1968). On the generalized stress-strain behaviour of 'wet' clay. in *Engineering Plasticity (eds. Heyman & Leckie),* Cambridge University Press, 535-609.

Roscoe, K. H. (1970). The influence of strains in soil mechanics. *Géotechnique* **20**, No.2, 129-170.

Rowe, P. W. (1962). The stress dilatancy relationship for static equilibrium of an assembly of particles in contact. *Proc. Royal Society, **A269***, 500-527.

Rowe, P. W. & Barden, L. (1964). Importance of free ends in triaxial testing. *J. Soil Mech. Found. Div., ASCE* **90**, No.1, 1-15.

Rowe, P. W. (1969). The relation between the shear strength of sands in triaxial compression, plane strain, and direct shear. *Géotechnique* **19**, No.1, 75-86.

Rowe, P. W. (1971). Theoretical meaning and observed values of deformation parameters for soil. *Proc. Roscoe Memorial Symposium: "Stress-strain behaviour of soils"*, Cambridge University, 143-194.

Rudnicki, J. W. & Rice, J. R. (1975). Conditions for the localization of deformation in pressure-sensitive dilatant materials. *J. Mech. Phys. Solids* **23**, 371-394.

Saada, A.S. & Townsend, F.C. (1981). State of art: Laboratory strength testing of soils. *Laboratory shear strength of soil, ASTM STP **740***, 7-77.

Saada, A. S., Bianchini, G. F. & Liang, L. (1994). Cracks, bifurcation and shear bands propagation in saturated clays. *Géotechnique* **44**, No.1, 35-64.

Saada, A.S., Liang, L., Figueroa, J.L. & Cope, C.T. (1999). Bifurcation and shear propagation in sands. *Géotechnique* **39**, No.3, 367-385.

Sadrnejad, S. A. & Pande, G. N. (1989). A multilaminate model for sands. *Proc. NUMOG III (Numerical Models in Geomechanics),* Elsevier, Niagara Falls, 17-27.

Sarsby, R. W., Kalteziotis, N. & Haddad, E. H. (1980). Bedding error in triaxial tests on granular media. *Géotechnique* **30**, No.3, 302-309.

Sarsby, R. W., Kalteziotis, N. & Haddad, E. H. (1982). Comparison of "free-ends" during triaxial testing. *J. Geotech. Engng, ASCE* **108**, No.1, 83-107.

Sasitharan, S., Robertson, P. K., Sego, D. C. & Morgenstern, N. R. (1993). Collapse behaviour of sand. *Can. Geotech. J.* **30**, 569-577.

Sasitharan, S., Robertson, P. K., Sego, D. C. & Morgenstern, N. R. (1994). State-boundary surface for very loose sand and its practical implication. *Can. Geotech. J.* **31**, 321-334.

Sassa, K. (1989). Geotechnical classification of landslides. *Landslides News*, No.3, 21-24.

Sassa, K. (2000). Mechanisms of flows in granular soils. *Proc. GeoEng 2000: An Int. Conf. on Geotech. and Geol. Engng, Melbourne*, **1**, 1671-1702.

Schofield, A. N. & Wroth, C. P. (1968). *Critical State Soil Mechanics*. McGraw-Hill, London.

Seed, H. B. & Lundgren, R. (1954). Investigation of the effects of transient loading on the strength and deformation characteristics of saturated sands. *Proc. ASTM* **54**, 1288-1306.

Seed, H. B., Singh, S., Chan, C. K. & Vilela, T. F. (1982). Consideration in undisturbed sampling of sands. *J. Geotech. Engng, ASCE* **108**, No.2, 265-283.

Sento, N., Kazama, M., Uzuoka, R., Ohmura, H. & Ishimaru, M. (2004). Possibility of postliquefaction flow failure due to seepage. *J. Geotech. Geoenviron. Engng, ASCE* **130**, No.7, 707-716.

Shapiro, S. & Yamamuro, J. A. (2003). Effects of three-dimensional stress-strain behaviour of loose sand. *J. Geotech. Geoenviron. Engng, ASCE* **129**, No.1, 1-11.

Shibata, T. & Karube, D. (1965). Influence of the variation of the intermediate principal stress on the mechanical properties of normally consolidated clays. *Proc. 6th Int. Conf. Soil Mech. Found. Engng, Montreal*, **1**, 359-363.

Shibuya, S. & Hight, D. W. (1987). On the stress path in simple shear. *Géotechnique* **37**, No.4, 511-515.

Simo, J. C., Oliver, J. & Armero, F. (1993). An analysis of strong discontinuities induced by strain-softening in rate-independent inelastic solids. *Comp. Mech.* **12**, 277–296.

Sivathayalan, S. & Vaid, Y. P. (2002). Influence of generalized initial state and principal stress rotation on the undrained response of sands. *Can. Geotech. J.* **39**, 63-76.

Skempton, A. W. (1986). Standard penetration test procedures and effects in sand of overburden pressure, relative density, particle size, ageing, and overconsolidation. *Géotechnique* **36**, 425-447.

Sladen, J. A., D'Hollander, R.D., Krahn, J. & Mitchell, D. E. (1985a). Back analysis of the Nerlerk berm liquefaction slides. *Can. Geotech. J.* **22**, 579-588.

Sladen, J. A., D'Hollander, R.D. & Krahn, J. (1985b). The liquefaction of sands, a collapse surface approach. *Can. Geotech. J.* **22**, 564-578.

Sladen, J. A., & Handford, G. (1987). A potential systematic error in laboratory testing of very loose sands. *Can. Geotech. J.* **24**, 462-466.

Sluys, L. J. & De Borst, R. (1992). Wave propagation and localization in a rate-dependent cracked medium – model formulation and one-dimensional examples. *Int. J. Solids Struct.* **29**, 2945-2958.

Sture, S. & Desai, C. S. (1979). Fluid cushion truly triaxial or multiaxial testing device. *Geotech. Testing J., ASTM* **2**, No.1, 20-33.

Sun, H., Chen, J. F. & Ge, X. R. (2004). Deformation characteristics of silty clay subjected by triaxial loading, by computerised tomography. *Géotechnique* **54**, No.5, 307-314.

Sutherland, H. B. & Mesdary, M. S. (1969). The influence of the intermediate principal stress on the strength of sand. *Proc. 7th Int. Conf. Soil Mech. Found. Engng, Mexico,* **2**, 391-399.

Symes, M. J. P. R., Gens, A. & Hight, D. W. (1984). Undrained anisotropy and principal stress rotation in saturated sand. *Géotechnique* **34**, No.1, 11-27.

Tatsuoka, F. & Ishihara, K. (1974). Yielding of sand in triaxial compression. *Soils Found.* **14**, No.3, 51-65.

Tatsuoka, F., Sakamoto, M., Kawamura, T., & Fukushima, S. (1986). Strength and deformation characteristics of sand in plane strain compression at extremely low pressures. *Soils Found.* **26**, No.1, 65-84.

Tatsuoka, F., Nakamura, S., Huang, C.-C. & Tani, K. (1990). Strength anisotropy and shear band direction in plane strain tests of sand. *Soils Found.* **30**, No.1, 35-54.

Tatsuoka, F., Sato, T., Park, C.-S, Kim, Y.-S., Mukabi, J. N. & Kohata, Y. (1994). Measuring of elastic properties of geomaterials in laboratory compression tests. *Geotech. Testing J., ASTM* **17**, No. 1, 80-94.

Tejchman, J. & Wu, W. (1993). Numerical study of shear band patterning in a Cosserat continuum. *Acta Mech.* **99**, 61-74.

Tejchman, J. & Bauer, E. (1996). Numerical simulation of shear band formation with a polar hypoplastic model. *Comput. Geotech.* **19**, No.3, 221-244.

Tejchman, J. & Wu, W. (1996). Numerical simulation of shear band formation with a hypoplastic model. *Comput. Geotech.* **18**, No.1, 71-84.

Thomas, T. (1961). Plastic flow and fracture in solids. *Academic Press,* New York.

Topolnicki, M., Gudehus, G. & Mazurkiewicz, B. K. (1990). Observed stress-strain behaviour of remoulded saturated clay under plane-strain conditions. *Géotechnique* **42**, No.2, 155-187.

Torrey, V. H. III & Weaver, F. J. (1984). Flow failures in Mississippi riverbanks. *Proc. 3rd Int. Symposium on Landslides,* Toronto, **2**, 335-360.

Vaid, Y. P. & Negussey, D. (1984). A critical assessment of membrane penetration in triaxial test. *Geotech. Testing J., ASTM* **7**, No.2, 70-76.

Vaid, Y. P., Chung, E. K. F. & Kuerbis, R. H. (1990). Stress path and steady state. *Can. Geotech. J.* **27**, 1-7.

Vaid, Y. P. & Sivathayalan, S. (1996). Errors in estimates of void ratio of laboratory sand specimens. *Can. Geotech. J.* **33**, 1017-1020.

Vaid, Y. P. & Eliadorani, A. A. (1998). Instability and liquefaction of granular soils under undrained and partially drained states. *Can. Geotech. J.* **35**, 1053-1062.

Valanis, K. C. (1985). On the uniqueness of solution of the initial value problem in strain softening materials. *J. Appl. Mech., ASME* **52**, No.3, 649-653.

Vardoulakis, I. (1979). Bifurcation analysis of the triaxial test on sand samples. *Acta Mechanica* **32**, 35-54.

Vardoulakis, I. (1980). Shear band inclination and shear modulus of sand in biaxial test. *Int. J. Num. Anal. Meth. Geomech.* **4**, 103-119.

Vardoulakis, I. & Graf, B. (1982). Imperfection sensitivity of the biaxial test on dry sand. *Proc. IUTAM Conf. on Deformation and Failure of Granular Materials,* (*eds. Vermeer & Luger),* Delft, 485-491.

Vardoulakis, I. (1983). Rigid granular plasticity model and bifurcation in the triaxial test. *Acta Mechanica* **49**, 57-79.

Verdugo, R. & Ishihara, K. (1996). The steady state of sandy soils. *Soils Found.* **36**, No.2, 81-91.

Vermeer, P. A. (1982). A simple shear-band analysis using compliances. *Proc. IUTAM Conf. on Deformation and Failure of Granular Materials,* (*eds. Vermeer & Luger),* Delft, 493-499.

Vermeer, P. A. (1990). The orientation of shear bands in biaxial tests. *Géotechnique* **40**, No.2, 223-236.

Wang, Q. & Lade, P. V. (2001). Shear banding in true triaxial tests and its effect on failure in sand. *J. Engng Mech., ASCE* **127**, No.8, 754-761.

Whitman, R. V. & Healy, K. A. (1962). Shear strength of sands during rapid loadings. *J. Soil Mech. Found. Div., ASCE* **88**, No. 2, 99-132.

Whittle, A. J. (1993). Evaluation of a constitutive model for overconsolidated clays. *Géotechnique* **43**, No.2, 289-313.

Whittle, A. J. & Kavvadas, M. J. (1994). Formulation of MIT-E3 constitutive model for overconsolidated clays. *J. Geotech. Engng, ASCE* **120**, No.1, 173-198.

Wood, D. M. (1990). *Soil behaviour and critical state soil mechanics*. Cambridge University Press, New York.

Wu, W. & Kolymbas, D. (1990). Numerical testing of the stability criterion for hypoplastic constitutive equations. *Mech. Mater.* **9**, 245-253.

Wu, W. & Sikora, Z. (1991). Localized bifurcation in hypoplasticity. *Int. J. Eng. Sci.* **29**, 195-201.

Wu, W., Bauer, E. & Kolymbas, D. (1996). Hypoplastic constitutive model with critical state for granular materials. *Mech. Mater.* **23**, 45-69.

Wu, W. & Niemunis, A. (1996). Failure criterion, flow rule and dissipation function derived from hypoplasticity. *Mech. Cohesive-Frictional Mater.* **1**, 145-163.

Wu, W. & Niemunis, A. (1997). Beyond failure in granular materials. *Int. J. Numer. Anal. Meth. Geomech.* **21**, 153-174.

Wu, W. & Kolymbas, D. (2000). Hypoplasticity now and then. In *Constitutive Modelling of Granular Materials, (ed. Kolymbas)*, Springer, Berlin, 56-105.

Yamada, Y. & Ishihara, K. (1979). Anisotropic deformation characteristics of sand under three dimensional stress conditions, *Soils Found.* **19**, No.2, 79-91.

Yamamuro, J. A. & Lade, P. V. (1995). Strain localization in extension tests on granular materials. *J. Engng Mech., ASCE* **121**, No.7, 828-836.

Yamamuro, J. A. & Lade, P. V. (1996). Drained sand behavior in axisymmetric tests at high pressures. *J. Geotech. Engng, ASCE* **122**, No.2, 109-119.

Yamamuro, J. A. & Lade, P. V. (1997a). Instability of granular materials at high pressures. *Soils Found.* **37**, No.1, 41-52.

Yamamuro, J. A. & Lade, P. V. (1997b). Static liquefaction of very loose sands. *Can. Geotech. J.* **34**, 905-917.

Yamamuro, J. A. & Lade, P. V. (1998). Steady-state concepts and static liquefaction of silty sands. *J. Geotech. Geoenviron. Engng, ASCE* **124**, No.9, 868-877.

Yang, J. (2002). Non-uniqueness of flow liquefaction line for loose sand. *Géotechnique* **52**, No.10, 757-760.

Yasin, S. J. M., Umetsu, K., Tatsuoka, F., Arthur, J. R. F. & Dunstan, T. (1999). Plane-strain strength and deformation of sands affected by batch variations and different apparatus types. *Geotech. Testing J., ASTM* **22**, No.1, 80-100

Yoshida, T., Tatsuoka, F., Kamegai, Y., Siddiquee, M. S. A. & Park, C.-S. (1994). Shear banding in sands observed in plane strain compression. *Localization and Bifurcation Theory for Soils and Rocks (eds. Chambon, Desrues & Vardoulakis)*, Balkema, Rotterdam, 165-179.

Yoshimine, M., Ozay, R., Sezen, A. & Ansal, A. (1999). Undrained plane strain shear tests on saturated sand using Hollow Cylinder Torsional Shear Apparatus. *Soils Found.* **39**, No.2, 131-136.

Zdravkovic, L. (1996). *The stress-strain-strength anisotropy of a granular medium under general stress conditions.* PhD thesis, Imperial College, London, England.

Zdravkovic, L. & Jardine, R. J. (2000). Undrained anisotropy of K_0-consolidated silt. *Can. Geotech. J.* **37**, 178-200.

Zdravkovic, L. & Jardine, R. J. (2001). The effect on anisotropy of rotating the principal stress axes during consolidation. *Géotechnique* **51**, No.1, 69-83.

Zhang, H. & Garga, V. K. (1997). Quasi-steady state: a real behaviour? *Can. Geotech. J*. **34**, 749-761.

Zienkiewicz, O. C., Pastor, M. & Huang, M. (1995). Softening, localisation and adaptive remeshing. Capture of discontinuous solutions. *Comp. Mech.* **17**, 98–106.

APPENDICES

APPENDIX A

THE K_0 OF SAND UNDER PLANE-STRAIN CONDITIONS

A.1 Introduction

The coefficient of lateral pressure at rest, K_0, is one of the most important parameters for geotechnical design. The K_0 is normally defined as the principal stress ratio at a state under zero lateral strain condition and can be determined as

$$K_0 = \frac{\sigma'_{ho}}{\sigma'_{vo}} \qquad (A-1)$$

where σ'_{ho} – the horizontal effective stress in situ; σ'_{vo} – vertical effective stress in situ.

For normally consolidated soils, Jaky's equation (Jaky, 1944)

$$K_0 = 1 - \sin\varphi' \qquad (A-2)$$

where φ' is the effective friction angle of soil, can also be used to determine K_0 value.

The K_0 consolidation in this research was conducted by controlling $d\varepsilon_v/d\varepsilon_1 = 1$.. Therefore, the effective stress path or K_0 value was measured as a result of the strain path control. It has been shown by Chu & Gan (2004) that for very loose specimens prepared by the MT method, the effective stress path can be affected by

the void ratio of the specimen. For the medium loose to medium dense specimens prepared using the WS method, the influence of void ratio on the effective stress paths is small. However, these observations have been made under axisymmetric conditions. Therefore, further studies were conducted in this research to investigate whether the K_0 is affected by the void ratio of sand or the specimen preparation method under plane-strain conditions. The summary of testing conditions is given in Table A-1.

Table A-1 Summary of the K_0 tests conducted under plane-strain conditions.

Test No	Specimen preparation method	e_0	e_c	p_c' (kPa)	q_c (kPa)	$(q/p')_c$	σ_2' (kPa)	σ_3' (kPa)	K_0
K_0MT1	MT	0.765	0.750	200.2	232.7	1.16	87.5	86.0	0.25
K_0MT2		0.788	0.769	202.2	226.2	1.12	91.5	90.5	0.27
K_0MT3		0.813	0.795	199.4	219.6	1.10	99.8	97.0	0.29
K_0MT4		0.888	0.868	198.3	205.4	1.04	96.9	94.5	0.36
K_0MT5		0.910	0.884	198.8	190.8	0.96	108.7	111.0	0.39
K_0MT6		0.946	0.902	198.4	168.4	0.85	123.6	120.0	0.44
K_0MT7		0.978	0.915	198.0	157.2	0.79	137.0	135.0	0.48
K_0WS1	WS	0.676	0.665	200.6	230.0	1.15	105.7	106.0	0.36
K_0WS2		0.689	0.679	200.0	222.4	1.11	106.7	107.5	0.36
K_0WS3		0.707	0.694	202.9	218.1	1.07	121.7	122.0	0.35
K_0WS4		0.768	0.756	202.9	203.5	1.00	129.0	130.0	0.39
K_0WS5		0.802	0.784	200.4	190.1	0.95	120.1	120.5	0.37

It was described in Chapter 3 that the PSA used in this study allows direct measurement of lateral pressure, σ_2. As a result, in shearing stage of all the plane-strain tests $\sigma_2' \neq \sigma_3'$. However, it was observed that during K_0 consolidation under plane-strain conditions σ_2' was almost identical with σ_3'. Therefore, in terms of K_0 value there is no difference whether σ_2' or σ_3' is used. The examples of σ_2' versus ε_1 and σ_3' versus ε_1 curves obtained during K_0 consolidation are presented in Fig. A.1.

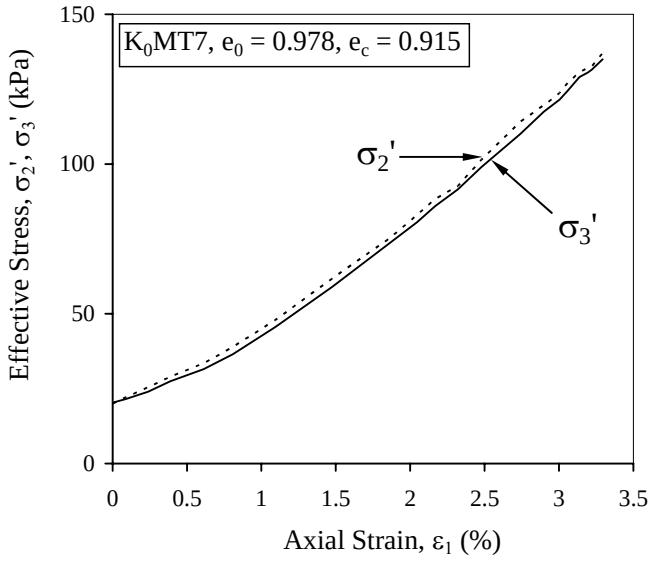

(a)

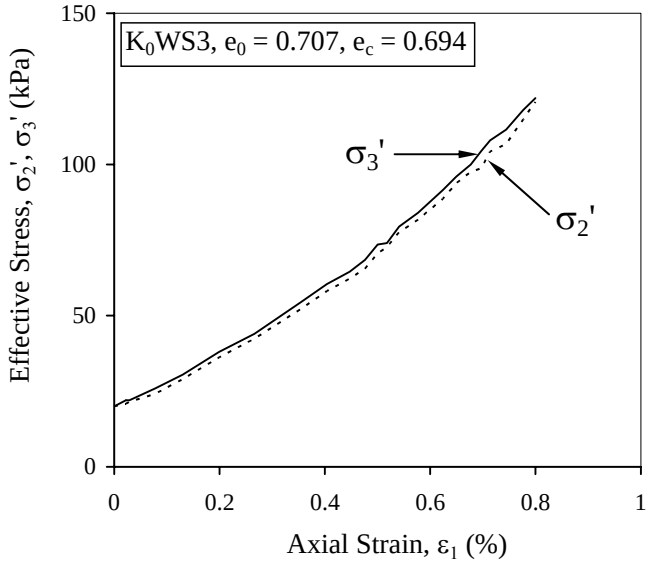

(b)

Fig. A.1 The lateral stress response obtained from K_0 consolidation tests under plane-strain conditions: (a) the MT method; (b) the WS method

A.2 The Moist Tamping Method

The results of seven K_0 consolidation tests obtained from very loose to medium loose specimens are presented in Fig. A.2. All the specimens were prepared using the MT method. The initial void ratios, e_0, of the specimens were in the range between 0.978 and 0.765. As shown in Fig. A.2(a), the effective K_0 paths obtained

from the seven tests are affected by the variation of void ratio. The looser the soil, the lower the effective stress path.

The variation of K_0 with the axial strain in the seven tests is plotted in Fig. A.2(b). As the tests started from the isotropic stress states, there was an initial transition from the isotropic state to K_0 state. After the initial period K_0 decreased slowly and reached more or less constant value at the end of consolidation. It can be observed that the looser the specimen, the larger axial strain developed during K_0 consolidation. Moreover, the higher the void ratio, the higher the K_0 value.

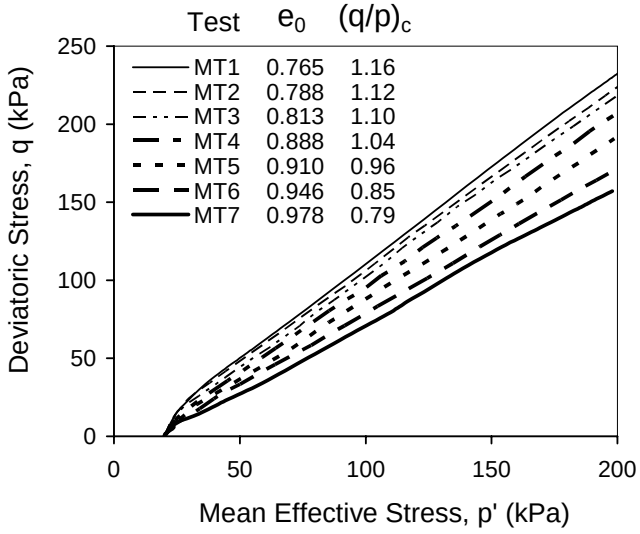

(a)

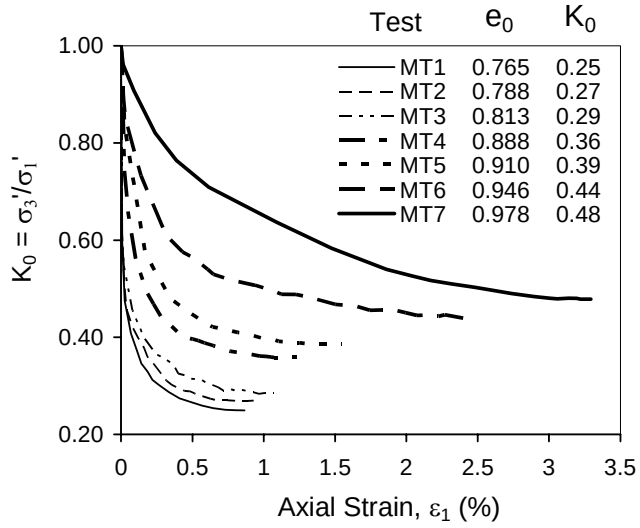

(b)

Fig. A.2 Results of K_0 consolidation tests for specimens prepared using the MT method: (a) effective stress paths; (b) K_0 versus axial strain curves

A.3 The Water Sedimentation Method

Typical results of five K_0 consolidation tests obtained from medium loose to medium dense specimens prepared using the WS method are given in Fig. A.3. The initial void ratios of the specimens varied from 0.802 to 0.676. The effective stress paths are plotted in Fig. A.3(a) and the variation of K_0 with axial strain is presented in Fig. A.3(b). It can be seen from Fig. A.3(a) that the effective stress paths are affected by the void ratio. The larger the initial void ratio, the lower the effective stress path. However, the data presented in Fig. A.3(b) indicate that within the range of void ratio, K_0 values do not vary much.

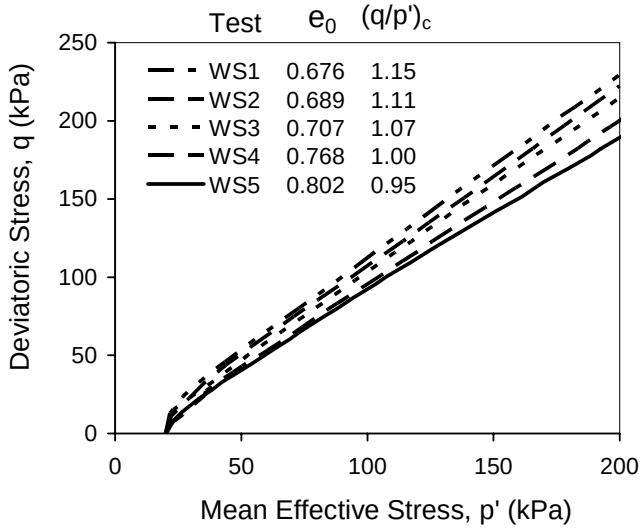

(a)

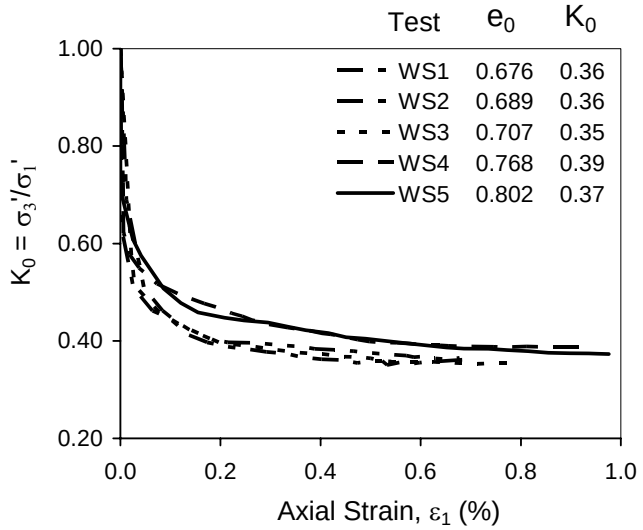

(b)

Fig. A.3 Results of K_0 consolidation tests for specimens prepared using the WS method: (a) effective stress paths; (b) K_0 versus axial strain curves

A.4 Discussion

The relationship between K_0 and the initial void ratio of specimens under plane-strain conditions is presented in Fig. A.4. The data obtained from triaxial tests by Chu & Gan (2004) is also plotted in Fig. A.4. The K_0 value was calculated at the end of each test. It can be seen from Fig. A.4 that for specimens prepared by the MT method a linear relationship between K_0 and e_0 can be fitted:

$$K_0 = 1.432\ e_0 - 0.885 \text{ (for } 0.765 < e_0 < 0.978) \qquad \text{(A – 3)}$$

However, for the specimens prepared using by the WS method, K_0 does not seem to be related to the initial void ratio. The K_0 values obtained from these specimens with e_0 between 0.676 and 0.802 are in the range 0.35–0.39. It can also be observed from Fig. A.4 that given the same e_0, the K_0 values obtained from the WS specimens are higher than those obtained from the MT specimens. The differences in the K_0 values may indicate that the WS method produces a less structured soil specimen than the MT method, as discussed by Chu & Gan (2004). It can be seen from Fig. A.4 that K_0 values obtained from plane-strain and triaxial tests are in good agreement. Therefore, the type of testing apparatus does not affect the K_0 measurement for the tested soil if the proper boundary conditions are imposed in the tests.

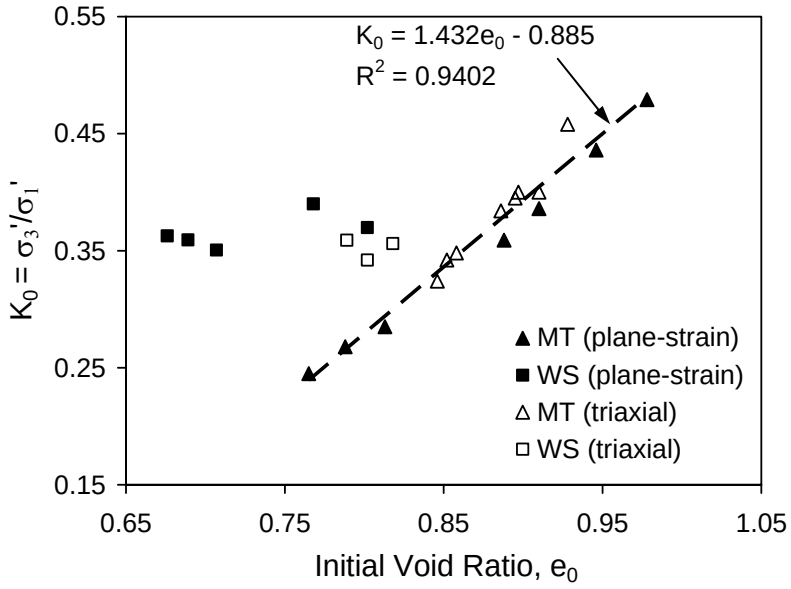

Fig. A.4 Plot of K_0 versus initial void ratio

APPENDIX B

THE CLASSIFICATION OF RELATIVE DENSITY

Table B-1 The classification of relative density (after Skempton, 1986)

D_r (%)	Classification
≤ 15	Very loose
15 – 35	Loose
35 – 50	Medium loose
50 – 65	Medium dense
65 – 85	Dense
85 – 100	Very dense

APPENDIX C

DEVELOPMENT OF SHEAR BANDS

Test CK_0D03 (e_c = 0.699; p_c' = 299 kPa)

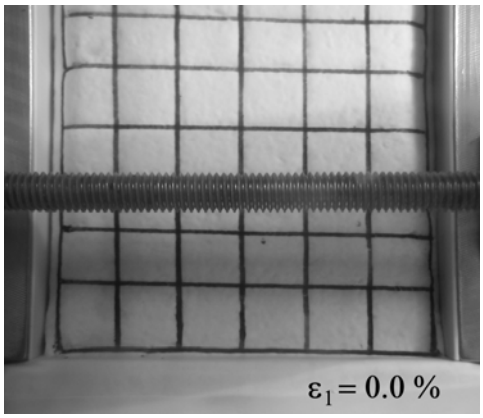

Fig. C.1(a) CK_0D03 (point 0)

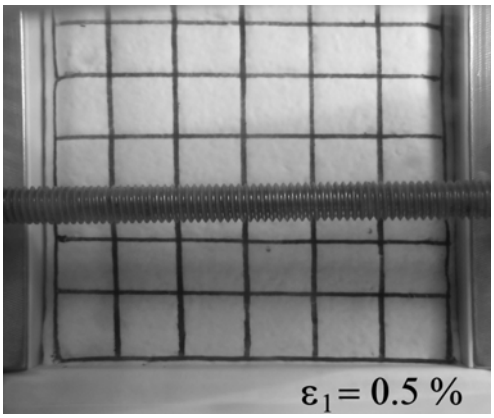

Fig. C.1(b) CK_0D03 (point 1)

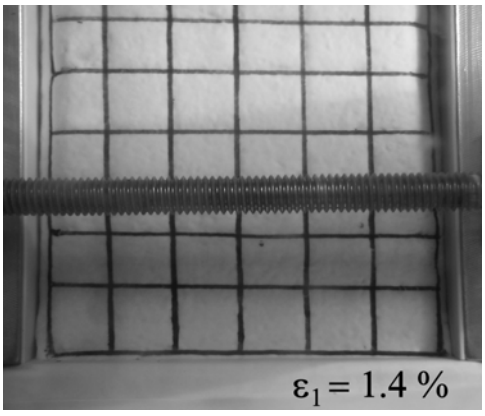

Fig. C.1(c) CK_0D03 (point 2)

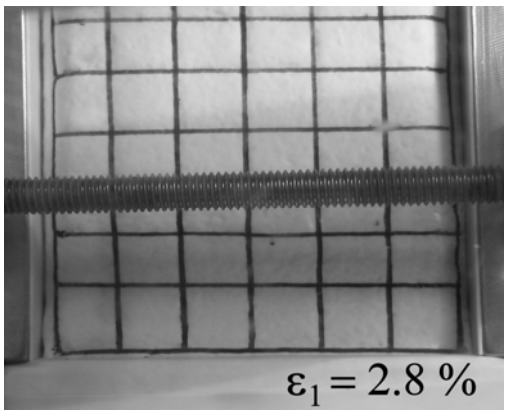

Fig. C.1(d) CK_0D03 (point 3)

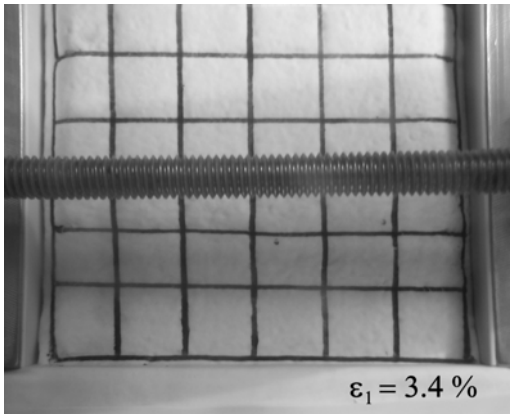

Fig. C.1(e) CK_0D03 (point 4 (O))

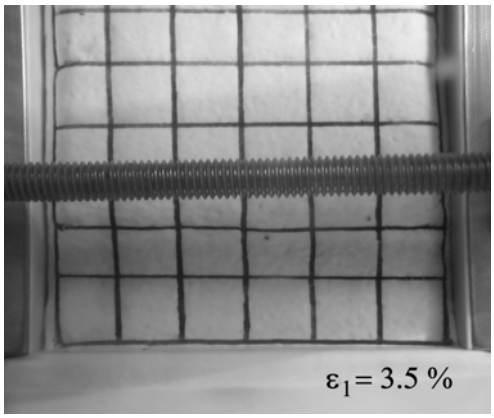

Fig. C.1(f) CK_0D03 (point 5 (B))

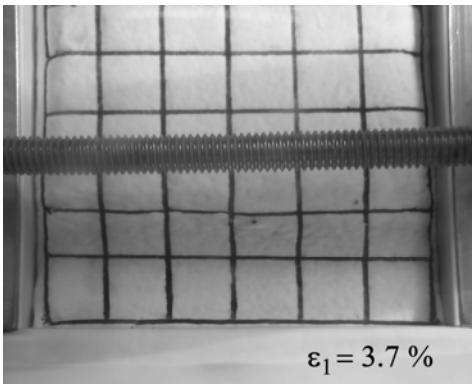

Fig. C.1(g) CK_0D03 (point 6 (F))

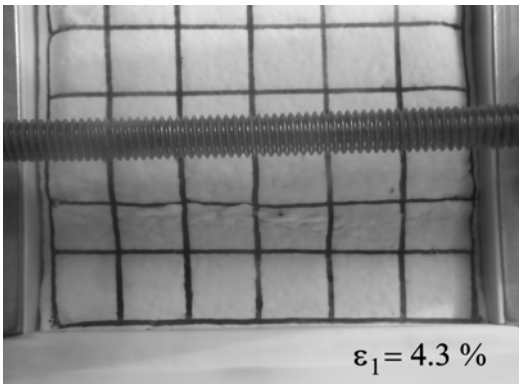

Fig. C.1(h) CK_0D03 (point 7)

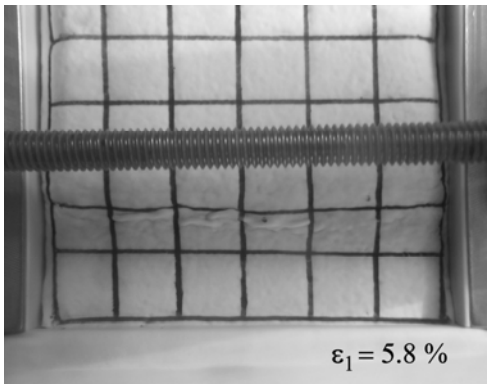

Fig. C.1(i) CK_0D03 (point 8)

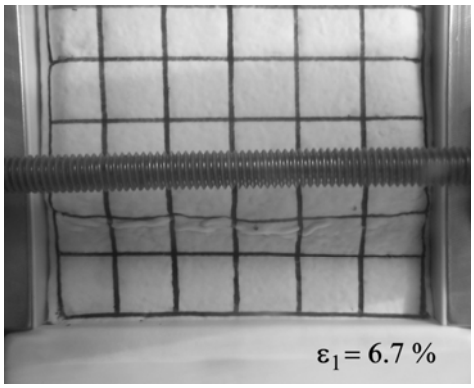

Fig. C.1(j) CK_0D03 (point 9)

Fig. C.1(k) CK_0D03 (point 10:σ_3 surface)

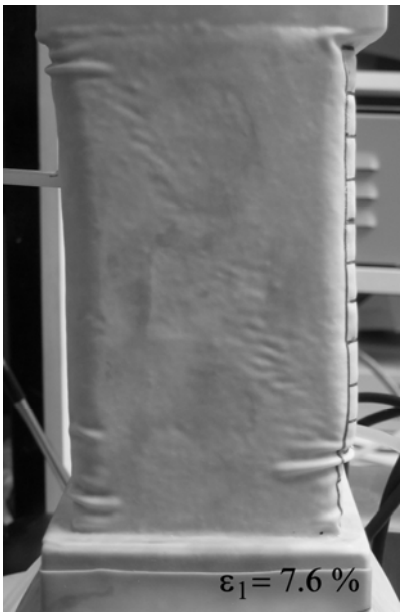

Fig. C.1(l) CK_0D03 (point 10: σ_2 surface)

Test CK_0D08 (e_c = 0.914; p_c' = 202 kPa)

Fig. C.2(a) Test CK_0D08 (point 0)

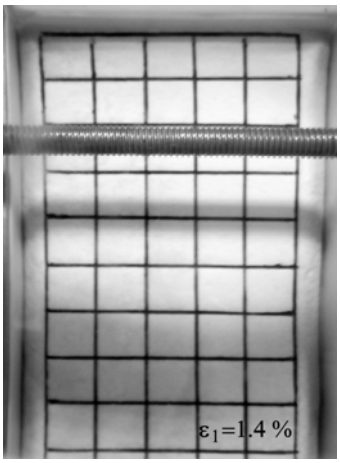

Fig. C.2(b) Test CK_0D08 (point 1)

Fig. C.2(c) Test CK_0D08 (point 2)

Fig. C.2(d) Test CK_0D08 (point 3)

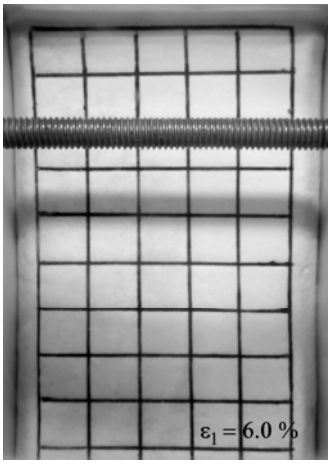

Fig. C.2(e) Test CK_0D08 (point 4)

Fig. C.2(f) Test CK_0D08 (point 5)

Fig. C.2(g) Test CK_0D08 (point 6)

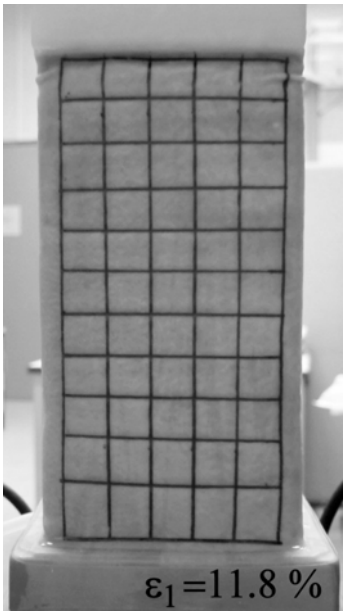

Fig. C.2(h) CK_0D08 (point 7(F): σ_3 surface)

Fig. C.2(i) CK_0D08 (point 7(F): σ_3 surface)

Test CK_0U02 (e_c = 0.695; p_c' = 202 kPa)

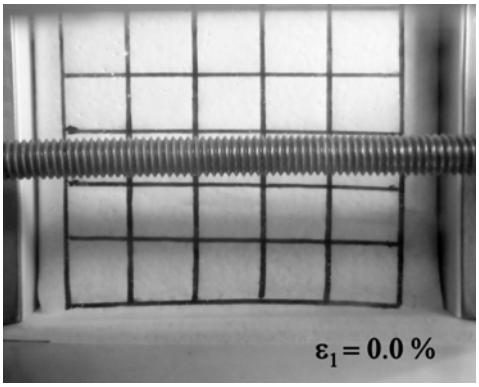

Fig. C.3(a) CK_0U02 (point 0)

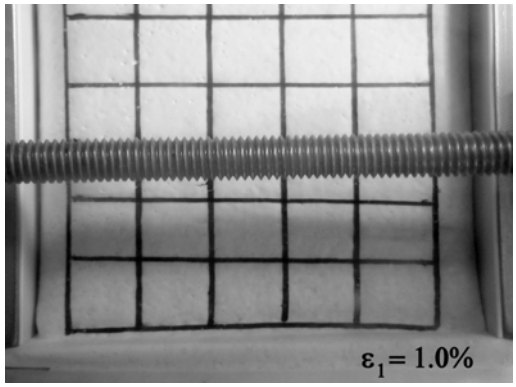

Fig. C.3(b) CK_0U02 (point 1)

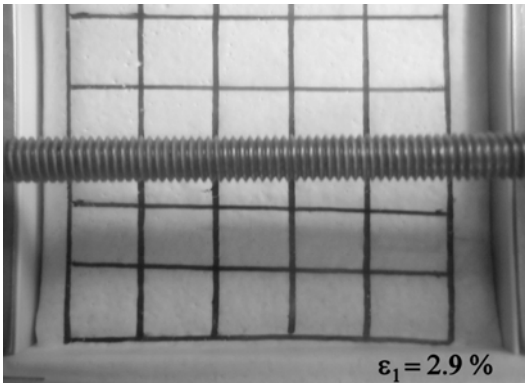

Fig. C.3(c) CK_0U02 (point 2)

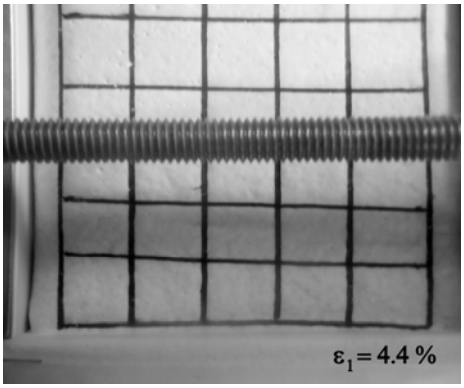

Fig. C.3(d) CK_0U02 (point 3(O))

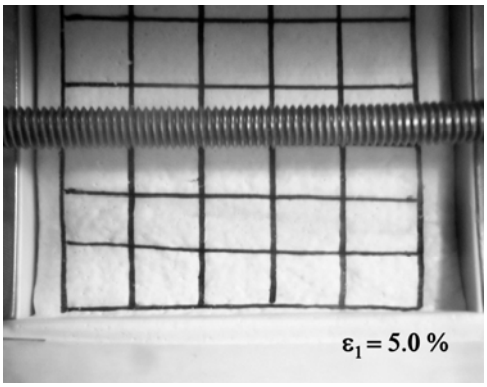

Fig. C.3(e) CK_0U02 (point 4)

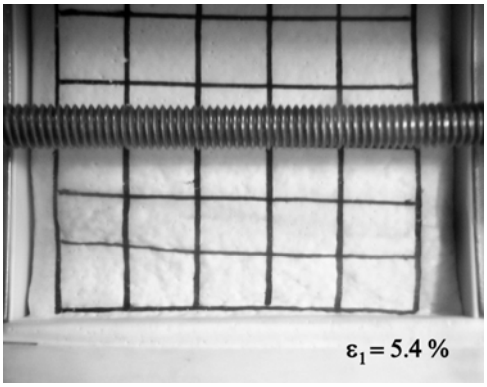

Fig. C.3(f) CK_0U02 (point 5 (P,B))

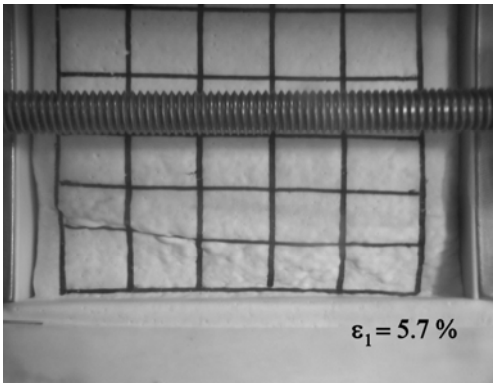

Fig. C.3(g) CK_0U02 (point 6)

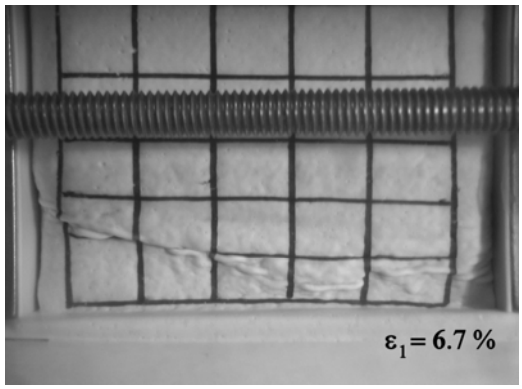

Fig. C.3(h) CK_0U02 (point 7)

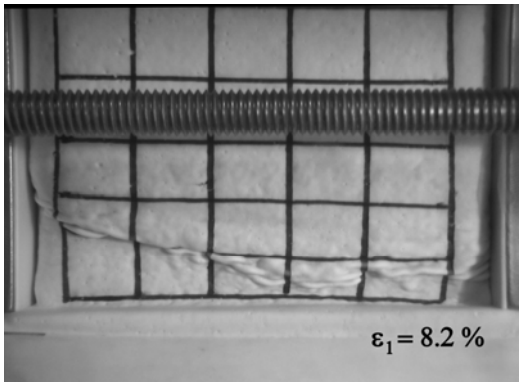

Fig. C.3(i) CK_0U02 (point 8)

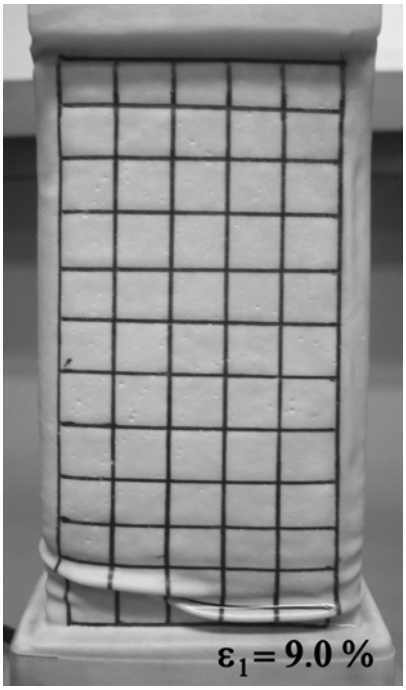

Fig. C.3(j) CK_0U02 (point 9: σ_3 surface)

Fig. C.3(k) CK_0U02 (point 9: σ_2 surface)

Test CK_0U05 (e_c = 0.915; p_c' = 198 kPa)

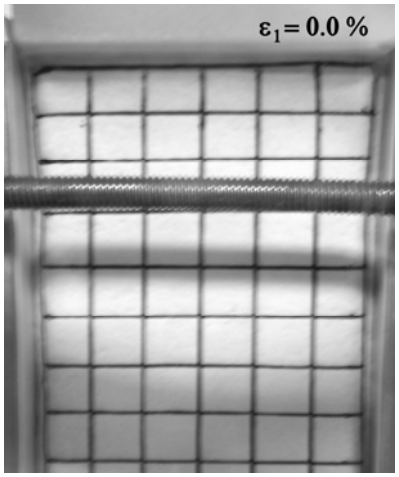

Fig. C.4(a) CK_0U05 (point 0)

Fig. C.4(b) CK_0U05 (point 1(P))

Fig. C.4(c) CK_0U05 (point 2)

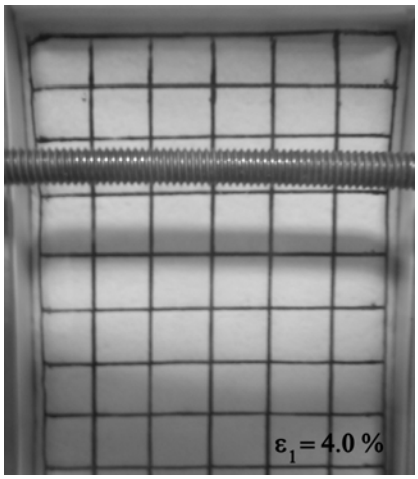

Fig. C.4(d) CK_0U05 (point 3)

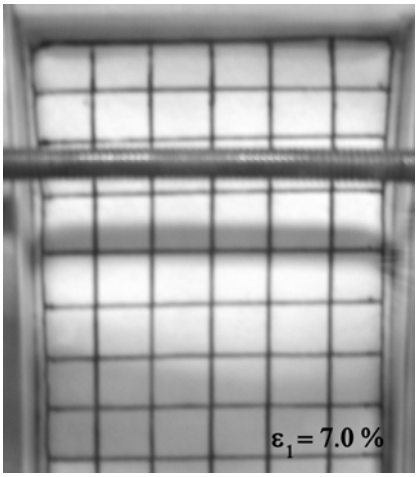

Fig. C.4(e) CK_0U05 (point 4)

Fig. C.4(f) CK_0U05 (point 5)

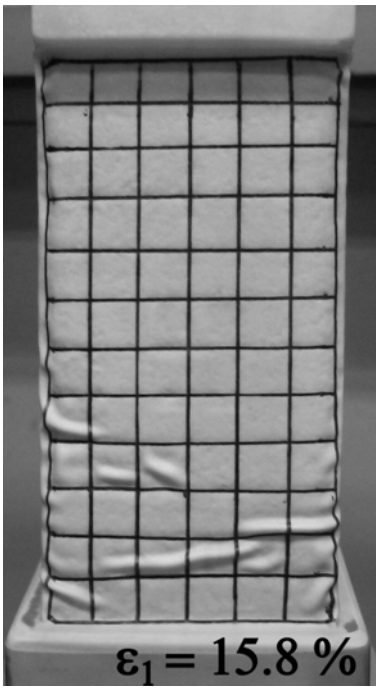

Fig. C.4(g) CK_0U05 (point 6: σ_3 surface)

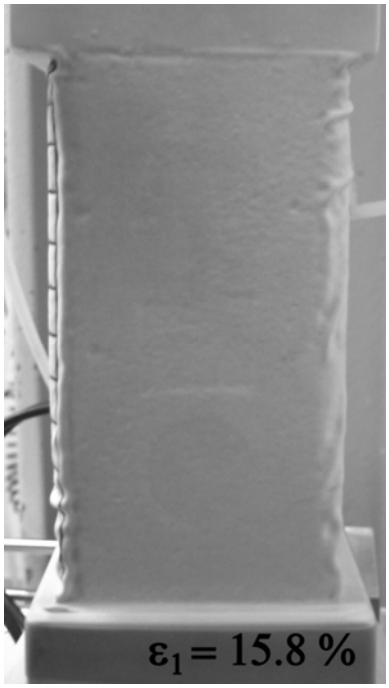

Fig. C.4(h) CK_0U05 (point 6: σ_2 surface)

Test CK_0U12 (e_c = 0.868; p_c' = 198 kPa)

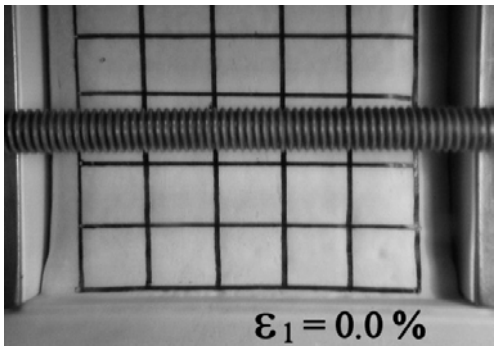

Fig. C.5(a) CK_0U12 (point 0)

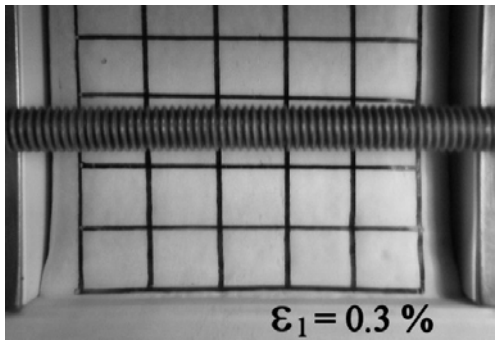

Fig. C.5(b) CK_0U12 (point 1)

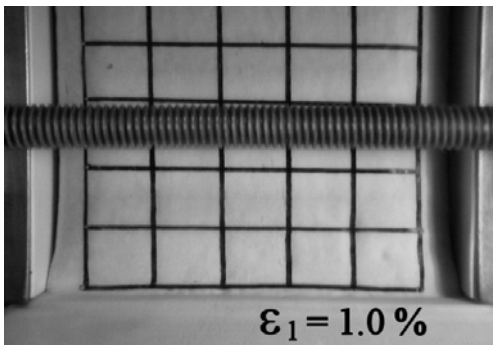

Fig. C.5(c) CK_0U12 (point 2(O))

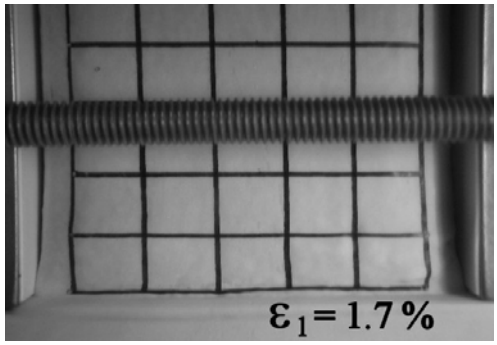

Fig. C.5(d) CK_0U12 (point 3(B))

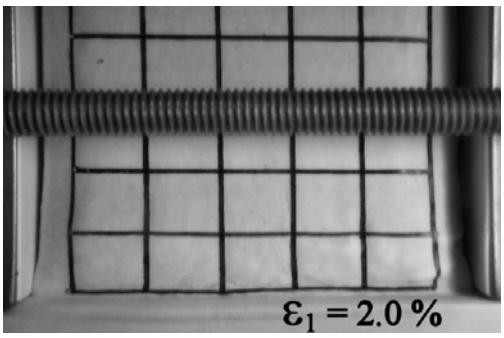

Fig. C.5(e) CK_0U12 (point 4(P))

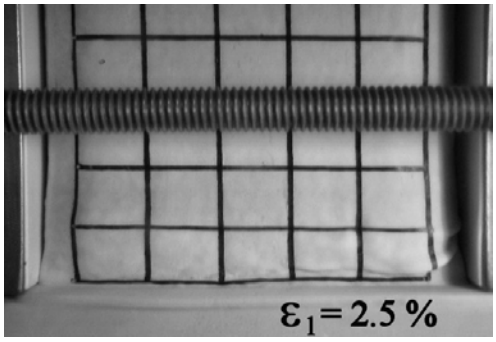

Fig. C.5(f) CK_0U12 (point 5)

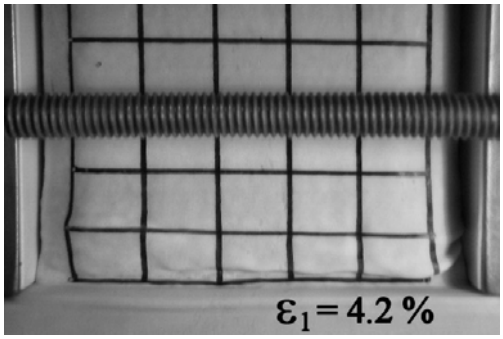

Fig. C.5(g) CK_0U12 (point 6)

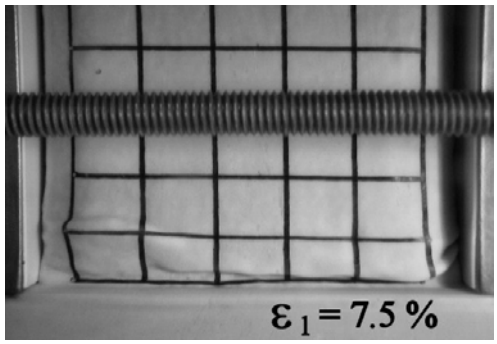

Fig. C.5(h) CK_0U12 (point 7)

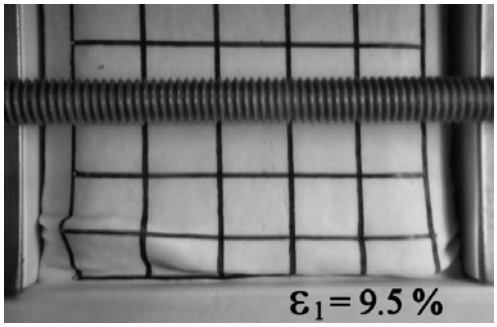

Fig. C.5(i) CK_0U12 (point 8)

Test SP05 (e_c = 0.677; p_c' = 198 kPa)

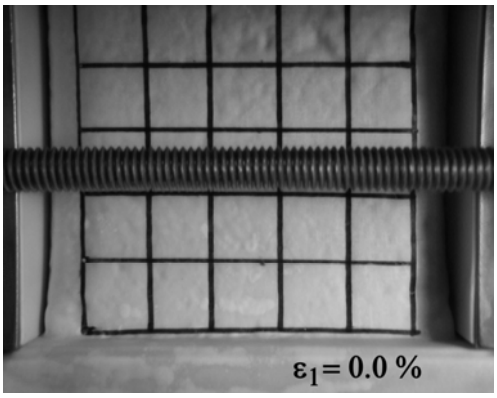

Fig. C.6(a) SP05 (point 0)

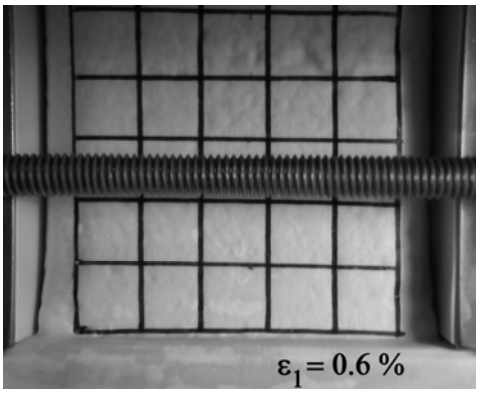

Fig. C.6(b) SP05 (point 1)

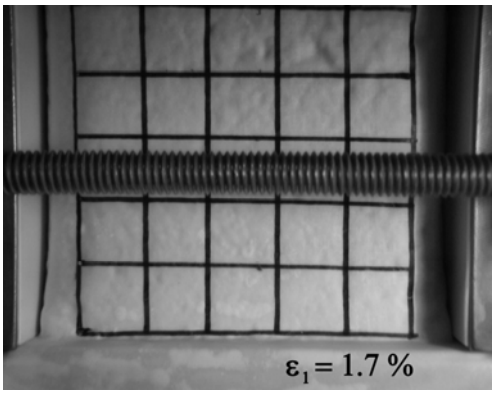

Fig. C.6(c) SP05 (point 2)

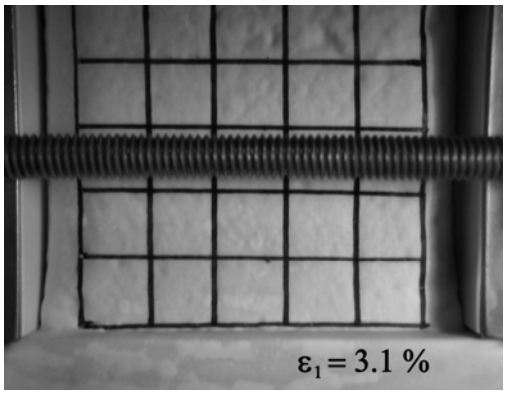

Fig. C.6(d) SP05 (point 3)

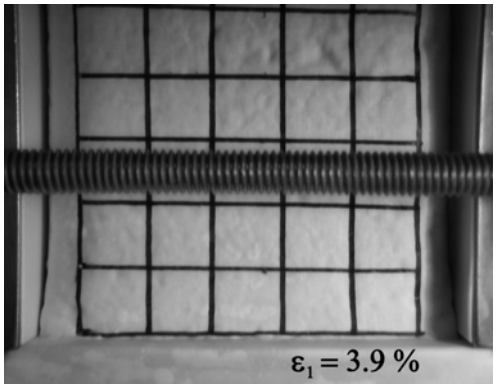

Fig. C.6(e) SP05 (point 4 (O))

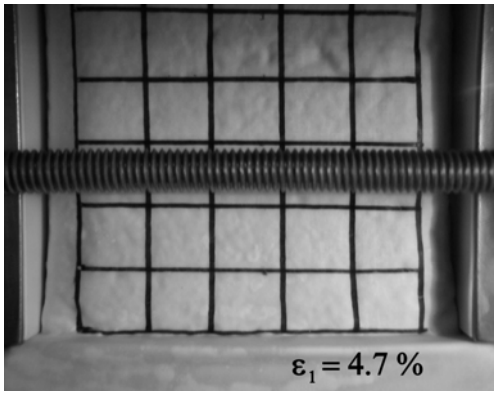

Fig. C.6(f) SP05 (point 5 (P,B))

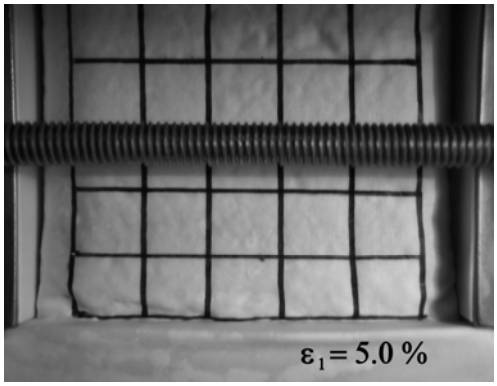

Fig. C.6(g) SP05 (point 6)

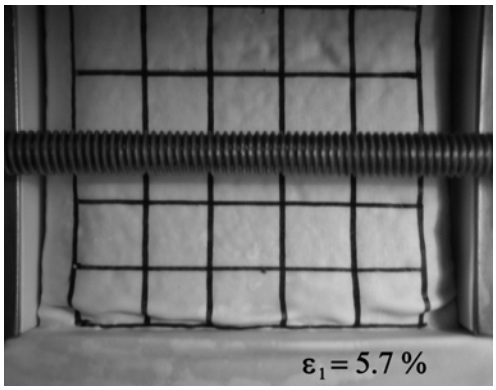

Fig. C.6(h) SP05 (point 7)

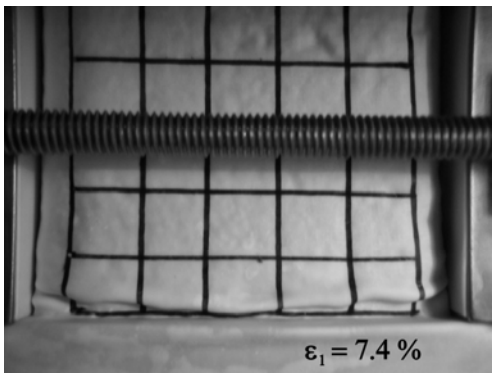

Fig. C.6(i) SP05 (point 8)

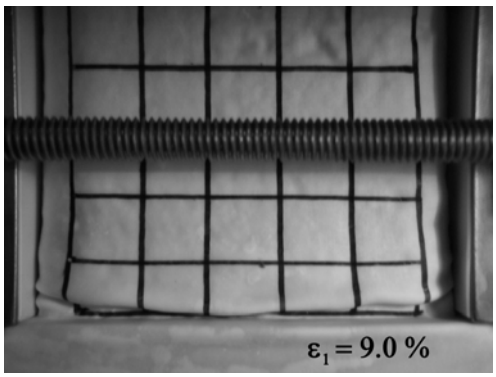

Fig. C.6(j) SP05 (point 9)

Test SP26 (e_c = 0.731; p_c' = 405 kPa)

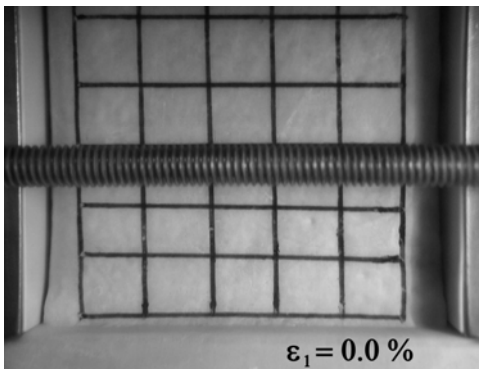

Fig. C.7(a) SP26 (point 0)

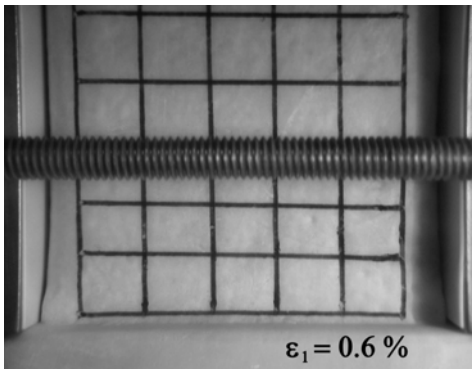

Fig. C.7(b) SP26 (point 1)

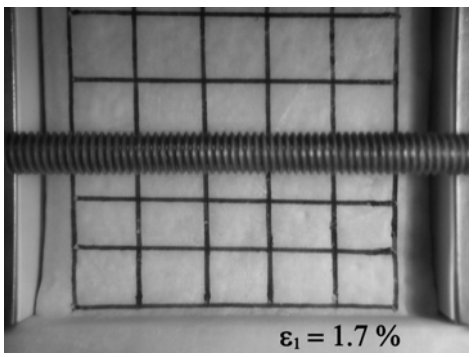

Fig. C.7(c) SP26 (point 2)

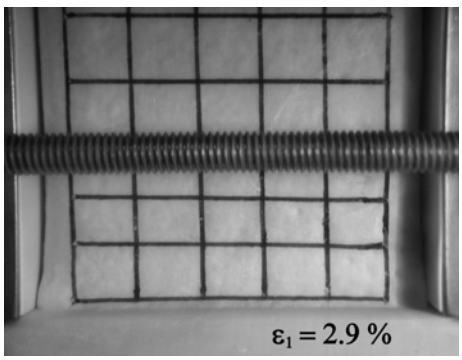

Fig. C.7(d) SP26 (point 3(O))

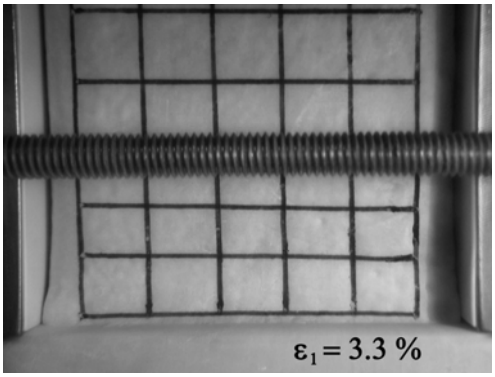

Fig. C.7(e) SP26 (point 4(P))

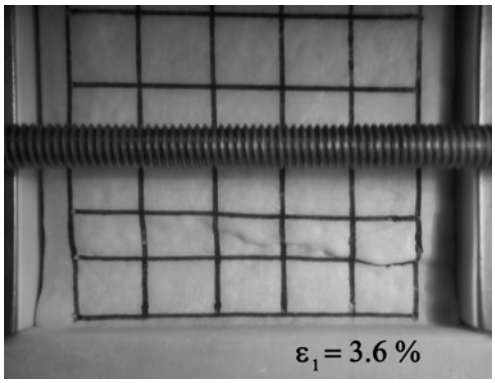

Fig. C.7(f) SP26 (point 5(B))

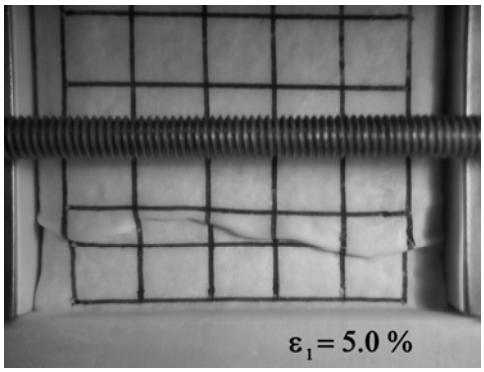

Fig. C.7(g) SP26 (point 6)

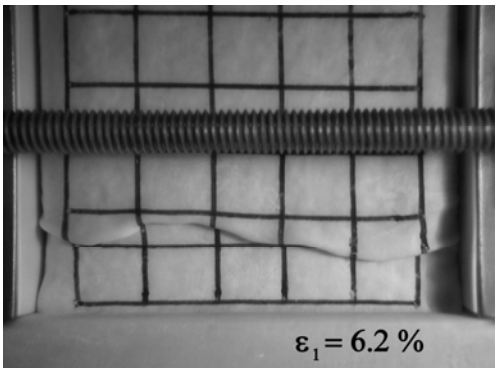

Fig. C.7(h) SP26 (point 7)

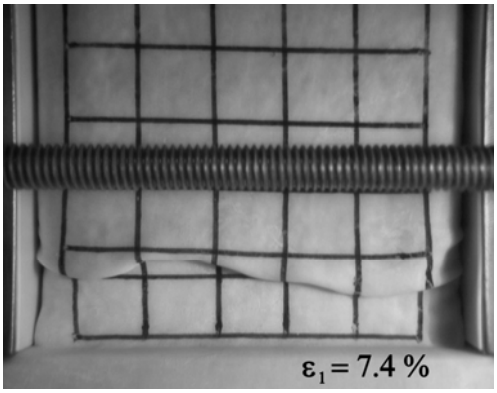

Fig. C.7(i) SP26 (point 8)

Test SP28 (e_c = 0.750; p_c' = 880 kPa)

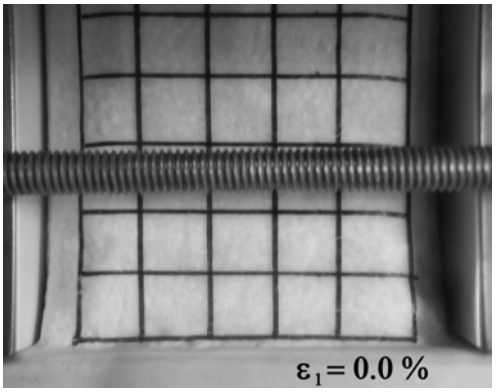

Fig. C.8(a) SP28 (point 0)

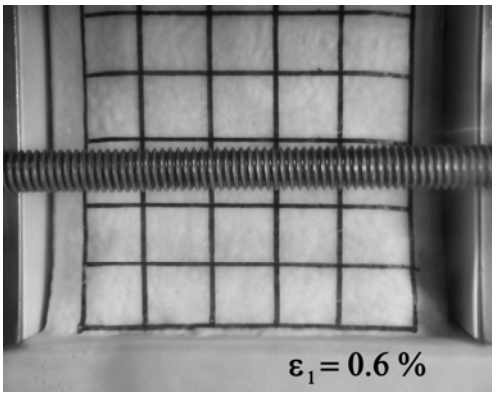

Fig. C.8(b) SP28 (point 1(P))

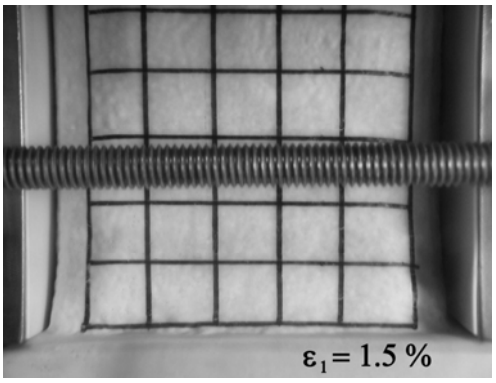

Fig. C.8(c) SP28 (point 2)

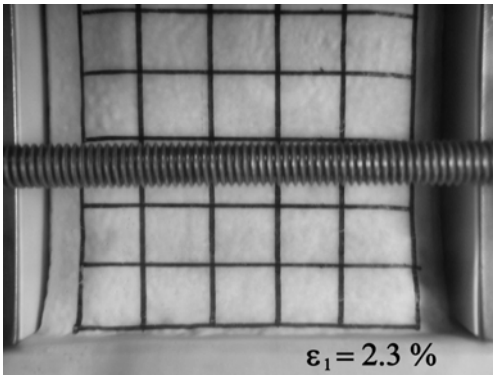

Fig. C.8(d) SP28 (point 3(O))

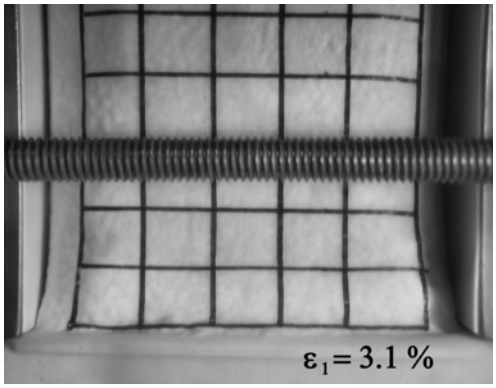

Fig. C.8(e) SP28 (point 4(B))

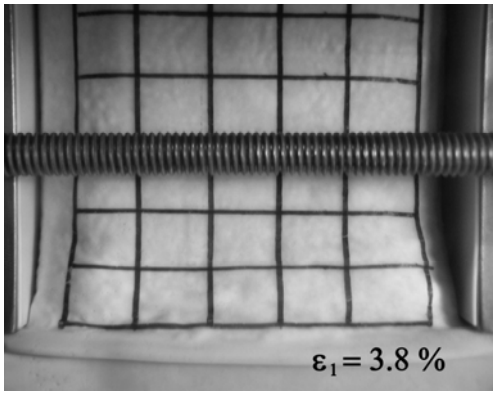

Fig. C.8(f) SP28 (point 5)

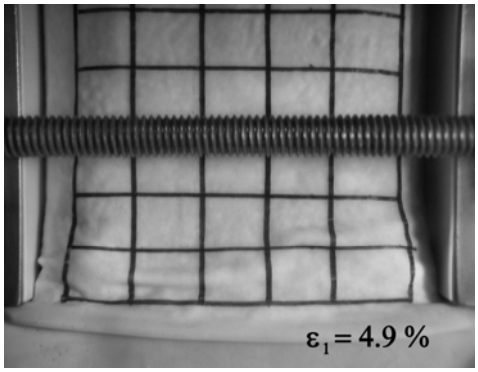

Fig. C.8(g) SP28 (point 6)

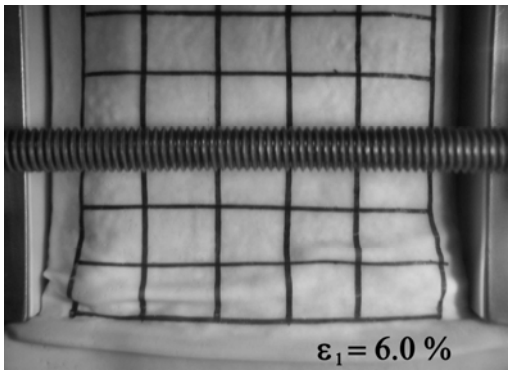

Fig. C.8(h) SP28 (point 7)

Test IND03 (e_c = 0.679; p_c' = 206 kPa)

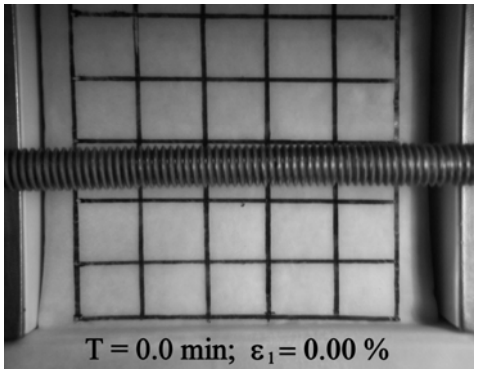

Fig. C.9(a) IND03 (point 0)

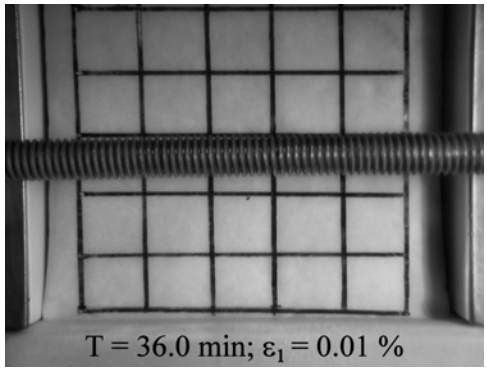

Fig. C.9(b) IND03 (point 1)

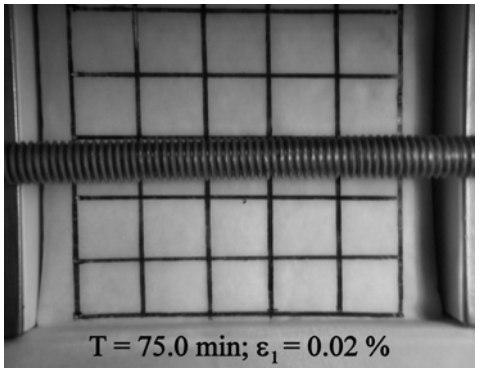

Fig. C.9(c) IND03 (point 2)

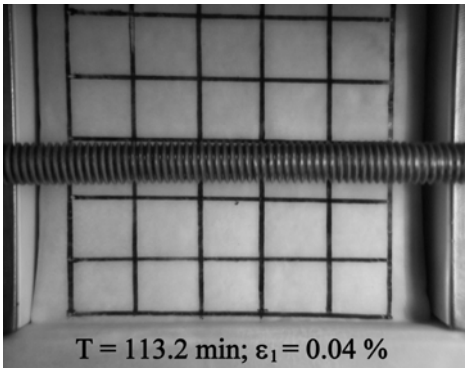

Fig. C.9(d) IND03 (point 3)

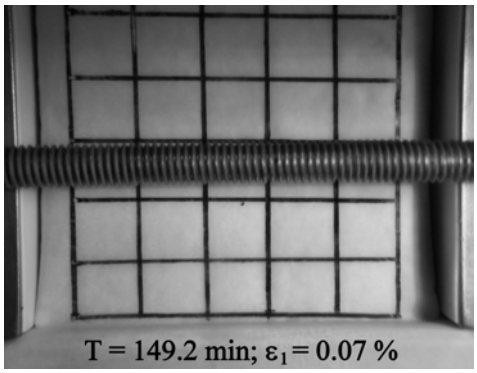

Fig. C.9(e) IND03 (point 4)

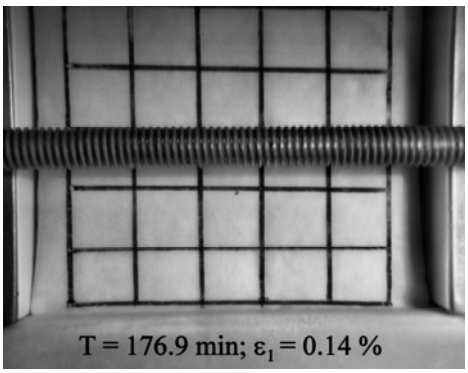

Fig. C.8(f) IND03 (point 5(O))

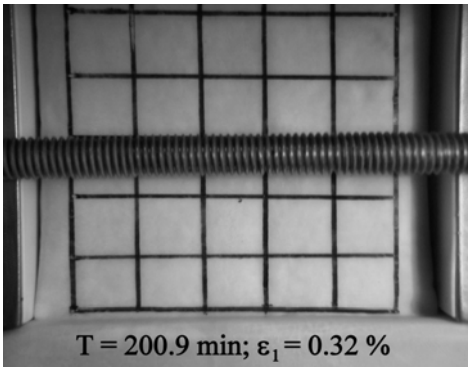

Fig. C.9(g) IND03 (point 6)

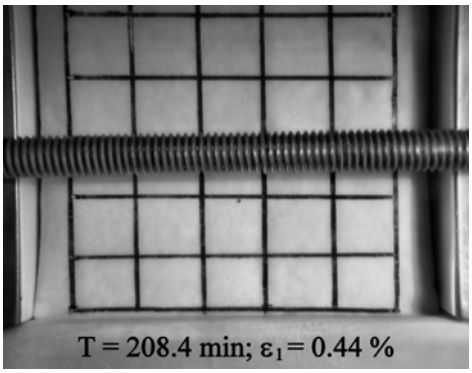

Fig. C.9(h) IND03 (point 7(I))

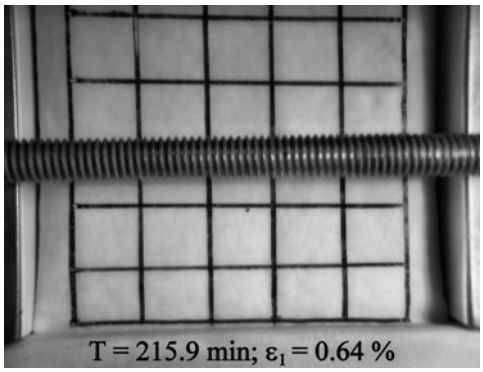

Fig. C.9(i) IND03 (point 8)

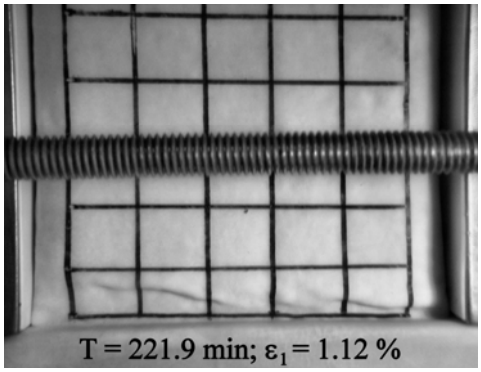

Fig. C.8(j) IND03 (point 9(B))

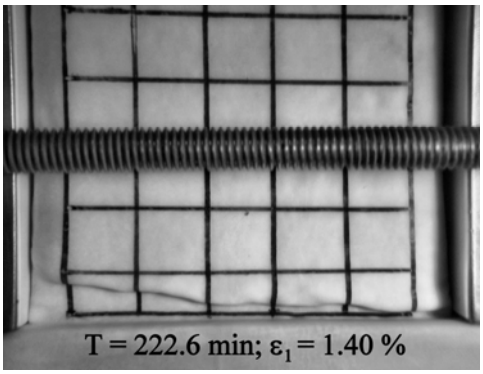

Fig. C.9(k) IND03 (point 10)

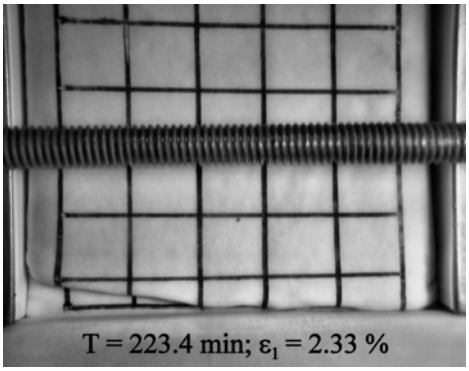

Fig. C.9(l) IND03 (point 11)

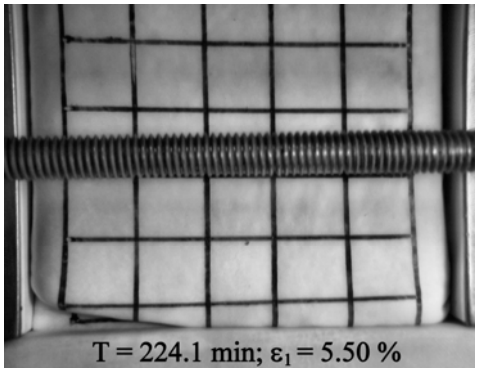

Fig. C.9(m) IND03 (point 12)

Test INSP06 (e_c = 0.685; p_c' = 201 kPa)

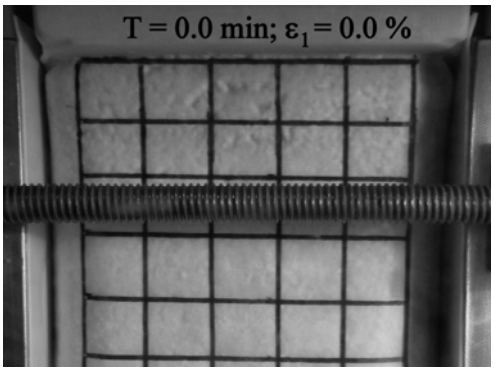

Fig. C.10(a) INSP06 (point 0)

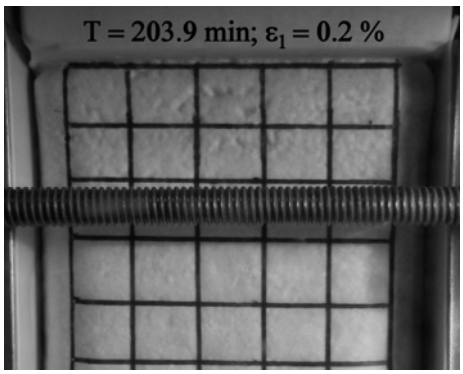

Fig. C.10(b) INSP06 (point 1)

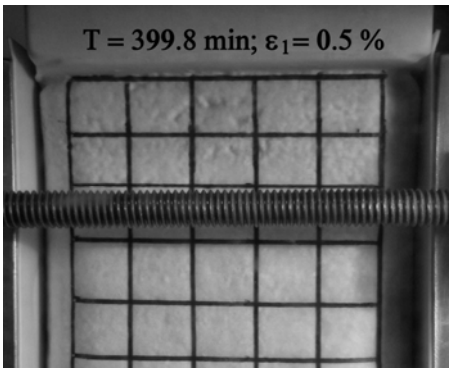

Fig. C.10(c) INSP06 (point 2)

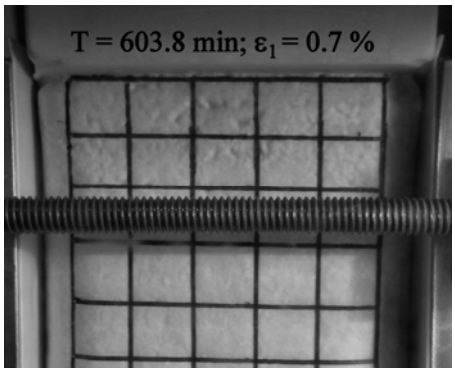

Fig. C.10(d) INSP06 (point 3)

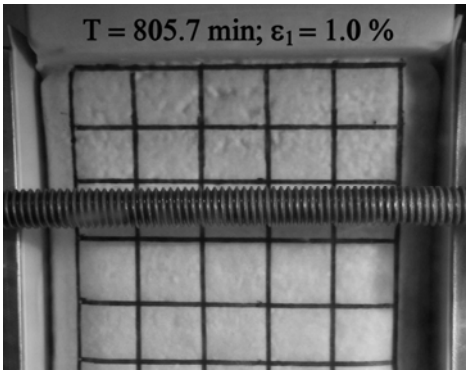

Fig. C.10(e) INSP06 (point 4)

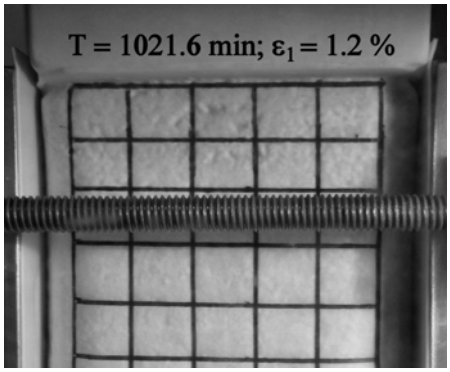

Fig. C.10(f) INSP06 (point 5)

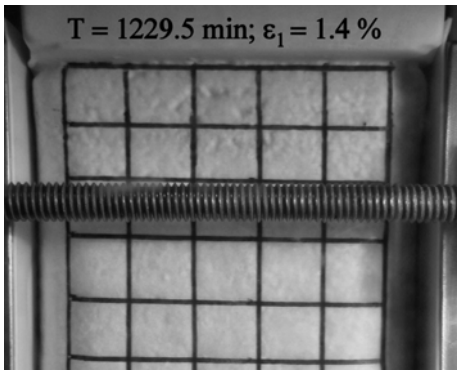

Fig. C.10(g) INSP06 (point 6)

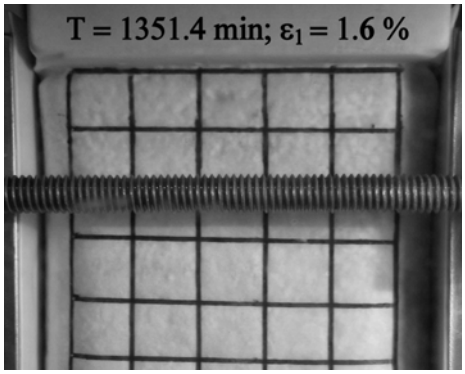

Fig. C.10(h) INSP06 (point 7(O))

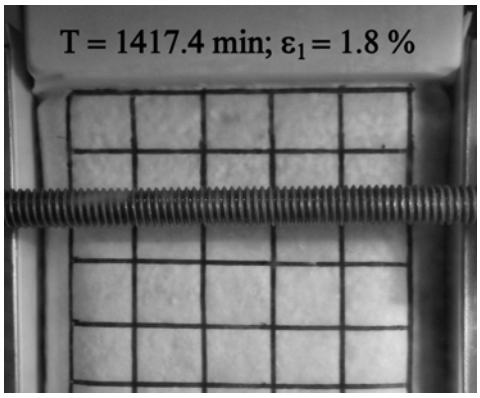

Fig. C.10(i) INSP06 (point 8)

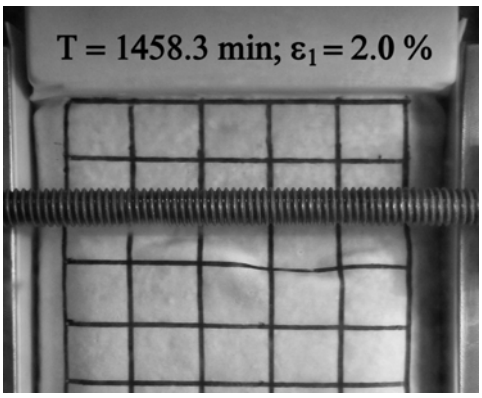

Fig. C.10(j) INSP06 (point 9(B))

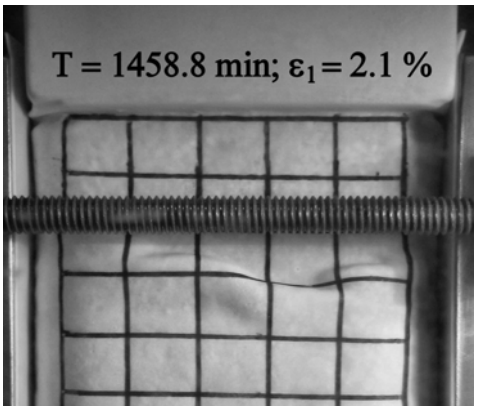

Fig. C.10(k) INSP06 (point 10(F))

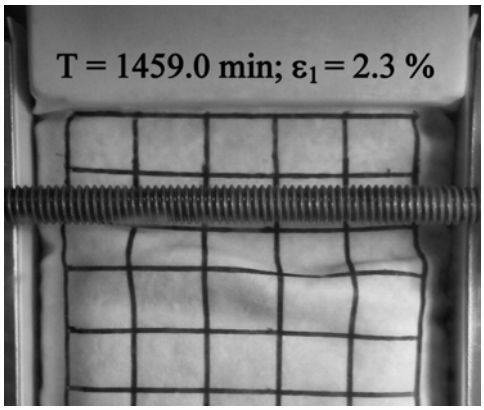

Fig. C.10(l) INSP06 (point 11)

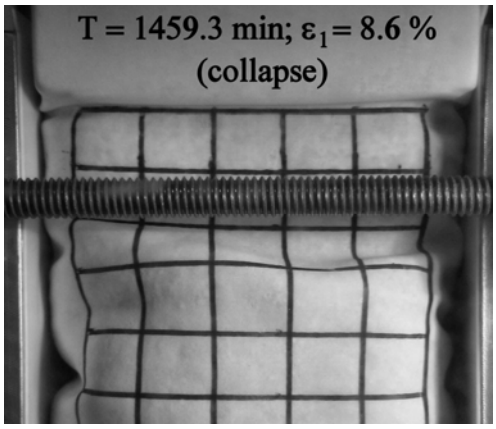

Fig. C.10(m) INSP06 (point 12)